Localization Matters: New Insights into Spatio-Temporal Regulation of Type VI Secretion Systems

INAUGURALDISSERTATION

zur
Erlangung der Würde eines Doktors der Philosophie
vorgelegt der
Philosophisch-Naturwissenschaftlichen Fakultät
der Universität Basel

von
Maj Brodmann
aus Basel-Stadt, Schweiz
2019

Genehmigt von der Philosophisch-Naturwissenschaftlichen Fakultät

auf Antrag von

Prof. Dr. Marek Basler

(Fakultätsverantwortlicher)

Prof. Dr. Julia Vorholt

(Korrreferentin)

Basel, den 17.09.2019

Prof. Dr. Martin Spiess

(Dekan)

“Don't let anyone rob you of your imagination, your creativity, or your curiosity. It's your place in the world; it's your life. Go on and do all you can with it, and make it the life you want to live.”

Mae Jemison

Pinky: "Gee Brain, what do you want to do tonight?"

Brain: "The same thing we do every night, try to take over the world!"

Pinky and the Brain

To Marco

SUMMARY

Subcellular organization is important for bacterial cell physiology. Especially, bacterial secretion systems are tightly regulated in a temporal and spatial manner to efficiently fulfill their function. Among them, the contact-dependent Type VI secretion (T6SS) has an important role in inter-bacterial competitions and pathogenicity of Gram-negative bacteria.

T6SS translocates effector proteins into target cells using the contraction of a long cytosolic sheath, which pushes an inner tube together with a sharp tip and associated effectors across target cell membranes. This mode of action allows bacteria to use T6SS against a broad range of prokaryotic and eukaryotic organisms. However, the contact-dependency limits the target range and the efficiency of effector translocation is low because only a small number of effectors can be delivered per one round of T6SS assembly.

Recent advances in live-cell fluorescence and super resolution microscopy led to the revelation that T6SS activation patterns and dynamics are surprisingly diverse in different bacteria. These differences in T6SS assembly dynamics likely reflect different strategies to overcome the disadvantages of T6SS mode of action. However, the spatio-temporal regulation behind these different T6SS firing patterns are not well understood.

My PhD thesis provides new insights into how different subcellular localizations of T6SS assembly are achieved.

The Threonine phosphorylation pathway (TPP) is a unique posttranslational regulation mechanism, which allows *Pseudomonas aeruginosa* to activate its T6SS apparatus in response to membrane damage inflicted by an attack from neighboring bacteria and to localize it to the site of attack. While the involved components are identified, it is not clear how the periplasmic sensor module integrates spatial and temporal information for precise and fast T6SS assembly initiation. To test if relocation of TPP components from outer to inner membrane (IM) is important for

T6SS activation, I changed their subcellular localization by mutating their N-terminal signal sequences. Relocation of one TPP component to IM indeed hyper-activated T6SS assembly, however, the exact mechanism of T6SS localization remains to be elucidated.

In collaboration with Prof. Kevin Foster, University of Oxford, we tested the benefit and cost of TPP-dependent localization of T6SS during bacterial competitions. Our results from *in silico* and imaging experiments suggested that *P. aeruginosa* uses TPP to kill competing bacteria by localized and repeated T6SS assemblies and thus inflicting more damage than it encounters from attacking competitors.

In collaboration with Prof. Petr Broz, University of Lausanne, we characterized the unique *Francisella* pathogenicity island (FPI), which encodes a non-canonical T6SS essential for phagosomal escape. The FPI lacks a specialized unfoldase required for recycling of contracted sheaths and for dynamics of canonical T6SS. Furthermore, the FPI encodes genes with unknown function. By live-cell fluorescence microscopy, we showed that *F. novicida* T6SS dynamics is comparable to canonical T6SS dynamics. Moreover, we found that general-purpose unfoldase ClpB recycles contracted sheaths and is essential for phagosomal escape *in vivo*. By analyzing T6SS dynamics and virulence of single deletion mutants *in vitro* and *in vivo*, we could group FPI components with unknown function into structural components, which are required for T6SS function, and putative effectors, which are critical for virulence but not for T6SS assembly.

Moreover, we showed that *F. novicida* T6SS assembles exclusively at bacterial poles. This unique polar localization raised the question of how *Francisella* T6SS is localized to the poles and whether it is important for T6SS function. I analyzed the dynamics of membrane complex formation, which is the first step of T6SS assembly, by live-cell fluorescence microscopy and structured illumination microscopy. I showed that the membrane complex is stably formed on the poles even in the absence of other FPI components. In addition, the membrane complex formation was insufficient to initiate sheath assembly indicating that additional signals are required to activate T6SS in *F. novicida*.

To investigate the contribution of FPI components and localization of T6SS to *Francisella* virulence in more detail, I established *Galleria mellonella* larvae as

infection model. Besides, I constructed two expression plasmids for *F. novicida*, which are mobilized by conjugation and have tetracyline inducible promoters for tunable gene expression. These new tools will be invaluable in the future research of mechanism required for *F. novicida* pathogenesis.

ACKNOWLEDGEMENTS

This PhD thesis would not have been possible without the support of many different people.

First, I would like to thank my doctoral supervisor Prof. Dr. Marek Basler for his constant support during my PhD thesis and for the scientific freedom to explore my own ideas. His joy for science and his curiosity is inspiring and has always been motivating me to give my best. I also learned a lot in all the scientific discussions. Moreover, I am very grateful for his mentoring and career support, which included the possibility to attend seminars and courses as well as to present my work at multiple conferences important to the field. In addition, I highly appreciate the support for finding a postdoctoral position.

I want to thank my PhD advisory committee member Prof. Dr. Julia Vorholt for coming to my PhD committee meeting every year and for the valuable scientific inputs for my projects. Furthermore, I would like to thank her for being my external reviewer of my PhD thesis.

Many thanks go to my PhD advisory committee member Prof. Dr. Petr Broz for his valued scientific inputs as well as for his collaboration in my *Francisella* projects. I also want to thank him for giving me the opportunity to rotate in his research group at the beginning of my PhD studies. Furthermore, I thank his whole group for the warm welcome and for the very productive collaborations. Especially, I want to thank Dr. Roland F. Dreier for his excellent introduction into the inflammasome field during my rotation project as well as the great teamwork later on. My PhD thesis would not have been as successful without him. Particular thanks go to Rosalie Heilig for accommodating me when I stayed in Lausanne and for her outstanding expertise and help in *Francisella* infections experiments.

Next, I would like to thank all the present and former members of the Basler research group for the excellent working atmosphere as well as their scientific support and willingness to help with problems. Special thanks go to Dr. Mihai Ionescu, Dr. Lin

Lin and Dr. Johannes Schneider for their dedication in keeping the laboratory and the microscope running. In addition, I highly appreciate the help of Linnéa Persson and Laurent Dubois for my different projects. Last, my PhD thesis would only have been half as enjoyable without my peers Dr. Maximilian Brackmann, who introduced me to the microscope as well to most of the laboratory techniques, Dr. Peter Ringel, who wrote a Fiji plug-in for me, Dr. Andrea Vettiger and Dr. Anna Hagmann, who was not only my roommate on all of the study trips but also my soulmate in the scientific world and beyond.

Furthermore, I want to thank the group of Timm Maier for inviting me to apéros and 3rd-floor events. In addition, I am very grateful for the constant supply of Phusion polymerase.

I also want to acknowledge Dr. Thomas Bock from the Protein Core Facility for his assistance with my mass spectrometry samples and Dr. Alexia Loynton-Ferrand from the Imaging Core Facility for her help with structured illumination microscopy. Moreover, I am very grateful for the support from the whole 4th-floor, especially the 4th-floor media kitchen and floor management team were a great help. I also highly appreciate the support from the 4th-floor administrative assistants Michaela Hanisch and Sarah Thomforde.

In addition, I want to express my gratitude towards my funding by the “Fellowship for excellence” program during the first three years and the Werner Siemens-Foundation for financing the amazing study trips every year.

Importantly, I want to thank my father Jan, my mother Silvia and my brother David for believing in me and for the constant support all my life long. You give me the confidence and back-up to live my dreams.

Moreover, I want to thank my friends for all the good times beyond science.

This whole PhD adventure was only possible with the endless support of my partner Marco. He comforts and motivates me when I am frustrated and he is critical when I am too easily satisfied. Moreover, he supports my decision to pursue my career including working on weekends, travelling a lot and moving abroad. Most importantly, he makes life enjoyable no matter what will happen in future.

STATEMENT TO MY THESIS

The work included in this thesis was carried out in the research group of Prof. Dr. Marek Basler in the Focal Area Infection Biology at the Department Biozentrum, University of Basel, Switzerland.

My PhD advisory committee includes:

Prof. Dr. Marek Basler
Biozentrum, University of Basel, Switzerland

Prof. Dr. Petr Broz
Department of Biochemistry, University of Lausanne, Switzerland

Prof. Dr. Julia Vorholt
Institute of Microbiology, ETH Zürich, Switzerland

This thesis is written as a cumulative dissertation with a general introduction on the mechanisms of subcellular organization in bacteria and a special focus on polar macromolecular complexes. Furthermore, a detailed introduction is given on the Type VI secretion system and the two studied model organisms *Pseudomonas aeruginosa* and *Francisella novicida*. The result section contains my work on the threonine phosphorylation pathway in *P. aeruginosa* and a manuscript in preparation about the costs and benefits of the spatio-temporal regulation of the T6SS in *P. aeruginosa*. Then a published research article characterizing the unique T6SS in *F. novicida* follows. A manuscript in preparation analyzing subcellular localization dynamics of *Francisella* T6SS membrane complex as well as additional results for establishing *Galleria mellonella* as infection model for *Francisella* T6SS research are included. Last, a published research article describing a newly designed expression plasmid for *F. novicida* follows. The appendix contains a published

review with recent insights in T6SS structure and in how certain bacteria regulate T6SS localization. To finish, I discuss my findings from the result section and give an outlook about limitations and possibilities to study bacterial subcellular localization in future.

CONTENT

I. INTRODUCTION

1. Subcellular organization in bacteria

Life requires organization in order to create the necessary environment to perform all biochemical reactions for growth and replication. The most basic way to organize a confined space is to separate it from the abiotic environment. Thus, the cytosol of every cell is surrounded by at least one biological membrane. It is commonly accepted that eukaryotic cells are highly spatially as well as temporally organized and compartmentalized. In contrast, prokaryotes to whom bacteria belong, were previously defined by the lack of a nucleus and thus compartmentalization (Woese et al., 1990). The average bacterial cytosol has a volume of 0.7 μm^3 and is therefore very limited in space (Kubitschek, 1990). Yet it contains everything which is required for successful propagation in diverse niches. Therefore, it is not surprising that bacterial cells are also highly organized in a temporal and spatial manner although the appreciation of this fact came only recently (Surovtsev and Jacobs-Wagner, 2018). Technical advances in electron microscopy and light based microscopy reveal much higher intracellular organization in prokaryotes than appreciated before (Cornejo et al., 2014; Glaeser, 2019; Schermelleh et al., 2019; Surovtsev and Jacobs-Wagner, 2018).

The most striking compartmentalization feature of bacteria is their cell envelope. Gram-positive bacteria are enclosed by one membrane while Gram-negative bacteria possess two membranes. (Gupta, 1998). In both cases, they possess a rigid cell wall made of a peptidoglycan layer, a meshwork of glycan strands cross-linked by peptides, surrounding the cytoplasmic or inner membrane (IM) (Typas et al., 2011). The outer membrane (OM) and IM of Gram-negative bacteria also create an additional compartment called periplasm. Furthermore, the surface of Gram-negative bacteria is covered by lipopolysaccharide (LPS) anchored to the OM by Lipid A, which acts as a barrier to small hydrophobic and hydrophilic molecules (Ruiz et al., 2009).

The cell wall is also responsible for the diverse shapes of bacteria, which can range from coccus to rod shaped including more sophisticated shapes like spirals, filaments, curved, Y-shaped or star formed bacteria (Young, 2006). The bacterial cell shape defines not only the surface to volume ratio, which has implications in nutrient acquisition, motility and niche colonization, but is also an important feature to

organize a cell (Surovtsev and Jacobs-Wagner, 2018; Young, 2006). Defined cellular compartments as consequence of the cell shape include prosthecae; thin appendages which contain little cytoplasm (e.g. stalk of *Caulobacter crecentus*) or specialized nitrogen fixing cells in filamentous *Cyanobacteria* (Rossetti et al., 2010). The most prominent compartment in rod-shaped bacteria are the poles. In chapter 1.6., the polar compartment including mechanisms to localize proteins to poles will be discussed in more detail.

1.1. Crossing the cell envelope

While the cell envelope is necessary to define the intracellular milieu and may protect the bacterial cell from environmental influences, it also restricts bacteria in the interaction with the extracellular environment. In order to scavenge nutrients, communicate or compete, bacteria possess highly regulated channels, porins and secretion systems to bridge the cell envelope (Costa et al., 2015; Lasica et al., 2017; Nikaido, 2003; van Wely et al., 2001). The most prominent pathways to secrete unfolded or folded proteins to periplasm are the general secretory (Sec-) and Twin-arginine (Tat-) pathways, respectively (Palmer and Berks, 2012; Tsirigotaki et al., 2017). Proteins secreted by these two pathways encode specific peptides for secretion. The essential Sec-Pathway recognizes a N-terminal positively charged signal sequence which is cleaved by a signal peptidase in periplasm (Tsirigotaki et al., 2017). Tat-pathway targeting is mediated by a N-terminal signal sequence, which contains a twin arginine motif (Palmer and Berks, 2012).

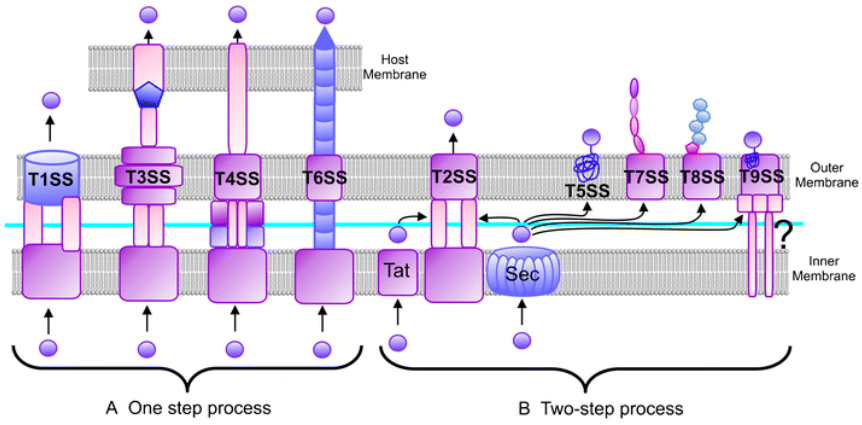

Figure 1: Summary of known bacterial secretion systems. T1SS, T3SS, T4SS and T6SS translocate their cargo in one step while T2SS, T5SS, T7SS, T8SS and T9SS require Sec- or Tat-pathway. *Source: Bocian-Ostrzycka et al., 2017, licensed under Creative Commons Attribution 4.0 International License (http://creativecommons.org/licenses/by/4.0/).*

In addition, nine specialized secretion systems are characterized so far (Type I-IX, figure 1) (Abdallah et al., 2007; Costa et al., 2015; Desvaux et al., 2009; Lasica et al., 2017; van Wely et al., 2001). The secretion systems differ in substrate recognition and type of substrate (unfolded/folded proteins and/or deoxyribonucleic acid (DNA)) (Costa et al., 2015). In Gram-negative bacteria, most secretion systems span across both IM and OM (Type I (T1SS), Type II (T2SS), Type III (T3SS), Type IV (T4SS) and Type VI (T6SS)). Type V (T5SS), Type VIII (T8SS) and Type IX (T9SS) secretion systems translocate their substrates across the OM after they are transported into periplasm via Sec- or Tat-pathway (Costa et al., 2015; Desvaux et al., 2009; Lasica et al., 2017). Type VII secretion systems (T7SS) are exclusively found in Gram-positive bacteria, especially in *Mycobacteria* (Abdallah et al., 2007). One particular secretion system, the T6SS will be discussed in more detail in chapter 2.

1.2. Periplasmic organization

The periplasmic space in Gram-negative bacteria includes the peptidoglycan layer and is defined by its oxidizing environment and lack of adenosine triphosphate (ATP) (Merdanovic et al., 2011). It is used to compartmentalize and sequester potentially harmful enzymes such as alkaline phosphatase (Silhavy et al., 2010). Many periplasmic proteins are lipoproteins which are anchored to either the IM or OM by a lipid moiety. Lipoproteins are transported to periplasm by the Sec-pathway, then a localization of lipoprotein (Lol) machinery localizes lipoproteins to their final destinations (figure 2) (Okuda and Tokuda, 2011). In *Escherichia coli*, membrane specificity is given by the second and third amino acid and after the cleavage site of the signal peptide for Sec-pathway dependent transport (Gennity and Inouye, 1991; Seydel et al., 1999). Especially, an aspartate at the second position after the cleavage site yields in IM localization in *E. coli* (Okuda and Tokuda, 2011). However, the specific IM retention signal may differ in different species. In *Pseudomonas aeruginosa*, the multidrug efflux pump component MexA sits in the IM facing periplasm but has a glycine at the second positions after the cleavage site. In addition, membrane specificity in *P. aeruginosa* is rather determined by position 3 and 4 (Narita and Tokuda, 2007).

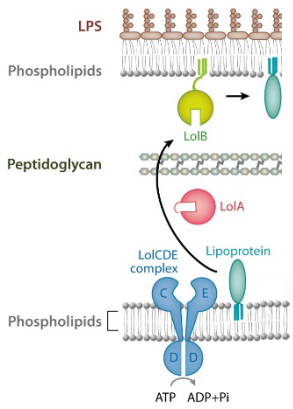

Figure 2: Overview of lipoprotein sorting. The Lol complex localizes lipoproteins to their final destination. *Source: Adapted from Okuda and Tokuda, 2011. Reproduced with permission of Annual Reviews in the format Thesis/Dissertation via Copyright Clearance Center.*

Periplasm also harbors many signaling cascades transducing information from the OM to the cytosol, which allows the bacterial cell to monitor the extracellular environment. For example, *E. coli* possesses several sensors for sensing envelope stress. The σ^E stress-response integrates unassembled OM proteins as well as disturbed LPS biogenesis and induces upregulation of an array of genes involved in assembly and transport of OM proteins and LPS (Lima et al., 2013). The Rcs phosphorelay monitors β-barrel assembly in the OM by OM lipoprotein RcsF, IM proteins IgaA, RcsC and RcsD (figure 3) (Cho et al., 2014). Normally, lipoprotein RcsF is transported to the inner leaflet of the outer membrane by the chaperone LolA and then is shuffled together with OmpA to the cell surface by BamA. Upon envelope stress, RcsF fails to bind BamA and is exposed to periplasm, where IgaA binds RcsF and initiates the downstream RcsC/D cascade and upregulation of genes involved in periplasmic quality control, motility and virulence (Cho et al., 2014).

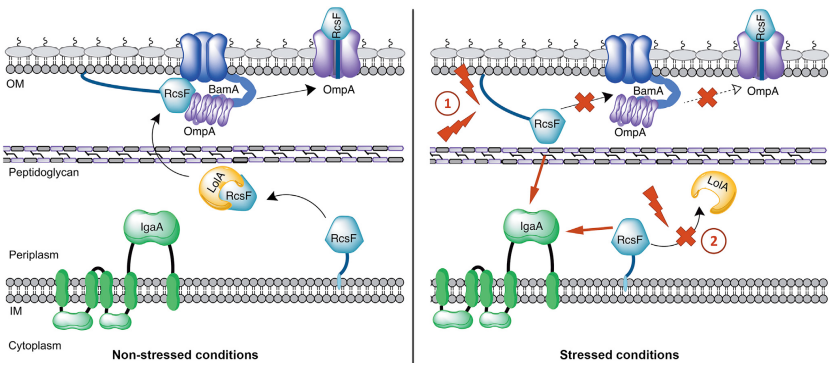

Figure 3: Model for sensing envelope stress by Rcs phosphorelay. Under normal conditions. lipoprotein RcsF is shuffled to the cell surface via BamA and OmpA. Upon envelope stress, BamA does not have the capacity to bind RcsF. Thus, RcsF binds IgaA and triggeres the downstream RcsC/D cascade. *Source: Cho et al., 2014. Reprinted with permission from Elsevier.*

1.3. Remodeling the cell wall

Crucial for maintaining and adapting the cell shape to environmental stimuli is the constant synthesis and remodeling of the peptidoglycan layer (figure 4) (Surovtsev and Jacobs-Wagner, 2018; Typas et al., 2011). Intensive remodeling of the peptidoglycan layer occurs during growth and division of a bacterial cell. However, loss of peptidoglycan integrity may be detrimental and thus, the modulation of peptidoglycan is tightly regulated. Peptidoglycan precursors (uridine diphosphate-*N*-acetylglucosamine and uridine diphosphate-*N*-acetylmuramylpentapeptide) are first synthesized in the cytosol and then flipped across the IM after forming lipid-anchored disaccharide pentapeptide monomer subunits (Barreteau et al., 2008; Bouhss et al., 2008). Then these subunits are polymerized into glycan strands by glycosyltransferases (penicillin binding proteins) and incorporated into the existing peptidoglycan layer, where crosslinking of the peptides by *DD*-transpeptidases occurs. (Typas et al., 2011; Vollmer and Bertsche, 2008). To insert new glycan strands, the existing peptidoglycan layer is cleaved by periplasmic peptidoglycan hydrolases, amidases, and lytic transglycosylases (Typas et al., 2011; Vollmer et al., 2008). Peptides are cleaved by *DD*- and *LD*-carboxypeptidases. Cleavage by amidases occurs mainly during septum cleavage (Typas et al., 2011). In general, peptidoglycan cleavage is controlled by incorporating the cleaving enzymes into the peptidoglycan synthesis machinery, so that they cannot hydrolyze peptidoglycan at locations without simultaneous peptidoglycan synthesis (Höltje, 1998). In addition, bacteria encode specific activators or inhibitors located in the periplasm to modulate hydrolase activity (Clarke et al., 2010; Morlot et al., 2010).

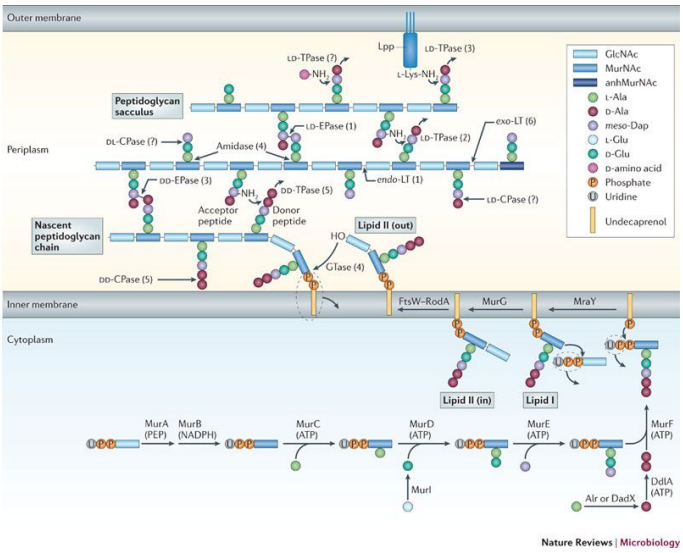

Figure 4: Overview of peptidoglycan synthesis and remodeling. Peptidoglycan precursors are synthesized in the cytosol and then flipped across the membrane into the periplasm. Peptidoglycan precursors are polymerized into glycan strands by glycosyltransferases (Gtases). Newly formed glycan strands are inserted in the peptidoglycan layer by *DD*-transpeptidases (*DD*-TPases). Lytic transglycosylases (LTs) cleave glycan chains Amidases remove peptides from glycan chains while peptides are trimmed by carboxypeptidases (CPases). Crosslinks between peptides are cleaved by endopeptidases (EPases). *Source: Typas et al., 2011. Reprinted by permission of Springer Nature.*

During cell elongation, circular peptidoglycan insertion into multiple sites of the lateral cell wall is coordinated by the actin-like protein MreB (figure 5) (Errington, 2015; Jones et al., 2001). MreB filaments recognize negative curvature and move along the cytoplasmic side of the IM orthogonal to the long axis together with the peptidoglycan synthesis machinery (Hussain et al., 2018; Olshausen et al., 2013). The two complexes are connected by transmembrane proteins RodZ and MreC/D (Typas et al., 2011). Although, it is clear that MreB motion is dependent on peptidoglycan synthesis, it is not known, how exactly MreB spatially controls peptidoglycan insertion and how for example the diameter of the cell is regulated (Surovtsev and Jacobs-Wagner, 2018). Nevertheless, MreB is crucial for maintaining the rod-shaped form in many bacteria. Interestingly, MreB does not exist in all rod-shaped bacteria and on the other hand also some coccoid bacteria possess MreB (Daniel and Errington, 2003). Rod-shaped bacteria lacking MreB may grow at the poles, such as *Agrobacterium tumefaciens* or *Mycobacterium smegmatis* (Surovtsev and Jacobs-Wagner, 2018).

Peptidoglycan remodeling during cell division is coordinated by the tubulin-like protein FtsZ, the master regulator of bacterial cell division (figure 5) (Adams and Errington, 2009). FtsZ forms a dynamic ring-like structure at the future division site and recruits proteins essential for the division including FtsA/K/W and ZipA (Aarsman et al., 2005; Erickson et al., 2010). Moreover, FtsZ also recruits enzymes of the peptidoglycan synthesis machinery for formation of the septum and synthesis of the new polar peptidoglycan (Aaron et al., 2007; den Blaauwen et al., 2017; Typas

et al., 2011). Polar peptidoglycan is characterized by fewer stem peptides compared to the lateral cell wall due to the activity of *N*-acetylmuramyl-*L*-alanine amidases (Peters et al., 2011).

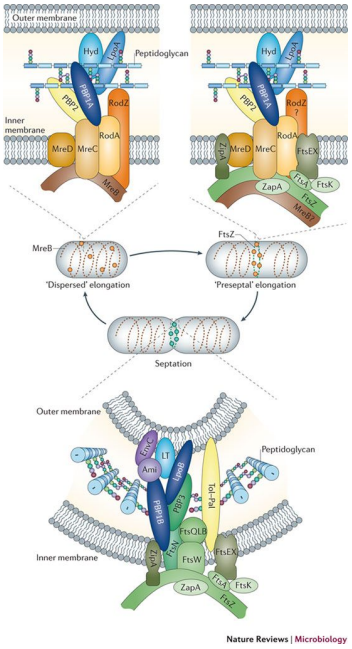

Figure 5: Protein complexes for remodeling peptidoglycan during growth and septation. For lateral growth, MreB coordinates peptidoglycan insertion by controlling the activity of glycosyltransferases and hydrolases. For septation, FtsZ organizes the divisome complex which includes cell division proteins, glycosyltransferases, amidases with their activators and proteins of the Tol-Pal complex for OM constriction. *Source: Typas et al., 2011. Reprinted by permission of Springer Nature.*

Next to MreB and FtsZ, many other cytoskeleton-like proteins sculpt the bacterial cell (Lin and Thanbichler, 2013). One example is crescentin in *C. crescentus*, which is anchored to the IM by MreB and is responsible for curved cell shape. Crescentin generates a compressive force to reduce the peptidoglycan insertion rate (Cabeen et al., 2009; Charbon et al., 2009). Other scaffold proteins include bactofilins, which are for example required for the helical shape of *Helicobacter plyori* by modulating the peptidoglycan crosslink hydrolases (Sycuro et al., 2010) or for generating the stalk in *C. crescentus* (Kühn et al., 2010).

1.4. Cytosolic organization

At first sight, bacteria do not have any cytoplasmic organization. However, they evolved many mechanisms to organize their cytosol. A prominent structural feature in the cytosol is the nucleoid. The nucleoid contains the compacted chromosome(s), is highly organized and occupies different amount of space in different bacteria (Gray

et al., 2019). For example, transcription and translation are partially separated in *E. coli* because messenger ribonucleic acids (mRNAs) loaded with multiple ribosomes locate in the nucleoid free poles as they are probably too big to diffuse through the compact nucleoid (Bakshi et al., 2012). Similarly, also mRNA degradation takes place more at the membranes as the ribonucleases are located outside of the nucleoid region in *E. coli* (Surovtsev and Jacobs-Wagner, 2018). This stands in contrast to *C. crescentus*, in which the nucleoid spans through the whole cell. There the ribosomes as well as the RNAses are located more inside the nucleoid (Surovtsev and Jacobs-Wagner, 2018). Nucleoid occlusion is also used to control the site of division. Nucleoid occlusion factors such as SlmA in *E. coli* and Noc in *Bacillus subtilis* bind to DNA and inhibit FtsZ-ring polymerization at locations where the chromosome is (Wu and Errington, 2011).

Another system for positioning the division site is the Min system in *E. coli* (figure 6) (Hu and Lutkenhaus, 1999). FtsZ-inhibitor MinC oscillates between the two poles resulting in a minimal MinC concentration in the mid-cell area over time, where the FtsZ-ring can polymerize (Raskin and de Boer, 1999). MinC oscillation is driven by the interaction between ATPase MinD in an ATP-bound state and MinE, which induces ATPase activity of MinD. Then, MinD is released from the membrane and so is MinC, which is bound to MinD (Park et al., 2011). After nucleotide exchange, MinD can re-enter 7the ATP-bound stage and associates with the membrane again. This antagonism between MinD and MinE yields in an oscillation of MinD and MinE between the two poles (Surovtsev and Jacobs-Wagner, 2018). Fascinatingly, the Min system can also be artificially reconstituted resulting in the same oscillation behavior as observed inside bacterial cells (Vecchiarelli et al., 2016).

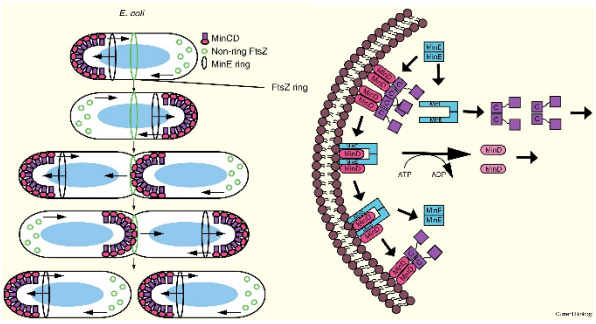

Figure 6: Positioning the site of division. Z-ring formation is inhibited at the poles by MinC (left), which oscillates from pole to pole driven by antagonistic interactions between MinD and MinE (right). *Source: Adapted from Rowlett and Margolin, 2013. Reprinted with permission from Elsevier.*

While high copy number cellular components are distributed by diffusion during cell division, it is a particular challenge to distribute low copy number components. Random distribution would likely result in one cell without or too little of these low copy components. Therefore, bacterial cells have several mechanisms to ensure equal distribution of low copy number components such as plasmids. The ParM/R system actively transports these plasmids to both poles by cytoskeletal filaments made of actin homologs (figure 7) (Gayathri and Harne, 2017). Thereby the actin-like filament consisting of ParM is stabilized as soon as the tip of the filaments binds a plasmid via ParR. The other end of the filament is stabilized through binding to another ParM filament in an antiparallel manner. Thus, plasmid binding yields in polymerization of two stable ParM filaments in an antiparallel manner thereby the plasmids are pushed towards each pole (Gayathri and Harne, 2017).

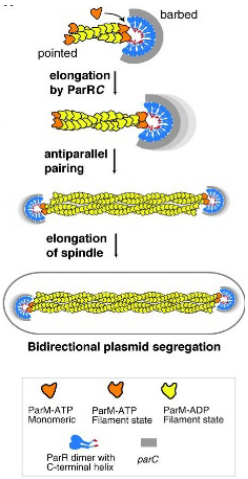

Figure 7: Plasmid distribution to poles by the ParM/R system. A bipolar spindle formed by ParM subunits pushes plasmid bound to ParR towards the poles. *Source: Gayathri et al., 2012. Reprinted with permission from AAAS.*

Another partitioning system consists of ParA/B, which results in a regularly spaced distribution of plasmids inside the bacterial cell (figure 8). ATPase ParA non-specifically binds to the nucleoid in an ATP dependent manner. Plasmid bound ParB recognizes ParA and is pulled towards ParA (Baxter and Funnell, 2014). Binding of ParA by ParB results in ATPase activity of ParA and thereby the ParA/B complex falls apart. These transient interactions between ParA and ParB lead to a recurrent pulling along an ATP-bound ParA gradient (Ringgaard et al., 2009). When multiple plasmids are present, the ATP-bound ParA gradient is eventually depleted between plasmids resulting in an evenly spaced pattern. Chromosome segregation may also

be driven by the ParA/B system, or by hub proteins located at the poles (see chapter 1.6.) (Surovtsev and Jacobs-Wagner, 2018).

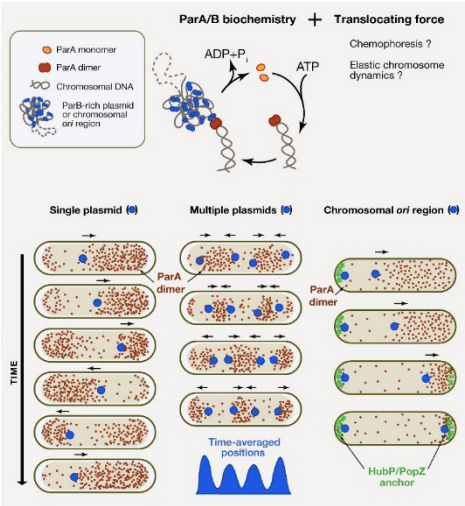

Figure 8: Plasmid segregation by the ParA/B system. Plasmids bound to ParB are pulled towards dimers of ParA. Eventually, ParB binding to ParA results in ParA monomerization and the ParA/B complex falls apart. Thus, translocation of plasmids bound to ParB towards gradient of dimerized ParA results in segregation of plasmids. *Source: Surovtsev and Jacobs-Wagner, 2018. Reprinted with permission from Elsevier.*

1.5. Organelles and microcompartments

Bacteria use also specialized cytosolic compartments to perform biochemical reactions which may be potentially harmful to the bacterial cell due to toxic intermediates or unwanted side-reactions (Cornejo et al., 2014; Grant et al., 2018; Kerfeld et al., 2018).

Organelles are one class of these intracellular compartments, which are surrounded by a lipid bilayer. A particularly well studied example is spore formation in *B. subtilis*. First, an asymmetric septum is formed leading to a big mother cell and a small forespore. Then the mother cell engulfs the forespore by remodeling the membrane and the peptidoglycan layer (Higgins and Dworkin, 2012). Proteins involved in formation of this internal, double membraned compartment include cell wall synthesis and degradation proteins as well as proteins required for membrane remodeling (Cornejo et al., 2014; Higgins and Dworkin, 2012). One of these proteins, SpoVM, recognizes positive curved membranes (Ramamurthi et al., 2009).

Another lipid-bound organelle is the magnetosome in magnetotactic bacteria, which allows navigation along magnetic fields (Blakemore, 1975). Magnetosomes are formed by invagination of the IM and contain magnetite or greigite, which are both iron-based crystals (Cornejo et al., 2014; Grant et al., 2018). Interestingly, the magnetosomes are aligned as chains inside the bacterial cell. Essential for positioning

of individual magnetosomes is MamK, a homolog of actin-like MreB (figure 9) (Grant et al., 2018).

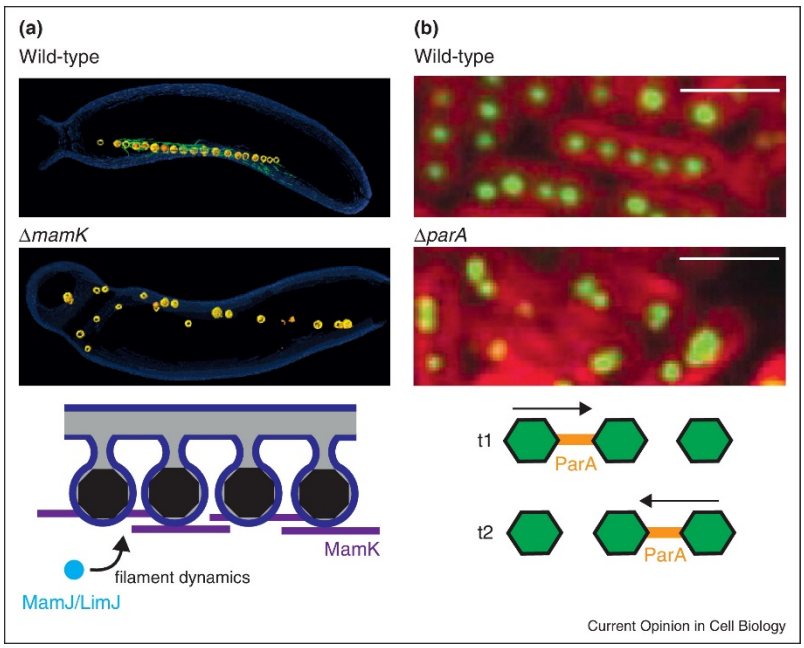

Figure 9: Positioning of magnetosomes and carboxysomes. Positioning of magnetosomes relies on MamK, a homolog of actin-like MreB. ParA is required for equal spacing of carboxysomes. *Source:Cornejo et al., 2014. Reprinted with permission from Elsevier.*

Anammoxosomes in some chemolithoautotrophic bacteria are used to convert ammonium and nitrite into nitrogen gas generating a proton-motive force by anaerobic ammonium oxidation (Grant et al., 2018). The lipid-surrounded organelle occupies about 60 % of the total cell volume and the membrane is enriched in ladderanes, required to restrict passive diffusion of protons and thus limiting energy loss (Neumann et al., 2014). Widely spread are also membrane-bounded storage granules, the best-characterized ones are polyphosphate granules from *A. tumefaciens* and *Rhodospirillum rubrum* (López-Marqués et al., 2004; Seufferheld et al., 2003).

Bacterial microcompartments consist entirely out of proteins encapsulating metabolic enzymes. A well-studied example is the carboxysome, which is found in *Cyanobacteria* and some chemoautotrophic bacteria. This microcompartment is required for producing 3-phospho-glycerate from CO_2 (Kerfeld et al., 2018). Carboxysomes contain the most abundant enzyme in the world called RuBisCo (ribulose-1,5-bisphosphate carboxylase/oxygenase) required for the first step of fixing CO_2 (Spreitzer and Salvucci, 2002). Like magnetosomes, carboxysomes are

arranged linearly in a regular pattern in *Cyanobacteria*. The subcellular arrangement of carboxysomes relies on the cytoskeletal protein ParA, which is involved in plasmid and chromosomal DNA segregation (figure 9) (Savage et al., 2010). Interestingly, some of these microcompartments are linked to virulence and fitness advantage in the gut for some enteric pathogens (e.g. *Salmonella typhimurium*, *Listeria monocytogenes* and enterohemorrhagic *E. coli*) (Bertin et al., 2011; Jakobson and Tullman-Ercek, 2016; Joseph et al., 2006; Kerfeld et al., 2018).

1.6. Organization of the polar compartment

An important compartment in rod-shape bacteria are the poles. They provide biochemical and physical cues required for proper subcellular localization of hub proteins. Hub proteins act as scaffold proteins for many different cellular components involved in chemotaxis, motility, cell differentiation, cell-cycle regulation and secretion (figure 10).

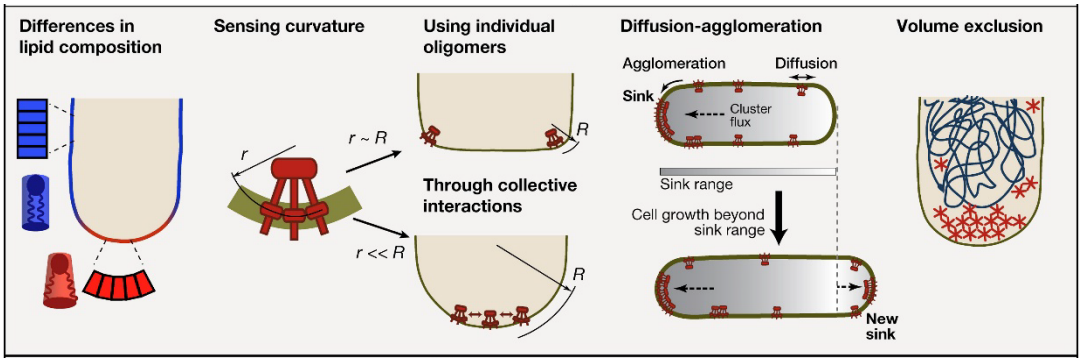

Figure 10: Cues to localize proteins to the poles. Bacterial poles have a different lipid composition, which can be recognized by some proteins. Other proteins sense the negative curvature of the poles. Poles may also act as sink for big protein clusters. Furthermore, the nucleoid can exclude big protein clusters and thus promote polar localization. *Source: Adapted from Surovtsev and Jacobs-Wagner, 2018. Reprinted with permission from Elsevier.*

The most prominent physical cue at the poles is the negative curvature of the membrane. Certain proteins such as MreB in rod-shaped bacteria or hub protein DivIVa in *B. subtilis* recognize negatively curved membranes (Hussain et al., 2018; Lenarcic et al., 2009). However, MreB does not localize to poles as the lipid composition at poles with its anionic phospholipids, such as cardiolipins, likely repels MreB (Kawazura et al., 2017). Thus, polar peptidoglycan is much more stable in rod-shaped bacteria with MreB dependent peptidoglycan insertion (Young, 2006). Therefore, the polar compartment is ideal for OM proteins or proteins inserted into

the peptidoglycan, which need to be in close proximity (e.g. chemoreceptors or large protein complexes) as they will not be separated during growth (de Pedro et al., 2004).

DivIVa is specifically localized to the poles as a function of its intrinsic physical properties, which allows molecular bridging of the negative curvature by DivIVa multimers. Therefore DivIVa clusters more likely at maturated and newly forming poles (Lenarcic et al., 2009). Although a membrane protein, chemoreceptor TlpA in *E. coli* also specifically recognizes the negative curvature due to its conical shape as trimer (Strahl et al., 2015). Other chemoreceptors, however, may cluster at the poles based on their ability to act as a sink for smaller clusters. As the two poles have the maximum distance possible between each other, large clusters will likely agglomerate there (Thiem and Sourjik, 2008). Bacteria also use the advantage of spatial separation through the poles. For example, *Rhodobacter sphaeroides* possesses two sets of chemoreceptors with different functions. One is localized at the poles and one is inserted into the lateral wall. Thus, crosstalk between the two sets of chemoreceptors is avoided (Wadhams et al., 2003).

Self-assembling hub protein PopZ in *C. crescentus* is localized to the poles by a volume exclusion mechanism. In *C. crescentus*, the nucleoid is spread throughout the bacterial cell, thus big PopZ oligomers are limited to the DNA-free poles (Ebersbach et al., 2008; Saberi and Emberly, 2010). Another known hub protein is HubP in *Vibrio cholerae*, which controls the polar localization of chromosome origin of replication, chemotactic machinery and flagellum (Yamaichi et al., 2012). However, it is not clear how transmembrane protein HubP is recruited to nascent poles; one possibility could be that HubP recognizes features of polar peptidoglycan via its LysM domain as it was shown for hub protein FimV in *P. aeruginosa* and for many other LysM domain containing proteins (Buist et al., 2008; Wehbi et al., 2011; Yamaichi et al., 2012).

Next to the known hub proteins, several other cellular components are localized to the poles by various mechanisms. A possible way to localize proteins to the poles is the “diffusion and capture” mechanism in which a protein randomly diffuses through the bacterial cell until a target protein or hub protein at the pole transiently or persistently captures it (Shapiro et al., 2009). PleC in *C. crescentus*, a histidine kinase

required for developing two asymmetric daughter cells, is localized at one pole while PleC proteins in the midcell area diffuse randomly suggesting that PleC is captured at the poles (Deich et al., 2004). Another example is how the origin of replication of the chromosome is localized to the poles prior chromosome segregation in some bacteria. In *C. crescentus* and *V. cholerae* (large chromosome), ParB binds the origin of replication region and is then captured by PopZ or HubP, respectively (figure 8) (Bowman et al., 2008; Yamaichi et al., 2012).

1.6.1. Polar localization of macromolecular complexes

Interestingly, many adhesins and pili are located at the poles. One explanation for this accumulation of attachment complexes at the poles may be the charge repulsion created by the negatively charged surfaces of bacteria and their natural attachment surfaces (van Loosdrecht et al., 1989; Young, 2006). By approaching the surface with the polar site first, bacteria may minimize and overcome the charge repulsion before aligning the rest of the cell in a second step (Agladze et al., 2005; Burrows, 2012; Hogan and Kolter, 2002; Sangermani et al., 2019).

In *P. aeruginosa*, polar localization of Type IVa pilus machinery is achieved by inserting it at future division sites. Hub protein FimV and non-polar protein PocA recruit components of the Type IVa pilus (Carter et al., 2017; Cowles et al., 2013). Pre-installing the Type IVa pilus at nascent poles has the advantage that no peptidoglycan hydrolases are required to make space in the already existing peptidoglycan layer. PocA is also required for polar localization of the *P. aeruginosa* flagellum (Cowles et al., 2013).

In general, many flagella are polarly localized; likely because they have advantages for directed movement in liquid and viscous environments (Young, 2006). Localization of polar flagella depends on hub proteins such as HubP in *V. cholerae* or TipN in *C. crescentus*, which marks the newly synthesized pole (Huitema et al., 2006; Yamaichi et al., 2012).

Polar secretion systems (T2SS-T7SS) are reported for Gram-negative and Gram-positive bacteria. Many of them are involved in host-pathogen interactions (Carlsson et al., 2009; Chakravortty et al., 2005; Charles et al., 2001; Jain et al., 2006; Jeong et

al., 2017; Morgan et al., 2010; Rosch and Caparon, 2004; Scott et al., 2001). However, most reports using fluorescence or electron microscopy are only descriptive regarding the polar localization of these secretion systems.

The T2SS (extracellular protein secretion apparatus) required for secretion of cholera toxin and proteases is predominately localized to the old pole in *V. cholerae* (Scott et al., 2001). However, eventually the T2SS becomes bipolar in old cells, suggesting that the recognized properties may include markers of matured poles. Interestingly, one T2SS component EpsM can localize to the poles independently from the other T2SS components (Scott et al., 2001). Nevertheless, it is still an open question how the secreted substrates are localized to the polar periplasm, since the Sec-pathway is not polarly distributed in *V. cholerae* (Scott et al., 2001). Similarly, one T2SS (Xcp system) in *P. aeruginosa* is also localized at one cell pole (Senf et al., 2008).

The T3SS (*Salmonella* pathogenicity island 2) in *S. typhimurium* promotes intracellular survival in enterocytes of the intestinal mucosa (Chakravortty et al., 2005). Strikingly, secreted effectors as well as the secretion apparatus is localized at one of the poles inside eukaryotic cells (Chakravortty et al., 2005; Nikolaus et al., 2001). Translocon component IpaC in *Shigella flexneri* is accumulated at the pole before it is polarly secreted in a T3SS dependent manner and then inserted into the host cell membrane (Jaumouillé et al., 2008). Interestingly, IpaC is targeted to the same pole as IcsA which is required for the actin-based motility inside eukaryotic cells (Jaumouillé et al., 2008).

Several T4SS secretion systems were found to be polarly localized, for example in *Coxiella burnetii* (Dot/Icm), *A. tumefaciens* (VirB/D4) as well as in *Legionella pneumophila* (Dot/Icm) (Jeong et al., 2017; Judd et al., 2005; Kumar and Das, 2002; Morgan et al., 2010). *Coxiella burnettii* T4SS is required for modulation of the parasitophorous vacuole, the intracellular niche of *C. burnettii* inside macrophages (Winchell et al., 2014). Localization of *C. burnettii* T4SS to one or both poles is suggested to enhance secretion of effector proteins across the vacuolar membrane (Morgan et al., 2010). On the other hand, the function of the unipolar T4SS in *A. tumefaciens* T4SS seems to be easily explained by the observation that *A. tumefaciens* polarly attaches to plant cells for T4SS dependent transfer of DNA and effector proteins (Judd et al., 2005; Matthysse, 1987). However, a newer report using

deconvolution microscopy suggests a more helical localization pattern of T4SS in *A. tumefaciens* and its co-localization with cytoskeletal protein MinD (Aguilar et al., 2010). Nevertheless, four components of the VirB/D4 T4SS (VirB4, VirB8, VirB11 and VirD4) in *A. tumefaciens* are capable of independently localizing to the pole in a so far unknown manner (Judd et al., 2005). The best-studied polar T4SS resides in *L. pneumophila* and is required for maintaining the *Legionella* containing vacuole inside eukaryotic cells (Qiu and Luo, 2017). *L. pneumophila* T4SS is localized to both poles. Interestingly, it is also the first polar secretion system for which it was shown that the polar localization is required for virulence (Jeong et al., 2017). Jeong et al., 2017 showed that mislocalization of the T4SS results in decreased virulence inside eukaryotic cells despite functional effector secretion. Polar localization of *L. pneumophila* T4SS likely depends on cell division proteins as T4SS were observed at newly formed septa. However, the exact mechanism is not known (Jeong et al., 2017). In addition, polar localization also depends on structural components DotU and IcmF, which localize to the poles on their own (Ghosal et al., 2019).

Polar T5SS or auto-transporters are found in several bacterial species including *Bordetella pertussis* (BrkA), *E. coli* (AIDA-I) or *S. flexneri* (SepA and IcsA) (Jain et al., 2006). The best-studied example is IcsA in *S. flexneri*, which is required for intra- and intercellular mobility (Goldberg et al., 1993). IcsA exhibits interesting subcellular localization dynamics; as it first inserts into the OM at the old pole, where it mediates the assembly of an actin tail, and then laterally diffuses towards the new pole (Steinhauer et al., 1999). Important for maintaining polar localization at the old pole in *S. flexneri* is the non-localized cleavage of IcsA by OM serine protease IcsP at the bacterial surface. In absence of IcsP, IcsA is distributed over the entire surface (Egile et al., 1997). In addition, polar localization of periplasmic acid phosphatase PhoN2 in *S. flexneri* seems to be required for wild-type levels of polar IcsA (Scribano et al., 2014). Recently, it was also shown that cytoskeleton protein MreB, which is normally distributed throughout the bacterial cell, in *S. flexneri* localizes to the same pole as IcsA in infected Hela cells (Krokowski et al., 2019). Nevertheless, it is not clear how IcsA is targeted to the pole. It is thought that the C-terminal part recognizes a putative polar target prior secretion (Charles et al., 2001). Interestingly, the C-terminal part of IcsA localizes to the pole also in a variety of *Enterobacteriacae* as well as in *V. cholerae*, suggesting that the recognized polar target is conserved

(Charles et al., 2001). Polar localization in non-native *E. coli* was also reported for BrkA, AIDA-I and SepA (Jain et al., 2006). Strikingly, even auto-transporter NalP from *Neisseria meningitidis*, a spherical shaped bacterium, localizes to the poles in *E. coli*, confirming that polar T5SS likely use a conserved mechanism to target the poles (Jain et al., 2006).

The vast majority of T6SS are localized at variable sites in bacterial cells. However, there is one report suggesting that *Burkholderia thailandensis* T6SS-5, which is required for formation of multinucleated giant cells inside host cells, is polarly localized (Schwarz et al., 2014). In addition, we characterized a polar T6SS in *Francisella novicida* required for phagosomal escape in chapter 3.3. (Brodmann et al., 2017). Polar localization of T6SS will be discussed in more detail in chapter "2.3.5. Polar localization".

The T7SS (ESX-1) in *Mycobacterium marinum* and *M. smegmatis*, required for intracellular survival in macrophages, is preferentially assembled at the pole, where peptidoglycan synthesis is active (Carlsson et al., 2009; Wirth et al., 2012). Polar localization depends on scaffold protein SaeC, however, it remains to be determined how SaeC localization is controlled (Wirth et al., 2012).

Furthermore, polar secretion of a toxin was reported (Geiger et al., 2018). Pathogenicity of *Salmonella enterica* subspecies *typhi* depends on the secretion of the typhoid toxin (Galán, 2016). The individual components of the typhoid toxin are secreted to periplasm by the Sec-pathway, where they assemble to a holotoxin complex. In order to cross the peptidoglycan layer, the typhoid toxin requires peptidoglycan cleavage by TtsA muramidase localized at the poles (Geiger et al., 2018). However, TtsA activity requires specific *LD*-crosslinked peptidoglycan, which is carried out by *LD*-transpeptidase YcbB. Interestingly, exponentially growing bacterial cells contain much more *DD*-crosslinks than *LD*-crosslinks, suggesting that environmental cues may change the overall architecture of the peptidoglycan layer in the *Salmonella* containing vacuole (Quintela et al., 1997). Therefore, the remarkable substrate specificity of TtsA may be a mechanism to regulate typhoid toxin secretion in a temporal and spatial in response to environmental cues manner (Geiger et al., 2018).

In *Streptococcus pyogenes*, a single microdomain inserted in the cytoplasmic membrane called ExPortal is used to polarly secrete proteins in a Sec-pathway dependent manner (Rosch and Caparon, 2004). The ExPortal is located either at the old pole or at the newly formed septum. Its polar localization may facilitate the organization and concentration of accessory factors which help with the folding of the secreted protein on the bacterial cell surface of Gram-positive bacteria (Rosch and Caparon, 2005).

Interestingly, there is one report showing that also some bacteriophages tend to infect bacteria at the poles, especially at low multiplicity of infection (MOI) (Edgar et al., 2008). While it is not elucidated how these bacteriophages target the bacterial poles, it is striking that bacterial proteins involved in the infection process such as ManY and FtsH are also localized at the poles (Edgar et al., 2008).

2. Type VI Secretion System

The T6SS, found in over 25 % of all sequenced Gram-negative bacteria, is a contractile nano-machine to deliver effector proteins into prokaryotic and eukaryotic target cells in a contact-dependent manner (Bingle et al., 2008; Ho et al., 2014). Originally, the T6SS was found in a transposon screen to identify new virulence factors in *V. cholerae* required for killing *Dictyostelium discoideum* (Pukatzki et al., 2006). Before its actual discovery, mutations inside T6SS gene clusters of pathogens were associated with decreased virulence in various infection models (Bladergroen et al., 2003; Das and Chaudhuri, 2003; Folkesson et al., 2002; Golovliov et al., 1997; Parsons and Heffron, 2005; Williams et al., 1996). Therefore, T6SS was initially thought to be mainly required for host-pathogen interactions, later on it became evident that T6SS is primarily used for competition between Gram-negative bacteria (Cianfanelli et al., 2016; Hood et al., 2010; Mougous et al., 2006; Russell et al., 2011).

2.1. T6SS mode of action

The T6SS is structurally and functionally related to contractile bacteriophages such as *Myoviridae* bacteriophages, R-type pyocins of *P. aeruginosa* and other extracellular contractile elements (Ge et al., 2015; Leiman et al., 2009; Shneider et al., 2013; Taylor et al., 2018).

Cryo-electron tomography was used to reveal the overall architecture of the T6SS apparatus inside an intact bacterial cell suggesting that the T6SS consists of three subassemblies (Basler et al., 2012; Chang et al., 2017). A membrane complex tethers the whole apparatus to the cell envelope. Then a baseplate complex including the spike and effectors connects the membrane complex with a long cytosolic sheath containing an inner tube (figure 11A-D) (Ho et al., 2014). Live-cell fluorescence microscopy of sheath subunit T6SS component B (TssB) and ATPase ClpV showed that the assembly and contraction of the sheath as well as disassembly of the contracted sheath is a dynamic process (figure 11) (Basler and Mekalanos, 2012). The sheath contracts in less than 2 ms and thus releases energy equivalent to the conversion of 1000 molecules of ATP to ADP (Vettiger et al., 2017; Wang et al.,

2017). Thereby sufficient force is generated to drill the inner tube of the sheath with spike and associated effectors into the cytosol of a target cell (figure 11 E-F) (Brackmann et al., 2017a; Vettiger and Basler, 2016). Then the contracted sheath is recycled by an ATPase ClpV (figure 11G-H) (Basler and Mekalanos, 2012; Bönemann et al., 2009).

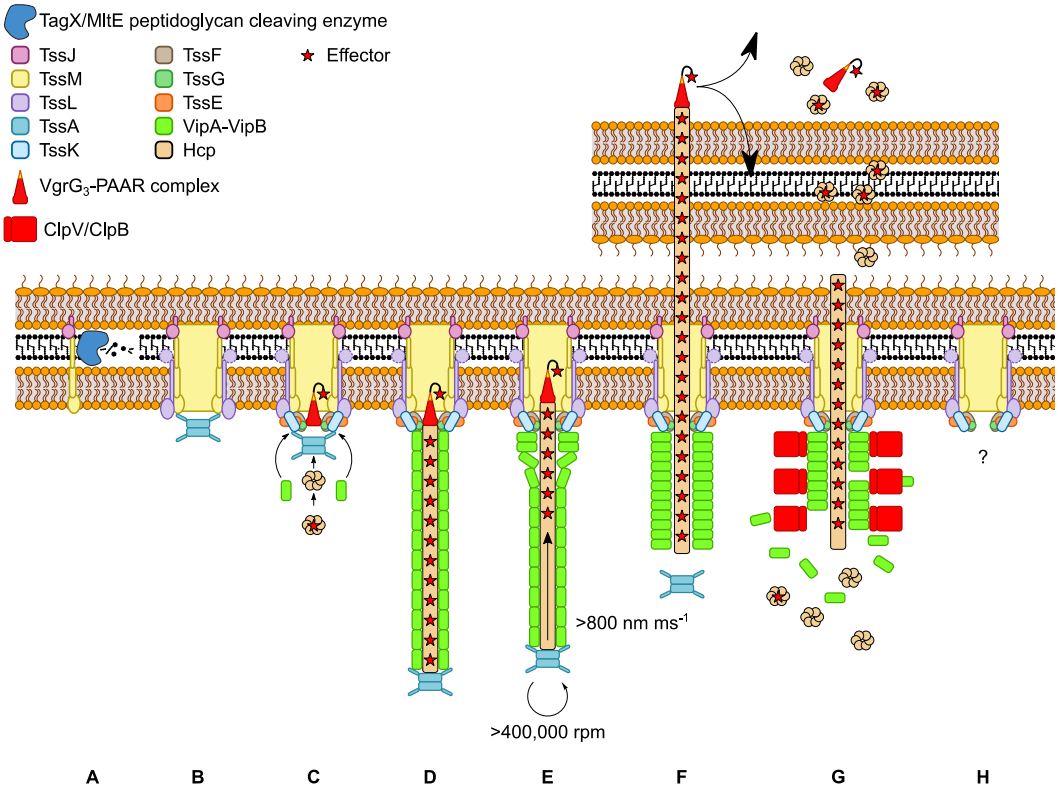

Figure 11: Overview of T6SS assembly and dynamics. A) Insertion of the membrane complex (TssJ/TssL/TssM) into the cell envelope may require local cleavage of peptidoglycan. **B)** The membrane complex serves as a scaffold for assembly of the baseplate (TssE/TssF/TssG/TssK) and may be coordinated by TssA. **C)** The baseplate complex harbors the spike complex (VgrG, PAAR and effectors) and initiates the assembly of a cytosolic sheath (TssB/TssC) with inner tube (Hcp). **D)** Sheath polymerizes by addition of subunits at its distal end. Sheath assembly may be coordinated by TssA and extended sheaths may be stabilized by TagA. **E)** Conformational changes of the baseplate triggers sheath contraction. **F)** Sheath contraction drills the inner tube together with the spike complex and the associated effectors into a target cell. **G)** Unfoldase ClpV recycles contracted sheath subunits under ATP consumption. **H)** The fates of membrane and baseplate complex are unknown, either they are disassembled or reused for a next round of firing. *Source Adpated from:Schneider et al., 2019, licensed under Creative Commons Attribution 4.0 International License (http://creativecommons.org/licenses/by/4.0/).*

Since T6SS dependent intoxication does not rely on a specific target cell receptor as it is the case for other secretion systems, diverse targets, ranging from eukaryotic cells over fungi to Gram-negative bacteria, can be killed (Brackmann et al., 2017). Interestingly however, Gram-positive bacteria seem to be immune against T6SS attacks (Alcoforado Diniz et al., 2015; Hachani et al., 2016; Trunk et al., 2018). The reason for this immunity is not clear, however, either T6SS fails to deliver effector

proteins through the thick peptidoglycan layer of Gram-positive bacteria or translocated effectors fail to find appropriate targets (Ho et al., 2014).

2.2. T6SS structure and assembly

The canonical T6SS consists of 13 conserved components required for its function and various accessory proteins involved in regulation and assembly (Boyer et al., 2009). Electron microscopy, crystallography and fluorescence live-cell microscopy were used to solve structures of subcomplexes or single proteins as well as to reveal the hierarchal assembly process of the T6SS.

2.2.1. Membrane complex

T6SS assembly starts with the membrane complex consisting of TssJ, TssM and TssL (figure 12) (Brunet et al., 2015; Durand et al., 2015; Gerc et al., 2015; Rapisarda et al., 2019). TssM and TssL are IcmF and IcmH homologs of the T4SS (Cianfanelli et al., 2016; Das and Chaudhuri, 2003). First, OM lipoprotein TssJ interacts with IM protein TssM, so that they span across the cell envelope (Aschtgen et al., 2008; Felisberto-Rodrigues et al., 2011; Zheng and Leung, 2007). Then the TssM-TssJ complex oligomerizes via the peptidoglycan-binding domain of TssM into a five-fold symmetry forming the core of the membrane complex (Durand et al., 2015; Rapisarda et al., 2019; Yin et al., 2019). Finally, dimers of IM protein TssL are recruited (Aschtgen et al., 2012; Durand et al., 2012, 2015; Ma et al., 2009; Zheng and Leung, 2007).

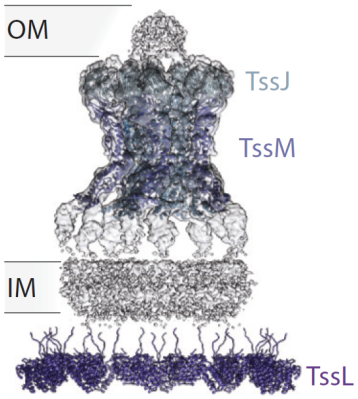

Figure 12: Structure of membrane complex. Three TssJ subunits bind one TssM component. Upon TssJ binds, TssM assembles into a complex with a five-fold symmetry, which spans across both membranes. Then, dimers of IM protein TssL bind to each TssM subunit. *Source: Adapted from Wang et al., 2019 with permission from the Annual Review of Microbiology, Volume 73 © 2019 by Annual Reviews, http://www.annualreviews.org/.*

Interestingly, the peptidoglycan meshwork is too tight to accommodate the whole membrane complex without peptidoglycan remodeling. Therefore, some T6SS clusters contain a specific peptidoglycan hydrolase, however, most do not (Santin et al., 2019; Weber et al., 2016). The role of these peptidoglycan hydrolases for T6SS localization is discussed in chapter 2.3.4. In addition, some membrane complexes are anchored to the cell wall by a peptidoglycan binding domain of TssL or by accessory proteins such as TagL or TagN (Aschtgen et al., 2010a, 2010b; Ma et al., 2009). Nevertheless, the role of peptidoglycan binding for assembly and stabilization of the membrane complex is debatable as peptidoglycan is dispensable for T6SS activity at least in *V. cholerae* (Vettiger et al., 2017).

The membrane complex likely undergoes some structural changes in order to accommodate the spike complex with effectors and the inner tube during secretion (Durand et al., 2015; Lin et al., 2014; Ma et al., 2012). Since some TssMs have NTPase activity, TssM might actively trigger the conformational change of the membrane complex; however, how the opening of the membrane complex is achieved is not clear yet (Ma et al., 2012).

2.2.2. Baseplate and spike complex

The baseplate is assembled in the cytosol on top of the membrane complex. However, the baseplate complex has a six-fold symmetry in contrast to the membrane complex (Brunet et al., 2015; Nazarov et al., 2018; Zoued et al., 2016). How this symmetry mismatch is resolved, remains to be elucidated. In general, the T6SS baseplate shares close homology to the baseplate of T4 bacteriophage (Nazarov et al., 2018; Taylor et al., 2016). A central hub consisting of trimeric VgrG and one PAAR protein is connected to six wedges made out of TssE, TssF, TssG and TssK in a 1:2:1:6 stoichiometry (figure 13) (Cherrak et al., 2018; Nazarov et al., 2018; Pukatzki et al., 2007; Shneider et al., 2013). TssE is highly conserved among contractile injection systems and is thought to connect the sheath subunits to the baseplate as it contains a similar handshake domain (Basler et al., 2012; Clemens et al., 2015; Kudryashev et al., 2015; Leiman et al., 2009; Lossi et al., 2011; Nazarov et al., 2018). Surprisingly, a *tssE* deletion mutant in *V. cholerae* is able to assemble T6SS sheaths with low frequency (Vettiger and Basler, 2016). Two molecules of TssF interconnect

TssE with TssG (Cherrak et al., 2018; Nazarov et al., 2018; Park et al., 2018). A TssK dimer binds to TssG connecting the baseplate to the membrane complex by interactions with TssL and TssM (Cherrak et al., 2018; Park et al., 2018).

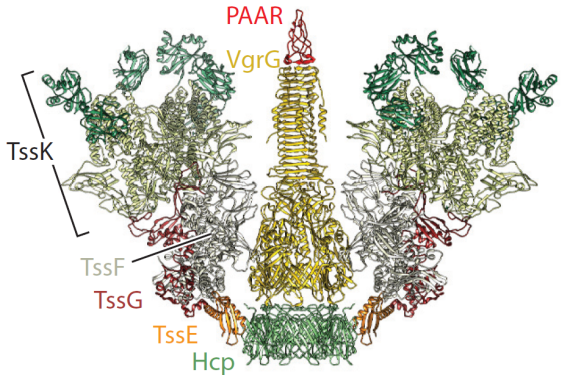

Figure 13: Structure of baseplate and spike complex. The baseplate consists of TssE/TssF/TssG/TssK in a 1:2:1:6 ratio and accommodates the spike complex made of VgrG and PAAR protein. *Source: Adapted from Wang et al., 2019 with permission from the Annual Review of Microbiology, Volume 73 © 2019 by Annual Reviews, http://www.annualreviews.org/.*

In general, it is thought that a conformational change in the baseplate triggers contraction of extended sheath (Brackmann et al., 2017b; Taylor et al., 2016; Wang et al., 2017). However, what exactly triggers sheath contraction remains unknown. Interestingly, TssK shares no homology to contractile bacteriophages, but to the receptor binding-protein of non-contractile phages and TssK dimers are mobile relative to the other wedge components suggesting that TssK may propagate the contraction signal from the membrane complex to the baseplate and thus to the extended sheath (Nguyen et al., 2017; Park et al., 2018). In addition, the T6SS baseplate lacks a LysM-domain protein, which clamps the T4 baseplate wedges together, suggesting that the T6SS baseplate is rather unstable (Arisaka et al., 2016).

2.2.3. Sheath and inner tube

The sheath and inner tube are polymerized onto the baseplate. The trimer of VgrG serves as a template for assembly of inner tube, which is formed by hexameric Hcp rings stacked together (Renault et al., 2018; Wang et al., 2017). The inner tube is surrounded by sheath subunits TssB and TssC. TssB and TssC form heterodimers and stack into hexameric rings which are interconnected (Clemens et al., 2015; Kudryashev et al., 2015; Salih et al., 2018; Wang et al., 2017). In contractile injection systems, TssB and TssC are fused into one gene product (Aksyuk et al., 2009). TssB

and TssC heterodimers are connected by a conserved handshake domain, which also mediates interaction with Hcp (Clemens et al., 2015; Kudryashev et al., 2015; Salih et al., 2018; Wang et al., 2017). TssC contains a domain (domain 3) which is unique for T6SS and is required for disassembly by ClpV (Bönemann et al., 2009; Clemens et al., 2015; Kudryashev et al., 2015; Salih et al., 2018; Wang et al., 2017).

The assembly of sheath and inner tube into an extended, meta-stable state starts at the baseplate and proceeds at the distal end of the growing structure (Vettiger et al., 2017). Since T6SS does not contain a tape measure protein unlike other contractile injection system, the sheath and inner tube assembly normally proceeds until the membrane opposite of the baseplate is reached (Basler et al., 2012; Brunet et al., 2013; Gerc et al., 2015; Leiman et al., 2010).

So far, the structure of the extended sheath with the inner tube inside was only solved from a sheath mutant, which was unable to contract. In this mutant, the N-terminal linker region of TssB was elongated by three amino acids, which resulted in an aberrant linkage of sheath rings (Brackmann et al., 2017b; Wang et al., 2017). The extended sheath structure revealed that the Hcp tube follows the same helical parameters as the sheath surrounding it in contrast to the previously solved crystal structures (Brunet et al., 2014; Mougous et al., 2006; Sun et al., 2007). Various structures of contracted sheaths suggest an overall conserved sheath architecture despite sequence variations (Clemens et al., 2015; Kudryashev et al., 2015; Salih et al., 2018).

2.2.4. Sheath contraction and recycling

The comparison of the extended with empty contracted sheath combined with T6SS dynamics observed by live-cell fluorescence microscopy revealed a translocation mechanism of inner tube with spike complex and effectors according to the inverted contractile phage model (Basler et al., 2012; Chang et al., 2017). Thereby, the conformational change of the baseplate translates into collapse of sheath rings nearest at the baseplate, then contraction ring by ring propagates along the sheath (Brackmann et al., 2017b; Ge et al., 2015; Wang et al., 2017).

Upon contraction, the sheath compresses to half of its original size while the diameter increases (figure 14) (Basler et al., 2012). Interactions with Hcp are abrogated along the contraction wave while they are still present in the remaining extended structure, thus the inner tube with the spike complex and effector is pushed forwards at a rotational speed of at least 477 000 revolutions per minute (Wang et al., 2017). Until now, it was never possible to measure the velocity of contraction, however it was shown to be faster than 800 nm/ms (Vettiger et al., 2017). Interestingly, the signal for contraction and as well, whether the membrane or the baseplate complex triggers contraction is still unknown.

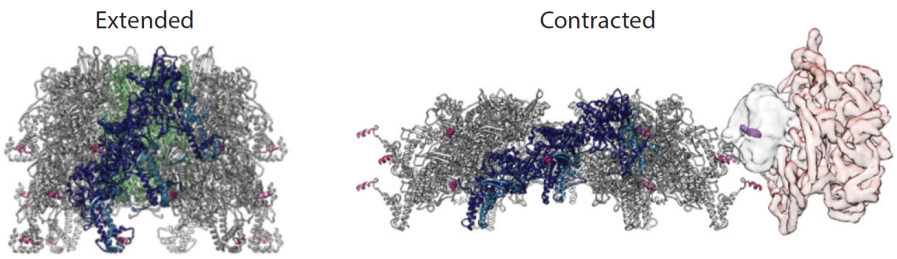

Figure 14: Structures of extended and contracted T6SS sheath. The T6SS sheath is made of hexameric heterodimers of TssB and TssC subunits. Upon contraction, the sheath compresses to half of its size and increases its diameter in order to translocate the inner tube (Hcp) forwards. In the contracted conformation, the N-terminal domain 3 in TssC (in red) gets exposed and is accessible by ClpV. ClpV recycles contracted sheath subunits under ATP consumption. *Source: Adapted from Wang et al., 2019 with permission from the Annual Review of Microbiology, Volume 73 © 2019 by Annual Reviews, http://www.annualreviews.org/.*

Sheath contraction leads to unfolding of N-terminal domain 3 in TssC (figure 14). Exposed domain 3 is recognized by hexameric ATPase associated with diverse cellular activites (AAA^+) ATPase ClpV, which under ATP consumption restores the high energy state conformation of sheath protomers (Bönemann et al., 2009; Kapitein et al., 2013; Pietrosiuk et al., 2011). However, the exact mechanism how ClpV recycles sheath subunits, remains to be elucidated. ClpV is neither essential for T6SS assembly nor contraction. Yet, killing efficiency is decreased in a *clpV* deletion mutant in *V. cholerae* highlighting the importance of T6SS dynamics and multiple firing events (Basler et al., 2012). Interestingly, *Francisella tularensis* and *Pseudomonas putida* encode T6SS clusters lacking ClpV (Bernal et al., 2017; Bröms et al., 2010). Some organisms have an accessory protein TagJ proposed to assist in contracted sheath disassembly. However, *tagJ* deletion did not result in an observable phenotype in *P. aeruginosa* (Förster et al., 2014; Lossi et al., 2012).

2.2.5. TssA family

Furthermore, members of the TssA protein family belong to the conserved T6SS components. They all contain a conserved N-terminal ImpA domain but have various structures, functions and subcellular localizations (Dix et al., 2018; Planamente et al., 2016; Zoued et al., 2016). *P. aeruginosa* TssA interacts with baseplate components and is proposed to serve as seed for assembly of the baseplate complex (Planamente et al., 2016). On the other hand, it also interacts with TagJ and ClpV. In contrast, *Burkholderia cenocepacia* and *E. coli* TssA seems to interact with almost all T6SS subassemblies (Dix et al., 2018; Zoued et al., 2016). *E. coli* TssA also coordinates copolymerization of sheath with inner tube (Zoued et al., 2016). Another TssA family member TagA sits at the membrane opposite of the baseplate and is required for ending sheath polymerization and stabilizing the extended sheath in *E. coli* (Santin et al., 2018; Szwedziak and Pilhofer, 2019).

2.2.6. Effectors

The T6SS effector protein repertoire is highly diverse and consists of anti-prokaryotic (e.g. peptidoglycan hydrolases), anti-eukaryotic (e.g. actin crosslinkers) and trans-kingdom effectors (e.g. phospholipases) (Alcoforado Diniz et al., 2015; Lien and Lai, 2017). In addition, non-toxic T6SS effectors required for zinc, iron and manganese scavenging were reported (Lin et al., 2017; Si et al., 2017; Wang et al., 2015). Cargo effectors are loaded on spike proteins VgrG, PAAR or Hcp by non-covalent binding while evolved effectors are part of C-terminal domains of VgrG or PAAR proteins (Liang et al., 2015; Ma et al., 2017; Shneider et al., 2013; Unterweger et al., 2015). Since the spike complex consists only of three VgrGs and one PAAR protein, which each can load only a limited number of effectors, the maximum number of loaded effectors per firing event is small (Shneider et al., 2013). Consequently, repeated T6SS firing, precise and efficient effector translocation as well as highly potent effectors may be crucial for successful killing of target cells (LaCourse et al., 2018).

Interestingly, some peptidoglycan hydrolases encode an internal secretion signal for Tat-dependent secretion in order to reach their target in periplasm as effectors may

be translocated into the cytoplasm of the target cell (Ho et al., 2017; Vettiger and Basler, 2016). In addition, some effectors have dedicated chaperones or adaptor proteins required for loading on the spike complex (Cianfanelli et al., 2016; Liang et al., 2015; Unterweger et al., 2015). How effector loading is regulated, and if the effector composition changes between firing events, is not known. However, T6SS effectors are often encoded in close proximity to their dedicated VrgG or PAAR proteins (Alcoforado Diniz et al., 2015; Dong et al., 2013; Ringel et al., 2017).

Anti-prokaryotic effectors also have an immunity protein encoded down or upstream to prevent self-intoxication before translocation or intoxication by T6SS attacks of neighboring sister cells (Dong et al., 2013; Miyata et al., 2013; Ringel et al., 2017). Immunity proteins bind to cognate effectors in order to prevent their toxic activity (Li et al., 2012). Thus, they are localized to periplasm or cytosol depending on the target of the corresponding effectors (Russell et al., 2011). Interestingly, immunity proteins are expressed independently of the core T6SS cluster for immediate protection by T6SS attacks from neighboring cells (Miyata et al., 2013). In *Proteus mirabilis*, variable sets of effectors and cognate immunity proteins are used for discrimination between self and non-self in inter-strain competitions resulting in a visible boundary between two strains called “Dienes line” (Alteri et al., 2013; Dienes, 1946).

2.3. Subcellular localization of T6SS

The contact-dependent mode of action together with the few effector molecules translocated per firing event are drawbacks which bacteria must overcome to efficiently kill target cells in a T6SS dependent manner. In addition, even the most active T6SS are fired only once per minute (Basler and Mekalanos, 2012). Thus, different strategies evolved for highly precise aiming, for quick repositioning of the T6SS apparatus as well as for optimization of target range.

2.3.1. T6SS diversity in regard of activation, dynamics and subcellular localization

Part of this chapter is published in the review "Assembly and Subcellular Localization of Bacterial Type VI Secretion System" in *Annual Review of Microbiology* 2019 (Wang et al., 2019) and is displayed here with permission from the Annual Review of Microbiology, Volume 73 © 2019 by Annual Reviews, http://www.annualreviews.org/.

Up to date, four phylogenetically different T6SS subtypes are identified (Russell et al., 2014). Subtype T6SS^{i} consists of the canonical, well-studied T6SS in *P. aeruginosa* and *V. cholera*. T6SS clusters in subtype T6SS^{i} can be very diverse regarding effector repertoire and accessory proteins (Alcoforado Diniz et al., 2015; Boyer et al., 2009). Besides, multiple clusters of subtype T6SS^{i} may be encoded on one genome. *B. thailandensis* encodes five different T6SS with distinct roles in targeting bacteria, host cells or manganese scavenging (Schwarz et al., 2010, 2014a; Si et al., 2017). T6SS in *Francisella* belongs to subtype T6SS^{ii} and lacks canonical T6SS components such as ClpV, TssA as well as TssE and TssG (Bröms et al., 2010; Russell et al., 2014). T6SS of Bacteroidetes phylum group in subtype T6SS^{iii} which is characterized by a lack of membrane complex (Russell et al., 2014). Recently, a subtype T6SS^{iv} was discovered in *Amoebophilus*, which also lacks a membrane complex as well as ClpV, but has a tail terminator as well as tape measure proteins similar to the ones in bacteriophages (Böck et al., 2017).

Next to genetic diversity, differential T6SS regulation on a transcriptional, post-transcriptional and post-translational level lead to highly diverse T6SS activity and dynamics patterns. In general, T6SS activity is regulated by controlling expression of the T6SS genes on a transcriptional or posttranscriptional level as a response to diverse environmental stimuli (Chen et al., 2015; Joshi et al.; Leung et al., 2011; Miyata et al., 2013). Strikingly, relative protein abundance of structural components is conserved in *P. aeruginosa*, *V. cholerae* and *Acinetobacter baylyi* despite of their different T6SS activation and dynamics patterns (see below) (Lin et al., 2019). However, some T6SS components in *V. cholerae* were proposed to be actively degraded suggesting additional post-translational regulation (Lin et al., 2019). These

findings highlight that single T6SS components can be differentially abundant despite of being part of the same genetic operon.

Interestingly, live-cell imaging of TssB or ClpV dynamics showed that bacteria have different T6SS assembly patterns and may dynamically localize the T6SS within the bacterial cell. *V. cholerae* and *Acinetobacter baylyi* build several T6SS sheaths per cell and fire constantly in apparently random directions (Basler and Mekalanos, 2012; Ringel et al., 2017). EAEC repeatedly assembles the Sci-1 T6SS at one or two apparently random positions within the cell (Durand et al., 2015). *P. aeruginosa* assembles one of its three T6SS within seconds of an attack from other bacteria at the site of the inflicted damage to quickly retaliate (Basler et al., 2013). The majority of *Serratia marcescens* cells assemble one T6SS sheath at random positions in the cell; however, they rely on regulated T6SS assembly for efficient killing of prey cells (Gerc et al., 2015; Ostrowski et al., 2018). In addition, intracellular pathogens *F. novicida* and *B. thailandensis* assemble their anti-eukaryotic T6SS on the poles (Brodmann et al., 2017; Schwarz et al., 2014).

2.3.2. Threonine Phosphorylation Pathway Mediates T6SS Repositioning

This chapter including subchapters and figure is published in the review “Assembly and Subcellular Localization of Bacterial Type VI Secretion System” in *Annual Review of Microbiology* 2019 (Wang et al., 2019) and is displayed here with permission from the Annual Review of Microbiology, Volume 73 © 2019 by Annual Reviews, http://www.annualreviews.org/.

The first example of posttranslational regulation of T6SS assembly by a threonine phosphorylation pathway (TPP) was described in *P. aeruginosa* (Mougous et al., 2007). Later, TPPs were shown to regulate initiation and positioning of T6SS assembly in several organisms (figure 15) (Basler et al., 2013; Fritsch et al., 2013; Lin et al., 2014; Ostrowski et al., 2018). TPPs have a sensor module that senses a signal and activates a kinase (PpkA). An activated kinase then phosphorylates a target protein, which in turn initiates T6SS assembly. Finally, a phosphatase (PppA) dephosphorylates the target protein and thus prevents further T6SS assembly

initiation. *P. aeruginosa* cluster H1-T6SS encodes a complete TPP with a sensor module composed of TagQ/TagR/TagS/TagT; a kinase PpkA phosphorylating Fha; and a cognate phosphatase, PppA. Other species like *S. marcescens* and *A. tumefaciens* possess only PpkA, PppA, and Fha. In addition, T6SS assembly in these three organisms is blocked by TagF, and deactivation of TagF can trigger T6SS assembly in a TPP-independent manner (Lin et al., 2014, 2018; Ostrowski et al., 2018; Silverman et al., 2011).

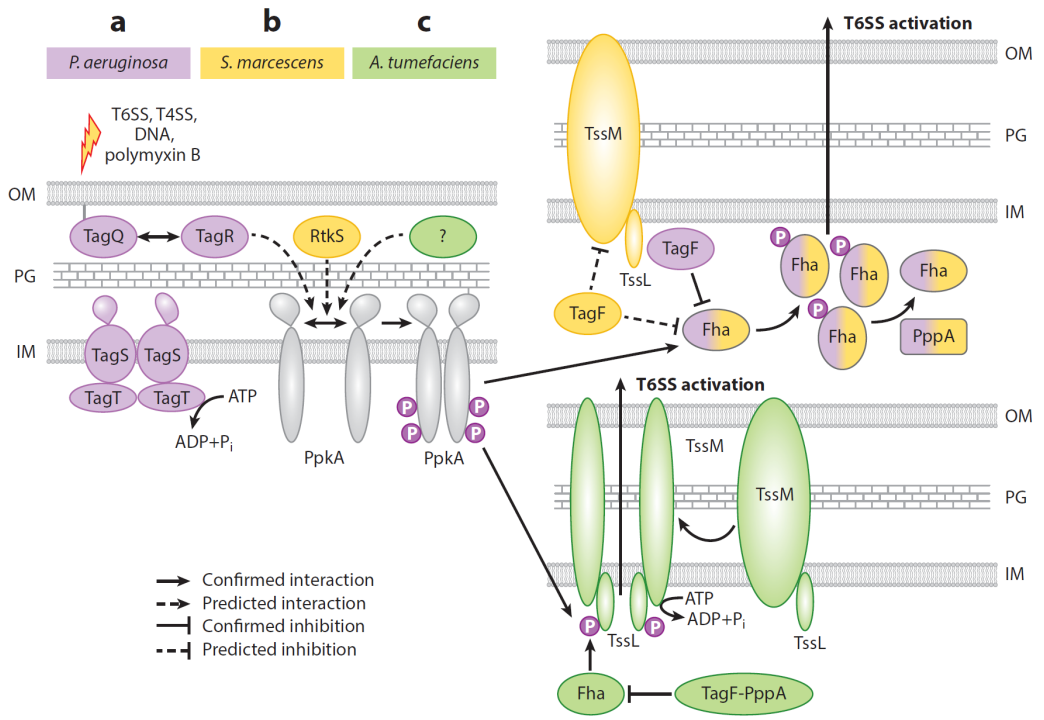

Figure 15: Posttranslational regulation of T6SS activity. A) In *Pseudomonas aeruginosa* (*purple*), membrane damage (*lightning bolt*) leads to activationof PpkA by TagQ/TagR/TagS/TagT and to phosphorylation of Fha. Phosphorylated Fha multimerizes and promotes T6SS assembly. PppA dephosphorylates Fha and stops T6SS assembly. TagF represses T6SS activity independently of the threonine phosphorylation pathway by interacting with Fha. (*b*) In *Serratia marcescens* (*yellow*), PpkA interacts with RtkS and subsequently phosphorylates Fha, which multimerizes and activates T6SS assembly. PppA dephosphorylates Fha and thus blocks T6SS activity. TagF blocks T6SS activity, likely by acting on the membrane complex. (*c*) In *Agrobacterium tumefaciens* (*green*), PpkA phosphorylates TssL, which triggers a conformational change in TssM and ATP hydrolysis. Binding of Fha to phosphorylated TssL induces T6SS activity. TagF-PppA blocks T6SS activity by interaction with Fha. Abbreviations: IM, inner membrane; OM, outer membrane; PG, peptidoglycan. *Source: Wang et al., 2019 with permission from the Annual Review of Microbiology, Volume 73 © 2019 by Annual Reviews, http://www.annualreviews.org/.*

2.3.2.1. Signal sensing and kinase activation

The sensor module TagQ/TagR/TagS/TagT in *P. aeruginosa* was shown to be required for sensing T6SS attacks from either sister cells or other bacteria as well as cell envelope stress induced by polymyxin B, the type 4 secretion system, chelation of ions, or extracellular DNA (Basler and Mekalanos, 2012; Basler et al., 2013; Ho et al., 2013; Wilton et al., 2016). Lipoprotein TagQ with a conserved lipobox is anchored to the periplasmic side of the OM and binds periplasmic TagR (Casabona et al., 2013). Interaction of TagR with the periplasmic domain of PpkA might result in activation of its kinase activity (Hsu et al., 2009). This suggests that TagQ might be sequestering TagR to the OM to prevent its binding to PpkA and thus T6SS activation; however, TagQ likely has an additional role since deletion of either TagQ or TagR prevents T6SS assembly (Casabona et al., 2013).

The components TagS and TagT form a putative ABC transporter with homology to the Lol complex, which transports lipoproteins (Narita and Tokuda, 2006). TagS forms an integral membrane protein with a long periplasmic loop, and TagT is an ATPase and contains Walker A and B motifs, which are required to hydrolyze ATP in vitro (Casabona et al., 2013). TagS or TagT is required for full T6SS activation (Basler et al., 2013; Casabona et al., 2013); however, despite homology to the Lol complex, it is unclear whether TagS and TagT transport any substrates. An obvious candidate would be TagQ or TssJ; however, deletion of TagS and TagT does not seem to alter their membrane localization (Casabona et al., 2013).

In *S. marcescens*, periplasmic RtkS (regulator of T6SS kinase in *Serratia*) was shown to be required for efficient killing of prey cells but dispensable for T6SS activity in liquid culture. Signals sensed by RtkS are unknown, and it is also unclear whether RtkS directly interacts with PpkA; however, deletion of rtkS resulted in destabilization and degradation of PpkA (Ostrowski et al., 2018).

The serine/threonine kinase PpkA is an IM protein with a periplasmic domain and cytosolic kinase domain. PpkA may be activated by interaction with a periplasmic protein (e.g., TagR) that results in PpkA dimerization. The PpkA dimer autophosphorylates and activates T6SS assembly by phosphorylating a T6SS component (Fritsch et al., 2013; Hsu et al., 2009; Lin et al., 2014; Motley and Lory, 1999; Mougous et al., 2007). While the kinase domain is conserved, the structure of

the periplasmic domain differs between *S. marcescens* and *P. aeruginosa* (Fritsch et al., 2013). This is likely because each PpkA responds to a different signal and binds a different periplasmic protein.

2.3.2.2. Activation of T6SS assembly by protein phosphorylation

In both *P. aeruginosa* and *S. marcescens*, activated PpkA phosphorylates Fha, which likely recognizes phosphorylated PpkA via its FHA domain, known to bind phosphopeptides (Mougous et al., 2007). However, it is unclear how phosphorylation of Fha promotes T6SS assembly (Hsu et al., 2009; Mougous et al., 2007; Ostrowski et al., 2018). Interestingly, Fha forms foci in *P. aeruginosa* independently of its phosphorylation status (Mougous et al., 2007); however, membrane-anchored PpkA is still required for formation of these foci (Hsu et al., 2009). This suggests that PpkA might have an additional structural role in Fha foci formation and T6SS assembly initiation. In *P. aeruginosa*, Fha phosphorylation is increased when cells are incubated on a solid surface, suggesting that cell-cell interactions result in PpkA activation (Casabona et al., 2013). This activation might be a consequence of T6SS dueling between sister cells (Basler and Mekalanos, 2012). In contrast, the majority of Fha in *S. marcescens* is phosphorylated also in liquid culture, where there are minimal or no cell-cell interactions (Fritsch et al., 2013).

In *A. tumefaciens*, PpkA phosphorylates the membrane complex component TssL, leading to a conformational change in TssM (Lin et al., 2014). TssM is an IM ATPase with Walker A and B motifs, and the conformational change triggers ATP hydrolysis. However, TssL-TssM interaction is independent of ATPase activity of TssM (Ma et al., 2012). Phosphorylated TssL interacts with Fha, and the Fha-pTssL complex promotes recruitment of secretion substrates Hcp and effector Atu4347 to TssL (Lin et al., 2014). It is unclear how ATPase activity of TssM is involved in recruiting the secreted proteins and whether formation of this complex requires additional proteins (Lin et al., 2014; Ma et al., 2012). TssM of *P. aeruginosa*, *V. cholerae*, and *Edwardsiella tarda* also contains Walker A and B motifs (Ma et al., 2012); however, ATP hydrolysis does not seem to be important for T6SS activity in *E. tarda* (Zheng and Leung, 2007).

An interesting case is *Vibrio alginolyticus*, which uses the TPP of its second T6SS cluster to regulate T6SS assembly as well as gene expression. As in *A. tumefaciens*, PpkA phosphorylates TssL, which results in binding of Fha and an increase in T6SS activity. In addition, PpkA phosphorylates a non-T6SS substrate, VtsR. Phosphorylated VtsR activates LuxO and subsequently promotes expression of T6SS-2 and quorum sensing (Yang et al., 2018).

2.3.2.3. T6SS assembly deactivation

In *P. aeruginosa* and *S. marcescens*, phosphatase PppA is responsible for dephosphorylation of Fha and thus shutting down T6SS activity. Since T6SS activity is low in *P. aeruginosa*, deletion of PppA results in an increase of T6SS activity and Hcp secretion (Basler et al., 2013; Casabona et al., 2013; Hsu et al., 2009; Mougous et al., 2007). However, *in S. marcescens*, deletion of PppA does not increase Hcp secretion in liquid medium, suggesting that the system is already at maximum activity. Interestingly, in both species, *pppA* deletion strains repeatedly assemble T6SS at the same location within the cells for several rounds of firing (Basler et al., 2013; Ostrowski et al., 2018). This has a major consequence for interaction with competing bacteria, because a *P. aeruginosa pppA*-negative strain cannot distinguish between T6SS-positive attackers and T6SS-negative bystander cells and kills both to a similar extent. Importantly, the killing rate of T6SS-positive attackers by a *pppA*-negative strain is low, even though a *pppA*-negative strain secretes significantly more effectors than the wild-type strain (Basler et al., 2013; Ho et al., 2013). A similar observation was also made for *S. marcescens*, where a *pppA*-negative strain kills prey cells poorly despite high T6SS activity (Fritsch et al., 2013; Ostrowski et al., 2018). This suggests that PppA activity is important to preventing excessive firing of T6SS in one direction and by stopping the assembly allows T6SS to reposition to a new subcellular location upon sensing a signal, which in turn is required for efficient killing of target cells.

2.3.3. TPP-independent regulation

This chapter is published in the review "Assembly and Subcellular Localization of Bacterial Type VI Secretion System" in *Annual Review of Microbiology* 2019 (Wang et al., 2019) and is displayed here with permission from the Annual Review of Microbiology, Volume 73 © 2019 by Annual Reviews, http://www.annualreviews.org/.

In addition to the TPP, TagF regulates T6SS assembly in *P. aeruginosa* and *S. marcescens*, by a poorly understood mechanism. For *P. aeruginosa*, it was shown that TagF sequesters Fha to prevent T6SS assembly (Lin et al., 2018), and indeed, deletion of TagF activates T6SS even in the absence of TagQ/TagR/TagS/TagT and PpkA (Silverman et al., 2011). Importantly, even strains lacking TPP, like *V. cholerae*, also require Fha for T6SS activity, suggesting that Fha is an important scaffold protein for assembly of other T6SS components (Zheng et al., 2011). Similarly to the case of *P. aeruginosa*, when *tagF* is deleted in the *ppkA*-negative strain of *S. marcescens*, T6SS assembly is restored. It is, however, unclear whether TagF interacts with Fha or other T6SS components.

In *A. tumefaciens*, TagF and PppA are fused into a single polypeptide; however, both independently block T6SS activity (Lin et al., 2014, 2018). The TagF domain binds Fha; however, this seems insufficient to prevent T6SS assembly, as a TagF domain mutant, which is still able to bind Fha, loses its ability to repress T6SS activity. This suggests that the TagF domain is also involved in Fha-independent repression (Lin et al., 2018). Similarly to the case of *S. marcescens*, efficiency of target-cell killing is decreased in the absence of PpkA and TagF-PppA even though the overall T6SS activity remains high (Lin et al., 2018), suggesting that TPP components and TagF are important for sensing prey cells and/or repositioning the T6SS apparatus.

2.3.4. Regulation of T6SS localization by peptidoglycan-cleaving enzymes

This chapter is published in the review "Assembly and Subcellular Localization of Bacterial Type VI Secretion System" in *Annual Review of Microbiology* 2019 (Wang et al., 2019) and is displayed here with permission from the Annual Review of Microbiology, Volume 73 © 2019 by Annual Reviews, http://www.annualreviews.org/.

Many cell envelope–spanning complexes, like flagella, the T3SS, or the T4SS, require specialized lytic transglycosylases for insertion into the peptidoglycan layer (Dik et al., 2017; Scheurwater and Burrows, 2011; Typas et al., 2011). Interestingly, two dedicated peptidoglycan-cleaving enzymes were shown to be required for T6SS assembly, and thus their control in response to certain signals or stimuli might, in principle, allow for dynamic localization of T6SS assembly. EAEC requires the general lytic transglycosylase MltE to insert membrane complexes of the Sci-1 T6SS. The lipoprotein MltE is located at the OM and interacts with the periplasmic domain of TssM. How MltE is activated by TssM and whether additional components are required is unknown (Santin and Cascales, 2017). In *Acinetobacter*, the *L,D*-endopeptidase TagX is encoded in the T6SS cluster and is required for T6SS activity (Ringel et al., 2017; Weber et al., 2016). Since T6SS assembles at low frequency also in a *tagX*-negative strain, it is likely that additional mechanisms allow for assembly initiation or peptidoglycan cleavage and that TagX is only required for integration of the T6SS apparatus into the peptidoglycan layer and not for T6SS function (Ringel et al., 2017).

2.3.5. Polar localization

This chapter is published in the review "Assembly and Subcellular Localization of Bacterial Type VI Secretion System" in *Annual Review of Microbiology* 2019 (Wang et al., 2019) and is displayed here with permission from the Annual Review of Microbiology, Volume 73 © 2019 by Annual Reviews, http://www.annualreviews.org/.

B. thailandensis and *F. novicida* were shown to assemble a polarly localized T6SS required for host-pathogen interactions (Brodmann et al., 2017; Schwarz et al., 2014). *B. thailandensis* T6SS-5 is required for formation of a multinucleated giant cell (French et al., 2011; Schwarz et al., 2010, 2014; Toesca et al., 2014), while *F. novicida* requires the T6SS for phagosomal escape and assembles one polar T6SS per cell in vitro and inside macrophages (Brodmann et al., 2017; Bröms et al., 2010). For the T6SS, sheath length defines the reach of T6SS attack, as the sheath contracts to half of its extended length (Basler et al., 2012). Therefore, polar T6SS assembly might allow assembly of longer sheaths in rod-shaped bacteria and thus increase efficiency of effector delivery. In the case of *F. novicida* it would be delivery across a phagosomal membrane, and in the case of *B. thailandensis* it would be the ability to induce membrane fusion of neighboring host cells. However, polar localization could also be required for coordination with other polarly localized complexes such as adhesins or pili to bring the target membrane closer to the bacterial cell and thus facilitate protein translocation by the T6SS.

2.4. T6SS model organisms

The T6SS is widespread among Gram-negative bacteria and the core components are mostly conserved. Nevertheless, T6SS dynamics and activation as well as subcellular localization vary largely in different bacteria and it is poorly understood what causes these differences. In order to further elucidate these spatio-temporal regulation mechanisms, I chose *P. aeruginosa* and *Francisella novicida*, both with unique T6SS dynamics to study different T6SS activation patterns and subcellular localizations.

2.4.1. Pseudomonas aeruginosa

P. aeruginosa is an environmental Gram-negative bacterium found ubiquitously in soil and water. It is also associated with different diseases such as cystic fibrosis and pneumonia as opportunistic human pathogen and causes life-threatening infections (Moradali et al., 2017). *P. aeruginosa* is capable to occupy many niches due to its sophisticated regulatory networks and array of virulence factors including a broad range of soluble antimicrobials as well as TypeIVa pili, T3SS and T6SS (Mathee et al., 2008; Moradali et al., 2017). High tolerance and persistence to antibiotics as well

as intrinsic and acquired antibiotic resistance mechanisms make *P. aeruginosa* one of the major threats for public health in future (Breidenstein et al., 2011; Hancock and Speert, 2000).

P. aeruginosa encodes three T6SS clusters (H1-H3) (Mougous et al., 2006). H1-T6SS has anti-prokaryotic properties, while H2-T6SS and H3- T6SS encode anti-prokaryotic as well as anti-eukaryotic effectors (Basler et al., 2013; Lesic et al., 2009; Mougous et al., 2006; Russell et al., 2013; Sana et al., 2015). All three T6SS clusters are differentially transcriptionally regulated by quorum sensing (Lesic et al., 2009). Besides, H1-T6SS (hereafter T6SS) is controlled on a post-transcriptional level by LadS and RetS in a reciprocal manner (Mougous et al., 2006). LadS leads to activation of the two-component signaling cascade GacS/GacA, which results in transcription of two small regulatory RNAs (srRNA) RsmY and RsmZ. These two srRNAs antagonize RsmA, which inhibits translation of T6SS genes among many others. Therefore inhibition of RsmA yields in upregulated T6SS expression (Brencic and Lory, 2009). Since T6SS is only expressed upon surface contact in a LadS/GacS dependent manner, wild type cells rarely assemble T6SS under laboratory conditions. For this reason, most T6SS studies are carried out in a Δ*retS* background, in which the repressor RetS of GacS is deleted and thus the antibacterial T6SS cluster overexpressed (Goodman et al., 2004; Mougous et al., 2006).

In contrast to all other studied T6SS model organisms, *P. aeruginosa* uses the T6SS as defensive weapon and only assembles T6SS if envelope stress is sensed (Basler and Mekalanos, 2012; Basler et al., 2013; Ho et al., 2013; Wilton et al., 2016). *P. aeruginosa* senses envelope stress within seconds, which may be caused by a T6SS attack of a neighboring cell, and strikes back at the attacker with great precision (Basler et al., 2013; Vettiger and Basler, 2016). This “tit-for-tat” behavior depends on the TPP described in chapter 2.3.2. However, in order to strike back, *P. aeruginosa* must survive initial T6SS attacks. It is not known how this defensive strategy evolved and what makes *P. aeruginosa* resilience to initial T6SS attacks.

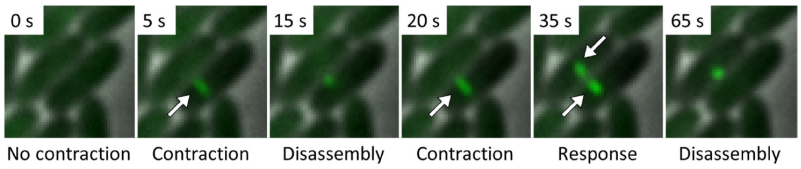

Figure 16: T6SS dueling between neighboring *P. aeruginosa* cells. T6SS activity in *P. aeruginosa ΔretS clpV-sfgfp* is monitored by live-cell fluorescence microscopy. T6SS activation of one cell triggers T6SS dependent retaliation of the neighboring cell. Arrows mark contraction of T6SS sheaths. *Source: Adapted from Basler and Mekalanos, 2012. Reprinted with permission from AAAS.*

Due to T6SS overexpression in the Δ*retS* background, accidental firings may happen leading to a quick counterattack of neighboring sister cells. This phenomenon of sensing a T6SS attack and firing back between sister cells is called dueling (figure 16) (Basler and Mekalanos, 2012). This defensive T6SS strategy allows co-existence for other species with *P. aeruginosa* as long as they do not inflict any harm (Basler et al., 2013).

2.4.2. Francisella novicida

The Gram-negative bacterium *Francisella tularensis* causes the zoonotic disease tularemia. Tularemia manifests in swollen lymph nodes and fever, and may be deadly if not treated (McLendon et al., 2006). Four subspecies of *F. tularensis* exist; subspecies *tularensis*, subspecies *holarctica*, subspecies *novicida* and subspecies *mediasiatica* (Keim et al., 2007). The most virulent subspecies are *F. tularensis* subspecies *tularensis* (hereafter *F. tularensis*), which is predominately found in North America, and *F. tularensis* subspecies *holarctica* (hereafter *F. holarctica*), the major cause of tularemia in Europe (Keim et al., 2007). For *F. tularensis*, 10 colony-forming units (CFU) are enough to causes disease, which may have a mortality rate up to 60 % if left untreated (Kingry and Petersen, 2014). This high infectivity together with easy transmission by aerosols and arthropod vectors led to the classification of *F. tularensis* as potential bioweapon (Oyston et al., 2004). On the other hand, *F. tularensis* subspecies *novicida* (hereafter *F. novicida*) only infects immuno-compromised humans and rodents (Kingry and Petersen, 2014).

The primary niche of *Francisella* are phagocytic cells such as macrophages. Once taken up by host cells, *Francisella* delays phagolysosome maturation and escapes from acidified phagosomes, which acquired early and late endosomal markers such

as LAMPs (Santic et al., 2005). In the cytosol, *Francisella* reaches its replicative niche and replicates to high number until host cell death occurs (Chong and Celli, 2010). However, it is not clear if phagosomal acidification triggers *Francisella* phagosomal escape as there are conflicting reports (Chong et al., 2008; Clemens et al., 2009; Santic et al., 2008). Interestingly, *Francisella* does not escape into the cytosol in infected amoeba but resides inside non-acidified vacuoles (Ozanic et al., 2015; Santic et al., 2011). Nevertheless, *Francisella* survival in amoeba is still dependent on the FPI (Ozanic et al., 2015).

Cytosolic replication of *Francisella* allows the host cell to mount anti-microbial immune defenses such as type1 interferons, guanylate-binding proteins and the Absent in melanoma 2 (AIM2) inflammasome (Henry et al., 2007; Jones et al., 2010; Meunier et al., 2015). The AIM2 inflammasome recognizes double-stranded DNA and acts as activation platform for caspase-1 leading to a cell death called pyroptosis and pro-inflammatory cytokine release (Fernandes-Alnemri et al., 2010). On the other hand, *Francisella* has different mechanisms to evade the immune system. *Francisella* LPS modifications to avoid the immune system include tetraacylated instead of hexaacylated Lipid A, longer acyl chains (16-18 carbons instead of 12-14) and masked phosphorylation of sugar backbones (Gunn and Ernst, 2007; Hajjar et al., 2006; Kanistanon et al., 2012). In addition, *F. tularensis* expresses a capsule and actively suppresses all pro-inflammatory signaling (Apicella et al., 2010; Kirimanjeswara et al., 2008; Lindemann et al., 2011). On the other hand, *F. novicida* fails to avoid immune recognition (Kingry and Petersen, 2014; Lagrange et al., 2018). In general, pathogenicity of the four *Francisella* subspecies correlates with the successful evasion from the immune system. Astonishingly, *F. novicida* uses CRISPR/Cas9 to downregulate a lipoprotein with unknown function during infection in order to enhance integrity of the bacterial cell envelope and prevent inflammasome activation (Jones et al., 2012; Ratner et al., 2019; Sampson et al., 2014).

2.4.2.1. The *Francisella* pathogenicity island

Essential for phagosomal escape, intracellular survival and thus infectivity is the *Francisella* pathogenicity island (FPI) (figure 17) (Bröms et al., 2010). Interestingly, *F. tularensis* and *F. holarctica* encode two identical FPIs which can complement each other, while *F. novicida* only encodes one FPI (Golovliov et al., 2003; Larsson et al., 2009; Nano et al., 2004). Thus, *F. novicida* is often used as model organism for studying the FPI. Furthermore, FPI gene *anmK* is likely expressed as two separate open reading frames in *F. tularensis* while the full-length proteins is expressed in *F. novicida* (Nano and Schmerk, 2007). In *F. holarctica*, *anmK* is missing and *pdpD* truncated and likely not functional (Ludu et al., 2008; Nano and Schmerk, 2007). On the other hand, *F. novicida* encodes an additional putative T6SS cluster called *Francisella novicida* island (FNI) (Larsson et al., 2009; Rigard et al., 2016). Many studies showed that disruption of single FPI genes by transposon mutagenesis or with in-frame deletions results in defects in phagosomal escape and intracellular survival defects inside host cells (Ahlund et al., 2010; Bönquist et al., 2008; Brunton et al., 2015; Gray et al., 2002; Kraemer et al., 2009; Meyer et al., 2015; Santic et al., 2005; Su et al., 2007). Yet, the relevance of *pdpD* may vary in different subspecies and for *pdpE* and *anmK* deletions no decrease in virulence was observed (Bröms et al., 2011; de Bruin et al., 2011; Ludu et al., 2008).

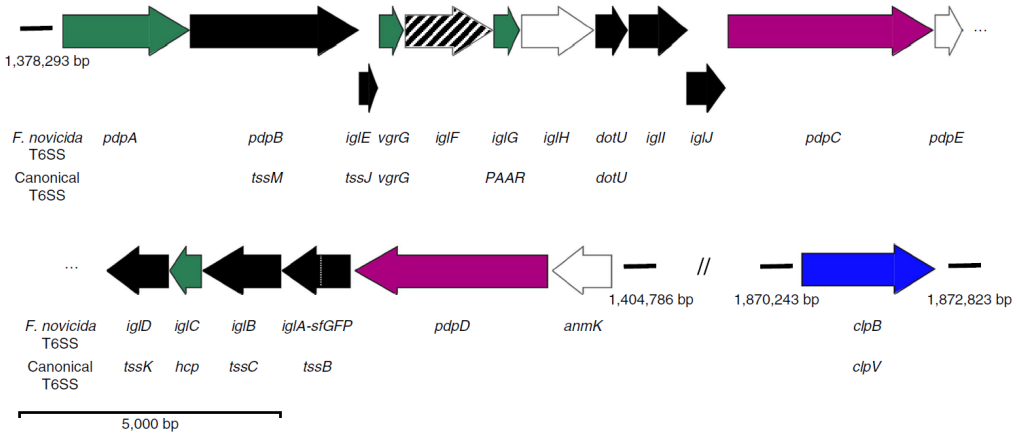

Figure 17: Schematic overview of *Francisella* pathogenicity island (FPI) encoding a non-canonical T6SS. Black genes are structural T6SS components. Secreted components are drawn in green and effectors in magenta. White components have unknown function. Unfoldase responsible for recycling of contracted sheath subunits is depicted in blue. *F. novicida* FPI nomenclature is shown with the corresponding canonical T6SS nomenclature below. *Source: Brodmann et al., 2017, licensed under Creative Commons Attribution 4.0 International License (http://creativecommons.org/licenses/by/4.0/).*

FPI transcription is regulated by at least six regulatory proteins involved in different pathways (Bröms et al., 2010). MglA and SspA are members of the stringent starvation response pathway and induce expression of FevR among others (Baron and Nano, 1998; Brotcke et al., 2006). Then, MglA, SspA and FevR form a complex in the presence of the alarmone ppGpp and induce FPI gene expression (Brotcke and Monack, 2008). MigR indirectly induces FPI gene expression through FevR (Buchan et al., 2009). In addition, the two-component signaling cascade PmrA/KpdD is involved in inducing FPI gene expression (Bell et al., 2010). Moreover, Hfq negatively represses a subset of FPI genes (*pdpA-iglJ*) concluding that the FPI consists of two operons (*pdpA-iglJ* and *pdpD-iglD*) (Meibom et al., 2009). How environmental stimuli modulate theses different transcriptional regulators is not known. However, there are several reports suggesting cues encountered during host cell infection such as iron depletion, oxidative stress or uptake of host cell arginine may upregulate *iglC* expression (Deng et al., 2006; Lenco et al., 2005; Ramond et al., 2015). Interestingly, transcription of FPI genes reaches its maximum 24 h post infection whereas phagosomal escape normally occurs 1 to 4 hours post infection (Wehrly TD et al., 2009).

Although the importance of the FPI for intracellular survival was recognized more than 20 years ago (Golovliov et al., 1997), it was only recently established that the FPI encodes a non-canonical T6SS (Bingle et al., 2008; de Bruin et al., 2007). FPI genes have only little homology to canonical T6SS core components and important components such as ClpV are missing. On the other hand, the FPI encodes additional genes with unknown function (Bingle et al., 2008). Therefore, T6SS function as well as T6SS dynamics were initially questionable. In chapter 3.4, I will characterize *Francisella* T6SS dynamics and reveal that general purpose unfoldase ClpB, a close homolog of ClpV, recycles contracted T6SS sheaths in *Francisella* (Brodmann et al., 2017).

Nevertheless, the structure of the contracted T6SS sheath consisting of IglA and IglB subunits looks overall similar to canonical contracted T6SS sheaths (Clemens et al., 2015; Kudryashev et al., 2015; Salih et al., 2018). Also, tube protein IglC has a similar fold as canonical Hcp despite of having no detectable sequence homology(Sun et al., 2007). *Francisella* membrane complex consists of IglE (TssJ), PdpB (TssM) and DotU (TssL) (de Bruin et al., 2011; Nguyen et al., 2014). PdpB

sits in the IM and bridges through periplasm (de Bruin et al., 2011; Nguyen et al., 2014). The C-terminus of PdpB interacts with lipoprotein IglE located at the OM despite lacking an aspartate at position 2 after the cleavage site (Nguyen et al., 2014). PdpB also interacts with IM protein DotU. Noteworthy to mention is that DotU is required for PdpB stability (de Bruin et al., 2011).

Francisella homologs of baseplate components based on bioinformatics analysis include IglH (TssE) and IglD (TssK), still homologs of TssF and TssG are missing although they are essential for canonical T6SS assembly (Brunet et al., 2015; Rigard et al., 2016).

The spike complex consists of VgrG and IglG (PAAR). *Francisella* VgrG contains only the structural C-terminal part of canonical VgrGs and lacks additional C-terminal domains with enzymatic activity (Bröms et al., 2010; Rigard et al., 2016). Interestingly, PdpA, a FPI component with unknown function, was shown to cap a trimer of VgrG *in vitro*, suggesting that PdpA may substitute the lacking N-terminal part of canonical VgrG (Eshraghi et al., 2016). Indeed, PdpA was found to be secreted together with VgrG in a T6SS dependent manner (Eshraghi et al., 2016). The PAAR motif in IglG is not strictly conserved, however, the structure of IglG is also coordinated by either a zinc or iron similar to canonical PAAR proteins (Rigard et al., 2016; Shneider et al., 2013). Also, IglG was shown to interact with IglF, another FPI component with unknown function, by a N-terminal helix (Rigard et al., 2016).

Identified secreted FPI components include IglC, VgrG, PdpA, PdpD and PdpC as well as OpiA and OpiB1-3 encoded outside of the FPI (Eshraghi et al., 2016). While IglC, VgrG and PdpA are likely purely structural components, the others may be effector proteins. Indeed, PdpC and PdpD are essential for phagosomal escape and intracellular survival (Ludu et al., 2008; Uda et al., 2014). Moreover, electron microscopy revealed that a *pdpC* deletion mutant is still partially covered by phagosomal membranes while a *iglC* deletion mutant resided in an intact vacuole (Lindgren et al., 2013). Since PdpC and PdpD have no homologs, it remains to be elucidated how they promote phagosomal escape and intracellular survival. In contrast, OpiA was shown to be a bacterial phosphatidylinositol 3-kinase, which is required to delay phagosomal maturation (Ledvina et al., 2018). Yet, activity of OpiA likely overlaps with other effector proteins as for example PdpC, since single *opiA*

deletion does not inhibit phagosomal escape (Eshraghi et al., 2016; Ledvina et al., 2018).

IglI and IglJ have both unknown function but are required for *Francisella* virulence (Bröms et al., 2011; Long et al., 2013).

II. AIM OF RESEARCH

Over 25 % of all sequenced Gram-negative bacteria encode at least one T6SS. These bacteria all live in diverse habitats. Different T6SS evolved for various types of antagonistic interactions, which are directed either against other prokaryotes or against eukaryotes. Despite of being a major virulence factor for inter-bacterial competition as well as for host-pathogen interactions, T6SS mode of action has serious drawbacks. First, T6SS dependent killing is contact dependent. Therefore, there is a limited reach for targeting competitors and the chances of being hit are high, too. Second, only few effector molecules are secreted per translocation event. Thus, T6SS dynamics are crucial for repeated firings in order translocate enough effectors. Third, the contracted sheath needs to be recycled and a part of the inner tube as well as the whole spike complex is lost during secretion and must be re-synthesized. Hence, each firing event should be as precise as possible for efficient translocation and minimizing costs.

Recent advances in live-cell fluorescence microscopy and super resolution microscopy allow precise subcellular localization of proteins in bacteria. Thereby it becomes evident that T6SS activity, dynamics and subcellular localization are remarkably diverse. This diversity in spatio-temporal regulation of T6SS firing likely reflects different strategies to resolve the above-mentioned drawbacks of T6SS. Nevertheless, it is poorly understood what causes these differences in T6SS dynamics and how subcellular localization is achieved, maintained and regulated.

This doctoral thesis aims at understanding how different spatial-temporal regulations of T6SS activity are achieved and what the consequences of different subcellular localizations are. In order to understand how certain bacteria dynamically localize T6SS to increase translocation efficiency, we will investigate the unique post-translational regulation mechanism called Threonine phosphorylation pathway (TPP)

in *P. aeruginosa*. TPP is required for rapid localization of attackers and for quick T6SS dependent retaliation. In detail, we will change subcellular localization of one TPP component and assess the change in T6SS activity and localization by live-cell fluorescence microscopy. Furthermore, we will investigate *in silico* when *P. aeruginosas* tit-for-tat T6SS strategy is successful for killing attackers, which exploit a constitutive active T6SS such as *V. cholerae*, and compare the *in silico* results with experimental data.

Next, we aim at characterizing the unique FPI architecture in *F. novicida*. Especially, we want to answer the question if and how *Francisella* T6SS is dynamic despite lacking the canonical ATPase required for recycling of contracted sheaths. By assessing T6SS dynamics and virulence *in vitro* and *in vivo* in single deletion mutants, we will gain insights in order to group unknown components into structural components and putative effector proteins. Furthermore, since *Francisella* T6SS has anti-eukaryotic activity and many secretion systems required for host-pathogen interactions are localized at bacterial poles, we want to determine the subcellular localization of *Francisella* T6SS. In order to identify the subcellular localization, we will analyze membrane complex dynamics with live-cell fluorescence microscopy by labelling single components in combination with different deletions. These results will provide insights about the hierarchy of membrane complex assembly and about which components are crucial for subcellular localization. In case *Francisella* T6SS is also polar, we aim at understanding how polar localization is achieved and whether there is a biological role for this specific subcellular localization. To answer these questions, we would need to find the mechanisms localizing *Francisella* T6SS to the poles. Therefore, we would make single deletions of components known to localize to the poles in other bacteria and analyze subcellular localization of *Francisella* T6SS in these mutants. Moreover, since *Francisella* T6SS is exclusively required for host-pathogen interactions, we aim at establishing an easy to use infection model for *Francisella* T6SS research. Thus, we will use *Galleria mellonella* larvae and characterize the contribution of single FPI components to *Francisella* virulence in these larvae.

III. RESULTS

3.1. Detection of envelope stress by TagQ/R/S/T in *Pseudomonas aeruginosa*

Maj Brodmann and Marek Basler

Biozentrum, University of Basel, Basel, Switzerland

Report

Statement of contribution:

I generated all TPP relocalization strains and performed all imaging experiments as well as the T6SS mediated killing assays. Furthermore, I prepared the samples for LC-MS. I arranged the figures and wrote the report.

Introduction

The threonine phosphorylation pathway (TPP) including the sensor module TagQ/R/S/T enables *Pseudomonas aeruginosa* to sense T6SS attacks and to launch quick counterattacks (Basler et al., 2013). A detailed description is found in chapter 3.2.3. Furthermore, *P. aeruginosa* senses not only T6SS attacks with this signaling cascade but also various envelope stresses induced by polymyxin B, Type 4 secretion system, chelation of ions or extracellular DNA (Basler and Mekalanos, 2012; Basler et al., 2013; Ho et al., 2013; Wilton et al., 2016). Therefore, it is possible that *P. aeruginosa* detects and localizes membrane perturbation or LPS rearrangement. However, it is not clear how the spatial and temporal information integrated by the TPP leads to a highly precise retaliation. Besides, the interplay between TagQ/TagR/TagS/TagT and PpkA and the detailed mode of action how membrane damage is sensed is not elucidated to date.

In recent years, a membrane damage sensing system in *E. coli* was discovered. Normally, lipoprotein RcsF is transported to the inner leaflet of the outer membrane by the chaperone LolA and then is shuffled together with OmpA to the cell surface by BamA. Upon envelope stress, RcsF fails to bind BamA and is exposed to periplasm, where IgaA binds RcsF and initiates the downstream Rcs cascade (Cho et al., 2014). In *P. aeruginosa* TPP, lipoprotein TagQ is anchored to the outer membrane and sequesters TagR in periplasm (Casabona et al., 2013) analogous to BamA sequestering RcsF (Cho et al., 2014). In addition, TagQ, is about 60 times more abundant than other members of the TPP suggesting that TagQ could serve as a sink for TagR (Lin et al., 2019). Therefore, we hypothesized that translocation of TagQ or TagR from outer to inner membrane due to membrane damage may lead to activation of the TPP.

Results

To test this idea, we changed the native N-terminal signal sequences of TagQ and TagR in order to achieve different subcellular localizations. The LipoP algorithm (Juncker et al., 2003) was used to determine the N-terminal signal sequence of TagQ and TagR (figure 1). The prediction revealed that the native TagQ N-terminal signal sequence is cleaved between G29 and C30. In accordance with this prediction, it is described that C30 is required to anchor TagQ to the outer membrane (Casabona et al., 2013). The N-terminal signal sequence of TagR is presumably cleaved between A23 and E24. New N-terminal signal sequences were designed in order to target outer membrane, periplasm, inner membrane and cytosol (figure 1). For outer membrane localization, the signal sequence of TagQ was used to replace the native N-terminal signal sequence of TagR. Periplasmic localization was achieved for both TagQ and TagR by replacing the native N-terminal signal sequences with the N-terminal signal sequence of Tsi1, the periplasmic immunity protein of Tse1 (Russell et al., 2011). For targeting the inner membrane, the 2^+ rule was applied, which concludes that the second amino acid after the cleavage site determines lipoprotein translocation to outer or inner membrane in *Escherichia coli* (Seydel et al., 1999). The second amino acid after the cleavage site in TagQ is an alanine, which should result in outer membrane localization according the 2^+ rule. This prediction was in accordance with experimentally determined outer membrane localization of TagQ (Casabona et al., 2013). Therefore, the native N-terminal signal sequences of TagQ and TagR were replaced with a modified TagQ signal sequence, in which the second amino acid after the cleavage site was substituted to an aspartate (D). Cytosolic localization was achieved by removing the N-terminal signal sequences.

pPSV35 expression plasmid, which is isopropyl-β-D-thiogalactopyranosid (IPTG) inducible (Rietsch et al., 2005), was used to express the different TagQ and TagR constructs in *P. aeruginosa* PAO1Δ*retS clpV-sfGFP* Δ*tagQ* or Δ*tagR* respectively. Δ*retS* background leads to upregulated T6SS activity (Mougous et al., 2006) and ensures that enough T6SS assemblies take place during experiments. Deletion of *tagQ* or *tagR* abolishes T6SS activity completely (Casabona et al., 2013), therefore the capability of the different constructs to restore T6SS activity was assessed by monitoring ClpV-sfGFP dynamics. In addition, dueling was quantified as a measure how well the different strains are able to sense T6SS attacks. Dueling was defined as

T6SS activities of two neighboring cells in close spatial and temporal (2 frames) proximity pointing at each other.

Native TagQ on plasmid already led to normal T6SS activity without inducing expression indicating that pPSV35 was leaky and even a small amount of TagQ was enough to restore T6SS activity (figure 2). However, only very little dueling was observed, suggesting that a certain level of TagQ is required for a fully functioning sensing system. Expression of native TagQ from plasmid induced with up to 500 µM IPTG led to T6SS activity and dueling comparable to chromosomal expression of TagQ (figure 2A). No matter how much expression of $TagQ_{periplasm}$ and $TagQ_{cytosol}$ was induced, T6SS activity and dueling was almost completely abolished (figure 2A), suggesting that these constructs were either not properly expressed or that they failed to activate T6SS due to their subcellular localization. $TagQ_{IM}$ had the most striking phenotype, namely already high activation of T6SS without induction by IPTG but no dueling (figure 2A and C). The T6SS activation pattern of $TagQ_{IM}$ looked very similar to the increased T6SS activity in a Δ*pppA* strain, which assembles very short structures at the same location for several rounds (Basler et al., 2013). The only difference was that $TagQ_{IM}$ did not result in assemblies locked in one position.

Native TagR on plasmid was not able to restore T6SS activity nor dueling without induced expression (figure 2B). In addition, TagR expression was even toxic for *P. aeruginosa* when induced in liquid culture. Therefore, expression of TagR constructs was induced on agarose pads for 15 min with 1 mM IPTG. While T6SS activity was restored with native TagR, $TagR_{periplasm}$ and $TagR_{IM}$, dueling was never observed (figure 2B). Interestingly, expression of native TagR and $TagR_{periplasm}$ led to long T6SS structures whereas expression of $TagR_{IM}$ yielded in short T6SS structures (figure 2B). $TagR_{OM}$ and $TagR_{cytosol}$ were not able to activate T6SS (figure 2B).

To avoid artificial expression levels and toxicity in case of the TagR constructs, all TagQ and TagR versions were introduced into the chromosome of *P. aeruginosa ΔretS clpV-sfGFP tssB-mCherry2*. *P. aeruginosa ΔretS clpV-sfGFP tssB-mCherry2* (parental strain) has both ClpV and TssB labelled with sfGFP and mCherry2, respectively (figure 3A). Again, mutant phenotypes were assessed by observing TssB-mCherry2 and ClpV-sfGFP dynamics. However, it did not make a difference if sheath (TssB-mCherry2) or ClpV (ClpV-sfGFP) was used for quantification of

T6SS activity and dueling as both quantifications led to very similar numbers (figure 4A and B).

As additional measure for the capability of *P. aeruginosa* to react to T6SS attacks, a T6SS mediated killing assay was designed. *P. aeruginosa* PAO1 strains harboring the chromosomal TagQ and TagR variants were mixed with $T6SS^+$ and $T6SS^-$ *Acinetobacter baylyi* ADP1 prey strains in a 5:1:1 ratio on a non-selective agar plate for 2 h. Then the bacteria were recovered and plated on three different selective plates as each strain had a different antibiotic resistance. Since *P. aeruginosa* embarks on a defensive T6SS strategy and only counterattacks, the $T6SS^+$ *A. baylyi* ADP1 should be killed more frequently than the $T6SS^-$ *A. baylyi* ADP1. Indeed, significantly more $T6SS^-$ prey cells than $T6SS^+$ prey cells were recovered from mixtures containing the parental *P. aeruginosa* PAO1 strain.

Live-cell fluorescence microscopy together with the T6SS mediated killing assay suggested that both $TagQ_{periplasm}$ and $TagQ_{cytosol}$ are not capable of T6SS activation (figure 3A and 4C). In contrast, $TagQ_{IM}$ triggered T6SS assembly more than 5-fold in average compared to the parental strain (figure 3A and 4A). The increase in T6SS activity in a $tagQ_{IM}$ mutant was still TPP dependent as the knockout of *tagR*, *tagT* or *ppkA* in a $tagQ_{IM}$ background completely abolished T6SS activity or abolished dueling in case of *ΔtagT* (figure 3C). Strikingly, $TagQ_{IM}$ yielded in less dueling and less efficient killing of *A. baylyi* despite higher T6SS activity (figure 4B-C). In addition, both *A. baylyi* strains were killed in equal amounts suggesting that a $tagQ_{IM}$ strain cannot distinguish between $T6SS^+$ and $T6SS^-$ prey cells (figure 4C). Similar results are reported for the Δ*pppA* strain, which kills less well than the parental strain despite its higher T6SS activity (Basler et al., 2013).

$TagR_{OM}$ and $TagR_{IM}$ expressed from the chromosome yielded in T6SS activity lower than the parental strain while $TagR_{periplasm}$ led to a more than 2-fold significant increase in T6SS activity (figure 3D and 4A). However, dueling cells were observed in all of these mutants (figure 3D and 4B). In agreement, these TagR mutants killed more $T6SS^+$ prey cells than $T6SS^-$ prey cells although the differences were not significant (figure 4C). Noteworthy to mention is that T6SS activity in a $tagR_{cytosol}$ mutant and in a $tagQ_{periplasm}$ $tagR_{IM}$ strain was not rescued (figure 3C).

To confirm that the different N-terminal signal sequences did not change protein abundance, whole-cell samples of TagQ and TagR mutants were analyzed by shotgun liquid chromatography-mass spectrometry (LC-MS) and compared to the parental strain. In general, over 2000 proteins were identified in each sample. The protein levels were considered to be significantly different at a 2-fold change with a q-value of under 0.01 (1 % false discovery rate).

Importantly, the IM N-terminal signal sequence did not affect protein levels in the $TagQ_{IM}$ mutant (figure 5A) suggesting that differences in protein levels could not explain the hyper-activated T6SS phenotype of this mutant. However, periplasmic and cytosolic N-terminal signal sequences of $TagQ_{periplasm}$ and $TagQ_{cytosol}$ led to a 16-fold decrease in TagQ protein abundance compared to the parental strain (figure 5A), which may also contribute to the abolished T6SS activity in these mutants observed by microscopy (figure 3B).

In addition, mutants with deletions of single TPP (*tagR*, *tagT* or *ppkA*) components in parental and $TagQ_{IM}$ background were analysed by LC-MS to rule out alternations in protein levels of downstream genes (figure 6). While deletion of *tagT* and *ppkA* did not influence expression of downstream genes, *tagR* deletion resulted in a 32-fold decrease of TagQ in both parental strain and $TagQ_{IM}$ background (figure 6). To test if *tagR* deletion led to a polar effect on *tagQ*, which is encoded directly downstream of *tagR*, a longer *ΔtagR* peptide scar was used to create a new *tagR* deletion strain. Indeed, the longer *tagR* peptide scar no longer affected TagQ protein abundance in both backgrounds (figure 6).

Interestingly, all altered N-terminal signal sequences in TagR mutants decreased TagR protein levels about 4-16 fold (figure 5). However, these decreases in TagR protein abundance did apparently not affect T6SS activity in these mutants as observed by microscopy and T6SS mediated killing assay (figure 3D and figure 4C).

Since the $TagQ_{IM}$ N-terminal signal did not affect protein levels, the next step was to confirm IM localization of TagQ in this mutant. Therefore, cellular fractionation was performed to separate OM, IM periplasmic and cytosolic content of the parental strain, $TagQ_{IM}$ strain and *ΔtagT* in both backgrounds. The different fractions were analyzed by LC-MS and compared to the corresponding parental strain fraction. Surprisingly, TagQ was up to 32 fold less abundant in the OM and IM fraction of the

$TagQ_{IM}$ background compared to the parental strain (figure 7A and C). Periplasmic and cytosolic fractions were comparable in both $TagQ_{IM}$ background and parental strain (figure 7B and D). These results indicate that TagQ was lost during cellular fractionation as the $TagQ_{IM}$ whole cell samples had comparable TagQ levels to the parental strain (figure 5A).

One explaination could be that $TagQ_{IM}$ was localized in inclusion bodies, which were likely discarded during cellular fractionation. To test this hypothesis, TagQ was labelled with mCherry2 in both $TagQ_{IM}$ and parental strain background. Most of TagQ-mCherry2 was localized at the membrane as reported previously (Casabona et al., 2013) (figure 8A). In addition, TagQ-mCherry2 was fully functional, as T6SS dueling was observable (figure 8B). However, in the $TagQ_{IM}$ background additional cytosolic TagQ-mCherry spots were observed, which were not present in the parental strain (figure 8A), suggesting that indeed TagQ was localized in inclusion bodies in $TagQ_{IM}$ background. Furthermore, T6SS dynamics were comparable to unlabeled $TagQ_{IM}$ (figure 8C).

In order to prevent formation of inclusion bodies, I replaced the N-terminal signal sequence of TagQ with the one of MexA. IM protein MexA is part of the well-studied MexAB-OprM multidrug efflux pump in *P. aeruginosa* (Masuda et al., 2000). The N-terminal signal sequence was previously used to localize lipoproteins to the IM (Narita and Tokuda, 2007). Unfortunately, TagQ with MexA IM-signal did not reproduce $TagQ_{IM}$ phenotype (figure 9A). While T6SS activity was higher in the $TagQ_{MexA}$ compared to the parental strain, dueling was still observed to a significant amount (figure 9B and C). Besides, T6SS sheaths were as long as the ones of the parental strain. These findings suggest that the TPP signaling cascade was still functional in this mutant. It remains to be determined whether the higher T6SS activity is a result of IM localization of $TagQ_{MexA}$.

Summary and outlook

In summary, although changing the N-terminal signal sequence of OM lipoprotein TagQ in order to localize TagQ to IM resulted in a striking T6SS phenotype with short random T6SS assemblies, my experiments could not confirm that IM localization of TagQ is the cause for this phenotype. Cellular fractionation combined with LC-MS as well as fluorescence microscopy revealed that $TagQ_{IM}$ was not enriched at the IM but sequestered in inclusion bodies. Thus, it is impossible to distinguish whether the observed phenotype derived from a general decrease in TagQ components due to sequestering in inclusion bodies or if the IM signal sequences led to altered folding properties and thus caused envelope stress. However, $TagQ_{IM}$ was least partially functional as T6SS is still activated compared to abrogated T6SS activity in a *tagQ* deletion mutant. Unfortunately, the $TagQ_{IM}$ phenotype could not be reproduced with another IM localization N-terminal signal sequence. Although the N-terminal signal sequence of IM lipoprotein MexA was previously used to localize proteins to the IM (Narita and Tokuda, 2007), $TagQ_{Mex}$ still enabled dueling and long T6SS structures. However, the overall T6SS activity was increased. It is worth mentioning that no cellular fractionation was performed for $TagQ_{MexA}$ to check its exact subcellular localization. Nevertheless, it is questionable if the initial hypothesis that TagQ relocation in response to envelope stress triggers the TPP is still valid.

Bioinformatics analysis (HHpred, Zimmermann et al., 2018) recently detected homology of TagQ to *Pseudomonas* lipoprotein YfiB. YfiB is part of a three-component signaling system involved in modulation of intracellular c-di-GMP levels in response to envelope stress (Li et al., 2015; Malone et al., 2010). Interestingly, YfiB is anchored to the OM and binds peptidoglycan via its OmpA-like domain (Malone et al., 2010). Thus, YfiB spans from OM to the peptidoglycan layer. Changes in distance between these two layers triggers a conformational change of YfiB and thus enhances its ability to bind YfiR. YfiR is the repressor of the IM integrated diguanylate cyclase YfiN. Therefore, as soon envelope stress leads to changes in distance between OM and peptidoglycan layer, YfiB is able to bind YfiR, and c-di-GMP production by YfiN is activated (Li et al., 2015; Malone et al., 2010, 2012). Since TagQ also contains a predicted putative OmpA peptidoglycan-binding domain, it is tempting to speculate that TagQ might sense cell envelope stress in a

similar manner. Thus, affinity of binding TagR may be affected by changes in the cell envelope.

In order to test whether the distance between OM and peptidoglycan is important for TagQ function, I plan to shorten the sequence between OM anchor and putative OmpA-like domain of TagQ. In addition, changing the distance between OM and peptidoglycan by osmotic shock will allow to further test this hypothesis. Furthermore, subcellular localization of TagR remains to be elucidated. Thus, I plan to tag TagR with mCherry2 to see where TagR is localized and whether localization changes upon dueling.

Material and methods

Bacterial strains and growth conditions

Pseudomonas aeruginosa PAO1 and derivative strains were grown aerobically in Luria broth (LB) or on LB agar plates at 37 °C. The medium was either supplemented with irgasan (20 µg/ml, Sigma-Aldrich) or with gentamycin (30 µg/ml, AppliChem) when strains harbored expression plasmids. *Acinetobacter baylyi* ADP1 and derivative strains were grown aerobically in LB or on LB agar plates at 30 °C. The medium was either supplemented with streptomycin (100 µg/ml, AppliChem) and spectinomycin (300 µg/ml, Sigma-Aldrich) or with streptomycin (100 µg/ml, AppliChem) and kanamycin (50 µg/ml, AppliChem). All strains are listed in table 1.

Bacterial mutagenesis

To introduce in-frame deletions and different N-terminal signal sequences on the chromosome of *Pseudomonas aeruginosa* PAO1, suicide vector pEXG2 (Rietsch et al., 2005) was used. Expression plasmid pPSV35 (Rietsch et al., 2005) was used for isopropyl-β-D-thiogalactopyranoside (IPTG, AppliChem) inducible expression of TagQ and TagR variants. All plasmids, remaining peptides of in-frame deletions, N-terminal sequences and primers are listed in table 2. All cloning products and sites of homologous recombination were verified by polymerase chain reaction (PCR) and sequencing.

Fluorescence live cell imaging

Microscope set up was described previously (Brodmann et al., 2017; Kudryashev et al., 2015; Vettiger and Basler, 2016). For imaging, day cultures of *P. aeruginosa* PA01 Δ*retS clpV-sfGFP tssB-mCherry2* parental and mutant strains were inoculated from plate at an optical density$_{600}$ (OD_{600}) of 0.2 without any antibiotics. For strains harboring an expression plasmid, the medium was supplemented with gentamycin and 0, 250, 500 and 1000 µM IPTG to induce gene expression. Expression of TagR constructs on plasmid was induced with 1000 µM IPTG directly on the agarose pad for 15 minutes. At an OD_{600} of 1, the cultures were concentrated to an OD_{600} of 10.

1.5 µl of the concentrated cultures was then spotted on a pad consisting of 1 % agarose in 2/3 phosphate buffered saline (PBS) and 1/3 LB. The agarose pad was incubated at 37 °C for 10 min before imaging at 30 °C and 95 % humidity. Most images were collected every 20 s for 3 min. The exposure time for each channel was set to 150 ms.

Image analysis

Image analysis was carried out with Fiji software (Schindelin et al., 2012) as previously described (Basler et al., 2013; Vettiger and Basler, 2016). The total number of bacteria in a field of view was counted with the plugin "Find Maxima". T6SS activity and dueling was quantified manually with the help of the plugin "Temporal-Color Code", with which all events of a time series are displayed on one image. Dueling was defined as T6SS activities of two neighboring cells in close spatial and temporal (2 frames) proximity pointing at each other.

Three-strain T6SS mediated killing assay

Overnight cultures of *P. aeruginosa* PA01 Δ*retS clpV-sfGFP tssB-mCherry2* parental strain and the different mutant strains, T6SS+ *A. baylyi* ADP1 *rpsL-K89R PAAR1-2::specR* and T6SS- *A. baylyi* ADP1 *rpsL-K89R Δ2'644'572-2'653'574::kanR* were grown with corresponding antibiotics. The next day, day cultures were inoculated at an OD_{600} of 0.2 and incubated at 37 °C for P. aeruginosa PA01 strains and at 30 °C for A. baylyi ADP1 strains. After 3 h, OD_{600} was measured and the cells were concentrated to OD_{600} of 10 accordingly. *P. aeruginosa* PA01 strains were mixed with T6SS+ and T6SS- *A. baylyi* ADP1 in a 5:1:1 ratio (50 µl:10 µl:10 µl). Then 5 µl of the mixtures were spotted in duplicates on a LB agar plate without any antibiotics. The plates were incubated at 37 °C for 2 h. Afterwards, the agar with the spots were cut out and the bacteria were recovered in 0.5 ml LB. 100 µl of the recovered bacteria were used for 1:10 dilution series. 5 µl of each dilution was spotted on three different LB agar plates containing either irgasan, streptomycin and spectinomycin or streptomycin and kanamycin to recover the predator strains as well as the two different prey strains. The LB agar plates were incubated at 37 °C for

P. aeruginosa PA01 strains and at 30 °C for *A. baylyi* ADP1 strains overnight. The next day, the number of recovered colony forming units (CFU) was calculated for each strain with the following formula:

$$\frac{CFU}{ml} = \frac{Average\ of\ counted\ colonies \times 10^{Dilution\ step}}{0.005\ ml}$$

Cellular fractionation

Cellular fractionation was performed as described previously (Hoang et al., 2011). 200 ml day cultures of *P. aeruginosa* PA01 Δ*retS clpV-sfGFP tssB-mCherry2* parental and mutant strains were inoculated from overnight cultures without antibiotics at 37 °C. After 4 h, OD_{600} was measured and adjusted to OD_{600} of 1. Then the cultures were concentrated by centrifugation at 3'000 g for 20 min and resuspendend in 2 ml of sucrose-Tris buffer (0.5 M sucrose, Fluka; 40 mM Tris-HCl, pH 7.5, AppliChem). Lysozyme (Sigma-Aldrich) was added to a final concentration of 0.5 mg/ml. Then the samples were incubated for 5 min. Afterwards, the cells were centrifuged at 1'500 g for 15 min. The supernatants containing periplasmic proteins were collected and immediately frozen. The pellets were resuspended in 2 ml lysis buffer (20 mM Tris-HCl, pH 7.5; 0.1 M NaCl, Merck; 1 mM Ethylenediaminetetraacetic acid (EDTA), pH 8, Calbiochem) and sonicated 30 s with 30 s break for 10 cycles in a Bioruptor Pico (Diagenode). Unbroken cells were concentrated at 10'000 g and 4 °C for 10 min. The supernatants were centrifuged at 200'000 g and 4 °C for 1 h for recovering cytoplasmic proteins. The pellet was washed twice with 20 mM Tris-HCl buffer (pH 7.5) with centrifugation at 200'000 g and 4 °C for 1 h in between. After washing, the pellets were resuspended in IM extraction buffer (20 mM Tris-HCl, 7.5, 0.5 % Sarkosyl (sodium N-lauroylsarcosinate, Sigma-Aldrich) and incubated at room temperature for 30 min. Then the samples were centrifuged at 200'000 g and 4 °C for 1 h. The supernatants containing the inner membrane proteins were collected. The remaining pellets containing the outer membrane proteins were resuspended in 20 mM Tris-HCl buffer (pH 7.5). Experiment was performed in biological triplicates.

Shotgun liquid chromatography-mass spectrometry

For whole cell analysis, 2 ml day cultures of *P. aeruginosa* PA01 Δ*retS clpV-sfGFP tssB-mCherry2* parental and mutant strains were inoculated at OD_{600} of 0.2 from plate. After 3 h, OD_{600} was measured and adjusted to OD_{600} of 1. 1 ml of these samples was concentrated and resuspended in 100 µl lysis buffer (8 M Urea, Sigma-Adrich; 0.1 M Ammonium bicarbonate, Sigma Aldrich) and heat inactivated at 95 °C for 10 min. Then the samples were sonicated 30 s with 30 s break for 10 cycles in a Bioruptor Pico and heated again at 95 °C for 10 min. Afterwards, the samples were centrifuged at 4'500 g for 10 s and the protein concentration was measured with a BCA protein assay kit (Pierce). In parallel, 2 µl of chloroacetamide (Sigma-Aldrich) was added and the samples were incubated at 37 °C for 30 min. Again, the samples were centrifuged at 4'500 g for 10 s.

For whole cell samples as well as for the different cellular fractions 50 µg of protein was used for overnight digestion at 37 °C with 1 µg of porcine Trypsin (Promega). The next day, the samples were centrifuged at 4'500 g for 10 s. For solid phase extraction, 50 µl of 5 % Trifluoroacetic acid (TFA, Thermo) in H_2O was added. Then 100 µl of 1 % TFA in isopropanol (Sigma-Aldrich) was added and the samples were loaded on PR-sulfonate cartridges (Styrenedivinylbenzene-reverse phase sulfonate (SDB-RPS), PreOmics). The cartridges were centrifuged at 1'800 g for 3 min and the flow-through was discarded. Then the cartridges were washed twice with 200 µl of 1 % TFA in isopropanol with centrifugation at 1'800 g for 3 min in between. A second washing step with 200 µl of 0.2 % TFA in H_2O was also carried out twice with centrifugation at 1'800 g for 3 min in between. The peptides were eluted in 200 µl elution buffer (1 % (v/v) ammonium hydroxide, Sigma-Aldrich; 19 % H_2O; 80 % acetonitrile, Thermo Scientific). The eluted peptides were dried under vacuum and resuspended in 20 µl LC-MS/MS buffer (0.15 % formic acid, Sigma-Adrich; 2 % acetonitrile). To dissolve the peptides, ultrasonication (Hielscher) for 10 s was used. Afterwards, the samples were incubated at 25 °C shaking for 5 min. Then concentration of the samples was measured and adjusted to 0.5 µg/µl before transferring the samples into LC-vials. A 1:10 iRT-peptide mix (Biognosys) was added (ThermoFisher).

1 µg of total peptides were used for LC-MS analysis with a dual pressure LTQ-Orbitrap Elite mass spectrometer connected to an electrospray ion source (both

Thermo Fisher Scientific) and a custom-made column heater set to 60°C. Peptides were separated with an an EASY nLC-1000 system (Thermo Fisher Scientific) equipped with a RP-HPLC column (75µm × 30cm) packed in-house with C18 resin (ReproSil-Pur C18–AQ, 1.9 µm resin; Dr. Maisch GmbH, Germany) using a linear gradient from 95% solvent A (0.1% formic acid in water) and 5% solvent B (80% acetonitrile, 0.1% formic acid, in water) to 35% solvent B over 50 min to 50% solvent B over 10 min to 95% solvent B over 2 min and 95% solvent B over 18min at a flow rate of 0.2 µl/min.

One high resolution MS scan in the FT part of the mass spectrometer at a resolution of 240,000 full width at half maximum (at 400 m/z, MS1) was acquired. Then MS/MS (MS2) scans followed in the linear ion trap for the 20 most intense MS signals. Unassigned and singly charged ions were excluded with the charged state screening modus. The dynamic exclusion duration was set to 30 s. The collision energy was set to 35%, and one microscan was acquired for each spectrum.

Protein identification and label-free quantification

The peptide precursor ion intensites across all samples were extracted with the Progenesis QI software (v2.0, Nonlinear Dynamics Limited) using the default parameters. MASCOT was used to search the generated mfg-gfiles against a decoy database containing normal and reverse sequences of the *P. aeruginosa* PAO1 proteome (source: UniProt) and commonly observed contaminants generated using the SequenceReverser tool from the MaxQuant software (Version 1.0.13.13). The search criteria included full tryptic specificity (cleavage after lysine or arginine residues, unless followed by proline); 3 missed cleavages were allowed; fixed modification of carbamidomethylation (C); variable oxidation (M) and protein N-terminal acetylation modifications; mass tolerance of 10 ppm (precursor) and 0.6 Da (fragments). The ion score was used to set a false discovery rate (FDR) of 1% on the peptide and protein level, respectively, based on the number of reverse protein sequence hits in the datasets.

Statistical analysis

Statistical analysis of most data was performed with Prism7 (GraphPad Software). To test if T6SS$^+$ *A. baylyi* ADP1 is killed significantly more than T6SS$^-$ *A. baylyi* ADP1 by *P. aeruginosa* PAO1 strains, multiple *t*-tests ($\alpha = 0.05$) with correction for multiple comparison (Holm-Sidak method) were used.

LC-MS data was analysed with the Quantsafe R package (version 2.3.4.). Data was globally normalized by equalizing the total peak/reporter areas across all LC-MS runs. The peak areas per protein and LC MS/MS run was summed followed by calculation of protein abundance ratios. Quantification was carried out for isoform specific peptide ion signals. Empirical Bayes moderated *t*-Tests were applied for the summarized protein expression values, as implemented in the R/Bioconductor limma package. Benjamini-Hochberg method was used to adjust the resulting per protein and condition comparison *p*-values for multiple testing. Changes in relative protein abundance were considered significantly different between two strains when the change was 2-fold or higher and the false discovery rate (q-value) was below 1 %.

References

Basler, M., and Mekalanos, J.J. (2012). Type 6 secretion dynamics within and between bacterial cells. Science (New York, N.Y.) *337*, 815–815.

Basler, M., Ho, B.T., and Mekalanos, J.J. (2013). Tit-for-tat: Type VI secretion system counterattack during bacterial cell-cell interactions. Cell *152*, 884–894.

Brodmann, M., Dreier, R.F., Broz, P., and Basler, M. (2017). Francisella requires dynamic type VI secretion system and ClpB to deliver effectors for phagosomal escape. Nat Commun *8*, 15853.

Casabona, M.G., Silverman, J.M., Sall, K.M., Boyer, F., Couté, Y., Poirel, J., Grunwald, D., Mougous, J.D., Elsen, S., and Attree, I. (2013). An ABC transporter and an outer membrane lipoprotein participate in posttranslational activation of type VI secretion in *Pseudomonas aeruginosa*. Environ. Microbiol. *15*, 471–486.

Cho, S.-H., Szewczyk, J., Pesavento, C., Zietek, M., Banzhaf, M., Roszczenko, P., Asmar, A., Laloux, G., Hov, A.-K., Leverrier, P., et al. (2014). Detecting Envelope Stress by Monitoring β-Barrel Assembly. Cell *159*, 1652–1664.

Ho, B.T., Basler, M., and Mekalanos, J.J. (2013). Type 6 Secretion System-Mediated Immunity to Type 4 Secretion System-Mediated Horizontal Gene Transfer. Science (New York, N.Y.) *342*, 250–253.

Hoang, H.H., Nickerson, N.N., Lee, V.T., Kazimirova, A., Chami, M., Pugsley, A.P., and Lory, S. (2011). Outer membrane targeting of Pseudomonas aeruginosa proteins shows variable dependence on the components of Bam and Lol machineries. MBio *2*.

Juncker, A.S., Willenbrock, H., Von Heijne, G., Brunak, S., Nielsen, H., and Krogh, A. (2003). Prediction of lipoprotein signal peptides in Gram-negative bacteria. Protein Sci. *12*, 1652–1662.

Kudryashev, M., Wang, R.Y.-R., Brackmann, M., Scherer, S., Maier, T., Baker, D., DiMaio, F., Stahlberg, H., Egelman, E.H., and Basler, M. (2015). Structure of the type VI secretion system contractile sheath. Cell *160*, 952–962.

Li, S., Li, T., Xu, Y., Zhang, Q., Zhang, W., Che, S., Liu, R., Wang, Y., and Bartlam, M. (2015). Structural insights into YfiR sequestering by YfiB in Pseudomonas aeruginosa PAO1. Sci Rep *5*, 16915.

Lin, L., Lezan, E., Schmidt, A., and Basler, M. (2019). Abundance of bacterial Type VI secretion system components measured by targeted proteomics. Nat Commun *10*, 2584.

Malone, J.G., Jaeger, T., Spangler, C., Ritz, D., Spang, A., Arrieumerlou, C., Kaever, V., Landmann, R., and Jenal, U. (2010). YfiBNR mediates cyclic di-GMP dependent small colony variant formation and persistence in Pseudomonas aeruginosa. PLoS Pathog. *6*, e1000804.

Malone, J.G., Jaeger, T., Manfredi, P., Dötsch, A., Blanka, A., Bos, R., Cornelis, G.R., Häussler, S., and Jenal, U. (2012). The YfiBNR signal transduction mechanism reveals novel targets for the evolution of persistent Pseudomonas aeruginosa in cystic fibrosis airways. PLoS Pathog. *8*, e1002760.

Masuda, N., Sakagawa, E., Ohya, S., Gotoh, N., Tsujimoto, H., and Nishino, T. (2000). Substrate Specificities of MexAB-OprM, MexCD-OprJ, and MexXY-OprM Efflux Pumps in Pseudomonas aeruginosa. Antimicrobial Agents and Chemotherapy *44*, 3322–3327.

Mougous, J.D., Cuff, M.E., Raunser, S., Shen, A., Zhou, M., Gifford, C.A., Goodman, A.L., Joachimiak, G., Ordoñez, C.L., Lory, S., et al. (2006). A Virulence Locus of Pseudomonas aeruginosa Encodes a Protein Secretion Apparatus. Science (New York, N.Y.) *312*, 1526–1530.

Narita, S., and Tokuda, H. (2007). Amino Acids at Positions 3 and 4 Determine the Membrane Specificity of Pseudomonas aeruginosa Lipoproteins. J. Biol. Chem. *282*, 13372–13378.

Rietsch, A., Vallet-Gely, I., Dove, S.L., and Mekalanos, J.J. (2005). ExsE, a secreted regulator of type III secretion genes in Pseudomonas aeruginosa. Proc. Natl. Acad. Sci. U.S.A. *102*, 8006–8011.

Russell, A.B., Hood, R.D., Bui, N.K., LeRoux, M., Vollmer, W., and Mougous, J.D. (2011). Type VI secretion delivers bacteriolytic effectors to target cells. Nature *475*, 343–347.

Schindelin, J., Arganda-Carreras, I., Frise, E., Kaynig, V., Longair, M., Pietzsch, T., Preibisch, S., Rueden, C., Saalfeld, S., Schmid, B., et al. (2012). Fiji: an open-source platform for biological-image analysis. Nat. Methods *9*, 676–682.

Seydel, A., Gounon, P., and Pugsley, A.P. (1999). Testing the "+2 rule" for lipoprotein sorting in the Escherichia coli cell envelope with a new genetic selection. Molecular Microbiology *34*, 810–821.

Vettiger, A., and Basler, M. (2016). Type VI Secretion System Substrates Are Transferred and Reused among Sister Cells. Cell *167*, 99-110.e12.

Wilton, M., Wong, M.J.Q., Tang, L., Liang, X., Moore, R., Parkins, M.D., Lewenza, S., and Dong, T.G. (2016). Chelation of Membrane-Bound Cations by Extracellular DNA Activates the Type VI Secretion System in Pseudomonas aeruginosa. Infect. Immun. *84*, 2355–2361.

Zimmermann, L., Stephens, A., Nam, S.-Z., Rau, D., Kübler, J., Lozajic, M., Gabler, F., Söding, J., Lupas, A.N., and Alva, V. (2018). A Completely Reimplemented MPI Bioinformatics Toolkit with a New HHpred Server at its Core. J. Mol. Biol. *430*, 2237–2243.

Figures

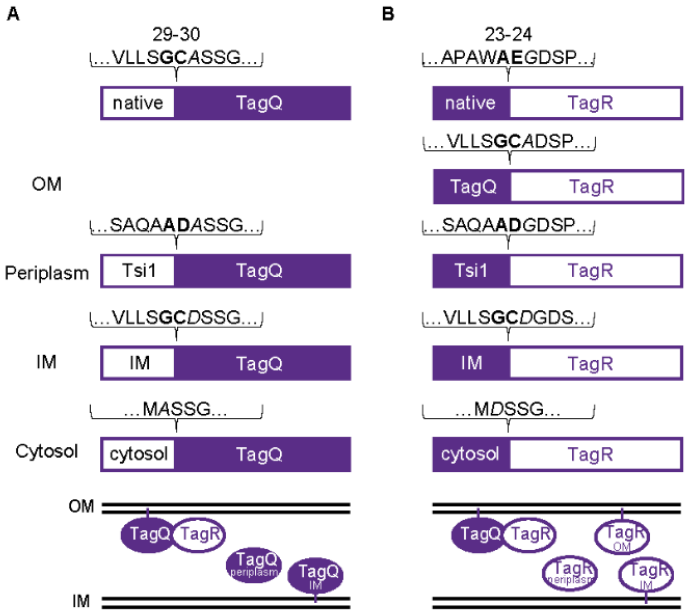

Figure 1: Overview of different signal sequences designed for TagQ and TagR. A) Native N-terminal signal sequence of TagQ is predicted to be cleaved between amino acids 29-30. Brackets display cleavage site in bold, the second amino acid after cleavage site in italic and 4 amino acids before and after cleavage site. Periplasmic localization was achieved by replacing the native N-terminal signal with the first 20 amino acids of Tsi1, a periplasmic immunity protein of T6SS effector Tse1. For IM localization, the second amino acid after the cleavage site A31 was exchanged with D31. The whole signal sequence was removed for cytosolic localization. An overview of subcellular localizations is shown below. **B)** Native N-terminal signal sequence of TagR is predicted to be cleaved between amino acids 23-24. Brackets display cleavage site in bold, the second amino acid after cleavage site in italic and 4 amino acids before and after cleavage site. OM localization was accomplished by replacing amino acids 1-25 by native N-terminal signal sequence of TagQ (amino acids 1-31). Periplasmic localization was achieved by replacing the native N-terminal signal with the first 20 amino acids of Tsi1, a periplasmic immunity protein of T6SS effector Tse1. For IM localization, the IM signal for TagQ was used to replace amino acids 1-31 of TagR. The whole signal sequence was removed for cytosolic localization. An overview of subcellular localizations is shown below.

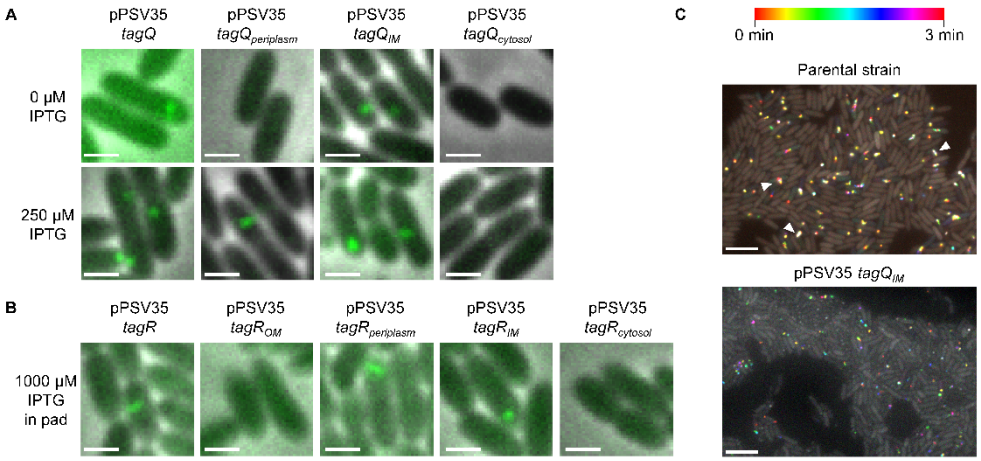

Figure 2: T6SS phenotypes of TagQ and TagR N-terminal signal sequence mutants expressed on plasmid. A) T6SS phenotypes of *P. aeruginosa* PAO1 Δ*retS clpV-sfGFP* Δ*tagQ* with TagQ, $TagQ_{periplasm}$, $TagQ_{IM}$ and $TagQ_{cytosol}$ expressed on pPSV35. Protein expression was induced with 250 µM IPTG. Merge of phase contrast and GFP channel is shown. 3.3 x 3.3 µm fields of view are shown. Scale bar represents 1 µm. **B)** T6SS phenotypes of *P. aeruginosa* PAO1 Δ*retS clpV-sfGFP* Δ*tagR* with TagR, $TagR_{OM}$, $TagR_{periplasm}$, $TagR_{IM}$ and $TagR_{cytosol}$ expressed on pPSV35. Protein expression was induced with 1000 µM IPTG in the agarose pad. Merge of phase contrast and GFP channel is shown. 3.3 x 3.3 µm fields of view are shown. Scale bar represents 1 µm. **C)** Summary of T6SS activity of *P. aeruginosa* PAO1 Δ*retS clpV-sfGFP* and *P. aeruginosa* PAO1 Δ*retS clpV-sfGFP* Δ*tagQ* pPSV35 $tagQ_{IM}$ in the GFP channel over 3 minutes with "Temporal-Color Code" function. Time color scale bar indicates at which time point the event appeared. Arrows highlight 3 dueling events for *P. aeruginosa* PAO1 Δ*retS clpV-sfGFP*. 13 x 9.8 µm fields of view are shown. Scale bar represents 5 µm.

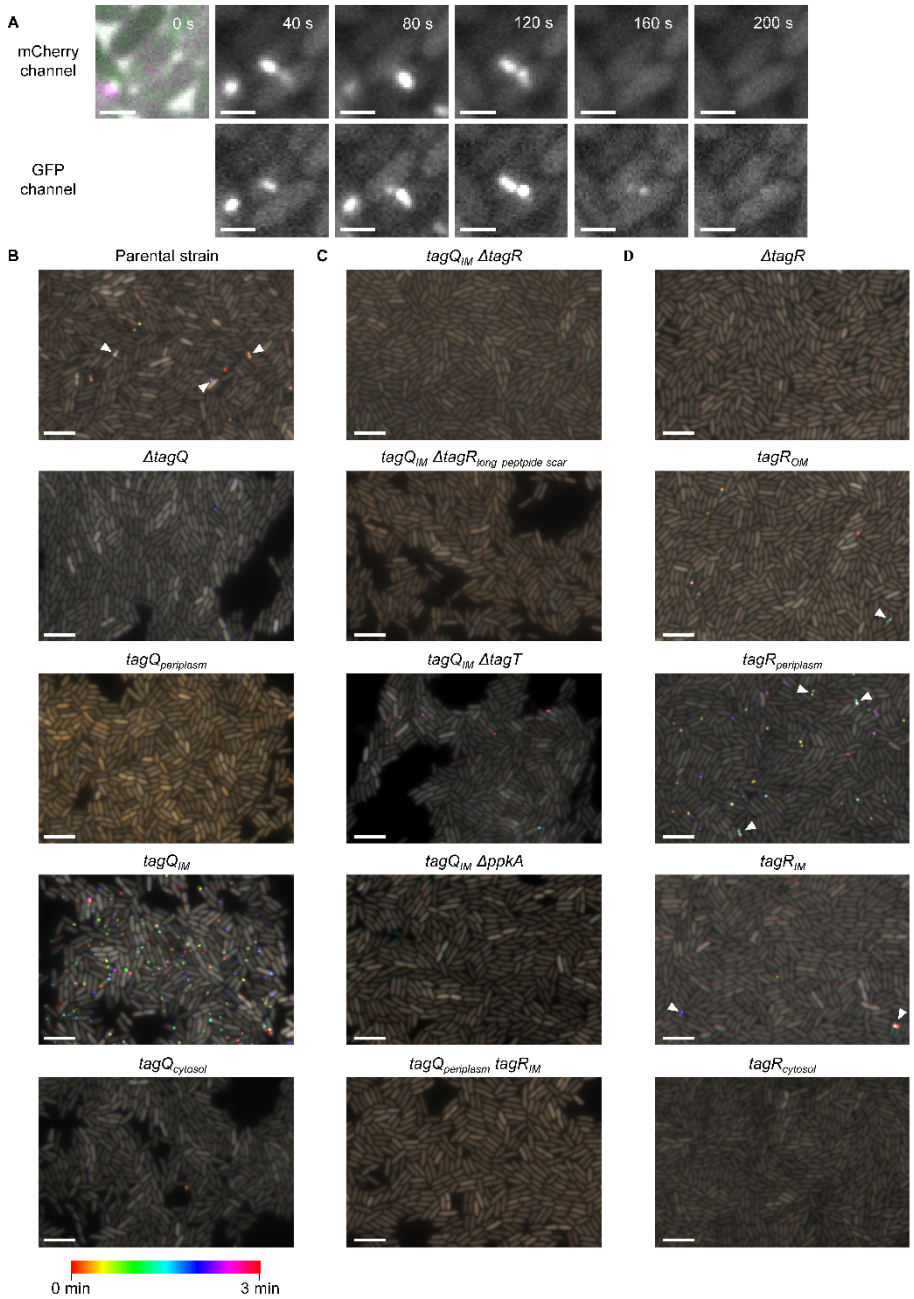

Figure 3: T6SS phenotypes of chromosomal TagQ and TagR N-terminal signal sequence mutants. A) T6SS dueling event of *P. aeruginosa* PAO1 Δ*retS clpV-sfGFP tssB-mCherry2*. First image shows merge of phase contrast, GFP channel and mCherry channel, followed by GFP channel (upper panel) and mCherry channel (lower panel). 3.3 x 3.3 µm fields of view are shown. Scale bar represents 1 µm. **B)** Summary of T6SS activity of *P. aeruginosa* PAO1 Δ*retS clpV-sfGFP tssB-mCherry2*, Δ*tagQ*, $tagQ_{periplasm}$, $tagQ_{IM}$ and $tagQ_{cytosol}$ in the mCherry channel over 3 minutes with "Temporal-Color Code" function. **C)** Summary of T6SS activity of *P. aeruginosa* PAO1 Δ*retS clpV-sfGFP tssB-mCherry2* $tagQ_{IM}$ Δ*tagR*, $tagQ_{IM}$ Δ*tagT*, $tagQ_{IM}$ Δ*ppkA* and $tagQ_{periplasm}$ $tagR_{IM}$ in the mCherry channel over 3 minutes with "Temporal-Color Code" function. **D)** Summary of T6SS activity of *P. aeruginosa* PAO1 Δ*retS clpV-sfGFP tssB-mCherry2* Δ*tagR*, $tagR_{OM}$, $tagR_{periplasm}$, $tagR_{IM}$ and $tagR_{cytosol}$ in the mCherry channel over 3 minutes with "Temporal-Color Code" function. **B-D)** Time color scale bar indicates at which time point the event appeared. Arrows highlight dueling events. 13 x 9.8 µm fields of view are shown. Scale bar represents 5 µm.

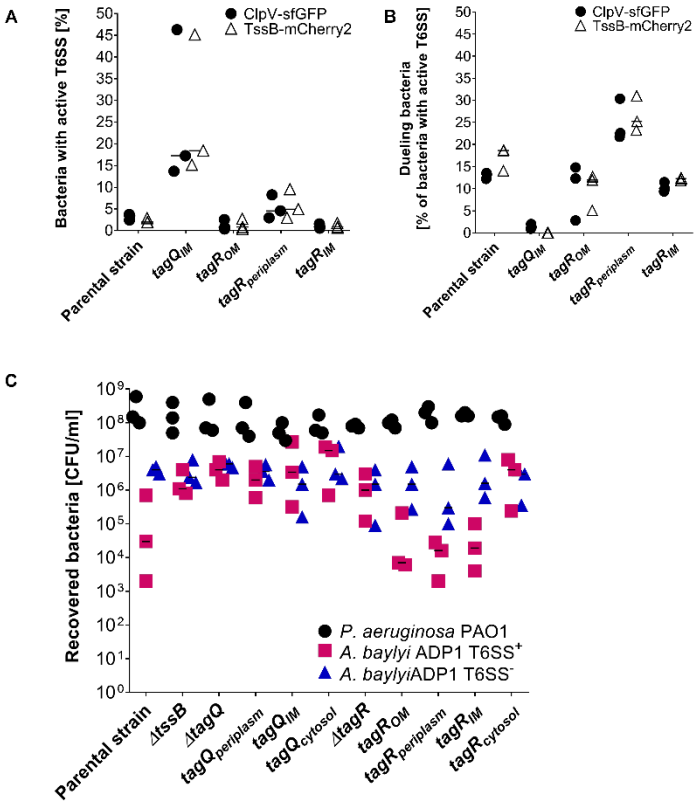

Figure 4: Quantification of T6SS activity, dueling and killing for TagQ and TagR N-terminal signal sequence mutants. **A)** Quantification of bacteria with T6SS assembly within 3 minutes of imaging for *P. aeruginosa* PAO1 Δ*retS clpV-sfGFP tssB-mCherry2*, $tagQ_{IM}$, $tagR_{OM}$, $tagR_{periplasm}$ and $tagR_{IM}$. Quantification was carried out based on ClpV-sfGFP (black circle) and TssB-mCherry2 (white triangle). Three biological replicates with at least 5000 bacteria each were analyzed. Black line represents median. **B)** Quantification of dueling bacteria, which had active T6SS in **A)** during 3 minutes of imaging. Quantification was carried out based on ClpV-sfGFP (black circle) and TssB-mCherry2 (white triangle). Black line represents median. **C)** Three-strain T6SS mediated killing assay carried out with *P. aeruginosa* PAO1 Δ*retS clpV-sfGFP tssB-mCherry2*, Δ*tssB*, Δ*tagQ*, $tagQ_{periplasm}$, $tagQ_{IM}$, $tagQ_{cytosol}$, Δ*tagR*, $tagR_{OM}$, $tagR_{periplasm}$, $tagR_{IM}$ and $tagR_{cytosol}$ (black circles) competing against $T6SS^+$ *A. baylyi* ADP1 *rpsL-K89R PAAR1-2::specR* (magenta squares) and $T6SS^-$ *A. baylyi* ADP1 *rpsL-K89R Δ2'644'572-2'653'574::kanR* (blue trinangles). Three biological replicates were performed. Black line represents median.

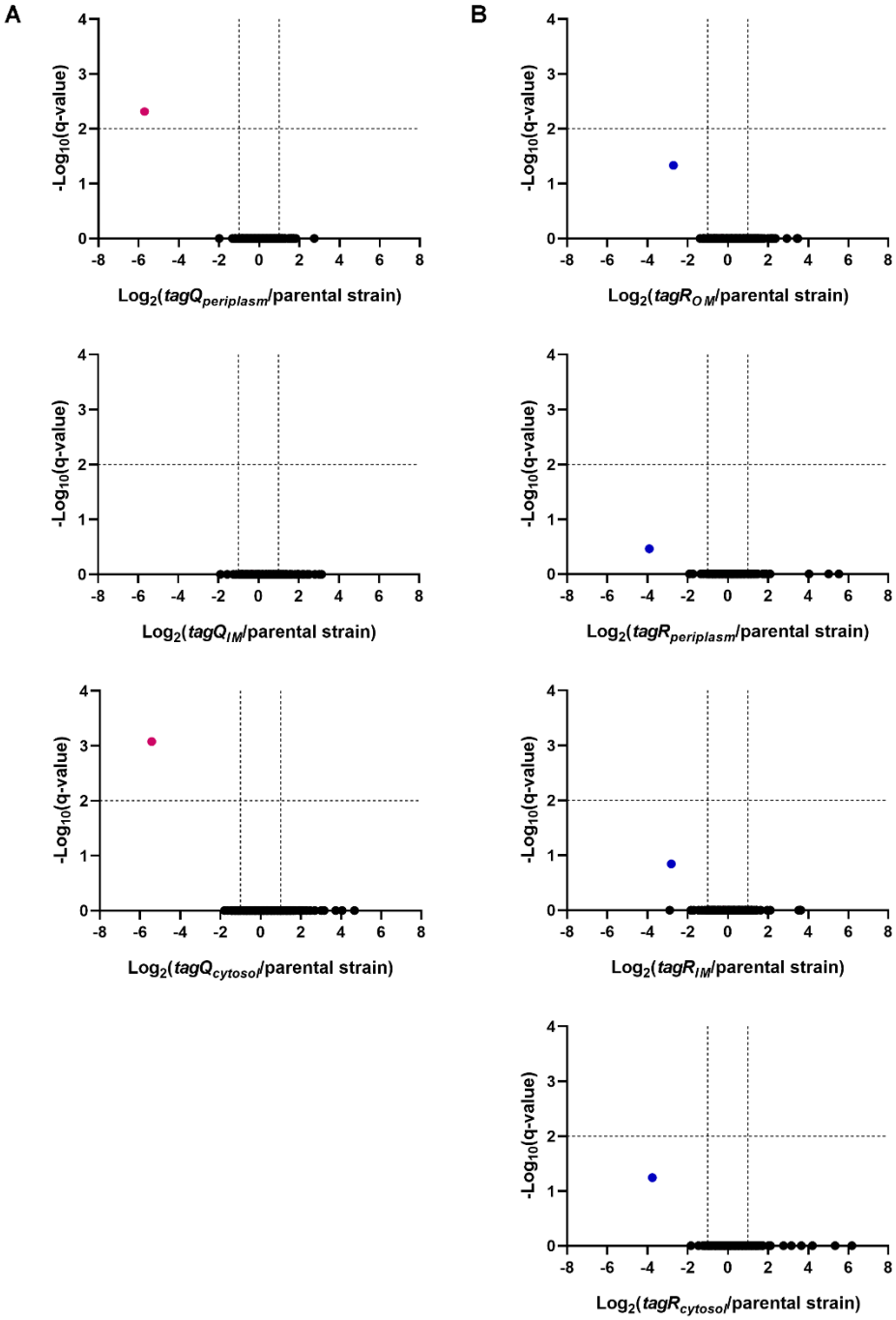

Figure 5: Relative protein abundancies in whole cell-samples of TagQ and TagR N-terminal signal sequence mutants. Protein abundancies were measured by LS-MS. For each identified protein, the fold change (x-axis) is plotted against -$\log_{10}$(*q*-value) as measure for significance (y-axis). The dotted lines on the x-axis represent 2-fold changes of the protein of the corresponding mutant compared to *P. aeruginosa* PAO1 Δ*retS clpV-sfGFP tssB-mCherry2*. The lines on the y-axis represent the false discovery rate of 1 % (*q*-values below 0.01). Value for TagQ is shown in magenta and for TagR in blue. Summary of three biological replicates. **A)** Relative protein abundancies for $tagQ_{periplasm}$, $tagQ_{IM}$ and $tagQ_{cytosol}$. **B)** Relative protein abundancies for $tagR_{OM}$, $tagR_{periplasm}$, $tagR_{IM}$ and $tagR_{cytosol}$.

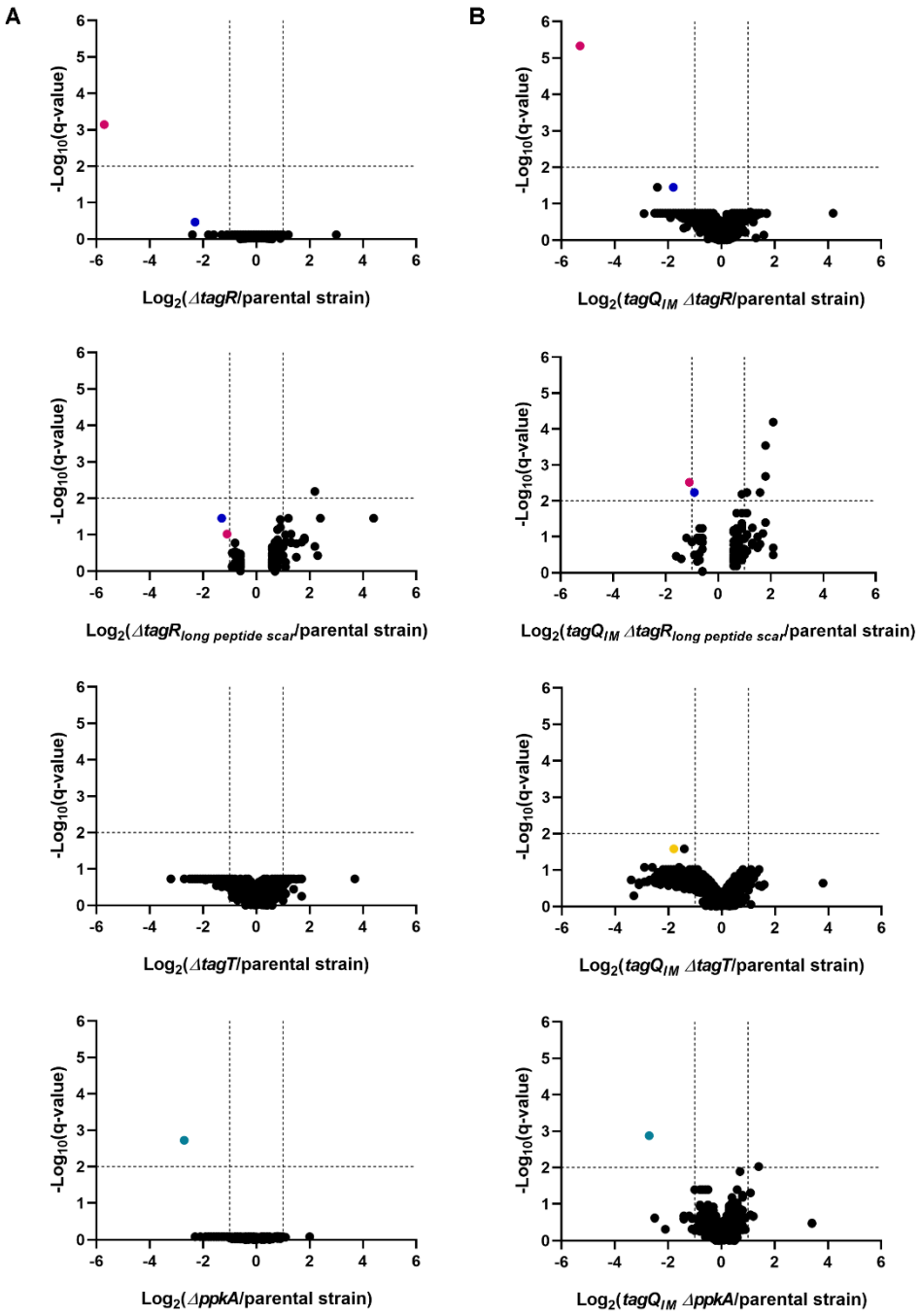

Figure 6: Relative protein abundancies in whole-cell samples of different gene deletions in parental strain and TagQ$_{IM}$ backgrounds. Protein abundancies were measured by LS-MS. For each identified protein, the fold change (x-axis) is plotted against -log$_{10}$ (*q*-value) as measure for significance (y-axis). The dotted lines on the x-axis represent 2-fold changes of the protein of the corresponding mutant compared to *P. aeruginosa* PAO1 Δ*retS clpV-sfGFP tssB-mCherry2*. The lines on the y-axis represent the false discovery rate of 1 % (*q*-values below 0.01). Values for TagQ, TagR, TagT and PpkA are shown in magenta, blue, yellow and turquoise, respectively. Summary of three biological replicates. **A)** Relative protein abundancies for Δ*tagR*, Δ*tagR*$_{long\ peptide\ scar}$, Δ*tagT* and Δ*ppkA*. **B)** Relative protein abundancies for *tagQ*$_{IM}$ Δ*tagR*, *tagQ*$_{IM}$ Δ*tagR*$_{long\ peptide\ scar}$, *tagQ*$_{IM}$ Δ*tagT* and *tagQ*$_{IM}$ Δ*ppkA*.

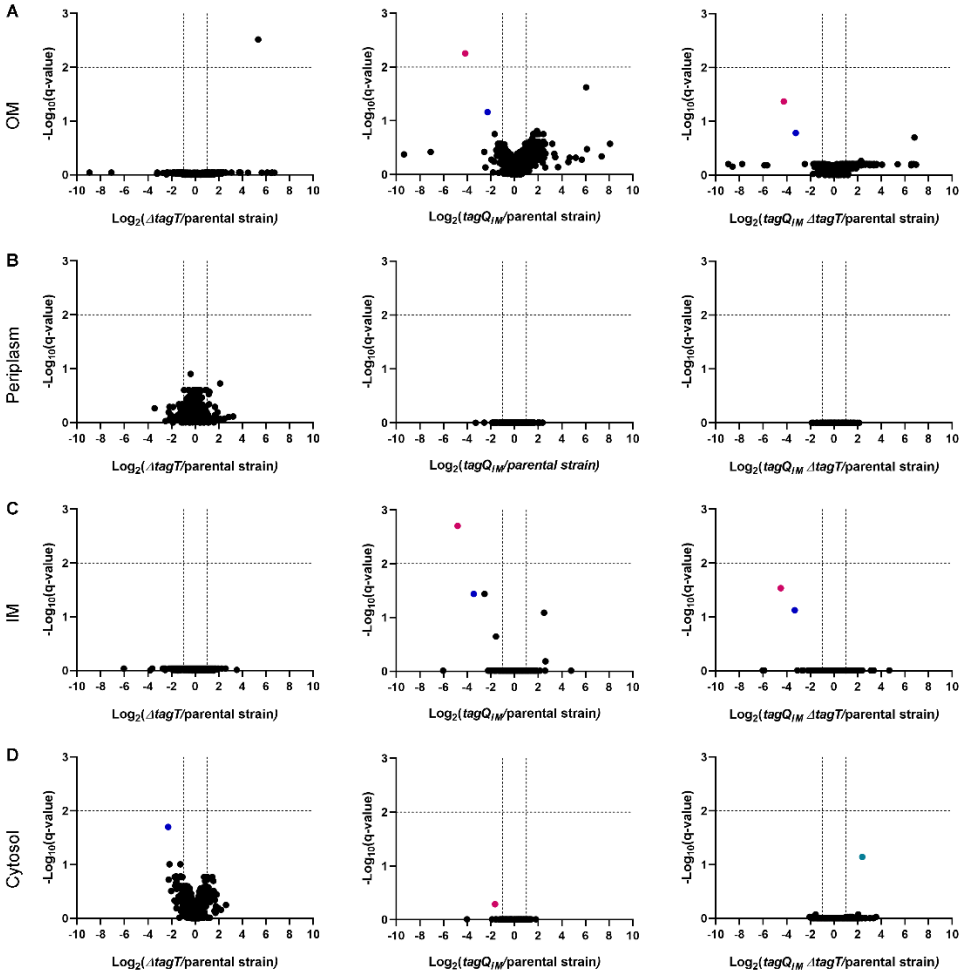

Figure 7: Relative protein abundancies in OM, periplasmic, IM and cytosolic fractions of parental strain and TagQ$_{IM}$ background. Protein abundancies were measured by LS-MS. For each identified protein, the fold change (x-axis) is plotted against -log$_{10}$ (*q*-value) as measure for significance (y-axis). The dotted lines on the x-axis represent 2-fold changes of the protein of corresponding mutant fraction compared to the fraction of *P. aeruginosa* PAO1 Δ*retS clpV-sfGFP tssB-mCherry2*. The lines on the y-axis represent the false discovery rate of 1 % (*q*-values below 0.01). Value for TagQ is shown in magenta and for TagR in blue. Summary of three biological replicates. **A)** Relative protein abundancies in OM fractions of Δ*tagT*, *tagQ$_{IM}$* and *tagQ$_{IM}$* Δ*tagT*. **B)** Relative protein abundancies in periplasmic fractions for Δ*tagT*, *tagQ$_{IM}$* and *tagQ$_{IM}$* Δ*tagT*. **C)** Relative protein abundancies in IM fractions of Δ*tagT*, *tagQ$_{IM}$* and *tagQ$_{IM}$* Δ*tagT*. **D)** Relative protein abundancies in the cytosolic fractions of Δ*tagT*, *tagQ$_{IM}$* and *tagQ$_{IM}$* Δ*tagT*.

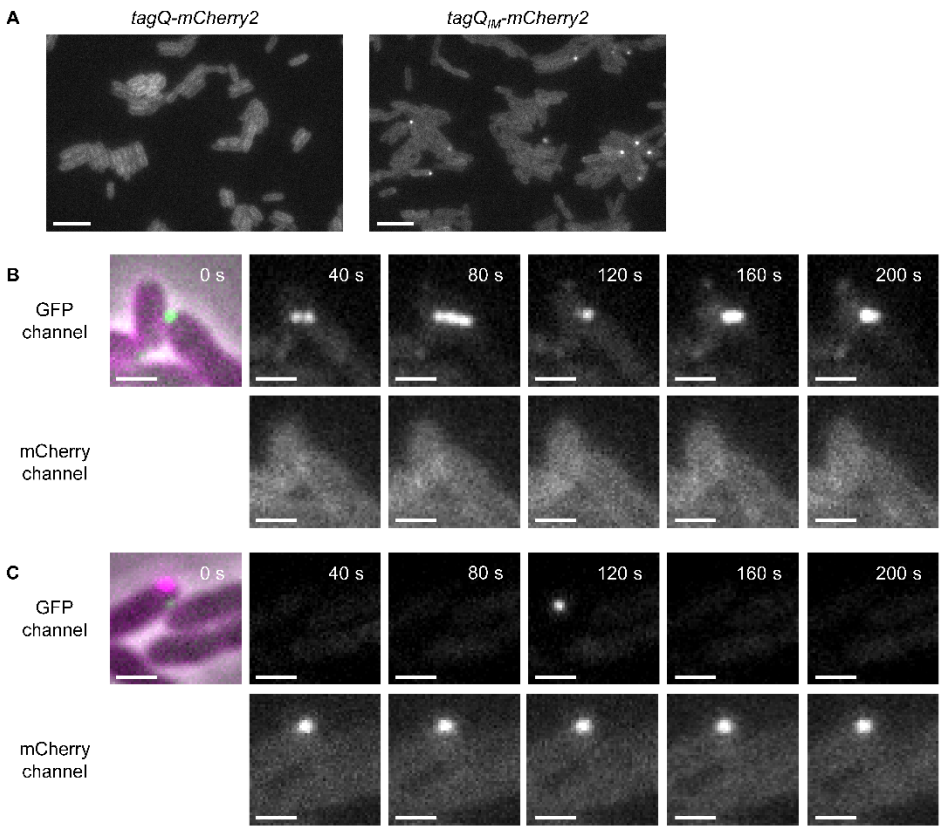

Figure 8: Localization of TagQ-mCherry2 and TagQ$_{IM}$-mCherry2. A) Membrane localization of TagQ-mCherry2 in *P. aeruginosa* PAO1 Δ*retS clpV-sfGFP tagQ-mCherry2* (right image) and formation of TagQ$_{IM}$-mCherry2 spots in *tagQ$_{IM}$-mCherry2* (left image). 13 x 9.8 µm fields of view are shown. Scale bar represents 5 µm. **B)** T6SS dueling event in *tagQ-mCherry2* background. **C)** T6SS assembly in *tagQ$_{IM}$-mCherry2* background. **C-D)** First image shows merge of phase contrast, GFP channel and mCherry channel, followed by GFP channel (upper panel) and mCherry channel (lower panel). of 3.3 x 3.3 µm fields of view are shown. Scale bar represents 1 µm.

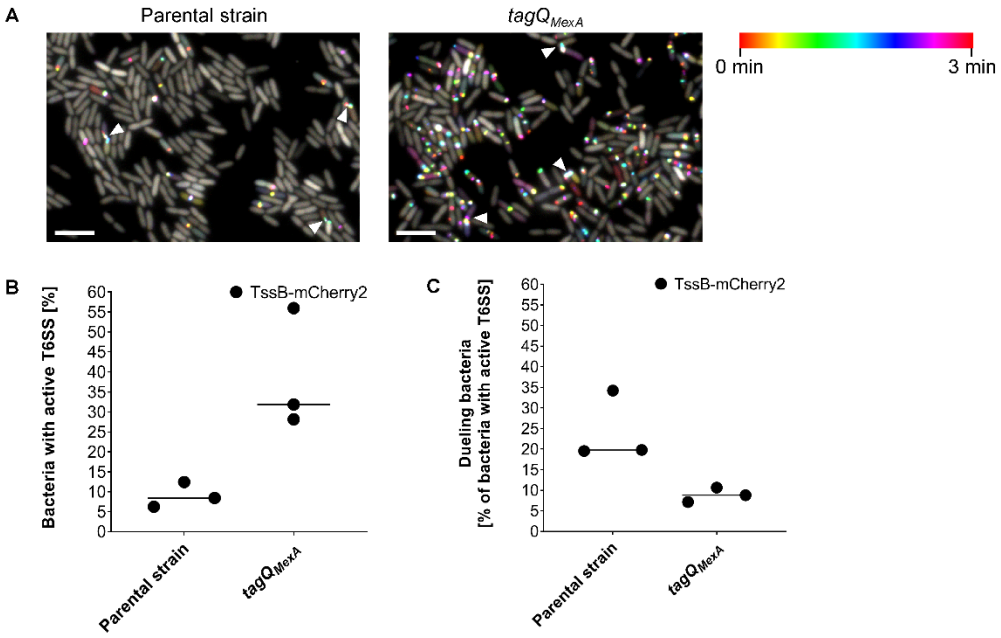

Figure 9: T6SS phenotyps of chromosomal TagQ MexA N-terminal signal sequence. A) Summary of T6SS activity of *P. aeruginosa* PAO1 Δ*retS clpV-sfGFP tssB-mCherry2* and $tagQ_{MexA}$ in the mCherry channel over 3 minutes with "Temporal-Color Code" function. Time color scale bar indicates at which time point the event appeared. Arrows highlight dueling events. 13 x 9.8 µm fields of view are shown. Scale bar represents 5 µm. **B)** Quantification of bacteria with T6SS assembly within 3 minutes of imaging for *P. aeruginosa* PAO1 Δ*retS clpV-sfGFP tssB-mCherry2* and $tagQ_{MexA}$. Quantification was carried out based on TssB-mCherry2. Three biological replicates with at least 1500 bacteria each were analyzed. Black line represents median. **B)** Quantification of dueling bacteria, which had active T6SS in **A)** during 3 minutes of imaging. Quantification was carried out based on TssB-mCherry2. Black line represents median.

Tables

Table 1: Strains used in this study, related to Material and methods

Organism	Genotype	Plasmid	Relevant features	Source
Pseudomonas aeruginosa PAO1	*tssB-mNeongreen*		C-terminal chromosomal fusion of *mNeongreen* to *tssB*	This study
	Δ*retS clpV-sfGFP*		Parental strain, C-terminal chromosomal fusion of *sfGFP* to *clpV*	Basler and Mekalanos, 2012
	Δ*retS clpV-sfGFP* Δ*tssB*		Deletion of *tssB*, T6SS-	Marek Basler
	Δ*retS clpV-sfGFP* Δ*tagQ*		Deletion of *tagQ*	Marek Basler
	Δ*retS clpV-sfGFP* Δ*tagQ*	pPSV35 *tagQ*	Inducible expression of *tagQ*	This study
	Δ*retS clpV-sfGFP* Δ*tagQ*	pPSV35 $tagQ_{periplasm}$	Inducible expression of $tagQ_{periplasm}$	This study
	Δ*retS clpV-sfGFP* Δ*tagQ*	pPSV35 $tagQ_{IM}$	Inducible expression of $tagQ_{IM}$	This study
	Δ*retS clpV-sfGFP* Δ*tagQ*	pPSV35 $tagQ_{cytosol}$	Inducible expression of $tagQ_{cytosol}$	This study
	Δ*retS clpV-sfGFP* Δ*tagR*		Deletion of *tagR*, polar effect on TagQ	Marek Basler
	Δ*retS clpV-sfGFP* Δ*tagR*	pPSV35 *tagR*	Inducible expression of *tagR*	This study
	Δ*retS clpV-sfGFP* Δ*tagR*	pPSV35 $tagR_{OM}$	Inducible expression of $tagR_{OM}$	This study
	Δ*retS clpV-sfGFP* Δ*tagR*	pPSV35 $tagR_{periplasm}$	Inducible expression of $tagR_{periplasm}$	This study
	Δ*retS clpV-sfGFP* Δ*tagR*	pPSV35 $tagR_{IM}$	Inducible expression of $tagR_{IM}$	This study
	Δ*retS clpV-sfGFP* Δ*tagR*	pPSV35 $tagR_{cytosol}$	Inducible expression of $tagR_{cytosol}$	This study
	Δ*retS clpV-sfGFP tssB-mCherry2*		Parental strain, C-terminal chromosomal fusion of *sfGFP* to *clpV* and C-terminal chromosomal fusion of *mCherry2* to *tssB*	This study
	Δ*retS clpV-sfGFP tssB-mCherry2* Δ*tagQ*		Deletion of *tagQ*	This study
	Δ*retS clpV-sfGFP tssB-mCherry2* Δ*tagQ* Δ*tagS*		Deletion of *tagQ* and *tagS*	This study
	Δ*retS clpV-sfGFP tssB-mCherry2* Δ*tagQ* Δ*tagT*		Deletion of *tagQ* and *tagT*	This study
	Δ*retS clpV-sfGFP tssB-mCherry2* Δ*tagQ* Δ*ppkA*		Deletion of *tagQ* and *ppkA*	This study

	Δ*retS clpV-sfGFP tssB-mCherry2* Δ*tagQ* Δ*pppA*		Deletion of *tagQ* and *pppA*	This study
	Δ*retS clpV-sfGFP tssB-mCherry2* Δ*tagQ*	pPSV35 *tagQ*	Inducible expression of *tagQ*	This study
	Δ*retS clpV-sfGFP tssB-mCherry2* Δ*tagQ*	pPSV35 $tagQ_{IM}$	Inducible expression of $tagQ_{IM}$	This study
	Δ*retS clpV-sfGFP tssB-mCherry2* $tagQ_{periplasm}$		Chromosomal $tagQ_{periplasm}$	This study
	Δ*retS clpV-sfGFP tssB-mCherry2* $tagQ_{periplasm}$ $tagR_{IM}$		Chromosomal $tagQ_{periplasm}$ and $tagR_{IM}$	This study
	Δ*retS clpV-sfGFP tssB-mCherry2* $tagQ_{IM}$		Chromosomal $tagQ_{IM}$	This study
	Δ*retS clpV-sfGFP tssB-mCherry2* $tagQ_{IM}$ Δ*tagR*		Chromosomal $tagQ_{IM}$, deletion of *tagR*	This study
	Δ*retS clpV-sfGFP tssB-mCherry2* $tagQ_{IM}$ Δ*tagS*		Chromosomal $tagQ_{IM}$, deletion of *tagS*	This study
	Δ*retS clpV-sfGFP tssB-mCherry2* $tagQ_{IM}$ Δ*tagT*		Chromosomal $tagQ_{IM}$, deletion of *tagT*	This study
	Δ*retS clpV-sfGFP tssB-mCherry2* $tagQ_{IM}$ Δ*ppkA*		Chromosomal $tagQ_{IM}$, deletion of *ppkA*	This study
	Δ*retS clpV-sfGFP tssB-mCherry2* $tagQ_{IM}$ Δ*pppA*		Chromosomal $tagQ_{IM}$, deletion of *pppA*	This study
	Δ*retS clpV-sfGFP tssB-mCherry2* $tagQ_{cytosol}$		Chromosomal $tagQ_{cytosol}$	This study
	Δ*retS clpV-sfGFP tssB-mCherry2* $tagQ_{MexA}$		Signal sequence of *mexA*	This study
	Δ*retS clpV-sfGFP tssB-mCherry2* Δ*tagR*		Deletion of *tagR*	This study
	Δ*retS clpV-sfGFP tssB-mCherry2* Δ$tagR_{long\ peptide\ scar}$		Deletion of *tagR* with no polar effect on TagQ	This study
	Δ*retS clpV-sfGFP tssB-mCherry2* Δ*tagR*	pPSV35 *tagQ*	Inducible expression of *tagQ*	This study
	Δ*retS clpV-sfGFP tssB-mCherry2* Δ*tagR*	pPSV35 $tagQ_{IM}$	Inducible expression of $tagQ_{IM}$	This study
	Δ*retS clpV-sfGFP tssB-mCherry2* $tagR_{OM}$		Chromosomal $tagR_{OM}$	This study
	Δ*retS clpV-sfGFP tssB-mCherry2* $tagR_{periplasm}$		Chromosomal $tagR_{periplasm}$	This study
	Δ*retS clpV-sfGFP tssB-mCherry2* $tagR_{IM}$		Chromosomal $tagR_{IM}$	This study
	Δ*retS clpV-sfGFP tssB-mCherry2* $tagR_{cytosol}$		Chromosomal $tagR_{cytosol}$	This study
Acinetobacter baylyi ADP1	*rpsL-K89R PAAR1-2::specR*		T6SS+	Marek Basler
	rpsL-K89R Δ2'644'572-2'653'574::kanR		T6SS-	Marek Basler

Table 2: Plasmids and primers used to generate mutants, related to Material and methods. Amino acids in bold represent N-terminal cleavage site.

Plasmid Name	Peptide scar, linker or N-terminal signal [Amino acids]	Primers	Sequence 5'-3' [base pairs]
pPSV35 *tagQ*	MSQPSENRLITSARY ALCLLTASGVLLS**GC** ASSG	PA0070_OM_EcoR1_Fw	GAATTCAGGAGGAAACTAGTATGAGCCAACCCAGCGAAAAC
		PA0070_HindIII_Rv	GTGCCAAGCTTTCAGGCCTTGGCGCAGCTC
		pPSV35_Seq_Fw	CGTGCTTTACACTTTATGCTTCC
		pPSV35_Seq_Rv	GGCCTCTTCGCTATTACGC
pPSV35 $tagQ_{periplasm}$	MKLLAGSFAALFLSL SAQA**AD**ASSG	PA0070_Periplasm_Spe1_Fw	ACTAGTATGAAACTGCTCGCCGGCAGCTTCGCCGCTCTCTTCCTGAGCCTTTCGGCCCAGGCGGCGGACG CCAGCAGCGGCGTC
		PA0070_HindIII_Rv	GTGCCAAGCTTTCAGGCCTTGGCGCAGCTC
		pPSV35_Seq_Fw	CGTGCTTTACACTTTATGCTTCC
		pPSV35_Seq_Rv	GGCCTCTTCGCTATTACGC
pPSV35 $tagQ_{IM}$	MSQPSENRLITSARY ALCLLTASGVLLS**GC** DSSG	PA0070_IM_Spe1_Fw	ACTAGTATGAGCCAACCCAGCGAAAACCGTTTGATCACCTCGGCGCGCTACGCGCTCTGCCTGTTGACCG CCAGCGGCGTGCTGCTCAGCGGCTGCGATAGCAGCGGCGTCGG
		PA0070_HindIII_Rv	GTGCCAAGCTTTCAGGCCTTGGCGCAGCTC
		pPSV35_Seq_Fw	CGTGCTTTACACTTTATGCTTCC
		pPSV35_Seq_Rv	GGCCTCTTCGCTATTACGC
pPSV35 $tagQ_{cytosol}$	MASSG	PA0070_Cytoplasm_Spe1_Fw	ACTAGTATGGCCAGCAGCGGCGTC
		PA0070_HindIII_Rv	GTGCCAAGCTTTCAGGCCTTGGCGCAGCTC
		pPSV35_Seq_Fw	CGTGCTTTACACTTTATGCTTCC
		pPSV35_Seq_Rv	GGCCTCTTCGCTATTACGC
pPSV35 *tagR*	MFEKAILPLALGACL AFAAPAW**AE**GDS	PA0071_OM_EcoR1_Fw	GAATTCAGGAGGAAACTAGTATGTTTGAGAAAGCCATTCTTCCGC
		PA0071_HindIII_Rv	GTGCCAAGCTTTTCAACGCCCGCTGGACGC
		pPSV35_Seq_Fw	CGTGCTTTACACTTTATGCTTCC
		pPSV35_Seq_Rv	GGCCTCTTCGCTATTACGC
pPSV35 $tagR_{OM}$	MSQPSENRLITSARY ALCLLTASGVLLS**GC** ADS	PA0071_OM forced_Spe1_Fw	ACTAGTATGAGCCAACCCAGCGAAAACCGTTTGATCACCTCGGCGCGCTACGCGCTCTGCCTGTTGACCG CCAGCGGCGTGCTGCTCAGCGGCTGCGCCGACTCGCCGGACAATCCCAAG
		PA0071_HindIII_Rv	GTGCCAAGCTTTTCAACGCCCGCTGGACGC
		pPSV35_Seq_Fw	CGTGCTTTACACTTTATGCTTCC
		pPSV35_Seq_Rv	GGCCTCTTCGCTATTACGC
pPSV35 $tagR_{periplasm}$	MKLLAGSFAALFLSL SAQA**AD**GDS	PA0071_Periplasm_Spe1_Fw	ACTAGTATGAAACTGCTCGCCGGCAGCTTCGCCGCTCTCTTCCTGAGCCTTTCGGCCCAGGCGGCGGACG GCGACTCGCCGGACAA
		PA0071_HindIII_Rv	GTGCCAAGCTTTTCAACGCCCGCTGGACGC
		pPSV35_Seq_Fw	CGTGCTTTACACTTTATGCTTCC
		pPSV35_Seq_Rv	GGCCTCTTCGCTATTACGC
pPSV35 $tagR_{IM}$	MSQPSENRLITSARY ALCLLTASGVLLS**GC** GDS	PA0071_IM_Spe1_Fw	ACTAGTATGAGCCAACCCAGCGAAAACCGTTTGATCACCTCGGCGCGCTACGCGCTCTGCCTGTTGACCG CCAGCGGCGTGCTGCTCAGCGGCTGCGATGGCGACTCGCCGGACAA
		PA0071_HindIII_Rv	GTGCCAAGCTTTTCAACGCCCGCTGGACGC

		pPSV35_Seq_Fw	CGTGCTTTACACTTTATGCTTCC
		pPSV35_Seq_Rv	GGCCTCTTCGCTATTACGC
pPSV35 *tagR*$_{cytosol}$	MGDS	PA0071_Cytoplasm_Spe1_Fw	ACTAGTATGGGCGACTCGCCGGACAA
		PA0071_HindIII_Rv	GTGCCAAGCTTTTCAACGCCCGCTGGACGC
		pPSV35_Seq_Fw	CGTGCTTTACACTTTATGCTTCC
		pPSV35_Seq_Rv	GGCCTCTTCGCTATTACGC
pEXG2 *tssB-mCherry2*	AAAGGG	PA0083_EcoRI_For	AAAAGAATTCATGGGAAGCACTACCAGCAG
		Ct-Link_rv	CTCACTCCTCCTCCTGCG
		mCherry2_link_For	GCGGCCGCAGGAGGAGGAGTGAGCAAGGGCGAGGAGGATA
		Up_rv_mCh2 link_PA0083_Rev	GCGGCTCGTCCTTGTACAGCTCGTCCATGCC
		Int_ PA0083_mCH2_do_fw	CTGTACAAGGACGAGCCGCAGGCGTAA
		PA0083_Del_4_Rev	AAGCTAAAGCTTGGGGTGGTGAAGATCTTGGT
		PA0084_Det_For	CCGAAATCGTGAGGAATCTC
		PA0083_Det_Rev	CATGGTCAGGCCGATGTAG
pEXG2 Δ*tagQ*	MSQPA*	PA0070_Del_1_For	TCAGTATCTAGAAACGAGACCACCGGTTTCC
		PA0070_Del_2_Rev	CCGATCAGGCGGGTTGGCTCATTGCATCTC
		PA0070_Del_3_For	GAGCCAACCCGCCTGATCGGCCTCGTTACC
		PA0070_Del_4_Rev	AAGCTAAAGCTTGATGATCAGCCTGACCACCC
		PA0070_Det_For	ACTCTATTCACCGGGATGCG
		PA0070_Det_Rev	GATCCTTCGCGACCTCGAC
pEXG2 *tagQ*$_{periplasm}$	MKLLAGSFAALFLSL SAQA**AD**ASSG	PA0070_Del_4_Rev	AAGCTAAAGCTTGATGATCAGCCTGACCACCC
		PA0070_Mis_1.REV	GGCCTGATCGGCCTCGTTACCG
		PA0070_Mis_2.FOR	CGGTAACGAGGCCGATCAGGCCTTGGCGCA
		PA0070_Peri_3.FOR	CAGTTTCATTGCATCTCACTCCTG
		PA0070_Del_1_For	TCAGTATCTAGAAACGAGACCACCGGTTTCC
		PA0070_Det_For	ACTCTATTCACCGGGATGCG
		PA0070_Det_Rev	GATCCTTCGCGACCTCGAC
pEXG2 *tagQ*$_{IM}$	MSQPSENRLITSARY ALCLLTASGVLLS**GC** DSSG	PA0070_Del_4_Rev	AAGCTAAAGCTTGATGATCAGCCTGACCACCC
		PA0070_Mis_1.REV	GGCCTGATCGGCCTCGTTACCG
		PA0070_Mis_2.FOR	CGGTAACGAGGCCGATCAGGCCTTGGCGCA
		PA0070_Mis_2.REV	CAGGAGTGAGATGCAATGAGCCAACCCAGC
		PA0070_Mis_3.FOR	TGGCTCATTGCATCTCACTCCTG
		PA0070_Det_For	ACTCTATTCACCGGGATGCG
		PA0070_Det_Rev	GATCCTTCGCGACCTCGAC
pEXG2 *tagQ*$_{cytosol}$	MGDS	PA0070_Del_4_Rev	AAGCTAAAGCTTGATGATCAGCCTGACCACCC
		PA0070_Mis_1.REV	GGCCTGATCGGCCTCGTTACCG
		PA0070_Mis_2.FOR	CGGTAACGAGGCCGATCAGGCCTTGGCGCA
		PA0070_Cyto_2.REV	CAGGAGTGAGATGCAATGGCCAGCAGC

		PA0070_Cyto_3.FOR	CTGGCCATTGCATCTCACTCCTG
		PA0070_Del_1_For	TCAGTATCTAGAAACGAGACCACCGGTTTCC
		PA0070_Det_For	ACTCTATTCACCGGGATGCG
		PA0070_Det_Rev	GATCCTTCGCGACCTCGAC
pEXG2 *tagQ*$_{MexA}$	MQRTPAMRVLVPAL LVAISALS**GC**GKSG	PA0070_Del_4_Rev	AAGCTAAAGCTTGATGATCAGCCTGACCACCC
		PA0070_Mis_1.REV	GGCCTGATCGGCCTCGTTACCG
		PA0070_Mis_2.FOR	GGCCGATCAGGCCTTGGCGCA
		PA0070-MexA_For	TGTACTGGTTCCGGCCCTGCTGGTCGCGATTTCGGCCCTTTCCGGGTGCGGAAAAAGCGGCGTCGGCTCG GTCGC
		PA0070-MexA_Rev	GGCCGGAACCAGTACACGCATGGCTGGCGTTCGTTGCATTGCATCTCACTCCTGGTTTGA
		PA0070_Del_1_For	TCAGTATCTAGAAACGAGACCACCGGTTTCC
		PA0070_Det_For	ACTCTATTCACCGGGATGCG
		PA0070_Det_Rev	GATCCTTCGCGACCTCGAC
pEXG2 Δ*tagR*	MFEKAILPLKELLASS GR*	PA0071_Del_1_For	TCAGTATCTAGAGAAGCCGCCGAGGACTATC
		PA0071_Del_2_Rev	ATTCCTTCAAGAGCGGAAGAATGGCTTTC
		PA0071_Del_3_For	TCTTCCGCTCTTGAAGGAATTGCTCGCGTC
		PA0071_Del_4_Rev	AAGCTAAAGCTTGCCTGGGTGTAGTTGCTGAT
		PA0071_Det_For	GGATGGCCAGGCACAGAG
		PA0071_Det_Rev	CTTGCTGCCGCCTTTCGTAG
pEXG2 Δ*tagR*$_{long\ peptide\ scar}$		PA0071_HindIII_Rv	GTGCCAAGCTTTTCAACGCCCGCTGGACGC
		dPA0071_long_1.REV	CCGCTCGCCGCCGCCACCCGCGACC
		dPA0071_long_2.FOR	GTGGCGGCGGCGAGCGGAAGAATGG
		PA0071_Del_1_For	TCAGTATCTAGAGAAGCCGCCGAGGACTATC
		PA0071_Det_For	GGATGGCCAGGCACAGAG
		PA0071_Det_Rev	CTTGCTGCCGCCTTTCGTAG
pEXG2 *tagR*$_{OM}$	MFEPSENRLITSARYA LCLLTASGVLLS**GC**A DS	PA0071_Del_4_Rev	AAGCTAAAGCTTGCCTGGGTGTAGTTGCTGAT
		PA0071_Mis_1.REV	GGCGTTGAAGGAGTTCCGTCCGG
		PA0071_Mis_2.FOR	CGGACGGAACTCCTTCAACGCCCGCT
		PA0071_IM2_new.REV	CGATGTTTGAGCCCAGCGAAAACCGTTTGATCACCT
		PA0071_IM3_new.FOR	TTTTCGCTGGGCTCAAACATCGCGTAATCCCTCTGC
		PA0071_Del_1_For	TCAGTATCTAGAGAAGCCGCCGAGGACTATC
		PA0071_Det_For	GGATGGCCAGGCACAGAG
		PA0071_Det_Rev	GGATGGCCAGGCACAGAG
pEXG2 *tagR*$_{periplasm}$	MFELAGSFAALFLSL SAQA**AD**GDS	PA0071_Del_4_Rev	AAGCTAAAGCTTGCCTGGGTGTAGTTGCTGAT
		PA0071_Mis_1.REV	GGCGTTGAAGGAGTTCCGTCCGG
		PA0071_Mis_2.FOR	GAACTCCTTCAACGCCCGCT
		PA0071_Peri2_new.REV	CGATGTTTGAGCTCGCCGGCAGCTTCGCC
		PA0071_Peri3_new.FOR	GCCGGCGAGCTCAAACATCGCGTAATCCC
		PA0071_Del_1_For	TCAGTATCTAGAGAAGCCGCCGAGGACTATC
		PA0071_Det_For	GGATGGCCAGGCACAGAG

		PA0071_Det_Rev	GGATGGCCAGGCACAGAG
pEXG2 *tagR*$_{IM}$	MFEPSENRLITSARYALCLLTASGVLLS**GC**GDS	PA0071_Del_4_Rev	AAGCTAAAGCTTGCCTGGGTGTAGTTGCTGAT
		PA0071_Mis_1.REV	GGCGTTGAAGGAGTTCCGTCCGG
		PA0071_Mis_2.FOR	GAACTCCTTCAACGCCCGCT
		PA0071_IM2_new.REV	CGATGTTTGAGCCCAGCGAAAACCGTTTGATCACCT
		PA0071_IM3_new.FOR	TTTTCGCTGGGCTCAAACATCGCGTAATCCCTCTGC
		PA0071_Del_1_For	TCAGTATCTAGAGAAGCCGCCGAGGACTATC
		PA0071_Det_For	GGATGGCCAGGCACAGAG
		PA0071_Det_Rev	GGATGGCCAGGCACAGAG
pEXG2 *tagR*$_{cytosol}$	MFEGDS	PA0071_Del_4_Rev	AAGCTAAAGCTTGCCTGGGTGTAGTTGCTGAT
		PA0071_Mis_1.REV	GGCGTTGAAGGAGTTCCGTCCGG
		PA0071_Mis_2.FOR	GAACTCCTTCAACGCCCGCT
		PA0071_Cyto2_new.REV	GATGTTTGAGGGCGACTCGCCGGACAATC
		PA0071_Cyto3_new.FOR	GCGAGTCGCCCTCAAACATCGCGTAATCCC
		PA0071_Del_1_For	TCAGTATCTAGAGAAGCCGCCGAGGACTATC
		PA0071_Det_For	GGATGGCCAGGCACAGAG
		PA0071_Det_Rev	GGATGGCCAGGCACAGAG
pEXG2 Δ*tagS*	MRAGLLLSLAWADYRAEGLRDV*	PA0072_Del_1_For	TCAGTATCTAGAGAATTCCTCGCCGGGGAAC
		PA0072_Del_2_Rev	ATCCCTCTGCGCGGTAGTCGGCCCAGGC
		PA0072_Del_3_For	CGACTACCGCGCAGAGGGATTACGCGATGT
		PA0072_Del_4_Rev	AAGCTAAAGCTTCAGTTCCGGGTGGTTCTTCA
		PA0072_Det_For	CTGTCGACGCTGCCATGATC
		PA0072_Det_Rev	CGAACTCCCACTCGACCTC
pEXG2 Δ*tagT*	(Basler and Mekalanos, 2012)	PA0073_Seq_For	TCTGGTTGTCGAACAGGTGG
		PA0073_Seq_Rev	TCTCCAGCCACTCGTTCAAC
pEXG2 Δ*ppkA*	(Basler et al., 2013)	PA0074_Seq_For	GGGAATCATCTCGACGCTCA
		PA0074_Seq_Rev	CGCATCGAACAATCGCTGAT
pEXG2 Δ*pppA*	(Basler et al., 2013)	PA0075_Seq_For	GACGGATCTGGGTGGCTTC
		PA0075_Seq_Rev	CGCCTTCAACCCCTTCAAGA

3.2.

The evolution of tit-for-tat in bacterial warfare

William P. J. Smith[1], Maj Brodmann[2], Daniel Unterweger[3], Yohan Davit[4], Laurie E. Comstock[5], Marek Basler[2], and Kevin R. Foster[1] *

1. Department of Zoology, University of Oxford, OX1 3PS, UNITED KINGDOM

2. Biozentrum, University of Basel, Klingelbergstrasse 50/70, CH-4056 Basel, SWITZERLAND

3. Christian Albrechts Universität zu Kiel, Christian-Albrechts-Platz 4, 24118 Kiel, GERMANY

4. Institut de Mécanique des Fluides de Toulouse (IMFT), Université de Toulouse, 31400 Toulouse, FRANCE

5. Brigham and Women's Hospital, Boston, MA 02115l, UNITED STATES

* Corresponding author. Email: kevin.foster@zoo.ox.ac.uk

Manuscript in preparation

Statement of contribution:

I performed and analyzed the imaging experiments as well as prepared figure 4 and S5. I reviewed and edited the manuscript.

The evolution of tit-for-tat in bacterial warfare

William P. J. Smith[1], Maj Brodmann[2], Daniel Unterweger[3], Yohan Davit[4], Laurie E. Comstock[5], Marek Basler[2], and Kevin R. Foster[1] *

1. Department of Zoology, University of Oxford, OX1 3PS, UNITED KINGDOM

2. Biozentrum, University of Basel, Klingelbergstrasse 50/70, CH-4056 Basel, SWITZERLAND

3. Christian Albrechts Universität zu Kiel, Christian-Albrechts-Platz 4, 24118 Kiel, GERMANY

4. Institut de Mécanique des Fluides de Toulouse (IMFT), Université de Toulouse, 31400 Toulouse, FRANCE

5. Brigham and Women's Hospital, Boston, MA 02115l, UNITED STATES

* Corresponding author. Email: kevin.foster@zoo.ox.ac.uk

Abstract

Many bacteria inject toxins into competitors using the Type VI Secretion System (T6SS), which resembles a poison-tipped molecular speargun. While many species simply fire T6SS needles randomly in space, the opportunistic pathogen *Pseudomonas aeruginosa* engages in tit-for-tat, shooting in retaliation to incoming T6SS attacks. Although the regulatory components for this response are identified, we do not understand when or why tit-for-tat will evolve. Here, we combine computational modelling and evolutionary game theory to study the competitive value of different patterns of T6SS firing. We were surprised to find that our models predict that the tit-for-tat strategy almost never evolves. This occurs for two reasons. Most simply, tit-for-tat loses against unarmed cells because it fails to fire. Moreover, tit-for-tat cells are also outcompeted by randomly firing strains who always hit them first. However, we then show that if a tit-for-tat strain retaliates strongly with many hits, they always win against a random firer. This occurs because tit-for-tat cells have an information advantage: they 'know' where and when to hit. We test our key prediction of strong retaliation by comparing *P. aeruginosa* (tit-for-tat) with *Vibrio cholerae* (random). While *V. cholerae* only fires once from each position, *P. aeruginosa* fires many times. Our work reveals that *P. aeruginosa* does *not* engage in strict tit-for-tat; rather, it gives more than it gets. More generally, we show how

the outcome of bacterial competition rests not only upon the weapons that cells carry, but exactly how they use them.

Significance Statement

Tit-for-tat, or 'an eye-for-an-eye', is a well-known principle from humans and other animals. Amazingly, some bacteria have also evolved a tit-for-tat behavior; they stab other cells with poisoned molecular needles (the type VI secretion system) – but only if stabbed. However, we do not understand how this remarkable behavior evolved. We have developed a realistic model of the type VI secretion system to study its evolution. We show that strict tit-for-tat is a poor evolutionary strategy for bacteria, because it lacks the first-strike advantage of random firing. By contrast, our model predicts that aggressive cells that hit back many times can always win, which led us to discover that this is how *P. aeruginosa* bacteria actually retaliate. In the brutal world of bacteria, therefore, the principle appears to be '*eyes*-for-an-eye'.

Introduction

The Type VI Secretory System (T6SS) is a contact-dependent nanoweapon, found in numerous proteobacterial and Bacteroidetes species (*1–4*) and used to inject effector proteins into neighboring cells (*5–7*). Structurally and functionally homologous to a phage's tail (*8*) the T6SS consists of a membrane-bound baseplate complex, an effector-tipped needle, and a surrounding sheath whose contraction drives the needle through the membranes of target cells (*9*, *10*). Used by many notorious plant and animal pathogens, the T6SS is a potent anti-competitor weapon: T6SS activity can determine whether a strain can invade, or defend, its niche in both environmental and host-associated microbial communities (*11–15*).

There is remarkable variation in the regulation and use of T6 weaponry across species. Bacteria activate and deploy the T6SS in a variety of environmental contexts (*16*, *17*) and against both prokaryotic and eukaryotic targets (*18*, *19*). The manner of firing also varies: whereas placement of T6SS assembly appears to be random in

some species, such as *Vibrio cholerae*, *Serratia marcescens* and *Acinetobacter baylyi* (*20–22*) other bacteria are known to fire from specific locations on their cell membranes. The most striking example of this spatiotemporal control is the retaliatory firing strategy observed in *Pseudomonas aeruginosa*, whose T6 apparatus (encoded at the HSI-I locus) is activated only in cells that are themselves attacked by T6SS needles (*23*, *24*). While the molecular regulation of the T6SS has received further attention (*25*), however, its evolution has not – leaving open the question of why the different firing strategies have evolved.

The evolution of reciprocation—tit-for-tat strategies—has a long history of study in evolutionary biology (*26–29*). However, the focus has been on the evolution of reciprocal cooperation rather than competition. Understanding the evolution of T6SS regulation then is important both for understanding bacterial warfare, and as a distinct case in evolutionary biology. On this basis, we developed an agent-based modelling framework to simulate competition between different T6SS strategists. By combining modelling with game theory, we have been able explore the evolution of T6SS regulation, including tit-for-tat firing, across a wide range of conditions. This reveals that tit-for-tat has major limitations as a strategy for T6SS warfare. It fails to fire against unarmed strains and, in addition, always fires second against aggressive strains, such that it rarely wins in direct competitions. However, we show that a strong retaliator, which fires multiple times in response to an attack, is a powerful competitor against random T6SS attackers. This led us to reanalyze the firing patterns of *P. aeruginosa*, which employs retaliatory firing, and to discover that it actually fires many times in response to an incoming attack.

Results

Agent-based modelling of different T6SS firing strategies

To study the interactions and evolution of different T6SS firing strategies, we extended an existing agent-based model of T6SS competition (*30–32*). Briefly, our model represents rod-shaped bacteria as sessile, elongating cylinders with hemispherical caps, which can intoxicate neighboring cells by firing T6SS needles. Importantly, different modes of T6SS firing (Table S1) can be represented and compared using this system: cells can be programmed not to fire (T6SS- 'Unarmed' strain), or to fire constantly and in random directions (T6SS+ 'Random' strain), or to fire in more elaborate patterns (Table S1). We assume each strategist is immune only to its own toxins, and that both carriage and expression of T6SS genes are costly, such that the specific growth rate of a T6SS+ strain is reduced in proportion to its firing rate. Further details are provided in the Supporting Information (Figure S1), and the model's variables and parameters are summarized in Tables S2 and S3.

Random T6SS firing is effective against unarmed strains

First, we used our agent-based model to study competition between Random T6SS attackers (R) and susceptible Unarmed cells (U). We simulated community growth within 2-D 'patch' environments, beginning with a randomly-scattered, 1:1 mixture of R and U cells. Each patch simulation begins with a finite, uniform resource quota that is consumed as cells grow, and simulations end once a patch becomes depleted of resources (Figure S1A). Would-be weapon users therefore face a trade-off: attacking one's competitors prevents them from using up a patch's resources, but at the costs of both reduced reproductive rate and efficiency.

Figure 1A shows two patch simulations between R and U strategists, carried out for different starting cell densities. In the left example (at low cell density), T6SS-mediated killing marginally increases the final frequency of R strategists; to the right (high cell density), this competitive advantage is greatly enhanced. Strong density dependence is consistent with empirical studies of T6SS competition – higher cell density results in increased (and earlier) contact between R and U cells, increasing

overall killing (*33*). We also observed that T6SS activity resulted in increased spatial segregation (*34*) between competing strains (Figure 1A), compared with T6SS-controls (Figure S1A).

To further explore the competitive value of Random T6SS firing, we compared R vs. U competition outcomes for a wide range of input parameters: varying initial cell density, T6SS firing rate, weapon cost, lysis rate and toxin potency. These analyses confirmed that random T6SS firing can indeed offer a competitive advantage (evidenced by increased R frequency after competition) under a broad set of conditions. As well as being favored by high cell density (Figure 1B, S2), natural selection for Random T6SS attackers is increased for low weapon costs (Figure S1C), and high toxin potency (Figure S1D). However, using lytic T6SS toxins is crucial for efficient killing (Figure S1D), as highlighted in a recent study (*32*).

Firing the T6SS at random can help a bacterial strain to increase its frequency in the short term. But when are Random T6SS attackers expected to invade an Unarmed population on longer timescales? To answer this question, we embedded our model in a game-theoretic framework called adaptive dynamics (*35*). This approach considers the fate of an initially rare, novel strategist placed in a metapopulation (large set of patches) dominated by another, resident strategist. If the relative fitness of the rare strategist is greater than that of the resident, its frequency in the metapopulation will increase, until it eventually replaces the resident altogether. Figure 1C shows the fate of an invading Random T6SS attacker as a function of its attack rate, $k_{fire,R}$, for two different competition scenarios (see Methods). For local competition, Random attackers compete only within niches with the resident Unarmed strain. For global competition, they must also compete with Unarmed cells in neighboring niches where Random attackers are absent. In both scenarios, we find that R can successfully invade U for all non-zero firing rates, assuming a high initial cell density (Figure 1C, 200:200 cells). For lower cell densities, the range of viable $k_{fire,R}$ values narrows, and is generally smaller for global competition than for local competition (Figure S3).

Random T6SS firing improves fitness against another random attacker

Our models predict that Random T6SS attackers will readily evolve in a population of Unarmed cells, under a range of conditions. As Random attackers become more abundant, they will begin to encounter one another, and so we must also consider the outcomes of battles between different R-type strategists. When can one Random attacker invade another? Here as before, we applied adaptive dynamics to study competition between pairs of R-type strategists, R1 and R2, each having its own attack rate $k_{fire,R1}$, $k_{fire,R2}$, and each being susceptible to the other's toxins[1]. Figure 1D shows a 'pairwise invasion plot' (*35*), indicating which of R1, R2 invades the other as a function of their respective attack rates, for local (within-patch) competition. We find that either strain can invade the other by firing faster than it, but only up to a point. Beyond the yellow diagonal line, having a higher attack rate than one's competitor makes one vulnerable to invasion, since the increased costs of the higher attack rate outweigh any additional benefits conferred. Figure 1E shows a similar pairwise invasion plot, this time computed for the case of global competition.

What firing rate $k_{fire,R}$ is predicted to evolve during competition between Random T6SS attackers? We can compute the Evolutionary Stable State (ESS) value of $k_{fire,R}$, denoted $k_{fire,R}^{ESS,local}$, as follows (Figure 1D): suppose we begin with a resident strain R1, which possesses the T6SS but does not use it ($k_{fire,R1} = 0$). Suppose a mutant strain R2 appears in this population with $k_{fire,R2} = \delta$, where $\delta > 0$ represents some small increment in firing rate. Since $k_{fire,R2} > k_{fire,R1}$, R2 can invade R1, and $k_{fire,R1} = \delta$ becomes the resident strategy. The same outcome occurs with $k_{fire,R2} = 2\delta$, 3δ … such that successive invasions by incrementally more aggressive mutants increase the firing rate in the resident population (Figure 1D, black arrows). Similarly, a resident population with a very high firing rate (e.g. $k_{fire,R1} = 250$ firings cell^{-1} h^{-1}) will be displaced by mutants with *lower* firing rates (Figure 1D, yellow arrows). $k_{fire,R}^{ESS,local}$ is the point where these progressions meet

[1] For cases where neither strain is vulnerable to the other's toxins, the outcome of competition is simple: the strain with the lowest k_{fire} wastes the least energy on futile firing, and wins. For cases where one strain is vulnerable to the other but not vice-versa, the outcome will be similar to the R vs. U battles shown in Figure 1, with the susceptible R strain in the role of the U strategist (except slightly worse-off on account of bearing the cost of T6SS carriage).

(Figure 1D, white circle) – mutants with higher or lower firing rates than this cannot displace residents that fire at this rate. Note that global competition (Figure 1E) favors a reduced level of aggression than local competition (i.e. $k_{fire,R}^{ESS,local} > k_{fire,R}^{ESS,global}$); similar trends can be seen for other strategist pairs at various initial densities (Figure S3).

'Tit-for-tat' retaliation is insufficient to beat a random attacker

So far, our results indicate that Random T6SS firing is often a successful strategy, enabling invasion of Unarmed populations, and offering better defense against other Random T6SS attackers than for T6SS- susceptible strains. Now, we consider a second T6SS firing strategy: the 'Tit-for-tat' (TFT) firing model for *P. aeruginosa* (*24*). TFT differs from R in two key respects: i) TFT does not fire its T6SS continuously, but counterattacks once per incident attack (retaliatory firing); ii) TFT does not fire from randomly-chosen sites on its cell membrane, but instead from the points where incident attacks struck (spatial sensing). We assume TFT to be identical to R in all other respects (toxin potency, lysis delay, weapon costs per T6SS firing, costs of weapon carriage).

Figure 2A shows our implementation of a TFT strategist in our agent-based model. To assess conditions favoring TFT strategists, we competed TFT against R for different initial cell densities, as before (Figure 2B, C). We were surprised to find that, while TFT generally does better against R than U (cf. Figure 1B), R can still outcompete TFT, particularly at higher cell densities. Consequently, R can invade and displace TFT for lower $k_{fire,R}$ values, for both local and global competition scales (Figures 2D, S3), provided cell density is sufficient.

Retaliatory T6SS firing is optimized by multiple counter-attacks and resilience towards initial attacks

A wide range of conditions preclude the evolution of TFT retaliatory T6SS firing from a population of Random attackers. Trivially, TFT is also guaranteed to lose against U, since the latter never triggers retaliatory T6SS attacks, and is spared the cost of T6SS carriage (*21*). How then could TFT evolve if it is often outcompeted by U or R?

To resolve this apparent paradox, we considered ways in which the TFT strategist might be improved. When we tried increasing the number of counterattacks launched by retaliators, we found that the resulting strategist—dubbed 2-Tits-For-Tat (2TFT)—is highly successful against a Random T6SS attacker (Figure 2E), outcompeting it for all T6SS firing rates and cell densities studied (Figure 2F). Intriguingly, swapping TFT for 2TFT also reversed the trend in competition outcome with respect to initial cell density, with higher cell densities now favoring 2TFT instead of R (Figure 2F, cf. Figure 2C). We interpret this as meaning that 2TFT is superior to R in a cell-on-cell battle, unlike U and TFT. As discussed above, increasing initial density simultaneously creates more fronts between competing cell groups and increases the time for which competing strains are in physical contact – both of which favor the strain with the best contact-dependent attack.

Accordingly, we also found that 2TFT is able to invade a population of R cells for all $k_{fire,R} > 0$ (Figures 2G), and for all cell densities studied (Figure S3). However, this robust competitive advantage disappeared when we reduced the resilience of both strategists (N_{hits} reduced to 1 from 2), such that a single T6SS hit is sufficient to disable a cell (Figure 2F, dotted lines; Figure S3): here, 2TFT performs no better than TFT.

Retaliator success stems from geometric and economic advantages

Mechanistically, how is it that 2TFT outcompetes R robustly, in contrast to the standard model of T6SS retaliation (TFT)? We identified two key advantages offered by retaliatory T6SS firing, and used our models to compare their relative contributions to 2TFT's fitness in competition with R (Figure 3). Firstly, the ability to sense *where* incident attacks are coming from allows T6SS counterattacks to be aimed specifically at attackers. By contrast, Random attackers have no information on where target cells are (*9*), and so miss most of the time (Figure 3A). Indeed, when we measured T6SS hit:miss ratios in fixed, well-mixed configurations of cells, we found that attacks by 2TFT cells were significantly more likely to hit R cells than vice versa (Figure 3B, see Methods).

Secondly, the ability to sense *when* one is being attacked prevents costly use of the T6SS when it is not needed. Examination of cell growth rates during R vs. 2TFT competitions showed that only 2TFT cells in actually in contact with competitors actually pay for T6SS firing – compared with R cells, which must pay for constant T6SS firing whether or not competitors are actually in range (Figure 3C). We found that this resulted in significantly higher specific growth rates for 2TFT cells than for R cells (Figure 3D).

To determine which of these advantages—improved aim or lower cost—drives 2TFT's success in a given scenario, we created three new retaliator phenotypes with one or both advantages removed (Figure 3E, F). To remove the advantage of T6SS aiming through spatial sensing, we configured TFT cells to counterattack from randomly-chosen sites on their membranes, instead of from the points at which incident attacks struck (Figure 3F). To remove the advantage of reduced T6SS cost, we configured TFT cells to pay the same growth costs as Random T6SS attackers, for any given attack rate $k_{fire,R}$. Comparing the single 'knockout' cases (loss of aiming or loss of cost saving) against a normal R vs. 2TFT competition, we found that removing cost-saving (Figure 3E, right column) still allowed 2TFT to beat R (albeit by a reduced margin) irrespective of weapon cost factor c. By contrast, eliminating T6SS aiming (Figure 3F, left column) allowed R to beat 2TFT, except

where weapon costs were very high. Similar trends appeared when cell density was varied instead of weapon costs (Figure S4) – here, removal of T6SS aiming resulted in reduced 2TFT fitness at higher cell density, confirming that aiming is generally required for 2TFT to beat R in a cell-on-cell battle.

Pseudomonas aeruginosa launches multiple counterattacks during retaliatory T6SS firing

Overall then, a key prediction emerging from our model is that retaliatory T6SS firing is only generally favorable if each hit sustained by the retaliating cell produces multiple counterattacks. As a test of this prediction, we analyzed the T6SS counterattacks of *Pseudomonas aeruginosa* bacteria, in response to random attacks by *Vibrio cholerae*. Both cell types express functional T6SS apparatus, the sheaths of which (TssB subunits in the case of *P. aeruginosa* and VipA subunits in the case of *V. cholerae*) carry fluorescent tags (see Methods). These tags allow individual T6SS firing events to be tracked using time-lapse fluorescence microscopy, as described in previous studies (*22*, *24*, *36*). When the two grown are together on agarose pads, *V. cholerae* antagonizes *P. aeruginosa* and causes it to launch counterattacks (Figure S5), such that T6SS dynamics of the two species can be compared directly in the same setting.

Figure 4 shows example kymographs for individual T6SS firing sites (baseplate complexes) imaged in *P. aeruginosa* (Figure 4A) and in *V. cholerae* (Figure 4B) cells during these co-culture experiments. In agreement with our model's predictions, *P. aeruginosa* is observed to fire repeatedly (between 1-6 firings over a 5-minute time-lapse, with median 2 firings per site, see Figure 4-C). By contrast, we could detect no instances of repeated T6SS firing within the same time window, confirming that repeated T6SS firing is not simply a universal trait among ɣ-Proteobacteria. These observations support the prediction that multiple counterattacks from the same T6SS site are necessary to extract maximum benefit from a retaliatory firing strategy.

Discussion

In this study, we have used agent-based modelling to compare bacterial strategies for T6SS attack. In addition to recapitulating previous studies' observations on the dynamics of T6SS competition (*33*, *34*), our models make several new predictions about the evolution of T6SS spatio-temporal regulation. Overall, our work characterizes random and retaliatory firing as generalist and specialist strategies, respectively. Random constitutive firing can readily evolve in unarmed populations, provided that i) weapon costs are not excessive and ii) initial mixing provides enough inter-strain contact.

By contrast, retaliatory firing is successful only against other T6SS users, and then only if additional constraints are met. Specifically, we predict that retaliation can evolve robustly provided that the retaliator i) survives multiple rounds of exogenous T6SS attack (resilience), and ii) deals more damage to an attacker than it sustains itself (disproportionate retribution). Ultimately, both additional constraints stem from the 'first-strike advantage' possessed by random attackers: having already been struck by at least one T6SS needle, a retaliator always enters combat at a disadvantage, requiring that retaliation be disproportionate to be generally successful.

The additional constraints limiting retaliator evolution may explain why *P. aeruginosa* is, to our knowledge, the only example of a T6SS retaliator found so far – whereas many species are known to use random T6SS firing (*20–22*). However, it is also clear that *P. aeruginosa* is a perfect fit to these constraints. Firstly, *P. aeruginosa* can resist oncoming T6SS attacks from other species like *V. cholerae*, perhaps because of its (in)famously impermiable cell membrane (*24*). Secondly, we have shown that *P. aeruginosa*'s ability to 'aim' T6SS firing—through spatially-resolved, TagQRST-mediated attack sensing—is a key contributor to its success as a retalitor (Figure 3E,F), because it provides cells with additional information on the location of attackers. By placing T6SS assemblies at attack sites, *P. aeruginosa* can substantially improve its hit efficiency, compared with a random firer that has no information on the location of its target.

Thirdly, our models show that *P. aeruginosa* cells can only fully exploit this 'aiming' if they also launches multiple counterattacks from a given site of impact, in contrast to the current 'Tit-for-tat' model (*24*). Otherwise, they still stand to lose more cells per pairwise T6SS battle than their competitors, such that the latter can win overall if the two strains are sufficiently well-mixed. Our experiments confirm that *P. aeruginosa* does indeed fire repeatedly from T6SS assemblies placed at hit sites, a pattern not observed in random-firing *V. cholerae*. In light of this observation, we suggest that *P. aeruginosa*'s retaliatory T6SS strategy is better thought of as "Tits-for-Tat" than the original 'Tit-for-tat' nomenclature drawn from evolutionary biology (*37*).

Like all models, ours make simplifying assumptions that trade degrees of realism for tractability. Among these is our coarse-grained representation of T6SS expression regulation: specifically, we assume that any constitutive T6SS activity becomes fully activated at the start of a given simulation and maintained thereafter at a constant level until the simulation's end. In reality, T6SS activation likely has a more gradual onset that decreases activity and costs in pre-confluent colonies (*17*), potentially reducing wastage and expanding the range of conditions estimated to support constitutive T6SS activity. While beyond the scope of the present study, evaluating the relative benefits of sensing other environmental cues (e.g. kin-lysate or damage sensing (*17*, *38*, *39*)) provides further applications for our model framework.

Another key assumption is that competitions involve only two T6SS strategists at a time. While many theoretical approaches (e.g. ecological network theory (*40*)) deconvolve the dynamics of multistrain communities into pairwise interactions such as these, our simulations so far ignore behaviors that might emerge only when three or more strategists are present within the same spatial niche. Intriguingly, parameter combinations exist such that unarmed strains are beaten by random attackers (T6SS killing trumps growth advantage), who are beaten by Tits-for-tat retaliators (superior killing and growth advantage trumps T6SS aggression), who can be beaten in turn by unarmed strains (growth advantage trumps unused costly T6SS). This 'rock-paper-scissors' relationship, also suggested in a recent study (*41*), could potentially

support non-transitive dynamics between competing bacterial strains, and thereby stabilize variation in T6SS firing patterns (*42*, *43*).

These limitations notwithstanding, a key strength of the model presented here is its geometric detail: by explicitly incorporating cell polarity, packing effects and discrete firing events, absent in previous models (*33*, *34*, *44*), it enables the effectiveness of different T6SS firing patterns to be measured and compared. We have so far applied our model to just three T6SS firing strategies – yet more are known (for example, polar firing used to manipulate eukaryotic cell structures by *Francisella* and *Burkholderia* spp. (*45*, *46*)), and others may soon be discovered. Moreover, different temporal patterns of firing are also now being characterized: Ostrowski et al. hypothesize that a T6SS firing delay, made possible by the TagF element of the PPI pathway, is necessary in *Serratia marcescens* for efficient killing (*47*). These findings generate further questions about the mechanisms governing T6SS site placement and firing strategy: how many sites, firing how fast, and for how long, are optimal against a given target? Models such as ours offer the opportunity to address these questions, and to learn more about variability in bacterial interference competition.

Conclusion

Bacteria differ widely in how they deploy T6SS weaponry in space and time. We have applied agent-based modelling and game theory to study competition between these contrasting strategies, revealing the strengths and weakness of each, and the environmental and physiological factors governing their evolution. Our analyses show that retaliatory T6SS firing by *P. aeruginosa* can be highly effective against speculative random firing: by exploiting cues indicating *when* to fire (i.e. only when in contact with a rival) and *where* to fire (i.e. in the direction of the rival cell), retaliators can outmatch competitors, delivering a disproportionate counterattack with superior T6SS efficiency and economy. By contrast, constitutive T6SS firing is a more generalist strategy, effective against both T6SS-armed and unarmed competitors. Overall, our work helps us to better understand the dynamics and

evolution of T6SS-mediated bacterial warfare, offering new routes to manipulate competiton for technological or therapeutic purposes.

Methods

Agent-based model

As in previous studies (*30*, *32*, *48*), we model bacterial communities as collections of 3-D rod-shaped cells, growing in independent niches on a flat surface (Figure S1A). Every cell is an independent 'agent' whose behavior depends on its phenotype, and on its interactions with neighboring cells. Each model simulation tracks cell growth, movement and death within a single niche. Niches have an allotted quota (E_0) of growth-limiting resources, which cells consume until the niche becomes depleted, thereby ending the simulation. Cell phenotypes, model variables and model parameters are summarized in Tables S1, S2 and S3, respectively.

Cell growth and division: Each cell's volume V_i increases exponentially through elongation, from initial volume V_0, according to the equation $dV_i/dt = k_{grow,i}V_i$, where $k_{grow,i}$ is a (phenotype-dependent) cell growth rate with maximum k_{max} . All living cells deplete niche resources E at a rate proportional to their volume: $dE/dt = -k_{max} \sum_i V_i$. Cells divide lengthwise into two identical daughter cells once they reach volume $2V_0 + \eta_{division}$, with $\eta_{division}$ a uniform random noise term. Each daughter's axis vector $\hat{\boldsymbol{a}}_i$ is perturbed slightly by a noise term with weight $\eta_{orientations}$, to represent spatial imperfections in the division process. Following the cell-growth phase, the cell configuration is returned to a quasi-stationary mechanical equilibrium using an energy minimization algorithm, described previously (*30*, *31*, *48–50*).

T6SS firing and costs. T6SS+ cells can fire toxin-laden needles of length L_{needle} outwards from points on their surface. Every timestep dt, a focal T6SS+ cell i may fire $N_{firings,i} \geq 0$ times. The number and spatial orientations of firings depend on the phenotype of the focal cell (Table S1). If the focal cell is a Random-firing ('R'-type) strategist, $N_{firings,i}$ is drawn from a Poisson distribution with mean k_{fire}; these needles emanate from randomly-chosen points on the focal cell's surface (Figure S1B). For retaliatory Tit-For-Tat ('TFT'-type) strategists, needles instead emanate from surface points at which the focal cell was struck; $N_{firings,i}$ is then the

number hits sustained by the focal cell in a given timestep. Similarly, Two-Tits-For-Tat ('2TFT'-type) strategists fire back twice for every hit they sustain. To reflect the material and energetic costs of T6SS carriage and use, T6SS+ cells reduce their growth rate to $k_{grow,i} = k_{max}\left(1 - c_{Total,i}\right)$, where $c_{Total,i} = c_{upfront} + c\left(N_{firings,i}/dt\right)$. Here, $c_{upfront}$ represents the cost of T6SS gene carriage, while the latter term reflects the 'running' costs of T6SS firing.

T6SS hit detection. To determine whether a given firing event is successful, we run a two-step hit detection algorithm (*32*) to determine i) whether that needle intersected any other cell in the population, and if so ii) where on the target cell the needle struck (Figure S1B). Both checks involve standard methods in computational geometry (*51*): i) involves computing the shortest distance d_{min} between the needle and cell line segments; $d_{min} < R - L_{penetration}$ indicates contact between the needle and the cell, where R is the cell radius of the victim, and $L_{penetration}$ a small tolerance factor. Test ii) involves checking whether a needle vector passes through the cylindrical midsection of the cell, or through spheres of radius R placed at its poles; whichever intercept lies closest to the needle's origin is logged as the entry point (Figure S1B, middle, yellow stars). Here, we show an example of a needle (red arrow) that intercepts only the cell midsection, and a second example (magenta arrow) intercepting both the left polar sphere and the midsection.

T6SS intoxication. Any cell struck by a T6SS needle fired from a non-kin cell becomes intoxicated (cells of the same genotype are assumed mutually immune). Cells respond to T6SS intoxication with a step-like dose-response: once a cell's cumulative translocation count reaches threshold N_{hits}, that cell begins to lyse. N_{hits} therefore parameterizes both the potency of a given T6SS effector, and the capacity of a victim cell to withstand it. Lysing cells die—and are immediately removed from the simulation—after a delay of $1/k_{lysis}$, where k_{lysis} is the victim cell lysis rate. Lysing cells do not grow or consume niche resources.

Adaptive dynamics

As in previous studies (*52*, *53*), we use Adaptive Dynamics (*35*) to determine whether a focal strategy (U, R, TFT or 2TFT) could evolve from a given bacterial metapopulation, subject to different scales of ecological competition. This method uses short-term competition outcomes to infer the evolutionary fate of a rare, novel strategy in a metapopulation where a different 'resident' strategy predominates. If the novel strategist can reproduce faster than the resident strategist even when rare, its frequency in the metapopulation will increase, until eventually it supplants the resident. For example: to test whether an R strategist can invade a population of U strategists, we compare their effective fitnesses where one is rare, and the other common. For R to invade U, we require

$$W_{rel}(rare\ R \mid common\ U) > 1, \qquad W_{rel}(common\ R \mid rare\ U) \geq 1,$$

where $W_{rel}(X \mid Y)$ is the relative fitness of X against Y. The first inequality specifies that R can invade U from rarity; the second checks that R is resistant to re-invasion by U once R becomes common. The definition of relative fitness W_{rel} depends upon the spatial scale of competition within the metapopulation. If competition is localized, then R competes primarily with nearby residents. Here, invasion is predicted simply from the ratio of strategists' fitness within a spatial niche: R invades U provided that

$$\frac{\omega_R(R \mid U)}{\omega_U(R \mid U)} > 1,$$

where $\omega_X(X \mid Y)$ is the fitness of strategist X in competition with strategist Y, with ω_X defined as $\omega_X = log_e(\sum V_X\ (t_{end}) / \sum V_X\ (t_{start}))$. Alternatively, competition may occur on much greater spatial scales, such that R must also compete with U strategists in other niches in the metapopulation. Assuming that R is initially rare, its encounters will predominately be with resident strategists, so its effective fitness is its reproductive capacity when in competition with U. Meanwhile, residents will encounter the novel strategy only rarely, and so will have an effective fitness based on reproduction when in competition with other residents. For R to invade U under these conditions, we require

$$\frac{\omega_R(R \mid U)}{\omega_U(U \mid U)} > 1, \qquad \frac{\omega_R(R \mid R)}{\omega_U(R \mid U)} \geq 1.$$

We refer to these two sets of inequalities as 'local' and 'global' invasion constraints.

To create the 1-D invasion plots shown in Figure 1C, we computed mean values of $\omega_R(R \mid R)$, $\omega_U(U \mid U)$, $\omega_R(R \mid U)$ and $\omega_U(R \mid U)$ for the R-strategist firing rates k_{fire} shown in Figure 1B, linearly interpolating one additional value between each pair of adjacent data points. We then classified each firing rate according to which of the local and global invasion constraints held true. We used the same methodology for other pairs of strategists (replacing U with TFT, 2TFT or a second R strategist; cf. Figure S3). For global invasion analyses of R1 vs. R2 competition (Figure 1E), we have the special case that the two global invasion constraints are equivalent (i.e. R1 invading R2 precludes R2 invading R1). Here, both strategists are characterized by their own independent firing rates $k_{fire,R1}, k_{fire,R2}$, and so invasion outcome is summarized by the 2-D colormap,

$$I_{inv}^{global}\left(k_{fire,R1}, k_{fire,R2}\right) = \omega_{R2}(R2 \mid R1)/\omega_{R1}(R1 \mid R1).$$

The corresponding invasion index for local competition scales (Figure 1D) is

$$I_{inv}^{local}\left(k_{fire,R1}, k_{fire,R2}\right) = \omega_{R2}(R2 \mid R1)/\omega_{R1}(R2 \mid R1).$$

Computation and Postprocessing

Agent-based model simulations were run on a 2017 Apple ® MacBook Pro laptop computer, with simulations distributed between an Intel ® 3.1GHz quadcore i7-7920HQ CPU, an Intel ® HD 630 Graphics card, and an AMD Radeon Pro 560 Compute Engine. Simulation data was analyzed using custom Matlab ® scripts (Version R2017a 9.2.0.556344), and visualized using Paraview software (Version 4.3.1) (*54*).

Bacterial strains and growth conditions for fluorescence microscopy

P. aeruginosa PAO1 *tssB-mNeonGreen*, *V. cholerae* 2740-80 *vipA-mCherry2* and *V. cholerae* 2740-80 *vipA-mCherry2 Δhcp1 Δhcp2* were inoculated from Luria broth (LB) agar plates and grown aerobically at 37 °C in LB to an OD600 of 1 (about 3 h).

1 ml of each day culture was then pelleted at 11,000 g for 1.5 min and resuspended in LB to reach OD600 of 10. *P. aeruginosa* PAO1 *tssB-mNeonGreen* was mixed with *V. cholerae* 2740-80 *vipA-mCherry2* or *V. cholerae* 2740-80 *vipA-mCherry2 Δhcp1 Δhcp2* in a 1:5 ratio (10 µl to 50 µl). 1.5 µl of both mixtures were spotted on a pad of 1 % agarose in 1/3 LB and 2/3 phosphate buffered saline (PBS). The pad was covered with a glass coverslip and incubated for 30 minutes at 30 °C before imaging.

Fluorescence microscopy

For live-cell fluorescence microscopy, the same equipment was used as described previously (*55*, *56*); a Nikon Ti-E inverted microscope with Perfect Focus System and a Plan Apo 1003 Oil Ph3 DM (NA 1.4) objective lens, a SPECTRA X light engine (Lumencore) and ET-GFP (Chroma #49002) and ET-mCherry (Chroma #49008) filter sets to excite and filter fluorescence. Exposure time was set to 150 ms and LED powers to 20 %. Images were recorded with a sCMOS camera pco.edge 4.2 (PCO, Germany; 65 nm pixel size) and VisiView software (Visitron Systems, Germany). Imaging was carried out at 30 °C and 95 % humidity controlled by an Okolab T-unit (Okolab) and images were collected every 2 s for 5 min. The imaging experiments were performed in two biological replicates.

Image analysis

Image analysis and manipulation was carried out with Fiji (*57*). Contrasts were set equally for a set of compared images. Intensity of GFP and mCherry channels were corrected with the 'simple ratio' bleach correction function. Numbers of *P. aeruginosa* PAO1 *tssB-mNeonGreen* cells in contact with *V. cholerae* 2740-80 *vipA-mCherry2* or *V. cholerae* 2740-80 *vipA-mCherry2 Δhcp1 Δhcp2* cells were counted based on the phase contrast and GFP channel. The number of T6SS structures per cell in *P. aeruginosa* PAO1 *tssB-mNeonGreen* was counted in the maximum intensity projection image of the GFP channel. Only T6SS structures of cells in contact with *V. cholerae* were counted. To quantify the number of repeated T6SS assemblies in kymograms, the "reslice" function was used. Only repeated T6SS assemblies directed towards *V. cholerae* cells were analyzed. Kymograms of V.

cholerae were used to calculate the time without new T6SS after contraction (2 s per pixel). Only T6SS assemblies directed towards *P. aeruginosa* cells were included in the analysis. All quantifications were performed manually. GraphPad Prism7 was used to display the histogram of repeated T6SS assemblies. The number of cells analyzed, averages with standard deviations and medians are given in the figure legend.

Statistical analyses

Unless indicated otherwise, the number of simulation replicates is five for each parameter combination shown. 2 biological replicates were used in all experiments. For comparative statistics (Figures 3B, 3D), we used a two-sample t-test. All statistical calculations were performed in Matlab ® (Version R2017a 9.2.0.556344).

References

1. F. Boyer, G. Fichant, J. Berthod, Y. Vandenbrouck, I. Attree, Dissecting the bacterial type VI secretion system by a genome wide in silico analysis: what can be learned from available microbial genomic resources? *BMC Genomics*. **10**, 1–14 (2009).

2. S. J. Coulthurst, The Type VI secretion system - a widespread and versatile cell targeting system. *Res. Microbiol.* **164**, 640–654 (2013).

3. S. S. Abby *et al.*, Identification of protein secretion systems in bacterial genomes. *Sci. Rep.* **6**, 23080 (2016).

4. M. J. Coyne, L. E. Comstock, Type VI Secretion Systems and the Gut Microbiota. *Microbiol. Spectr.* **7** (2019), doi:10.1128/microbiolspec.PSIB-0009-2018.

5. S. Pukatzki *et al.*, Identification of a conserved bacterial protein secretion system in Vibrio cholerae using the Dictyostelium host model system. *Proc. Nat. Acad. Sci.* **103**, 1528–1533 (2006).

6. T. R. D. Costa *et al.*, Secretion systems in Gram-negative bacteria: structural and mechanistic insights. *Nat. Rev. Microbiol.* **13**, 343 (2015).

7. E. Durand, C. Cambillau, E. Cascales, L. Journet, VgrG, Tae, Tle, and beyond: the versatile arsenal of Type VI secretion effectors. *Trends Microbiol.* **22**, 498–507 (2014).

8. V. S. Nguyen *et al.*, Towards a complete structural deciphering of Type VI secretion system. *Curr. Opin. Struct. Biol.* **49**, 77–84 (2018).

9. B. T. Ho, T. G. Dong, J. J. Mekalanos, A View to a Kill: The Bacterial Type VI Secretion System. *Cell Host Microbe*. **15**, 9–21 (2014).

10. M. Brackmann, S. Nazarov, J. Wang, M. Basler, Using Force to Punch Holes: Mechanics of Contractile Nanomachines. *Trends Cell Biol.* **27**, 623–632 (2017).

11. A. L. Hecht *et al.*, Strain competition restricts colonization of an enteric pathogen and prevents colitis. *EMBO Rep.* **17**, 1281–1291 (2016).

12. A. G. Wexler *et al.*, Human symbionts inject and neutralize antibacterial toxins to persist in the gut. *Proc. Natl. Acad. Sci. U. S. A.* **113**, 3639–44 (2016).

13. M. Chatzidaki-Livanis, N. Geva-Zatorsky, L. E. Comstock, Bacteroides fragilis type VI secretion systems use novel effector and immunity proteins to antagonize human gut Bacteroidales species. *Proc. Natl. Acad. Sci.* **113**, 3627–3632 (2016).

14. P. Bernal, L. P. Allsopp, A. Filloux, M. A. Llamas, The Pseudomonas putida T6SS is a plant warden against phytopathogens. *ISME J.* **11**, 972–987 (2017).

15. W. Zhao, F. Caro, W. Robins, J. J. Mekalanos, Antagonism toward the intestinal microbiota and its effect on Vibrio cholerae virulence. *Science*. **359**, 210–213 (2018).

16. C. S. Bernard, Y. R. Brunet, E. Gueguen, E. Cascales, Nooks and crannies in type VI secretion regulation. *J. Bacteriol.* **192**, 3850–60 (2010).

17. M. Lazzaro, M. F. Feldman, E. García Véscovi, A Transcriptional Regulatory Mechanism Finely Tunes the Firing of Type VI Secretion System in Response to Bacterial Enemies. *MBio*. **8**, e00559-17 (2017).

18. S. Schwarz *et al.*, Burkholderia Type VI Secretion Systems Have Distinct Roles in Eukaryotic and Bacterial Cell Interactions. *PLoS Pathog.* **6** (2010), doi:10.1371/journal.ppat.1001068.

19. A. Hachani, T. E. Wood, A. Filloux, Type VI secretion and anti-host effectors. *Curr. Opin. Microbiol.* **29**, 81–93 (2016).

20. M. Basler, J. J. Mekalanos, Type 6 Secretion Dynamics Within and Between Bacterial Cells. *Science (80-.).*, 1–2 (2012).

21. A. J. Gerc *et al.*, Visualization of the Serratia Type VI Secretion System Reveals Unprovoked Attacks and Dynamic Assembly. *Cell Rep.* **12**, 2131–2142 (2015).

22. P. D. Ringel, D. Hu, M. Basler, The Role of Type VI Secretion System Effectors in Target Cell Lysis and Subsequent Horizontal Gene Transfer. *Cell Rep.* **21**, 3927–3940 (2017).

23. M. Basler, M. Pilhofer, G. P. Henderson, G. J. Jensen, J. J. Mekalanos, Type VI secretion requires a dynamic contractile phage tail-like structure. *Nature*. **483** (2012), doi:10.1038/nature10846.

24. M. Basler, B. T. Ho, J. J. Mekalanos, Tit-for-Tat: Type VI Secretion System Counterattack during Bacterial Cell-Cell Interactions. *Cell*. **152**, 884–894 (2013).

25. D. Liebl, M. Robert-Genthon, V. Job, V. Cogoni, I. ATTREE, Baseplate component TssK and spatio-temporal assembly of T6SS in Pseudomonas aeruginosa. *Front. Microbiol.* **10**, 1615 (2019).

26. R. L. Trivers, The Evolution of Reciprocal Altruism. *Q. Rev. Biol.* **46**, 35–57 (1971).

27. R. Axelrod, W. D. Hamilton, The Evolution of Cooperation. *Science (80-.).* **211**, 1390–1396 (1981).

28. M. A. Nowak, Five rules for the evolution of cooperation. *Science*. **314**, 1560–3 (2006).

29. H. Zhang, M. Perc, Evolution of conditional cooperation under multilevel selection. *Sci. Rep.* **6**, 23006 (2016).

30. T. J. Rudge, P. J. Steiner, A. Phillips, J. Haseloff, Computational Modeling of Synthetic Microbial Biofilms. *ACS Synth. Biol.* **1**, 345–352 (2012).

31. W. P. J. Smith *et al.*, Cell morphology drives spatial patterning in microbial communities. *Proc. Natl. Acad. Sci.*, E280–E286 (2016).

32. W. P. J. Smith *et al.*, The Evolution of the Type VI Secretion System as a Lytic Weapon. *TBC* (2019).

33. D. B. Borenstein, P. Ringel, M. Basler, N. S. Wingreen, Established Microbial Colonies Can Survive Type VI Secretion Assault. *PLoS Comput. Biol.* **11**, 1–16 (2015).

34. L. McNally *et al.*, Killing by Type VI secretion drives genetic phase separation and correlates with increased cooperation. *Nat. Commun.* **8**, 14371 (2017).

35. Å. Brännström *et al.*, The Hitchhiker's Guide to Adaptive Dynamics. *Games*. **4**, 304–328 (2013).

36. A. Vettiger, J. Winter, L. Lin, M. Basler, The type VI secretion system sheath assembles at the end distal from the membrane anchor. *Nat. Commun.* **8**, 16088 (2017).

37. R. Axelrod, W. D. Hamilton, The Evolution of Cooperation. *Science (80-.).* **211**, 1390–1396 (1981).

38. M. Leroux *et al.*, Kin cell lysis is a danger signal that activates antibacterial pathways of Pseudomonas aeruginosa. *Elife*. **4**, 1–25 (2015).

39. D. M. Cornforth, K. R. Foster, Competition sensing: the social side of bacterial stress responses. *Nature*. **11**, 285–293 (2013).

40. K. Z. Coyte, J. Schluter, K. R. Foster, The ecology of the microbiome: Networks, competition, and stability. *Science*. **350**, 663–6 (2015).

41. B. Chassaing, E. Cascales, Antibacterial Weapons: Targeted Destruction in the Microbiota. *Trends Microbiol.* **26**, 329–338 (2018).

42. B. Kerr, M. A. Riley, M. W. Feldman, B. J. M. Bohannan, Local dispersal promotes biodiversity in a real-life game of rock–paper–scissors. *Nature*. **418**, 171–174 (2002).

43. J. M. Biernaskie, A. Gardner, S. A. West, Multicoloured greenbeards, bacteriocin diversity and the rock-paper-scissors game. *J. Evol. Biol.* **26**, 2081–2094 (2013).

44. M. J. Q. Wong *et al.*, Microbial Herd Protection Mediated by Antagonistic Interaction in Polymicrobial Communities. *Appl. Environ. Microbiol.* **82**, 6881–6888 (2016).

45. S. Schwarz *et al.*, VgrG-5 is a Burkholderia type VI secretion system-exported protein required for multinucleated giant cell formation and virulence. *Infect. Immun.* (2014), doi:10.1128/IAI.01368-13.

46. M. Brodmann, R. F. Dreier, P. Broz, M. Basler, Francisella requires dynamic type VI secretion system and ClpB to deliver effectors for phagosomal escape. *Nat. Commun.* **8** (2017), doi:10.1038/ncomms15853.

47. A. Ostrowski *et al.*, Killing with proficiency: Integrated post-translational regulation of an offensive Type VI secretion system. *PLOS Pathog.*, 1–25 (2018).

48. T. J. Rudge, P. J. Steiner, A. Kan, J. Haseloff, Cell Polarity-Driven Instability Generates Self-Organized, Fractal Patterning of Cell Layers. *ACS Synth. Biol*, 705–714 (2013).

49. I. N. Nuñez *et al.*, Artifical Symmetry-Breaking for Morphogenetic Engineering Bacterial Colonies. *ACS Synth. Biol.* **6**, 256–265 (2016).

50. I. Frost *et al.*, Cooperation, competition and antibiotic resistance in bacterial colonies. *ISME J.* **12**, 1582–1593 (2018).

51. P. J. Schneider, D. H. Eberly, *Geometric Tools For Computer Graphics* (Elsevier, 2002; http://cds.cern.ch/record/1085063/files/1558605940_TOC.pdf).

52. S. Mitri, J. B. Xavier, K. R. Foster, Social evolution in multispecies biofilms. *Proc. Natl. Acad. Sci. U. S. A.* **108 Suppl 2**, 10839–46 (2011).

53. K. Z. Coyte, H. E. Tabuteau, E. A. Gaffney, K. R. Foster, W. M. Durham, Microbial competition in porous environments can select against rapid biofilm growth. *Proc. Natl. Acad. Sci.*, E161–E170 (2017).

54. J. Ahrens, B. Geveci, C. Law, in *Visualization Handbook* (Elsevier, 2005; www.paraview.org.).

55. M. Kudryashev *et al.*, Structure of the type VI secretion system contractile sheath. *Cell*. **160**, 952–962 (2015).

56. A. Vettiger, M. Basler, Type VI Secretion System Substrates Are Transferred and Reused among Sister Cells. *Cell.* **167**, 99–110.e12 (2016).

57. J. Schindelin *et al.*, Fiji: an open-source platform for biological-image analysis. *Nat. Methods*. **9**, 676–682 (2012).

Figures

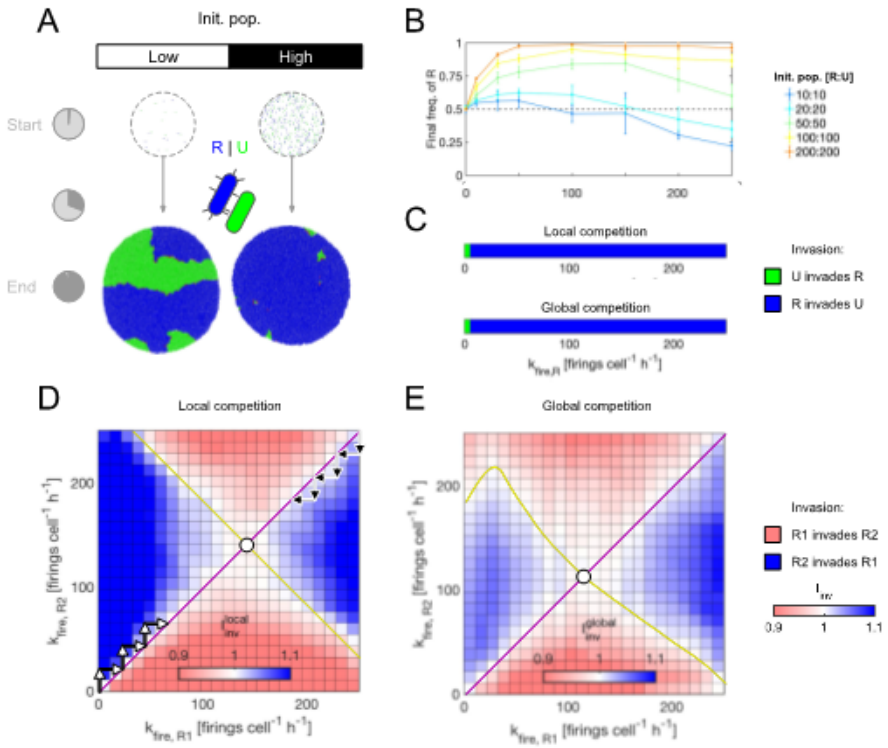

Figure 1: Random T6SS firing is effective against both Unarmed strains and other Random attackers. (**A**) simulation snapshots showing initial and final cell configurations for surfacial competition between T6SS- 'Unarmed' strain (U, green) and a Random-firing T6SS+ strain (R, blue). Simulations are carried out for both low and high initial cell densities (left and right columns; initial cell populations 10 vs. 10 and 200 vs. 200 cells respectively); pie charts (left) chart the consumption of niche resources. Firing rate $k_{fire,R} = 50$ firings cell^{-1} h^{-1}. (**B**) Competition outcomes, measured by final R cell proportion, as a function of firing rate $k_{fire,R}$ for increasing initial cell densities (see legend, right). (**C**) Invasion plots showing outcomes of local and global invasion analyses for R vs. U competition (see Methods), as a function of firing rate $k_{fire,R}$, for high initial cell density (200 vs. 200 cells); additional cases shown in Figure S4. (**D,E**) Pairwise invasion plots for competing R-type strategists (R1, R2), showing invasion outcomes for local (D) and global (E) competition scales for intermediate cell density (50 vs 50 cells). Arrows mark progression of evolving firing rates $k_{fire,R}$, converging on evolutionary stable strategy firing rates (ESS, white circles). Simulation parameters used throughout: $N_{hits} = 2$, $c = 0.001$; 5 simulation replicates per case in B, C and 10 per case in D, E.

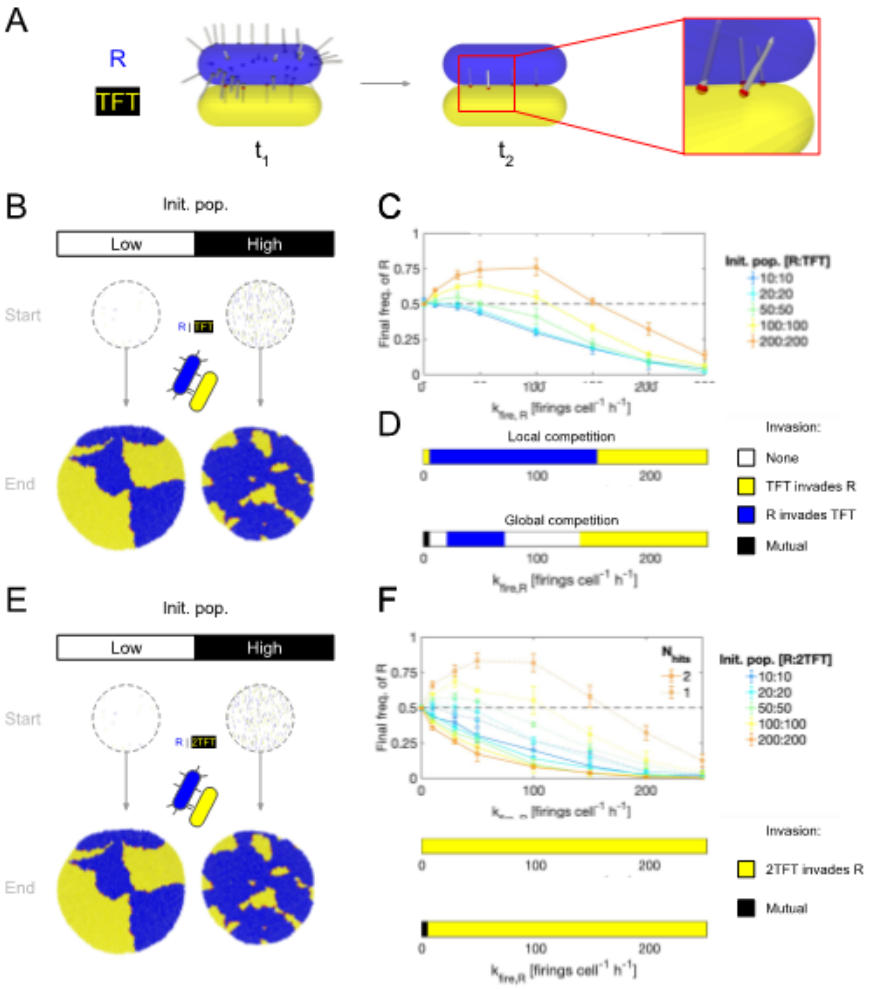

Figure 2: 'Tit-for-tat' retaliatory T6SS firing is insufficient to robustly defeat random T6SS attackers (**A**): Model representation of retaliatory T6SS firing in response to a random attacker (R, blue). Following R's initial attack (t_1), the retaliator cell (TFT, yellow) fires T6SS needles outwards from the points on its surface where initial attacks struck (t_2, magnified box). (**B**) Simulation snapshots showing initial and final cell configurations for competitions between R and TFT strategists ('low' and 'high' initial cell populations correspond to 10 vs. 10 and 200 vs. 200 cells as in Figure 1). (**C**) Competition outcome, measured by final R cell proportion, as a function of firing rate $k_{fire,R}$ for increasing initial cell densities (see legend, right). (**D**) Invasion plots showing outcomes of local and global invasion analyses for R vs. TFT competition, as a function of firing rate, $k_{fire,R}$, for high initial cell density (200 vs. 200 cells). (**E,F,G**): analogous to B,C,D except with TFT replaced by 2TFT, which counterattacks twice per successful oncomong attack. Simulation parameters: $N_{hits} = 2$, $c = 0.001$. 5 simulation replicates per case in C,D,F,G.

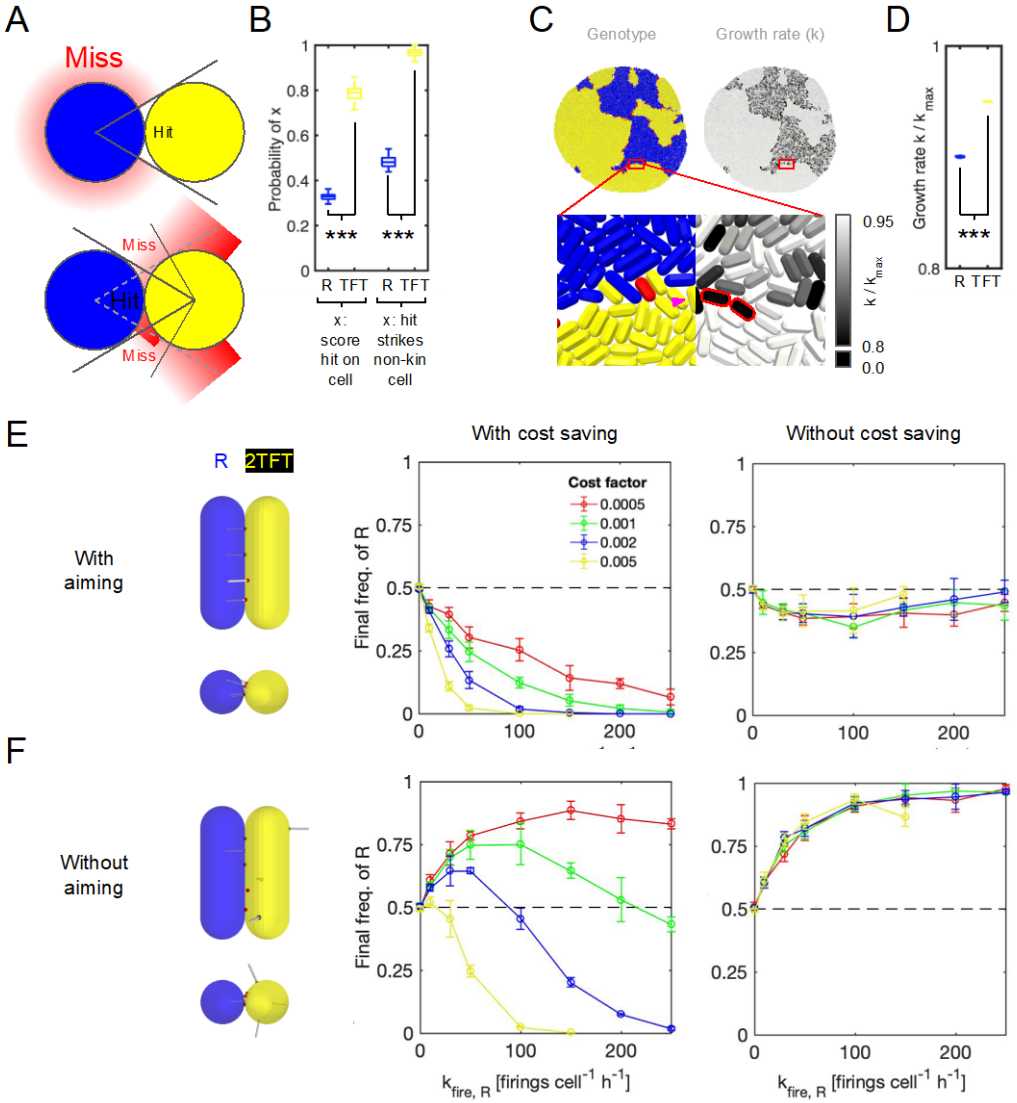

Figure 3: T6SS aiming and cost-saving allow 2-shot retaliators to beat random attackers. (**A**) Diagram comparing likelihood of successful T6SS attack for random firing (top) and retaliatory firing (bottom). (**B**) Measurements of absolute and non-kin cell hit probabilities from static, mixed cell populations, for random (R, blue) and retaliatory (2TFT, yellow) T6SS firing (*** = p <0.001, 2-way Student's t-test). (**C**) Visual comparison of R and 2TFT cell growth rates during competition. Cell configuration and magnified sections are colored by cell type (left) or by growth rate (right). Magenta arrow highlights a single TFT cell whose growth rate is reduced by active firing; dead cells are outlined in red in the right-hand. (**D**) Comparison of R and 2TFT cell growth rates, measured at the end of 5 separate R vs. 2TFT competitions. (**E,F**) Comparison of R vs. 2TFT competition outcomes, in which 2TFT strategists are modified to remove T6SS aiming (F) and/or cost saving (E,F, right column), for increasing weapon costs c (see legend in E, left column).

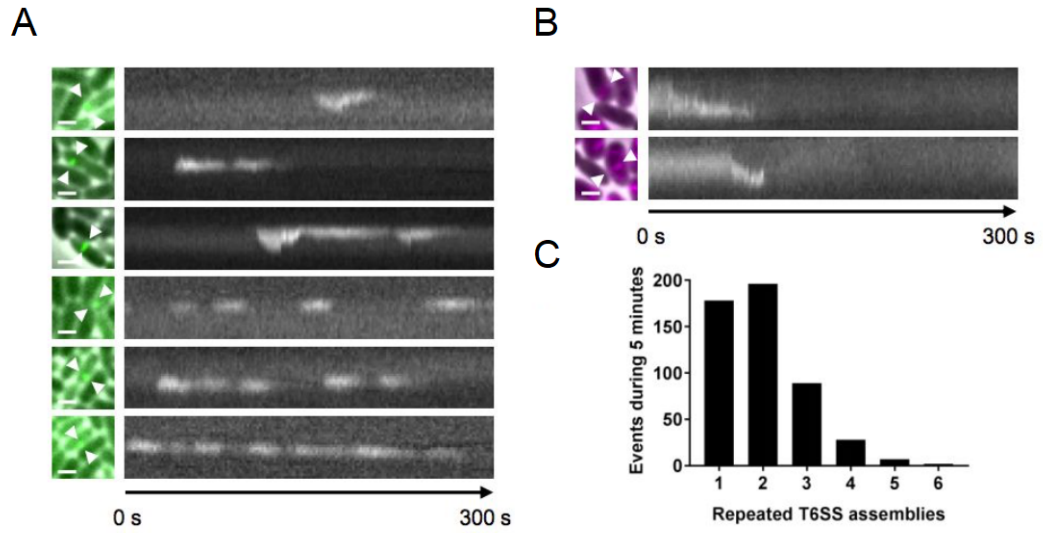

Figure 4: Repeated T6SS assemblies of *P. aeruginosa*. (**A**): Mixture of *P. aeruginosa* PAO1 *tssB-mNeonGreen* (green) with T6SS+ *V. cholerae* 2740-80 *vipA-mCherry2* (black). A merge of phase contrast and GFP channels is shown (left). 3.3 x 3.3 µm field of view is shown; scale bar 1 µm. Arrows point to assembled T6SS for which the contraction event is shown in the kymogram (2 s per pixel, 5 minutes in total, GFP channel). Kymograms show 1 to 6 repeated T6SS assemblies during 5 minutes. (**B**) Mixture of *P. aeruginosa* PAO1 *tssBmNeonGreen* (black) with T6SS+ *V. cholerae* 2740-80 *vipA-mCherry2* (magenta). A merge of phase contrast and mCherry channels is shown (left). 3.3 x 3.3 µm field of view is shown and scale bar represent 1 µm. Arrows point to assembled T6SS for which the contraction event is shown in the kymogram (2 s per pixel, 5 minutes in total, mCherry channel). For at least 3 minutes after contraction, no T6SS assembly at the same location was observed (n = 100, 2 biological replicates). (**C**) Histogram of repeated T6SS assemblies of *P. aeruginosa* PAO1 *tssB-mNeonGreen* cells in contact with *V. cholerae* 2740-80 *vipA-mCherry2* (average of repeated firings = 1.992, standard deviation of 0.975, Median: 2, n = 500, 2 biological replicates).

Supplementary Information

SI Tables

Table S1: T6SS strategists used in our agent-based model.

T6SS phenotype	$N_{firings}$	Growth rate	Firing pattern
U = Unarmed	0	k_{max}	None
R = Random attacker	$k_{fire,R}$ dt	$k_{max}(1 - c_{upfront} - cN_{firings,i} / dt)$	Random
TFT = Tit-for-tat	1 x num. incident attacks	$k_{grow}(1 - c_{upfront} - cN_{firings,i} / dt)$	From incident attack points
2TFT = 2-Tits-for-tat	2 x num. incident attacks	$k_{grow}(1 - c_{upfront} - cN_{firings} / dt)$	From incident attack points

Table S2: Table of agent-based model variables.

Category	Variable	Symbol	Units
Geometric	Position vector	$\mathbf{p_i} = (p_x, p_y, p_z)_i$	µm
	Orientation unit vector	$\mathbf{a_i} = (a_x, a_y, a_z)_i$	-
	Segment length	L_i	µm
	Volume	$V_i = 4\pi R^3/3 + \pi L_i R^2$	μm^3
	Specific growth rate	$k_{grow,i} = k_{grow,max}(1-c_{total,i})$	h^{-1}
T6SS	Total cost	$c_{total,i} = c_{upfront} + c(k_{fire,i})$	%
	Firing rate	$k_{fire,i} = N_{firings,i}(t) / dt$	Firings h^{-1}
	Firings this timestep	$N_{firings,i}$	Firings
	Cumulative hits	$N_{hits,i}$	Hits
Genetic	Cell genotype	U, R, TFT or 2TFT	-

Table S3: Table of agent-based model parameters.

Type	Parameter	Symbol	Value(s)	Units	Source
Domain	Inoculum zone size	$D_{homeland}$	100	µm	This study
	Inoculum population	N_{cells}	20-400	cells	This study
	Domain carrying capacity	E_0	10,000 V_0	-	This study
Cell-based	Max. growth rate	k_{max}	1.0	h^{-1}	Rudge2012
	Upfront T6SS cost	$c_{upfront}$	5	%	This study
	Pro rata T6SS cost	c	0.05 -0.5	% per k_{fire}	This study
	T6SS firing rate	k_{fire}	0-250.0	firings $cell^{-1}$ h^{-1}	Estimated from Basler2013
	Lysis delay	k_{lysis}	0.8-8.0	h^{-1}	Estimated from Basler2013
	Lethal hit threshold	N_{hits}	1-3	-	This study
	Needle length	L_{needle}	0.5	µm	Estimated from Basler2013
	Min. needle penetration	$L_{penetration}$	10	nm	Estimated from membrane width
	Cell radius	R	0.5	µm	Estimated from Basler2013
	Cell volume at birth	V_0	1.16	μm^3	Estimated from Basler2013
	Cell division volume noise	$\eta_{division}$	9	%	Smith2016
	Cell division orientation noise	$\eta_{orientation}$	0.2	%	Smith2016
Numerical	Simulation timestep	dt	0.025	h	Rudge2012
	Grid element size	h	10	µm	Smith2016
	CG absolute tolerance	ϵ_{CG}	0.001	-	Smith2016
	Max. contact iterations	$M_{Iter, max}$	8	-	Rudge2012
Mechanical	Regularization weight	α	0.04	-	Smith2016
	Growth restriction factor	1 / ɣ	0.002	-	Smith2016

SI Figures

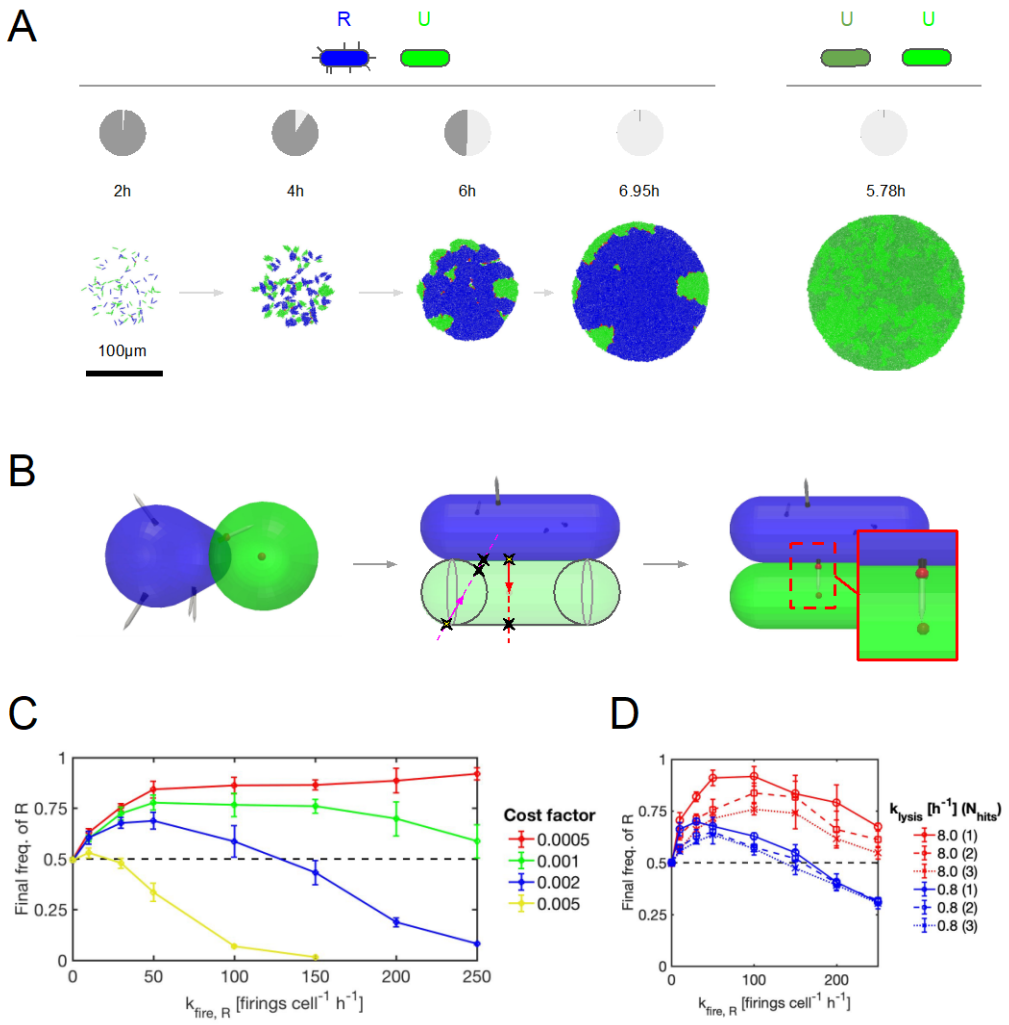

Figure S1: Agent-based modelling of T6SS-mediated competition. (**A**) Simulation time-lapse showing competition between Random T6SS attackers (R, blue) and T6SS- Unarmed cells (U, green) in a resource-limited niche. Final state (6.95 h) compared with that for U vs. U competition (right, 5.78 h). Pie charts track resource depletion; simulation parameters $N_{hits} = 2$, $c = 0.001$, $k_{fire,R} = 50.0$ firings cell^{-1} h^{-1}. (**B**) Overview of hit detection system: each T6SS needle is checked for intersection with neighbor cells' midsections and polar spheres (middle). (**C,D**) Parameter sweeps for R vs. U competitions, plotting final R proportion against firing rates $k_{fire,R}$ for different cost factors c (C), lysis rates k_{lysis} (D) and effector potencies N_{hits} (D). Parameters: $N_{hits} = 2$, $k_{lysis} = 8.0$ h^{-1} (C), $c = 0.001$ (D); 5 replicates per case. Initial cell density 50 vs. 50 cells throughout.

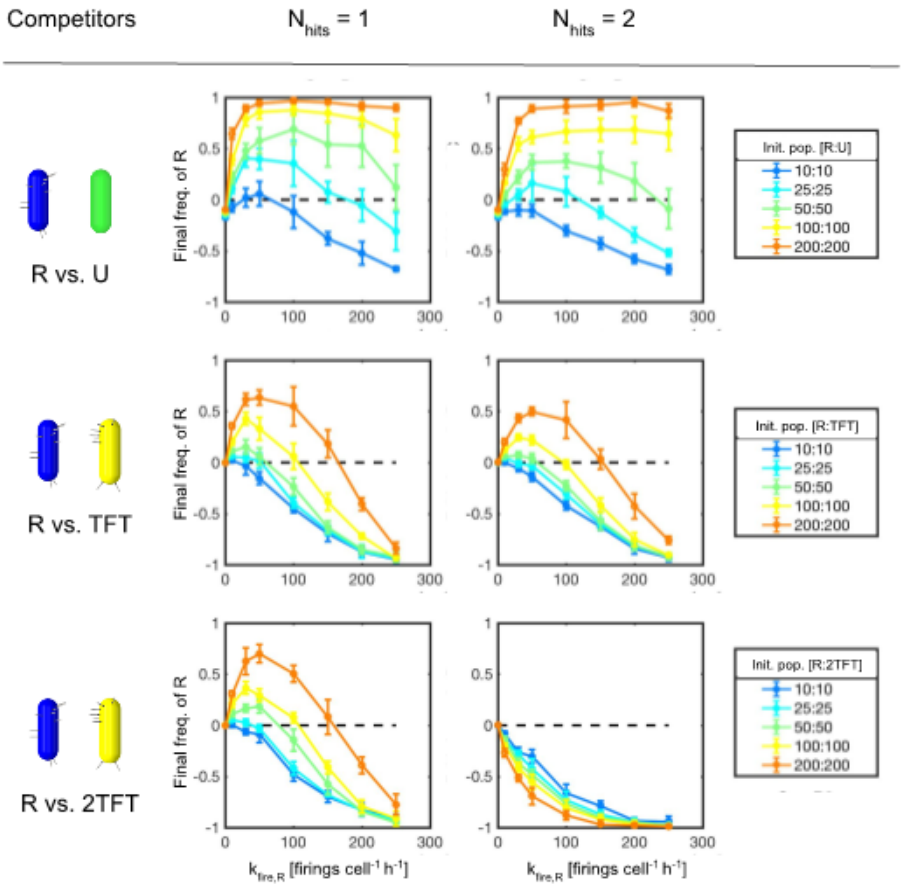

Figure S2: Comparison of competition simulations between T6SS strategists. Repeats of $k_{fire,R}$ vs. cell density parameter sweeps, showing competition outcomes for different competitors (rows) and T6SS effector potencies N_{hits} (columns). Panels analogous to those shown in Figures 1 and 2; N_{hits} = 2 cases repeated here for reference. k_{lysis} = 8.0 h^{-1}, c = 0.001 and 5 replicates per case throughout.

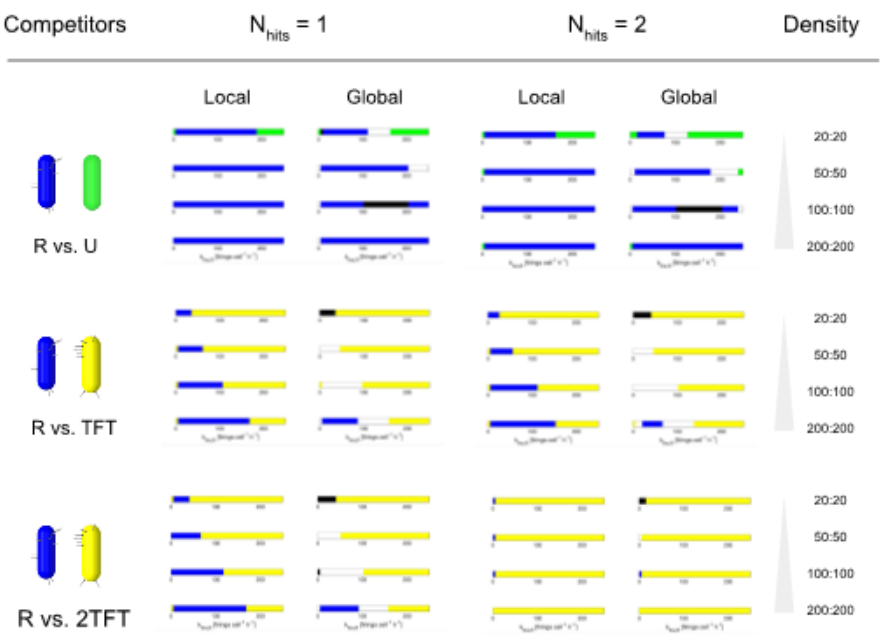

Figure S3: Comparison of invasion analyses between T6SS strategists. 1-D invasion plots show outcomes of local and global invasion analyses, analogous to those shown in Figures 1 and 2, for different competitors (left column) intial cell densities (right column), and T6SS effector potencies (middle two columns). N_{hits} = 2 cases repeated here for reference; color legends as in Figures 1 and 2. $k_{lysis} = 8.0$ h^{-1}, $c = 0.001$ and 5 replicates per case throughout.

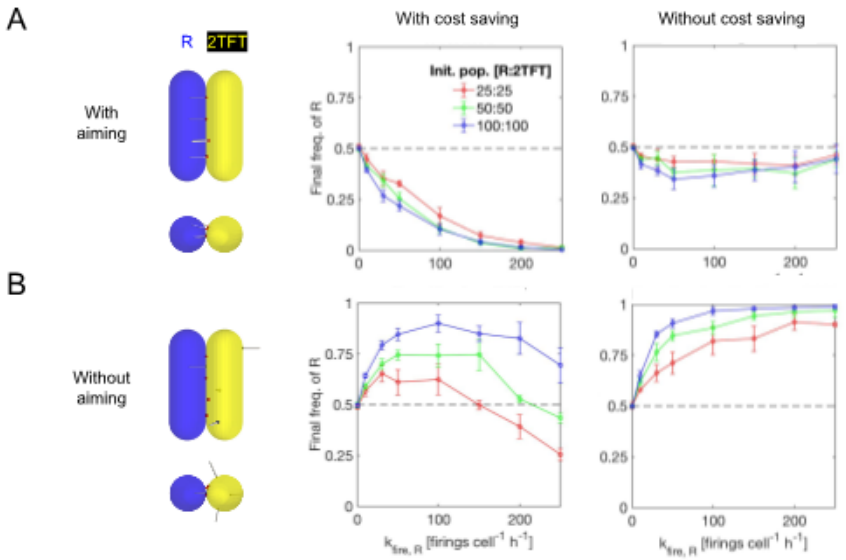

Figure S4: Additional 2TFT 'Knockout' competitions. Repeats of R vs. 2TFT advantage 'knockout' parameter sweeps from Figure 3, showing variation in competition outcome with initial cell density (see legend). $k_{lysis} = 8.0$ h^{-1}, $c = 0.001$ and 5 replicates per case throughout.

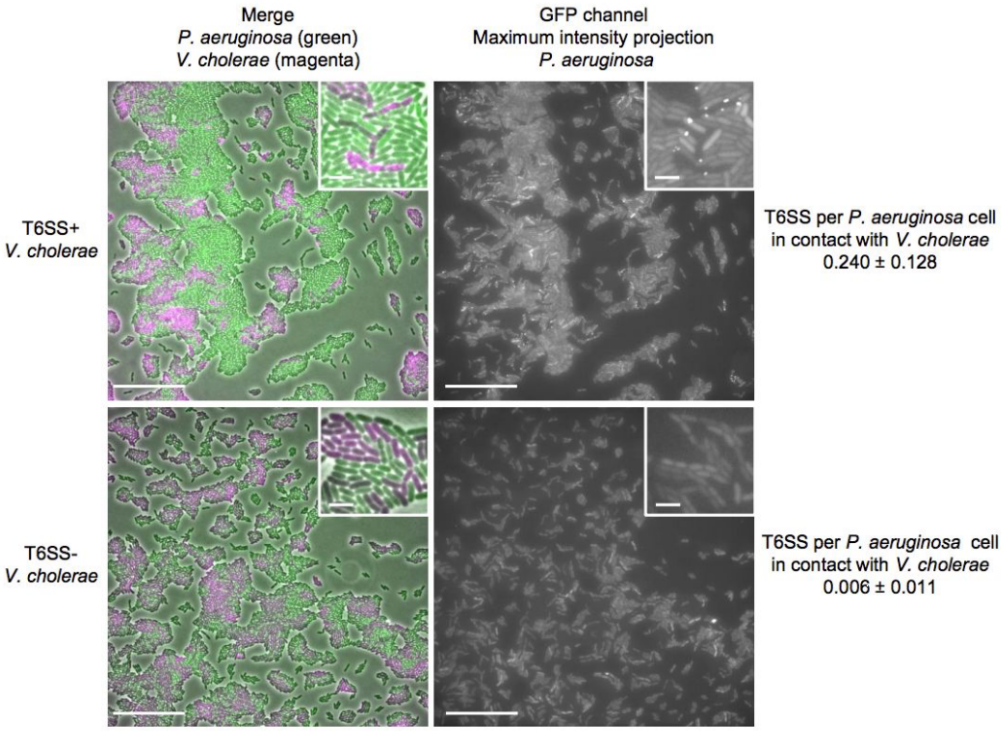

Figure S5: Activation of *P. aeruginosa* T6SS by *V. cholerae* T6SS. Mixture of *P. aeruginosa* PAO1 *tssB-mNeonGreen* with T6SS+ *V. cholerae* 2740-80 *vipA-mCherry2* (top) or with T6SS- *V. cholerae* 2740-80 *vipA-mCherry2 Δhcp1 Δhcp2* (bottom). A merge of phase contrast, GFP and mCherry channels is shown (left) as well as the maximum intensity projection of the GFP channel with the accumulated T6SS events of *P. aeruginosa* PAO1 *tssBmNeonGreen* within 5 minutes (right). Large images have a field of view of 133.2 x 133.2 µm and the scale bars represent 30 µm. Small images are close ups and show a field of view of 13 x 13 µm and the scale bars represent 3 µm. T6SS structures per *P. aeruginosa* PAO1 *tssB-mNeongreen* cell in contact with either *V. cholerae* 2740-80 *vipA-mCherry2* (top) or *V. cholerae* 2740-80 *vipA-mCherry2 Δhcp1 Δhcp2* (bottom) is shown (average with standard deviation, n > 6500 cells, 2 biological replicates).

3.3. *Francisella* requires dynamic type VI secretion system and ClpB to deliver effectors for phagosomal escape

Maj Brodmann1*, Roland F. Dreier1*, Petr Broz1[#] and Marek Basler1[#]

1 Focal Area Infection Biology, Biozentrum, University of Basel, Klingelbergstrasse 50/70, CH - 4056 Basel, Switzerland

* contributed equally

[#] correspondence to: petr.broz@unibas.ch, marek.basler@unibas.ch

Nature Communications volume 8, Article number: 15853 (2017)

DOI: 10.1038/ncomms15853

Statement of contribution:

I generated all strains except *F. novicida iglA-sfGFP* and *F. novicida iglA-sfGFP ΔpdpC ΔpdpD-anmK*. In addition, I performed and analyzed all imaging experiments. Furthermore, I helped with the *in vivo* experiments. I prepared figures and wrote the manuscript together with the other authors.

nature COMMUNICATIONS

ARTICLE

Received 22 Dec 2016 | Accepted 8 May 2017 | Published 16 Jun 2017

DOI: 10.1038/ncomms15853 OPEN

Francisella requires dynamic type VI secretion system and ClpB to deliver effectors for phagosomal escape

Maj Brodmann[1,*], Roland F. Dreier[1,*], Petr Broz[1] & Marek Basler[1]

Francisella tularensis is an intracellular pathogen that causes the fatal zoonotic disease tularaemia. Critical for its pathogenesis is the ability of the phagocytosed bacteria to escape into the cell cytosol. For this, the bacteria use a non-canonical type VI secretion system (T6SS) encoded on the *Francisella* pathogenicity island (FPI). Here we show that in *F. novicida* T6SS assembly initiates at the bacterial poles both *in vitro* and within infected macrophages. T6SS dynamics and function depends on the general purpose ClpB unfoldase, which specifically colocalizes with contracted sheaths and is required for their disassembly. T6SS assembly depends on *iglF*, *iglG*, *iglI* and *iglJ*, whereas *pdpC*, *pdpD*, *pdpE* and *anmK* are dispensable. Importantly, strains lacking *pdpC* and *pdpD* are unable to escape from phagosome, activate AIM2 inflammasome or cause disease in mice. This suggests that PdpC and PdpD are T6SS effectors involved in phagosome rupture.

[1] Focal Area Infection Biology, Biozentrum, University of Basel, Klingelbergstrasse 50/70, CH-4056 Basel, Switzerland. * These authors contributed equally to this work. Correspondence and requests for materials should be addressed to P.B. (email: petr.broz@unibas.ch) or to M.Ba. (email: marek.basler@unibas.ch).

Francisella tularensis is a Gram-negative bacterium that causes the zoonotic disease tularaemia in human and animal host. The severity of tularaemia varies depending on the route of infection and the type of strain. The *Francisella tularensis* subsp. *tularensis* is the most virulent strain and aerosol transmission of a few bacteria can cause lethal pneumonia in humans[1]. Given the low infectious dose and the severity of the infection, subsp. *tularensis* has been classified as Tier 1 select agent. The related strain *Francisella tularensis* subsp. *novicida* (*F. novicida*) has in contrast low virulence in humans, but is highly virulent in mice and thus often used as a laboratory model for tularaemia[2]. The pathogenicity of both *Francisella* species is linked to their ability to replicate in the cytosol of phagocytes, such as macrophages or dendritic cells. After phagocytosis, the bacteria shortly reside within a membrane-bound phagosome, but subsequently disrupt the phagosomal membrane and escape into the host cell cytosol, where they replicate[3].

While phagosomal escape is essential for *Francisella* intracellular replication and virulence *in vivo*, it also allows the host to mount anti-microbial and innate immune defenses. Among these are the production of type I interferons (type I IFNs) via the cGAS-STING-IRF3 axis, the production of antimicrobial guanylate-binding proteins (GBPs) and the activation of the AIM2 (absent in melanoma 2) inflammasome, which controls the release of mature IL-1β and IL-18 as well as the induction of host cell death through pyroptosis[4–11]. Interferon production and inflammasome activation require the recognition of bacterial DNA in the cytosol, and have been linked to the lysis of cytosolic *Francisella*. Mice deficient in these responses fail to control bacterial replication, resulting in a fatal disease[4–6,8,9]. *Francisella* virulence and the escape from the phagosomal compartment requires a gene cluster referred to as the *Francisella* Pathogenicity Island (FPI)[12]. Two nearly identical copies of the FPI are found in subspecies *tularensis*, *holarctica* and *mediasiatica*. The *F. novicida* genome contains only a single FPI copy[13], but features a related island called '*Francisella novicida* Island (FNI)'[14,15]. The FPI has been suggested to encode a non-canonical type VI secretion system (T6SS)[16,17], which based on gene content and phylogeny is proposed to represent a unique T6SS subtype (T6SS^{ii})[18].

T6SS is a nanomachine capable of delivery of effector proteins across target cell membranes of both bacterial and eukaryotic cells and thus is often required for bacterial competition and pathogenesis[19–23]. One of the hallmarks of this system is its highly dynamic assembly that can be visualized by live-cell fluorescence microscopy[24,25]. Assembly of T6SS starts by formation of a membrane complex formed of TssJ, TssL and TssM[26]. This is followed by assembly of a baseplate complex from TssE, TssF, TssG, TssK and also VgrG, PAAR spike as well as TssA in some organisms[27–31]. Baseplate complex then initiates assembly of a long Hcp tube and TssB, TssC (or VipA, VipB) sheath wrapped around the tube[32]. Both spike and Hcp tube can associate with effectors and are delivered together into target cells upon rapid sheath contraction[33–39].

Even though the *F. novicida* sheath is structurally similar to the sheath of canonical T6SS of *V. cholerae*[40,41], it is unclear to what extent the canonical T6SS assembly mechanisms apply to *Francisella*. The reason is that *Francisella* T6SS is highly divergent and clear homologues of several core components are missing, such as TssE, TssF and TssG. In addition, many components such as TssK, VgrG, Hcp and PAAR have only low primary sequence homology to the canonical T6SS components. For example, IglG was recently shown to be structurally similar to PAAR proteins, which are required for T6SS function[15,29]. On the other hand, the FPI cluster contains many genes of unknown function, such as *iglF*, *iglI*, *iglJ*, *pdpA*, *pdpC*, *pdpE*, *pdpD* and *anmK*. PdpA, PdpC and PdpD were identified by mass-spectrometry as secreted by *Francisella* T6SS and PdpC/PdpD were proposed to be effectors required for phagosomal escape, intracellular growth and virulence[42–48]. Interestingly, the FPI cluster lacks a homologue of an unfoldase ClpV, which is present in all canonical T6SS clusters and recycles contracted sheaths[14,24,49,50]. Overall, the non-canonical gene composition suggests a unique mode of action of the *Francisella* T6SS.

Here we show that *F. novicida* T6SS sheath cycles between assembly, contraction and disassembly. Interestingly, the vast majority of T6SS sheath assemblies initiate close or at the cell pole. We show that ClpB colocalizes with contracted sheaths and is required for sheath disassembly, however, is dispensable for

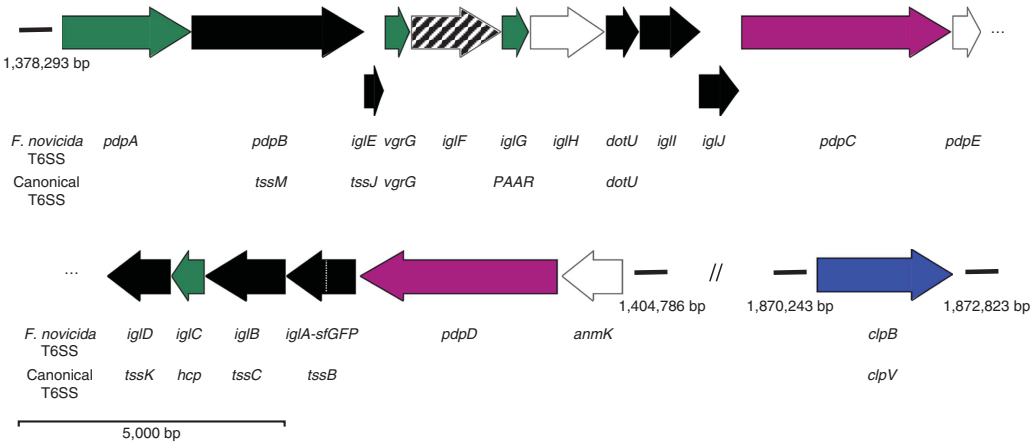

Figure 1 | A schematic overview of *Francisella* T6SS genes. Assignments for gene functions are based on previous studies cited in the main text and our observations: Black—structural components; Green—secreted structural components; Purple—secreted effectors; Blue—unfoldase; White—no clear evidence for function; Shaded—required for efficient assembly. The *Francisella* FPI (*pdpA–anmK*) nomenclature and the canonical T6SS nomenclature for the *F. novicida* genes is shown. Genes are drawn in scale.

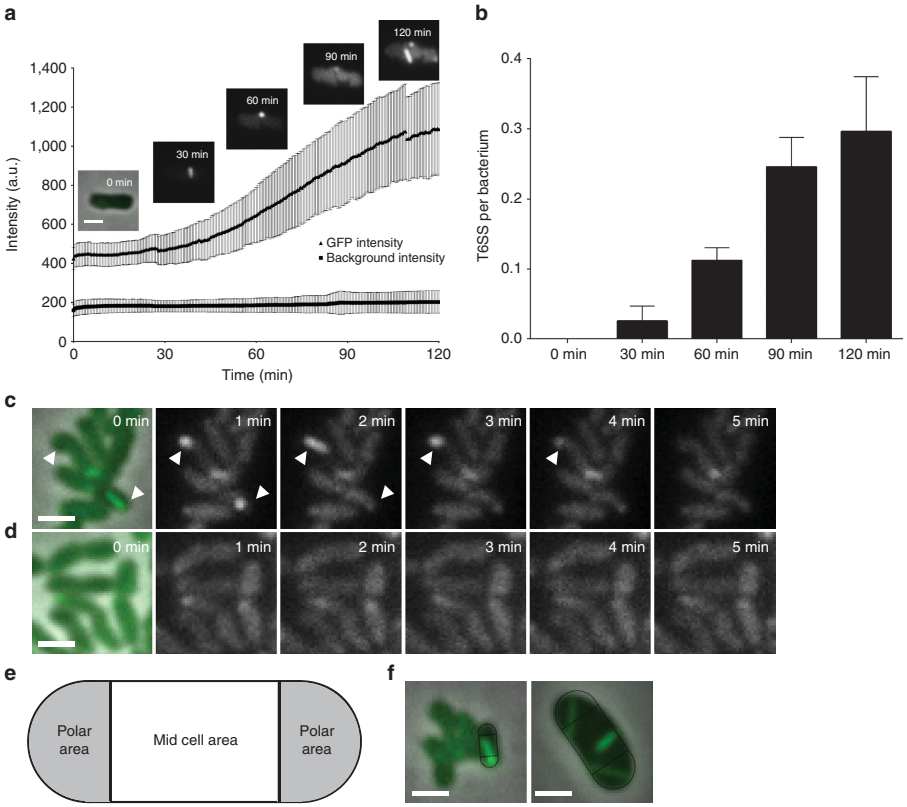

Figure 2 | Increase of GFP intensity correlates with increased number of dynamic T6SS per bacterium. (**a**) GFP signal intensities of *F. novicida* U112 *iglA-sfGFP* and fluorescence background were measured every minute for three regions of interest containing 1–30 bacteria. Two independent experiments were carried out. GFP intensity increase in a single *F. novicida* U112 *iglA-sfGFP* bacterium is shown at different time points. First image is a merge of phase contrast and GFP channels, following images represent GFP channel only. (**b**) Number of bacteria and T6SS structures were counted at time points between 0 and 120 min in three regions of interest containing 36–191 bacteria. Two independent experiments were carried out. Error bars represent s.d. (**c**,**d**) IglA-sfGFP localization in *F. novicida* U112 *iglA-sfGFP* wild type (**c**) and Δ*pdpB* (**d**). Arrowheads indicate T6SS sheath assembly and contraction. First image is a merge of phase contrast and GFP channels, following images represent GFP channel only. (**e**) Model for quantification of T6SS assembly position. Pole area was determined as 50% of total surface area equally distributed to both poles. (**f**) Model from **e** applied to *F. novicida* U112 *iglA-sfGFP* and *V. cholerae* 2740-80 *vipA-msfGFP*. Merge of phase contrast and GFP channels is shown. For **a**,**c**,**d** and **f** 3.3 × 3.3 μm fields of view are shown. Scale bar, 1 μm.

sheath assembly and contraction. T6SS dynamics and function depends on *iglF*, *iglG*, *iglI* and *iglJ*, while *pdpC* and *pdpD* are specifically required for phagosomal escape and virulence in a mouse model of tularaemia, but also for the engagement of the host innate immune response.

Results

***Francisella* T6SS is dynamic and assembles on the cell pole.** *Francisella* T6SS has a non-canonical gene composition and lacks ClpV suggesting unique mode of action (Fig. 1). To understand *Francisella* T6SS assembly and function, we searched for conditions that would allow us to image subcellular localization of TssB homologue IglA. We have serendipitously discovered that *F. novicida iglA-sfGFP* grown to an exponential phase in BHI media induced expression of IglA-sfGFP upon prolonged incubation on an agarose pad under a glass coverslip. Importantly, the increase in expression correlated with an increase in number of IglA-sfGFP structures detected in the bacteria (Fig. 2a,b). Time-lapse imaging at a rate of 20 frames per minute showed that IglA-sfGFP structures extended across the bacteria within 30 and 120 s with assembly speeds between 5 and 15 nm s^{-1}. After full assembly, the IglA-sfGFP structures immediately contracted to approximately half of their original length and became brighter (Fig. 2c; Supplementary Fig. 1a; Supplementary Movies 1 and 4). After contraction, the sheath structures were disassembled during the next ∼2–3 min (Fig. 2c; Supplementary Fig. 1a). The average fluorescence intensity of the bacteria before and after one cycle of assembly, contraction and disassembly was similar, suggesting that IglA-sfGFP remained stable and folded during this cycle (Supplementary Fig. 1b). Importantly, no IglA-sfGFP structures were detected in the bacteria lacking the TssM homologue encoded by *pdpB* (Fig. 1), suggesting that assembly of IglA-sfGFP structures is dependent

on the function of the whole T6SS (Fig. 2d; Supplementary Movie 2). The dynamics of IglA-sfGFP localization is similar to that of VipA-sfGFP in *V. cholerae* and is consistent with the fact that IglA and IglB form a structure closely resembling *V. cholerae* T6SS sheath[25,40,41].

Interestingly, we also noticed that IglA-sfGFP sheaths were preferentially assembled from the bacterial pole and thus often formed structures as long as the bacterial length. To quantify the preference for subcellular localization, we divided the bacterial perimeter equally to a polar region and a mid-cell region (Fig. 2e) and counted assemblies initiated in these two equally large regions. Out of 851 assemblies, 821 assemblies (96.5%) were initiated in the polar region. As a control, we performed the same analysis for *V. cholerae* and show that only 53.8% (425 from 790) assemblies were initiated in the polar region (Fig. 2f) as expected for assemblies without preferred localization[24,25,51]. Taken together, we show that *F. novicida* assembles a dynamic T6SS sheath on the cell poles and that the sheath cycles through assembly, contraction and disassembly similarly to what was previously described for other canonical T6SSs.

ClpB is required for disassembly of contracted sheaths. The fact that contracted sheaths were quickly disassembled without apparent degradation of IglA-sfGFP suggested that *F. novicida* recycles contracted sheaths using a mechanism similar to the canonical ClpV-mediated sheath disassembly. The closest homologue of *V. cholerae* ClpV in *F. novicida* genome is ClpB (FTN_1743) (36% sequence identity). Interestingly, *clpB* was previously shown to be required for survival of various stresses[52] but also essential for intracellular replication and virulence of *F. novicida*[53,54].

Here we show that *F. novicida* lacking *clpB* mainly contained bright IglA-sfGFP foci (Fig. 3a). Time-lapse imaging showed that the *F. novicida* Δ*clpB* occasionally assembled new sheaths with kinetics similar to that of the parental strain but after contraction, the sheaths were never disassembled and remained intact in the bacteria (Fig. 3a,b; Supplementary Movies 1 and 4). Such assembly was still dependent on functional T6SS, as no sheath extensions and contractions were detected in *F. novicida* Δ*clpB*/*pdpB*. However, some bright, non-dynamic IglA-sfGFP foci were detected in the absence of both *clpB* and *pdpB* (Supplementary Fig. 2a; Supplementary Movie 2). This indicates that activity of ClpB is required for recycling of contracted sheaths, however, in case of a defect in ClpB function, some non-dynamic IglA-sfGFP foci may form also in the absence of a fully functional T6SS.

To test directly the role of ClpB in disassembly of the contracted sheaths, we introduced *clpB-mCherry2* fusion to the native locus on the chromosome of the *iglA-sfGFP* or wild-type strain. Fusing mCherry2 to ClpB had no influence on the ability of *F. novicida* to survive heat shock indicating that such fusion is fully functional (Supplementary Fig. 2d). ClpB-mCherry2 subcellular localization cycled between uniform cytosolic and punctate localization and this dynamics was dependent on the presence of *pdpB* (Supplementary Fig. 2b,c, Supplementary Movie 3). When IglA-sfGFP and ClpB-mCherry2 were imaged simultaneously, ClpB spots colocalized specifically with the contracted sheaths (Fig. 3c; Supplementary Movies 3 and 5).

F. novicida uses the T6SS to escape from phagosome of cells like macrophages and consistently IglA-sfGFP spots could be detected in intracellular bacteria, implying the assembly of T6SS sheaths[40]. To test whether sheath assembly is dynamic under physiological conditions during infection, we infected primary murine bone marrow-derived macrophages (BMDMs) from wild-type C57BL/6 mice for 1 h with exponentially grown *F. novicida*. After washing away non-phagocytosed bacteria, the infected cells were fixed, stained with phalloidin and anti-*F. novicida* LPS antibody and analysed by super resolution structured illumination microscopy (SIM) to determine the relative localization of actin, bacteria and T6SS sheaths (Fig. 4a,b). This analysis confirmed that *F. novicida* reside inside the macrophage and assemble T6SS sheaths.

Next, we imaged IglA-sfGFP and ClpB-mCherry2 dynamics within *F. novicida* in live macrophages and observed that the sheaths cycled through assembly, contraction and disassembly. Importantly, ClpB-mCherry2 dynamically localized into spots that colocalized with the contracted sheaths, suggesting that ClpB is responsible for disassembly of the contracted sheaths also within phagosomes of infected macrophages (Fig. 4c; Supplementary Movie 6). In total, we analysed 30 sheath assembly, contraction and disassembly events inside live macrophages and all of the assemblies originated from the cell pole (Fig. 4c; Supplementary Movie 6). Together, these data suggest that sheath dynamics and subcellular localization observed during imaging of *F. novicida* on agarose pads is similar to that of the sheath in the bacteria residing inside of live macrophages.

To determine the importance of ClpB for *F. novicida* pathogenesis, we infected BMDMs with *F. novicida* wild-type, Δ*pdpB* and Δ*clpB* and determined the percentage of phagosomal and cytosolic bacteria using a phagosome-protection assay based on selective permeabilization of the plasma membrane with digitonin[9]. *F. novicida* Δ*clpB* had a significant defect in phagosomal escape at 4 h post infection, similarly to bacteria lacking the essential structural component PdpB (Fig. 3d; Supplementary Fig. 3a). Consistent with reduced cytosolic localization, we observed significantly reduced levels of pyroptosis induction and cytokine release in LPS-primed BMDMs infected for 10 h with *F. novicida* Δ*pdpB* and Δ*clpB*, while the wild-type strain elicited strong immune responses (Fig. 3e). Finally, we evaluated the role of ClpB *in vivo* in a mouse model of tularaemia. We infected age- and sex-matched wild-type C57BL/6 mice subcutaneously with 10^4 colony-forming units (CFUs) of *F. novicida* wild-type, Δ*pdpB* and Δ*clpB* and measured the bacterial burden at 2 days post infection. Mice infected with *F. novicida* Δ*clpB* displayed significantly reduced bacterial counts in the liver and spleen as compared to the mice infected with *F. novicida* wild type, and in many cases no bacteria could be recovered, similarly to what was observed with *F. novicida* Δ*pdpB* (Supplementary Fig. 3b). Overall these results indicate that ClpB acts as an unfoldase for the FPI-encoded T6SS sheath, and that its activity is essential for T6SS dynamics and consequently *F. novicida* virulence.

Differential requirement of FPI genes for sheath dynamics. Almost all FPI genes were shown to be required for intracellular replication probably due to a lack of phagosomal escape, however, many genes of the FPI cluster have no known homologues or were not characterized in detail[14]. Importantly, both structural components of T6SS as well as putative effectors secreted by T6SS are in principle essential for overall T6SS function, however, effectors may be to a certain degree dispensable for T6SS assembly. To provide an insight into which FPI genes are required for assembly of T6SS and which may potentially encode secreted effectors, we generated in-frame deletions of genes for which we were unable to predict function based on homology to known canonical T6SS components (Fig. 1). IglA-sfGFP subcellular localization was then imaged in those strains under the same conditions as used before for the parental strain.

In Δ*iglF* and Δ*iglG* strains, we detected on average 1 dynamic sheath assembly per 400 and 500 cells, respectively, in 5 min (Supplementary Movie 2). This suggests that IglF and IglG may

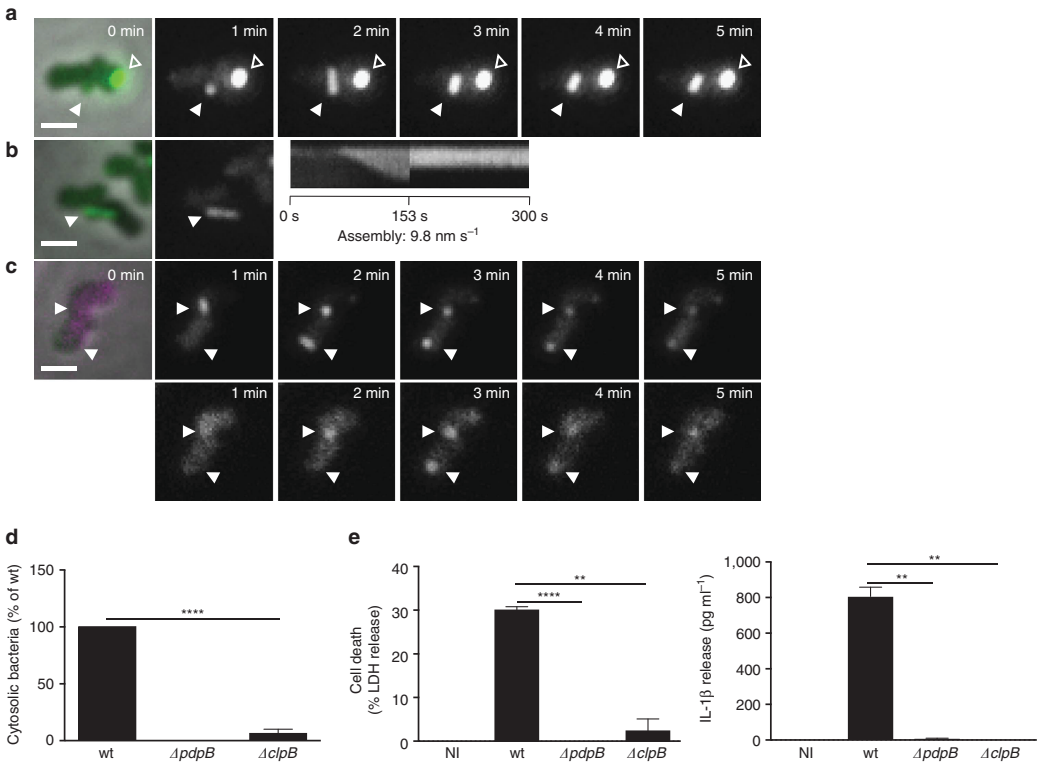

Figure 3 | Phagosomal rupture and AIM2 inflammasome activation is dependent on disassembly of T6SS sheaths by ClpB. (**a**) T6SS dynamics in *F. novicida* U112 *iglA-sfGFP ΔclpB*. Arrowheads indicate T6SS sheath assembly, contraction and location of sheath after contraction. Empty arrowheads indicate non-dynamic IglA-sfGFP foci. First image is a merge of phase contrast and GFP channels, following images represent GFP channel only. (**b**) Kymogram of *F. novicida* U112 *iglA-sfGFP ΔclpB* over 5 min (3 s per pixel). First image is a merge of phase contrast and GFP channels, following images represent GFP channel only. (**c**) Colocalization of ClpB-mCherry2 with IglA-sfGFP (arrows) in *F. novicida* U112 *iglA-sfGFP clpB-mCherry2*. First image is a merge of phase contrast, GFP and mCherry channels, following images represent GFP channel (upper panel) and mCherry channel (lower panel). (**d**) Quantification of cytosolic bacteria in unprimed wild-type BMDMs 4 h after infection with *F. novicida* U112 *iglA-sfGFP* wild type, *ΔpdpB* or *ΔclpB* (normalized to wild type). (**e**) Release of LDH and mature IL-1β from primed wild-type BMDMs 10 h after infection with *F. novicida* U112 *iglA-sfGFP* wild type, *ΔpdpB or ΔclpB* (NI—noninfected control). (**a**–**c**) 3.3 × 3.3 μm fields of view are shown. Scale bars, 1 μm. (**d**,**e**) Data are pooled from three independent experiments (**d**) (mean and s.d. are shown) or representatives of three independent experiments (**e**) (mean and s.d. of triplicate wells are shown). $^{**}P<0.01$ and $^{****}P<0.0001$ (two-tailed unpaired *t*-test with Welch's correction).

be required for efficient initiation of T6SS assembly. On the other hand, *iglI* and *iglJ* are essential for sheath assembly as no sheath assemblies were detected in more than 1,000 cells in 5 min even though IglA-sfGFP was expressed to the same level as in the parental strain (Fig. 5a; Supplementary Movie 2). Consistent with the defect in T6SS assembly, we found that Δ*iglF*, Δ*iglG*, Δ*iglI* and Δ*iglJ* strains were unable to escape into the cytosol of the infected macrophages, and consequently failed to activate cytosolic innate immune signalling (Fig. 5b,c). We cannot completely rule out the possibility that the observed phenotypes of mutants are due to polar effects on expression of other T6SS genes. However, defect in intracellular growth was previously successfully complemented for *iglF*, *iglG* and *iglI* genes[55].

Single deletion of *pdpE*, *pdpC*, *pdpD* and *anmK* or deletion of both *pdpD* and *anmK* (Δ*pdpD*/*anmK*) or *pdpC* and *pdpD* (Δ*pdpC*/*pdpD*) had no significant influence on sheath dynamics or localization (Fig. 6a; Supplementary Movie 1). Only deletion of all three genes *pdpC*, *pdpD* and *anmK* in the same strain decreased frequency of sheath assembly by 30% from an average of one structure per three cells to about one structure per five cells (Supplementary Fig. 4a). Nevertheless, sheath assemblies in Δ*pdpC*/*pdpD*/*anmK* still preferentially localized to the cell pole, assembled with a similar speed and cycled through extension, contraction and disassembly like in the parental strain (Supplementary Fig. 4b,c; Supplementary Movie 1). Importantly, Δ*pdpE* and Δ*pdpC*/*pdpD*/*anmK* assembled sheaths with dynamics undistinguishable from the parental strain within infected macrophages (Supplementary Fig. 5e,f). In conclusion, our analysis allowed us to identify FPI genes (*iglF*, *iglG*, *iglI* and *iglJ*) essential for T6SS assembly and a distinct set of FPI genes (*pdpE*, *pdpC*, *pdpD* and *anmK*) that are dispensable for T6SS assembly.

PdpC and PdpD are required for phagosomal escape. To test whether *pdpE*, *pdpC*, *pdpD* and *anmK* genes are required for the escape of *F. novicida* from phagosome, we infected BMDMs with

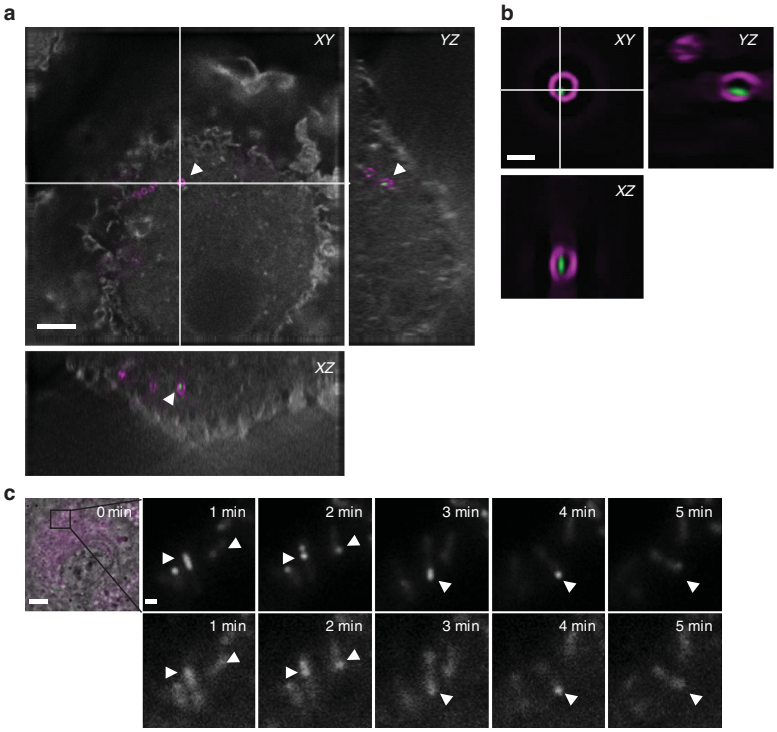

Figure 4 | T6SS dynamics in bone marrow-derived macrophages (BMDMs). (**a**) Merged wide field image and orthogonal view of BMDMs infected for 1 h with *F. novicida* U112 *iglA-sfGFP clpB-mCherry2*; in grey: actin staining, in magenta: LPS staining, in green: IglA-sfGFP. 41 × 41 µm field of view, scale bar, 5 µm. (**b**) Close up and orthogonal SIM view of bacterium highlighted with arrowheads in **a**; magenta: LPS staining, green: IglA-sfGFP. 5.1 × 5.1 µm field of view, scale bar, 1 µm. (**c**) Time-lapse images of unprimed wild-type BMDMs infected with *F. novicida* U112 *iglA-sfGFP clpB-mCherry2* for 1 h. First image consists of merged phase contrast, GFP and mCherry channels. 30 × 30 µm field of view is shown. Scale bar, 5 µm. Close ups consist of GFP channel (upper panel) and mCherry channel (lower panel). Close ups show 5 × 5 µm. Scale bar, 1 µm. Arrowheads indicate T6SS sheath assembly, contraction and location of sheath after contraction.

F. novicida Δ*pdpE*, Δ*anmK*, Δ*pdpC*, Δ*pdpD*, Δ*pdpD*/*anmK* or Δ*pdpC*/*pdpD*/*anmK* and determined the percentage of phagosomal and cytosolic bacteria compared to wild-type and Δ*pdpB* bacteria as outlined above (Supplementary Fig. 3a). Interestingly, we found that deletion of *pdpC* resulted in a very strong defect in phagosomal escape in comparison to wild-type bacteria, although the reduction was smaller than with bacteria lacking the structural component PdpB (Fig. 6b). *F. novicida* Δ*pdpD* and Δ*pdpD*/*anmK* also showed a defect in phagosomal escape, which was however less severe than the phenotype of a *pdpC* or *pdpB* deletion. No significant difference in phagosomal escape was observed between Δ*pdpD* and Δ*pdpD*/*anmK* strains, indicating that AnmK plays no role in phagosomal escape, consistent with the finding that phagosomal escape of the Δ*anmK* strain was indistinguishable from the wild-type strain (Fig. 6b). To determine whether the effect of a *pdpC* and *pdpD* deletion was additive, we generated a strain lacking *pdpC*, *pdpD* and also *anmK*. Interestingly, bacteria lacking *pdpC*/*pdpD*/*anmK* were unable to escape from the phagosomal compartment similarly to the Δ*pdpB* strain. In contrast, deletion of *pdpE* had no significant effect on phagosomal escape (Fig. 6b).

Next, we tested the role of *pdpE*, *pdpC*, *pdpD* and *anmK* in cytosolic innate immune detection of *F. novicida*. Consistent with the reduced level of cytosolic localization, we found that *F. novicida* Δ*pdpC* and Δ*pdpC*/*pdpD*/*anmK* induced significantly lower levels of type I IFN production in unprimed BMDMs infected for 10 h at an MOI of 100 (Supplementary Fig. 5c). The triple mutant Δ*pdpC*/*pdpD*/*anmK* had the most severe phenotype and only elicited IFN levels in the range of the Δ*pdpB* strain (Supplementary Fig. 5c).

Since type I IFNs control the activation of the AIM2 inflammasome during *F. novicida* infection[5], we examined the level of inflammasome activation in LPS-primed infected macrophages at different time points (Fig. 6c; Supplementary Fig. 5a). While infection with *F. novicida* lacking *pdpC* or *pdpD* resulted in significantly reduced levels of inflammasome activation, only the deletion of both *pdpC* and *pdpD* completely abrogated cell death induction and cytokine production in infected macrophages, which was consistent with the reduced levels of cytosolic localization and type I IFN induction in macrophages infected with mutants lacking both proteins (Fig. 6b; Supplementary Fig. 5c). Cell death induction and cytokine production in infected macrophages was unchanged between cells infected with wild-type and *ΔanmK* bacteria indicating that AnmK is not involved in modulating inflammasome activation (Fig. 6c). Consistently, cell death and cytokine production was comparable between cells infected with *F. novicida* Δ*pdpC*/*pdpD* and *Δpdp*C/*pdpD*/*anmK* or *F. novicida* Δ*pdpD* and Δ*pdpD*/*anmK*. Importantly, the observed

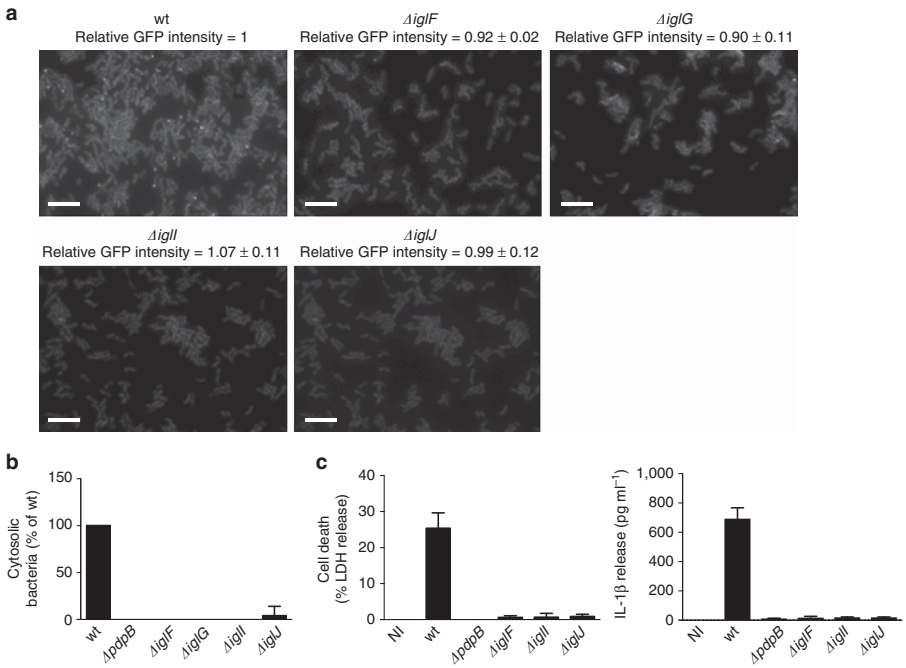

Figure 5 | Identification of genes required for assembly and function of *F. novicida* T6SS. (**a**) IglA-sfGFP localization in *F. novicida* U112 *iglA-sfGFP* wild type, *ΔiglF*, *ΔiglG*, *ΔiglI* and *ΔiglJ*. The GFP channel is shown. The numbers above the images represent the ratio of average GFP intensity of mutants compared to the parental strain with s.d. The average GFP intensities were quantified in three independent experiments. Thirty bacteria were analysed per experiment; 39 × 26 μm fields of view are shown. Scale bars, 5 μm. (**b**) Quantification of cytosolic bacteria in unprimed wild-type BMDMs 4 h after infection with *F. novicida* U112 *iglA-sfGFP* wild type, *ΔpdpB*, *ΔiglF*, *ΔiglG*, *ΔiglI* or *ΔiglJ* (normalized to wild type). (**c**) Release of LDH and IL-1β from primed wild-type BMDMs 10 h after infection with *F. novicida* U112 *iglA-sfGFP* wild type, *ΔpdpB*, *ΔiglF*, *ΔiglI* or *ΔiglJ* (NI—noninfected control). (**b**,**c**) Data are pooled from three independent experiments (**b**) (mean and s.d. are shown) or are representatives of three independent experiments (**c**) (mean and s.d. of triplicate wells are shown).

changes in inflammasome activation were independent of macrophage priming, since unprimed macrophages infected with wild-type or mutant *F. novicida* responded similarly (Supplementary Fig. 5b). Deletion of *pdpE* had no significant effect on the level of type I IFN induction, pyroptosis and cytokine release (Supplementary Fig. 5a–c).

Previous work has implicated the FPI in intracellular replication[55], therefore, we also examined intracellular replication of wild-type or mutant *F. novicida*. We monitored growth over 24 h of infection in BMDMs lacking the inflammasome adaptor protein ASC as they fail to trigger pyroptosis in response to bacterial infection[8]. *F. novicida* wild-type and Δ*pdpE* replicated over the course of the infection (Supplementary Fig. 5d), while bacteria that lacked a dynamic T6SS (Δ*pdpB* or Δ*clpB*) or bacteria that had a dynamic T6SS, but were deficient in phagosomal escape (Δ*pdpC* or Δ*pdpC*/*pdpD*/*anmK*), were cleared over the course of the infection. Consistent with reduced phagosomal escape, *pdpD*/*anmK*-deficient bacteria also displayed a reduced rate of replication compared to wild-type bacteria, however, the difference was not significant.

Finally, we examined the role of potential T6SS effectors *in vivo*. Age- and sex-matched wild-type C57BL/6 mice were infected subcutaneously with 10^4 CFUs of *F. novicida* wild-type or strains deficient for the putative effectors, and the bacterial burden in the liver and spleen as well as serum IL-18 levels were assessed at 2 days post infection (Fig. 6d,e). The bacterial burden closely correlated with phagosomal escape, in that a partial reduction in virulence could be observed in Δ*pdpC* and Δ*pdpD*/*anmK*-infected mice. Deletion of *pdpC* alone had a stronger effect than deletion of *pdpD*/*anmK* although this difference was only significant in the liver. Deleting all three potential effectors, Δ*pdpC*/*pdpD*/*anmK*, rendered the bacteria largely avirulent, similarly to the deletion of the T6SS structural component *pdpB*. Consistent with the reduced levels of inflammasome activation *in vitro* (Fig. 6c; Supplementary Fig. 5a), we found that deletion of *pdpB*, *pdpC*, *pdpD*/*anmK* or *pdpC*/*pdpD*/*anmK* resulted in significantly lower levels of serum IL-18. A deficiency in *pdpE* appeared to have no effect on virulence or host response, since infection with *F. novicida* Δ*pdpE* resulted in bacterial burden and cytokine levels that were comparable to infections with *F. novicida* wild type (Fig. 6d,e). In summary, these results confirm previous studies indicating that PdpC and PdpD are T6SS-secreted effectors. Moreover, we show that PdpC and PdpD are dispensable for T6SS dynamics and specifically facilitate the escape of *F. novicida* from the phagosome into the host cell cytosol and therefore are essential for *Francisella* virulence.

Discussion

We show here that *Francisella* T6SS sheath is under certain conditions highly dynamic and ClpB is necessary for sheath disassembly. Since ClpB-mCherry2 specifically colocalizes with

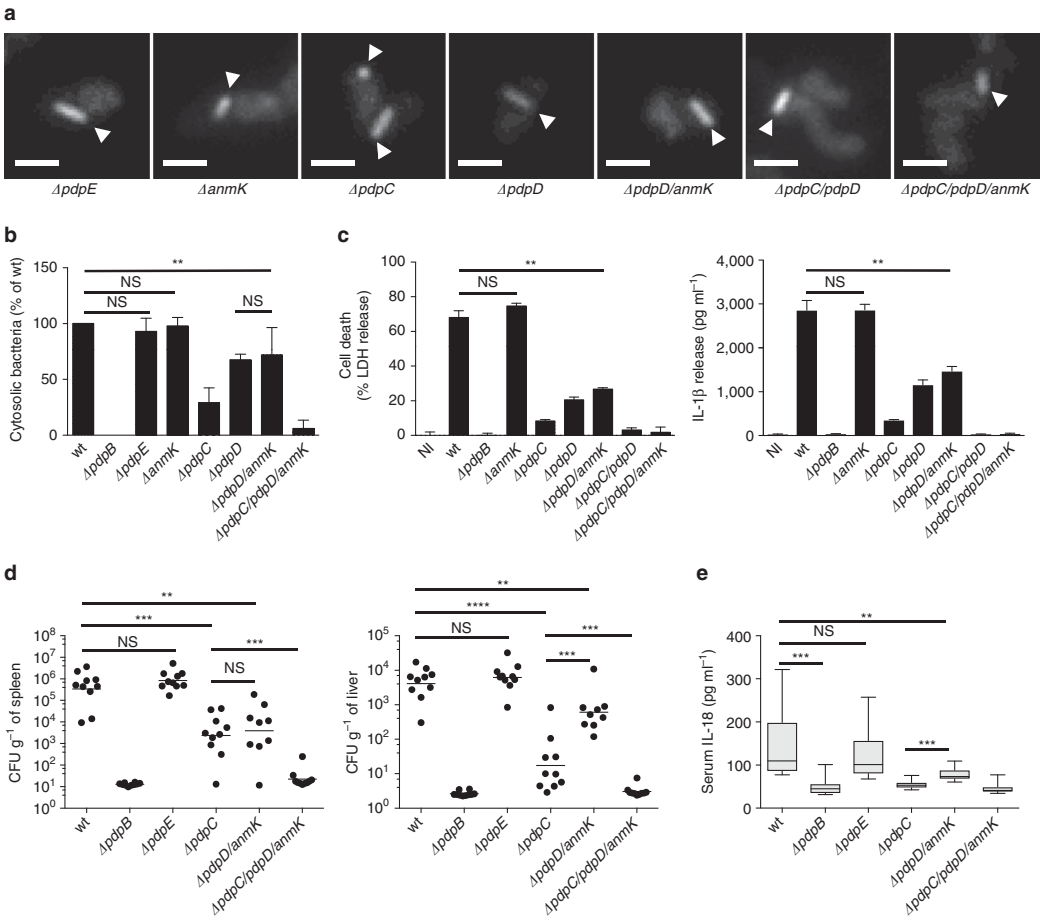

Figure 6 | Contribution of uncharacterized FPI genes to T6SS function. (**a**) T6SS sheath assembly (arrowheads) in *F. novicida* U112 *iglA-sfGFP* Δ*pdpE*, Δ*anmK*, Δ*pdpC*, Δ*pdpD*, Δ*pdpD/anmK*, Δ*pdpC/pdpD* and Δ*pdpC/pdpD/anmK*. GFP channel and 3.3 × 3.3 μm fields of view are shown. Scale bars, 1 μm. (**b**) Quantification of cytosolic bacteria in unprimed wild-type BMDMs 4 h after infection with *F. novicida* U112 *iglA-sfGFP* wild type, Δ*pdpB*, Δ*pdpE*, Δ*anmK*, Δ*pdpC*, Δ*pdpD*, Δ*pdpD/anmK* or Δ*pdpC/pdpD/anmK* (normalized to wild type). (**c**) Release of LDH and IL-1β from primed wild-type BMDMs 10 h after infection with *F. novicida* U112 *iglA-sfGFP* wild type, Δ*pdpB*, Δ*anmK*, Δ*pdpC*, Δ*pdpD*, Δ*pdpD/anmK*, Δ*pdpC/pdpD* or Δ*pdpC/pdpD/anmK* (NI—noninfected control). (**d**,**e**) Bacterial burden (as colony-forming units (CFUs) per gram tissue) in the spleen and liver (**d**) and serum IL-18 levels (**e**) of wild-type C57BL/6JRj mice infected subcutaneously for 2 days with 1×10^4 *F. novicida* U112 *iglA-sfGFP* wild type, Δ*pdpB*, Δ*pdpE*, Δ*pdpC*, Δ*pdpD/anmK* and Δ*pdpC/pdpD/anmK*. Small horizontal lines indicate the mean. Each symbol represents an individual mouse ($n = 5$ per experiment). Graphs show pooled data from two independent biological replicates with $n = 5$ per experiment ($n = 10$ total per group); small horizontal lines indicate the mean. (**b**–**e**) Data are pooled from three independent experiments (**b**) (mean and s.d. are shown) or two independent experiments (**d**,**e**) or are representatives of three independent experiments (**c**) (mean and s.d. of triplicate wells are shown). $^{**}P < 0.01$, $^{***}P < 0.001$ and $^{****}P < 0.0001$ (two-tailed unpaired *t*-test with Welch's correction (**b**,**c**) or Mann–Whitney test (**d**,**e**)).

the contracted sheaths, our data suggest that ClpB is directly involved in *Francisella* sheath disassembly similarly to ClpV in canonical T6SS (refs 24,49,50,56,57). Interestingly, *Francisella* ClpB was also shown to alter the immune response *in vivo*[58] and to be required for heat shock survival[52]. However, we show here that T6SS activity is dispensable for heat shock survival (Supplementary Fig. 2d). This suggests that, in contrast to canonical T6SS where ClpV is apparently solely dedicated to sheath disassembly, *Francisella* ClpB has a dual role. This raises the question how ClpB recognizes different substrates and whether a specific adaptor protein is required to recognize contracted sheaths similarly to adaptor proteins that recognize substrates for AAA+-mediated unfolding[59–62]. We show that ClpB is important for *F. novicida* virulence, which is consistent with what was shown previously[52–54,58]. Since all virulence related phenotypes of *clpB*-negative strain correlated with the phenotypes of the other strains with impaired T6SS dynamics (Fig. 3; Supplementary Figs 2 and 3), we propose that *in vivo* ClpB is mainly important for T6SS sheath disassembly. However, refolding of substrates unrelated to T6SS may be required to

survive certain stresses, which *Francisella* encounter during pathogenesis.

Detailed analysis of subcellular localization of dynamic T6SS sheath shows that *Francisella* T6SS assembles on the bacterial cell poles both *in vitro* as well as during infection of macrophages (Figs 2e,f and 3c; Supplementary Fig. 5e,f). Interestingly, similarly to what we show here for *Francisella*, ClpV-5 from T6SS-5 of *Burkholderia thailandensis* was found to preferentially localize to spots on bacterial poles[63]. Those spots were however less dynamic than ClpB spots in *Francisella* and thus it remains to be directly tested if assembly of T6SS-5 of *B. thailandensis* indeed initiates at the poles. Interestingly, both T6SS-5 of *B. thailandensis* and *Francisella* T6SS are required for manipulation of the eukaryotic cells after bacterial internalization. However, unlike in *Francisella*, T6SS-5 of *B. thailandensis* is only required for formation of multinucleated giant cells after bacteria escape from endosomes using T3SS[63–67]. Since T6SS sheaths almost always assemble as long as the bacteria, one possible advantage of the polar localization could be that the sheaths assembled from the pole in rod shaped bacteria would be generally longer than the sheaths assembled from the side of the cells. Given that the T6SS sheaths only contract to about half of their extended size[25], longer sheaths may increase the distance to which T6SS can deliver effectors. Interestingly, restricted subcellular localization was shown to decrease T6SS efficiency in inter-bacterial competitions despite increased overall activity[51]. However, since *F. novicida* is completely surrounded by phagosome membrane, restricted directionality of T6SS assembly should have no consequences for delivery of effectors to the host cell. In addition, polar localization of T6SS may increase chances of puncturing phagosomal membranes, as those may be physically closer to the bacterial poles when bacteria are in a tight membrane compartment. As it was shown previously for inter-bacterial interactions, proper aiming of the T6SS apparatus at the target bacteria increases efficiency of substrate translocation[37,51].

The primary function of the *Francisella* T6SS is to promote the escape of *Francisella* from the phagosome. We show that phagosome escape depends entirely on PdpC and PdpD, which are dispensable for T6SS assembly and dynamics (Fig. 6a,b; Supplementary Movie 1), suggesting that these proteins function as effectors necessary for phagosomal escape. It is also possible that PdpD and PdpC are required for activity or secretion of yet uncharacterized T6SS effectors to promote phagosomal escape, however previous work by Eshraghi *et al.*[42] has shown that *F. novicida* PdpC and PdpD are released by the T6SS in an *in vitro* secretion assay, supporting the hypothesis that these proteins function as secreted effectors in the target cell. Moreover, *F. tularensis* and *F. holarctica* lacking *pdpC* are unable to escape from the phagosome, induce cytotoxicity and replicate intracellularly, and they are avirulent in a mouse model of tularaemia[43,44,46–48]. These observations support our conclusions that PdpC contribute to *Francisella* virulence, independent of the *Francisella tularensis* subspecies. Whereas *pdpC* is conserved in all subspecies of *Francisella tularensis*, *pdpD* is differentially encoded[45]. Therefore, PdpD might have subspecies-specific virulence related functions.

PdpC and PdpD share no homology with known effectors or pore forming toxins, such as Listeriolysin O, type C phospholipases or phenol-soluble modulins, that allow other cytosolic bacteria (*Listeria monocytogenes*, *Shigella flexneri*, *Burkholderia thailandensis or Staphylococcus aureus*) to escape from the phagosome, and thus might represent a novel class of effectors with membranolytic function[68,69]. The exact mechanism of how these effectors destabilize the phagosomal membrane and if this results in the recruitment of galectin-8, a marker of ruptured vacuoles that recruits antimicrobial autophagy[70], remains to be analysed. The *Francisella* O-antigen allows the bacteria to avoid ubiquitination and uptake into LC3-positive compartments[71], but whether *Francisella* can actively inhibit or escape autophagy by injected effectors, as reported for *Listeria* and *Shigella* is unknown[72].

PdpE and AnmK, which are dispensable for T6SS assembly and phagosomal escape (Fig. 6a,b), might be effectors whose function is required once the bacteria enter the cytosol. However, their contribution to overall bacterial replication and virulence *in vivo* is minor (Fig. 6d,e; Supplementary Fig. 5d). In addition, OpiA and OpiB, encoded outside of the FPI cluster, were recently identified as T6SS secreted proteins, however, their contribution to intracellular replication is also minimal in comparison to the effects of a *pdpC* or *pdpD* deletion[42]. It is possible that these effectors have tissue-specific functions, or that they are required for *Francisella* replication in amoeba or within arthropod hosts[73,74].

Live-cell imaging of T6SS sheath dynamics suggests that IglF, IglG, IglI and IglJ are putative structural components required for T6SS assembly in *Francisella* (Fig. 5a; Supplementary Movie 2). These proteins could be homologues of components of canonical T6SS baseplate, which are difficult to identify using homology modelling[14,75] (Fig. 1). However, it is also conceivable that some of these proteins may be secreted effectors or be required for effector secretion, because deletion of certain effectors decreases T6SS function in *V. cholerae*[37,76]. Nonetheless, our finding that the dynamics of *Francisella* T6SS is possible to image *in vitro* will help to dissect the assembly of this non-canonical T6SS and to differentiate between structural components and translocated substrates. Further analysis of the structural components will reveal principles of T6SS evolution and defining the molecular mechanisms by which *Francisella* effectors modulate host cell signalling will significantly contribute to our understanding of *Francisella* virulence.

Methods

Bacterial strains and growth conditions. *Francisella tularensis* subsp. *novicida* strain U112 (hereafter *F. novicida*) and the derivative strains were grown at 37 °C with aeration in brain heart infusion (BHI) medium supplemented with 0.2% L-cysteine (Sigma) and appropriate antibiotics. Antibiotic concentrations used were 100 μg ml^{-1} ampicillin (AppliChem) or 15 μg ml^{-1} kanamycin (AppliChem). A detailed strain list can be found in Supplementary Table 1. For infection with *F. novicida*, BHI medium was inoculated with bacteria from BHI agar plate (supplemented with 0.2% L-cysteine (Sigma) and appropriate antibiotics) and were grown overnight at 37 °C with aeration.

Bacterial mutagenesis. All in-frame deletions were generated by homologous recombination using the suicide vector pDMK3 as previously described[77]. A list of plasmids, primers as well as remaining peptides encoded by deleted genes can be found in Supplementary Table 2. To obtain single colonies after recombination, bacteria were grown overnight at 37 °C on Mueller-Hinton agar (MHA) supplemented with 0.1% D-glucose (Millipore), 0.1% FCS (BioConcept), 100 μg ml^{-1} ampicillin (AppliChem) and 0.1% L-cysteine (Sigma) (hereafter MHA plate). Cloning product sequences were verified and chromosomal mutations were tested by PCR using primers located outside of the replaced region. Sites of homologous recombination of the chromosomal mutations were verified by sequencing.

Heat shock survival assay. Heat shock survival assay was adapted from ref. 52. In brief, bacteria were grown overnight as described above, diluted 1:40 in BHI medium and grown for 3 h at 37 °C with aeration. Then bacteria were diluted 1:10 in 250 μl BHI in a 1.5 ml tube and incubated in a water bath at 50 °C for 0, 15 or 30 min. At each time point the bacteria were transferred on ice and serial dilutions were plated on MHA plates. The next day, CFUs were counted and the concentration of surviving bacteria was calculated.

Fluorescence microscopy. Procedures and settings to detect a fluorescence signal in *F. novicida* were employed as previously described[37,41]. All imaging was carried out at 37 °C and humidity was regulated to 95% using a T-unit (Oko-lab). The exposure time was set to 150 ms for all channels. For bacterial imaging on agarose pads, *F. novicida* strains from BHI plate were washed once with BHI, diluted

1:40 in BHI medium and grown at 37 °C with aeration for 3–4 h. Bacteria from 1 ml culture were re-suspended in 50–100 µl phosphate-buffered saline (PBS), spotted on a pad of 1% agarose in PBS, covered with a cover glass (Roth) and either imaged directly or incubated at 37 °C for 1 h before imaging. Images were collected every 3 s for T6SS assembly speed quantification and every 30 s for assessment of T6SS dynamics. For imaging of infected macrophages, BMDMs were seeded onto cover glass (VWR) in 24-well plates at a density of 1.5×10^5 cells per well and infected with *F. novicida* at a multiplicity of infection of 100 in 1 ml OptiMEM (Life Technologies) as described below. Thirty minutes post infection, the BMDMs were washed three times with OptiMEM and the cover glass was mounted on a pad of 1% agarose in PBS BMDMs facing down. Images were collected every 30 s for assessment of T6SS dynamics.

Image analysis. Fiji[78] was used for all image analysis and manipulations as described previously[37,51]. The 'Time Series Analyzer V3.0' plugin was used for quantification of GFP signal intensity. For comparison of GFP signal intensities of mutants and wild type, only bacteria without assembled T6SS structures were considered. For quantification of T6SS activity in different mutants from 5 min time-lapse movies the 'temporal colour code' function was used. For kymograms and T6SS assembly speed quantification the 'reslice' function was used. For determination of subcellular localization of T6SS assembly the surface area of bacteria was divided into an equally sized polar and mid cell area. The surface area was calculated based on the model of a capsule using the manually measured length and width of the bacteria (see formulas below). T6SS assemblies initiating in one of the two pole areas were considered as T6SS assemblies at pole.

$$h_{\mathrm{m}} = \mathrm{Height}_{\mathrm{measured}}$$

$$l_{\mathrm{m}} = \mathrm{Length}_{\mathrm{measured}}$$

$$r = \frac{h_{\mathrm{m}}}{2}$$

$$l_{\mathrm{Cylinder}} = l_{\mathrm{m}} - h_{\mathrm{m}}$$

$$A_{\mathrm{total}} = A_{\mathrm{Sphere}} + A_{\mathrm{Cylinder}} = 4\pi r^2 + 2\pi r l_{\mathrm{Cylinder}}$$

$$A_{0.5} = 0.5 \times A_{\mathrm{total}}$$

For determination of subcellular localization of T6SS assembly, images of *V. cholerae* 2740-80 were reanalysed from ref. 37. Contrast on compared sets of images was adjusted equally. All imaging experiments were performed with at least two biological replicates.

Structured illumination microscopy. BMDMs were seeded onto cover glass (VWR) in 24-well plates at a density of 1.25×10^5 cells per well and infected with *F. novicida* at a multiplicity of infection of 100 for 1 h as described below. BMDMs were washed three times with PBS and fixed for 10 min at 37 °C with 4% paraformaldehyde (Electron Microscopy Science). Cover glass was incubated with chicken anti-*F. novicida* (1:2,000; a gift from D.M. Monack, Stanford University) for 1 h at room temperature, then was washed three times with PBS, incubated with goat anti-chicken coupled to Alexa 568 (1:500; Life Technologies) and DY-647-Phalloidin (1:500; Dyomics) for another 45 min at room temperature, washed three times with PBS and was mounted on glass slides with Vectashield (Vector labs). 3D-SM was performed on a microscope system DeltaVision OMX-Blaze version 4 (Applied Precision, Issaquah, WA). Images were acquired using a Plan Apo N 60 × 1.42 numerical aperture oil immersion objective lens (Olympus) and four liquid-cooled sCMOS cameras (pco Edge, full frame 2,560 × 2,160; Photometrics). Optical *z*-sections were separated by 0.125 µm. The laser lines 488 and 568 were used for 3D-SIM acquisition. Exposure times were typically between 10 and 140 ms, and the power of each laser was adjusted to achieve optimal intensities of between 5,000 and 8,000 counts in a raw image of 15-bit dynamic range at the lowest laser power possible to minimize photobleaching. Phalloidin Alexa-647 was acquired using the widefield mode of the system. Raw 3D-SIM images were processed and reconstructed using the DeltaVision OMX SoftWoRx software package (Applied Precision).

Cell culture and infection. Primary wild-type BMDMs from C57BL/6JRj mice (Janvier) were differentiated in DMEM (Sigma) with 20% M-CSF (supernatants of L929 mouse fibroblasts), 10% v/v FCS, 10 mM HEPES, nonessential amino acids and penicillin (100 IU ml^{-1})/streptomycin (100 µg ml^{-1}) (all BioConcept). One day before infection, BMDMs were seeded into 24- or 96-well plates (Eppendorf) at a density of 1.5×10^5 or 5×10^4 cells per well in DMEM (Sigma) with 10% M-CSF (supernatants of L929 mouse fibroblasts), 10% v/v FCS, 10 mM HEPES and nonessential amino acids (all BioConcept). Where required, BMDMs were pre-stimulated overnight with LPS (from *Escherichia coli* strain O111:B4 (InvivoGen; tlr-3pelps)). *F. novicida* were grown overnight at 37 °C with aeration as described above. The bacteria were added to the BMDMs at a multiplicity of infection of 100 or the indicated value. The plates were centrifuged for 5 min at 500*g* to ensure similar adhesion of the bacteria to the cells and were incubated for 120 min at 37 °C. Next, the medium was replaced with fresh medium containing 10 µg ml^{-1} gentamicin (BioConcept) to kill extracellular bacteria, then plates were incubated at 37 °C for the indicated length of time.

Cytokine and LDH release measurement. IL-1β and IL-18 were measured by enzyme-linked immunosorbent assay (eBioscience). Lactate dehydrogenase (LDH) was measured with an LDH Cytotoxicity Detection Kit (Takara). To correct for spontaneous cell lysis and to normalize the values, the percentage of LDH release was calculated as follows:

$$\frac{\mathrm{LDH\ value}_{\mathrm{infected}} - \mathrm{LDH\ value}_{\mathrm{uninfected}}}{\mathrm{LDH\ value}_{\mathrm{total\ lysis}} - \mathrm{LDH\ value}_{\mathrm{uninfected}}} \times 100$$

Phagosome protection assay. The amount of cytoplasmic and vacuolar bacteria was measured as previously described[79]. In brief, BMDMs were seeded into 24-well plates at a density of 1.5×10^5 cells per well and *F. novicida* were grown for 4 h at 37 °C with aeration as described above. BMDMs were infected with *F. novicida* at a multiplicity of infection of 100 for 4 h as outlined above. BMDMs were washed three times with KHM buffer (110 mM potassium acetate, 20 mM Hepes, 2 mM $MgCl_2$) and incubated for 1 min with 75 µg ml^{-1} digitonin (Sigma) followed by differential staining of cytoplasmic and total bacteria. Antibodies used for staining were chicken anti-*F. novicida* (1:2,000; a gift from D.M. Monack, Stanford University) and goat anti-chicken coupled to Alexa 647 (cytoplasmic bacteria) or Alexa 488 (total bacteria) (1:500; both from Life Technologies). Stained bacteria were analysed on a FACS-Canto-II. Percentage of cytosolic bacteria were normalized to wild-type *F. novicida* as follows:

$$\frac{\mathrm{FACS\ value} - \mathrm{FACS\ value}_{\Delta pdpB}}{\mathrm{FACS\ value}_{wt} - \mathrm{FACS\ value}_{\Delta pdpB}} \times 100$$

Intracellular bacterial growth assay. BMDMs were seeded into 24-well plates at a density of 1.5×10^5 cells per well and infected with *F. novicida* at a multiplicity of infection of 1 as described above. After 2 and 24 h of infection, the BMDMs were washed three times with PBS and lysed with 0.1% Triton-X 100 (Promega) for 10 min at 37 °C. The bacteria were stained for 10 min with chicken anti-*F. novicida* (1:2,000; a gift from D.M. Monack, Stanford University), washed once with PBS and stained for 10 min with goat anti-chicken coupled to Alexa 647 and Alexa 488 (1:500 each; both from Life Technologies). A volume of 20 µl 123count eBeads (eBioscience) was added to each sample. The samples were analysed on a FACS-Canto-II by counting the number of bacteria per 5,000 beads. The CFU ratio was calculated by dividing the number of bacteria at 24 h (output) with the number of bacteria at 2 h (input).

Type I interferon measurement. One day before infection, ISRE-L929 reporter cells (a gift from D.M. Monack, Stanford University) were seeded into black 96-well plates with micro-clear bottom (Greiner) at a density of 1×10^5 cells per well in DMEM (Sigma) with 10% v/v FCS and penicillin (100 IU ml^{-1})/streptomycin (100 µg ml^{-1}) (both BioConcept). BMDMs were seeded into 96-well plates at a density of 5×10^4 cells per well and infected with *F. novicida* at a multiplicity of infection of 100 as described above. After 10 h of infection, type I IFN production was measured with the Bright-Glo Luciferase Assay System (Promega) as previously described[80].

Animal infection. All animal experiments were approved (licence 2535-26742, Kantonales Veterinäramt Basel-Stadt) and were performed according to local guidelines (Tierschutz-Verordnung, Basel-Stadt) and the Swiss animal protection law (Tierschutz-Gesetz). Female 10 weeks old wt C57BL/6JRj mice (Janvier) were infected subcutaneously with 10^4 CFUs of indicated stationary-phase *F. novicida* strain in 50 µl PBS. Mice were killed 48 h post infection. Bacterial load of spleen and liver was analysed by plating the bacteria on MHA plates. The plates were incubated for 24 h at 37 °C. IL-18 levels in the blood were measured by enzyme-linked immunosorbent assay (eBioscience). No randomization or 'blinding' of researchers to sample identity was used.

Statistical analysis. Statistical data analysis was done using Prism 6.0h (GraphPad Software, Inc.). To evaluate the difference between two groups (T6SS per cell, T6SS assembly speed, subcellular localization of T6SS, bacterial survival, cell death, cytokine release, phagosomal escape, bacterial growth and IFN production) the unpaired two-tailed *t*-test with Welch's correction was used. Animal experiments were evaluated with a two-tailed Mann–Whitney test. *P* values are given in the figure legends.

Data availability. The authors declare that the data supporting the findings of this study are available within the paper and its Supplementary Information files.

References

1. Oyston, P. C. F., Sjostedt, A. & Titball, R. W. Tularaemia: bioterrorism defence renews interest in *Francisella tularensis*. *Nat. Rev. Microbiol.* **2,** 967–978 (2004).
2. Kingry, L. C. & Petersen, J. M. Comparative review of *Francisella tularensis* and *Francisella novicida*. *Front. Cell Infect. Microbiol.* **4,** 35 (2014).
3. Chong, A. & Celli, J. The Francisella intracellular life cycle: toward molecular mechanisms of intracellular survival and proliferation. *Front. Microbiol.* **1,** 138 (2010).
4. Fernandes-Alnemri, T. *et al.* The AIM2 inflammasome is critical for innate immunity to *Francisella tularensis*. *Nat. Immunol.* **11,** 385–393 (2010).
5. Henry, T., Brotcke, A., Weiss, D. S., Thompson, L. J. & Monack, D. M. Type I interferon signaling is required for activation of the inflammasome during Francisella infection. *J. Exp. Med.* **204,** 987–994 (2007).
6. Jones, J. W. *et al.* Absent in melanoma 2 is required for innate immune recognition of *Francisella tularensis*. *Proc. Natl Acad. Sci. USA* **107,** 9771–9776 (2010).
7. Man, S. M. *et al.* The transcription factor IRF1 and guanylate-binding proteins target activation of the AIM2 inflammasome by Francisella infection. *Nat. Immunol.* **16,** 467–475 (2015).
8. Mariathasan, S., Weiss, D. S., Dixit, V. M. & Monack, D. M. Innate immunity against *Francisella tularensis* is dependent on the ASC/caspase-1 axis. *J. Exp. Med.* **202,** 1043–1049 (2005).
9. Meunier, E. *et al.* Guanylate-binding proteins promote activation of the AIM2 inflammasome during infection with *Francisella novicida*. *Nat. Immunol.* **16,** 476–484 (2015).
10. Rathinam, V. A. K. *et al.* The AIM2 inflammasome is essential for host defense against cytosolic bacteria and DNA viruses. *Nat. Immunol.* **11,** 395–402 (2010).
11. Storek, K. M., Gertsvolf, N. A., Ohlson, M. B. & Monack, D. M. cGAS and Ifi204 cooperate to produce type I IFNs in response to Francisella infection. *J. Immunol.* **194,** 3236–3245 (2015).
12. Nano, F. E. *et al.* A *Francisella tularensis* pathogenicity island required for intramacrophage growth. *J. Bacteriol.* **186,** 6430–6436 (2004).
13. Nano, F. E. & Schmerk, C. The Francisella pathogenicity island. *Ann. NY Acad. Sci.* **1105,** 122–137 (2007).
14. Bröms, J. E., Sjöstedt, A. & Lavander, M. The role of the *Francisella Tularensis* pathogenicity island in type VI secretion, intracellular survival, and modulation of host cell signaling. *Front. Microbiol.* **1,** 136 (2010).
15. Rigard, M. *et al. Francisella tularensis* IglG belongs to a novel family of PAAR-like T6SS proteins and harbors a unique N-terminal extension required for virulence. *PLoS Pathog.* **12,** e1005821 (2016).
16. Bingle, L. E., Bailey, C. M. & Pallen, M. J. Type VI secretion: a beginner's guide. *Curr. Opin. Microbiol.* **11,** 3–8 (2008).
17. de Bruin, O. M., Ludu, J. S. & Nano, F. E. The Francisella pathogenicity island protein IglA localizes to the bacterial cytoplasm and is needed for intracellular growth. *BMC Microbiol.* **7,** 1 (2007).
18. Russell, A. B. *et al.* A type VI secretion-related pathway in Bacteroidetes mediates interbacterial antagonism. *Cell Host Microbe* **16,** 227–236 (2014).
19. Alcoforado Diniz, J., Liu, Y.-C. & Coulthurst, S. J. Molecular weaponry: diverse effectors delivered by the type VI secretion system. *Cell. Microbiol.* **17,** 1742–1751 (2015).
20. Durand, E., Cambillau, C., Cascales, E. & Journet, L. VgrG, Tae, Tle, and beyond: the versatile arsenal of type VI secretion effectors. *Trends Microbiol.* **22,** 498–507 (2014).
21. Hachani, A., Wood, T. E. & Filloux, A. Type VI secretion and anti-host effectors. *Curr. Opin. Microbiol.* **29,** 81–93 (2016).
22. Ho, B. T., Dong, T. G. & Mekalanos, J. J. A view to a kill: the bacterial type VI secretion system. *Cell Host Microbe* **15,** 9–21 (2014).
23. Russell, A. B., Peterson, S. B. & Mougous, J. D. Type VI secretion system effectors: poisons with a purpose. *Nat. Rev. Microbiol.* **12,** 137–148 (2014).
24. Basler, M. & Mekalanos, J. J. Type 6 secretion dynamics within and between bacterial cells. *Science* **337,** 815 (2012).
25. Basler, M., Pilhofer, M., Henderson, G. P., Jensen, G. J. & Mekalanos, J. J. Type VI secretion requires a dynamic contractile phage tail-like structure. *Nature* **483,** 182–186 (2012).
26. Durand, E. *et al.* Biogenesis and structure of a type VI secretion membrane core complex. *Nature* **523,** 555–560 (2015).
27. Brunet, Y. R., Zoued, A., Boyer, F., Douzi, B. & Cascales, E. The type VI secretion TssEFGK-VgrG phage-like baseplate is recruited to the TssJLM membrane complex via multiple contacts and serves as assembly platform for tail tube/sheath polymerization. *PLoS Genet.* **11,** e1005545 (2015).
28. Planamente, S. *et al.* TssA forms a gp6-like ring attached to the type VI secretion sheath. *EMBO J.* **35,** 1613–1627 (2016).
29. Shneider, M. M. *et al.* PAAR-repeat proteins sharpen and diversify the type VI secretion system spike. *Nature* **500,** 350–353 (2013).
30. Zoued, A. *et al.* TssK is a trimeric cytoplasmic protein interacting with components of both phage-like and membrane anchoring complexes of the type VI secretion system. *J. Biol. Chem.* **288,** 27031–27041 (2013).
31. Zoued, A. *et al.* Architecture and assembly of the type VI secretion system. *Biochim. Biophys. Acta* **1843,** 1664–1673 (2014).
32. Brunet, Y. R., Henin, J., Celia, H. & Cascales, E. Type VI secretion and bacteriophage tail tubes share a common assembly pathway. *EMBO Rep.* **15,** 315–321 (2014).
33. Flaugnatti, N. *et al.* A phospholipase A1 antibacterial type VI secretion effector interacts directly with the C-terminal domain of the VgrG spike protein for delivery. *Mol. Microbiol.* **99,** 1099–1118 (2016).
34. Hachani, A., Allsopp, L. P., Oduko, Y. & Filloux, A. The VgrG proteins are 'à la carte' delivery systems for bacterial type VI effectors. *J. Biol. Chem.* **289,** 17872–17884 (2014).
35. Liang, X. *et al.* Identification of divergent type VI secretion effectors using a conserved chaperone domain. *Proc. Natl Acad. Sci. USA* **112,** 9106–9111 (2015).
36. Silverman, J. M. *et al.* Haemolysin coregulated protein is an exported receptor and chaperone of type VI secretion substrates. *Mol. Cell* **51,** 584–593 (2013).
37. Vettiger, A. & Basler, M. Type VI secretion system substrates are transferred and reused among sister cells. *Cell* **167,** 99–110.e12 (2016).
38. Whitney, J. C. *et al.* Genetically distinct pathways guide effector export through the type VI secretion system. *Mol. Microbiol.* **92,** 529–542 (2014).
39. Whitney, J. C. *et al.* An interbacterial NAD(P)(+) glycohydrolase toxin requires elongation factor Tu for delivery to target cells. *Cell* **163,** 607–619 (2015).
40. Clemens, D. L., Ge, P., Lee, B.-Y., Horwitz, M. A. & Zhou, Z. H. Atomic structure of T6SS reveals interlaced array essential to function. *Cell* **160,** 940–951 (2015).
41. Kudryashev, M. *et al.* Structure of the type VI secretion system contractile sheath. *Cell* **160,** 952–962 (2015).
42. Eshraghi, A. *et al.* Secreted effectors encoded within and outside of the francisella pathogenicity island promote intramacrophage growth. *Cell Host Microbe* **20,** 573–583 (2016).
43. Lindgren, M., Eneslätt, K., Bröms, J. E. & Sjöstedt, A. Importance of PdpC, IglC, IglI, and IglG for modulation of a host cell death pathway induced by *Francisella tularensis*. *Infect. Immun.* **81,** 2076–2084 (2013).
44. Lindgren, M., Bröms, J. E., Meyer, L., Golovliov, I. & Sjöstedt, A. The *Francisella tularensis* LVS ΔpdpC mutant exhibits a unique phenotype during intracellular infection. *BMC Microbiol.* **13,** 20 (2013).
45. Ludu, J. S. *et al.* The Francisella pathogenicity island protein PdpD is required for full virulence and associates with homologues of the type VI secretion system. *J. Bacteriol.* **190,** 4584–4595 (2008).
46. Ozanic, M., Marecic, V., Lindgren, M., Sjöstedt, A. & Santic, M. Phenotypic characterization of the *Francisella tularensis* ΔpdpC and ΔiglG mutants. *Microbes Infect.* **18,** 768–776 (2016).
47. Uda, A. *et al.* Role of pathogenicity determinant protein C (PdpC) in determining the virulence of the *Francisella tularensis* subspecies tularensis SCHU. *PLoS ONE* **9,** e89075 (2014).
48. Long, M. E., Lindemann, S. R., Rasmussen, J. A., Jones, B. D. & Allen, L.-A. H. Disruption of *Francisella tularensis* Schu S4 iglI, iglJ, and pdpC genes results in attenuation for growth in human macrophages and *in vivo* virulence in mice and reveals a unique phenotype for pdpC. *Infect. Immun.* **81,** 850–861 (2013).
49. Bönemann, G., Pietrosiuk, A., Diemand, A., Zentgraf, H. & Mogk, A. Remodelling of VipA/VipB tubules by ClpV-mediated threading is crucial for type VI protein secretion. *EMBO J.* **28,** 315–325 (2009).
50. Förster, A. *et al.* Coevolution of the ATPase ClpV, the sheath proteins TssB and TssC, and the accessory protein TagJ/HsiE1 distinguishes type VI secretion classes. *J. Biol. Chem.* **289,** 33032–33043 (2014).
51. Basler, M., Ho, B. T. & Mekalanos, J. J. Tit-for-tat: type VI secretion system counterattack during bacterial cell-cell interactions. *Cell* **152,** 884–894 (2013).
52. Meibom, K. L. *et al.* The heat-shock protein ClpB of *Francisella tularensis* is involved in stress tolerance and is required for multiplication in target organs of infected mice. *Mol. Microbiol.* **67,** 1384–1401 (2008).
53. Ahlund, M. K., Rydén, P., Sjöstedt, A. & Stöven, S. Directed screen of *Francisella novicida* virulence determinants using Drosophila melanogaster. *Infect. Immun.* **78,** 3118–3128 (2010).
54. Gray, C. G., Cowley, S. C., Cheung, K. K. M. & Nano, F. E. The identification of five genetic loci of *Francisella novicida* associated with intracellular growth. *FEMS Microbiol. Lett.* **215,** 53–56 (2002).
55. de Bruin, O. M. *et al.* The biochemical properties of the Francisella pathogenicity island (FPI)-encoded proteins IglA, IglB, IglC, PdpB and DotU suggest roles in type VI secretion. *Microbiology* **157,** 3483–3491 (2011).
56. Gerc, A. J. *et al.* Visualization of the serratia type VI secretion system reveals unprovoked attacks and dynamic assembly. *Cell Rep.* **12,** 2131–2142 (2015).
57. Kapitein, N. *et al.* ClpV recycles VipA/VipB tubules and prevents non-productive tubule formation to ensure efficient type VI protein secretion. *Mol. Microbiol.* **87,** 1013–1028 (2013).
58. Barrigan, L. M. *et al.* Infection with *Francisella tularensis* LVS clpB leads to an altered yet protective immune response. *Infect. Immun.* **81,** 2028–2042 (2013).

59. Kirstein, J., Molière, N., Dougan, D. A. & Turgay, K. Adapting the machine: adaptor proteins for Hsp100/Clp and AAA+ proteases. *Nat. Rev. Microbiol.* **7,** 589–599 (2009).
60. Mogk, A. *et al.* Broad yet high substrate specificity: the challenge of AAA+ proteins. *J. Struct. Biol.* **146,** 90–98 (2004).
61. Sauer, R. T. & Baker, T. A. AAA+ proteases: ATP-fueled machines of protein destruction. *Annu. Rev. Biochem.* **80,** 587–612 (2011).
62. Sauer, R. T. *et al.* Sculpting the proteome with AAA(+) proteases and disassembly machines. *Cell* **119,** 9–18 (2004).
63. Schwarz, S. *et al.* VgrG-5 is a Burkholderia type VI secretion system-exported protein required for multinucleated giant cell formation and virulence. *Infect. Immun.* **82,** 1445–1452 (2014).
64. French, C. T. *et al.* Dissection of the Burkholderia intracellular life cycle using a photothermal nanoblade. *Proc. Natl Acad. Sci. USA* **108,** 12095–12100 (2011).
65. Galyov, E. E., Brett, P. J. & DeShazer, D. Molecular insights into Burkholderia pseudomallei and Burkholderia mallei pathogenesis. *Annu. Rev. Microbiol.* **64,** 495–517 (2010).
66. Schwarz, S. *et al.* Burkholderia type VI secretion systems have distinct roles in eukaryotic and bacterial cell interactions. *PLoS Pathog.* **6,** e1001068 (2010).
67. Toesca, I. J., French, C. T. & Miller, J. F. The type VI secretion system spike protein VgrG5 mediates membrane fusion during intercellular spread by pseudomallei group Burkholderia species. *Infect. Immun.* **82,** 1436–1444 (2014).
68. Grosz, M. *et al.* Cytoplasmic replication of *Staphylococcus aureus* upon phagosomal escape triggered by phenol-soluble modulin α. *Cell. Microbiol.* **16,** 451–465 (2014).
69. Hybiske, K. & Stephens, R. S. Exit strategies of intracellular pathogens. *Nat. Rev. Microbiol.* **6,** 99–110 (2008).
70. Thurston, T. L. M., Wandel, M. P., von Muhlinen, N., Foeglein, A. & Randow, F. Galectin 8 targets damaged vesicles for autophagy to defend cells against bacterial invasion. *Nature* **482,** 414–418 (2012).
71. Case, E. D. R. *et al.* The Francisella O-antigen mediates survival in the macrophage cytosol via autophagy avoidance. *Cell. Microbiol.* **16,** 862–877 (2014).
72. Deretic, V., Saitoh, T. & Akira, S. Autophagy in infection, inflammation and immunity. *Nat. Rev. Immunol.* **13,** 722–737 (2013).
73. Akimana, C. & Kwaik, Y. A. Francisella-arthropod vector interaction and its role in patho-adaptation to infect mammals. *Front. Microbiol.* **2,** 34 (2011).
74. Santic, M. *et al.* Intra-vacuolar proliferation of *F. novicida* within *H. vermiformis*. *Front. Microbiol.* **2,** 78 (2011).
75. Boyer, F., Fichant, G., Berthod, J., Vandenbrouck, Y. & Attree, I. Dissecting the bacterial type VI secretion system by a genome wide *in silico* analysis: what can be learned from available microbial genomic resources? *BMC Genomics* **10,** 104–104 (2009).
76. Dong, T. G., Ho, B. T., Yoder-Himes, D. R. & Mekalanos, J. J. Identification of T6SS-dependent effector and immunity proteins by Tn-seq in Vibrio cholerae. *Proc. Natl Acad. Sci. USA* **110,** 2623–2628 (2013).
77. Lindgren, H. *et al.* Resistance of *Francisella tularensis* strains against reactive nitrogen and oxygen species with special reference to the role of KatG. *Infect. Immun.* **75,** 1303–1309 (2007).
78. Schindelin, J. *et al.* Fiji: an open-source platform for biological-image analysis. *Nat. Methods* **9,** 676–682 (2012).
79. Meunier, E. *et al.* Caspase-11 activation requires lysis of pathogen-containing vacuoles by IFN-induced GTPases. *Nature* **509,** 366–370 (2014).
80. Peng, K., Broz, P., Jones, J., Joubert, L.-M. & Monack, D. Elevated AIM2-mediated pyroptosis triggered by hypercytotoxic Francisella mutant strains is attributed to increased intracellular bacteriolysis. *Cell. Microbiol.* **13,** 1586–1600 (2011).

Acknowledgements

We thank M.A. Horwitz (UCLA) for providing the strain *F. novicida* U112 *iglA-sfGFP*, D.M. Monack (Stanford University) for the conjugation plasmid, the anti-*Francisella* primary antibody and the ISRE-L929 cells, A. Harms and C. Dehio (Biozentrum, University of Basel) for the *E. coli* conjugation strain and the Imaging Core Facility and FACS Core Facility (Biozentrum, University of Basel) for technical support. We thank P.D. Ringel for his help with the analysis of subcellular localization of T6SS assembly. The work was supported by SNSF Starting Grant BSSGI0_155778 (to M.Ba.), SNSF grant 31003A_159525 (to M.Ba.), SNSF grant PP00P3_139120/1 (to P.B.) and the University of Basel. M.Br. was supported by the Biozentrum Basel International PhD Program 'Fellowships for Excellence'.

Author contributions

M.Br., R.F.D., P.B. and M.Ba. designed experiments, analysed and interpreted the results. M.Br. and R.F.D. generated strains and acquired all data. All authors wrote and approved the manuscript.

Additional information

Supplementary Information accompanies this paper at http://www.nature.com/naturecommunications

Competing interests: The authors declare no competing financial interests.

Reprints and permission information is available online at http://npg.nature.com/reprintsandpermissions/

How to cite this article: Brodmann, M. *et al. Francisella* requires dynamic type VI secretion system and ClpB to deliver effectors for phagosomal escape. *Nat. Commun.* **8,** 15853 doi: 10.1038/ncomms15853 (2017).

Publisher's note: Springer Nature remains neutral with regard to jurisdictional claims in published maps and institutional affiliations.

Supplemental files

Type of file: PDF
Size of file: 0 KB
Title of file for HTML: Supplementary Information
Description: Supplementary Figures and Supplementary Tables

Type of file: MP4
Size of file: 0 KB
Title of file for HTML: Supplementary Movie 1
Description: T6SS sheath dynamics in wild-type and mutant strains. IglAsfGFP was monitored in F. novicida U112 iglA-sfGFP wild-type, ΔpdpE, ΔanmK, ΔpdpC, ΔpdpD, ΔpdpD/anmK, ΔpdpC/pdpD, ΔpdpC/pdpD/anmK and ΔclpB for 5 min at a frame rate of 20 frames per minute. 2 representative time-lapse image series for each strain are shown. Merge of phase contrast and GFP channel is shown. Fields of view are 39 x 26 µm. Videos play at a frame rate of 10 frames per second.

Type of file: MP4
Size of file: 0 KB
Title of file for HTML: Supplementary Movie 2
Description: Knockout of critical components abolishes T6SS dynamics. IglAsfGFP was monitored in F. novicida U112 iglA-sfGFP ΔpdpB, ΔclpB/pdpB, ΔiglF, ΔiglG, ΔiglI and ΔiglJ for 5 min at a frame rate of 2 frames per minute. 2 representative time-lapse image series for each strain are shown. Merge of phase contrast and GFP channel is shown. Fields of view are 39 x 26 µm. Videos play at a frame rate of 5 frames per second.

Type of file: MP4
Size of file: 0 KB
Title of file for HTML: Supplementary Movie 3
Description: ClpB spots co-localize with contracted sheaths. IglA-sfGFP and ClpB-mCherry2 was monitored in F. novicida U112 iglA-sfGFP clpB-mCherry2, iglA-sfGFP clpBmCherry2 ΔpdpB and clpB-mCherry2 for 5 min at a frame rate of 2 frames per minute. 2 representative time-lapse image series for each strain are shown. Merge of phase contrast, GFP and mCherry channels is shown. Fields of view are 39 x 26 µm. Videos play at a frame rate of 5 frames per second.

Type of file: MP4
Size of file: 0 KB
Title of file for HTML: Supplementary Movie 4
Description: Examples of wild-type and ΔclpB T6SS sheath dynamics. IglAsfGFP was monitored in F. novicida U112 iglA-sfGFP wild-type and ΔclpB for 5 min at a frame rate of 20 frames per minute. 10 representative time-lapse image series for each strain are shown. GFP channel is shown. Fields of view are 3.3 x 3.3 µm. Videos play at a frame rate of 10 frames per second.

Type of file: MP4
Size of file: 0 KB
Title of file for HTML: Supplementary Movie 5
Description: Examples of co-localization of ClpB with contracted sheath. IglAsfGFP and ClpB-mCherry2 was monitored in F. novicida U112 iglA-sfGFP clpB-mCherry2 for 5 min at a frame rate of 20 frames per minute. 10 representative time-lapse image series are shown. Left fields show GFP channel and right fields show mCherry channel. Fields of view are

3.3 x 3.3 µm. Videos play at a frame rate of 10 frames per second.

Type of file: MP4
Size of file: 0 KB
Title of file for HTML: Supplementary Movie 6
Description: Examples of T6SS dynamics in infected bone marrow derived macrophages. IglA-sfGFP and ClpB-mCherry2 was monitored in F. novicida U112 iglA-sfGFP clpB-mCherry2 for 10 min at a frame rate of 2 frames per minute. 5 representative time-lapse image series are shown. Left fields show phase contrast channel, middle fields show GFP channel and right fields show mCherry channel. Fields of view are 30 x 30 µm. Videos play at a frame rate of 5 frames per second.

Type of file: PDF
Size of file: 0 KB
Title of file for HTML: Peer Review File
Description:

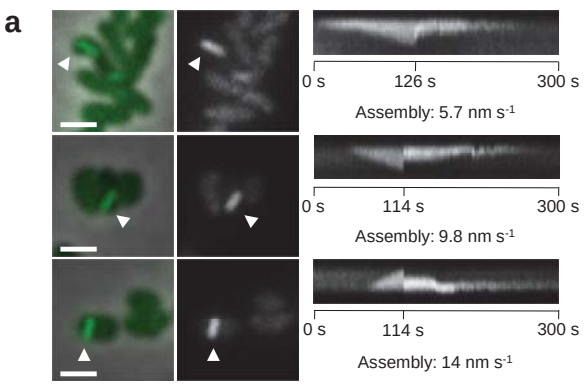

b

$$\frac{GFP\ intensity_{\text{Before assembly}}}{GFP\ intensity_{\text{After assembly}}} = 1.06 \pm 0.07$$

$$\frac{GFP\ intensity_{F.novicida\ \text{U112}-sfGFP\ \Delta pdpB}}{GFP\ intensity_{F.novicida\ \text{U112}-sfGFP}} = 0.96 \pm 0.23$$

Supplementary Figure 1 : Assembly speed varies between bacteria. (a) Kymograms of slow (~ 5 nm s^{-1}) to fast (~ 14 nm s^{-1}) T6SS assemblies (arrowheads) over 5 minutes (3 s per pixel) in *F. novicida* U112 *iglA-sfGFP*. First image is a merge of phase contrast and GFP channel, following images represent GFP channel only. 3.3 x 3.3 µm fields of view are shown. Scale bars represent 1 µm. **(b)** GFP intensities were measured a frame before and a frame after a complete assembly-disassembly cycle in two independent experiments. 30 bacteria were analyzed per experiment. GFP intensities measured in *F. novicida* U112 *iglA-sfGFP* wild-type *and ΔpdpB* were compared in four independent experiments. 30 bacteria were analyzed per experiment. Standard deviation was calculated.

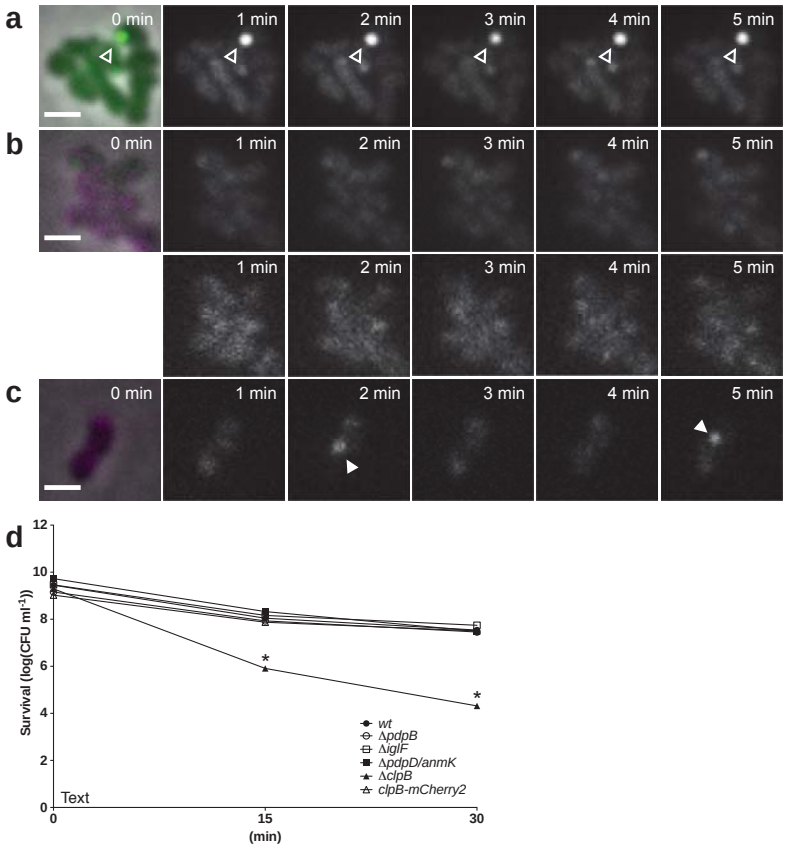

Supplementary Figure 2: T6SS activity is required for ClpB spot localization but dispensable for ClpB-dependent heat tolerance. (a) IglA-sfGFP localization and foci (empty arrowheads) in *F. novicida U112 iglA-sfGFP ΔclpB/pdpB*. First image is a merge of phase contrast and GFP channels, following images represent GFP channel only. 3.3 x 3.3 µm fields of view are shown. Scale bars represent 1 µm. **(b)** IglA-sfGFP and ClpB-mCherry2 localization in *F. novicida* U112 *iglA-sfGFP clpB-mCherry2 ΔpdpB*. First image is a merge of phase contrast, GFP and mCherry channels, following images represent GFP channel (upper panel) and mCherry channel (lower panel). **(c)** ClpB-mCherry2 localization dynamics in *F. novicida* U112 *clpB-mCherry2*. First image is a merge of phase contrast and mCherry channels, following images represent mCherry channel only. Arrowheads indicate ClpB recruitment. **(d)** Heat shock survival assay performed with *F. novicida U112 iglA-sfGFP* wild-type, *ΔpdpB*, *ΔiglF*, *ΔpdpD/anmK*, *ΔclpB* and *clpB-mCherry2* at 50 °C for 0, 15 and 30 min. Data are pooled from three independent experiments. *P < 0.05 (two-tailed unpaired *t*-test with Welch's correction). (a-c) 3.3 x 3.3 µm fields of view are shown. Scale bar represents 1 µm.

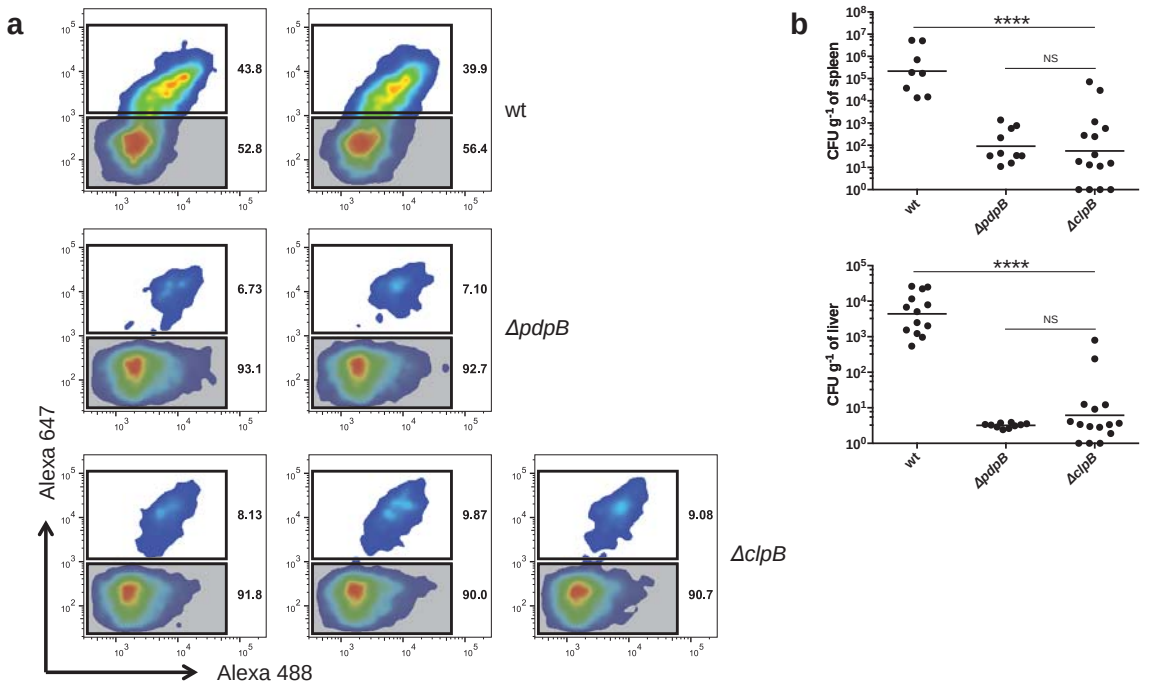

Supplementary Figure 3: *F. novicida* U112 *iglA-sfGFP ΔclpB* fails to escape into the cytosol and is avirulent *in vivo*. (a) Representative FACS blots from the quantification of cytosolic (white gates) and vacuolar bacteria (grey gates) by flow cytometry in unprimed wild-type BMDMs 4 h after infection with *F. novicida* U112 *iglA-sfGFP* wild-type, *ΔpdpB* or *ΔclpB.* Numbers next to the gates indicate the percentage of cytosolic and vacuolar bacteria. **(b)** Bacterial burden (as colony-forming units (CFU) per gram tissue) in the spleen and liver of wild-type C57BL/6JRj mice infected subcutaneously for 2 days with 1 x 10^4 *F. novicida* U112 *iglA-sfGFP* wild-type, *ΔpdpB* or *ΔclpB.* Each symbol represents an individual mouse (n = 8 (wild-type), 10 (*ΔpdpB)*, 15 (*ΔclpB*) (spleen), or n = 13 (wild-type), 10 (*ΔpdpB),* 15 (*ΔclpB*) (liver)); small horizontal lines indicate the mean. Data are pooled from two independent experiments. ****$P < 0.0001$; NS - not significant (Mann-Whitney test).

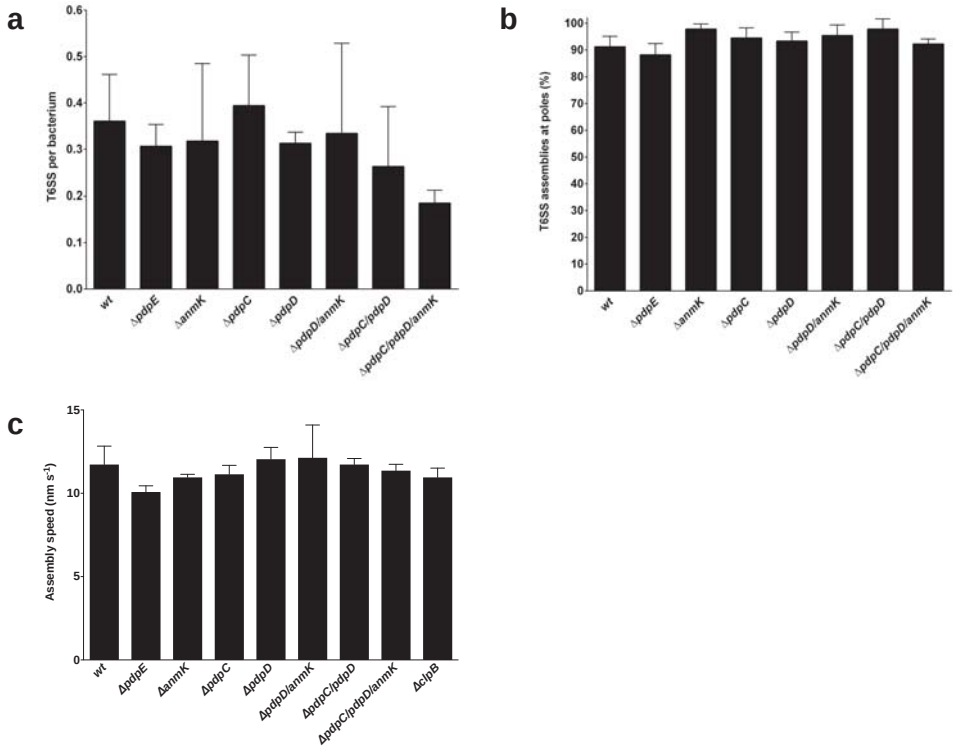

Supplementary Figure 4: *pdpE*, *anmK, pdpC* and *pdpD* and play no role in T6SS sheath localization and dynamics. (a) Quantification of number of T6SS sheath structures per bacterium within 5 min of imaging. **(b)** Quantification of T6SS sheath assembly at poles. **(c)** Quantification of T6SS assembly speed. Averages of three independent experiments. 30 bacteria per experiment were analyzed. Error bars represent standard deviation. No significant differences to wild-type (two-tailed unpaired *t*-test with Welch's correction).

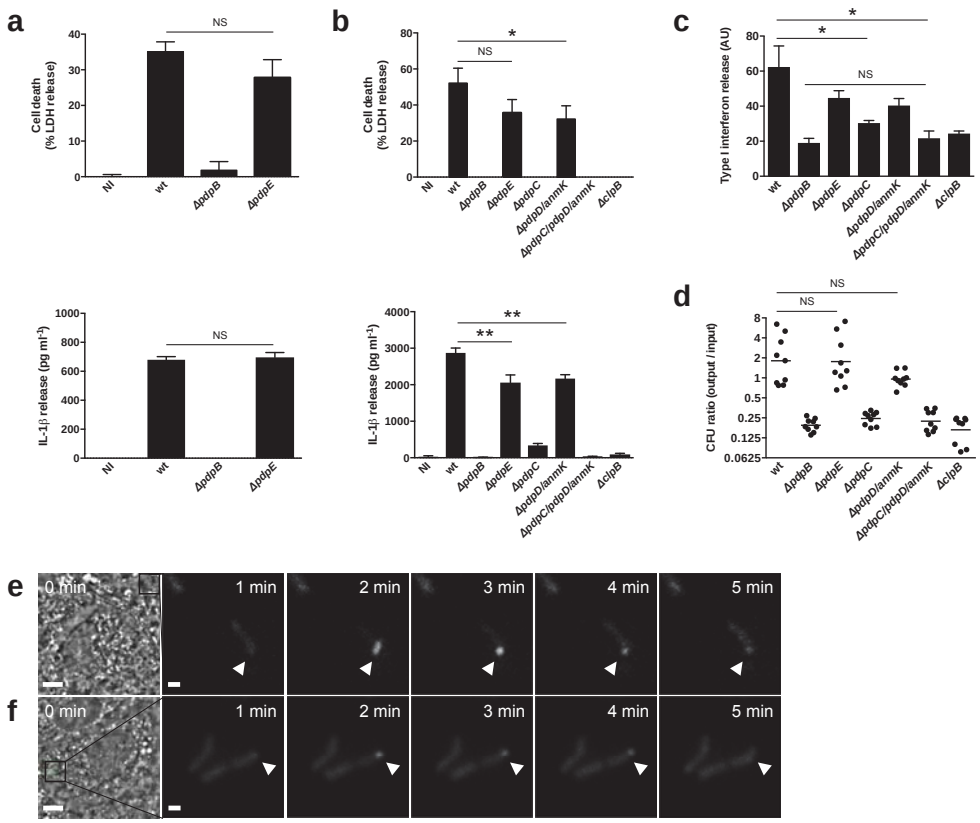

Supplementary Figure 5: Putative effector mutants show distinct innate immune activation and survival within macrophages. Release of LDH and IL-1β from **(a)** LPS-primed wild-type BMDMs 10 h or **(b)** unprimed wild-type BMDMs 24 h after infection with *F. novicida* U112 *iglA-sfGFP* wild-type, *ΔpdpB, ΔpdpE, ΔpdpC, ΔpdpD, ΔpdpD/anmK, ΔpdpC/pdpD/anmK* or *ΔclpB* (NI - noninfected control). **(c)** Quantification of type-I-interferon release in the supernatant of unprimed wild-type BMDMs infected for 10 h with *F. novicida* U112 *iglA-sfGFP* wild-type, *ΔpdpB, ΔpdpE, ΔpdpC, ΔpdpD, ΔpdpD/anmK, ΔpdpC/pdpD/anmK* or *ΔclpB.* **(d)** Intracellular growth within *Asc*$^{-/-}$ BMDMs during the first 24 h of infection with *F. novicida* U112 *iglA-sfGFP* wild-type, *ΔpdpB, ΔpdpE, ΔpdpC, ΔpdpD/anmK, ΔpdpC/pdpD/anmK* or *ΔclpB.* Growth was calculated as ratio of number of bacteria at 24 h (output) divided by the number of bacteria at 2 h (input). **(f, e**) Timelapse images from BMDMs infected for 1 h with *F. novicida* U112 *iglA-sfGFP ΔpdpE* **(e)** and *ΔpdpC/pdpD/anmK* **(f)**. 30 x 30 µm fields of view are shown. First image consists of merged phase contrast channel and GFP channel. Scale bar represents 5 µm. The close ups show 5 x 5 µm. Scale bar represents 1 µm. Close ups consist of GFP channel. (a-d) Data are representatives of three independent experiments (a-c) (mean and standard deviation of triplicate wells are shown) or pooled from three independent experiments (small horizontal lines indicate the mean) (d). *$P < 0.05$ and **$P < 0.01$; NS - not significant (two-tailed unpaired *t*-test with Welch's correction).

Supplementary Table 1: Strains used in this study, related to Material and Methods

Organism	Genotype	Relevant features	Source
Francisella novicida U112	*iglA-sfGFP*	Parental strain, C-terminal chromosomal fusion of *sfGFP* to *iglA*	(Clemens et al., 2015)
	iglA-sfGFP ΔpdpB	Deletion of *pdpB*	This study
	iglA-sfGFP ΔclpB	Deletion of *clpB*	This study
	iglA-sfGFP ΔclpB/pdpB	Deletion of *clpB* and *pdpB*	This study
	iglA-sfGFP clpB-mCherry2	C-terminal chromosomal fusion of *mCherry2* to *clpB*	This study
	iglA-sfGFP clpB-mCherry2 ΔpdpB	C-terminal chromosomal fusion of *mCherry2* to *clpB,* deletion of *pdpB*	This study
	clpB-mCherry2	C-terminal chromosomal fusion of *mCherry2* to *clpB*	This study
	iglA-sfGFP ΔiglF	Deletion of *iglF*	This study
	iglA-sfGFP ΔiglG	Deletion of *iglG*	This study
	iglA-sfGFP ΔiglI	Deletion of *iglI*	This study
	iglA-sfGFP ΔiglJ	Deletion of *iglJ*	This study

iglA-sfGFP ΔpdpE	Deletion of *pdpE*	This study
iglA-sfGFP ΔanmK	Deletion of *anmK*	This study
iglA-sfGFP ΔpdpC	Deletion of *pdpC*	This study
iglA-sfGFP ΔpdpD	Deletion of *pdpD*	This study
iglA-sfGFP ΔpdpD/anmK	Deletion of *pdpD* and *anmK*	This study
iglA-sfGFP ΔpdpC/pdpD	Deletion of *pdpC* and *pdpD*	This study
iglA-sfGFP ΔpdpC/pdpD/anmK	Deletion of *pdpC*, *pdpD* and *anmK*	This study

Supplementary Table 2: Plasmids used to generate in-frame deletions in this study, related to Material and Methods

Plasmid Name	Peptide scar left on the chromosome after allelic exchange	Primers used to generate in-frame deletion	
pDMK3-Δ*pdpB*	MNFIQKQGEVNVQ*	dFTN_1310_Del1_Xho1.FOR	TCAGTACTCGAGCAACTATATGAAAACTTACATAATT
		dFTN_1310_Del1.REV	CTCCTTGTTTTTGAATAAAATTCATACTTTTAATTT
		dFTN_1310_Del2_.FOR	ATGAATTTTATTCAAAAACAAGGAGAAGTTAATGT
		dFTN_1310_Del2.REV	ATAATAGCGGCCGCTTAGCAGAGCTTTTTATATT
		dFTN_1310_Det_FOR	ACATCAAGAAATACTCTGCCCTTC
		dFTN_1310_Det_REV	TATTATTATCCAACCATTGTTGCTG
pDMK3-Δ*clpB*	MNINKFTIKLANNNITFSK*	dFTN_1743_1_Spe1.FOR	TCAGTAACTAGTAGATAAATGCGACTATTGATG
		dFTN_1743_1.REV	TAATATTGTTATTAGCTAGTTTTATTGTAAATTTATTTATATTCATTATTT

	dFTN_1743_2.FOR	ATTTACAATAAAACTAGCTAATAACAATATTACATTCTCTAAA
	dFTN_1743_2_Sac1.REV	TCAGTAGAGCTCTCTTTTGTCATTGCAAAAGA
	dFTN_1743_Det.FOR	CAAGAATTCCATCAACCCAGA
	FTN_1743-mCherry_Det_REV	CCATCAAACTTAACAAAAGCTCCT
pDMK3-*clpB-mCherry2*	FTN_1743-mcherry1_Spe1.FOR	TCAGTAACTAGTGGTGTCGGTAAAACTGA
	FTN_1743-mcherry1.REV	CGGCCGCTTTAGAGAATGTAATATTGTTATTAGCG
	FTN_1743-mcherry2.FOR	CTCTAAAGCGGCCGCAGGA
	FTN_1743-mcherry2.REV	ATTAAACCGATTTTACTTGTACAGCTCGTC
	FTN_1743-mcherry3.FOR	CTGTACAAGTAAAATCGGTTTAATCAATATCTAAATTAT
	FTN_1743-mcherry3_Sac1.REV	TCAGTAGAGCTCGCTTTATAAGTTAGATTAATAGAGTTTG
	FTN_1743-mcherry_Det_FOR	GATGGAAGGCGAAAAAGACA
	FTN_1743-mcherry_Det_REV	CCATCAAACTTAACAAAAGCTCCT

pDMK3-Δ*iglF*	MNNDIDKWFESKQEAYWKI*	dFTN_1313_1_Spe1.FOR	TCAGTAACTAGTTTTCTCAAAGAATATATGATGATAATG
		dFTN_1313_1.REV	TTGCTTGCTTTCAAACCATTTATCAATATCATTATT
		dFTN_1313_2.FOR	TGGTTTGAAAGCAAGCAAGAAGC
		dFTN_1313_2_Sac1.REV	TCAGTAGAGCTCTATTTCTAATAAGCATGATTTA GGAA
		dFTN1313_Det.FOR	CTGGGTAATCAAGCACAAAGGT
		dFTN1313_Det.REV	GTGGCAAAGCTAGGATCTTCT
pDMK3-Δ*iglG*	MLNIINDSLKGGQINVKTS*	dFTN_1314_1_Xho1.FOR	TCAGTACTCGAGATAAAAAATCAACTCTACAAAAACC
		dFTN_1314_1.REV	TTTGTCCACCTTTTAAGGAGTCATTTATAATATTTAACATT
		dFTN_1314_2.FOR	CTCCTTAAAAGGTGGACAAATAAATGTAAA
		dFTN_1314_2_Not1.REV	TCAGTAGCGGCCGCTAATTTTTCGTCATTATAGTTTTCAG
		dFTN_1314_Det.FOR	TTTCGCTAACGTCACTACAAGC
		dFTN_1314_Det.REV	TCATCGAAGCAAATGAGGTG

pDMK3-Δ*iglI*	MSQIISTLNNDSVEKISNEIDED YFEDLFDI*	dFTN_1317_1_Xho1.FOR	TCAGTACTCGAGAAATTTATAAATCAAAACACCTTTAGC
		dFTN_1317_1.REV	TTCTACCGAATCATTATTTAGTGTAGATATTATCTGACT
		dFTN_1317_2.FOR	ACACTAAATAATGATTCGGTAGAAAAAATTT
		dFTN_1317_2_NotI.REV	TCAGTAGCGGCCGCATTTCAAGTTCTATCTTAAATGGG
		dFTN_1317_Det.FOR	ATCGCAGCACACAATCTTTAAA
		dFTN_1317_Det.REV	TCAGATAGTGATTCGGATTTTTCA
pDMK3-Δ*iglJ*	MKTILKIFLTYKQQIYLGYFNL*	dFTN_1318_1_Xho1.FOR	TCAGTACTCGAGATAACATAGATTCTATTATAGAAATTGTACA
		dFTN_1318_1.REV	CCTAGATATATCTGTTGTTTATATGTCAAAAAGATCTTCAAA
		dFTN_1318_2.FOR	GATCTTTTTGACACAGATATATCTAGGTTATTTTAATTTATG
		dFTN_1318_2_NotI.REV	TCAGTAGCGGCCGCATCATTTGCGCTTATTTCAA
		dFTN_1318_Det.For	CGCAAATGCAGAATCAAGAA
		dFTN_1318_Det.Rev	CGACTAGCGCGTCTAAAAATG
pDMK3-Δ*pdpE*	MSKKVFQLLLHYEKKITII*	dFTN_1320_1_Xho1.FOR	TCAGTACTCGAGACCAACAGAAGAAAACTTTG
		dFTN_1320_1.REV	ATTTTCTTTTCATAATGTAATAATAATTGAAATACTTTTTTACTCATATT

		dFTN_1320_2.FOR	ATTTCAATTATTATTACATTATGAAAAGAAAATTACTATAATATAAC
		dFTN_1320_2_Not1.REV	TCAGTAGCGGCCGCGGTGATATTTTTGTAAAACTTAATAGG
		dFTN_1320_Det.FOR	GGGTTGGGCTATCACATCAA
		dFTN_1320_Det.REV	GTT AAGTTTGCAGACAGGTC
pDMK3-Δ*anmK*	LSEYKYCVGIIPSATGAKSRVIL GQINFF*	dFTN_1326_1_Xho1.FOR	TCAGTACTCGAGCTTAGGTATAATGGAATAAATGATTTAAC
		dFTN_1326_1.REV	GTGTAGGAATCATACCATCTGCAACCG
		dFTN_13125-26_2.FOR	CTATACTTTCTGATTCCTACACAATATTTATATTCAC
		dFTN_1325-26_2_Sac1.REV	TCAGTAGAGCTCGTGTATCTGCTAAAAAATTAGAGT
		dFTN_1326_Det.For	GCCGATGAAGCTTTACCACT
		dFTN_1325-26_Det.REV	TGCCTGCAGTAATATTCAAAGC
pDMK3-Δ*pdpC*	MNDKYELNIYSDFFKKISS*	dFTN_1319_1_Xho1.FOR	TCAGTACTCGAGCTAAATAACTTTGTGAGCCTTC
		dFTN_1319_1.REV	TTTAAAAAAGTCTGAATAGATATTTAGTTCATATTTGTCG
		dFTN_1319_2.FOR	GAACTAAATATCTATTCAGACTTTTTTAAAAAAATATCGTC
		dFTN_1319_2_Not1.REV	TCAGTAGCGGCCGCTGATAATATCGATGCAATATATGAAA

		dFTN_1319_Det.For	CCAGAATGATTCGGTAGAAAAA
		dFTN_1319_Det.Rev	AAAGGAAAGCAACAGCTCCA
pDMK3-Δ*pdpD*	MDQDINDLLYDTDDLKKEKVR KYRPMIWV*	dFTN_1325_1_Xho1.FOR	TCAGTACTCGAGCACTATCAACTTCTGTAGATCC
		dFTN_1325-26_1.REV	TGTGTAGGAATCAGAAAGTATAGACCAATGATC
		dFTN_13125.FOR	GTCTATACTTTCTTACTTTTTCTTTTTTGAGGTCA
		dFTN_1325_2_Not1.REV	TCAGTAGCGGCCGCCTAAAAATGCAAATATTGATGATATTTATG
		dFTN_1325-26_Det.FOR	GCACCTTTAGCCATTCTTGCT
		dFTN_1325_Det.Rev	AGGAGATATCGCTGCTGGAG
pDMK3-Δ*pdpD/anmK*	LSEYKYCVGIRKYRPMIWV*	dFTN_1325-26_1_Spe1.FOR	TCAGTAACTAGTCACTATCAACTTCTGTAGATCC
		dFTN_1325-26_1.REV	TGTGTAGGAATCAGAAAGTATAGACCAATGATC
		dFTN_13125-26_2.FOR	CTATACTTTCTGATTCCTACACAATATTTATATTCAC
		dFTN_1325-26_2_Sac1.REV	TCAGTAGAGCTCGTGTATCTGCTAAAAAATTAGAGT

dFTN_1325-26_Det.FOR	GCACCTTTAGCCATTCTTGCT
dFTN_1325-26_Det.REV	TGCCTGCAGTAATATTCAAAGC

3.4. Spatio-temporal dynamics of *Francisella* Type VI secretion system assembly

Maj Brodmann1, Linnéa Persson2, Laurent Dubois3 and Marek Basler1[#]

1 Focal Area Infection Biology, Biozentrum, University of Basel, Basel, Switzerland

2 Wallenberg Centre for Molecular and Translational Medicine, University of Gothenburg, Gothenburg, Sweden

3 Department of Microbiology, Harvard Medical School, Boston, United States of America.

[#] correspondence to: marek.basler@unibas.ch

Manuscript in preparation

Statement of contribution:

I generated most strains, designed, performed most experiments and analyzed the collected data. Furthermore, I trained and supervised BSc student Linnéa Persson. I prepared figures and wrote the manuscript together with Marek Basler.

Spatio-temporal dynamics of *Francisella* Type VI secretion system assembly

Maj Brodmann[1], Linnéa Persson[2], Laurent Dubois[3], Marek Basler[1*]

[1]Biozentrum, University of Basel, Switzerland.

[2]Wallenberg Centre for Molecular and Translational Medicine, University of Gothenburg, Gothenburg, Sweden.

[3]Department of Microbiology, Harvard Medical School, Boston, United States of America.

[*]Correspondence: Dr. Marek Basler, marek.basler@unibas.ch

Abstract

Many bacterial secretions systems required for host-pathogen interactions reside at bacterial poles. Nonetheless, little is known about how these secretion systems are localized to the poles and whether polar localization is important for their function. *Francisella* Type VI secretion system (T6SS) is localized to the poles and is essential for phagosomal escape and thus *Francisella* virulence. Here we characterize the spatio-temporal dynamics of T6SS membrane complex biogenesis, which is the first step in T6SS assembly. We show that membrane complex biogenesis at bacterial poles depends on PdpB, IglE and DotU but is independent of other FPI components. Furthermore, membrane complex formation does not depend on protein synthesis in contrast to T6SS sheath assembly suggesting differential regulation of FPI components. In addition, we show that IglI, a member of the TssA family, localizes at the poles and co-localizes with the distal end of growing T6SS sheaths.

Introduction

Subcellular organization of bacterial cells was long underappreciated. Due to advances in electron and fluorescence microscopy, it became evident that bacteria are highly organized in a temporal and spatial manner (Surovtsev and Jacobs-Wagner, 2018). A compartment with distinct properties are the poles in rod-shaped bacteria. The poles provide physical and biochemical cues important for the organization of the whole bacterial cell (Surovtsev and Jacobs-Wagner, 2018; Young, 2006). In addition, because new peptidoglycan is laterally inserted in most rod-shaped bacteria, the polar peptidoglycan is more stable (Typas et al., 2011;

Young, 2006). Thus, it is favorable to localize large protein complexes as well as proteins, which need to be in close proximity of each other, at the poles as they will not be separated during cell growth (de Pedro et al., 2004). Indeed, complexes such as Type IVa pili, flagella, chemoreceptors and secretion systems we shown to be polarly localized (Carter et al., 2017; Huitema et al., 2006; Surovtsev and Jacobs-Wagner, 2018; Thiem and Sourjik, 2008; Yamaichi et al., 2012). Polar secretion systems became of special interest as they are often important for host-pathogen interactions (Carlsson et al., 2009; Chakravortty et al., 2005; Charles et al., 2001; Jain et al., 2006; Jeong et al., 2017; Morgan et al., 2010; Rosch and Caparon, 2004; Scott et al., 2001).

One of the best-studied polar secretion system is the Type IV secretion system (T4SS) in *Legionella pneumophila*, which requires the T4SS for maintaining the *Legionella* containing vacuole (LCV) inside eukaryotic cells (Qiu and Luo, 2017). Interestingly, polar localization of *Legionella* T4SS is required for full virulence as a mislocalized secretion apparatus leads to virulence defects despite of functional effector secretion (Jeong et al., 2017). A possible advantage of polar secretion could be that the local concentration of effector protein is higher if they are secreted from single site, or that *Legionella* is in close contact with the membrane of the LCV at the poles. While the exact mechanism of how *Legionella* T4SS is localized to the poles is unknown, cell division proteins are likely involved as T4SS were observed at newly formed septa (Jeong et al., 2017). In addition, polar localization depends on the structural components of T4SS, DotU and IcmF (Ghosal et al., 2019).

Previously, we showed that *Francisella tularensis* subspecies *novicida* (*F. novicida*) assembles a polar Type VI secretion system (T6SS), which is essential for phagosomal escape and intracellular survival (Brodmann et al., 2017; Bröms et al., 2010; Chong and Celli, 2010). This non-canonical T6SS is encoded on the *Francisella* pathogenicity island (FPI) (Bröms et al., 2010). While the causative agents of the deadly zoonotic disease tularemia *Francisella tularensis* subspecies *tularensis* and subspecies *holarctica* harbor two identical FPIs, *F. novicida* encodes only one (Bröms et al., 2010; Oyston et al., 2004). On the other hand, *F. novicida* encodes an additional putative T6SS on the *Francisella novicida* island (FNI) (Bröms et al., 2010; Rigard et al., 2016).

In general, FPI genes have low sequence homology to canonical T6SS core components and important components such as a specific unfoldase are missing. Conversely, the FPI contains several genes with unknown function (Bingle et al., 2008; Bröms et al., 2010). Nevertheless, *Francisella* T6SS sheath dynamics was shown to be similar to canonical T6SS when visualized by live-cell fluorescence microscopy (Basler and Mekalanos, 2012; Basler et al., 2012; Brodmann et al., 2017). Canonical T6SS assembly starts with assembly of a membrane complex (Durand et al., 2015; Rapisarda et al., 2019). In *Francisella*, the membrane complex is formed by IglE (homolog of TssJ), PdpB (TssM) and DotU (TssL) (de Bruin et al., 2011; Durand et al., 2015; Nguyen et al., 2014; Rapisarda et al., 2019). The membrane complex anchors the baseplate to the cell envelope (Wang et al., 2019). Based on bioinformatic analysis, *Francisella* base plate consists of IglH (TssE) and IglD (TssK) (Brunet et al., 2015; Cherrak et al., 2018; Rigard et al., 2016). However, clear homologs of TssF and TssG are missing. The baseplate harbors the spike complex with associated effectors and serves as scaffold for the assembly of a long cytosolic sheath with an inner tube. In *Francisella*, the spike complex consists of VgrG and IglG (homolog of canonical PAAR proteins) as well as PdpA, which was shown to interact with VgrG (Eshraghi et al., 2016; Rigard et al., 2016; Shneider et al., 2013). In addition, IglG was shown to interact with IglF but the function of IglF remains unknown (Rigard et al., 2016). Upon an unknown signal, the extended sheath made of IglA (TssB) and IglB (TssC) subunits contracts and expels the inner IglC (Hcp) tube together with the spike complex and effectors PdpC and PdpD towards a target (Brodmann et al., 2017; Brunet et al., 2014; Clemens et al., 2015; Eshraghi et al., 2016; Kudryashev et al., 2015; Sun et al., 2007; Wang et al., 2017). Then, general purpose unfoldase ClpB recycles the contracted *Francisella* T6SS sheath (Alam et al., 2018; Bönemann et al., 2009; Brodmann et al., 2017; Pietrosiuk et al., 2011). Additional FPI components with unknown function IglI and IglJ are required for T6SS assembly while PdpE and AnmK are not (Brodmann et al., 2017). On the other hand, in some organisms, baseplate and sheath assembly is coordinated by TssA, which is missing in *Francisella* (Abdelrahim Zoued et al., 2016; Dix et al., 2018; Planamente et al., 2016)

Up to date, polar localization of dynamic T6SS is unique to *F. novicida* (Brodmann et al., 2017). Interestingly, *Burkholderia thailandensis*, which requires T6SS-5 for

pathogenesis and formation of multinucleated giant cells, was shown to polarly localize ClpV-5 (Schwarz et al., 2014). However, ClpV-5 foci were less dynamics and localize to poles also in the absence of a functional T6SS-5 (Lennings et al., 2019; Schwarz et al., 2014). Since polar secretion systems are often required for host-pathogen interactions (Carlsson et al., 2009; Chakravortty et al., 2005; Charles et al., 2001; Jain et al., 2006; Jeong et al., 2017; Morgan et al., 2010; Rosch and Caparon, 2004; Scott et al., 2001), it is likely that polar localization of T6SS in *Francisella* is important for virulence. However, little is known about how *Francisella* T6SS is localized to the poles. Although the membrane complex is formed as first step in canonical T6SS assembly and defines subcellular localization, nothing is known about *Francisella* membrane complex biogenesis. In addition, the role of FPI components with unknown function for polar localization of the T6SS remains to be elucidated.

Here we show that *F. novicida* membrane complex is stably formed at one or both poles even in the absence of other FPI components and known proteins involved in cell division. Membrane complex biogenesis depends on PdpB, IglE and DotU. Membrane complex starts forming after 20 minutes incubated on an agarose pad and does not require protein synthesis in contrast to sheath assembly. Furthermore, we show that ImpA domain containing IglI is polarly localized, is required for T6SS sheath assembly and may co-localize with the distal end of a growing sheath. Last, we show that while the putative T6SS on the FNI is not assembled under our conditions, FNI component FTN_0045 forms distinct foci and its deletion affects *Francisella* T6SS dynamics.

Results

To characterize the formation of polar T6SS membrane complex in *F. novicida* in a temporal and spatial manner, we first tagged membrane complex components PdpB and DotU with fluorescent proteins to follow membrane complex dynamics using live-cell fluorescence imaging (figure 1 B-E). Since non-functional proteins are also often localized to the poles (Stewart et al., 2005), we tested msfGFP and mScarlet-I fusions to minimize the possibility that the polar localization is due to aggregation. In addition, we checked for proper T6SS function in the PdpB and DotU tagged mutants by monitoring sheath assembly by live-cell fluorescence microscopy. After 1 h incubation on an agarose pad, we saw distinct PdpB or DotU foci at either one pole or both poles in a cell (figure 1 A-E). Both msfGFP and mScarlet-I fusions showed similar polar localization and sheath assembly was unaffected. While PdpB and DotU tagged with msfGFP or mScarlet-I behaved similarly, tagged sheath subunit IglA with sfGFP or mCherry2 showed differences in assembly speed and sheath length. T6SS sheaths were significantly shorter and assembly was significantly slower with IglA-mCherry2 than with IglA-sfGFP (figure 1 G).

Interestingly, PdpB and DotU foci were stable before, during and after T6SS sheath assembly and contraction (figure 1 B-E). As reported previously only approximately 30 % of cells assemble sheath after 120 min incubation on an agarose pad (Brodmann et al., 2017), however, most cells lacking detectable sheath assembly still formed stable PdpB or DotU foci. Since *F. novicida* is small compared to other bacteria, we verified subcellular localization of DotU-mScarlet-I with live-cell structural illumination microscopy (SIM) (figure 1 F). Indeed, most bacterial cells contained one or two DotU-mScarlet-I foci at the poles. In addition, sheath assemblies were observed originating from a labelled membrane complex.

To identify proteins required for subcellular localization of PdpB-mScarlet-I and DotU-mScarlet-I, we monitored their localization in various mutant backgrounds (figure 2 A-B). Polar localization of PdpB-mScarlet-I was abolished in a *ΔdotU* mutant (figure 2 A). Polar localization of DotU-mScarlet-I depended on PdpB or IglE but remained polar in the absence of IglF, IglI or IglJ (figure 2 B). However, signal intensity of DotU-mScarlet-I in *ΔpdpB* and *ΔiglF* mutants was lower than in the parental strain suggesting that protein stability is affected in these mutants and thus

could have contributed to delocalization of DotU-mScarlet-I in the *ΔpdpB* mutant. A polar effect of *iglF* deletion can be ruled out, as we previously restored T6SS activity by expressing IglF from a plasmid (Brodmann et al., 2018).

In order to follow biogenesis of the *Francisella* membrane complex, we imaged PdpB-mScarlet-I or DotU-mScarlet-I immediately after the bacterial cells were taken from liquid cultures and spotted on an agarose pad (figure 2 C-F). Interestingly, PdpB and DotU were already expressed and localized at the cell periphery when imaging started (figure 2 C-F). After 20 minutes of imaging, stable polar PdpB or DotU foci were formed (figure 2 C, E). During the time course of 1 h, signal intensity of both fusion proteins only slightly increased in contrast to the gradual increase in signal intensity of IglA-sfGFP. Most sheath assemblies were detected after 1h of incubation on the pad. Most PdpB or DotU foci remained stable over the time course of imaging.

Since signal intensity of the membrane complex remained similar over time, we wanted to know if membrane complex formation depends on protein synthesis. Thus, we supplemented the liquid culture with 1000 µg/ml chloramphenicol (4x MIC (Ikäheimo et al., 2000)) for 1 h and spotted the bacterial cells on an agarose pad also containing 1000 µg/ml chloramphenicol in order to inhibit protein synthesis. Surprisingly, stable PdpB or DotU foci still formed in the presence of chloramphenicol after 20 min of incubation on the pad (figure 2 D, F). In contrast, IglA-sfGFP signal intensity remained unchanged and no sheath assemblies were observed (figure 2 D, F). These results suggest that expression of membrane complex components and sheath components are differently regulated and that polar localization of the membrane complex is independent of protein synthesis despite the fact that PdpB and DotU foci form only after 20 minutes of encountering an agarose pad.

Since polar localization of *Legionella* T4SS was suggested to depend on cell division proteins (Jeong et al., 2017), we deleted several genes implicated in cell division or in subcellular organization and which had decreased virulence in transposon screens (figure 3) (Ahlund et al., 2010; Brunton et al., 2015; Kraemer et al., 2009; Su et al., 2007). We found three different phenotypes. First, deletion of *minD*, *parB*, *FTN_0340*, *FTB_0938* and *FTN_1507* led to neither localization defect nor decreased T6SS activity (figure 3 A). Second, deletion of *ftsA*, *virK*, *fipA* and *dsbB* decreased T6SS activity without altering subcellular localization (figure 3 B-C). FtsA

and VirK were not associated with *Francisella* T6SS activity before. FtsA interacts with the FtsZ ring at the inner membrane during cell division and is required for its stabilization (Aarsman et al., 2005). Function of VirK is unknown, however it is associated with virulence in *Shigella* and *Salmonella* (Detweiler et al., 2003; Nakata et al., 1992). Interestingly, *virK* is encoded downstream of $opiB_{1-3}$, components secreted in a T6SS dependent manner in *F. novicida* (Eshraghi et al., 2016). FipA and DsbB are both involved in disulfide bridge formation in periplasm and are required for proper folding of IglC (Lo et al., 2016; Qin et al., 2016). Thus, decreased T6SS activity in these deletion mutants is likely due to decreased stability of T6SS components such as IglC. Third set of deletions included *minC*, *ispZ* and *slt* (figure 3 D). These deletions resulted in aberrant cell shapes (*ΔminC* and *ΔispZ*) and formation of minicells (*ΔminC*) and importantly also abrogated sheath assemblies. Interestingly, deletion of *minD* has no observable phenotype. IspZ is a putative intracellular septation protein A, which was shown to be required for normal intracellular cell division in *Shigella* (Mac Síomóin et al., 1996). In a *Δslt* mutant, polar T6SS sheath assemblies were observed but only in rod-shaped cells suggesting that the soluble lytic murein transglycosylase is not directly required for inserting the membrane complex into the cell wall. It is unclear if decreased or abrogated T6SS activity in *minC*, *ispZ* and *slt* mutants is caused by the deletion of these genes or if it is a consequence of aberrant cell shapes.

HHpred analysis (Zimmermann et al., 2018) of FPI components with unknown function revealed that IglI has a putative N-terminal ImpA domain (amino acid 40 – 182) similar to proteins of the TssA family (Dix et al., 2018; Planamente et al., 2016; Schneider et al., 2019; Zoued et al., 2016). Therefore, we tagged IglI with mScarlet-I and analyzed its subcellular localization using live-cell wide-field fluorescence microscopy and SIM (figure 4 A-B). Despite rapid bleaching of IglI-mScarlet-I, we detected its localization to the poles even in cells containing no sheath assemblies (figure 4). Interestingly, using deconvolution and SIM, we observed two different subcellular localizations for IglI-mScarlet-I in the cells with ongoing sheath assembly (figure 4 A-B). In some cases, IglI-mScarlet-I localized to the distal end of an assembling sheath (figure 4 A-B, example 1). In other examples, IglI-mScarlet-I stayed at the pole during sheath assembly (figure 4 A-B, example 2). In order to investigate whether polar localization of IglI-mScarlet-I in cells without sheath

assembly depends on any other FPI components, we deleted *pdpB*, *dotU*, *iglE*, *iglF* and *iglJ* in IglI-mScarlet-I background and assessed its subcellular localization. Interestingly, IglI-mScarlet-I was polarly localized in all of these deletion mutants, suggesting that IglI-mScarlet-I localizes to the poles independently of other structural T6SS components (figure 4 C)..

Since *F. novicida* encodes an additional putative T6SS on the FNI (figure 5 A), we wondered if $T6SS_{FNI}$ is functional. Therefore, we tagged $IglA_{FNI}$ with msfGFP in an $IglA_{FPI}$-mCherry2 background. However, we did not find any conditions in which we could observe $T6SS_{FNI}$ assembly (figure 5 B). Since the membrane complex is assembled before T6SS assemblies occur (figure 2 C-F), we also tagged $DotU_{FNI}$ with mScarlet-I, however, we did not see any distinct $DotU_{FNI}$-mScarlet-I foci (figure 5 C). In order to trigger $T6SS_{FNI}$ assembly, we reasoned that one of the FNI genes with unknown function might encode a post-translational repressor of T6SS similar to TagF in *Pseudomonas aeruginosa* or *Serratia marcescens* (Lin et al., 2018; Silverman et al., 2011). Thus, we deleted *FTN_0045*, *FTN_0046*, *FTN_0047*, *FTN_0052* and *FTN_0053*, however, we observed no $T6SS_{FNI}$ sheath assembly in any of these deletion mutants after incubation on an agarose pad for 1 h (figure 5 D).

Interestingly, when we tagged FTN_0045, which harbors a putative N-terminal ImpA domain (amino acid 27-189) similarly to IglI, we observed dynamic FTN_0045-mScarlet-I spots (figure 6 A). In addition, SIM revealed that FTN_0045-mScarlet-I foci never overlapped with $IglA_{FPI}$-sfGFP foci (figure 6 B, two examples). To find if FTN_0045-mScarlet-I foci formation is dependent on any FNI or FPI genes, we tested several deletion mutants in FTN_0045-mScarlet-I background. Deletion of $pdpB_{FNI}$, *pdpB*, *dotU*, *iglI*, *iglB*, *clpB* and *ftsA* did not alter FTN_0045-mScarlet-I foci formation (figure 6 C). Interestingly, deletion of *FTN_0045* resulted in the increase of the time between $T6SS_{FPI}$ sheath assembly and contraction (figure 6 D). Such stalled sheath assemblies are not regularly observed in the presence of FTN_0045 as the sheaths tend to contract immediately after full length assembly similar to sheath dynamics in *P. aeruginosa* and *Acinetobacter baylyi* (Brodmann et al., 2017; Ringel et al., 2017; Schneider et al., 2019). Importantly, deletion of *FTN_0045* did not cause a polar effect as expression of FTN_0045 from pFNMB2 in a *FTN_0045* deletion mutant had a retention time between sheath assembly and contraction comparable to the parent stain (figure 6 D).

Discussion

We showed that *Francisella* T6SS membrane complex is stably formed at the poles before sheath assemblies occur (figure 1). This is similar to *Escherichia coli*, where stable membrane complexes also form albeit at random subcellular localizations (Durand et al., 2015). In *E. coli*, the assembly of TssM depends on the outer membrane TssJ but is independent of TssL (Durand et al., 2015). Interestingly, formation of the PdpB membrane complex spot is dependent on DotU in *Francisella* (figure 2 A). Since PdpB stability decreases without DotU (de Bruin et al., 2011), it is possible that polar localization is required for its stability, however, it is also possible that we failed to detect low amount of polarly localized PdpB. In addition, formation of DotU foci was dependent on PdpB (figure 2 B). Only one PdpB or DotU spot was resolved at one particular pole by either wide field fluorescence microscopy or SIM, however, there could be several membrane complexes assembled at one locus. Indeed, there is an example of T6SS arrays in *Amoebophilus asiaticus*, which encodes another non-canonical but unrelated T6SS (Böck et al., 2017).

Strikingly, most *Francisella* cells assembled a membrane complex at one or both poles (figure XX). However, only about 30 % of cells assembled a dynamic sheath under the same conditions despite apparently having the same amount of IglA-sfGFP (Brodmann et al., 2017). This indicates that there are additional regulation mechanisms that activate T6SS sheath assembly or that some low copy number essential components are limiting T6SS assembly. FPI transcription is regulated by at least six transcriptional regulators, which integrate signals from different pathways (Bröms et al., 2010). This complex regulatory network may also explain the observation that DotU and IglA expression is apparently differently regulated (Fig XX). Indeed, *dotU* and *iglA* lie on two different operons, which are differentially repressed by Hfq (Meibom et al., 2009).

In canonical T6SS, membrane complex formation requires 5-12 copies of each component, while sheath and inner tube assembly require up to thousands copies per structure (Lin et al., 2019; Wang et al., 2017). Thus, it would be cost-effective for *Francisella* to express components of the membrane complex first and only express high copy number subunits after sensing additional stimuli. Accordingly,

phagosomal escape occurs 1 – 4 h post infection (Chong et al., 2008), leaving enough time to synthesize sheath and inner tube components. However, it also raises the question why membrane complex components are already expressed in liquid culture. One explanation could be that, components of the membrane complex are inserted into the cell envelope during cell division as suggested for *Legionella* T4SS (Jeong et al., 2017). However, this seems unlikely for PdpB and DotU as we showed that membrane complex foci formed after 20 min of incubation on an agarose pad (figure 2 C-F). In agreement, deletion of several genes involved in cell division did not abrogate polar T6SS assembly (figure 3). In canonical T6SS, the whole membrane complex cannot be inserted without peptidoglycan remodeling. Thus, some T6SS clusters encode specific peptidoglycan hydrolases (Santin and Cascales, 2017; Weber et al., 2016). Since the FPI does not encode a peptidoglycan hydrolase, it is possible that a general peptidoglycan hydrolase makes space for T6SS membrane complex insertion.

Interestingly, time-lapse imaging suggested that membrane complex foci are only formed after 20 min incubation on an agarose pad suggesting that there is additional regulation for membrane complex biogenesis (Figure 2 C and E). In addition, we usually observed T6SS sheath assemblies only at one pole even if both poles harbored a membrane complex focus, suggesting that T6SS sheath assembly is regulated. This could be similar to a threonine phosphorylation pathway that regulates initiation and positioning of T6SS assembly on a post-translational level in some organisms (Basler et al., 2013; Casabona et al., 2013; Fritsch et al., 2013; Lin et al., 2014; Mougous et al., 2007; Ostrowski et al., 2018; Silverman et al., 2011).

Next, we showed that IglI is localized to the poles and may co-localize with the distal end of an assembling sheath. Bioinformatics analysis showed a putative N-terminal ImpA domain similar to members of the TssA protein family, which have diverse structures and functions (Dix et al., 2018; Planamente et al., 2016; Santin et al., 2018; Schneider et al., 2019; Zoued et al., 2016). Similarly to TssA in *E. coli*, IglI is essential for T6SS function in *F. novicida* (Brodmann et al., 2017, 2018; Zoued et al., 2016). TssA in *E. coli* initiates sheath assembly at the baseplate and then co-localizes with its distal end during sheath assembly (Zoued et al., 2016). In contrast, IglI was observed both at the distal end of a sheath and also at the membrane during on-going sheath assembly (figure 4 A-B). SIM imaging showed that IglI often co-

localizes with small pre-assembled IglA foci in cells without fully assembled sheaths (figure 4 A), however, IglI also localizes at the poles in cells with no apparent sheath assemblies (figure 4 B-C). In addition, unlike TssA in *E. coli*, IglI localizes to foci in the absence of the membrane complex (figure 4 C), however IglI is not required for polar localization of the membrane complex (figure 2 B). It is also interesting that IglI is not always localized at the distal end of an assembling sheath but sometimes only localizes to the membrane as was previously reported for *P. aeruginosa* TssA1 (Schneider et al., 2019).

Lastly, we checked subcellular localization of $T6SS_{FNI}$, the additional putative T6SS encoded on the FNI (Bröms et al., 2010; Rigard et al., 2016). Unfortunately, $T6SS_{FNI}$ sheath or membrane complex assembly was never observed under our conditions (figure 5 B,C). In addition, we found no repressor in the FNI cluster (figure 5 D) that would function similarly to a post-translational repressor TagF in *P. aeruginosa* and *S. marcescens* (Lin et al., 2018; Silverman et al., 2011). It is likely that either not all necessary $T6SS_{FNI}$ components are expressed or that additional positive stimuli are missing under our test conditions.

Since FTN_0045 is the only FNI component, which was identified in a transposon screen for intracellular virulence factors (Kraemer et al., 2009), we were interested in its subcellular localization. Interestingly, FTN_0045 contains a putative N-terminal ImpA domain and formed dynamic foci, which were formed independently of other FNI or FPI components (figure 6 A-C). Surprisingly, deletion of *FTN_0045* affected T6SS sheath dynamics and elongated the time sheaths remained extended (figure 6 D). In *E. coli* and *V. cholerae*, an additional TssA-like protein called TagA is localized to the membrane opposite of the baseplate and stabilizes the extended sheath (Santin et al., 2018; Schneider et al., 2019; Szwedziak and Pilhofer, 2019). Deletion of TagA results in sheaths contracting immediately upon full assembly (Santin et al., 2018). Thus, deletion of *FTN_0045* seems to have the opposite phenotype of *tagA* deletion, however the mechanism of how FNI component FTN_0045 affects $T6SS_{FPI}$ sheath dynamics remains to be elucidated.

In summary, we characterized dynamics of *Francisella* T6SS membrane complex assembly, which occurs at one or both poles, which is dependent on PdpB, IglE or DotU but independent of other FPI components. In addition, we showed that IglI is required to initiate T6SS sheath assembly similar to TssA in *E. coli*. Future

experiments will have to elucidate the necessary components for localizing *Francisella* T6SS to the poles and answer the question if *Francisella* possesses post-translational regulation for initiating T6SS activity. Nevertheless, understanding the spatial-temporal dynamics of *Francisella* T6SS assembly will allow better inhibition of *Francisella* pathogenicity in future.

Material and Methods

Bacterial strains and growth conditions

Francisella novicida U112 (*F. novicida*) and derivative strains were grown aerobically in brain heart infection (BHI) broth or on BHI agar plates at 37 °C. The medium was always supplemented with 0.1 % L-cysteine (Acros Organics) and either with ampicillin (100 µg/ml AppliChem) or with kanamycin (15 µg/ml, AppliChem) when strains harbored expression plasmids. To induce gene expression, 100 ng/ml anhydrotetracycline (ATc, IBA) was added to the liquid culture at OD_{600} of 0.02 for 3 h. *Escherichia coli* DH5α λpir (*E. coli*) and derivative strains were aerobically grown in Luria broth (LB) or on LB agar plates supplemented with 50 µg/ml kanamycin at 37 °C. All strains are listed in table 1.

Bacterial mutagenesis

To introduce in-frame deletions and tag genes with fluorophores on the chromosome of *F. novicida*, suicide vector pDMK3 was used (Lindgren et al., 2007). Fluorophores were c-terminally linked to corresponding genes by an Ala-Ala-Ala-Gly-Gly-Gly linker. After the end codon of the fluorophore, 10 amino acids of the tagged gene was added in order to avoid polar effects on downstream genes. Expression plasmid pFNMB2 was used for gene expression under a tetracycline inducible promoter (Brodmann et al., 2018). Mutagenesis and conjugation was carried out as reported previously (Brodmann et al., 2017, 2018). For conjugation, a donor *E. coli* strain from A. Harms and C. Dehio (Harms et al., 2017) was used. In short, recipient *F. novicida* and donor *E. coli* strains were grown in liquid cultures until OD_{600} of 1. 1 ml of each culture was washed once in LB broth and mixed together in 20 µl of LB. The mixture was spotted on a LB agar plate supplemented with 300 µM 2,6-Diaminopimelic acid and incubated at 25 °C over night. Then, the mixture was plated on Muller Hinton agar plates supplemented with 0.1 % L-cysteine, 0.1 % *D*-glucose (Millipore), 0.1 % fetal calf serum (BioConcept), 100 µg/ml ampicillin and 15 µg/ml kanamycin. The plates were incubated at 37 °C for 2 days. *F. novicida* colonies harboring the plasmid were restreaked on BHI agar plates supplemented with 0.1 % L-cysteine, 100 µg/ml ampicillin and 15 µg/ml kanamycin. For negative selection, colonies were restreaked on LB agar plates supplemented with 0.1 % L-cysteine, 10

% sucrose and 100 µg/ml ampicillin and incubated at room temperature for a couple of days. All plasmids and remaining peptides of in-frame deletions are listed in table 2. All cloning products were sequenced and sites of homologous recombination were verified by PCR.

Fluorescence live cell imaging

Microscope set up was described previously (Brodmann et al., 2017; Kudryashev et al., 2015; Vettiger and Basler, 2016). A Nikon Ti-E inverted motorized microscope was used for live-cell fluorescence imaging. The microscope was equipped with Perfect Focus System and a Plan Apo 1003 Oil Ph3 DM (NA 1.4) objective lens. Fluorescence was excited and filtrated with SPECTRA X light engine (Lumencor) along with ET-GFP (Chroma #49002) and ET-mCherry (Chroma #49008) filter sets. The exposure time for each channel was set to 150 ms. Images were collected with a sCMOS camera pco.edge 4.2 with a pixel size of 65 nm (PCO) and VisiView software (Visitron). For imaging, day cultures of *F. novicida* parental and mutant strains were inoculated from plate at an OD_{600} of 0.02 without any antibiotics. For strains harboring an expression plasmid, the medium was supplemented with 15 µg/ml, kanamycin and 100 ng/ml ATc to induce expression. At an OD_{600} of 1, the cultures were concentrated in phosphate saline buffer (PBS) to an OD_{600} of 10. 1.5 µl of the concentrated cultures was then spotted on a pad consisting of 1 % agarose in PBS. The agarose pad was incubated at 37 °C for 1 h before imaging at 30 °C and 95 % humidity (T-unit, Okolab). For long-term imaging, the liquid cultures were supplemented with 1000 µg/ml chloramphenicol in dimethylsulfoxid (DMSO, Sigma-Aldrich) or just the similar volume of DMSO as control at OD_{600} of 0.8 and incubated aerobically for 1 h. The concentrated cultures were spotted on a pad consisting of 1 % agarose in PBS supplemented with or without 1000 µg/ml chloramphenicol in DMSO. Then, imaging started immediately. In general, images were collected every 5 s for 3 min. For the long-term imaging, images were collected every 5 min for 1 h.

Image analysis

Image analysis was carried out with Fiji software (Schindelin et al., 2012) as previously described (Basler et al., 2013; Vettiger and Basler, 2016). For comparison of fluorescent signal intensities, the contrast was set to same values for sets of compared images. Kymograms were made with the "Reslice" function. If not stated otherwise, no deconvolution was applied. In necessary, Huygens Remote Manager (http://huygensrm.org) was used for deconvolving images. "Classic maximum likelihood estimation "algorithm was applied with background estimation set to auto. 40 iterations were run and quality change stopping criterion was 0.1.

Quantification of T6SS activity from 3 min time-lapse movies was carried out with the "temporal colour code" function. T6SS activity is shown as relative T6SS activity of mutants compared to parental strain in order to account for daily variations. Three biological replicates were analyzed with at least 1000 cells per field of view. Determination of the time between stopped assembly and contraction was performed with the "Reslice" function. Only events were taken into account with visible assembly stop and contraction. Analysis included three biological replicates with at least 105 events per strain in total. T6SS sheath length and assembly speed was quantified with "Reslice" function. Three biological replicates were analysed with at least 67 events in total.

Live-cell structural illumination microscopy (SIM)

Samples were prepared as described above. 3D SIM was performed with on a microscope system DeltaVision OMX-Blaze version 4 (GE Healthcare) equipped with a Plan Apo N 60x (NA 1.42) oil immersion objective lens (Olympus) and four liquid-cooled sCMOS cameras (Edge 5.5, full frame 2.560 x 2160; PCO). 488 nm and 568 nm solid state laser lines were used for excitation of fluorescence with 10 % laser intensity. Exposure time was between 12 - 120 ms. Exciting light was directed through a movable optical grating to generate a fine-striped interference pattern on the sample plane. The pattern was shifted laterally through five phases and three angular rotations of 60° for each Z-section. Z-sections were spaced by 0.125 µm. Raw 2D-SIM images were processed and reconstructed using DeltaVision OMX SoftWoRx software package (v6.1.3, GE Healthcare). The resulting size of the

reconstructed images was of 512 x 512 pixels from an initial set of 256 x 256 raw images.

Homology predictions

Amino acid sequences of FNI genes (uniprot.org) were used for homology detection and structure prediction by HMM-HMM comparison (HHpred) with the online MPI Bioinformatics Toolkit (Zimmermann et al., 2018).

Statistical analysis

Statistical analysis of data was performed with Prism8 (GraphPad Software). To test if the retardation of T6SS sheath contraction is significantly different in mutants compared to parental strain, one-way ANOVA ($\alpha = 0.05$) with correction for multiple comparison (Tukey's multiple comparisons test) was used. *p*-values and *q*-values are given in the figure legend. Differences in T6SS sheath length and assembly speed were tested with an unpaired two-tailed *t*-test with Welch's correction. *p*-values are given in the figure legend.

Author contributions

M.Br. and M.Ba. designed experiments, analyzed and interpreted the results. M.Br., L.P. and L.D. generated strains and acquired data. M.Br. and M.Ba. wrote the manuscript. All authors approved the manuscript.

Acknowledgment

We thank M.A. Horwitz (UCLA) for providing the strain *F. novicida* U112 *iglA-sfGFP*, D.M. Monack (Stanford University) for the conjugation plasmid pDMK3, A. Harms and C. Dehio (Biozentrum, University of Basel) for the *E. coli* conjugation strain and the Imaging Core Facility (Biozentrum, University of Basel), in particular Alexia Ferrand, for the technical assistance provided on the OMX microscope. The work was supported by Swiss National Science Foundation (SNSF) grant XX and

the University of Basel. M.Br. was supported by the Biozentrum Basel International PhD Program "Fellowships for Excellence”. L.P. was supported by the Biozentrum Basel "Bachelor Research Summer Internship" program.

Declaration of interests

The authors declare no competing interests.

References

Aarsman, M.E.G., Piette, A., Fraipont, C., Vinkenvleugel, T.M.F., Nguyen-Distèche, M., and den Blaauwen, T. (2005). Maturation of the Escherichia coli divisome occurs in two steps. Mol. Microbiol. *55*, 1631–1645.

Abdelrahim Zoued, E.D., Yannick R. Brunet, S.S., Badreddine Douzi, M.G., Nicolas Flaugnatti, P.L., Laure Journet, R.F., Tâm Mignot, C.C., and Eric Cascales (2016). Priming and polymerization of a bacterial contractile tail structure. Nature.

Ahlund, M.K., Rydén, P., Sjöstedt, A., and Stöven, S. (2010). Directed screen of Francisella novicida virulence determinants using Drosophila melanogaster. Infect. Immun. *78*, 3118–3128.

Alam, A., Golovliov, I., Javed, E., and Sjöstedt, A. (2018). ClpB mutants of Francisella tularensis subspecies holarctica and tularensis are defective for type VI secretion and intracellular replication. Sci. Rep. *8*, 11324.

Basler, M., and Mekalanos, J.J. (2012). Type 6 secretion dynamics within and between bacterial cells. Science *337*, 815–815.

Basler, M., Pilhofer, M., Henderson, P., Jensen, J.G., and Mekalanos, J. (2012). Type VI secretion requires a dynamic contractile phage tail-like structure. Nature *483*, 182–186.

Basler, M., Ho, B.T., and Mekalanos, J.J. (2013). Tit-for-tat: Type VI secretion system counterattack during bacterial cell-cell interactions. Cell *152*, 884–894.

Bingle, L.E., Bailey, C.M., and Pallen, M.J. (2008). Type VI secretion: a beginner's guide. Curr. Opin. Microbiol. *11*, 3–8.

Böck, D., Medeiros, J.M., Tsao, H.-F., Penz, T., Weiss, G.L., Aistleitner, K., Horn, M., and Pilhofer, M. (2017). In situ architecture, function, and evolution of a contractile injection system. Science *357*, 713–717.

Bönemann, G., Pietrosiuk, A., Diemand, A., Zentgraf, H., and Mogk, A. (2009). Remodelling of VipA/VipB tubules by ClpV-mediated threading is crucial for type VI protein secretion. EMBO J. *28*, 315–325.

Brodmann, M., Dreier, R.F., Broz, P., and Basler, M. (2017). Francisella requires dynamic type VI secretion system and ClpB to deliver effectors for phagosomal escape. Nat. Commun. *8*, 15853.

Brodmann, M., Heilig, R., Broz, P., and Basler, M. (2018). Mobilizable Plasmids for Tunable Gene Expression in Francisella novicida. Front. Cell. Infect. Microbiol. *8*.

Bröms, J.E., Sjöstedt, A., and Lavander, M. (2010). The Role of the Francisella Tularensis Pathogenicity Island in Type VI Secretion, Intracellular Survival, and Modulation of Host Cell Signaling. Front. Microbiol. *1*, 136.

de Bruin, O.M., Duplantis, B.N., Ludu, J.S., Hare, R.F., Nix, E.B., Schmerk, C.L., Robb, C.S., Boraston, A.B., Hueffer, K., and Nano, F.E. (2011). The biochemical properties of the Francisella pathogenicity island (FPI)-encoded proteins IglA, IglB, IglC, PdpB and DotU suggest roles in type VI secretion. Microbiol. Read. Engl. *157*, 3483–3491.

Brunet, Y.R., Hénin, J., Celia, H., and Cascales, E. (2014). Type VI secretion and bacteriophage tail tubes share a common assembly pathway. EMBO Rep. *15*, 315–321.

Brunet, Y.R., Zoued, A., Boyer, F., Douzi, B., and Cascales, E. (2015). The Type VI Secretion TssEFGK-VgrG Phage-Like Baseplate Is Recruited to the TssJLM Membrane Complex via Multiple Contacts and Serves As Assembly Platform for Tail Tube/Sheath Polymerization. PLoS Genet. *11*, e1005545.

Brunton, J., Steele, S., Miller, C., Lovullo, E., Taft-Benz, S., and Kawula, T. (2015). Identifying Francisella tularensis genes required for growth in host cells. Infect. Immun. *83*, 3015–3025.

Carlsson, F., Joshi, S.A., Rangell, L., and Brown, E.J. (2009). Polar localization of virulence-related Esx-1 secretion in mycobacteria. PLoS Pathog. *5*, e1000285.

Carter, T., Buensuceso, R.N.C., Tammam, S., Lamers, R.P., Harvey, H., Howell, P.L., and Burrows, L.L. (2017). The Type IVa Pilus Machinery Is Recruited to Sites of Future Cell Division. MBio *8*.

Casabona, M.G., Silverman, J.M., Sall, K.M., Boyer, F., Couté, Y., Poirel, J., Grunwald, D., Mougous, J.D., Elsen, S., and Attree, I. (2013). An ABC transporter and an outer membrane lipoprotein participate in posttranslational activation of type VI secretion in Pseudomonas aeruginosa. Environ. Microbiol. *15*, 471–486.

Chakravortty, D., Rohde, M., Jäger, L., Deiwick, J., and Hensel, M. (2005). Formation of a novel surface structure encoded by Salmonella Pathogenicity Island 2. EMBO J. *24*, 2043–2052.

Charles, M., Pérez, M., Kobil, J.H., and Goldberg, M.B. (2001). Polar targeting of Shigella virulence factor IcsA in Enterobacteriacae and Vibrio. Proc. Natl. Acad. Sci. U. S. A. *98*, 9871–9876.

Cherrak, Y., Rapisarda, C., Pellarin, R., Bouvier, G., Bardiaux, B., Allain, F., Malosse, C., Rey, M., Chamot-Rooke, J., Cascales, E., et al. (2018). Biogenesis and structure of a type VI secretion baseplate. Nat. Microbiol.

Chong, A., and Celli, J. (2010). The francisella intracellular life cycle: toward molecular mechanisms of intracellular survival and proliferation. Front. Microbiol. *1*, 138.

Chong, A., Wehrly, T.D., Nair, V., Fischer, E.R., Barker, J.R., Klose, K.E., and Celli, J. (2008). The Early Phagosomal Stage of Francisella tularensis Determines Optimal Phagosomal Escape and Francisella Pathogenicity Island Protein Expression. Infect. Immun. *76*, 5488–5499.

Clemens, D.L., Ge, P., Lee, B.-Y., Horwitz, M.A., and Zhou, Z.H. (2015). Atomic Structure of T6SS Reveals Interlaced Array Essential to Function. Cell *160*, 940–951.

Detweiler, C.S., Monack, D.M., Brodsky, I.E., Mathew, H., and Falkow, S. (2003). virK, somA and rcsC are important for systemic Salmonella enterica serovar Typhimurium infection and cationic peptide resistance. Mol. Microbiol. *48*, 385–400.

Dix, S.R., Owen, H.J., Sun, R., Ahmad, A., Shastri, S., Spiewak, H.L., Mosby, D.J., Harris, M.J., Batters, S.L., Brooker, T.A., et al. (2018). Structural insights into the function of type VI secretion system TssA subunits. Nat. Commun. *9*, 4765.

Durand, E., Nguyen, V.S., Zoued, A., Logger, L., Péhau-Arnaudet, G., Aschtgen, M.-S., Spinelli, S., Desmyter, A., Bardiaux, B., Dujeancourt, A., et al. (2015). Biogenesis and structure of a type VI secretion membrane core complex. Nature *523*, 555–560.

Eshraghi, A., Kim, J., Walls, A.C., Ledvina, H.E., Miller, C.N., Ramsey, K.M., Whitney, J.C., Radey, M.C., Peterson, S.B., Ruhland, B.R., et al. (2016). Secreted Effectors Encoded within and outside of the Francisella Pathogenicity Island Promote Intramacrophage Growth. Cell Host Microbe *20*, 573–583.

Fritsch, M.J., Trunk, K., Diniz, J.A., Guo, M., Trost, M., and Coulthurst, S.J. (2013). Proteomic Identification of Novel Secreted Antibacterial Toxins of the Serratia marcescens Type VI Secretion System. Mol. Cell. Proteomics MCP *12*, 2735–2749.

Ghosal, D., Jeong, K.C., Chang, Y.-W., Gyore, J., Teng, L., Gardner, A., Vogel, J.P., and Jensen, G.J. (2019). Molecular architecture, polar targeting and biogenesis of the Legionella Dot/Icm T4SS. Nat. Microbiol.

Harms, A., Segers, F.H.I.D., Quebatte, M., Mistl, C., Manfredi, P., Körner, J., Chomel, B.B., Kosoy, M., Maruyama, S., Engel, P., et al. (2017). Evolutionary Dynamics of Pathoadaptation Revealed by Three Independent Acquisitions of the VirB/D4 Type IV Secretion System in Bartonella. Genome Biol. Evol. *9*, 761–776.

Huitema, E., Pritchard, S., Matteson, D., Radhakrishnan, S.K., and Viollier, P.H. (2006). Bacterial birth scar proteins mark future flagellum assembly site. Cell *124*, 1025–1037.

Ikäheimo, I., Syrjälä, H., Karhukorpi, J., Schildt, R., and Koskela, M. (2000). In vitro antibiotic susceptibility of Francisella tularensis isolated from humans and animals. J. Antimicrob. Chemother. *46*, 287–290.

Jain, S., van Ulsen, P., Benz, I., Schmidt, M.A., Fernandez, R., Tommassen, J., and Goldberg, M.B. (2006). Polar localization of the autotransporter family of large bacterial virulence proteins. J. Bacteriol. *188*, 4841–4850.

Jeong, K.C., Ghosal, D., Chang, Y.-W., Jensen, G.J., and Vogel, J.P. (2017). Polar delivery of Legionella type IV secretion system substrates is essential for virulence. Proc. Natl. Acad. Sci. U. S. A.

Kraemer, P.S., Mitchell, A., Pelletier, M.R., Gallagher, L.A., Wasnick, M., Rohmer, L., Brittnacher, M.J., Manoil, C., Skerett, S.J., and Salama, N.R. (2009). Genome-wide screen in Francisella novicida for genes required for pulmonary and systemic infection in mice. Infect. Immun. *77*, 232–244.

Kudryashev, M., Wang, R.Y.-R., Brackmann, M., Scherer, S., Maier, T., Baker, D., DiMaio, F., Stahlberg, H., Egelman, E.H., and Basler, M. (2015). Structure of the type VI secretion system contractile sheath. Cell *160*, 952–962.

Lennings, J., Mayer, C., Makhlouf, M., Brötz-Oesterhelt, H., and Schwarz, S. (2019). Polar localization of the ATPase ClpV-5 occurs independent of type VI secretion system apparatus proteins in Burkholderia thailandensis. BMC Res. Notes *12*, 109.

Lin, J.-S., Wu, H.-H., Hsu, P.-H., Ma, L.-S., Pang, Y.-Y., Tsai, M.-D., and Lai, E.-M. (2014). Fha Interaction with Phosphothreonine of TssL Activates Type VI Secretion in Agrobacterium tumefaciens. PLoS Pathog. *10*, e1003991.

Lin, J.-S., Pissaridou, P., Wu, H.-H., Tsai, M.-D., Filloux, A., and Lai, E.-M. (2018). TagF-mediated repression of bacterial type VI secretion systems involves a direct interaction with the cytoplasmic protein Fha. J. Biol. Chem.

Lin, L., Lezan, E., Schmidt, A., and Basler, M. (2019). Abundance of bacterial Type VI secretion system components measured by targeted proteomics. Nat. Commun. *10*, 2584.

Lindgren, H., Shen, H., Zingmark, C., Golovliov, I., Conlan, W., and Sjöstedt, A. (2007). Resistance of Francisella tularensis strains against reactive nitrogen and oxygen species with special reference to the role of KatG. Infect. Immun. *75*, 1303–1309.

Lo, K.Y., Visram, S., Vogl, A.W., Shen, C.L.J., and Guttman, J.A. (2016). Morphological analysis of Francisella novicida epithelial cell infections in the absence of functional FipA. Cell Tissue Res. *363*, 449–459.

Mac Síomóin, R.A., Nakata, N., Murai, T., Yoshikawa, M., Tsuji, H., and Sasakawa, C. (1996). Identification and characterization of ispA, a Shigella flexneri chromosomal gene essential for normal in vivo cell division and intracellular spreading. Mol. Microbiol. *19*, 599–609.

Meibom, K.L., Forslund, A.-L., Kuoppa, K., Alkhuder, K., Dubail, I., Dupuis, M., Forsberg, A., and Charbit, A. (2009). Hfq, a novel pleiotropic regulator of virulence-associated genes in Francisella tularensis. Infect. Immun. *77*, 1866–1880.

Morgan, J.K., Luedtke, B.E., and Shaw, E.I. (2010). Polar localization of the Coxiella burnetii type IVB secretion system. FEMS Microbiol. Lett. *305*, 177–183.

Mougous, J.D., Gifford, C.A., Ramsdell, T.L., and Mekalanos, J.J. (2007). Threonine phosphorylation post-translationally regulates protein secretion in Pseudomonas aeruginosa. Nat Cell Biol *9*, 797–803.

Nakata, N., Sasakawa, C., Okada, N., Tobe, T., Fukuda, I., Suzuki, T., Komatsu, K., and Yoshikawa, M. (1992). Identification and characterization of virK, a virulence-associated large plasmid gene essential for intercellular spreading of Shigella flexneri. Mol. Microbiol. *6*, 2387–2395.

Nguyen, J.Q., Gilley, R.P., Zogaj, X., Rodriguez, S.A., and Klose, K.E. (2014). Lipidation of the FPI protein IglE contributes to Francisella tularensis ssp. novicida intramacrophage replication and virulence. Pathog. Dis. *72*, 10–18.

Ostrowski, A., Cianfanelli, F.R., Porter, M., Mariano, G., Peltier, J., Wong, J.J., Swedlow, J.R., Trost, M., and Coulthurst, S.J. (2018). Killing with proficiency: Integrated post-translational regulation of an offensive Type VI secretion system. PLoS Pathog. *14*, e1007230.

Oyston, P.C.F., Sjostedt, A., and Titball, R.W. (2004). Tularaemia: bioterrorism defence renews interest in Francisella tularensis. Nat. Rev. Microbiol. *2*, 967–978.

de Pedro, M.A., Grünfelder, C.G., and Schwarz, H. (2004). Restricted Mobility of Cell Surface Proteins in the Polar Regions of Escherichia coli. J. Bacteriol. *186*, 2594–2602.

Pietrosiuk, A., Lenherr, E.D., Falk, S., Bönemann, G., Kopp, J., Zentgraf, H., Sinning, I., and Mogk, A. (2011). Molecular basis for the unique role of the AAA+ chaperone ClpV in type VI protein secretion. J. Biol. Chem. *286*, 30010–30021.

Planamente, S., Salih, O., Manoli, E., Albesa-Jové, D., Freemont, P.S., and Filloux, A. (2016). TssA forms a gp6-like ring attached to the type VI secretion sheath. EMBO J. *35*, 1613–1627.

Qin, A., Zhang, Y., Clark, M.E., Moore, E.A., Rabideau, M.M., Moreau, G.B., and Mann, B.J. (2016). Components of the type six secretion system are substrates of Francisella tularensis Schu S4 DsbA-like FipB protein. Virulence *7*, 882–894.

Qiu, J., and Luo, Z.-Q. (2017). Legionella and Coxiella effectors: strength in diversity and activity. Nat. Rev. Microbiol. *15*, 591–605.

Rapisarda, C., Cherrak, Y., Kooger, R., Schmidt, V., Pellarin, R., Logger, L., Cascales, E., Pilhofer, M., Durand, E., and Fronzes, R. (2019). In situ and high-resolution cryo-EM structure of a bacterial type VI secretion system membrane complex. EMBO J.

Rigard, M., Bröms, J.E., Mosnier, A., Hologne, M., Martin, A., Lindgren, L., Punginelli, C., Lays, C., Walker, O., Charbit, A., et al. (2016). Francisella tularensis IglG Belongs to a Novel Family of PAAR-Like T6SS Proteins and Harbors a Unique N-terminal Extension Required for Virulence. PLoS Pathog. *12*, e1005821.

Ringel, P.D., Hu, D., and Basler, M. (2017). The Role of Type VI Secretion System Effectors in Target Cell Lysis and Subsequent Horizontal Gene Transfer. Cell Rep. *21*, 3927–3940.

Rosch, J., and Caparon, M. (2004). A microdomain for protein secretion in Gram-positive bacteria. Science *304*, 1513–1515.

Santin, Y.G., and Cascales, E. (2017). Domestication of a housekeeping transglycosylase for assembly of a Type VI secretion system. EMBO Rep. *18*, 138–149.

Santin, Y.G., Doan, T., Lebrun, R., Espinosa, L., Journet, L., and Cascales, E. (2018). In vivo TssA proximity labelling during type VI secretion biogenesis reveals TagA as a protein that stops and holds the sheath. Nat. Microbiol. *3*, 1304–1313.

Schindelin, J., Arganda-Carreras, I., Frise, E., Kaynig, V., Longair, M., Pietzsch, T., Preibisch, S., Rueden, C., Saalfeld, S., Schmid, B., et al. (2012). Fiji: an open-source platform for biological-image analysis. Nat. Methods *9*, 676–682.

Schneider, J.P., Nazarov, S., Adaixo, R., Liuzzo, M., Ringel, P.D., Stahlberg, H., and Basler, M. (2019). Diverse roles of TssA-like proteins in the assembly of bacterial type VI secretion systems. EMBO J. *0*, e100825.

Schwarz, S., Singh, P., Robertson, J.D., LeRoux, M., Skerrett, S.J., Goodlett, D.R., West, T.E., and Mougous, J.D. (2014). VgrG-5 is a Burkholderia type VI secretion system-exported protein required for multinucleated giant cell formation and virulence. Infect. Immun. *82*, 1445–1452.

Scott, M.E., Dossani, Z.Y., and Sandkvist, M. (2001). Directed polar secretion of protease from single cells of Vibrio cholerae via the type II secretion pathway. Proc. Natl. Acad. Sci. U. S. A. *98*, 13978–13983.

Shneider, M.M., Buth, S.A., Ho, B.T., Basler, M., Mekalanos, J.J., and Leiman, P.G. (2013). PAAR-repeat proteins sharpen and diversify the type VI secretion system spike. Nature *500*, 350–353.

Silverman, J.M., Austin, L.S., Hsu, F., Hicks, K.G., Hood, R.D., and Mougous, J.D. (2011). Separate inputs modulate phosphorylation-dependent and -independent type VI secretion activation. Mol. Microbiol. *82*, 1277–1290.

Stewart, E.J., Madden, R., Paul, G., and Taddei, F. (2005). Aging and death in an organism that reproduces by morphologically symmetric division. PLoS Biol. *3*, e45.

Su, J., Yang, J., Zhao, D., Kawula, T.H., Banas, J.A., and Zhang, J.-R. (2007). Genome-wide identification of Francisella tularensis virulence determinants. Infect. Immun. *75*, 3089–3101.

Sun, P., Austin, B.P., Schubot, F.D., and Waugh, D.S. (2007). New protein fold revealed by a 1.65 Å resolution crystal structure of Francisella tularensis pathogenicity island protein IglC. Protein Sci. *16*, 2560–2563.

Surovtsev, I.V., and Jacobs-Wagner, C. (2018). Subcellular Organization: A Critical Feature of Bacterial Cell Replication. Cell *172*, 1271–1293.

Szwedziak, P., and Pilhofer, M. (2019). Bidirectional contraction of a type six secretion system. Nat. Commun. *10*, 1565.

Thiem, S., and Sourjik, V. (2008). Stochastic assembly of chemoreceptor clusters in Escherichia coli. Mol. Microbiol. *68*, 1228–1236.

Typas, A., Banzhaf, M., Gross, C.A., and Vollmer, W. (2011). From the regulation of peptidoglycan synthesis to bacterial growth and morphology. Nat. Rev. Microbiol. *10*, 123–136.

Vettiger, A., and Basler, M. (2016). Type VI Secretion System Substrates Are Transferred and Reused among Sister Cells. Cell *167*, 99-110.e12.

Wang, J., Brackmann, M., Castaño-Díez, D., Kudryashev, M., Goldie, K.N., Maier, T., Stahlberg, H., and Basler, M. (2017). Cryo-EM structure of the extended type VI secretion system sheath-tube complex. Nat. Microbiol. *2*, 1507–1512.

Wang, J., Brodmann, M., and Basler, M. (2019). Assembly and Subcellular Localization of Bacterial Type VI Secretion Systems. Annu. Rev. Microbiol.

Weber, B.S., Hennon, S.W., Wright, M.S., Scott, N.E., de Berardinis, V., Foster, L.J., Ayala, J.A., Adams, M.D., and Feldman, M.F. (2016). Genetic Dissection of the Type VI Secretion System in Acinetobacter and Identification of a Novel Peptidoglycan Hydrolase, TagX, Required for Its Biogenesis. MBio *7*.

Yamaichi, Y., Bruckner, R., Ringgaard, S., Möll, A., Cameron, D.E., Briegel, A., Jensen, G.J., Davis, B.M., and Waldor, M.K. (2012). A multidomain hub anchors the chromosome segregation and chemotactic machinery to the bacterial pole. Genes Dev. *26*, 2348–2360.

Young, K.D. (2006). The selective value of bacterial shape. Microbiol. Mol. Biol. Rev. MMBR *70*, 660–703.

Zimmermann, L., Stephens, A., Nam, S.-Z., Rau, D., Kübler, J., Lozajic, M., Gabler, F., Söding, J., Lupas, A.N., and Alva, V. (2018). A Completely Reimplemented MPI Bioinformatics Toolkit with a New HHpred Server at its Core. J. Mol. Biol. *430*, 2237–2243.

Zoued, A., Durand, E., Brunet, Y.R., Spinelli, S., Douzi, B., Guzzo, M., Flaugnatti, N., Legrand, P., Journet, L., Fronzes, R., et al. (2016). Priming and polymerization of a bacterial contractile tail structure. Nature *531*, 59–63.

Figures

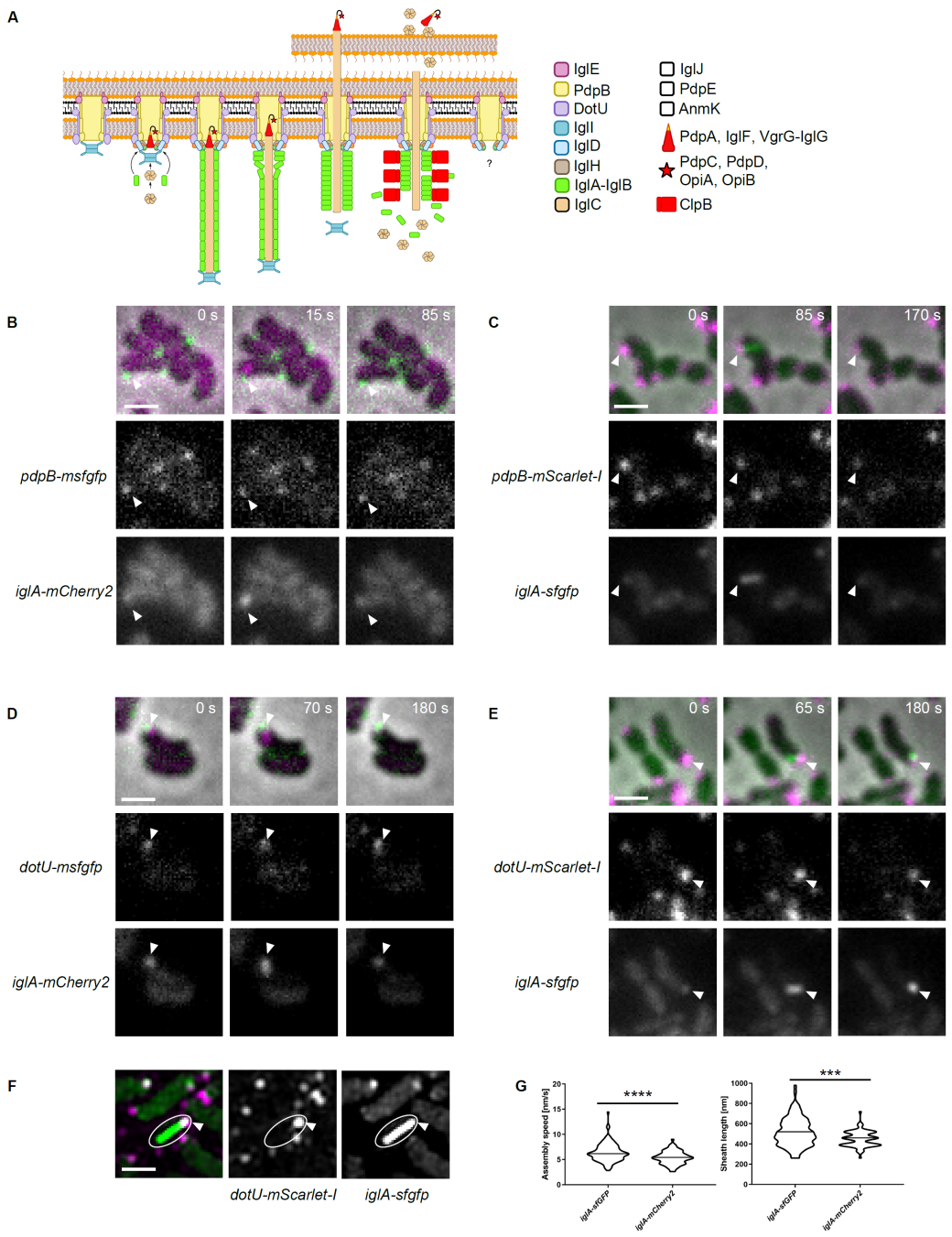

Figure 1: *Francisella* T6SS membrane complex is localized at poles. A) General T6SS biogenesis with *Francisella* T6SS components based on this study and cited articles in the main text. Membrane complex (IglE, PdpB and DotU) is assembled and serves as scaffold for baseplate (IglD and IglH) and spike complex (VgrG and IglG). PdpA and IglF were shown to be associated with VgrG and IglG, respectively. However, their exact functions are not known. IglI likely initiates and coordinates sheath (IglA and IglB) and inner tube (IglC) polymerization at the distal end of the baseplate. Contraction of T6SS sheath propels the inner tube together with the spike complex and associated effectors (PdpC, PdpD, OpiA and OpiB) into the extracellular space, whether this is the phagosomal cytosol or across the phagosomal membranes remains to be elucidated. The contracted sheath is recycled by ClpB. Whether the membrane and baseplate complex is disassembled or reused for another round of firing is not known. IglJ is a FPI component with unknown function but is essential for T6SS assembly. PdpE and AnmK are FPI components with unknown functions but dispensable for T6SS function. *Figure adapted from Schneider et al., 2019.* **B-E)** Subcellular localizations of membrane complex and sheath before, during and after T6SS assembly and contraction. Upper panels are merge of phase contrast, RFP channel and GFP channels. Middle and lower panels show GFP channel and RFP channel, respectively. Arrows highlight T6SS assemblies. 3.3 x 3.3. µm fields of view are shown. Scale bars represent 1 µm. **B)** Polar localization of membrane complex (PdpB-msfGFP) and extended sheath (IglA-mCherry2) in *F. novicida* U112 *iglA-mCherry2 pdpB-msfgfp*. **C)** Polar localization of membrane complex (PdpB-mScarlet-I) and extended sheath (IglA-sfGFP)

in *F. novicida* U112 *iglA-sfgfp pdpB-mScarlet-I*. **D)** Polar localization of membrane complex (DotU-msfGFP) and extended sheath (IglA-mCherry2) in *F. novicida* U112 *iglA-mCherry2 dotU-mScarlet-I*. **E)** Polar localization of membrane complex (DotU-mScarlet-I) and extended sheath (IglA-sfGFP) in *F. novicida* U112 *iglA-sfgfp dotU-mScarlet-I*. **F)** Polar membrane complex (DotU) and extended sheath in *F. novicida* U112 *iglA-sfgfp dotU-mScarlet-I*. Images acquired with SIM. First image is a merge of RFP and GFP channel, middle image shows RFP channel and last image shows GFP channel. 3.3 x 3.3. µm fields of view are shown. Arrows highlight T6SS assembly. White line outlines the shape of the bacterial cell. Scale bar represents 1 µm. **G)** Quantification of assembly speed and sheath length of T6SS sheaths tagged with sfGFP and mCherry2, respectively. Three biological replicates with at least 67 events in total were analyzed. Black bar represents median. $^{****}p<0.0001$, $^{***}p<0.001$.

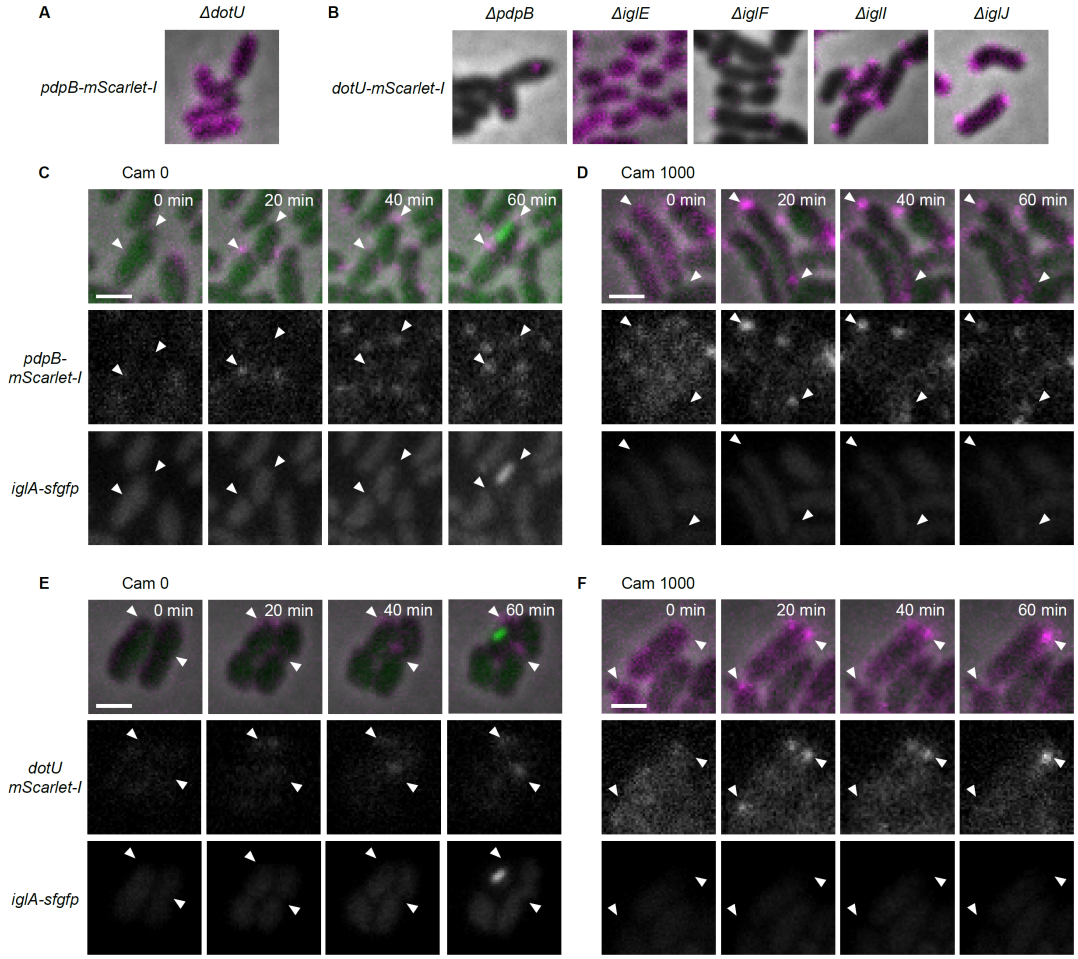

Figure 2: Dynamics of membrane complex formation. A-B) Images consist of merge of phase contrast and RFP channel is shown. 3.3 x 3.3 µm fields of view are shown. Scale bars represent 1 µm. **A)** Formation of polar PdpB-mScarlet-I subcomplex depends on DotU in *F. novicida* U112 *iglA-sfgfp pdpB-mScarlet-I ΔdotU*. **B)** Polar localization of DotU-mScarlet-I depends on PdpB or IglE in *F. novicida* U112 *iglA-sfgfp dotU-mScarlet-I ΔpdpB* or *ΔiglE* but not on other structural T6SS components in *F. novicida* U112 *iglA-sfgfp dotU-mScarlet-I ΔiglF*, *ΔiglI* or *ΔiglI*. **C-F)** Upper panels are merge of phase contrast, RFP channel and GFP channels. Middle and lower panels show RFP channel and GFP channel, respectively. Arrows highlight T6SS assemblies or formation of membrane complexes. 3.3 x 3.3. µm fields of view are shown. Scale bars represent 1 µm. **C-D)** Time-lapse images of *F. novicida* U112 *iglA-sfgfp pdpB-mScarlet-I* on agarose pads supplemented with **C)** 0 or **D)** 1000 µg/ml chloramphenicol. **E-F)** Time-lapse images of *F. novicida* U112 *iglA-sfgfp dotU-mScarlet-I* on agarose pads supplemented with **E)** 0 or **F)** 1000 µg/ml chloramphenicol. **C, E)** Assembly of polar membrane complex starts after 20 min and sheath assembly after 1h incubation on an agarose pad. **D, F)** Polar assembly of membrane complex is not dependent on protein synthesis in contrast to sheath assembly.

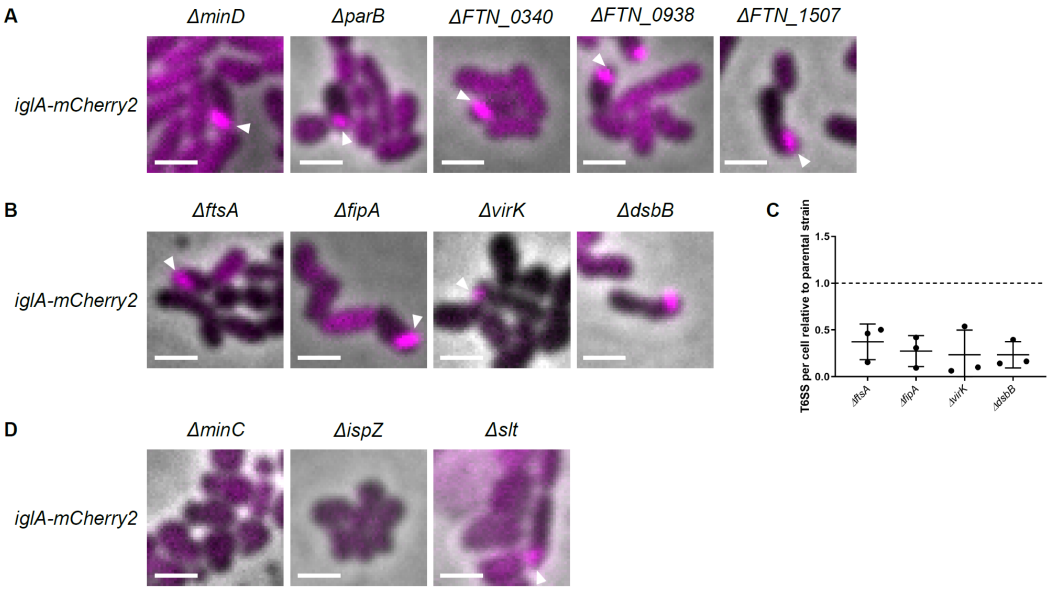

Figure 3: Polar localization of *Francisella* T6SS membrane complex is independent from several cellular components involved in subcellular organization. A-B, D) Images consist of merge of phase contrast and RFP channel is shown. Arrows highlight T6SS assemblies. 3.3 x 3.3 µm fields of view are shown. Scale bars represent 1 µm. **A)** Normal T6SS activity in *F. novicida* U112 *iglA-mCherry2 iglA*$_{FNI}$*-sfGFP ΔminD*, *ΔparB*, *ΔFTN_0340*, *ΔFTN_0938* or *ΔFTN_1507*. **B)** Decreased T6SS activity in *F. novicida* U112 *iglA-mCherry2 iglA*$_{FNI}$*-sfGFP ΔftsA*, *ΔfipA*, *ΔvirK* or *ΔdsbB*. **C)** Quantification of T6SS activity of mutants in **B)** compared to parental strain *F. novicida* U112 *iglA-mCherry2 iglA*$_{FNI}$*-sfGFP*. Black line represents mean. Error bars represent standard deviation. Three biological replicates with at least 1000 bacterial cells per field of view were analyzed for each mutant and parental strain. **D)** Aberrant cell shapes in *F. novicida* U112 *iglA-mCherry2 iglA*$_{FNI}$*-sfGFP ΔminC*, *ΔispZ* or *Δslt* lead to abolished T6SS activity.

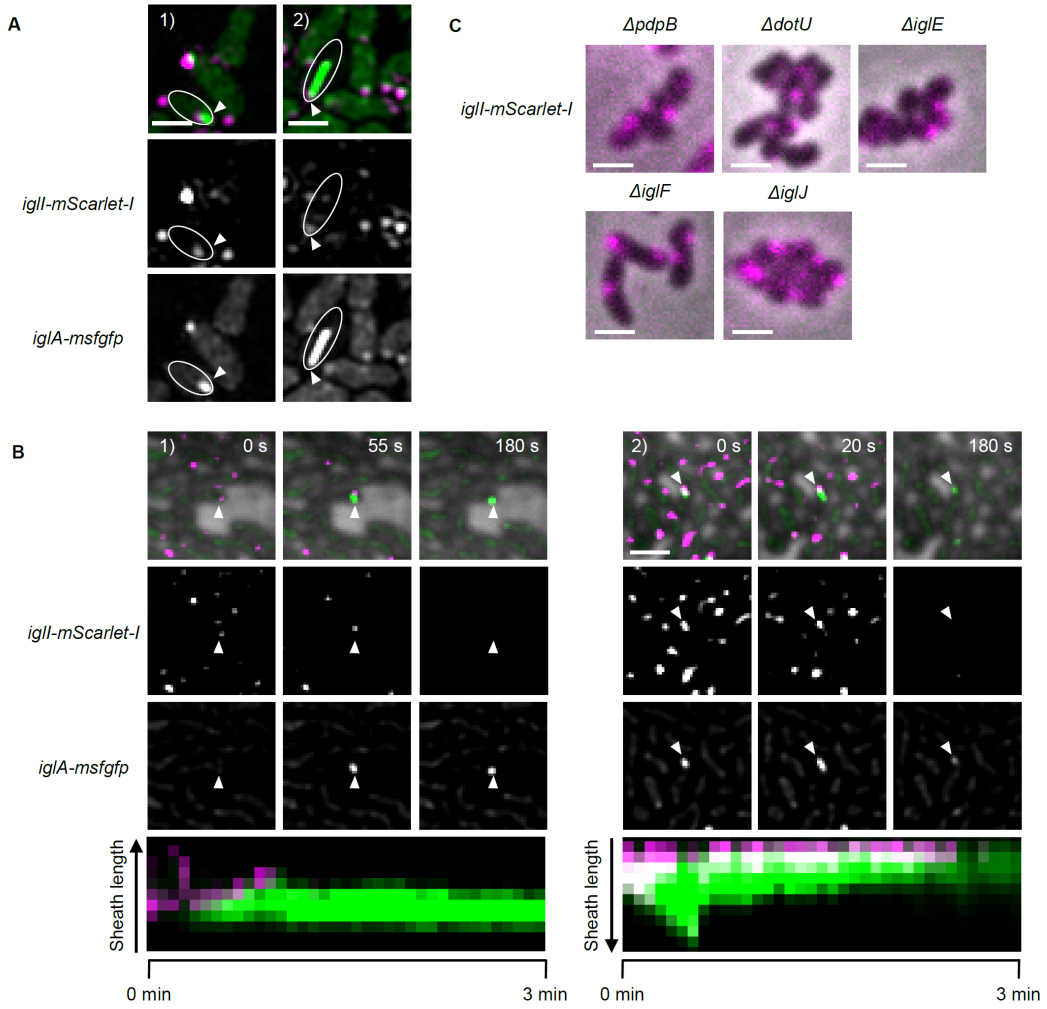

Figure 4: IglI colocalizes with poles and growing T6SS sheath. A) SIM images of *F. novicida* U112 *iglA-sfgfp iglI-mScarlet-I*. Example 1) shows IglI-mScarlet-I colocalizing with growing sheath (IglA-sfGFP) at distal end. Example 2) shows colocalization of IglI-mScarlet-I with cell pole during T6SS assembly (IglA-sfGFP). First images is a merge of RFP and GFP channel, middle images show RFP channel and lower images show GFP channel. Arrows highlight T6SS assembly. White line outlines the shape of the bacterial cell. 3.3 x 3.3 µm fields of view are shown. Scale bars represents 1 µm. **B)** Time-lapse images of before, during and after T6SS assembly and contraction in *F. novicida* U112 *iglA-sfgfp iglI-mScarlet-I*. Example 1) shows T6SS assembly with IglI-mScarlet-I colocalization with distal end of growing T6SS sheath (IglA-sfGFP). Example 2) shows IglI-mScarlet-I at the cell pole during T6SS assembly (IglA-sfGFP). Upper panels are merge of phase contrast, RFP channel and GFP channels. Middle and lower panels show RFP channel and GFP channel, respectively. RFP and GFP channels are deconvolved. Kymograms show IglI-mScarlet-I and IglA-sfGFP over 3 min (5s per pixel). Arrows highlight T6SS assemblies. 3.3 x 3.3. µm fields of view are shown. Scale bars represent 1 µm. **C)** Localization of IglI-mScarlet-I at the cell pole does not depend on structural T6SS components in *F. novicida* U112 *iglA-sfgfp iglI-mScarlet-I ΔpdpB*, *ΔdotU*, *ΔiglE*, *ΔiglF* or *ΔiglI*. Images consist of merge of phase contrast and RFP channel is shown. 3.3 x 3.3 µm fields of view are shown. Scale bars represent 1 µm.

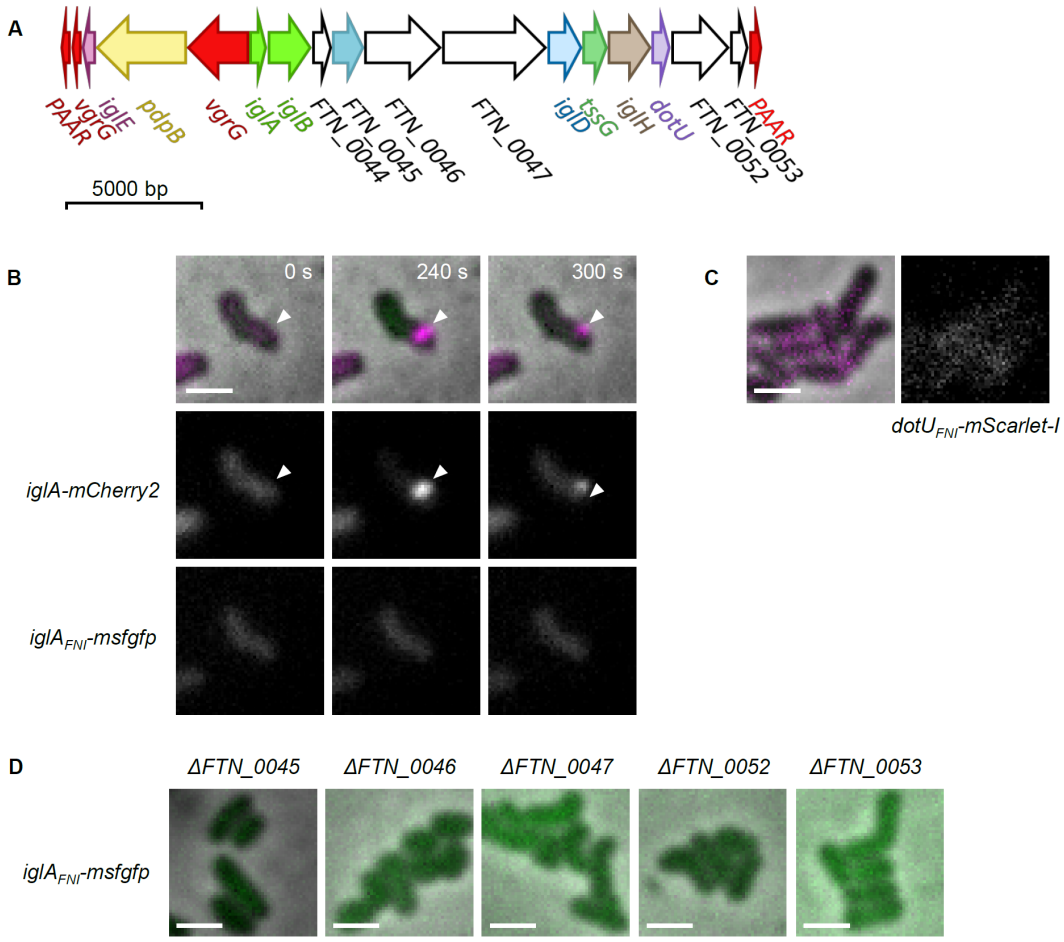

Figure 5: Characterization of putative T6SS encoded on the FNI. A) Schematic overview of FNI genes based on homology predictions (HHpred). Colors refer to overview figure in figure **1A)**. Genes are drawn in scale. **B-D)** Arrows highlight T6SS assemblies. 3.3 x 3.3 µm fields of view are shown. Scale bars represent 1 µm. **B)** Time-lapse images of before, during and after T6SS assembly and contraction in *F. novicida* U112 *iglA-mCherry2 iglA$_{FNI}$-sfGFP*. No T6SS$_{FNI}$ assemblies. Upper panels are merge of phase contrast, RFP channel and GFP channels. Middle and lower panels show RFP channel and GFP channel, respectively. **C)** No subcellular localization of DotU$_{FNI}$-mScarlet-I in *F. novicida* U112 *iglA-sfgfp dotU$_{FNI}$-mScarlet-I*. A merge of phase contrast and RFP channel (left image) and RFP channel (right image) is shown. **C)** Putative T6SS$_{FNI}$ assembly does not depend on FNI components with unknown function in *F. novicida* U112 *iglA-mCherry2 iglA$_{FNI}$-sfGFP ΔFTN_0045*, *ΔFTN_0046*, *ΔFTN_0047*, *ΔFTN_0052* or *ΔFTN_0053*. Images consist of a merge of phase contrast and GFP channel.

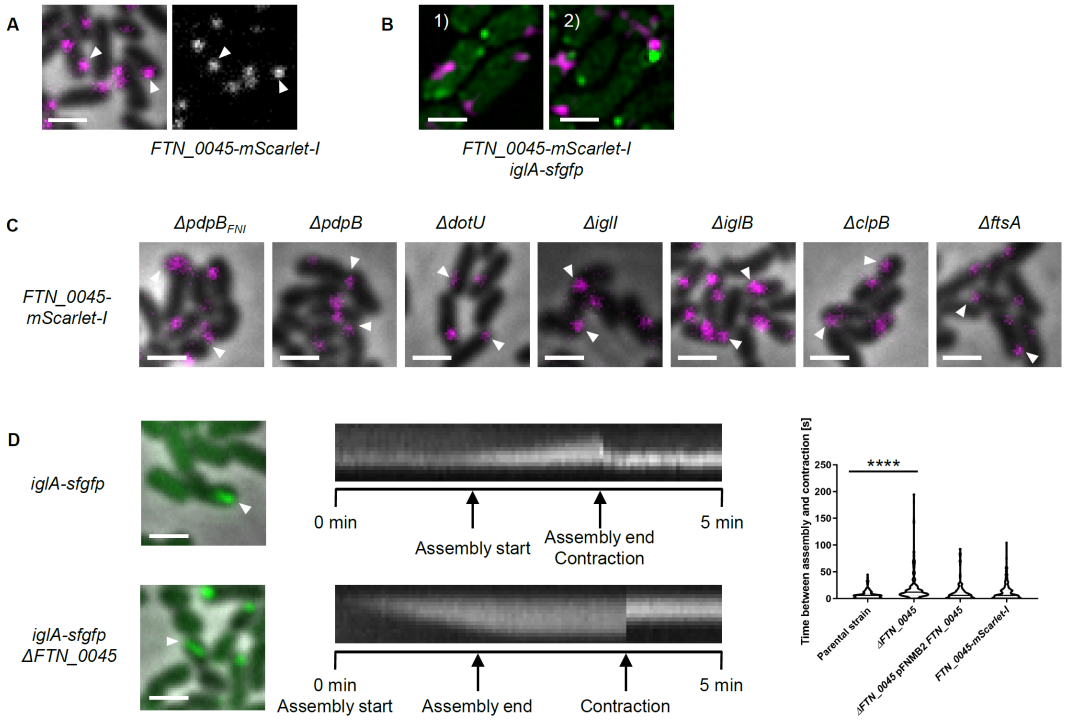

Figure 6: FTN_0045 forms distinct foci and influences T6SS sheath dynamics. Arrows highlight T6SS assemblies. 3.3 x 3.3 µm fields of view are shown. Scale bars represent 1 µm. **A)** FTN_0045-mScarlet-I forms distinct spots in *F. novicida* U112 *iglA-sfgfp FTN_0045-mScarlet-I*. A merge of phase contrast and RFP channel (left image) and RFP channel (right image) is shown. **B)** SIM images with two examples of *F. novicida* U112 *iglA-sfgfp FTN_0045-mScarlet-I*. Both examples show a merge of GFP and RFP channel. **C)** Foci formation of FTN_0045-mScarlet-I is independent from components important for T6SS function in *F. novicida* U112 *iglA-sfgfp FTN_0045-mScarlet-I* $\Delta pdpB_{FNI}$, *ΔpdpB*, *ΔdotU*, *ΔiglI*, *ΔiglB*, *ΔclpB* or *ΔftsA*. **D)** Deletion of *FTN_0045* in *F. novicida* U112 *iglA-sfgfp ΔFTN_0045* results in retardation of contraction compared to parental strain *F. novicida* U112 *iglA-sfgfp*. Images consist of merge of phase contrast with GFP channel. Kymograms show T6SS assemlies over 5 min (3 s per pixel) in GFP channel. Quantification of retardation time before contraction for *F. novicida* U112 *iglA-sfgfp, ΔFTN_0045*, *ΔFTN_0045* pFNMB2 *FTN_0045* and *FTN_0045-mScarlet-I*. Expression of FTN_0045 from plasmid was induced with 100 ng/ml ATc. Three biological replicates were analyzed with at least 105 events in total. ******** q>0.0001.

Tables

Table 1: Strains used in this study, related to Material and methods

Organism	Genotype	Plasmid	Relevant features	Source
Francisella novicida U112	*iglA-mCherry2*		C-terminal chromosomal fusion of *mCherry2* to *iglA*	This study
	iglA-mCherry2, pdpB-msfgfp		C-terminal chromosomal fusion of *mCherry2* to *iglA*, C-terminal chromosomal fusion of *msfgfp* to *pdpB*	This study
	iglA-sfgfp, pdpB-mScarlet-I		C-terminal chromosomal fusion of *sfgfp* to *iglA*, C-terminal chromosomal fusion of *mScarlet-I* to *pdpB*	This study
	iglA-sfgfp, pdpB-mScarlet-I, ΔdotU		In-frame deletion of *dotU*	This study
	iglA-mCherry2, dotU-msfgfp		C-terminal chromosomal fusion of *mCherry2* to *iglA*, C-terminal chromosomal fusion of *msfgfp* to *dotU*	This study
	iglA-sfgfp, dotU-mScarlet-I		C-terminal chromosomal fusion of *sfgfp* to *iglA*, C-terminal chromosomal fusion of *mScarlet-I* to *dotU*	This study
	iglA-sfgfp, dotU-mScarlet-I, ΔpdpB		In-frame deletion of *pdpB*	This study
	iglA-sfgfp, dotU-mScarlet-I, ΔiglE		In-frame deletion of *iglE*	This study
	iglA-sfgfp, dotU-mScarlet-I, ΔiglF		In-frame deletion of *iglF*	This study
	iglA-sfgfp, dotU-mScarlet-I, ΔiglI		In-frame deletion of *iglI*	This study
	iglA-sfgfp, dotU-mScarlet-I, ΔiglJ		In-frame deletion of *iglJ*	This study
	iglA-sfgfp, iglI-mScarlet-I		C-terminal chromosomal fusion of *sfgfp* to *iglA*, C-terminal chromosomal fusion of *mScarlet-I* to *iglI*	This study
	iglA-sfgfp, iglI-mScarlet-I, ΔpdpB		In-frame deletion of *pdpB*	This study
	iglA-sfgfp, iglI-mScarlet-I, ΔdotU		In-frame deletion of *dotU*	This study
	iglA-sfgfp, iglI-mScarlet-I, ΔiglE		In-frame deletion of *iglE*	This study
	iglA-sfgfp, iglI-mScarlet-I, ΔiglF		In-frame deletion of *iglF*	This study
	iglA-sfgfp, iglI-mScarlet-I, ΔiglJ		In-frame deletion of *iglJ*	This study
	iglA-mCherry2, $iglA_{FNI}$-msfgfp		C-terminal chromosomal fusion of *mCherry2* to *iglA*, C-terminal chromosomal fusion of *msfgfp* to $iglA_{FNI}$	This study
	iglA-mCherry2, $iglA_{FNI}$-msfgfp, ΔminD		In-frame deletion of *minD*	This study

iglA-mCherry2, iglA$_{FNI}$-msfgfp, ΔparB	In-frame deletion of *parB*	This study
iglA-mCherry2, iglA$_{FNI}$-msfgfp, ΔFTN_0340	In-frame deletion of *FTN_0340*	This study
iglA-mCherry2, iglA$_{FNI}$-msfgfp, ΔFTN_0938	In-frame deletion of *FTN_0938*	This study
iglA-mCherry2, iglA$_{FNI}$-msfgfp, ΔFTN_1507	In-frame deletion of *FTN_1507*	This study
iglA-mCherry2, iglA$_{FNI}$-msfgfp, ΔftsA	In-frame deletion of *ftsA*	This study
iglA-mCherry2, iglA$_{FNI}$-msfgfp, ΔfipA	In-frame deletion of *fipA*	This study
iglA-mCherry2, iglA$_{FNI}$-msfgfp, ΔvirK	In-frame deletion of *virK*	This study
iglA-mCherry2, iglA$_{FNI}$-msfgfp, ΔdsbB	In-frame deletion of *dsbB*	This study
iglA-mCherry2, iglA$_{FNI}$-msfgfp, ΔminC	In-frame deletion of *minC*	This study
iglA-mCherry2, iglA$_{FNI}$-msfgfp, ΔispZ	In-frame deletion of *ispZ*	This study
iglA-mCherry2, iglA$_{FNI}$-msfgfp, Δslt	In-frame deletion of *slt*	This study
iglA-mCherry2, iglA$_{FNI}$-msfgfp, ΔFTN_0045	In-frame deletion of *FTN_0045*	This study
iglA-mCherry2, iglA$_{FNI}$-msfgfp, ΔFTN_0046	In-frame deletion of *FTN_0046*	This study
iglA-mCherry2, iglA$_{FNI}$-msfgfp, ΔFTN_0047	In-frame deletion of *FTN_0047*	This study
iglA-mCherry2, iglA$_{FNI}$-msfgfp, ΔFTN_0052	In-frame deletion of *FTN_0052*	This study
iglA-mCherry2, iglA$_{FNI}$-msfgfp, ΔFTN_0053	In-frame deletion of *FTN_0053*	This study
iglA$_{FNI}$-msfgfp, dotU$_{FNI}$-mScarlet-I	C-terminal chromosomal fusion of *msfgfp* to *iglA$_{FNI}$*, C-terminal chromosomal fusion of *mScarlet-I* to *dotU$_{FNI}$*	This study
iglA-sfgfp, FTN_0045-mScarlet-I	C-terminal chromosomal fusion of *sfgfp* to *iglA*, C-terminal chromosomal fusion of *mScarlet-I* to *FTN_0045*	This study
iglA-sfgfp, FTN_0045-mScarlet-I, ΔpdpB$_{FNI}$	In-frame deletion of *pdpB$_{FNI}$*	This study
iglA-sfgfp, FTN_0045-mScarlet-I, ΔpdpB	In-frame deletion of *pdpB*	This study
iglA-sfgfp, FTN_0045-mScarlet-I, ΔdotU	In-frame deletion of *dotU*	This study
iglA-sfgfp, FTN_0045-mScarlet-I, ΔiglI	In-frame deletion of *iglI*	This study
iglA-sfgfp, FTN_0045-mScarlet-I, ΔiglB	In-frame deletion of *iglB*	This study

iglA-sfgfp, FTN_0045-mScarlet-I, ΔclpB		In-frame deletion of *clpB*	This study
iglA-sfgfp, FTN_0045-mScarlet-I, ΔftsA		In-frame deletion of *ftsA*	This study
iglA-sfgfp		C-terminal chromosomal fusion of *sfgfp* to *iglA*	Clemens et al., 2015
iglA-sfgfp, ΔFTN_0045		In-frame deletion of *FTN_0045*	This study
iglA-sfgfp, ΔFTN_0045	pFNMB2 *FTN_0045*	Inducible expression of *FTN_0045*	This study

Table 2: Plasmids and primers used to generate mutants, related to Material and Methods.

Plasmid Name	Peptide scar	Primers	Sequence 5'-3' [base pairs]
pDMK3 *iglA-mCherry2*		FTN_1324-mCh_1_Spe1.FOR	TCAGTAACTAGTGTCAAACCTATATATGCAGC
		FTN_1324-mCH_1.REV	CTGTACAAGTAAAGAGGATTTTGTTATGACAA
		FTN_1324-mCh_2.FOR	CAAAATCCTCTTTACTTGTACAGCTCGTC
		FTN_1324-mCh_2.REV	TGATAAGGCGGCCGCAGGA
		FTN_1324-mCH_3.FOR	CGGCCGCCTTATCATCTACTTGTTGATTACT
		FTN_1324-mCH_3_Sac1.REV	TCAGTAGAGCTCGTTTTGAACATGAAGAGATTAG
		FTN_1324-mCh_Det.FOR	TTGAAGCAGGTCCCCATAGA
		FTN_1324-mCh_Det.REV	CGACAAACACTAATAAAGCCGT
pDMK3 *pdpB-msfgfp*		dFTN_1311_1_Spe1.FOR	TCAGTAACTAGTAACATCTAGATATTGCCATTAATG
		FTN_1310-Neon_1new.REV	CCTCCTGCGGCCGCTTGTACATTAACTTCTCCTTGT
		FTN_1310-Neon_2.FOR	GTACAAGCGGCCGCAGGA
		FTN_1310-msfgfp_2.REV	CCATCCTAATACTTATTTGTAGAGCTCATCCATG
		FTN_1310-msfgfp_3.FOR	CTCTACAAATAAGTATTAGGATGGCAA
		FTN_1310-msfgfp_3_Xma1.REV	TCAGTACCCGGGCTTTATATTAATAGTTGCAGACTCTAG
		dFTN_1311_Det_FOR	CAATGTCATCAAAGGATTCTTCC
		FTN_1310_Det_Rev	TATTATTATCCAACCATTGTTGCTG
pDMK3 *pdpB-mScarlet-I*		dFTN_1311_1_Spe1.FOR	TCAGTAACTAGTAACATCTAGATATTGCCATTAATG
		FTN_1310-Neon_1new.REV	CCTCCTGCGGCCGCTTGTACATTAACTTCTCCTTGT
		FTN_1310-Neon_2.FOR	GTACAAGCGGCCGCAGGA
		FTN_1310-mScarlet-I_2.REV	GCCATCCTAATACTTATTTATACAGTTCATCCATACC
		FTN_1310-mScarlet-I_3.FOR	CTGTATAAATAAGTATTAGGATGGCAA
		FTN_1310-msfgfp_3_Xma1.REV	TCAGTACCCGGGCTTTATATTAATAGTTGCAGACTCTAG
		dFTN_1311_Det_FOR	CAATGTCATCAAAGGATTCTTCC
		FTN_1310_Det_Rev	TATTATTATCCAACCATTGTTGCTG
pDMK3 *dotU-msfgfp*		dFTN_1317-20_1_Xho1.FOR	TCAGTACTCGAGAAATTTATAAATCAAAACACCTTTAGC
		FTN_1316-mScarlet-I_1.REV	CCTGCGGCCGCCCAGCTTAATAAAATTAGTAAGC
		FTN_1316-mScarlet-I_2.FOR	TTAAGCTGGGCGGCCGCAGGAGGA
		FTN_1316-msfgfp_2.REV	TTAGTAAGCTTAATTATTTGTAGAGCTCATCCA
		FTN_1316-msfgfp_3.FOR	GAACTGTATAAATAATTAAGCTTACTAATTTTATTAAGCTG
		FTN_1316-mScarlet-I_3_Xma1.REV	TCAGTACCCGGGAGATGTTTCAAATATTCTTTCAC
		dFTN_1317-20_Det.FOR	ATCGCAGCACACAATCTTTAAA
		dFTN_1316_Det.REV	TTTTCGGGCATTCTCTCAAGA
pDMK3 *dotU-mScarlet-I*		dFTN_1317-20_1_Xho1.FOR	TCAGTACTCGAGAAATTTATAAATCAAAACACCTTTAGC
		FTN_1316-mScarlet-I_1.REV	CCTGCGGCCGCCCAGCTTAATAAAATTAGTAAGC
		FTN_1316-mScarlet-I_2.FOR	TTAAGCTGGGCGGCCGCAGGAGGA
		FTN_1316-mScarlet-I_2.REV	AAATTAGTAAGCTTAATTATTTATACAGTTCATCCATACC

		FTN_1316-mScarlet-I_3.FOR	GAACTGTATAAATAATTAAGCTTACTAATTTTATTAAGCTG
		FTN_1316-mScarlet-I_3_Xma1.REV	TCAGTACCCGGGAGATGTTTCAAATATTCTTTCAC
		dFTN_1317-20_Det.FOR	ATCGCAGCACACAATCTTTAAA
		dFTN_1316_Det.REV	TTTTCGGGCATTCTCTCAAGA
pDMK3 *iglI-mScarlet-I*		dFTN_1318_1_Xho1.FOR	TCAGTACTCGAGATAACATAGATTCTATTATAGAAATTGTACA
		FTN_1317-mScarlet-I_1.REV	CGGCCGCTATGTCAAAAAGATCTTCAAAATAGT
		FTN_1317-mScarlet-I_2.FOR	CTTTTTGACATAGCGGCCGCAGGA
		FTN_1317-mScarlet-I_2.REV	TTTCTACCGAATCTTATTTATACAGTTCATCCATACC
		FTN_1317-mScarlet-I_3.FOR	ACTGTATAAATAAGATTCGGTAGAAAAAATTTCAA
		FTN_1318_Sac1.REV	TCAGTAGAGCTCTCATAAATTAAAATAACCTAGATATATCTGAT
		dFTN_1318_Det.For	CGCAAATGCAGAATCAAGAA
		dFTN_1318_Det.Rev	CGACTAGCGCGTCTAAAAATG
pDMK3 *iglA$_{FNI}$-msfgfp*		FTN_0042-Fu_1_Xho1.FOR	TCAGTACTCGAGTGTGGTGAATTTTATTTGCTT
		FTN_0042-Fu_1.REV	GCTCCCGCATTTTCTCCCTC
		FTN_0042-GFP_2.For	GAGAAAATGCGGGAGCCGGAGCAGGAGGATCTAAAGGTGAAGAAC
		FTN_0042-GFP_2.REV	CATCAGAAACAATTTATTTGTAGAG
		FTN_0042-GFP_3.FOR	CTCTACAAATAAATTGTTTCTGATG
		FTN_0042-Fu_3_NotI.REV	TCAGTAGCGGCCGCGCAGCCTGTTCTGAC
		FTN_0042-fusion_det_FOR	TCTCTTTGATTGCATTTAAGACTATT
		FTN_0042-fusion_Det_REV	TTCCTCATTTGAAAGTGGATTT
pDMK3 *dotU$_{FNI}$-mScarlet-I*		FTN_0051-mScarlet-I_1_Xho1.FOR	TCAGTACTCGAGTATGTTGTCTACATAAGAACAGA
		FTN_0051-mScarlet_I_1.REV	TCCTCCTCCTGCGGCCGCGTGAATAAACCATAAGCCA
		FP-Link-Univ-FOR	GCGGCCGCAGGAGGAGGA
		FTN_0051-mScarlet-I_2.REV	GCCAAGATATGCTTATTTATACAGTTCATCCATACCAC
		FTN_0051-mScarlet-I_3.FOR	CTGTATAAATAAGCATATCTTGGCTTATG
		FTN_0051-mScarlet-I_3_Xma1.REV	TCAGTACCCGGGTATTGATATATCGAGCTGATTAAAG
		FTN_0051-mScarlet-I_Det.For	TCCGCCCTTTAAGCAGAAGT
		FTN_0051-mScarlet-I_Det.REV	ACAATAAATGGTTGCGGAGAAC
pDMK3 *FTN_0045-mScarlet-I*		FTN_0045-mScarlet-I_1_Xho1.FOR	TCAGTACTCGAGAGTATCACAACCTTAATTAATGA
		FTN_0045-mNeongreen_1.REV	GCGGCCGCTAAATCTAAAATATCGAATGCTGAACT
		FTN_0045-mNeongreen_2.FOR	TTTAGATTTAGCGGCCGCAGGAGG
		FTN_0045-mScarlet-I_2.REV	ATGCTGAACTAAATTATTTATACAGTTCATCCATACC
		FTN_0045-mScarlet-I_3.FOR	ACTGTATAAATAATTTAGTTCAGCATTCGATATT
		FTN_0045-mScarlet-I_3_Sac1.REV	TCAGTAGAGCTCAAAATACATTGATTAATTTTTTTTATTGTAT
		FTN0045_det_FOR	GCTCAAATAGCAGTTGAGCCT
		FTN0045_det_REV	AACCGTCGTTTTTATCAATAATAGC
pDMK3 *ΔpdpB*	MNFIQKQGEVNVQ*	dFTN_1310_Del1_Xho1.FOR	TCAGTACTCGAGCAACTATATGAAAACTTACATAATT
		dFTN_1310_Del1.REV	CTCCTTGTTTTTGAATAAAATTCATACTTTTAATTT
		dFTN_1310_Del2_.FOR	ATGAATTTTATTCAAAAACAAGGAGAAGTTAATGT

		dFTN_1310_Del2.REV	ATAATAGCGGCCGCTTAGCAGAGCTTTTTATATT
		dFTN_1310_Det_FOR	ACATCAAGAAATACTCTGCCCTTC
		dFTN_1310_Det_REV	TATTATTATCCAACCATTGTTGCTG
pDMK3 *ΔdotU*	MKDFKEIEIILSLLILLSW*	dFTN_1316_1_Xho1.FOR	TCAGTACTCGAGGTTAATTTAATACCTGTGTTTAATAGT
		dFTN_1316_1.REV	AAATTAGTAAGCTTAAAATAATTTCTATCTCTTTAAAGTCTTT
		dFTN_1316_2.FOR	GAGATAGAAATTATTTTAAGCTTACTAATTTTATTAAGCT
		dFTN_1316_2_Not1.REV	TCAGTAGCGGCCGCAGATGTTTCAAATATTCTTTCAC
		dFTN_1316_Det.FOR	GAAGATCCTAGCTTTGCCACA
		dFTN_1316_Det.REV	TTTTCGGGCATTCTCTCAAGA
pDMK3 *ΔiglE*	MYNKLLKNLCKNDSSIEKD*	dFTN_1310_Del1_Xho1.FOR	TCAGTACTCGAGCAACTATATGAAAACTTACATAATT
		dFTN_1311_1.REV	TGCTATCATTTTTACAAAGATTTTTCAATAATTTATTGT
		dFTN_1311_2.FOR	GAAAAATCTTTGTAAAAATGATAGCAGCATAGAA
		dFTN_1312_Not1.REV	TCAGTAGCGGCCGCTTATTTATAGAATATAAAGCTCTTAAAAGAAT
		dFTN_1310_Det_For	ACATCAAGAAATACTCTGCCCTTC
		dFTN_1312_Det.Rev	GCTTGTAGTGACGTTAGCGAAA
pDMK3 *ΔiglF*	MNNDIDKWFESKQEAYWKI*	dFTN_1313_1_Spe1.FOR	TCAGTAACTAGTTTTCTCAAAGAATATATGATGATAATG
		dFTN_1313_1.REV	TTGCTTGCTTTCAAACCATTTATCAATATCATTATT
		dFTN_1313_2.FOR	TGGTTTGAAAGCAAGCAAGAAGC
		dFTN_1313_2_Sac1.REV	TCAGTAGAGCTCTATTTCTAATAAGCATGATTTA GGAA
		dFTN1313_Det.FOR	CTGGGTAATCAAGCACAAAGGT
		dFTN1313_Det.REV	GTGGCAAAGCTAGGATCTTCT
pDMK3 *ΔiglI*	MSQIISTLNNDSVEKISNEIDEDYFEDLFDI*	dFTN_1317_1_Xho1.FOR	TCAGTACTCGAGAAATTTATAAATCAAAACACCTTTAGC
		dFTN_1317_1.REV	TTCTACCGAATCATTATTTAGTGTAGATATTATCTGACT
		dFTN_1317_2.FOR	ACACTAAATAATGATTCGGTAGAAAAAATTT
		dFTN_1317_2_NotI.REV	TCAGTAGCGGCCGCATTTCAAGTTCTATCTTAAATGGG
		dFTN_1317_Det.FOR	ATCGCAGCACACAATCTTTAAA
		dFTN_1317_Det.REV	TCAGATAGTGATTCGGATTTTTCA
		dFTN_1317_1_Xho1.FOR	TCAGTACTCGAGAAATTTATAAATCAAAACACCTTTAGC
pDMK3 *ΔiglJ*	MKTILKIFLTYKQQIYLGYFNL*	dFTN_1318_1_Xho1.FOR	TCAGTACTCGAGATAACATAGATTCTATTATAGAAATTGTACA
		dFTN_1318_1.REV	CCTAGATATATCTGTTGTTTATATGTCAAAAAGATCTTCAAA
		dFTN_1318_2.FOR	GATCTTTTTGACACAGATATATCTAGGTTATTTTAATTTATG
		dFTN_1318_2_NotI.REV	TCAGTAGCGGCCGCATCATTTGCGCTTATTTCAA
		dFTN_1318_Det.For	CGCAAATGCAGAATCAAGAA
		dFTN_1318_Det.Rev	CGACTAGCGCGTCTAAAAATG
		dFTN_1318_1_Xho1.FOR	TCAGTACTCGAGATAACATAGATTCTATTATAGAAATTGTACA
pDMK3 *ΔminD*	MSEKKQGKVFSFFKKLIGKS*	dFTN_0330_1_Xho1.FOR	TCAGTACTCGAGCAAGCTTTTCATTTCAAAGG
		dFTN_0330_1.REV	TTGAAGAAACTAAATACCTTGCCTTGTTT
		dFTN_0330_2.FOR	GCAAGGTATTTAGTTTCTTCAAAAAATTGATAGGT
		dFTN_0330_2_Not1.REV	TCAGTAGCGGCCGCGCCAGAAAGCTCACTT

		dFTN_0330_Det.FOR	TGCGAAAACAGGACACTTCT
		dFTN_0330_Det.REV	TTTCTGGTGAGTCGCTAGCT
pDMK3 *ΔparB*	MAKKVSLMNRKINKKILFDALIN*	dFTN_0434_1_Xho1.FOR	TCAGTACTCGAGAGCAGACAAATATAGACTATAATT
		dFTN_0434_1.REV	AGAGTATTTTCTTATTGATTTTACGGTTCATTAAG
		dFTN_0434_2.FOR	CCGTAAAATCAATAAGAAAATACTCTTTGATGCG
		dFTN_0434_2_Not1.REV	TCAGTAGCGGCCGCTCCTTGTACTCAAAAAAATTAGC
		dFTN_0434_Det.FOR	TTTGGCTGGAGACTCTACGA
		dFTN_0434_Det.REV	CAACGCTCCTCCAATTGCAT
pDMK3 *ΔFTN_0340*	MTIKKLSTLVIEKAKSDATE*	FTN0340_Xho1_FOR	TCAGTACTCGAGGGTGGTTGGTGTGATATTGATC
		FTN0340_REV	CTTTCAACACTAGTACTAATTGAAAAAGCAAAATCTGATGCA
		FTN0340_FOR	TGCTTTTTCAATTAGTACTAGTGTTGAAAGTTTCTTTATAGT
		FTN0340_NotI_REV	TCAGTAGCGGCCGCATTGGAGTGACTTTGTTCAAGCT
		FTN0340_det_FOR	GGAGTGCGCGTGGTTATATT
		FTN0340_det_REV	AGAAGTAATTTCTCCGGCACT
pDMK3 *ΔFTN_0938*	MSNELQNNNQPSGQARANAS*	FTN0938_XhoI_FOR	TCAGTACTCGAGAGGAATCGGCGCATTAGTTCAT
		FTN0938_REV	CAGAATAATAATGGTCAGGCGCGAGCAAAT
		FTN0938_FOR	TGCTCGCGCCTGACCATTATTATTCTGTAACTCATTTGACATACA
		FTN0938_NotI_REV	TCAGTAGCGGCCGCTAATTTCTGTTTAATGAAGTTAGCCGG
		FTN0938_det_FOR	GTTGAGTTACTTCCAAATGCAGA
		FTN0938_det_REV	GCTATGCAGAGCCTCCCATT
pDMK3 *ΔFTN_1507*	MLLQQIKSQAVKIIEREVKQDDNQAQ*	FTN1507_XhoI_FOR	CTCGAGCTCGAGGCCACTAGCTGCTATAAAGAAAAC
		FTN1507_REV	TCTCAGGCAGGCGTTGCAGATCGCGTTAAG
		FTN1507_FOR	ATCTGCAACGCCTGCCTGAGATTTTATCTG
		FTN1507_NotI_REV	TCAGTAGCGGCCGCGCTGTTATCGGTGGTTTGGC
		FTN1507_det_FOR	TCCGAGTCAGCAGAATTTTGT
		FTN1507_det_REV	GCCATCCTGATAGACCATATTTCA
pDMK3 *ΔftsA*	MGFGNSNFCASVKGWFSNNF*	dFTN_0163_1_Xho1.FOR	TCAGTACTCGAGTATTTTTGTTGCTGCTAAAACA
		dFTN_0163_1.REV	CCTTTACAGAAGCACAAAAATTACTATTCC
		dFTN_0163_2.FOR	TTTTTGTGCTTCTGTAAAGGGTTGGTTTT
		dFTN_0163_2_Not1.REV	TCAGTAGCGGCCGCATCATTGCTAGACCCATAT
		dFTN_0163_Det.For	CGAGTGGTTTATGCGAGCAA
		dFTN_0163_Det.REV	ACACCCTTAGCACCATCAAG
pDMK3 *ΔfipA*	MKLTKTLFIAQKQAMAAQKK*	dFTN_0772_1_Xho1.FOR	TCAGTACTCGAGGCTGAAAAAGCAGGAC
		dFTN_0772_1.REV	CTTGCTTTTGCGCTATAAATAGAGTTTTAG
		dFTN_0772_2.FOR	ATTTATAGCGCAAAAGCAAGCAATGG
		dFTN_0772_2_Not1.REV	TCAGTAGCGGCCGCCTTCACCTGTTGCAAA
		dFTN_0772_Det.FOR	AGTCCCTGGTACCAATAGTGTC
		dFTN_0772_Det.REV	CCAAGTTGACCAAAGCCCAT
pDMK3 *ΔvirK*	MKKIITLSTLTKDQASFFSN*	FTN1068_XhoI_FOR	TCAGTACTCGAGTCCATTCGGTGAATATTTCCCA

		FTN1068_REV	AGAAGCTAGCTAGTGTAATTATCTTTTTCATTTTATTCTCC
		FTN1068_FOR	AATTACACTAGCTAGCTTCTTCTCTAACTAAATAAAG
		FTN1068_NotI_REV	TCAGTAGCGGCCGCCAACTATTAGCTGCTAAAAAACAGAAT
		FTN1068_det_FOR	ATCATTATTGGAAATGGTCAAGGA
		FTN1068_det_REV	CGGGATTATATATTGCTTTGCAA
pDMK3 *ΔdsbB*	MKKLSNCIFIFNTLACFVALGVVIFTISVLD WKPNFLVRILKK*	FTN1608_XhoI_for	TCAGTACTCGAGAATTTCTCAATAGCCGAAGAA
		FTN1608_rev	TCTAACTAAAAAGTTTGGTTTCCAATCTAAAACACTAATTGT
		FTN1608_for	GATTGGAAACCAAACTTTTTAGTTAGAATTTTAAAAAAATAG
		FTN1608_NotI_rev	TCAGTAGCGGCCGCAGGTGCTCTAACCTCTTTAAA
		FTN1608_det_for	GCCAATGGCTATCATGGCTT
		FTN1608_det_r	AGTGTTGCAGCATTATCACCA
pDMK3 *ΔminC*	MKQAFHFKGGQDDKIHIEGF*	dFTN_0331_1_Xho1.FOR	TCAGTACTCGAGTAGACAATGATCCAACTGC
		dFTN_0331_1.REV	ATCATCTTGACCACCTTTGAAATGAAAA
		dFTN_0331_2.FOR	CAAAGGTGGTCAAGATGATAAGATACATATAGAAG
		dFTN_0331_2_Not1.REV	TCAGTAGCGGCCGCATTTGAAGCCTCTAGAATATC
		dFTN_0331_Det.FOR	ACTCCGGATCAACTCTTGCA
		dFTN_0331_Det.REV	TCATCTTTGAGTTCCGCAAGT
pDMK3 *ΔispZ*	MNKMINDLLPSIYLSKHIKR*	dFTN_0464_1_Xho1.FOR	TCAGTACTCGAGGATTATACTTATTTCAATTTTCGATTT
		dFTN_0464_1.REV	TAAATAGATAGATGGAAGCAAATCATTAATCAT
		dFTN_0464_2.FOR	TGATTTGCTTCCATCTATCTATTTATCCAAACATATTAAA
		dFTN_0464_2_Not1.REV	TCAGTAGCGGCCGCATATGATCAACCTGAATGTATG
		dFTN_0464_Det.FOR	CCCACCAACACCAAGCTTAG
		dFTN_0464_Det.REV	TGAGAGATTCTGTAGCGGCT
pDMK3 *Δslt*	MVINKKFITSISDKQSFRK*	FTN0496_Xho1_FOR	TCAGTACTCGAGGAAGAGAGTATAGTTTTAGGCTG
		FTN0496_REV	TTGTCAGATATACTTGTTATGAACTTTTTATTAATCACAAT
		FTN0496_FOR	AAAGTTCATAACAAGTATATCTGACAAGCAGAGTTTTAGA
		FTN00496_NotI_REV	TCAGTAGCGGCCGCCCACCTATAAGTATTTACAGCAGC
		FTN0496_det_FOR	TAGTTCGATTGCAGCCCCTC
		FTN0496_det_REV	GTGAGAACCTTTGCTGAATTGC
pDMK3 *ΔFTN_0040*	MNLYMIIILINIFMSLETK*	dFTN_0040_1_Xho1.FOR	TCAGTACTCGAGAGATTTATACTTAAGCTCTTAAGGT
		dFTN_0040_1.REV	GATAATAATTCTAATTAATATTTTTATGAGCCTTGAAACT
		dFTN_0040_2.FOR	GGCTCATAAAAATATTAATTAGAATTATTATCATATATAAATTCATAAA A
		dFTN_0040_2_Not1.REV	TCAGTAGCGGCCGCTTTGAATTTGAAAATAATGCTTTAAAAA
		dFTN_0040_Det.For	GGACATTGTATGTTCTGGTCATTT
		dFTN_0040_Det.Rev	TGGTTTTGCATAAGGCTGAA
pDMK3 *ΔFTN_0045*	MSKASKELQDDFSSAFDILDL*	FTN0045_XhoI_FOR	TCAGTACTCGAGAGTACTTCCACACGTGCAGT
		FTN0045_REV	TAAAATCATCTTGTAATTCTTTACTTGCTTTGCTCAT
		FTN0045_FOR	AGAATTACAAGATGATTTTAGTTCAGCATTCGAT
		FTN0045_NotI_REV	TCAGTAGCGGCCGCACAAACTTAGCTTTTAGATTCGCT

		FTN0045_det_FOR	GCTCAAATAGCAGTTGAGCCT
		FTN0045_det_REV	AACCGTCGTTTTTATCAATAATAGC
pDMK3 *ΔFTN_0046*	MFENKTVKELLNTKTNQHI*	FTN_0045-mScarlet-I_1_Xho1.FOR	TCAGTACTCGAGAGTATCACAACCTTAATTAATGA
		dFTN_0046_1.REV	TTTTAGTATTTAGAAGCTCTTTAACGGTTT
		dFTN_0046_2.FOR	CGTTAAAGAGCTTCTAAATACTAAAACAAATCAACATATTT
		dFTN_0046_2_Xma1.REV	TCAGTACCCGGGATTCAGAGTCTGATTTATCATC
		dFTN_0046_Det.FOR	TGTCTTTACTTGCAAGCTCACT
		dFTN_0046_Det.REV	TGTACTTATCGGAACAAGCCA
pDMK3 *ΔFTN_0047*	MANKYFIKPTVIERFSKIF*	dFTN_0047_1_Xho1.FOR	TCAGTACTCGAGTTTTCCATTCTTATCAGATCAAA
		dFTN_0047_1.REV	AATCTTTCAATAACTGTAGGTTTAATAAAATATTTATTAGC
		dFTN_0047_2.FOR	TTATTAAACCTACAGTTATTGAAAGATTTTCAAAAATTTT
		dFTN_0047_2_Xma1.REV	TCAGTACCCGGGGATAGCATGAAATATAAATACTGGA
		dFTN_0047_Det.FOR	TGGGAGCTTTAAACAGTAACAGT
		dFTN_0047_Det.REV	TGGATCCAACTCGTTAGACTCT
pDMK3 *ΔFTN_0052*	MNKEIFRQVSEIIRIISSL*	dFTN_0052_1_Sal1.FOR	TCAGTAGTCGACTTTAGTTTTTATACAAATTTAGTCCAAAA
		dFTN_0052_1.REV	AATTCTAATTATTTCAGATACTTGTCTAAATATTTCTTTATT
		dFTN_0052_2.FOR	TTAGACAAGTATCTGAAATAATTAGAATTATATCAAGTTTGTAG
		dFTN_0052_2_Xma1.REV	TCAGTACCCGGGTGCAAGCTGACCTTGAC
		FTN_0051-mScarlet-I_Det.For	TCCGCCCTTTAAGCAGAAGT
		dFTN_0052_Det.REV	TTAGTTGCAGGTGGTGTCCA
pDMK3 *ΔFTN_0053*	MDIEKIIRKINAKYLLQGGRNE*	dFTN_0053_1_Xho1.FOR	TCAGTACTCGAGTAGTCAGATTTTAATGACGTTAG
		dFTN_0053_1.REV	ATAAATATTTCGCATTAATTTTTCTAATTATTTTTTCAATATCCA
		dFTN_0053_2.FOR	AATAATTAGAAAAATTAATGCGAAATATTTATTACAAGG
		dFTN_0053_2_Xma1.REV	TCAGTACCCGGGAATGGAGTTAAACATCGTAG
		dFTN_0053_Det.FOR	TGGGAGCTTTAAACAGTAACAGT
		dFTN_0053_Det.REV	CGAAGCACATGATGAGGCAA
pFNMB2 *FTN_0045*		FTN_0045_Mlu1.For	TCAGTAACGCGTATGAGCAAAGCAAGTAAAGAATTACA
		FTN_0045_Sac1_Rev	TCAGTAGAGCTCTTATAAATCTAAAATATCGAATGCTGAACTAAAATC
		pJB_seq_For	TCATAGAAGCTTGCATGCCTG
		pJB_seq_REV	GAGACCCCACACTACCATCG

3.5. Establishing *Galleria mellonella* as infection model for *Francisella* T6SS research

Maj Brodmann and Marek Basler

Focal Area Infection Biology, Biozentrum, University of Basel, Basel, Switzerland

Report

Statement of contribution:

I generated the strain and performed all infection experiments. In addition, I prepared figures and wrote the report.

Introduction

Francisella tularensis is the causative agent of the deadly zoonotic disease called tularemia (Oyston et al., 2004). Tularemia is transmitted by arthropod vectors, infected animals or aerosols but *Francisella* is also found in aquatic and terrestrial environments (Hennebique et al., 2019; Ozanic et al., 2015). Thus, diverse infection routes are reported such as oral, subcutaneous or pneumonic transmission (Keim et al., 2007). The most virulence subspecies *Francisella tularensis* subspecies *tularensis* and subspecies *holarctica* are considered as Tier 1 select agents as they are highly infectious in humans (lethal $dose_{50} < 10$ colony forming units (CFU)) and cause a high mortality rate if left untreated (up to 60 %) (Kingry and Petersen, 2014; Oyston et al., 2004). In contrast, *Francisella tularensis* subspecies *novicida* (*F. novicida*) has a high infectivity in mice but not in humans (Kingry and Petersen, 2014). While the primary niche of *Francisella* are phagocytes such as macrophages, *Francisella* can infect a broad range of cells including non-phagocytic cells such as HeLa cells and erythrocytes (Chong and Celli, 2010; Jones et al., 2014; Schmitt et al., 2017). Interestingly, *Francisella* cannot trigger its own uptake but needs to be internalized with the help of various host-receptors.(Jones et al., 2014). Crucial for *Francisella* virulence is the *Francisella* pathogenicity island (FPI) which encodes a non-canonical Type VI secretion system (T6SS) and is required for phagosomal escape and intracellular survival (Brodmann et al., 2017; Bröms et al., 2010; Chong and Celli, 2010). Cytosolic replication allows the host cell to mount antimicrobial immune responses such as production of type 1 interferons, guanylate-binding proteins and the activation of the absent in melanoma 2 (AIM2) inflammasome resulting in pyroptotic cell death and pro-inflammatory cytokines (Henry et al., 2007; Jones et al., 2010; Meunier et al., 2015).

F. novicida is often used as model organism to study *Francisella* pathogenicity as it is closely related to the more virulent subspecies and encodes only one FPI instead of two (Kingry and Petersen, 2014). On the host side, *Francisella* pathogenicity is mainly studied in primary or immortalized macrophages derived from mice or humans (Elkins et al., 2007). In addition, also various amoebae and *Drosophila melanogaster* cells have been used to identify *Francisella* virulence factors (Abd et al., 2003; Ahlund et al., 2010; Lampe et al., 2015; Santic et al., 2011). *In vivo* models often include mice, Fischer rats or even macaques (Guina et al., 2018; Ray et al.,

2010; Rick Lyons and Wu, 2007). Interestingly, immune responses may differ between the subspecies and between different infection models (Elkins et al., 2007; Jones et al., 2014; Kingry and Petersen, 2014; Lagrange et al., 2018).

Most studies focus on aspects of *Francisella* pathogenicity important for humans or mammals, however *Francisella* often resides in the environment encountering various potential reservoir hosts such as arthropods (Keim et al., 2007). In addition, the usage of mammals as *in vivo* models for studying *Francisella* pathogenicity is ethnically difficult, space and time consuming and expensive. Conversely, *Galleria mellonella* (*G. mellonella*) larvae are increasingly used for studying host-pathogen interactions as well as for antimicrobial drug testing (Tsai et al., 2016). The advantage of *G. mellonella* is that the larvae require limited space and are cheap in maintenance compared to mammals, as they do not require any specific lab equipment (Ramarao et al., 2012). In addition, handling is easy and does not require specific training. Furthermore, *G. mellonella* is insensitive to incubation at 37 °C and thus can be used to study human pathogens (Tsai et al., 2016). Importantly, *G. mellonella* contains a complex innate immune system including phagocytic cells called hemocytes and a humoral response (Tsai et al., 2016). The humoral response consists of plasma proteins called opsonins, which recognize pathogen associated molecular patterns similar to pattern recognition receptors in mammals, and stimulate hemocyte activity or enhance antimicrobial properties of antimicrobial peptides (Tsai et al., 2016; Vogel et al., 2011). A part of the humoral response, which can be visually observed, is a melanization process required for encapsulation of pathogens (Tang, 2009). Thereby, the phenoloxidase pathway is activated by pattern recognition receptors resulting in melanin production. Melanization results in a color change of the larvae from a healthy yellow into different shades of brown and black depending on the strength of the immune response (Cerenius and Söderhäll, 2004).

While *Francisella* triggers an innate immune response including melanization in *G. mellonella* larvae, which subsequently leads to death of *G. mellonella* (Aperis et al., 2007; Thelaus et al., 2018), it is not clear whether *Francisella* virulence depends on the FPI and thus on the T6SS. In addition, *Francisella* was shown to be associated with hemocytes during infection (Aperis et al., 2007), but it is not known in which subcellular compartment *Francisella* resides.

Here we show that virulence of *F. novicida* in *G. mellonella* larvae depends on a functional T6SS. However, T6SS dynamics is less important than reported previously in mice and bone-marrow derived macrophages. In addition, known effectors were dispensable for killing the larvae. Only combined deletion of *pdpC*, *pdpD*, *anmK* and *opiA*, an effector encoded outside of the FPI, led to increased larvae survival.

Results

In order to determine if killing of *G. mellonella* larvae by *F. novicida* is T6SS dependent, I used 3 different concentrations (10^8 CFU/ml, 10^6 CFU/ml and 10^4 CFU/ml or 10^6, 10^4 and 10^2 bacteria per infection dose) for infection with the parental strain (*iglA-sfgfp*) and a *ΔpdpB* mutant, which does not have a functional T6SS. My results suggest that killing of *G. mellonella* larvae is concentration and T6SS dependent (figure 1A). Larvae infected with a high and middle dose were all dead after 2 days, while larvae infected with the low infection dose survived 3 days. In addition, larvae infected with the parental strain turned completely black due to melanization (figure 1B). On the other hand, almost all larvae infected with the T6SS-negative mutant were still alive after 5 days, although the larvae infected with the highest infection dose eventually started dying. In summary, I could reproduce concentration dependent survival dynamics similar to a previous report (Thelaus et al., 2018). I decided to use 10^4 bacteria per infection dose for all following infection experiments as a clear difference in larvae survival between the parental strain and the T6SS-negative mutant was observed.

Since T6SS dynamics are essential for *Francisella* virulence in bone-marrow derived macrophages (BMDMs) and in mice (Brodmann et al., 2017), I wanted to test if this is the case as well in *G. mellonella*. Therefore, I infected larvae with a *ΔclpB* mutant, which still had a functional T6SS but could not recycle contracted T6SS sheaths. Surprisingly, a *ΔclpB* mutant killed larvae as efficiently as the parental strain (figure 2A), suggesting that either less effector translocation events are required for intracellular survival or that *G. mellonella* is sensitive to a few surviving bacteria.

Next, I tested if the effector PdpC, which is secreted in a T6SS dependent manner and has a major role in phagosomal escape in BMDMs and mice, is important for

killing of *G. mellonella* larvae. Again, a *ΔpdpC* mutant killed as efficiently as the parental strain (figure 2A). Thus, I tested if the triple *pdpC pdpD-anmK* deletion mutant, which is completely avirulent in BMDMs and mice (Brodmann et al., 2017) is able to kill the *G. mellonella* larvae. Strikingly, even this mutant was as efficient in killing as the parental strain (figure 2B). In addition, single deletion of *opiA*, an effector encoded outside of the FPI involved in delaying phagosome maturation (Eshraghi et al., 2016; Ledvina et al., 2018), also did not decrease *Francisella* virulence (figure 2B). Then, I combined deletion of all four genes in a *ΔpdpC ΔpdpD-anmK ΔopiA* mutant. Interestingly, this mutant is avirulent in *G. mellonella* larvae (figure 3A). Thus, all four genes in combination are important for *Francisella* virulence in *G. mellonella* infections. In summary, my results suggest that T6SS is critical for virulence in *G. mellonella* and the model is sensitive to several T6SS effectors delivered in small amounts.

Outlook

Although all data are preliminary, my results suggest that *Francisella* virulence in *G. mellonella* also depends on a functional T6SS similar to reports in other model organisms (Brodmann et al., 2017; Bröms et al., 2010; Rick Lyons and Wu, 2007). Nevertheless, there are striking differences compared to the already established infection models. First, T6SS sheath recycling plays no role in *G. mellonella* despite of being crucial for intracellular survival in mice and BMDMs (Brodmann et al., 2017) (figure 1). Interestingly, a *ΔclpB* mutant was also attenuated in *D. melanogaster* (Ahlund et al., 2010). However, differences in infection dose or incubation temperature may account for these different disease outcomes. Thus, lowering the infection dose might result in attenuation of a *ΔclpB* mutant in *G. mellonella*.

More surprising was that the contributions of single or both effectors PdpC and PpdD were not detectable in *G. mellonella* (figure 2), while they clearly play an important role in all other *in vitro* and *in vivo* infection systems (Brodmann et al., 2017; Bröms et al., 2010; Lindgren et al., 2013; Long et al., 2013; Ludu et al., 2008; Ozanic et al., 2016; Uda et al., 2014). Only combined deletion of *pdpC pdpD-anmK opiA* resulted in decreased virulence (figure 3). These results suggest that *Francisella* might

manipulate different host-cell components in insects compared to mammal model systems. In accordance, single interruptions of *pdpC* and *pdpD* by transposons had no effect in *D. melanogaster* nor in a cell line derived from *Anopheles gambiae* (Ahlund et al., 2010; Read et al., 2008). Nevertheless, my results suggest that at least partially, PdpC, PdpD, AnmK and OpiA do contribute to *Francisella* virulence in insects. However, they may have redundant functions as suggested for PdpC and OpiA in macrophages (Ledvina et al., 2018).

In order to elucidate if all above-mentioned genes are equally important or have redundant activity, I plan to make different combinations of gene deletions. In addition, analysis of the localization of these different deletion mutants inside *G. mellonella* may give hints towards the function of the deleted genes.

In summary, *G. mellonella* is an easy to handle and cheap infection model suitable for studying *Francisella* virulence and its non-canonical T6SS. By investigating why some genes have differential importance in *G. mellonella* compared to BMDMs and mice, *Francisella* pathogenicity will be understood in more detail. In addition, tularemia transmission by arthropod vectors is the major infection route in Switzerland and Europe (Wittwer et al., 2018), thus it is important to understand *Francisella* pathogenicity in infection models, which resemble physiological reservoir hosts.

Material and Methods

Bacterial strains

Francisella novicida U112 (*F. novicida*) and derivative strains were in brain heart infusion (BHI) broth with aeration or on BHI agar plates at 37 °C. The medium was supplemented with 0.1 % L-cysteine (Acros Organics) and 100 µg/ml ampicillin (AppliChem). *Escherichia coli* DH5α λpir (*E. coli*) and derivative strains were aerobically grown in Luria broth (LB) or on agar plates supplemented with 50 µg/ml kanamycin at 37 °C. All strains are listed in table 1.

Bacterial mutagenesis

To introduce in-frame deletions on the chromosome of *F. novicida*, suicide vector pDMK3 was used (Lindgren et al., 2007). For conjugation, a donor *E. coli* strain from A. Harms and C- Dehio (Harms et al., 2017) was used. In short, liquid cultures of recipient *F. novicida* and donor *E. coli* strains were grown until OD_{600} of 1 was reached. Day cultures were washed once in LB and 1ml of both donor and recipient strain culture was concentrated and mixed together. Conjugation took place on a LB agar plate supplemented with 300 µM 2,6-Diaminopimelic acid at 25 °C over night. Then the mixture was transferred on Muller Hinton agar plates supplemented with 0.1 % L-cysteine, 0.1 % *D*-glucose (Millipore), 0.1 % fetal calf serum (BioConcept), 100 µg/ml ampicillin and 15 µg/ml kanamycin to select for recipients containing the suicide vector. Colonies regrew after 2 days of incubation at 37 °C and were restreaked on BHI agar plates supplemented with 0.1 % L-cysteine, 100 µg/ml ampicillin and 15 µg/ml kanamycin. Negative selection was carried out on LB agar plates supplemented with 0.1 % L-cysteine, 10 % sucrose and 100 µg/ml ampicillin, which were at room temperature for a couple of days. All plasmids and remaining peptides of in-frame deletions are listed in table 2. All cloning products were sequenced and sites of homologous recombination were verified by PCR.

Galleria mellonella infections

Weight and aged defined *Galleria mellonella* (*G. mellonella*) larvae from TruLarv (BioSystems Technology) were used for infection experiments. For each condition, 10 randomly chosen larvae were infected. Day cultures of different *F. novicida* strains were inoculated at OD_{600} of 0.02 and grown as described above for 3 h. Then, cultures were washed once with Dulbecco's phosphate saline buffer without $CaCl_2$ and $MgCl_2$ (DPBS, Sigma) and OD_{600} was adjusted to 1 in DPBS. 10-fold dilutions in DPBS were carried out until a concentration of 10^6 CFU/ml was reached. 10 µl of this concentration (roughly 10 000 CFUs) was used for injection into second left pro-leg with a Hamilton syringe (10 µl volume, 26s ga bevel tip, needle length 51 mm; Sigma-Aldrich). Infected larvae were incubated in one petri dish per condition at 37 °C for five days. Survival was scored every 24 h. Death was defined as no movement of legs, head or body. Pupated larvae were considered alive as long as they exhibited any movement. As control for proper handling, each experiment included larvae injected with DPBS.

Statistical analysis

Survival plots and median survival was calculated with Prism8 (GraphPad Software). Each infection experiment was only performed once so far.

References

Abd, H., Johansson, T., Golovliov, I., Sandström, G., and Forsman, M. (2003). Survival and growth of Francisella tularensis in Acanthamoeba castellanii. Appl. Environ. Microbiol. *69*, 600–606.

Ahlund, M.K., Rydén, P., Sjöstedt, A., and Stöven, S. (2010). Directed screen of Francisella novicida virulence determinants using Drosophila melanogaster. Infect. Immun. *78*, 3118–3128.

Aperis, G., Fuchs, B.B., Anderson, C.A., Warner, J.E., Calderwood, S.B., and Mylonakis, E. (2007). Galleria mellonella as a model host to study infection by the Francisella tularensis live vaccine strain. Microbes Infect. *9*, 729–734.

Brodmann, M., Dreier, R.F., Broz, P., and Basler, M. (2017). Francisella requires dynamic type VI secretion system and ClpB to deliver effectors for phagosomal escape. Nat. Commun. *8*, 15853.

Bröms, J.E., Sjöstedt, A., and Lavander, M. (2010). The Role of the Francisella Tularensis Pathogenicity Island in Type VI Secretion, Intracellular Survival, and Modulation of Host Cell Signaling. Front. Microbiol. *1*, 136.

Cerenius, L., and Söderhäll, K. (2004). The prophenoloxidase-activating system in invertebrates. Immunol. Rev. *198*, 116–126.

Chong, A., and Celli, J. (2010). The francisella intracellular life cycle: toward molecular mechanisms of intracellular survival and proliferation. Front. Microbiol. *1*, 138.

Elkins, K.L., Cowley, S.C., and Bosio, C.M. (2007). Innate and adaptive immunity to Francisella. Ann. N. Y. Acad. Sci. *1105*, 284–324.

Eshraghi, A., Kim, J., Walls, A.C., Ledvina, H.E., Miller, C.N., Ramsey, K.M., Whitney, J.C., Radey, M.C., Peterson, S.B., Ruhland, B.R., et al. (2016). Secreted Effectors Encoded within and outside of the Francisella Pathogenicity Island Promote Intramacrophage Growth. Cell Host Microbe *20*, 573–583.

Guina, T., Lanning, L.L., Omland, K.S., Williams, M.S., Wolfraim, L.A., Heyse, S.P., Houchens, C.R., Sanz, P., and Hewitt, J.A. (2018). The Cynomolgus Macaque Natural History Model of Pneumonic Tularemia for Predicting Clinical Efficacy Under the Animal Rule. Front. Cell. Infect. Microbiol. *8*.

Harms, A., Segers, F.H.I.D., Quebatte, M., Mistl, C., Manfredi, P., Körner, J., Chomel, B.B., Kosoy, M., Maruyama, S., Engel, P., et al. (2017). Evolutionary Dynamics of Pathoadaptation Revealed by Three Independent Acquisitions of the VirB/D4 Type IV Secretion System in Bartonella. Genome Biol. Evol. *9*, 761–776.

Hennebique, A., Boisset, S., and Maurin, M. (2019). Tularemia as a waterborne disease: a review. Emerg. Microbes Infect. *8*, 1027–1042.

Henry, T., Brotcke, A., Weiss, D.S., Thompson, L.J., and Monack, D.M. (2007). Type I interferon signaling is required for activation of the inflammasome during Francisella infection. J. Exp. Med. *204*, 987–994.

Jones, B.D., Faron, M., Rasmussen, J.A., and Fletcher, J.R. (2014). Uncovering the components of the Francisella tularensis virulence stealth strategy. Front. Cell. Infect. Microbiol. *4*, 32.

Jones, J.W., Kayagaki, N., Broz, P., Henry, T., Newton, K., O'Rourke, K., Chan, S., Dong, J., Qu, Y., Roose-Girma, M., et al. (2010). Absent in melanoma 2 is required for innate immune recognition of Francisella tularensis. Proc. Natl. Acad. Sci. U. S. A. *107*, 9771–9776.

Keim, P., Johansson, A., and Wagner, D.M. (2007). Molecular epidemiology, evolution, and ecology of Francisella. Ann. N. Y. Acad. Sci. *1105*, 30–66.

Kingry, L.C., and Petersen, J.M. (2014). Comparative review of Francisella tularensis and Francisella novicida. Front. Cell. Infect. Microbiol. *4*, 35.

Lagrange, B., Benaoudia, S., Wallet, P., Magnotti, F., Provost, A., Michal, F., Martin, A., Di Lorenzo, F., Py, B.F., Molinaro, A., et al. (2018). Human caspase-4 detects tetra-acylated LPS and cytosolic Francisella and functions differently from murine caspase-11. Nat. Commun. *9*.

Lampe, E.O., Brenz, Y., Herrmann, L., Repnik, U., Griffiths, G., Zingmark, C., Sjöstedt, A., Winther-Larsen, H.C., and Hagedorn, M. (2015). Dissection of Francisella-Host Cell Interactions in Dictyostelium discoideum. Appl. Environ. Microbiol. *82*, 1586–1598.

Ledvina, H.E., Kelly, K.A., Eshraghi, A., Plemel, R.L., Peterson, S.B., Lee, B., Steele, S., Adler, M., Kawula, T.H., Merz, A.J., et al. (2018). A Phosphatidylinositol 3-Kinase Effector Alters Phagosomal Maturation to Promote Intracellular Growth of Francisella. Cell Host Microbe *24*, 285-295.e8.

Lindgren, H., Shen, H., Zingmark, C., Golovliov, I., Conlan, W., and Sjöstedt, A. (2007). Resistance of Francisella tularensis strains against reactive nitrogen and oxygen species with special reference to the role of KatG. Infect. Immun. *75*, 1303–1309.

Lindgren, M., Bröms, J.E., Meyer, L., Golovliov, I., and Sjöstedt, A. (2013). The Francisella tularensis LVS ΔpdpC mutant exhibits a unique phenotype during intracellular infection. BMC Microbiol. *13*, 20.

Long, M.E., Lindemann, S.R., Rasmussen, J.A., Jones, B.D., and Allen, L.-A.H. (2013). Disruption of Francisella tularensis Schu S4 iglI, iglJ, and pdpC Genes Results in Attenuation for Growth in Human Macrophages and In Vivo Virulence in Mice and Reveals a Unique Phenotype for pdpC. Infect. Immun. *81*, 850–861.

Ludu, J.S., de Bruin, O.M., Duplantis, B.N., Schmerk, C.L., Chou, A.Y., Elkins, K.L., and Nano, F.E. (2008). The Francisella pathogenicity island protein PdpD is required for full virulence and associates with homologues of the type VI secretion system. J. Bacteriol. *190*, 4584–4595.

Meunier, E., Wallet, P., Dreier, R.F., Costanzo, S., Anton, L., Ruhl, S., Dussurgey, S., Dick, M.S., Kistner, A., Rigard, M., et al. (2015). Guanylate-binding proteins promote activation of the AIM2 inflammasome during infection with Francisella novicida. Nat Immunol *advance online publication*.

Oyston, P.C.F., Sjostedt, A., and Titball, R.W. (2004). Tularaemia: bioterrorism defence renews interest in Francisella tularensis. Nat. Rev. Microbiol. *2*, 967–978.

Ozanic, M., Marecic, V., Abu Kwaik, Y., and Santic, M. (2015). The Divergent Intracellular Lifestyle of Francisella tularensis in Evolutionarily Distinct Host Cells. PLoS Pathog. *11*, e1005208.

Ozanic, M., Marecic, V., Lindgren, M., Sjöstedt, A., and Santic, M. (2016). Phenotypic characterization of the Francisella tularensis ΔpdpC and ΔiglG mutants. Microbes Infect. *18*, 768–776.

Ramarao, N., Nielsen-Leroux, C., and Lereclus, D. (2012). The insect Galleria mellonella as a powerful infection model to investigate bacterial pathogenesis. J. Vis. Exp. JoVE e4392.

Ray, H.J., Chu, P., Wu, T.H., Lyons, C.R., Murthy, A.K., Guentzel, M.N., Klose, K.E., and Arulanandam, B.P. (2010). The Fischer 344 rat reflects human susceptibility to francisella pulmonary challenge and provides a new platform for virulence and protection studies. PloS One *5*, e9952.

Read, A., Vogl, S.J., Hueffer, K., Gallagher, L.A., and Happ, G.M. (2008). Francisella genes required for replication in mosquito cells. J. Med. Entomol. *45*, 1108–1116.

Rick Lyons, C., and Wu, T.H. (2007). Animal models of Francisella tularensis infection. Ann. N. Y. Acad. Sci. *1105*, 238–265.

Santic, M., Ozanic, M., Semic, V., Pavokovic, G., Mrvcic, V., and Kwaik, Y.A. (2011). Intra-Vacuolar Proliferation of F. Novicida within H. Vermiformis. Front. Microbiol. *2*, 78.

Schmitt, D.M., Barnes, R., Rogerson, T., Haught, A., Mazzella, L.K., Ford, M., Gilson, T., Birch, J.W.-M., Sjöstedt, A., Reed, D.S., et al. (2017). The Role and Mechanism of Erythrocyte Invasion by Francisella tularensis. Front. Cell. Infect. Microbiol. *7*, 173.

Tang, H. (2009). Regulation and function of the melanization reaction in Drosophila. Fly (Austin) *3*, 105–111.

Thelaus, J., Lundmark, E., Lindgren, P., Sjödin, A., and Forsman, M. (2018). Galleria mellonella Reveals Niche Differences Between Highly Pathogenic and Closely Related Strains of Francisella spp. Front. Cell. Infect. Microbiol. *8*.

Tsai, C.J.-Y., Loh, J.M.S., and Proft, T. (2016). Galleria mellonella infection models for the study of bacterial diseases and for antimicrobial drug testing. Virulence *7*, 214–229.

Uda, A., Sekizuka, T., Tanabayashi, K., Fujita, O., Kuroda, M., Hotta, A., Sugiura, N., Sharma, N., Morikawa, S., and Yamada, A. (2014). Role of Pathogenicity Determinant Protein C (PdpC) in Determining the Virulence of the Francisella tularensis Subspecies tularensis SCHU. PLOS ONE *9*, e89075.

Vogel, H., Altincicek, B., Glöckner, G., and Vilcinskas, A. (2011). A comprehensive transcriptome and immune-gene repertoire of the lepidopteran model host Galleria mellonella. BMC Genomics *12*, 308.

Wittwer, M., Altpeter, E., Pilo, P., Gygli, S.M., Beuret, C., Foucault, F., Ackermann-Gäumann, R., Karrer, U., Jacob, D., Grunow, R., et al. (2018). Population Genomics of Francisella tularensis subsp. holarctica and its Implication on the Eco-Epidemiology of Tularemia in Switzerland. Front. Cell. Infect. Microbiol. *8*, 89.

Figures

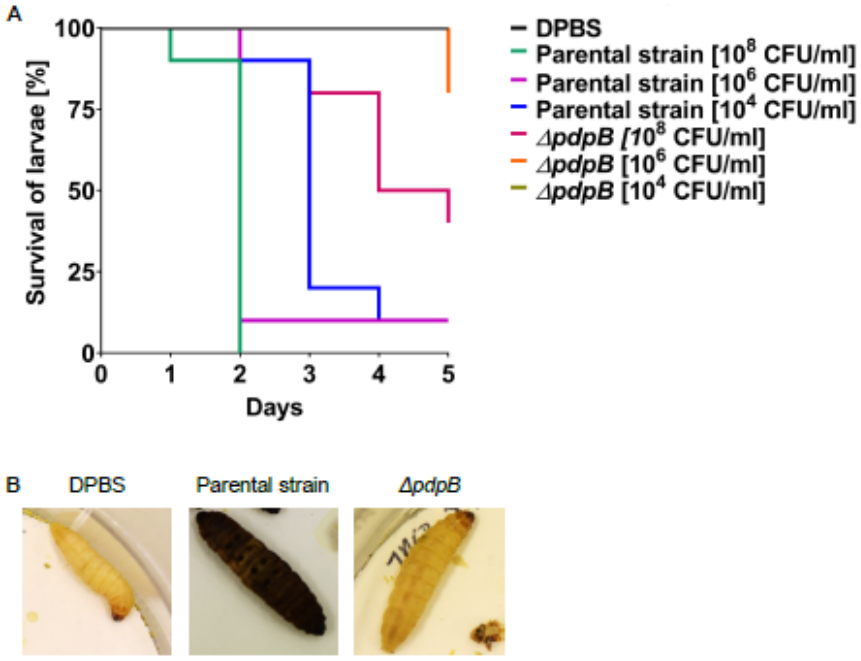

Figure 1: *Francisella* virulence in *G. mellonella* larvae depends on a functional T6SS. A) Survival of *G. mellonella* larvae infected with DPBS as control and different concentrations of *F. novicida* U112 *iglA-sfgp* (parental strain) and *ΔpdpB* (T6SS-negative). Olive line for *ΔpdpB* [10^4 CFU/ml] is underneath the black line for DPBS. 10 larvae per condition were infected. Experiment was performed once. **B)** Images of larvae infected with DPBS, parental strain and *ΔpdpB* at a concentration of 10^6 CFU/ml at day 5.

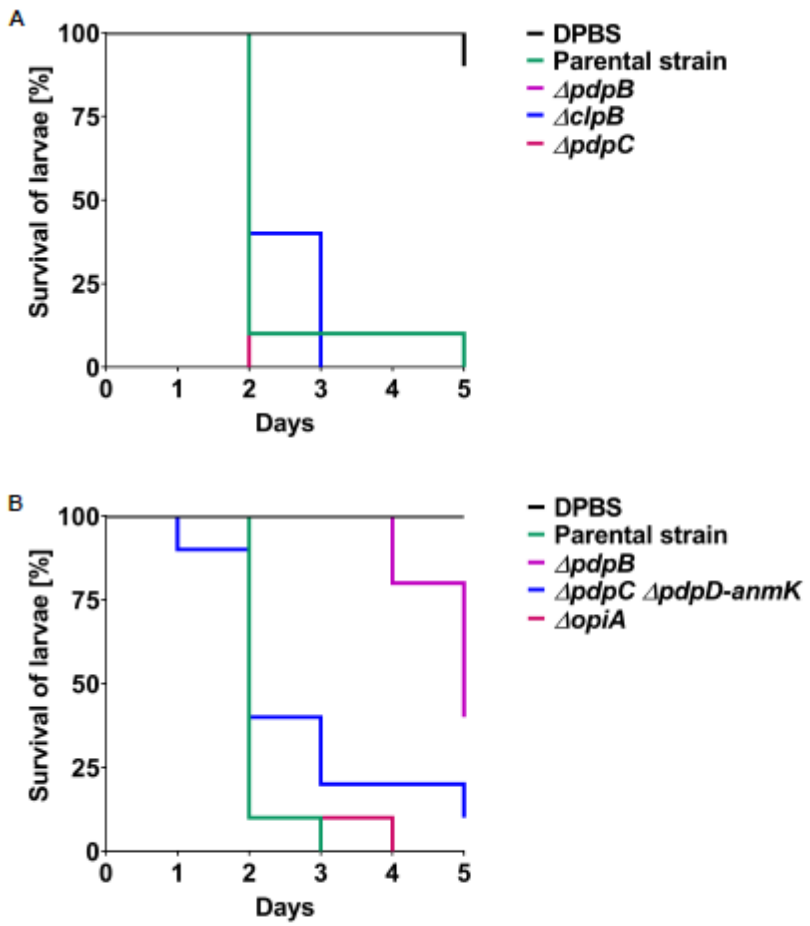

Figure 2: *Francisella* virulence in *G. mellonella* larvae is independent of T6SS dynamics and effectors important in other model systems. A-B) 10 larvae per condition were infected with bacteria at concentration of 10^6 CFU/ml. Experiments were performed once. **A)** Survival of *G. mellonella* larvae infected with DPBS as control and *F. novicida* U112 *iglA-sfgp* (parental strain), *ΔpdpB* (T6SS-negative), *ΔclpB* and *ΔpdpC*. **B)** Survival of *G. mellonella* larvae infected with DPBS as control and *F. novicida* U112 *iglA-sfgp* (parental strain), *ΔpdpB* (T6SS-negative), *ΔpdpC ΔpdpD-anmK* and *ΔopiA*.

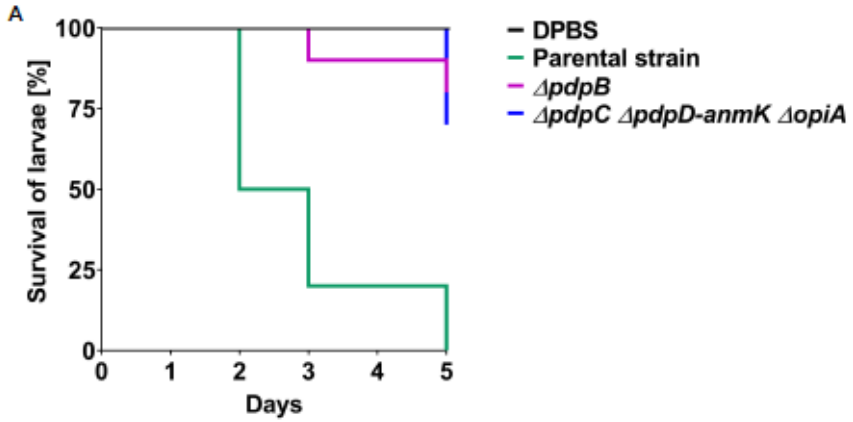

Figure 3: Combined deletion of *pdpC, pdpD-anmK* and *opiA* results in decreased *Francisella* virulence in *G. mellonella* larvae. A) Survival of *G. mellonella* larvae infected with DPBS as control and *F. novicida* U112 *iglA-sfgp* (parental strain), *ΔpdpB* (T6SS-negative), *ΔpdpC ΔpdpD-anmK ΔopiA*. 10 larvae per condition were infected with bacteria at concentration of 10^6 CFU/ml. Experiment was performed once.

Tables

Table 1: Strains used in this study, related to Material and methods

Organism	Genotype	Plasmid	Relevant features	Source
Francisella novicida U112	*iglA-sfgfp*		C-terminal chromosomal fusion of *sfgfp* to *iglA*	Clemens et al., 2015
	iglA-sfgfp ΔpdpB		In-frame deletion of *pdpB*	Brodmann et al., 2017
	iglA-sfgfp, ΔclpB		In-frame deletion of *clpB*	Brodmann et al., 2017
	iglA-sfgfp, ΔpdpC		In-frame deletion of *pdpC*	Brodmann et al., 2017
	iglA-sfgfp, ΔpdpC ΔpdpD-anmk		In-frame deletion of *pdpC*, *pdpD* and *anmK*	Brodmann et al., 2017
	iglA-sfgfp, ΔopiA		In-frame deletion of *opiA*	This study
	iglA-sfgfp, ΔpdpC ΔpdpD-anmk ΔopiA		In-frame deletion of *pdpC*, *pdpD*, *anmK* and *opiA*	This study

Table 2: Plasmids and primers used to generate mutants, related to Material and Methods.

Plasmid Name	Peptide scar	Primers	Sequence 5'-3' [base pairs]
pDMK3 *ΔopiA*	MKNFEVIRKDFFSHLCNLLN*	dFTN_0131_Xho1_1.FOR	TCAGTACTCGAGAGTTTATTTTTAATCCACATAAGC
		dFTN_0131_1.REV	TACGCAAAGATTTTTCTCATTTGTGTAATTTGTTG
		dFTN_0131_2.FOR	AAATGAGAAAAATCTTTGCGTATTACTTC
		dFTN_0131_Not1_2.REV	TCAGTAGCGGCCGCGTCAACCATATAACAAAGGC
		dFTN_0131_Det.FOR	TCCGGAAAATATCGTTGGAGT
		dFTN_0131_Det.REV	TGGCAGTCTTTAGAGGAGCT

3.6. Mobilizable Plasmids for Tunable Gene Expression in *Francisella novicida*

Maj Brodmann[1], Rosalie Heilig[2], Petr Broz[2] and Marek Basler[1*]

[1] Biozentrum, University of Basel, Basel, Switzerland

[2] Department of Biochemistry, University of Lausanne, Epalinges, Switzerland

[*] **Correspondence:** Dr. Marek Basler, marek.basler@unibas.ch

Frontiers in Cellular and Infection Microbiology

31 August 2018, Volume 8, Article 284

DOI: 10.3389/fcimb.2018.00284

Statement of contribution:

I designed and generated plasmids and strains. Furthermore, I performed and analyzed all imaging experiments. I prepared figures and wrote the manuscript with Marek Basler.

frontiers in Cellular and Infection Microbiology

ORIGINAL RESEARCH
published: 31 August 2018
doi: 10.3389/fcimb.2018.00284

Mobilizable Plasmids for Tunable Gene Expression in *Francisella novicida*

*Maj Brodmann[1], Rosalie Heilig[2], Petr Broz[2] and Marek Basler[1]**

[1] Biozentrum, University of Basel, Basel, Switzerland, [2] Department of Biochemistry, University of Lausanne, Épalinges, Switzerland

Francisella tularensis is the causative agent of the life-threatening disease tularemia. However, the molecular tools to study *Francisella* are limited. Especially, expression plasmids are sparse and difficult to use, as they are unstable and prone to spontaneous loss. Most *Francisella* expression plasmids lack inducible promoters making it difficult to control gene expression levels. In addition, available expression plasmids are mainly designed for *F. tularensis*, however, genetic differences including restriction-modification systems impede the use of these plasmids in *F. novicida*, which is often used as a model organism to study *Francisella* pathogenesis. Here we report construction and characterization of two mobilizable plasmids (pFNMB1 and pFNMB2) designed for regulated gene expression in *F. novicida*. pFNMB plasmids contain a tetracycline inducible promoter to control gene expression levels and *oriT* for RP4 mediated mobilization. We show that both plasmids are stably maintained in bacteria for more than 40 generations over 4 days of culturing in the absence of selection against plasmid loss. Expression levels are dependent on anhydrotetracycline concentration and homogeneous in a bacterial population. pFNMB1 and pFNMB2 plasmids differ in the sequence between promoter and translation start site and thus allow to reach different maximum levels of protein expression. We used pFNMB1 and pFNMB2 for complementation of *Francisella* Pathogenicity Island mutants Δ*iglF*, Δ*igIl*, and Δ*iglC in-vitro* and pFNMB1 to complement Δ*igIl* mutant in bone marrow derived macrophages.

Keywords: ***Francisella novicida*, expression plasmid, conjugation, ATc inducible, complementation, type VI secretion system, bacterial mutagenesis, tularemia**

OPEN ACCESS

Edited by:
Sophie Bleves,
Aix-Marseille Université, France

Reviewed by:
Gregory T. Robertson,
Colorado State University,
United States
Roger Derek Pechous,
University of Arkansas for Medical
Sciences, United States

***Correspondence:**
Marek Basler
marek.basler@unibas.ch

Received: 08 May 2018
Accepted: 25 July 2018
Published: 31 August 2018

Citation:
Brodmann M, Heilig R, Broz P and Basler M (2018) Mobilizable Plasmids for Tunable Gene Expression in Francisella novicida.
Front. Cell. Infect. Microbiol. 8:284.
doi: 10.3389/fcimb.2018.00284

INTRODUCTION

Francisella tularensis is the causative agent of tularemia and can cause life-threatening disease in animals and humans. Essential for *Francisella* virulence is the *Francisella* pathogenicity island (FPI), which encodes a dynamic type VI secretion system (T6SS) (Bröms et al., 2010; Chong and Celli, 2010; Clemens et al., 2015; Brodmann et al., 2017). The most virulent subspecies *F. tularensis* subspecies *tularensis*, classified as a Tier 1 agent (Oyston et al., 2004), and subspecies *holarctica* (hereafter *F. tularensis*) contain two FPIs. The related subspecies *F. tularensis* subspecies *novicida* (hereafter *F. novicida*) possesses only one FPI and is highly virulent in mice but rarely infects humans. These features make *F. novicida* an ideal model organism for investigating tularemia and *Francisella* T6SS (Kingry and Petersen, 2014).

Molecular tools to make chromosomal in-frame deletion mutations in *Francisella* are available and commonly used to study the role of a certain gene of interest on a particular phenotype (Anthony et al., 1991; Golovliov et al., 2003; Frank and Zahrt, 2007). However, gene deletion and insertions may alter the expression of neighboring genes and cause so called "polar effects". If expression of the gene of interest *in trans* from an inducible plasmid reverses the mutant phenotype, a possible polar effect can be ruled out. Unfortunately, only few expression plasmids are available for *Francisella*. Therefore, many recent studies lack *in trans* complementation of in-frame deletion mutations (Nano and Schmerk, 2007; Santic et al., 2011; Eshraghi et al., 2016; Brodmann et al., 2017) or use chromosomal complementation *in cis* (de Bruin et al., 2007; Weiss et al., 2007; Lindgren et al., 2013).

All available expression plasmids for *Francisella* are derived from the pFNL10 plasmid except for pCUG18, which is derived from pC194 and pUC18 (Rasko et al., 2007). pFNL10 was isolated from the *F. novicida*-like strain F6168 (Pavlov et al., 1996). The function of pFNL10 is unclear; however, the five encoding regions on the plasmid were identified. ORF1—ORF3 are required for plasmid replication and encode replication initiation protein RepA (ORF1), an ATP-dependent RNA helicase/endonuclease (ORF2), and an integrase/recombinase (ORF3). ORF4 and ORF5 encode a putative toxin-antitoxin system together with a possible regulatory feature ORFm (Pomerantsev et al., 2001a) (**Figure 1A**). Over the last 20 years, pFNL10 was modified to meet the needs of the *Francisella* research community. First, tetracycline and chloramphenicol resistance cassettes were introduced for selection resulting in pFNL200 (Pavlov et al., 1996). Since pFNL200 was restricted to replicate in *Francisella*, the p15A origin of replication of *Escherichia coli* was added thus obtaining a shuttle vector pKK202 (Norqvist et al., 1996). Later, the constitutively active *gro*ESL promoter was successfully used to express *gfp* and other genes (pKK214, pKK289Km, **Figure 1B**) *in-vitro* and in eukaryotic cells (Abd et al., 2003; Bönquist et al., 2008). Other pFNL10 derivatives are pFNLTP, which includes a version that only replicates at 32°C but not at 42°C due to a mutation in *repA* (Maier et al., 2004) and pMP, which includes a version of a *bla* promoter that is not recognized in *E. coli* to allow cloning of toxic genes in *E. coli* (LoVullo et al., 2006, 2009). So far, only two controllable *Francisella* promoter systems exist; a glucose repressible system (pTCD3) (Horzempa et al., 2008) and a tetracycline inducible or repressible version of the *gro*ESL promoter (pEDL) (LoVullo et al., 2012). The tetracycline inducible promoter system is a preferred choice for many bacterial model organisms because it allows tight and concentration dependent regulation of expression levels. It is also applicable for infection models such as cell cultures or animals since tetracycline passively penetrates most mammalian membranes (Bertram and Hillen, 2008). The tetracycline inducible promoter systems consists of constitutively expressed TetR, which binds to the *tetO* sequence and thereby transcriptionally represses the *tetA* promoter. Tetracycline or anhydrotetracycline (ATc), which is less toxic but has even higher affinity to TetR, binds TetR, and derepresses the *tetA* promoter (Gossen and Bujard, 1992). In the case of the tetracycline repressible promoter system, TetR binds *tetO* only if tetracycline or ATc is present, therefore, transcription is repressed upon addition of ATc (Scholz et al., 2004).

Despite the efforts in recent years, complementation from plasmid remains difficult in *Francisella*. Non-native expression levels (Santic et al., 2007; Zogaj and Klose, 2010) and spontaneous deletions in pFNL200 (Pomerantsev et al., 2001b) and pFNLTP (Maier et al., 2004) were reported. Another problem is the relatively low electroporation efficiency in *Francisella* and especially in *F. novicida* for plasmids isolated from *E. coli*. This is thought to be due to active restriction-modification systems in *Francisella* (Maier et al., 2004; LoVullo et al., 2006). In *F. novicida*, 4 restriction-modification systems were identified to restrict unmodified plasmid DNA, while in *F. tularensis* most restriction-modification system were annotated as pseudogenes (Gallagher et al., 2008). Expression plasmids were mainly tested in *F. tularensis* (Norqvist et al., 1996; Abd et al., 2003; LoVullo et al., 2006, 2009, 2012; Rasko et al., 2007) and consequently, in-frame deletions were more often complemented from plasmid in *F. tularensis* (Lai et al., 2004; Gil et al., 2006; Maier et al., 2006; Bönquist et al., 2008; Ark and Mann, 2011; Lindemann et al., 2011; Schmidt et al., 2013). On the other hand, suitable expression plasmids are mostly lacking in *F. novicida* and therefore only few studies include complementation experiments (Tempel et al., 2006; de Bruin et al., 2011).

Here we report construction of expression plasmids derived from pKK289Km specially designed for *F. novicida*. pFNMB1 and pFNMB2 plasmids can be mobilized by conjugation to overcome the need for electroporation. In addition, ATc induction allows homogeneous gene expression and the plasmids are stably maintained in a population for 4 days without selection pressure. As a proof of concept, we successfully complemented in-frame deletion of FPI genes *iglF*, *iglI,* and *iglC in-vitro* and *iglI* in bone marrow derived macrophages.

MATERIALS AND METHODS

Bacterial Strains and Growth Conditions

Francisella tularensis subsp. *novicida* strain U112 and the derivative strains were grown in brain heart infusion (BHI) broth supplemented with 0.2% L-cysteine (Sigma). Ampicillin (100 μg/ml, AppliChem) or kanamycin (15 μg/ml, AppliChem) were added if not stated otherwise. Liquid cultures were grown aerobically at 37°C. Gene expression from plasmid was induced by adding the indicated concentration of anhydrotetracycline (ATc, IBA) to the liquid culture at OD_{600} of 0.02 for 3 h. *Escherichia coli* DH5α λ*pir* and derivative strains were grown aerobically in Luria broth (LB) or on LB agar plates both supplemented with 50 μg/ml kanamycin at 37°C. All strains used are listed in **Supplementary Table 1**.

Construction of Plasmids

All plasmids and corresponding primers are listed in **Supplementary Table 2**. Expression plasmids pFNMB1 and pFNMB2 were constructed by using the backbone of pKK289Km *gfp* (Bönquist et al., 2008) and inserting the RP4 mobilization site of pDMK3 (Lindgren et al., 2007) at EcoRI and SbfI restriction

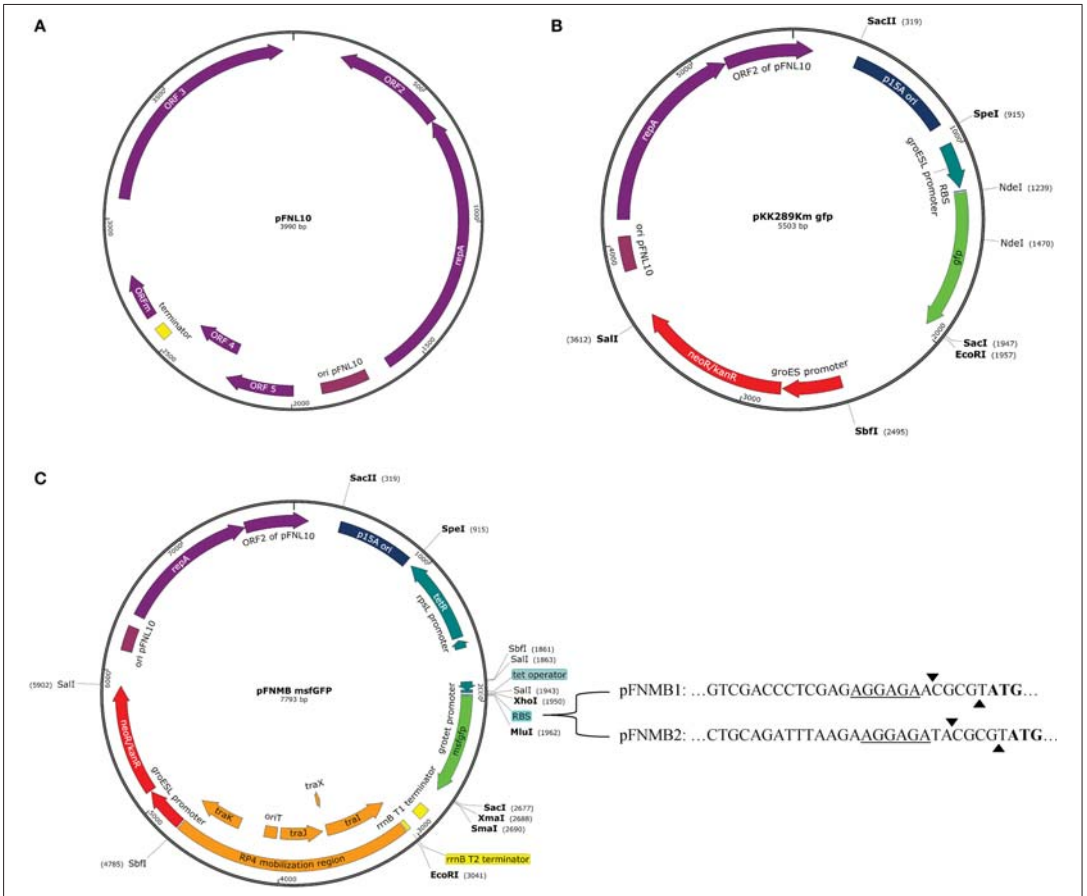

FIGURE 1 | Plasmid maps. Promoters, genes, terminators, and some relevant restriction sites are shown. Maps were designed with SnapGene Version 4.0.3. **(A)** Plasmid map of pFNL10 according to Pomerantsev et al. (2001a). **(B)** Plasmid map of pKK289Km *gfp* according to Bönquist et al. (2008). **(C)** Plasmid map of pFNMB *msfgfp* with variable RBS sequences. pFNMB1 contains the RBS sequence of *iglC* and pFNMB2 of pKK289Km. The underline highlights the RBS, the arrows mark the MluI restriction site and the start codon is represented in bold.

sites, thereby removing the truncated chloramphenicol resistance cassette, a leftover of pKK214CAT (Abd et al., 2003). Then the ATc inducible promoter cassette of pEDL17 (*tetR* with *rpsL* promoter and *groESL* promoter with *tetO*; LoVullo et al., 2012), the multiple cloning site of pDMK3 and the *E. coli rrnB* T1 and T2 terminators of pBAD24 (Guzman et al., 1995) were combined by overlap-extension PCR. The PCR product was placed into pKK289Km *gfp* at SpeI and EcoRI restriction sites to remove the original *groESL* promoter and *gfp* gene. For pFNMB1, the *iglC* RBS was inserted together with *msfgfp* at XhoI and XmaI restriction sites by amplification of *msfgfp* with primers containing the sequence of *iglC* RBS and an additional MluI restriction site in front of the *msfgfp* start codon (AGAGGAGAACGCGT). For pFNMB2, the *iglC* RBS was exchanged for the RBS of pKK289Km by combining the ATc inducible promoter cassette of pEDL17 and *msfgfp* by overlap-extension PCR using primers containing the RBS of pKK289Km with a MluI restriction site. The PCR product was placed into pFNMB1 at SpeI and XmaI restriction sites. All cloning products were sequenced. Plasmid maps were generated with SnapGene Version 4.0.3. pFNMB1 *msfgfp* (Addgene ID: 113191) and pFNMB2 *msfgfp* (Addgene ID: 113192) were deposited to Addgene.

Bacterial Mutagenesis

Suicide vector pDMK3 was used for generating in-frame deletions as reported previously (Lindgren et al., 2007; Brodmann et al., 2017), except that an optimized conjugation procedure

was used (described below). Various genes were cloned into pKK289Km using NdeI and EcoRI or SacI restriction sites and into pFNMB1 and pFNMB2 using MluI and SacI restriction sites. Plasmids, remaining peptides of in-frame deletions and primers are listed in **Supplementary Table 3**. Cloning products were sequenced and the site of homologous recombination was verified by PCR with primers located outside of the replaced regions.

pKK289Km and derivatives were transformed by electroporation as reported previously (Maier et al., 2004). Up to 1 μg of plasmid was used for electroporation. pFNMB1, pFNMB2 and derivatives were mobilized by conjugation as described below.

Conjugation

F. novicida was grown on BHI agar plates supplemented with 0.2 % L-cysteine and 100 μg/ml ampicillin and the donor *E. coli* strain (kind gift of A. Harms and C. Dehio, Harms et al., 2017) harboring the plasmid of interest was grown on Luria-Bertani (LB) agar plates supplemented with 300 μM 2,6-Diaminopimelic acid (Sigma) and 50 μg/ml kanamycin. Both plates were incubated over night at 37°C. The following day, about 100 μl of *F. novicida* and *E. coli* dense bacterial cultures were transferred to a fresh LB plate supplemented with 300 μM 2,6-Diaminopimelic acid and mixed thoroughly. After 2 h incubation at 37°C, about 50 μl of the mixture was resuspended in 100 μl Mueller–Hinton (MH) broth and plated on MH agar plates supplemented with 0.1% L-cysteine, 0.1% D-glucose (Millipore), 0.1% FCS (BioConcept), 100 μg/ml ampicillin, and 15 μg/ml kanamycin and incubated for 2 days at 37°C. Single *F. novicida* colonies were purified by passaging on selective plates.

To assess conjugation efficiency, the donor and recipient strains were first concentrated to an OD_{600} of 10 and then mixed in a 1 to 1 ratio (each 50 μl). Five microliters of the mixture was spotted on a LB agar plate supplemented with 300 μM 2,6-Diaminopimelic acid in two technical replicates. After 2 h, the spots were cut out and resuspended in 100 μl of MH broth. The resuspended bacteria were plated on MH agar plates supplemented with 0.1% L-cysteine, 0.1% D-glucose, 0.1% FCS, 100 μg/ml ampicillin, and 15 μg/ml kanamycin. The CFU per ml and the conjugation efficiency were calculated in the following manner:

$$Transformants\,(\frac{CFU}{ml}) = \frac{average\ colonies_{counted}}{0.1\ ml}$$

$$Conjugation\ efficency = \frac{calculated\ transformants}{used\ donor\ cells}$$

The assay was performed in three biological replicates.

Plasmid Stability Assay

On day 0, *F. novicida* harboring pFNMB1 *msfgfp* or pFNMB2 *msfgfp* were diluted to an OD_{600} of 0.02 and grown in liquid overnight (ON) cultures supplemented with 15 μg/ml kanamycin and 500 ng/ml ATc to induce gene expression. On days 1–4, the old ON cultures were diluted to an OD_{600} of 0.02 and supplemented with 100 μg/ml ampicillin and 500 ng/ml ATc. For every ON culture, OD_{600} was measured and aliquots were taken for imaging, serial dilutions and inoculation of new ON cultures. Serial dilutions were plated on MH agar plates supplemented with 0.1% L-cysteine, 0.1% D-glucose, 0.1% FCS, and 100 μg/ml ampicillin and on MH agar plates supplemented with 0.1% L-cysteine, 0.1% D-glucose, 0.1% FCS, and 100 μg/ml ampicillin and 15 μg/ml kanamycin. Colony forming units (CFU) were counted and the concentrations of CFU/ml were calculated. Number of generations were calculated with following formula:

$$N_0 = calculated\ concentration\ of\ bacteria\ used\ for\ inoculation$$

$$N = calculated\ concentration\ of\ bacteria\ after\ serial\ dilution$$

$$Number\ of\ generations\ n = \frac{\log \frac{N}{N_0}}{\log 2}$$

The experiment was carried out in three biological replicates.

Plasmid Recovery

pFNMB1 *msfgfp* and pFNMB2 *msfgfp* were recovered from *F. novicida* with a Zyppy Plasmid Miniprep Kit (Zymo Research) after passaging the cultures for 4 days in liquid BHI supplemented with 100 μg/ml ampicillin and 500 ng/ml ATc as described above. About 250 ng of each plasmid DNA was then transformed into chemo-competent *E. coli* DH5α *λpir*. The transformed *E. coli* were plated on LB agar plates supplemented with 50 μg/ml kanamycin. Three independent experiments were carried out. The next day, colonies were grown in liquid LB supplemented with 50 μg/ml kanamycin, plasmid DNA was isolated and 250 ng of each plasmid was digested with SacI-HF and SpeI restriction enzymes (New England BioLabs) for 1 h. As control, both plasmids were additionally isolated from *E. coli* directly, without passaging in *F. novicida*, and digested identically. After heat inactivation of the enzymes (80°C for 20 min), the digested plasmids were loaded on a 1% agarose gel (BioConcept) together with a 1 kb ladder (New England BioLabs). DNA was stained with RedSafe (iNtRON Biotechnology) and a Red imaging system (Alpha Innotech) was used for imaging.

Fluorescence Microscopy

Microscope set up was described previously (Kudryashev et al., 2015; Vettiger and Basler, 2016; Brodmann et al., 2017). *F. novicida* strains were prepared as described in Brodmann et al. (2017). For assessment of plasmid stability, 1.5 μl ON culture was spotted on a pad of 1% agarose in phosphate buffered saline (PBS) and imaged immediately. For measuring the GFP signal intensities after induction with ATc, the spotted bacteria were imaged immediately. For assessing T6SS function of complemented in-frame deletion mutants, the bacteria were incubated on a pad at 37°C for 1 h before imaging. All imaging experiments were performed in three independent experiments.

Image Analysis

Image analysis and manipulations were performed with Fiji software (Schindelin et al., 2012) as described previously (Basler

et al., 2013; Vettiger and Basler, 2016). For calculation of the GFP signal intensities after ATc induction, the background intensity was subtracted with the plugin "BackgroundSubstracter." Then the plugin "Time Series Analyzer V3.0" was used to quantify the total GFP signal intensity of the whole field of view. The total GFP signal intensity was divided by the number of bacteria in the field of view. Number of bacteria was calculated with the "Find Maxima" function from phase contrast images. Contrast on compared images was adjusted equally. For the **Supplementary Movies**, the contrast used for *F. novicida* U112 Δ*iglC* pFNMB2 *iglC* induced with 500 ng/ml was set to match the other strains.

Cell Culture and Infection Assay

The day before infection experiment, bone marrow derived macrophages (BMDMs) were seeded into 96-well plates (Eppendorf) at a density of $5*10^4$ cells/well in DMEM (Thermo Fisher) with 20% M-CSF (supernatant of L929 mouse fibroblasts, BioConcept), 10% FCS (BioConcept), 10 mM HEPES (BioConcept), and non-essential amino acids (Thermo Fisher). The BMDMs were primed with 100 ng/ml LPS from *E. coli* O111:B4 (InvivoGen). *F. novicida* strains were grown aerobically in liquid BHI culture supplemented with the corresponding antibiotics and with 0 or 500 ng/ml ATc at 37°C ON. The next day, the medium of the BMDMs was replaced with fresh medium supplemented with 0 or 1,000 ng/ml ATc and the bacteria were added to the BMDMs at a multiplicity of infection (MOI) of 100. The 96-well plates were centrifuged at 300 g for 5 min to synchronize the infection process and afterwards incubated at 37°C. After 2 h, the medium was replaced with fresh medium supplemented with 0 or 1,000 ng/ml ATC and with 10 μg/ml gentamycin (BioConcept). Then the 96-well plates were incubated for 10 h at 37°C. Afterwards, a lactate dehydrogenase (LDH) release assay was carried out with an LDH Cytotoxicity Detection Kit (Takara). The percentage of LDH release was calculated with the following formula:

$$\%\ of\ LDH\ release = \frac{LDH\ value_{infected} - LDH\ value_{\ uninfected}}{LDH\ value_{total\ lysis} - LDH\ value_{\ uninfected}} \times 100$$

Infection experiments were carried out in biological triplicates. The unpaired two-tailed *t*-test with Welch's correction was used to identify significant differences. *P*-values are given in the figure legend.

RESULTS

The need for expression plasmids for *F. novicida*, motivated us to construct the mobilizable and inducible expression plasmids pFNMB1 and pFNMB2 (**Figure 1C**). We constructed pFNMB1 and pFNMB2 by using the backbone of pKK289Km, which is transformed by electroporation and contains a constitutively active promoter *gro*ESL (Bönquist et al., 2008). As electroporation can be difficult in *F. novicida* (Maier et al., 2004; LoVullo et al., 2006), the need for electroporation was circumvented by inserting the RP4 mobilization site of pDMK3 (Lindgren et al., 2013) encoding *traI* (relaxase), *traX* (regulation of *traI* and *traJ*), *traJ,* and *traK* (*oriT* binding proteins) and origin of transfer (*oriT*) (Haase et al., 1995) at the site of the truncated chloramphenicol resistance cassette. The constitutively active *gro*ESL promoter was exchanged for the tetracycline inducible *grotet* promoter (LoVullo et al., 2012). Two different RBS were inserted to achieve a wider range of expression levels. pFNMB1 was designed for lower expression and contains the ribosomal binding site (RBS) of *iglC* in front of a MluI restriction site. Higher expression levels in pFNMB2 were reached by inserting the RBS of pKK289Km in front of a MluI restriction site. In addition, the well characterized *E. coli rrnB* T1 and T2 terminators from pBAD (Guzman et al., 1995) were inserted after a multiple cloning site.

First, we tested the conjugation efficiency of pFNMB1 *msfgfp* from an *E. coli* strain harboring a chromosomally encoded RP4 machinery (Harms et al., 2017) to *F. novicida*. Both strains were mixed in a 1:1 ratio and spotted on an agar plate. After 2 h incubation at 37°C, the bacteria were resuspended and plated on agar plates containing both ampicillin and kanamycin to select for *F. novicida* harboring the plasmid. On average, about $5.1*10^{-7} \pm 2.5*10^{-7}$ bacterial cells were transformed per donor cell.

As plasmid instability is reported for certain *Francisella* plasmids (Pomerantsev et al., 2001b; Maier et al., 2004), we tested the stability of pFNMB1 and pFNMB2 with *msfgfp* in *F. novicida* over 4 days by inducing expression with 500 ng/ml ATc but without addition of kanamycin to select for plasmid maintenance (**Figure 2**). To assess plasmid stability, we monitored msfGFP expression by fluorescence microscopy (**Figures 2A,B**) and counted the kanamycin resistant colonies (**Figure 2C**). Over 4 days and during ∼40 generations, the plasmids were stable in the bacterial population. Importantly both, the *msfgfp* and the kanamycin resistance cassette, which are located at different sites on the plasmid (**Figure 1C**), stayed fully functional. To exclude that the plasmids integrated into the chromosome, pFNMB1 *msgfp* and pFNMB2 *msfgfp* were recovered from *F. novicida* after passaging the bacteria for 4 days as described above. Then the isolated plasmid DNA was transformed into *E. coli*. The plasmids were recovered again, digested with SacI and SpeI restriction enzymes and loaded on an agarose gel to analyze the size of the DNA fragments. Two bands of the correct size (about 6,000 base pairs and 1,700 base pairs) were observed for pFNMB1 *msfgfp* and pFNMB2 *msfgfp* similarly to the controls pFNMB1 *msfgfp* and pFNMB2 *msfgfp*, which were not passaged in *F. novicida* (**Figures 2D,E**). These results strongly suggest that the plasmids are maintained extra-chromosomally in *F. novicida* without any rearrangements.

To test if the *grotet* promoters of pFNMB1 and pFNMB2 respond to ATc in *F. novicida*, we used different ATc concentrations to induce expression of msfGFP (**Figure 3**). Indeed, msfGFP intensity increased in a concentration dependent manner for both plasmids. However, the level of induction differed; GFP expression from pFNMB1 was in general lower than from pFNMB2 (**Figure 3D**) indicating that the pKK289Km RBS starts translation more efficiently than the *iglC* RBS. Furthermore, we compared GFP expression from pFNMB1, pFNMB2 and pKK289Km by fluorescence microscopy (**Figures 3A–C**). Interestingly, bacteria harboring pKK289Km *gfp* showed a heterogeneous expression of GFP (**Figure 3C**), while all bacteria harboring pFNMB1 *msfgfp* or pFNMB2 *msfgfp* expressed similar levels of GFP after induction with 500 ng/ml ATc. Without ATc, no GFP fluorescence was observed indicating that expression is well repressed by the TetR in the absence of ATc (**Figures 3A,B**). However, GFP expression was higher in some bacteria containing pKK289Km plasmid than in those with pFNMB1 and pFNMB2 (**Figures 3A–C**).

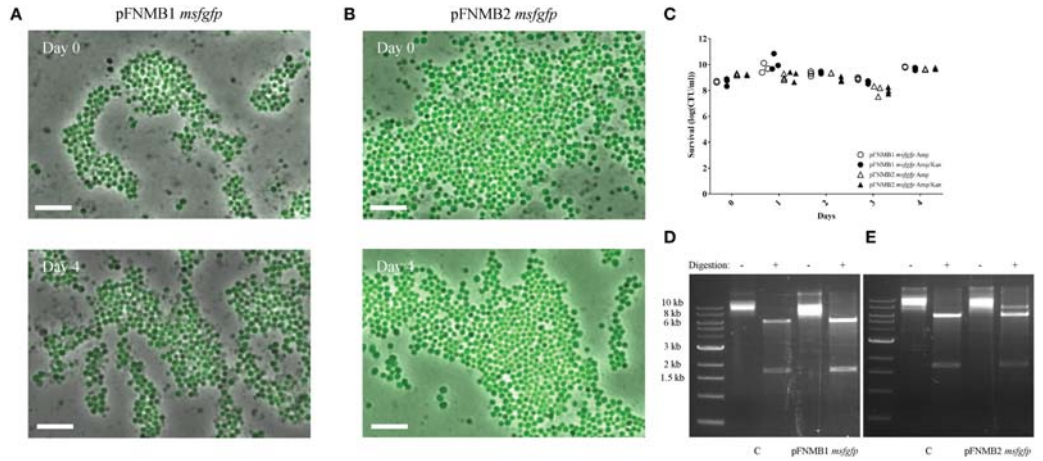

FIGURE 2 | Plasmid stability. GFP expression was induced with 500 ng/ml of ATc. ON culture of day 0 was supplemented with 15 μg/ml kanamycin, while ON cultures of days 1–4 were supplemented with 50 μg/ml ampicillin. **(A)** GFP expression in *F. novicida* U112 pFNMB1 *msfgfp* ON cultures of day 0 and day 4. **(B)** GFP expression in *F. novicida* U112 pFNMB2 *msfgfp* ON cultures of day 0 and day 4. **(A,B)** Images are a merge of phase contrast and GFP channel. 26 × 39 μm fields of view are shown. Scale bar represent 5 μm. Representative replicates are shown. Three independent experiments were performed. **(C)** Survival assay performed with ON cultures of *F. novicida* U112 pFNMB1 *msfgfp* and *F. novicida* U112 pFNMB2 *msfgfp* plated on ampicillin and ampicillin/kanamycin plates. Three independent experiments were performed. **(D)** Digestion of pFNMB1 *msfgfp* with SacI and SpeI restriction enzymes. **(E)** Digestion of pFNMB2 *msfgfp* with SacI and SpeI restriction enzymes. **(D,E)** Plasmids were passaged in *F. novicida* for 4 days before being transformed into *E. coli*. Controls were isolated directly from *E. coli*. Representative replicates are shown. Three independent experiments were performed.

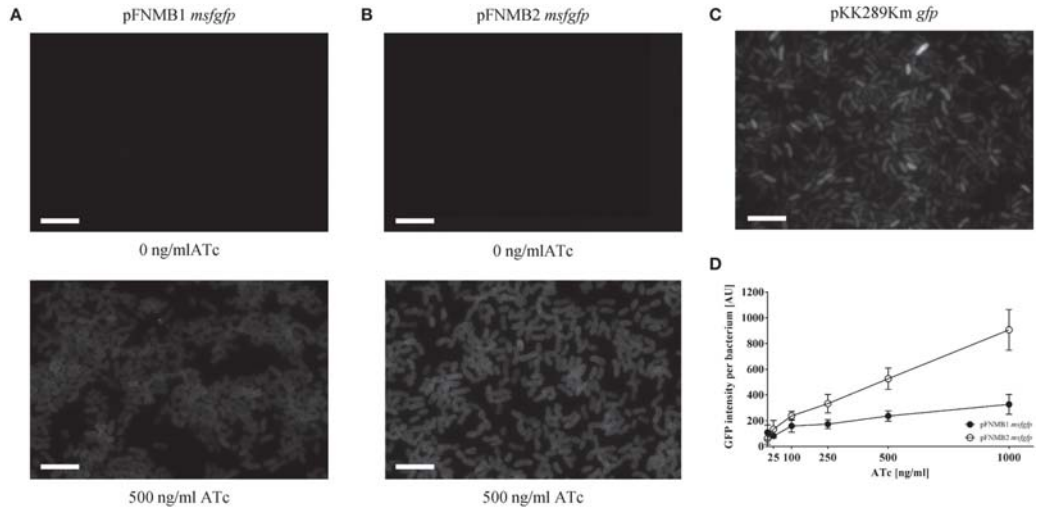

FIGURE 3 | GFP intensities of pFNMB1 *msfgfp*, pFNMB2 *msfgfp,* and pKK289Km *gfp*. **(A)** Homogeneous GFP expression in *F. novicida* U112 pFNMB1 *msfgfp* upon induction with 500 ng/ml ATc. **(B)** Homogeneous GFP expression in *F. novicida* U112 pFNMB2 *msfgfp* upon induction with 500 ng/ml ATc. **(C)** Heterogeneous GFP expression in *F. novicida* U112 pKK289Km *gfp*. **(A–C)** GFP expression was induced with 0 ng/ml ATc and 500 ng/ml of ATc. GFP channels are shown. 39 × 26 μm fields of view. Scale bars represent 5 μm. **(D)** GFP expression in *F. novicida* U112 pFNMB1 *msfgfp* and *F. novicida* U112 pFNMB2 *msfgfp* was induced with 0, 25, 100, 250, 500, and 1,000 ng/ml of ATc. GFP intensity per bacterium was calculated as described in the section Materials and Methods. Three independent experiments were performed. Standard deviations are shown.

In our previous study, we constructed several in-frame deletion mutants in *F. novicida* and assessed T6SS function using fluorescence microscopy (Brodmann et al., 2017). For two mutants (Δ*iglF* and Δ*iglI*) with abolished T6SS function, we were unable to exclude polar effects as the deletion of the downstream genes (*iglG* and *iglJ*) resulted in similar phenotypes. Here, we generated *F. novicida* mutants carrying the respective complementation plasmids and successfully restored T6SS sheath assembly in Δ*iglF* and Δ*iglI* mutants by expression of IglF or IglI from pFNMB1 after induction with 250 ng/ml ATc (**Figures 4C,D**, **Supplementary Movies 1**, **2**). Importantly, independently isolated colonies exhibited the same phenotypes. This was in contrast with several problems we experienced when using pKK289Km plasmid. First, electroporation of pKK289Km was very inefficient, as we routinely obtained only 1–10 transformed colonies even when using 1 μg of the plasmid DNA and $3*10^{10}$ *F. novicida* cells. In addition, independently isolated colonies exhibited different phenotypes such as no complementation, partial complementation or we only detected IglA-GFP aggregates in cells (**Figures 4A,B**, **Supplementary Movies 1**, **2**) suggesting spontaneous deletions or variable expression levels. As previously characterized (Brodmann et al., 2017), T6SS dynamics in *F. novicida* consists of assembly, contraction and disassembly of a long cytosolic sheath at the bacterial poles and thus non-dynamic GFP aggregates likely represent non-functional T6SS (**Supplementary Movies 1**, **2**). We also tested ATc inducible plasmid pEDL17 (LoVullo et al., 2012) for complementation, however, we failed to obtain any *F. novicida* colonies containing the plasmid.

To further test pFNMB1 and pFNMB2 plasmids, we attempted to restore T6SS function in a Δ*iglC* mutant. The IglC protein is likely forming the T6SS inner tube, which was shown to be required in a large copy number in canonical T6SS, e.g., up to ∼1,000 molecules for a single *Vibrio cholerae* T6SS sheath-tube complex (Wang et al.,

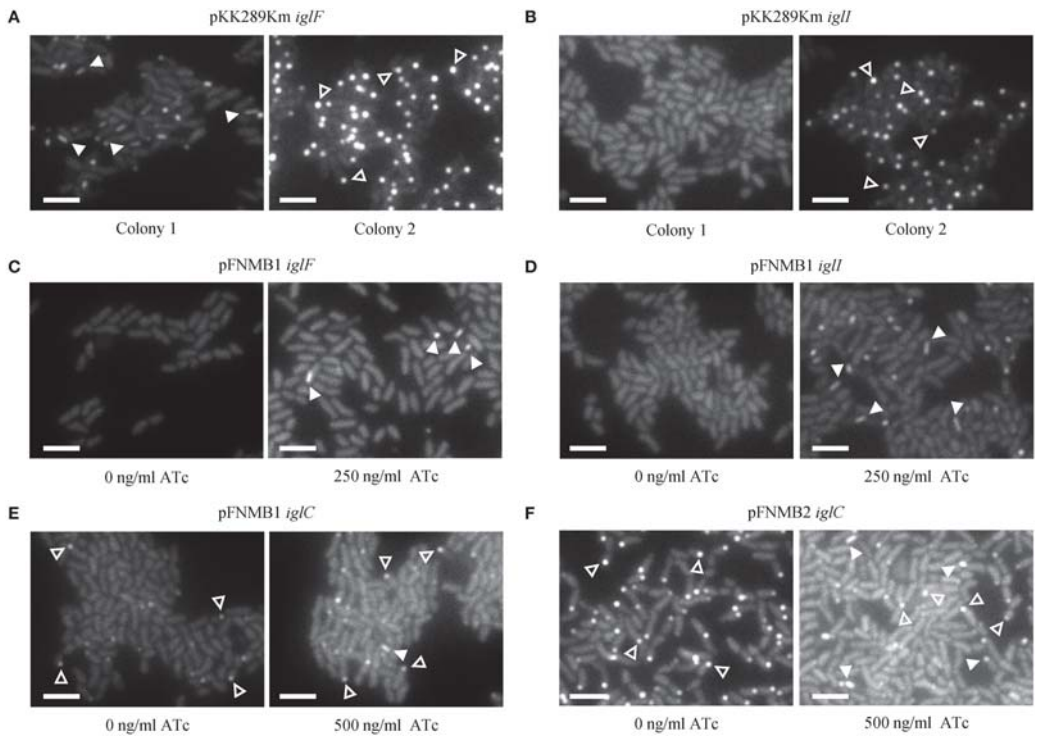

FIGURE 4 | Complementation of in-frame deletion mutants on agar pads. The first frame of the GFP channel of one of the examples in the **Supplementary Movie 2** is shown. T6SS assemblies were distinguished from GFP aggregates by analyzing dynamics in the movies. A maximum of 4 T6SS assemblies (arrow heads) and/or GFP aggregates (empty arrow heads) are highlighted. 13 × 9.75 μm fields of view. Scale bars represent 2 μm. **(A)** T6SS sheath assemblies (arrow heads) in *F. novicida* U112 *iglA-sfgfp* Δ*iglF* pKK289Km *iglF* colony 1 and GFP aggregates (empty arrow heads) in colony 2 **(B)** Failed T6SS sheath assembly in *F. novicida* U112 *iglA-sfgfp* Δ*iglI* pKK289Km *iglI* colony 1 and GFP aggregates (empty arrow heads) in colony 2. **(C)** T6SS sheath assemblies (arrow heads) in *F. novicida* U112 *iglA-sfgfp* Δ*iglF* pFNMB1 *iglF*, IglF expression induced with 250 ng/ml of ATc. **(D)** T6SS sheath assemblies (arrow heads) in *F. novicida* U112 *iglA-sfgfp* Δ*iglI* pFNMB1 *iglI*, IglI expression induced with 250 ng/ml of ATc. **(E)** One T6SS sheath assembly (arrow head) and GFP aggregates (empty arrow heads) in *F. novicida* U112 *iglA-sfgfp* Δ*iglC* pFNMB1 *iglC*, IglC expression induced with 500 ng/ml of ATc. **(F)** T6SS sheath assemblies (arrow heads) and GFP aggregates (empty arrow heads) in *F. novicida* U112 *iglA-sfgfp* Δ*iglC* pFNMB2 *iglC*, IglC expression induced with 500 ng/ml of ATc.

2017). As shown on **Figure 4E** and **Supplementary Movies 1**, **2**, T6SS sheath dynamics was only partially restored when inducing IglC expression from pFNMB1 with 500 ng/ml of ATc. However, T6SS sheath dynamics was restored to the levels similar to the parental strain when using pFNMB2 for IglC expression (**Figure 4F**, **Supplementary Movies 1**, **2**). Overall, this suggests that pFNMB plasmids are superior to the previously used plasmids for complementation in *F. novicida* and that pFNMB2 plasmid can be used to achieve high levels of protein expression.

Intracellular *F. novicida* require a functional T6SS to escape from the phagosome in order to reach the replicative niche in the cytosol (Chong and Celli, 2010). Cytosolic *F. novicida* bacteria activate the absent in melanoma 2 (AIM2) inflammasome among other defense mechanisms, which leads to pyroptotic cell death and pro-inflammatory cytokine release (Fernandes-Alnemri et al., 2010; Jones et al., 2010). To test whether pFNMB1 can be used for complementation in bone marrow derived macrophages (BMDMs), we analyzed in-frame deletion mutant Δ*iglI* and the respective complemented strain for induction of pyroptosis in infected cells as a measure for phagosomal escape and thus T6SS function. We pre-induced expression of IglI from pFNMB1 with 0 and 500 ng/ml ATc overnight and then infected BMDMs, which were supplemented with 0 and 1,000 ng/ml ATc. After 10 h of infection, we observed significantly higher cell death for the complemented strain than for the in-frame deletion mutant without induced gene expression or for the in-frame deletion mutant without the plasmid (**Figure 5**). This result indicates that pFNMB1 can be used to restore T6SS activity in *F. novicida* mutant in BMDMs.

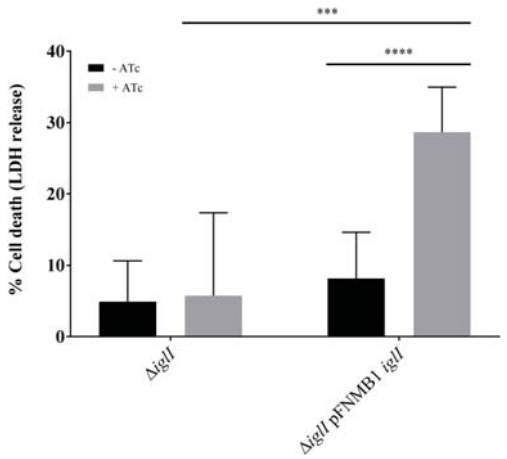

FIGURE 5 | Complementation of Δ*igll* mutant in BMDMs. Release of LDH from primed BMDMs supplemented with 0 and 1,000 ng/ml ATc 10 h after infection with *F. novicida* U112 *iglA-sfgfp* Δ*igll* and *F. novicida* U112 *iglA-sfgfp* Δ*igll* pFNMB1 *igll*. Bacterial cultures were supplemented with 0 and 500 ng/ml ATc overnight. Black columns represent conditions without induction by ATc and gray columns represent conditions with ATc. Means and standard deviations of nine measurements originating from three biological replicates are shown. The two-tailed unpaired *t*-test with Welch's correction was used to test significant differences between two groups. ***$P < 0.001$ and ****$P < 0.0001$.

DISCUSSION

We generated stable mobilizable expression plasmids pFNMB1 and pFNMB2 for *F. novicida*. There are two major advantages using these plasmids. First, they can be easily mobilized from *E. coli* to *F. novicida*; second, they allow for inducible and homogeneous expression of inserted genes *in-vitro* and inside eukaryotic cells. We modified pKK289Km by insertion of the RP4 mobilization site as we experienced great difficulties transforming *F. novicida* by electroporation similarly to what was reported previously (Maier et al., 2004; LoVullo et al., 2006). The low electroporation efficiency in *F. novicida* is probably caused by the capsule and restriction-modification systems (Maier et al., 2004; LoVullo et al., 2006; Frank and Zahrt, 2007; Gallagher et al., 2008). Gallagher et al. (2008) suggested to first transform plasmid DNA into a *F. novicida* strain with all restriction-modification systems deleted and then use this isolated plasmid DNA to transform wild-type *F. novicida*. Importantly, the high efficiency of mobilization of the pFNMB plasmids can be reached without this step and therefore may allow for generation of large libraries of mutants and thus facilitate future screens and selections.

To express genes in a controlled manner, pFNMB1 and pFNMB2 contain a tetracycline inducible promoter system, which was used for *F. tularensis* (LoVullo et al., 2012). We could show that expression levels were dependent on ATc concentration in *F. novicida* (**Figure 3D**). In contrast to *F. tularensis* (LoVullo et al., 2012), we observed no growth defects of *F. novicida* in the presence of 1,000 ng/ml ATc. However, we noticed that the expression levels achieved from pKK289Km were higher than those from our constructs. One possible explanation for the lower induction levels of pFNMB1 compared to pKK289Km are the different RBS. However, pFNMB2 has a similar RBS as pKK289Km (except for the MluI restriction site); therefore, it is also possible that pFNMB2 is still partially repressed even at 1,000 ng/ml of ATc. This may suggest that cytosolic concentration of ATc reaches lower level in *F. novicida* than in *F. tularensis*. Indeed, differences in resistance levels toward tetracycline antibiotics and number of transporters were reported (Kingry and Petersen, 2014; Sutera et al., 2014). Additionally, in contrast to pKK289Km, the expression from pFNMB1 and pFNMB2 is homogenous throughout the bacterial population (**Figures 3A–C**). The reason for the heterogeneous gene expression from pKK289Km in *F. novicida* is unknown; however, spontaneous deletions or differential activation of the *gro*ESL promoter could be responsible.

Other suitable inducible promoter systems are difficult to use in *Francisella*. The *araBAD* promoter requires the uptake of L-arabinose for induction (Guzman et al., 1995); similarly the *lac* promoter requires lactose or isopropyl-β-D-thiogalactopyranosid (Polisky et al., 1976). Since *Francisella* lacks the L-arabinose and lactose degradation pathway (NCBI, RefSeq NC_008601.1, Larsson et al., 2005), it is questionable if these inducers are taken up. In addition, *Francisella* has a unique RNA polymerase composition with two different α subunits, which may interfere with promoter recognition of these commonly used inducible promoter systems subunits (Charity et al., 2007). A glucose repressible promoter system was described for *F. tularensis* (Horzempa et al., 2008), however, since glucose is a common carbon source, the use of such repressor could be problematic. In addition, a temperature dependent promoter was constructed for *F. tularensis* (Maier et al., 2004). However, since *Francisella* is an intracellular

pathogen (Chong and Celli, 2010), many cell culture infections or *in vivo* experiments are performed at defined temperature and temperature shifting is impossible. Overall, the tetracycline inducible promoter system is likely the best option for *F. novicida* despite the apparent suboptimal level of derepression by ATc. Importantly, the possibility of inducing gene expression in cell culture or *in vivo* is a crucial advantage for testing the role of expressed genes during the pathogenesis of *F. novicida*.

In summary, we show that pFNMB1 and pFNMB2 are easy to mobilize into *F. novicida* and are stably maintained in the population. The tetracycline inducible promoter system is functional in *F. novicida* and can be used to tune gene expression levels. pFNMB1 and pFNMB2 exhibit homogeneous expression patterns in a population and can be used to complement chromosomal in-frame deletions. Overall, pFNMB1 and pFNMB2 may serve as useful tools for future studies of *F. novicida*.

AUTHOR CONTRIBUTIONS

MBr and MBa designed experiments, analyzed, and interpreted the results. MBr generated strains and acquired all data except for the BMDM infection experiments. PB and RH designed, analyzed, and interpreted the BMDM infection experiments. RH acquired the data for the BMDM infection experiments. MBr and MBa wrote the manuscript. All authors read and approved the manuscript.

ACKNOWLEDGMENTS

We thank M. A. Horwitz (UCLA) for providing the strain *F. novicida* U112 *iglA-sfGFP*, D. M. Monack (Stanford University) for the conjugation plasmid pDMK3, T. H. Kawula (University of North Carolina at Chapel Hill) for the inducible and repressible plasmids pEDL17 and pEDL47, A. Sjöstedt (Umeå University) for the expression plasmid pKK289Km *gfp* and A. Harms and C. Dehio (Biozentrum, University of Basel) for the *E. coli* conjugation strain. The work was supported by Swiss National Science Foundation (SNSF) grants 31003A_159525 and PP00P3_165893/1 and the University of Basel. MBr was supported by the Biozentrum Basel International Ph.D. Program Fellowships for Excellence.

SUPPLEMENTARY MATERIAL

The Supplementary Material for this article can be found online at: https://www.frontiersin.org/articles/10.3389/fcimb.2018.00284/full#supplementary-material

REFERENCES

Abd, H., Johansson, T., Golovliov, I., Sandström, G., and Forsman, M. (2003). Survival and growth of *Francisella tularensis* in *Acanthamoeba castellanii*. *Appl. Environ. Microbiol.* 69, 600–606. doi: 10.1128/AEM.69.1.600-606.2003

Anthony, L. S., Gu, M. Z., Cowley, S. C., Leung, W. W., and Nano, F. E. (1991). Transformation and allelic replacement in *Francisella* spp. *J. Gen. Microbiol.* 137, 2697–2703. doi: 10.1099/00221287-137-12-2697

Ark, N. M., and Mann, B. J. (2011). Impact of *Francisella tularensis* pilin homologs on pilus formation and virulence. *Microb. Pathog.* 51, 110–120. doi: 10.1016/j.micpath.2011.05.001

Basler, M., Ho, B. T., and Mekalanos, J. J. (2013). Tit-for-tat: type VI secretion system counterattack during bacterial cell-cell interactions. *Cell* 152, 884–894. doi: 10.1016/j.cell.2013.01.042

Bertram, R., and Hillen, W. (2008). The application of Tet repressor in prokaryotic gene regulation and expression. *Microb. Biotechnol.* 1, 2–16. doi: 10.1111/j.1751-7915.2007.00001.x

Bönquist, L., Lindgren, H., Golovliov, I., Guina, T., and Sjöstedt, A. (2008). MglA and Igl proteins contribute to the modulation of *Francisella tularensis* live vaccine strain-containing phagosomes in murine macrophages. *Infect. Immun.* 76, 3502–3510. doi: 10.1128/IAI.00226-08

Brodmann, M., Dreier, R. F., Broz, P., and Basler, M. (2017). *Francisella* requires dynamic type VI secretion system and ClpB to deliver effectors for phagosomal escape. *Nat. Commun.* 8:15853. doi: 10.1038/ncomms15853

Bröms, J. E., Sjöstedt, A., and Lavander, M. (2010). The role of the *Francisella tularensis* pathogenicity island in type VI secretion, intracellular survival, and modulation of host cell signaling. *Front. Microbiol.* 1:136. doi: 10.3389/fmicb.2010.00136

Charity, J. C., Costante-Hamm, M. M., Balon, E. L., Boyd, D. H., Rubin, E. J., and Dove, S. L. (2007). Twin RNA polymerase-associated proteins control virulence gene expression in *Francisella tularensis*. *PLoS Pathog.* 3:e84. doi: 10.1371/journal.ppat.0030084

Chong, A., and Celli, J. (2010). The *francisella* intracellular life cycle: toward molecular mechanisms of intracellular survival and proliferation. *Front. Microbiol.* 1:138. doi: 10.3389/fmicb.2010.00138

Clemens, D. L., Ge, P., Lee, B. Y., Horwitz, M. A., and Zhou, Z. H. (2015). Atomic structure of T6SS reveals interlaced array essential to function. *Cell* 160, 940–951. doi: 10.1016/j.cell.2015.02.005

de Bruin, O. M., Duplantis, B. N., Ludu, J. S., Hare, R. F., Nix, E. B., Schmerk, C. L et al. (2011). The biochemical properties of the *Francisella* pathogenicity island (FPI)-encoded proteins IglA, IglB, IglC, PdpB and DotU suggest roles in type VI secretion. *Microbiology* 157, 3483–3491. doi: 10.1099/mic.0.052308-0

de Bruin, O. M., Ludu, J. S., and Nano, F. E. (2007). The *Francisella* pathogenicity island protein IglA localizes to the bacterial cytoplasm and is needed for intracellular growth. *BMC Microbiol.* 7:1. doi: 10.1186/1471-2180-7-1

Eshraghi, A., Kim, J., Walls, A. C., Ledvina, H. E., Miller, C. N., Ramsey, K. M., et al. (2016). Secreted effectors encoded within and outside of the *Francisella* pathogenicity island promote intramacrophage growth. *Cell Host Microbe* 20, 573–583. doi: 10.1016/j.chom.2016.10.008

Fernandes-Alnemri, T., Yu, J. W., Juliana, C., Solorzano, L., Kang, S., Wu, J., et al. (2010). The AIM2 inflammasome is critical for innate immunity to *Francisella tularensis*. *Nat. Immunol.* 11, 385–393. doi: 10.1038/ni.1859

Frank, D. W., and Zahrt, T. C. (2007). Genetics and genetic manipulation in *Francisella tularensis*. *Ann. N.Y. Acad. Sci.* 1105, 67–97. doi: 10.1196/annals.1409.008

Gallagher, L. A., McKevitt, M., Ramage, E. R., and Manoil, C. (2008). Genetic dissection of the *Francisella novicida* restriction barrier. *J. Bacteriol.* 190, 7830–7837. doi: 10.1128/JB.01188-08

Gil, H., Platz, G. J., Forestal, C. A., Monfett, M., Bakshi, C. S., Sellati, T. J., et al. (2006). Deletion of TolC orthologs in *Francisella tularensis* identifies roles in multidrug resistance and virulence. *Proc. Natl. Acad. Sci. U.S.A.* 103, 12897–12902. doi: 10.1073/pnas.0602582103

Golovliov, I., Sjöstedt, A., Mokrievich, A., and Pavlov, V. (2003). A method for allelic replacement in *Francisella tularensis*. *FEMS Microbiol. Lett.* 222, 273–280. doi: 10.1016/S0378-1097(03)00313-6

Gossen, M., and Bujard, H. (1992). Tight control of gene expression in mammalian cells by tetracycline-responsive promoters. *Proc. Natl. Acad. Sci. U.S.A.* 89, 5547–5551. doi: 10.1073/pnas.89.12.5547

Guzman, L. M., Belin, D., Carson, M. J., and Beckwith, J. (1995). Tight regulation, modulation, and high-level expression by vectors containing the arabinose PBAD promoter. *J. Bacteriol.* 177, 4121–4130. doi: 10.1128/jb.177.14.4121-4130.1995

Haase, J., Lurz, R., Grahn, A. M., Bamford, D. H., and Lanka, E. (1995). Bacterial conjugation mediated by plasmid RP4: RSF1010 mobilization, donor-specific phage propagation, and pilus production require the same Tra2

core components of a proposed DNA transport complex. *J. Bacteriol.* 177, 4779–4791. doi: 10.1128/jb.177.16.4779-4791.1995

Harms, A., Segers, F. H., Quebatte, M., Mistl, C., Manfredi, P., Körner, J., et al. (2017). Evolutionary dynamics of pathoadaptation revealed by three independent acquisitions of the VirB/D4 type IV secretion system in *Bartonella*. *Genome Biol. Evol.* 9, 761–776. doi: 10.1093/gbe/evx042

Horzempa, J., Tarwacki, D. M., Carlson, P. E., Robinson, C. M., and Nau, G. J. (2008). Characterization and application of a glucose-repressible promoter in *Francisella tularensis*. *Appl. Environ. Microbiol.* 74, 2161–2170. doi: 10.1128/AEM.02360-07

Jones, J. W., Kayagaki, N., Broz, P., Henry, T., Newton, K., O'Rourke, K., et al. (2010). Absent in melanoma 2 is required for innate immune recognition of *Francisella tularensis*. *Proc. Natl. Acad. Sci. U.S.A.* 107, 9771–9776. doi: 10.1073/pnas.1003738107

Kingry, L. C., and Petersen, J. M. (2014). Comparative review of *Francisella tularensis* and *Francisella novicida*. *Front. Cell. Infect. Microbiol.* 4:35. doi: 10.3389/fcimb.2014.00035

Kudryashev, M., Wang, R. Y. R., Brackmann, M., Scherer, S., Maier, T., Baker, D., et al. (2015). Structure of the type VI secretion system contractile sheath. *Cell* 160, 952–962. doi: 10.1016/j.cell.2015.01.037

Lai, X. H., Golovliov, I., and Sjöstedt, A. (2004). Expression of IglC is necessary for intracellular growth and induction of apoptosis in murine macrophages by *Francisella tularensis*. *Microb. Pathog.* 37, 225–230. doi: 10.1016/j.micpath.2004.07.002

Larsson, P., Oyston, P. C. F., Chain, P., Chu, M. C., Duffield, M., Fuxelius, H. H., et al. (2005). The complete genome sequence of *Francisella tularensis,* the causative agent of tularemia. *Nat. Genet.* 37, 153–159. doi: 10.1038/ng1499

Lindemann, S. R., Peng, K., Long, M. E., Hunt, J. R., Apicella, M. A., Monack, D. M., et al. (2011). *Francisella tularensis* Schu S4 O-antigen and capsule biosynthesis gene mutants induce early cell death in human macrophages. *Infect. Immun.* 79, 581–594. doi: 10.1128/IAI.00863-10

Lindgren, H., Shen, H., Zingmark, C., Golovliov, I., Conlan, W., and Sjöstedt, A. (2007). Resistance of *Francisella tularensis* strains against reactive nitrogen and oxygen species with special reference to the role of KatG. *Infect. Immun.* 75, 1303–1309. doi: 10.1128/IAI.01717-06

Lindgren, M., Bröms, J. E., Meyer, L., Golovliov, I., and Sjöstedt, A. (2013). The *Francisella tularensis* LVS Δ*pdpC* mutant exhibits a unique phenotype during intracellular infection. *BMC Microbiol.* 13:20. doi: 10.1186/1471-2180-13-20

LoVullo, E. D., Miller, C. N., Pavelka, M. S., and Kawula, T. H. (2012). TetR-based gene regulation systems for *Francisella tularensis*. *Appl. Environ. Microbiol.* 78, 6883–6889. doi: 10.1128/AEM.01679-12

LoVullo, E. D., Sherrill, L. A., and Pavelka, M. S. (2009). Improved shuttle vectors for *Francisella tularensis* genetics. *FEMS Microbiol. Lett.* 291, 95–102. doi: 10.1111/j.1574-6968.2008.01440.x

LoVullo, E. D., Sherrill, L. A., Perez, L. L., and Pavelka, M. S. (2006). Genetic tools for highly pathogenic *Francisella tularensis* subsp. tularensis. *Microbiology* 152, 3425–3435. doi: 10.1099/mic.0.29121-0

Maier, T. M., Havig, A., Casey, M., Nano, F. E., Frank, D. W., and Zahrt, T. C. (2004). Construction and characterization of a highly efficient *Francisella* shuttle plasmid. *Appl. Environ. Microbiol.* 70, 7511–7519. doi: 10.1128/AEM.70.12.7511-7519.2004

Maier, T. M., Pechous, R., Casey, M., Zahrt, T. C., and Frank, D. W. (2006). *In vivo* Himar1-based transposon mutagenesis of *Francisella tularensis*. *Appl. Environ. Microbiol.* 72, 1878–1885. doi: 10.1128/AEM.72.3.1878-1885.2006

Nano, F. E., and Schmerk, C. (2007). The *Francisella* pathogenicity island. *Ann. N.Y. Acad. Sci.* 1105, 122–137. doi: 10.1196/annals.1409.000

Norqvist, A., Kuoppa, K., and Sandström, G. (1996). Construction of a shuttle vector for use in *Francisella tularensis*. *FEMS Immunol. Med. Microbiol.* 13, 257–260. doi: 10.1111/j.1574-695X.1996.tb00248.x

Oyston, P. C. F., Sjostedt, A., and Titball, R. W. (2004). Tularaemia: bioterrorism defence renews interest in *Francisella tularensis*. *Nat. Rev. Microbiol.* 2, 967–978. doi: 10.1038/nrmicro1045

Pavlov, V. M., Mokrievich, A. N., and Volkovoy, K. (1996). Cryptic plasmid pFNL10 from *Francisella novicida*-like F6168: the base of plasmid vectors for *Francisella tularensis*. *FEMS Immunol. Med. Microbiol.* 13, 253–256. doi: 10.1111/j.1574-695X.1996.tb00247.x

Polisky, B., Bishop, R. J., and Gelfand, D. H. (1976). A plasmid cloning vehicle allowing regulated expression of eukaryotic DNA in bacteria. *Proc. Natl. Acad. Sci. U.S.A.* 73, 3900–3904. doi: 10.1073/pnas.73.11.3900

Pomerantsev, A. P., Golovliov, I. R., Ohara, Y., Mokrievich, A. N., Obuchi, M., Norqvist, A., et al. (2001a). Genetic organization of the *Francisella* plasmid pFNL10. *Plasmid* 46, 210–222. doi: 10.1006/plas.2001.1548

Pomerantsev, A. P., Obuchi, M., and Ohara, Y. (2001b). Nucleotide sequence, structural organization, and functional characterization of the small recombinant plasmid pOM1 that is specific for *Francisella tularensis*. *Plasmid* 46, 86–94. doi: 10.1006/plas.2001.1538

Rasko, D. A., Esteban, C. D., and Sperandio, V. (2007). Development of novel plasmid vectors and a promoter trap system in *Francisella tularensis* compatible with the pFLN10 based plasmids. *Plasmid* 58, 159–166. doi: 10.1016/j.plasmid.2007.03.002

Santic, M., Molmeret, M., Barker, J. R., Klose, K. E., Dekanic, A., Doric, M., et al. (2007). A *Francisella tularensis* pathogenicity island protein essential for bacterial proliferation within the host cell cytosol. *Cell. Microbiol.* 9, 2391–2403. doi: 10.1111/j.1462-5822.2007.00968.x

Santic, M., Ozanic, M., Semic, V., Pavokovic, G., Mrvcic, V., and Kwaik, Y. A. (2011). Intra-vacuolar proliferation of *F. Novicida* within *H. Vermiformis*. *Front. Microbiol.* 2:78. doi: 10.3389/fmicb.2011.00078

Schindelin, J., Arganda-Carreras, I., Frise, E., Kaynig, V., Longair, M., Pietzsch, T., et al. (2012). Fiji: an open-source platform for biological-image analysis. *Nat. Methods* 9, 676–682. doi: 10.1038/nmeth.2019

Schmidt, M., Klimentova, J., Rehulka, P., Straskova, A., Spidlova, P., Szotakova, B., et al. (2013). *Francisella tularensis* subsp. holarctica DsbA homologue: a thioredoxin-like protein with chaperone function. *Microbiol. Read. Engl.* 159, 2364–2374. doi: 10.1099/mic.0.070516-0

Scholz, O., Henssler, E. M., Bail, J., Schubert, P., Bogdanska-Urbaniak, J., Sopp, S., et al. (2004). Activity reversal of Tet repressor caused by single amino acid exchanges. *Mol. Microbiol.* 53, 777–789. doi: 10.1111/j.1365-2958.2004.04159.x

Sutera, V., Levert, M., Burmeister, W. P., Schneider, D., and Maurin, M. (2014). Evolution toward high-level fluoroquinolone resistance in *Francisella* species. *J. Antimicrob. Chemother.* 69, 101–110. doi: 10.1093/jac/dkt321

Tempel, R., Lai, X. H., Crosa, L., Kozlowicz, B., and Heffron, F. (2006). Attenuated *Francisella novicida* transposon mutants protect mice against wild-type challenge. *Infect. Immun.* 74, 5095–5105. doi: 10.1128/IAI.00598-06

Vettiger, A., and Basler, M. (2016). Type VI secretion system substrates are transferred and reused among sister cells. *Cell* 167, 99–110.e12. doi: 10.1016/j.cell.2016.08.023

Wang, J., Brackmann, M., Castaño-Díez, D., Kudryashev, M., Goldie, K. N., Maier, T., et al. (2017). Cryo-EM structure of the extended type VI secretion system sheath-tube complex. *Nat. Microbiol.* 2, 1507–1512. doi: 10.1038/s41564-017-0020-7

Weiss, D. S., Brotcke, A., Henry, T., Margolis, J. J., Chan, K., and Monack, D. M. (2007). *In vivo* negative selection screen identifies genes required for *Francisella* virulence. *Proc. Natl. Acad. Sci. U.S.A.* 104, 6037–6042. doi: 10.1073/pnas.0609675104

Zogaj, X., and Klose, K. E. (2010). Genetic manipulation of *francisella tularensis*. *Front. Microbiol.* 1:142. doi: 10.3389/fmicb.2010.00142

Conflict of Interest Statement: The authors declare that the research was conducted in the absence of any commercial or financial relationships that could be construed as a potential conflict of interest.

Supplementary Material

Mobilizable plasmid for tunable gene expression in *Francisella novicida*.

Maj Brodmann[1] and Marek Basler[1*]

[1] Biozentrum, University of Basel, Basel, Switzerland

[*] **Correspondence:**

Dr. Marek Basler

marek.basler@unibas.ch

1. Supplementary tables

Table S1: Strains used in this study, related to Material and Methods

Organism	Genotype	Plasmid	Relevant features	Source
Francisella novicida U112	*iglA-sfGFP*		Parental strain, C-terminal chromosomal fusion of *sfGFP* to *iglA*	(Clemens et al., 2015)
	iglA-sfGFP ΔiglF		Deletion of *iglF*	(Brodmann et al., 2017)
	iglA-sfGFP ΔiglI		Deletion of *iglI*	(Brodmann et al., 2017)
	iglA-sfGFP ΔiglC		Deletion of *iglC*	This study
		pKK289Km *gfp*	Constitutive expression of GFP under *groESL* promoter	(Bönquist et al., 2008)
	iglA-sfGFP ΔiglF	pKK289Km *iglF*	Constitutive complementation *iglF*	This study
	iglA-sfGFP ΔiglI	pKK289Km *iglI*	Constitutive complementation *iglI*	This study
		pFNMB1 *msfgfp*	RP4 mobilization site, ATC inducible expression of *msfgfp*, *iglC* RBS	This study
		pFNMB2 *msfgfp*	RP4 mobilization site, ATC inducible expression of *msfgfp*, pKK289Km RBS	This study
	iglA-sfGFP ΔiglF	pFNMB1 *iglF*	Inducible expression of *iglF*	This study
	iglA-sfGFP ΔiglI	pFNMB1 *iglI*	Inducible expression of *iglI*	This study
	iglA-sfGFP ΔiglC	pFNMB1 *iglC*	Inducible expression of *iglC*	This study
	iglA-sfGFP ΔiglC	pFNMB2 *iglC*	Inducible expression of *iglC*	This study
Escherichia coli DH5α *λpir*		pFNMB1 *msfgfp*	RP4 mobilization site, ATC inducible expression of *msfgfp*, *iglC* RBS	This study
		pFNMB2 *msfgfp*	RP4 mobilization site, ATC inducible expression of *msfgfp*, pKK289Km RBS	This study

Table S2: Plasmids and primers used to generate plasmids pFNMB1 and pFNMB2, related to Material and Methods

Plasmid Name	Feature	Primers used		Restriction sites	Source
pKK289Km *gfp*	Backbone				(Bönquist et al., 2008)
pDMK3	RP4 mobilization site	oriT-long_EcoR1.FOR	TCAGTAGAATTCTTAGATCCAGCCGACCAG	EcoR1	(Lindgren et al., 2007)
		oriT-long_Sbf1.REV	TCAGTACCTGCAGGTCAATCCTTTTTGTCCGGTG	Sbf1	
pDMK3	MCS	Tet_MCS_2.FOR	CAGTGATAGAGAGTCGACCCTCGAGTACGCGTCTCTAG		(Lindgren et al., 2007)
		Tet_MCS_Term_2.REV	CAGACCGCCCCGGGAGAGCTCAGGT		
pEDL17	ATC inducible promoter cassette	Tet_MCS_Spe1.For	TCAGTAACTAGTTTAAGACCCACTTTCACATT	Spe1	(LoVullo et al., 2012)
		Tet_MCS_1.REV	CTCGAGGGTCGACTCTCTATCACTGATAGGGACAAGTCTAGATATTGAG		
pBAD24	*rnB* T1 terminator	Tet_MCS_Term_3.FOR	CTCTCCCGGGGCGGTCTGATAAAACAGAATTTGCCT	EcoR1	(Guzman et al., 1995)
		Tet_MCS_Term_3_EcoR1.REV	TCAGTAGAATTCAAAAGGCCATCCGTCAGGAT		

15 **Table S3: Plasmids and primers used to generate mutants, related to Material and Methods**

Plasmid Name	Peptide scar left on the chromosome after allelic exchange	Primers used	
pDMK3 Δ*iglC*	MSEMITRQQVVAKIG YIAAA*	dFTN_1322_1_Xho1.FOR	TCAGTACTCGAGGTTGAATTAAGCTGTAAATATCAT
		dFTN_1322_1.REV	ACAACAGGTAGTTGCTAAAATAGGATATATTG
		dFTN_1322_2.FOR	TTTTAGCAACTACCTGTTGTCTTGTTATCAT
		dFTN_1322_2_Not1.REV	TCAGTAGCGGCCGCTCCAGTTCAGTATAAACTTATG
		dFTN_1323_Det.FOR	ACCTGTCTGCAAACTTTCAACA
		dFTN_1322_Det.REV	GAAACCTTGATGTTGCTGCA
pKK289Km *iglF*		FTN_1313_Nde1.FOR	TCAGTACATATGAATAATGATATTGATAAATGGTTTG AA
		FTN_1313_Sac1_REV	TCAGTAGAGCTCTTAAATTTTCCAATAAGCTTCTTG
		pKK289Km_Seq1.FOR	CCCCAAACATCGCAAAAGGT
		pKK289Km_Seq1.REV	CACGCCACATCTTGCGAATA
pKK289Km *iglI*		FTN_1317_Nde1.FOR	TCAGTACATATGAGTCAGATAATATCTACACTAAATA AT
		FTN_1317_EcoR1.REV	TCAGTAGAATTCTATATGTCAAAAAGATCTTCAAAAT AGT
		pKK289Km_Seq1.FOR	CCCCAAACATCGCAAAAGGT
		pKK289Km_Seq1.REV	CACGCCACATCTTGCGAATA
pFNMB1 *msfgfp*		iglC_RBS_Mlu1_GFP.FOR	TCAGTACTCGAGAGGAGAACGCGTATGGGATCTAAA GGTGAAGAACT
		msfGFP_Xma_REV	TCAGTACCCGGGTTATTTGTAGAGCTCATCCATG
		pFNMB_seq_FOR	TCATAGAAGCTTGCATGCCTG
		pFNMB_seq_REV	GAGACCCCACACTACCATCG
pFNMB2 *msfgfp*		Tet_MCS_Spe1.For	TCAGTAACTAGTTTAAGACCCACTTTCACATT
		Tet_pKK289Km_RBS_Mlu1_gfp_1.REV	ACGCGTATCTCCTTCTTAAATCTGCAGTCTCTATCACT GATAGGGACAAG
		Tet_pKK289Km_RBS_Mlu1_gfp_2.FOR	ATTTAAGAAGGAGATACGCGTATGGGATCTAAAGGT GAAGAACTGTTCAC
		msfGFP_Xma_REV	TCAGTACCCGGGTTATTTGTAGAGCTCATCCATG
		pFNMB_seq_FOR	TCATAGAAGCTTGCATGCCTG

	pFNMB_seq_REV	GAGACCCCACACTACCATCG
pFNMB1 *iglF*	FTN_1313_Mlu1.FOR	TCAGTAACGCGTATGAATAATGATATTGATAAATGGTTTGAA
	FTN_1313_Sac1_REV	TCAGTAGAGCTCTTAAATTTTCCAATAAGCTTCTTG
	pFNMB_seq_FOR	TCATAGAAGCTTGCATGCCTG
	pFNMB_seq_REV	GAGACCCCACACTACCATCG
pFNMB1 *iglI*	FTN_1317_Mlu1.FOR	TCAGTAACGCGTATATGAGTCAGATAATATCTACACTAAATAAT
	FTN_1317_Sac1.REV	TCAGTAGAGCTCTTATATGTCAAAAAGATCTTCAAAATAGT
	pFNMB_seq_FOR	TCATAGAAGCTTGCATGCCTG
	pFNMB_seq_REV	GAGACCCCACACTACCATCG
pFNMB1 *iglC*	FTN_1322_Mlu1.FOR	TCAGTAACGCGTATGAGTGAGATGATAACAAG
	FTN_1322_Sac1.REV	TCAGTAGAGCTCCTATGCAGCTGCAATATATC
	pFNMB_seq_FOR	TCATAGAAGCTTGCATGCCTG
	pFNMB_seq_REV	GAGACCCCACACTACCATCG
pFNMB2 *iglC*	FTN_1322_Mlu1.FOR	TCAGTAACGCGTATGAGTGAGATGATAACAAG
	FTN_1322_Sac1.REV	TCAGTAGAGCTCCTATGCAGCTGCAATATATC
	pFNMB_seq_FOR	TCATAGAAGCTTGCATGCCTG
	pFNMB_seq_REV	GAGACCCCACACTACCATCG

16

2. Supplementary movies

Supplementary movie 1: Close up of T6SS sheath dynamics in complemented mutants. IglA-sfGFP was monitored in *F. novicida* U112 *iglA-sfgfp* Δ*iglF* pKK289Km *iglF, F. novicida* U112 *iglA-sfgfp* Δ*iglF* pFNMB1 *iglF*, F. novicida U112 *iglA-sfgfp* Δ*iglI* pKK289Km *iglI*, *F. novicida* U112 *iglA-sfgfp* Δ*iglI* pFNMB1 *iglI, F. novicida* U112 *iglA-sfgfp* Δ*iglC* pFNMB1 *iglC* and *F. novicida* U112 *iglA-sfgfp* Δ*iglC* pFNMB2 *iglC*. Gene expression was induced with 250 ng/ml of ATc except for IglC, which was induced with 500 ng/ml of ATc. The bacteria were imaged for 5 min at a frame rate of 2 frames per minutes and for each strain two representative time-lapse image series are shown. The movie consist of the GFP channel and the scale bar represents 1 µm. Fields of view are 3.3 x 3.3 µm. Movies play at a frame rate of 5 frames per second.

Supplementary movie 2: Overview of T6SS sheath dynamics in complemented mutants. IglA-sfGFP was monitored in *F. novicida* U112 *iglA-sfgfp* Δ*iglF* pKK289Km *iglF, F. novicida* U112 *iglA-sfgfp* Δ*iglF* pFNMB1 *iglF*, F. novicida U112 *iglA-sfgfp* Δ*iglI* pKK289Km *iglI*, *F. novicida* U112 *iglA-sfgfp* Δ*iglI* pFNMB1 *iglI, F. novicida* U112 *iglA-sfgfp* Δ*iglC* pFNMB1 *iglC* and *F. novicida* U112 *iglA-sfgfp* Δ*iglC* pFNMB2 *iglC*. Gene expression was induced with 250 ng/ml of ATc except for IglC, which was induced with 500 ng/ml of ATc. The bacteria were imaged for 5 min at a frame rate of 2 frames per minutes and for each strain two representative time-lapse image series are shown. The movie consist of the GFP channel and the scale bar represents 5 µm. Fields of view are 39 x 26 µm. Movies play at a frame rate of 5 frames per second.

3. Supplementary references

Bönquist, L., Lindgren, H., Golovliov, I., Guina, T., and Sjöstedt, A. (2008). MglA and Igl proteins contribute to the modulation of *Francisella tularensis* live vaccine strain-containing phagosomes in murine macrophages. *Infect. Immun. 76*, 3502–3510.

Brodmann, M., Dreier, R.F., Broz, P., and Basler, M. (2017). *Francisella* requires dynamic type VI secretion system and ClpB to deliver effectors for phagosomal escape. *Nat. Commun. 8*, 15853

Clemens, D.L., Ge, P., Lee, B.-Y., Horwitz, M.A., and Zhou, Z.H. (2015). Atomic Structure of T6SS Reveals Interlaced Array Essential to Function. *Cell 160*, 940–951.

Guzman, L.M., Belin, D., Carson, M.J., and Beckwith, J. (1995). Tight regulation, modulation, and high-level expression by vectors containing the arabinose PBAD promoter. *J. Bacteriol. 177*, 4121–4130.

Lindgren, H., Shen, H., Zingmark, C., Golovliov, I., Conlan, W., and Sjöstedt, A. (2007). Resistance of *Francisella tularensis* strains against reactive nitrogen and oxygen species with special reference to the role of KatG. *Infect. Immun. 75*, 1303–1309.

LoVullo, E.D., Miller, C.N., Pavelka, M.S., and Kawula, T.H. (2012). TetR-based gene regulation systems for *Francisella tularensis*. *Appl. Environ. Microbiol. 78*, 6883–6889.

IV.DISCUSSION

IV.DISCUSSION

Subcellular organization in bacteria is increasingly appreciated and considered important for the function of a bacterial cell (Shapiro et al., 2009; Surovtsev and Jacobs-Wagner, 2018; Updegrove and Ramamurthi, 2017; Young, 2006). Especially, bacterial secretion systems are tightly regulated for efficient substrate delivery (Basler et al., 2013; Bröms et al., 2010; Ellermeier and Slauch, 2007; Joshi et al.; Lacerda et al., 2013; Mougous et al., 2007; Yahr and Wolfgang, 2006).

The T6SS is a contact-dependent contractile nanomachine to deliver effector proteins into target cells (Wang et al., 2019). This recently discovered secretion system is a major contributor in shaping bacterial communities as well as in host-pathogen interactions (Alteri et al., 2013; Basler et al., 2013; Bingle et al., 2008; Brodmann et al., 2017; Chen et al., 2019; Gibbs et al., 2008; Schwarz et al., 2014). Although the T6SS is encoded in more than 25 % of all sequence Gram-negative bacteria (Bingle et al., 2008), it has several drawbacks. First, the contact-dependency limits the range of the T6SS and requires the attacker to come within the targets reach. Thus, the chances increase of being it oneself. In addition, the T6SS mode of action yields in only a few effector translocation events per round of firing while thousands of T6SS components are required for building the whole apparatus. Thus, bacteria evolved different strategies in order to overcome these above-mentioned drawbacks. These strategies are reflected in the diverse T6SS activation patterns, dynamics and subcellular localizations observed by live-cell fluorescence microscopy. Nevertheless, the regulation mechanisms behind these differences in T6SS dynamics are poorly understood.

This PhD thesis aimed at getting more insights into how different spatial-temporal T6SS activity patterns are accomplished. Besides, we wanted to understand what the consequences of different T6SS subcellular localizations are.

4.1. The importance of repositioning the T6SS apparatus

Live-cell fluorescence microscopy revealed that T6SS assemblies take place at several subcellular localizations inside a cell and that positioning of the T6SS is dynamic in most bacteria (Basler and Mekalanos, 2012; Basler et al., 2013; Gerc et al., 2015; Ostrowski et al., 2018; Ringel et al., 2017). The importance of T6SS repositioning is best described for *P. aeruginosa* and *S. marcescens*; when their T6SS is locked in one position, killing of prey cell significantly decreases despite of high T6SS activity (Basler et al., 2013; Fritsch et al., 2013; Ostrowski et al., 2018). These reports suggest that dynamical repositioning of the T6SS likely increases the chances of translocating enough effectors into to the right target.

P. aeruginosa, *S. marcescens* and *A. tumefaciens* evolved a specialized post-translational regulation for T6SS repositioning called Threonine phosphorylation pathway (TPP) (Basler et al., 2013; Fritsch et al., 2013; Lin et al., 2014; Mougous et al., 2007; Ostrowski et al., 2018). The TPP contains a periplasmic sensor module, which integrates extracellular signals and activates the IM kinase PpkA. Activated PpkA phosphorylates a cytosolic target protein and subsequently T6SS assembly is initiated. Eventually, phosphatase PppA dephosphorylates the target protein and T6SS activity is shut down. The unique sensor module composed of TagQ/TagR/TagS/TagT in *P. aeruginosa* senses membrane damage resulting in fast T6SS dependent retaliations (Basler and Mekalanos, 2012; Basler et al., 2013; Casabona et al., 2013; Ho et al., 2013; Silverman et al., 2011; Wilton et al., 2016). However, it is not clear how attackers are localized and how signals are integrated by TagQ/TagR/TagS/TagT.

My first project (chapter 3.1.) aimed at understanding how membrane damage is sensed by TagQ/TagR/TagS/TagT and subsequently initiates T6SS assembly. In *E. coli* envelope stress is sensed by mislocalized lipoprotein RcsF (Cho et al., 2014). Thus, we mutated the N-terminal signal sequence of lipoprotein TagQ in order to change its subcellular localization from OM to IM. Interestingly, we observed a hyperactive T6SS mutant which had similarities to a *pppA* deletion mutant (Basler et al., 2013). In agreement, this TagQ mutant was not able to distinguish between $T6SS^-$ and $T6SS^+$ prey cells. Unfortunately, we could not confirm that translocation of TagQ from OM to IM constitutively activated T6SS as mutant TagQ was also found in

inclusion bodies. Consequently, we failed to confirm that changes in subcellular localization of TagQ are important for initiating T6SS assembly in *P. aeruginosa*. Moreover, this hypothesis had several weaknesses. Based on bioinformatics analysis, TagR likely binds and subsequently activates PpkA (Hsu et al., 2009). Since TagQ is about 60 times more abundant than other TPP components and shown to localize TagR to the OM (Casabona et al., 2013; Lin et al., 2019), TagQ could potentially act as sink for TagR in order to prevent T6SS activation. In agreement, TagQ localized to IM would bring TagR in closer proximity of PpkA and thus increases T6SS activation. However, deletion of TagQ does not lead to expected hyperactive T6SS by freed TagR but to abrogation of T6SS activity (Casabona et al., 2013). Thus, TagQ likely has an additional function, which remains unknown so far. One possibility is that TagQ is required for TagR stability. However, my TagR mutants with mutated N-terminal signal sequences were less abundant compared to wild-type TagR but were still able to induce T6SS activity and quick retaliation responses.

Furthermore, the role of ABC transporter TagS/TagT was neglected for our hypothesis that subcellular localization changes of TagQ and TagR results in T6SS activation. Yet, TagS and TagT are required for proper sensing and full T6SS activity (Basler et al., 2013; Casabona et al., 2013). Since it is not known what TagS/TagT transport (Casabona et al., 2013), it is difficult to form a hypothesis regarding their function. In addition, recent bioinformatics predictions reveal that TagQ may have a peptidoglycan-binding domain. Thus, it may be necessary to refine our hypothesis and include newly gained insights. In general, I firmly believe that for elucidating how the TPP in *P. aeruginosa* works, it is necessary to have structures of the different TPP components. Solved structures will allow making educated guesses about interaction sites or transported substrates and will facilitate making mutants in order to confirm newly formed hypotheses.

Other bacteria reposition their T6SS apparatus without the TPP. For example, *V. cholerae* and *A. baylyi* have a constantly active T6SS which apparently assembles at random localizations of a cell (Basler and Mekalanos, 2012; Ringel et al., 2017). However, the question still arises what triggers the T6SS assembly at a particular localization. Interestingly, many cell envelope-spanning complexes such as flagella, T3SS or T4SS depend on a specialized lytic transglycosylase for insertion into the peptidoglycan layer (Dik et al., 2017; Scheurwater et al., 2008; Typas et al., 2011).

Indeed, *A. baylyi* encodes the specialized *LD*-endopeptidase TagX which is required for insertion of the membrane complex into the peptidoglycan layer (Weber et al., 2016). *E. coli* Sci-1 T6SS membrane complex is also inserted into the peptidoglycan layer by the general lytic transglycose MltE (Santin and Cascales, 2017). Interestingly, the Sci-1 T6SS in EAEC is an exception as it is not repositioned but repeatedly assembled at apparently random positions within a cell (Durand et al., 2015). Nevertheless, it remains to be elucidated how TagX and MltE are regulated.

In contrast, *V. cholerae* does not encode any peptidoglycan-cleaving enzyme in its T6SS cluster. Thus, one possibility could be that local weakening of the peptidoglycan due to general peptidoglycan remodeling or due to the activity of peptidoglycan targeting antibiotics or effectors might be enough for T6SS membrane complex insertion. Interestingly, T6SS in *V. cholerae* does not need an intact peptidoglycan layer for functional effector translocation (Vettiger et al., 2017), suggesting that its membrane complex may be assembled randomly without any regulation.

4.2. Consequences of T6SS repositioning in *P. aeruginosa*

The interplay between TPP components in *P. aeruginosa* results in a unique activation pattern, where *P. aeruginosa* only assembles its T6SS if membrane damaged caused by T6SS or other stimuli is sensed (Basler et al., 2013). This defensive T6SS strategy favors pacifistic bystanders while other neighboring T6SS$^+$ bacteria are killed. However, this “tit-for-tat strategy” has also consequences for *P. aeruginosa* itself. Chapter 3.2. of this PhD thesis investigated when the defensive T6SS strategy of *P. aeruginosa* is successful. By modelling T6SS based bacterial competitions *in silico*, it became evident that certain constraints have to be met in order for *P. aeruginosa* to kill T6SS$^+$ attackers successfully.

First, *P. aeruginosa* needs to survive initial attacks in order to localize an attacker and second, needs to efficiently retaliate and inflict more damage than encountered. While it was already known that the TPP ensures precise localization of attackers and thus efficient effector translocation, our live-cell fluorescence microscopy data suggest that indeed, *P. aeruginosa* inflicts maximal damage by quick multiple rounds of firing at the same site. Although, it is not clear if the T6SS is quickly reassembled

or several T6SS are assembled at the same position, SIM data of Dr. Andrea Vettiger suggest that T6SS sheaths are reassembled at the same position. On the other hand, it is still an open question, how *P. aeruginosa* becomes resilient to initial T6SS attacks.

While the defensive T6SS strategy of *P. aeruginosa* is likely more cost-efficient in regard of T6SS components, TPP components also need to be expressed and maintained at their proper localization. Especially, TagQ is present in 50'000 copies on average per *ΔretS* cell (comparable to the number of Hcp subunits) and requires transport to the OM (Casabona et al., 2013; Lin et al., 2019). In order to keep the T6SS assembly cost low, *P. aeruginosa* must avoid accidental firings such as observed in a *ΔretS* strain. A drawback of sensing general membrane damage is that sister cells and non-kin attackers are not distinguishable. Thus, additional T6SS regulation by TagF as well as by the complex transcriptional and post-transcriptional network described in chapter 2.4.1. may be a consequence of keeping the random T6SS activity low (LeRoux et al., 2015; Lesic et al., 2009; Lin et al., 2018; Mougous et al., 2006; Silverman et al., 2011). However, since *S. marcescens*, *A. tumefaciens* and *A. baylyi* also encode TagF (Lin et al., 2014, 2018; Silverman et al., 2011), its exact contribution to different T6SS activation strategies remains elusive.

4.3. *Francisella* T6SS dynamics and its role in pathogenesis

Thorough investigation of canonical T6SS led to the detailed understanding of T6SS we have today (Wang et al., 2019). However, *Francisella*, the causative agent of tularemia, encodes a non-canonical T6SS on the FPI required for phagosomal escape (Bröms et al., 2010). Especially, the lack of ATPase for disassembly of contracted sheath subunits as well as many genes with unknown function made it initially unclear if *Francisella* T6SS has as similar mode of action as canonical ones (Bröms et al., 2010; Clemens et al., 2015).

In chapter 3.3. we characterized *Francisella* T6SS dynamics by live-cell fluorescence microscopy. Furthermore, we assessed the contribution of unknown genes to T6SS function and *Francisella* virulence. In summary, *Francisella* T6SS sheath dynamics are comparable to canonical ones (Basler and Mekalanos, 2012; Brodmann et al., 2017; Ringel et al., 2017). Besides, we found that general unfoldase ClpB

disassembles contracted sheath subunits instead of canonical ClpV. These findings suggest that despite of sequence variations in individual components and the replacement of specialized T6SS components by more general components, *Francisella* T6SS functions as a normal T6SS. In agreement, the solved structure of contracted sheath as well as structures from individual FPI components harbor folds comparable to canonical T6SS components (Aschtgen et al., 2012; Clemens et al., 2015; Kudryashev et al., 2015; Mougous et al., 2006; Robb et al., 2012; Salih et al., 2018; Sun et al., 2007). Nevertheless, important baseplate components such as TssG and TssF are missing. However, it is likely that some of the genes with unknown function but which are essential for T6SS function may serve as replacements as for example IglI for TssA (chapter 3.4.). In order to find the missing baseplate components, solved structures of all FPI components might be essential.

The importance of ClpB-mediated T6SS sheath recycling for *Francisella* virulence highlighted that individual effector translocations events are not enough for phagosomal escape as a *clpB* deletion mutant is still able to fire at least once or twice. One possibility is that the local concentration of effectors at the target site is too low in general. However, it is also possible that *Francisella* sequentially secretes different effectors in a temporal hierarchy as observed for the T3SS (Deng et al., 2005; Winnen et al., 2008). Thus, it could be that eventually abrogated T6SS dynamics lead to the absence of one specific effector. Moreover, it is also possible that secondary effects of *clpB* deletion decreases *Francisella* virulence as ClpB is also involved in unfolding aggregated proteins in response to various stresses (Meibom et al., 2008). In order to detangle these two functions, it will be necessary to block ClpB-mediated sheath recycling specifically without blocking its other function.

In general, the effector repertoire of *Francisella* T6SS is poorly characterized. We and others identified two effectors encoded on the FPI, which are required for phagosomal escape (Brodmann et al., 2017; Eshraghi et al., 2016; Ludu et al., 2008; Uda et al., 2014). In addition, two components secreted in a T6SS dependent manner, which are not encoded on the FPI, were identified (Eshraghi et al., 2016). So far, only the mode of action of OpiA, a phosphatidylinositol 3-kinase for delaying phagosomal maturation, was resolved (Ledvina et al., 2018). Thus, it remains to be elucidated how the other known effectors contribute to *Francisella* virulence and if there are more effectors to be found.

In order to investigate the role of *Francisella* T6SS and its effectors *in vivo*, I established *G. mellonella* larvae as an easy to use infection-model (chapter 3.5). *G. mellonella* larvae combine the benefit of low maintenance costs and easy handling of *in vitro* systems with the advantage of being a multicellular organism with a complex innate immune system (Ramarao et al., 2012; Tsai et al., 2016). Furthermore, not only does *G. mellonella* allow the study of bacterial pathogenicity but also drug discovery and toxicity studies can be carried out in this model organism (Aperis et al., 2007; Megaw et al., 2015; Tsai et al., 2016). Most importantly, *G. mellonella* may also serve as *in vivo* model for *Francisella* arthropod reservoir hosts. To date, *Francisella* virulence studies focus mainly on pathogenicity in mammals. However, *Francisella* is often found in the environment and most tularemia cases are transmitted by arthropods (Wittwer et al., 2018). Thus, it is important to understand the role of *Francisella* T6SS in theses settings.

My initial results suggested that *Francisella* virulence in *G. mellonella* larvae is also dependent on a functional T6SS. However, the contribution of known effectors may be different from the one in mice. In addition, T6SS sheath recycling was not essential for killing *G. mellonella* larvae suggesting that less translocation events are necessary for full virulence. Nevertheless, I am certain that *Francisella* infections in *G. mellonella* larvae will add new insights to the *Francisella* effector repertoire as well as give valuable information about the importance different virulence factors in arthropods.

Although *Francisella* is studied for a long time, only a limited number of expression plasmids are available (Abd et al., 2003; Bönquist et al., 2008; LoVullo et al., 2006; Maier et al., 2004; Norqvist et al., 1996). Furthermore, all of them were designed for *F. tularensis* and *F. holarctica*, but worked poorly in *F. novicida* (LoVullo et al., 2006; Maier et al., 2004).

In chapter 3.6. I designed mobilizable and tunable expression plasmids tailored to *F. novicida* in order to express genes in a temporal controlled manner (Brodmann et al., 2018). These plasmids will help to gain further insights into *Francisella* physiology and virulence.

4.4. The unique polar localization of *Francisella* T6SS

A unique feature of the dynamic non-canonical *Francisella* T6SS is its restricted subcellular localization to the poles (chapter 3.3.) (Brodmann et al., 2017). Interestingly, there is one report for polar localization of ClpV-5 in *B. thailandensis* (Schwarz et al., 2014). However, ClpV-5 foci were less dynamic and were also polarly localized in the absence of a functional T6SS (Lennings et al., 2019; Schwarz et al., 2014). Nonetheless, many secretion systems required for host-pathogen interactions are reported to be at the poles (Carlsson et al., 2009; Chakravortty et al., 2005; Charles et al., 2001; Jain et al., 2006; Jeong et al., 2017; Morgan et al., 2010; Rosch and Caparon, 2004; Scott et al., 2001). The importance of polar localization was demonstrated for *L. pneumophila* T4SS; mislocalization led to decrease virulence despite of functional secretion (Jeong et al., 2017).

Chapter 3.4 aimed at elucidating how *Francisella* T6SS is localized to the poles in order to answer the question whether the subcellular localization of the T6SS is important for *Francisella* virulence. Analysis of membrane complex dynamics with live-cell fluorescence revealed that *Francisella* membrane complex is only assembled after 20 min incubation on an agarose pad. Interestingly, formation of membrane complex was not dependent on functional protein synthesis. In contrast, sheath assembly was dependent on protein synthesis and required expression of sheath subunits during 1-2 h incubation on an agarose pad. These findings suggest that there is differential expression of FPI components resulting in a two-step assembly of the T6SS apparatus. In this way, *Francisella* may control costs for T6SS assembly and only express high copy number subunits after sensing additional stimuli. Moreover, these results also suggest that the membrane complex is not pre-installed at nascent poles as observed for Type IVa pili in *P. aeruginosa* and suggested for the polar T4SS in *L. pneumophila* (Carter et al., 2017; Jeong et al., 2017). In agreement, deletion of several proteins involved in cell division did not abrogate polar T6SS activity.

Furthermore, we observed a striking difference between the number of formed membrane complexes, which was present in almost every cell, and the number of assembled T6SS sheaths, which were only present in every third cell, after 1 to 2 h incubation on an agarose pad. In addition, some cells had membrane complexes

formed at both poles but only assembled T6SS sheath at one pole. One explanation for these observations could be that there are limiting components. For example, limitation of spike protein VgrG results in fewer T6SS assemblies in *V. cholerae* (Vettiger and Basler, 2016). In agreement, a study of the abundancy of canonical T6SS components revealed that membrane complex components together with baseplate and spike complex components belong to the lowest abundant T6SS components (Lin et al., 2019). However, after 1 to 2 h incubation on agarose pads, enough sheath subunits are expressed to assemble a T6SS structure. Thus, it is unlikely that other, less abundant T6SS components are limiting. Another and more exciting possibility is that there is additional post-translational regulation. One possibility is that changes in c-di-GMP levels may activate membrane complex formation as response to surface encounter as shown for biogenesis of Type IVa pili in *P. aeruginosa* (Laventie et al., 2019). Indeed, *F. novicida* but not *F. tularensis* encodes a c-di-GMP regulon (Zogaj et al., 2012).

Studies presented in this thesis were carried out in *F. novicida*, which contains only one FPI (Brodmann et al., 2017; Bröms et al., 2010). The more virulent *F. tularensis* and F. *holarctica* encode both two identical FPIs, which can complement each other (Bröms et al., 2010). Therefore, it would be interesting to see, if they still assemble only one T6SS per cell and or if they simultaneously assemble T6SS at both poles.

As discussed above, antibacterial T6SS need to be repositioned for efficient killing of target cells. However, this seems not to be the case for the anti-eukaryotic T6SS in *Francisella*. Since *Francisella* is small and T6SS is a contact-dependent secretion system, polar assembly may increase the target range as it allows the assembly of longer sheaths. Furthermore, *Francisella* may come into closer contact with the phagosomal membrane at the poles or the local concentration of effectors may be increased by polar secretion as suggested for *L. pneumophila* T4SS (Jeong et al., 2017).

In general, there are several reasons for the accumulation of anti-eukaryotic secretion systems at the poles. First, bacteria have to overcome charge repulsion in order come in close contact with host cells (van Loosdrecht et al., 1989). Thus, bacteria approaching with the poles first minimize the surface area encountering these charge repulsions. In addition, many flagella and pili are polarly localized (Carter et al.,

2017; Young, 2006), thus it is likely that these bacteria encounter host cells again first via the pole. Moreover, polar peptidoglycan has the advantage that it is more stable compared to lateral peptidoglycan, which is constantly remodeled (Typas et al., 2011; Young, 2006). Therefore, large macromolecular complexes are more stable and less likely ripped apart if inserted at the poles.

In summary, polar localization of dynamic *Francisella* T6SS is unique among T6SS but not among other anti-eukaryotic secretion systems. Thus, polar localization of *Francisella* T6SS likely serves a specific function. Since the mechanism to localize *Francisella* T6SS to the poles is not identified yet, it was not possible to assess the contribution of polar localization to *Francisella* virulence. Nevertheless, our study brought new insights in membrane complex formation and regulation. Consequently, our results will serve as a starting point for future investigations.

4.5. The putative T6SS encoded on the FNI in *Francisella novicida*

F. novicida encodes, next to the characterized polar T6SS on the FPI, an additional putative T6SS on the FNI (Brodmann et al., 2017; Bröms et al., 2010; Rigard et al., 2016). However, the relevance of the FNI remains elusive, as most FNI genes were never found in transposon screens for virulence factors (Ahlund et al., 2010; Brunton et al., 2015; Kraemer et al., 2009; Su et al., 2007).

In chapter 3.4. we tried to investigate if the $T6SS_{FNI}$ encodes a functional T6SS by live-cell fluorescence microscopy. However, we never observed any T6SS assembly in our conditions. In accordance, fluorescently tagged membrane complex component DotU resulted in a diffuse signal in the cytosol. Either the FNI components were not expressed sufficiently or a trigger for initiating the assembly was missing. However, as we do not know in what conditions the $T6SS_{FNI}$ is required, it is difficult to predict the necessary triggers. Another possibility is that essential components are missing, as for example no inner tube FNI component (*iglC/hcp*) is identified yet.

In contrast, fluorescently tagged FNI component FTN_0045, which contains a putative ImpA domain, yielded in dynamic cytosolic foci. Surprisingly, deletion of *FTN_0045* affected T6SS sheath dynamics encoded on the FPI. The retention time

between assembly and contraction was significantly longer in a *FTN_0045* deletion mutant. In the parental *F. novicida* strain, T6SS sheath assemble and immediately contract afterwards (Brodmann et al., 2017). In some bacteria with canonical T6SS, an ImpA-domain containing protein called TagA is required to stabilize extended sheaths before contraction (Santin et al., 2018; Szwedziak and Pilhofer, 2019). Thus, FTN_0045 seems to have the opposite effect of TagA. Interestingly, deletion of *FTN_0045* resulted in decreased virulence in mice (Kraemer et al., 2009) suggesting again that abnormal T6SS dynamics may cause a virulence defect. However, it is not known if FTN_0045 has an additional role in *F. novicida* pathogenicity.

Although we were not able to elucidate the importance of the FNI in *F. novicida*, we have evidence that FNI components are expressed and some of them even have distinct subcellular localizations. Thus, I am confident that the FNI does have a role in *F. novicida* physiology, although future experiments will have to determine its exact function.

4.6. The study of subcellular localization in future

The T6SS is an excellent example that subcellular localization is also important in bacteria. Nevertheless, still not much is known in general about how bacteria achieve, maintain and regulate subcellular localization. But why is it such a difficult topic to investigate?

First, bacteria are small compared to eukaryotic cells. Thus, imaging techniques with enough resolution to resolve distinct loci inside bacteria are sparse and expensive. Next to cryo-electron microscopy, which cannot capture dynamic processes, light-based microscopy techniques are the method of choice to investigate bacteria. Dynamic processes inside bacterial cells are mostly investigated with live-cell fluorescence microscopy. However, there the resolution is limited by the diffraction barrier to 200-250 nm, which can already be a fourth of a bacterial cell (Huang et al., 2010; Schneider and Basler, 2016). In the last years, several super-resolution techniques were developed in order to break the resolution limit of light microscopes (Schermelleh et al., 2019). Especially, structured illumination microscopy (SIM) became very popular as it allows the use of conventional fluorophores (Gustafsson, 2000). SIM increases resolution through the addition of a fine-striped interference

pattern in different angles to the light path in order gain more high frequency information. Then, reconstruction algorithms are used to make the additional gained information visible (Gustafsson, 2000). Nowadays, SIM can push the lateral resolution limit to 60 nm or lower (Li et al., 2015).

Next to resolution, there is still the challenge of labelling the protein of interest. The fluorophore toolbox constantly expands in regards of wavelength, size, physical and biochemical properties (Schneider and Basler, 2016). However, the challenge remains to find a fluorophore, which is non-toxic, bright and stable enough and does not affect the labelled protein in your model organism of choice. Deconvolution algorithms may improve signal to noise ratio for weak signals, which are often the case for low copy number proteins (Swedlow, 2013). In order for deconvolution algorithms to work, at least three images in z-orientation per frame and channel are needed. For SIM, the number of images required for reconstruction is even 45x higher. Thus, fluorophore bleaching is still a major problem in some cases.

Furthermore, it may be difficult to screen and select for mislocalized proteins of interest, especially if involved proteins are essential or there is no obvious phenotype to select. Newly developed tools such as CRISPR interference (CRISPRi) may help to screen for essential proteins involved in subcellular localization. CRISPRi uses a mutant Cas9 protein (dCas9), which cannot cleave DNA any longer but still translocates to the DNA of interest guided by a given sgRNA. Thereby, dCas9 blocks transcription and thus the gene of interest is silenced (Larson et al., 2013). The advantage of CRISPRi compared to conventional gene deletion is that the silencing of a gene can be temporally regulated and thus allows to target essential genes (Peters et al., 2016).

Screening for phenotypes with differences in temporal or spatial expression of a protein of interest by time-lapse microscopy is time consuming and low-throughput. However, recently a new microscopy based screen called DuMPLING was reported, which combines a pooled CRISPRi library with live-cell fluorescence microscopy in a microfluidic device (Lawson et al., 2017). It allows automated screening for about 60 phenotypes at once depending the size of the mother machine. The advantage of this screen is that also transient as well as subcellular localization phenotypes are captured in contrast to conventional endpoint screens. Furthermore, barcodes for

different CRISPRi sequences allow identification of the corresponding genotypes by fluorescent *in situ* hybridization or *in situ* sequencing.

Another possible for selection of mislocalized T6SS or other proteins of interest in intracellular pathogens such as *Francisella* is to use a CRISPRi library and select for bacteria, which are not able to escape the phagosome. Since the phagosome is more acidic than the cytosol (Huynh and Grinstein, 2007), antibiotics sensitive to pH such as aminoglycosides will only kill cytosolic bacteria but not the ones trapped inside the phagosome. In contrast, selection for mutants, which reached the cytosol, could be achieved with chloroquine, which only accumulates to bactericidal concentrations in acidic vesicles (Finlay and Falkow, 1988; Thurston et al., 2016).

Summarized, the development of new tools and methods as well as further diversification of model systems will facilitate the study of subcellular localization in bacteria in future. This will be important to find new antimicrobial targets to overcome multidrug resistance pathogens and to end the antimicrobial drug discovery crisis.

V. ABBREVIATIONS

AAA	ATPase associated with diverse cellular activities
AD	Adaptive dynamics
AIM2	Absent in melanoma 2
ATc	Anhydrotetracycline
ATP	Adenosine triphosphate
BHI	Brain heart infusion
BMDM	Bone-marrow derived macrophage
CFU	Colony forming unit
CPase	Carboxypeptidase
CRISPRi	Clusterd regularly interspaced short palindromic repeats interference
DMSO	Dimethyl sulfoxide
DNA	Deoxyribonucleic acid
DPBS	Dulbecco's phosphate buffered saline
EAEC	Enteroaggreative *Escherichia coli*
EDTA	Ethylenediaminetetraacetic acid
EPase	Endopeptidase
FNI	*Francisella novicida* island
FPI	*Francisella* pathogenicity island
Gtase	Glycosyltransferase
HHpred	Structure prediction by hidden Markov model comparison
IbM	individual-based model
IM	Inner membrane
IPTG	Isopropyl-β-thiogalactopyranoside
LB	Luria broth
LC-MS	Liquid chromatography-mass spectrometry
LD_{50}	Lethal dose for 50 % of subjects

LOL	Localization of lipoproteins
LPS	Lipopolysaccharide
LT	Lytic transglycosylase
LVC	*Legionella* containing vacuole
MIC	Minimal inhibitory concentration
MOI	Multiplicity of infection
mRNA	messenger ribonucleic acid
NA	Numerical aperture
OD_{600}	Optical density at 600 nm
OM	Outer membrane
PBS	Phosphate buffered saline
PCR	Polymerase chain reaction
RuBisCo	Ribulose-1,5-bisphosphate carboxylase/oxygenase
SDB-RPS	Styrenedivinylbenzene-reverse phase sulfonate
SIM	Structured illumination microscopy
Sec	General secretory pathway
sgRNA	small guide ribonucleic acid
SNSF	Swiss National Science Foundation
T1SS	Type I secretion system
T2SS	Type II secretion system
T3SS	Type II secretion system
T4SS	Type III secretion system
T5SS	Type V secretion system
T6SS	Type VI secretion system
T7SS	Type VII secretion system
T8SS	Type VIII secretion system
T9SS	Type IX secretion system
TFA	Trifluoroacetic acid
TPase	Transpeptidase
TPP	Threonine phosphorylation pathway

VI.REFERENCES

VI.REFERENCES

Aaron, M., Charbon, G., Lam, H., Schwarz, H., Vollmer, W., and Jacobs-Wagner, C. (2007). The tubulin homologue FtsZ contributes to cell elongation by guiding cell wall precursor synthesis in Caulobacter crescentus. Mol. Microbiol. *64*, 938–952.

Aarsman, M.E.G., Piette, A., Fraipont, C., Vinkenvleugel, T.M.F., Nguyen-Distèche, M., and den Blaauwen, T. (2005). Maturation of the Escherichia coli divisome occurs in two steps. Mol. Microbiol. *55*, 1631–1645.

Abby, S.S., Cury, J., Guglielmini, J., Néron, B., Touchon, M., and Rocha, E.P.C. (2016). Identification of protein secretion systems in bacterial genomes. Sci. Rep. *6*, 23080.

Abd, H., Johansson, T., Golovliov, I., Sandström, G., and Forsman, M. (2003). Survival and growth of Francisella tularensis in Acanthamoeba castellanii. Appl. Environ. Microbiol. *69*, 600–606.

Abdallah, A.M., Gey van Pittius, N.C., Champion, P.A.D., Cox, J., Luirink, J., Vandenbroucke-Grauls, C.M.J.E., Appelmelk, B.J., and Bitter, W. (2007). Type VII secretion--mycobacteria show the way. Nat. Rev. Microbiol. *5*, 883–891.

Abdelrahim Zoued, E.D., Yannick R. Brunet, S.S., Badreddine Douzi, M.G., Nicolas Flaugnatti, P.L., Laure Journet, R.F., Tâm Mignot, C.C., and Eric Cascales (2016). Priming and polymerization of a bacterial contractile tail structure. Nature.

Adams, D.W., and Errington, J. (2009). Bacterial cell division: assembly, maintenance and disassembly of the Z ring. Nat. Rev. Microbiol. *7*, 642–653.

Agladze, K., Wang, X., and Romeo, T. (2005). Spatial periodicity of Escherichia coli K-12 biofilm microstructure initiates during a reversible, polar attachment phase of development and requires the polysaccharide adhesin PGA. J. Bacteriol. *187*, 8237–8246.

Aguilar, J., Zupan, J., Cameron, T.A., and Zambryski, P.C. (2010). Agrobacterium type IV secretion system and its substrates form helical arrays around the circumference of virulence-induced cells. Proc. Natl. Acad. Sci. U. S. A. *107*, 3758–3763.

Ahlund, M.K., Rydén, P., Sjöstedt, A., and Stöven, S. (2010). Directed screen of Francisella novicida virulence determinants using Drosophila melanogaster. Infect. Immun. *78*, 3118–3128.

Ahrens, J., Geveci, B., and Law, C. (2005). ParaView: An End-User Tool for Large Data Visualization. In Visualization Handbook, (Elsevier), p.

Aksyuk, A.A., Leiman, P.G., Kurochkina, L.P., Shneider, M.M., Kostyuchenko, V.A., Mesyanzhinov, V.V., and Rossmann, M.G. (2009). The tail sheath structure of bacteriophage T4: a molecular machine for infecting bacteria. EMBO J. *28*, 821–829.

Alam, A., Golovliov, I., Javed, E., and Sjöstedt, A. (2018). ClpB mutants of Francisella tularensis subspecies holarctica and tularensis are defective for type VI secretion and intracellular replication. Sci. Rep. *8*, 11324.

Alcoforado Diniz, J., Liu, Y.-C., and Coulthurst, S.J. (2015). Molecular weaponry: diverse effectors delivered by the Type VI secretion system. Cell. Microbiol. *17*, 1742–1751.

Alteri, C.J., Himpsl, S.D., Pickens, S.R., Lindner, J.R., Zora, J.S., Miller, J.E., Arno, P.D., Straight, S.W., and Mobley, H.L.T. (2013). Multicellular Bacteria Deploy the Type VI Secretion System to Preemptively Strike Neighboring Cells. PLoS Pathog *9*, e1003608.

Aperis, G., Fuchs, B.B., Anderson, C.A., Warner, J.E., Calderwood, S.B., and Mylonakis, E. (2007). Galleria mellonella as a model host to study infection by the Francisella tularensis live vaccine strain. Microbes Infect. *9*, 729–734.

Apicella, M.A., Post, D.M.B., Fowler, A.C., Jones, B.D., Rasmussen, J.A., Hunt, J.R., Imagawa, S., Choudhury, B., Inzana, T.J., Maier, T.M., et al. (2010). Identification, Characterization and Immunogenicity of an O-Antigen Capsular Polysaccharide of Francisella tularensis. PLoS ONE *5*.

Arisaka, F., Yap, M.L., Kanamaru, S., and Rossmann, M.G. (2016). Molecular assembly and structure of the bacteriophage T4 tail. Biophys. Rev. *8*, 385–396.

Aschtgen, M.-S., Bernard, C.S., De Bentzmann, S., Lloubès, R., and Cascales, E. (2008). SciN is an outer membrane lipoprotein required for type VI secretion in enteroaggregative Escherichia coli. J. Bacteriol. *190*, 7523–7531.

Aschtgen, M.-S., Thomas, M.S., and Cascales, E. (2010a). Anchoring the type VI secretion system to the peptidoglycan: TssL, TagL, TagP... what else? Virulence *1*, 535–540.

Aschtgen, M.-S., Gavioli, M., Dessen, A., Lloubès, R., and Cascales, E. (2010b). The SciZ protein anchors the enteroaggregative Escherichia coli Type VI secretion system to the cell wall. Mol. Microbiol. *75*, 886–899.

Aschtgen, M.-S., Zoued, A., Lloubès, R., Journet, L., and Cascales, E. (2012). The C-tail anchored TssL subunit, an essential protein of the enteroaggregative Escherichia coli Sci-1 Type VI secretion system, is inserted by YidC. MicrobiologyOpen *1*, 71–82.

Axelrod, R., and Hamilton, W.D. (1981). The Evolution of Cooperation. Science *211*, 1390–1396.

Bakshi, S., Siryaporn, A., Goulian, M., and Weisshaar, J.C. (2012). Superresolution imaging of ribosomes and RNA polymerase in live Escherichia coli cells. Mol. Microbiol. *85*, 21–38.

Baron, G.S., and Nano, F.E. (1998). MglA and MglB are required for the intramacrophage growth of Francisella novicida. Mol. Microbiol. *29*, 247–259.

Barreteau, H., Kovac, A., Boniface, A., Sova, M., Gobec, S., and Blanot, D. (2008). Cytoplasmic steps of peptidoglycan biosynthesis. FEMS Microbiol. Rev. *32*, 168–207.

Basler, M., and Mekalanos, J.J. (2012). Type 6 secretion dynamics within and between bacterial cells. Science *337*, 815–815.

Basler, M., Pilhofer, M., Henderson, P., Jensen, J.G., and Mekalanos, J. (2012). Type VI secretion requires a dynamic contractile phage tail-like structure. Nature *483*, 182–186.

Basler, M., Ho, B.T., and Mekalanos, J.J. (2013). Tit-for-tat: Type VI secretion system counterattack during bacterial cell-cell interactions. Cell *152*, 884–894.

Baxter, J.C., and Funnell, B.E. (2014). Plasmid Partition Mechanisms. Microbiol. Spectr. *2*.

Bell, B.L., Mohapatra, N.P., and Gunn, J.S. (2010). Regulation of Virulence Gene Transcripts by the Francisella novicida Orphan Response Regulator PmrA: Role of Phosphorylation and Evidence of MglA/SspA Interaction. Infect. Immun. *78*, 2189–2198.

Bernal, P., Allsopp, L.P., Filloux, A., and Llamas, M.A. (2017). The Pseudomonas putida T6SS is a plant warden against phytopathogens. ISME J. *11*, 972–987.

Bernard, C.S., Brunet, Y.R., Gueguen, E., and Cascales, E. (2010). Nooks and crannies in type VI secretion regulation. J. Bacteriol. *192*, 3850–3860.

Bertin, Y., Girardeau, J.P., Chaucheyras-Durand, F., Lyan, B., Pujos-Guillot, E., Harel, J., and Martin, C. (2011). Enterohaemorrhagic Escherichia coli gains a competitive advantage by using ethanolamine as a nitrogen source in the bovine intestinal content. Environ. Microbiol. *13*, 365–377.

Biernaskie, J.M., Gardner, A., and West, S.A. (2013). Multicoloured greenbeards, bacteriocin diversity and the rock-paper-scissors game. J Evol Biol *26*, 2081–2094.

Bingle, L.E., Bailey, C.M., and Pallen, M.J. (2008). Type VI secretion: a beginner's guide. Curr. Opin. Microbiol. *11*, 3–8.

den Blaauwen, T., Hamoen, L.W., and Levin, P.A. (2017). The divisome at 25: the road ahead. Curr. Opin. Microbiol. *36*, 85–94.

Bladergroen, M.R., Badelt, K., and Spaink, H.P. (2003). Infection-blocking genes of a symbiotic Rhizobium leguminosarum strain that are involved in temperature-dependent protein secretion. Mol. Plant-Microbe Interact. MPMI *16*, 53–64.

Blakemore, R. (1975). Magnetotactic bacteria. Science *190*, 377–379.

Bocian-Ostrzycka, K.M., Grzeszczuk, M.J., Banaś, A.M., and Jagusztyn-Krynicka, E.K. (2017). Bacterial thiol oxidoreductases - from basic research to new antibacterial strategies. Appl. Microbiol. Biotechnol. *101*, 3977–3989.

Böck, D., Medeiros, J.M., Tsao, H.-F., Penz, T., Weiss, G.L., Aistleitner, K., Horn, M., and Pilhofer, M. (2017). In situ architecture, function, and evolution of a contractile injection system. Science *357*, 713–717.

Bönemann, G., Pietrosiuk, A., Diemand, A., Zentgraf, H., and Mogk, A. (2009). Remodelling of VipA/VipB tubules by ClpV-mediated threading is crucial for type VI protein secretion. EMBO J. *28*, 315–325.

Bönquist, L., Lindgren, H., Golovliov, I., Guina, T., and Sjöstedt, A. (2008). MglA and Igl proteins contribute to the modulation of Francisella tularensis live vaccine strain-containing phagosomes in murine macrophages. Infect. Immun. *76*, 3502–3510.

Borenstein, D.B., Ringel, P., Basler, M., and Wingreen, N.S. (2015). Established Microbial Colonies Can Survive Type VI Secretion Assault. PLoS Comput. Biol. *11*, 1–16.

Bouhss, A., Trunkfield, A.E., Bugg, T.D.H., and Mengin-Lecreulx, D. (2008). The biosynthesis of peptidoglycan lipid-linked intermediates. FEMS Microbiol. Rev. *32*, 208–233.

Bowman, G.R., Comolli, L.R., Zhu, J., Eckart, M., Koenig, M., Downing, K.H., Moerner, W.E., Earnest, T., and Shapiro, L. (2008). A polymeric protein anchors the chromosomal origin/ParB complex at a bacterial cell pole. Cell *134*, 945–955.

Boyer, F., Fichant, G., Berthod, J., Vandenbrouck, Y., and Attree, I. (2009). Dissecting the bacterial type VI secretion system by a genome wide in silico analysis: what can be learned from available microbial genomic resources? BMC Genomics *10*, 104–104.

Brackmann, M., Nazarov, S., Wang, J., and Basler, M. (2017a). Using Force to Punch Holes: Mechanics of Contractile Nanomachines. Trends Cell Biol.

Brackmann, M., Wang, J., and Basler, M. (2017b). Type VI secretion system sheath inter-subunit interactions modulate its contraction. EMBO Rep.

Brännström, Å., Johansson, J., von Festenberg, N., Brännström, Å., Johansson, J., and von Festenberg, N. (2013). The Hitchhiker's Guide to Adaptive Dynamics. Games *4*, 304–328.

Breidenstein, E.B.M., de la Fuente-Núñez, C., and Hancock, R.E.W. (2011). Pseudomonas aeruginosa: all roads lead to resistance. Trends Microbiol. *19*, 419–426.

Brencic, A., and Lory, S. (2009). Determination of the regulon and identification of novel mRNA targets of Pseudomonas aeruginosa RsmA. Mol. Microbiol. *72*, 612–632.

Brodmann, M., Dreier, R.F., Broz, P., and Basler, M. (2017). Francisella requires dynamic type VI secretion system and ClpB to deliver effectors for phagosomal escape. Nat. Commun. *8*, 15853.

Brodmann, M., Heilig, R., Broz, P., and Basler, M. (2018). Mobilizable Plasmids for Tunable Gene Expression in Francisella novicida. Front. Cell. Infect. Microbiol. *8*.

Bröms, J.E., Sjöstedt, A., and Lavander, M. (2010). The Role of the Francisella Tularensis Pathogenicity Island in Type VI Secretion, Intracellular Survival, and Modulation of Host Cell Signaling. Front. Microbiol. *1*, 136.

Bröms, J.E., Lavander, M., Meyer, L., and Sjöstedt, A. (2011). IglG and IglI of the Francisella pathogenicity island are important virulence determinants of Francisella tularensis LVS. Infect. Immun. *79*, 3683–3696.

Brotcke, A., and Monack, D.M. (2008). Identification of fevR, a novel regulator of virulence gene expression in Francisella novicida. Infect. Immun. *76*, 3473–3480.

Brotcke, A., Weiss, D.S., Kim, C.C., Chain, P., Malfatti, S., Garcia, E., and Monack, D.M. (2006). Identification of MglA-regulated genes reveals novel virulence factors in Francisella tularensis. Infect. Immun. *74*, 6642–6655.

de Bruin, O.M., Ludu, J.S., and Nano, F.E. (2007). The Francisella pathogenicity island protein IglA localizes to the bacterial cytoplasm and is needed for intracellular growth. BMC Microbiol. *7*, 1.

de Bruin, O.M., Duplantis, B.N., Ludu, J.S., Hare, R.F., Nix, E.B., Schmerk, C.L., Robb, C.S., Boraston, A.B., Hueffer, K., and Nano, F.E. (2011). The biochemical properties of the Francisella pathogenicity island (FPI)-encoded proteins IglA, IglB, IglC, PdpB and DotU suggest roles in type VI secretion. Microbiol. Read. Engl. *157*, 3483–3491.

Brunet, Y.R., Espinosa, L., Harchouni, S., Mignot, T., and Cascales, E. (2013). Imaging type VI secretion-mediated bacterial killing. Cell Rep. *3*, 36–41.

Brunet, Y.R., Hénin, J., Celia, H., and Cascales, E. (2014). Type VI secretion and bacteriophage tail tubes share a common assembly pathway. EMBO Rep. *15*, 315–321.

Brunet, Y.R., Zoued, A., Boyer, F., Douzi, B., and Cascales, E. (2015). The Type VI Secretion TssEFGK-VgrG Phage-Like Baseplate Is Recruited to the TssJLM Membrane Complex via Multiple Contacts and Serves As Assembly Platform for Tail Tube/Sheath Polymerization. PLoS Genet. *11*, e1005545.

Brunton, J., Steele, S., Miller, C., Lovullo, E., Taft-Benz, S., and Kawula, T. (2015). Identifying Francisella tularensis genes required for growth in host cells. Infect. Immun. *83*, 3015–3025.

Buchan, B.W., McCaffrey, R.L., Lindemann, S.R., Allen, L.-A.H., and Jones, B.D. (2009). Identification of migR, a regulatory element of the Francisella tularensis live vaccine strain iglABCD virulence operon required for normal replication and trafficking in macrophages. Infect. Immun. *77*, 2517–2529.

Buist, G., Steen, A., Kok, J., and Kuipers, O.P. (2008). LysM, a widely distributed protein motif for binding to (peptido)glycans. Mol. Microbiol. *68*, 838–847.

Burrows, L.L. (2012). Pseudomonas aeruginosa twitching motility: type IV pili in action. Annu. Rev. Microbiol. *66*, 493–520.

Cabeen, M.T., Charbon, G., Vollmer, W., Born, P., Ausmees, N., Weibel, D.B., and Jacobs-Wagner, C. (2009). Bacterial cell curvature through mechanical control of cell growth. EMBO J. *28*, 1208–1219.

Carlsson, F., Joshi, S.A., Rangell, L., and Brown, E.J. (2009). Polar localization of virulence-related Esx-1 secretion in mycobacteria. PLoS Pathog. *5*, e1000285.

Carter, T., Buensuceso, R.N.C., Tammam, S., Lamers, R.P., Harvey, H., Howell, P.L., and Burrows, L.L. (2017). The Type IVa Pilus Machinery Is Recruited to Sites of Future Cell Division. MBio *8*.

Casabona, M.G., Silverman, J.M., Sall, K.M., Boyer, F., Couté, Y., Poirel, J., Grunwald, D., Mougous, J.D., Elsen, S., and Attree, I. (2013). An ABC transporter and an outer membrane lipoprotein participate in posttranslational activation of type VI secretion in Pseudomonas aeruginosa. Environ. Microbiol. *15*, 471–486.

Cerenius, L., and Söderhäll, K. (2004). The prophenoloxidase-activating system in invertebrates. Immunol. Rev. *198*, 116–126.

Chakravortty, D., Rohde, M., Jäger, L., Deiwick, J., and Hensel, M. (2005). Formation of a novel surface structure encoded by Salmonella Pathogenicity Island 2. EMBO J. *24*, 2043–2052.

Chang, Y.-W., Rettberg, L.A., Ortega, D.R., and Jensen, G.J. (2017). In vivo structures of an intact type VI secretion system revealed by electron cryotomography. EMBO Rep. e201744072.

Charbon, G., Cabeen, M.T., and Jacobs-Wagner, C. (2009). Bacterial intermediate filaments: in vivo assembly, organization, and dynamics of crescentin. Genes Dev. *23*, 1131–1144.

Charles, M., Pérez, M., Kobil, J.H., and Goldberg, M.B. (2001). Polar targeting of Shigella virulence factor IcsA in Enterobacteriacae and Vibrio. Proc. Natl. Acad. Sci. U. S. A. *98*, 9871–9876.

Chassaing, B., and Cascales, E. (2018). Antibacterial Weapons: Targeted Destruction in the Microbiota. Trends Microbiol. *26*, 329–338.

Chatzidaki-Livanis, M., Geva-Zatorsky, N., and Comstock, L.E. (2016). Bacteroides fragilis type VI secretion systems use novel effector and immunity proteins to antagonize human gut Bacteroidales species. Proc. Natl. Acad. Sci. *113*, 3627–3632.

Chen, C., Yang, X., and Shen, X. (2019). Confirmed and Potential Roles of Bacterial T6SSs in the Intestinal Ecosystem. Front. Microbiol. *10*, 1484.

Chen, L., Zou, Y., She, P., and Wu, Y. (2015). Composition, function, and regulation of T6SS in Pseudomonas aeruginosa. Microbiol. Res. *172*, 19–25.

Cherrak, Y., Rapisarda, C., Pellarin, R., Bouvier, G., Bardiaux, B., Allain, F., Malosse, C., Rey, M., Chamot-Rooke, J., Cascales, E., et al. (2018). Biogenesis and structure of a type VI secretion baseplate. Nat. Microbiol.

Cho, S.-H., Szewczyk, J., Pesavento, C., Zietek, M., Banzhaf, M., Roszczenko, P., Asmar, A., Laloux, G., Hov, A.-K., Leverrier, P., et al. (2014). Detecting Envelope Stress by Monitoring β-Barrel Assembly. Cell *159*, 1652–1664.

Chong, A., and Celli, J. (2010). The francisella intracellular life cycle: toward molecular mechanisms of intracellular survival and proliferation. Front. Microbiol. *1*, 138.

Chong, A., Wehrly, T.D., Nair, V., Fischer, E.R., Barker, J.R., Klose, K.E., and Celli, J. (2008). The Early Phagosomal Stage of Francisella tularensis Determines Optimal Phagosomal Escape and Francisella Pathogenicity Island Protein Expression. Infect. Immun. *76*, 5488–5499.

Cianfanelli, F.R., Monlezun, L., and Coulthurst, S.J. (2016). Aim, Load, Fire: The Type VI Secretion System, a Bacterial Nanoweapon. Trends Microbiol. *24*, 51–62.

Clarke, C.A., Scheurwater, E.M., and Clarke, A.J. (2010). The vertebrate lysozyme inhibitor Ivy functions to inhibit the activity of lytic transglycosylase. J. Biol. Chem. *285*, 14843–14847.

Clemens, D.L., Lee, B.-Y., and Horwitz, M.A. (2009). Francisella tularensis Phagosomal Escape Does Not Require Acidification of the Phagosome. Infect. Immun. *77*, 1757–1773.

Clemens, D.L., Ge, P., Lee, B.-Y., Horwitz, M.A., and Zhou, Z.H. (2015). Atomic Structure of T6SS Reveals Interlaced Array Essential to Function. Cell *160*, 940–951.

Cornejo, E., Abreu, N., and Komeili, A. (2014). Compartmentalization and organelle formation in bacteria. Curr. Opin. Cell Biol. *26*, 132–138.

Cornforth, D.M., and Foster, K.R. (2013). Competition sensing: the social side of bacterial stress responses. Nature *11*, 285–293.

Costa, T.R.D., Felisberto-Rodrigues, C., Meir, A., Prevost, M.S., Redzej, A., Trokter, M., and Waksman, G. (2015). Secretion systems in Gram-negative bacteria: structural and mechanistic insights. Nat. Rev. Microbiol. *13*, 343–359.

Coulthurst, S.J. (2013). The Type VI secretion system - a widespread and versatile cell targeting system. Res. Microbiol. *164*, 640–654.

Cowles, K.N., Moser, T.S., Siryaporn, A., Nyakudarika, N., Dixon, W., Turner, J.J., and Gitai, Z. (2013). The putative Poc complex controls two distinct Pseudomonas aeruginosa polar motility mechanisms. Mol. Microbiol. *90*, 923–938.

Coyne, M.J., and Comstock, L.E. (2019). Type VI Secretion Systems and the Gut Microbiota. Microbiol. Spectr. *7*.

Coyte, K.Z., Schluter, J., and Foster, K.R. (2015). The ecology of the microbiome: Networks, competition, and stability. Science *350*, 663–666.

Coyte, K.Z., Tabuteau, H.E., Gaffney, E.A., Foster, K.R., and Durham, W.M. (2017). Microbial competition in porous environments can select against rapid biofilm growth. Proc. Natl. Acad. Sci. E161–E170.

Daniel, R.A., and Errington, J. (2003). Control of cell morphogenesis in bacteria: two distinct ways to make a rod-shaped cell. Cell *113*, 767–776.

Das, S., and Chaudhuri, K. (2003). Identification of a unique IAHP (IcmF associated homologous proteins) cluster in Vibrio cholerae and other proteobacteria through in silico analysis. In Silico Biol. *3*, 287–300.

Deich, J., Judd, E.M., McAdams, H.H., and Moerner, W.E. (2004). Visualization of the movement of single histidine kinase molecules in live Caulobacter cells. Proc. Natl. Acad. Sci. U. S. A. *101*, 15921–15926.

Deng, K., Blick, R.J., Liu, W., and Hansen, E.J. (2006). Identification of Francisella tularensis genes affected by iron limitation. Infect. Immun. *74*, 4224–4236.

Deng, W., Li, Y., Hardwidge, P.R., Frey, E.A., Pfuetzner, R.A., Lee, S., Gruenheid, S., Strynakda, N.C.J., Puente, J.L., and Finlay, B.B. (2005). Regulation of type III secretion hierarchy of translocators and effectors in attaching and effacing bacterial pathogens. Infect. Immun. *73*, 2135–2146.

Desvaux, M., Hébraud, M., Talon, R., and Henderson, I.R. (2009). Secretion and subcellular localizations of bacterial proteins: a semantic awareness issue. Trends Microbiol. *17*, 139–145.

Detweiler, C.S., Monack, D.M., Brodsky, I.E., Mathew, H., and Falkow, S. (2003). virK, somA and rcsC are important for systemic Salmonella enterica serovar Typhimurium infection and cationic peptide resistance. Mol. Microbiol. *48*, 385–400.

Dienes, L. (1946). Reproductive processes in Proteus cultures. Proc. Soc. Exp. Biol. Med. Soc. Exp. Biol. Med. N. Y. N *63*, 265–270.

Dik, D.A., Marous, D.R., Fisher, J.F., and Mobashery, S. (2017). Lytic transglycosylases: concinnity in concision of the bacterial cell wall. Crit. Rev. Biochem. Mol. Biol. *52*, 503–542.

Dix, S.R., Owen, H.J., Sun, R., Ahmad, A., Shastri, S., Spiewak, H.L., Mosby, D.J., Harris, M.J., Batters, S.L., Brooker, T.A., et al. (2018). Structural insights into the function of type VI secretion system TssA subunits. Nat. Commun. *9*, 4765.

Dong, T.G., Ho, B.T., Yoder-Himes, D.R., and Mekalanos, J.J. (2013). Identification of T6SS-dependent effector and immunity proteins by Tn-seq in Vibrio cholerae. Proc. Natl. Acad. Sci. U. S. A. *110*, 2623–2628.

Durand, E., Zoued, A., Spinelli, S., Watson, P.J.H., Aschtgen, M.-S., Journet, L., Cambillau, C., and Cascales, E. (2012). Structural characterization and oligomerization of the TssL protein, a component shared by bacterial type VI and type IVb secretion systems. J. Biol. Chem. *287*, 14157–14168.

Durand, E., Cambillau, C., Cascales, E., and Journet, L. (2014). VgrG, Tae, Tle, and beyond: the versatile arsenal of Type VI secretion effectors. Trends Microbiol. *22*, 498–507.

Durand, E., Nguyen, V.S., Zoued, A., Logger, L., Péhau-Arnaudet, G., Aschtgen, M.-S., Spinelli, S., Desmyter, A., Bardiaux, B., Dujeancourt, A., et al. (2015). Biogenesis and structure of a type VI secretion membrane core complex. Nature *523*, 555–560.

Ebersbach, G., Briegel, A., Jensen, G.J., and Jacobs-Wagner, C. (2008). A self-associating protein critical for chromosome attachment, division, and polar organization in caulobacter. Cell *134*, 956–968.

Edgar, R., Rokney, A., Feeney, M., Semsey, S., Kessel, M., Goldberg, M.B., Adhya, S., and Oppenheim, A.B. (2008). Bacteriophage infection is targeted to cellular poles. Mol. Microbiol. *68*, 1107–1116.

Egile, C., d'Hauteville, H., Parsot, C., and Sansonetti, P.J. (1997). SopA, the outer membrane protease responsible for polar localization of IcsA in Shigella flexneri. Mol. Microbiol. *23*, 1063–1073.

Elkins, K.L., Cowley, S.C., and Bosio, C.M. (2007). Innate and adaptive immunity to Francisella. Ann. N. Y. Acad. Sci. *1105*, 284–324.

Ellermeier, J.R., and Slauch, J.M. (2007). Adaptation to the host environment: regulation of the SPI1 type III secretion system in Salmonella enterica serovar Typhimurium. Curr. Opin. Microbiol. *10*, 24–29.

Erickson, H.P., Anderson, D.E., and Osawa, M. (2010). FtsZ in bacterial cytokinesis: cytoskeleton and force generator all in one. Microbiol. Mol. Biol. Rev. MMBR *74*, 504–528.

Errington, J. (2015). Bacterial morphogenesis and the enigmatic MreB helix. Nat. Rev. Microbiol. *13*, 241–248.

Eshraghi, A., Kim, J., Walls, A.C., Ledvina, H.E., Miller, C.N., Ramsey, K.M., Whitney, J.C., Radey, M.C., Peterson, S.B., Ruhland, B.R., et al. (2016). Secreted Effectors Encoded within and outside of the Francisella Pathogenicity Island Promote Intramacrophage Growth. Cell Host Microbe *20*, 573–583.

Felisberto-Rodrigues, C., Durand, E., Aschtgen, M.-S., Blangy, S., Ortiz-Lombardia, M., Douzi, B., Cambillau, C., and Cascales, E. (2011). Towards a Structural Comprehension of Bacterial Type VI Secretion Systems: Characterization of the TssJ-TssM Complex of an Escherichia coli Pathovar. PLoS Pathog. *7*, e1002386.

Fernandes-Alnemri, T., Yu, J.-W., Juliana, C., Solorzano, L., Kang, S., Wu, J., Datta, P., McCormick, M., Huang, L., McDermott, E., et al. (2010). The AIM2 inflammasome is critical for innate immunity to Francisella tularensis. Nat. Immunol. *11*, 385–393.

Finlay, B.B., and Falkow, S. (1988). Comparison of the invasion strategies used by Salmonella cholerae-suis, Shigella flexneri and Yersinia enterocolitica to enter cultured animal cells: endosome acidification is not required for bacterial invasion or intracellular replication. Biochimie *70*, 1089–1099.

Folkesson, A., Löfdahl, S., and Normark, S. (2002). The Salmonella enterica subspecies I specific centisome 7 genomic island encodes novel protein families present in bacteria living in close contact with eukaryotic cells. Res. Microbiol. *153*, 537–545.

Förster, A., Planamente, S., Manoli, E., Lossi, N.S., Freemont, P.S., and Filloux, A. (2014). Coevolution of the ATPase ClpV, the sheath proteins TssB and TssC, and the accessory protein TagJ/HsiE1 distinguishes type VI secretion classes. J. Biol. Chem. *289*, 33032–33043.

French, C.T., Toesca, I.J., Wu, T.-H., Teslaa, T., Beaty, S.M., Wong, W., Liu, M., Schröder, I., Chiou, P.-Y., Teitell, M.A., et al. (2011). Dissection of the Burkholderia intracellular life cycle using a photothermal nanoblade. Proc. Natl. Acad. Sci. U. S. A. *108*, 12095–12100.

Fritsch, M.J., Trunk, K., Diniz, J.A., Guo, M., Trost, M., and Coulthurst, S.J. (2013). Proteomic Identification of Novel Secreted Antibacterial Toxins of the Serratia marcescens Type VI Secretion System. Mol. Cell. Proteomics MCP *12*, 2735–2749.

Frost, I., Smith, W.P.J., Mitri, S., Millan, A.S., Davit, Y., Osborne, J.M., Pitt-Francis, J.M., MacLean, R.C., and Foster, K.R. (2018). Cooperation, competition and antibiotic resistance in bacterial colonies. ISME J. *12*, 1582–1593.

Galán, J.E. (2016). Typhoid toxin provides a window into typhoid fever and the biology of Salmonella Typhi. Proc. Natl. Acad. Sci. U. S. A. *113*, 6338–6344.

Gayathri, P., and Harne, S. (2017). Structure and Dynamics of Actin-Like Cytomotive Filaments in Plasmid Segregation. Subcell. Biochem. *84*, 299–321.

Gayathri, P., Fujii, T., Møller-Jensen, J., van den Ent, F., Namba, K., and Löwe, J. (2012). A bipolar spindle of antiparallel ParM filaments drives bacterial plasmid segregation. Science *338*, 1334–1337.

Ge, P., Scholl, D., Leiman, P.G., Yu, X., Miller, J.F., and Zhou, Z.H. (2015). Atomic structures of a bactericidal contractile nanotube in its pre- and postcontraction states. Nat. Struct. Mol. Biol. *22*, 377–382.

Geiger, T., Pazos, M., Lara-Tejero, M., Vollmer, W., and Galán, J.E. (2018). Peptidoglycan editing by a specific LD-transpeptidase controls the muramidase-dependent secretion of typhoid toxin. Nat. Microbiol. *3*, 1243–1254.

Gennity, J.M., and Inouye, M. (1991). The protein sequence responsible for lipoprotein membrane localization in Escherichia coli exhibits remarkable specificity. J. Biol. Chem. *266*, 16458–16464.

Gerc, A.J., Diepold, A., Trunk, K., Porter, M., Rickman, C., Armitage, J.P., Stanley-Wall, N.R., and Coulthurst, S.J. (2015). Visualization of the Serratia Type VI Secretion System Reveals Unprovoked Attacks and Dynamic Assembly. Cell Rep. *12*, 2131–2142.

Ghosal, D., Jeong, K.C., Chang, Y.-W., Gyore, J., Teng, L., Gardner, A., Vogel, J.P., and Jensen, G.J. (2019). Molecular architecture, polar targeting and biogenesis of the Legionella Dot/Icm T4SS. Nat. Microbiol.

Gibbs, K.A., Urbanowski, M.L., and Greenberg, E.P. (2008). Genetic Determinants of Self Identity and Social Recognition in Bacteria. Science *321*, 256–259.

Glaeser, R.M. (2019). How Good Can Single-Particle Cryo-EM Become? What Remains Before It Approaches Its Physical Limits? Annu. Rev. Biophys. *48*, 45–61.

Goldberg, M.B., Bârzu, O., Parsot, C., and Sansonetti, P.J. (1993). Unipolar localization and ATPase activity of IcsA, a Shigella flexneri protein involved in intracellular movement. J. Bacteriol. *175*, 2189–2196.

Golovliov, I., Ericsson, M., Sandström, G., Tärnvik, A., and Sjöstedt, A. (1997). Identification of proteins of Francisella tularensis induced during growth in macrophages and cloning of the gene encoding a prominently induced 23-kilodalton protein. Infect. Immun. *65*, 2183–2189.

Golovliov, I., Sjöstedt, A., Mokrievich, A., and Pavlov, V. (2003). A method for allelic replacement in Francisella tularensis. FEMS Microbiol. Lett. *222*, 273–280.

Goodman, A.L., Kulasekara, B., Rietsch, A., Boyd, D., Smith, R.S., and Lory, S. (2004). A signaling network reciprocally regulates genes associated with acute infection and chronic persistence in Pseudomonas aeruginosa. Dev. Cell *7*, 745–754.

Grant, C.R., Wan, J., and Komeili, A. (2018). Organelle Formation in Bacteria and Archaea. Annu. Rev. Cell Dev. Biol. *34*, 217–238.

Gray, C.G., Cowley, S.C., Cheung, K.K.M., and Nano, F.E. (2002). The identification of five genetic loci of Francisella novicida associated with intracellular growth. FEMS Microbiol. Lett. *215*, 53–56.

Gray, W.T., Govers, S.K., Xiang, Y., Parry, B.R., Campos, M., Kim, S., and Jacobs-Wagner, C. (2019). Nucleoid Size Scaling and Intracellular Organization of Translation across Bacteria. Cell *177*, 1632-1648.e20.

Guina, T., Lanning, L.L., Omland, K.S., Williams, M.S., Wolfraim, L.A., Heyse, S.P., Houchens, C.R., Sanz, P., and Hewitt, J.A. (2018). The Cynomolgus Macaque Natural History Model of Pneumonic Tularemia for Predicting Clinical Efficacy Under the Animal Rule. Front. Cell. Infect. Microbiol. *8*.

Gunn, J.S., and Ernst, R.K. (2007). The structure and function of Francisella lipopolysaccharide. Ann. N. Y. Acad. Sci. *1105*, 202–218.

Gupta, R.S. (1998). What are archaebacteria: life's third domain or monoderm prokaryotes related to gram-positive bacteria? A new proposal for the classification of prokaryotic organisms. Mol. Microbiol. *29*, 695–707.

Gustafsson, M.G.L. (2000). Surpassing the lateral resolution limit by a factor of two using structured illumination microscopy. J. Microsc. *198*, 82–87.

Hachani, A., Wood, T.E., and Filloux, A. (2016). Type VI secretion and anti-host effectors. Curr. Opin. Microbiol. *29*, 81–93.

Hajjar, A.M., Harvey, M.D., Shaffer, S.A., Goodlett, D.R., Sjöstedt, A., Edebro, H., Forsman, M., Byström, M., Pelletier, M., Wilson, C.B., et al. (2006). Lack of In Vitro and In Vivo Recognition of Francisella tularensis Subspecies Lipopolysaccharide by Toll-Like Receptors. Infect. Immun. *74*, 6730–6738.

Hancock, R.E.W., and Speert, D.P. (2000). Antibiotic resistance in Pseudomonas aeruginosa: mechanisms and impact on treatment. Drug Resist. Updat. *3*, 247–255.

Harms, A., Segers, F.H.I.D., Quebatte, M., Mistl, C., Manfredi, P., Körner, J., Chomel, B.B., Kosoy, M., Maruyama, S., Engel, P., et al. (2017). Evolutionary Dynamics of Pathoadaptation Revealed by Three Independent Acquisitions of the VirB/D4 Type IV Secretion System in Bartonella. Genome Biol. Evol. *9*, 761–776.

Hecht, A.L., Casterline, B.W., Earley, Z.M., Goo, Y.A., Goodlett, D.R., and Bubeck Wardenburg, J. (2016). Strain competition restricts colonization of an enteric pathogen and prevents colitis. EMBO Rep. *17*, 1281–1291.

Hennebique, A., Boisset, S., and Maurin, M. (2019). Tularemia as a waterborne disease: a review. Emerg. Microbes Infect. *8*, 1027–1042.

Henry, T., Brotcke, A., Weiss, D.S., Thompson, L.J., and Monack, D.M. (2007). Type I interferon signaling is required for activation of the inflammasome during Francisella infection. J. Exp. Med. *204*, 987–994.

Higgins, D., and Dworkin, J. (2012). Recent progress in Bacillus subtilis sporulation. FEMS Microbiol. Rev. *36*, 131–148.

Ho, B.T., Basler, M., and Mekalanos, J.J. (2013). Type 6 Secretion System-Mediated Immunity to Type 4 Secretion System-Mediated Horizontal Gene Transfer. Science *342*, 250–253.

Ho, B.T., Dong, T.G., and Mekalanos, J.J. (2014). A View to a Kill: The Bacterial Type VI Secretion System. Cell Host Microbe *15*, 9–21.

Ho, B.T., Fu, Y., Dong, T.G., and Mekalanos, J.J. (2017). Vibrio cholerae type 6 secretion system effector trafficking in target bacterial cells. Proc. Natl. Acad. Sci. U. S. A. *114*, 9427–9432.

Hoang, H.H., Nickerson, N.N., Lee, V.T., Kazimirova, A., Chami, M., Pugsley, A.P., and Lory, S. (2011). Outer membrane targeting of Pseudomonas aeruginosa proteins shows variable dependence on the components of Bam and Lol machineries. MBio *2*.

Hogan, D.A., and Kolter, R. (2002). Pseudomonas-Candida interactions: an ecological role for virulence factors. Science *296*, 2229–2232.

Höltje, J.V. (1998). Growth of the stress-bearing and shape-maintaining murein sacculus of Escherichia coli. Microbiol. Mol. Biol. Rev. MMBR *62*, 181–203.

Hood, R.D., Singh, P., Hsu, F., Güvener, T., Carl, M.A., Trinidad, R.R.S., Silverman, J.M., Ohlson, B.B., Hicks, K.G., Plemel, R.L., et al. (2010). A type VI secretion system of Pseudomonas aeruginosa targets a toxin to bacteria. Cell Host Microbe *7*, 25–37.

Hsu, F., Schwarz, S., and Mougous, J.D. (2009). TagR Promotes PpkA-Catalyzed Type VI Secretion Activation in Pseudomonas aeruginosa. Mol. Microbiol. *72*, 1111–1125.

Hu, Z., and Lutkenhaus, J. (1999). Topological regulation of cell division in Escherichia coli involves rapid pole to pole oscillation of the division inhibitor MinC under the control of MinD and MinE. Mol. Microbiol. *34*, 82–90.

Huang, B., Babcock, H., and Zhuang, X. (2010). Breaking the diffraction barrier: super-resolution imaging of cells. Cell *143*, 1047–1058.

Huitema, E., Pritchard, S., Matteson, D., Radhakrishnan, S.K., and Viollier, P.H. (2006). Bacterial birth scar proteins mark future flagellum assembly site. Cell *124*, 1025–1037.

Hussain, S., Wivagg, C.N., Szwedziak, P., Wong, F., Schaefer, K., Izoré, T., Renner, L.D., Holmes, M.J., Sun, Y., Bisson-Filho, A.W., et al. (2018). MreB filaments align along greatest principal membrane curvature to orient cell wall synthesis. ELife *7*.

Huynh, K.K., and Grinstein, S. (2007). Regulation of vacuolar pH and its modulation by some microbial species. Microbiol. Mol. Biol. Rev. MMBR *71*, 452–462.

Ikäheimo, I., Syrjälä, H., Karhukorpi, J., Schildt, R., and Koskela, M. (2000). In vitro antibiotic susceptibility of Francisella tularensis isolated from humans and animals. J. Antimicrob. Chemother. *46*, 287–290.

Jain, S., van Ulsen, P., Benz, I., Schmidt, M.A., Fernandez, R., Tommassen, J., and Goldberg, M.B. (2006). Polar localization of the autotransporter family of large bacterial virulence proteins. J. Bacteriol. *188*, 4841–4850.

Jakobson, C.M., and Tullman-Ercek, D. (2016). Dumpster Diving in the Gut: Bacterial Microcompartments as Part of a Host-Associated Lifestyle. PLoS Pathog. *12*, e1005558.

Jaumouillé, V., Francetic, O., Sansonetti, P.J., and Tran Van Nhieu, G. (2008). Cytoplasmic targeting of IpaC to the bacterial pole directs polar type III secretion in Shigella. EMBO J. *27*, 447–457.

Jeong, K.C., Ghosal, D., Chang, Y.-W., Jensen, G.J., and Vogel, J.P. (2017). Polar delivery of Legionella type IV secretion system substrates is essential for virulence. Proc. Natl. Acad. Sci. U. S. A.

Jones, B.D., Faron, M., Rasmussen, J.A., and Fletcher, J.R. (2014). Uncovering the components of the Francisella tularensis virulence stealth strategy. Front. Cell. Infect. Microbiol. *4*, 32.

Jones, C.L., Sampson, T.R., Nakaya, H.I., Pulendran, B., and Weiss, D.S. (2012). Repression of bacterial lipoprotein production by Francisella novicida facilitates evasion of innate immune recognition. Cell. Microbiol. *14*, 1531–1543.

Jones, J.W., Kayagaki, N., Broz, P., Henry, T., Newton, K., O'Rourke, K., Chan, S., Dong, J., Qu, Y., Roose-Girma, M., et al. (2010). Absent in melanoma 2 is required for innate immune recognition of Francisella tularensis. Proc. Natl. Acad. Sci. U. S. A. *107*, 9771–9776.

Jones, L.J., Carballido-López, R., and Errington, J. (2001). Control of cell shape in bacteria: helical, actin-like filaments in Bacillus subtilis. Cell *104*, 913–922.

Joseph, B., Przybilla, K., Stühler, C., Schauer, K., Slaghuis, J., Fuchs, T.M., and Goebel, W. (2006). Identification of Listeria monocytogenes genes contributing to intracellular replication by expression profiling and mutant screening. J. Bacteriol. *188*, 556–568.

Joshi, A., Kostiuk, B., Rogers, A., Teschler, J., Pukatzki, S., and Yildiz, F.H. Rules of Engagement: The Type VI Secretion System in Vibrio cholerae. Trends Microbiol.

Judd, P.K., Kumar, R.B., and Das, A. (2005). Spatial location and requirements for the assembly of the Agrobacterium tumefaciens type IV secretion apparatus. Proc. Natl. Acad. Sci. U. S. A. *102*, 11498–11503.

Juncker, A.S., Willenbrock, H., Von Heijne, G., Brunak, S., Nielsen, H., and Krogh, A. (2003). Prediction of lipoprotein signal peptides in Gram-negative bacteria. Protein Sci. Publ. Protein Soc. *12*, 1652–1662.

Kanistanon, D., Powell, D.A., Hajjar, A.M., Pelletier, M.R., Cohen, I.E., Way, S.S., Skerrett, S.J., Wang, X., Raetz, C.R.H., and Ernst, R.K. (2012). Role of Francisella Lipid A Phosphate Modification in Virulence and Long-Term Protective Immune Responses. Infect. Immun. *80*, 943–951.

Kapitein, N., Bönemann, G., Pietrosiuk, A., Seyffer, F., Hausser, I., Locker, J.K., and Mogk, A. (2013). ClpV recycles VipA/VipB tubules and prevents non-productive tubule formation to ensure efficient type VI protein secretion. Mol. Microbiol. *87*, 1013–1028.

Kawazura, T., Matsumoto, K., Kojima, K., Kato, F., Kanai, T., Niki, H., and Shiomi, D. (2017). Exclusion of assembled MreB by anionic phospholipids at cell poles confers cell polarity for bidirectional growth. Mol. Microbiol. *104*, 472–486.

Keim, P., Johansson, A., and Wagner, D.M. (2007). Molecular epidemiology, evolution, and ecology of Francisella. Ann. N. Y. Acad. Sci. *1105*, 30–66.

Kerfeld, C.A., Aussignargues, C., Zarzycki, J., Cai, F., and Sutter, M. (2018). Bacterial microcompartments. Nat. Rev. Microbiol. *16*, 277–290.

Kerr, B., Riley, M.A., Feldman, M.W., and Bohannan, B.J.M. (2002). Local dispersal promotes biodiversity in a real-life game of rock–paper–scissors. Nature *418*, 171–174.

Kingry, L.C., and Petersen, J.M. (2014). Comparative review of Francisella tularensis and Francisella novicida. Front. Cell. Infect. Microbiol. *4*, 35.

Kirimanjeswara, G.S., Olmos, S., Bakshi, C.S., and Metzger, D.W. (2008). Humoral and Cell-Mediated Immunity to the Intracellular Pathogen Francisella tularensis. Immunol. Rev. *225*, 244–255.

Kraemer, P.S., Mitchell, A., Pelletier, M.R., Gallagher, L.A., Wasnick, M., Rohmer, L., Brittnacher, M.J., Manoil, C., Skerett, S.J., and Salama, N.R. (2009). Genome-wide screen in Francisella novicida for genes required for pulmonary and systemic infection in mice. Infect. Immun. *77*, 232–244.

Krokowski, S., Atwal, S., Lobato-Márquez, D., Chastanet, A., Carballido-López, R., Salje, J., and Mostowy, S. (2019). Shigella MreB promotes polar IcsA positioning for actin tail formation. J. Cell Sci. *132*.

Kubitschek, H.E. (1990). Cell volume increase in Escherichia coli after shifts to richer media. J. Bacteriol. *172*, 94–101.

Kudryashev, M., Wang, R.Y.-R., Brackmann, M., Scherer, S., Maier, T., Baker, D., DiMaio, F., Stahlberg, H., Egelman, E.H., and Basler, M. (2015). Structure of the type VI secretion system contractile sheath. Cell *160*, 952–962.

Kühn, J., Briegel, A., Mörschel, E., Kahnt, J., Leser, K., Wick, S., Jensen, G.J., and Thanbichler, M. (2010). Bactofilins, a ubiquitous class of cytoskeletal proteins mediating polar localization of a cell wall synthase in Caulobacter crescentus. EMBO J. *29*, 327–339.

Kumar, R.B., and Das, A. (2002). Polar location and functional domains of the Agrobacterium tumefaciens DNA transfer protein VirD4. Mol. Microbiol. *43*, 1523–1532.

Lacerda, T.L.S., Salcedo, S.P., and Gorvel, J.-P. (2013). Brucella T4SS: the VIP pass inside host cells. Curr. Opin. Microbiol. *16*, 45–51.

LaCourse, K.D., Peterson, S.B., Kulasekara, H.D., Radey, M.C., Kim, J., and Mougous, J.D. (2018). Conditional toxicity and synergy drive diversity among antibacterial effectors. Nat. Microbiol.

Lagrange, B., Benaoudia, S., Wallet, P., Magnotti, F., Provost, A., Michal, F., Martin, A., Di Lorenzo, F., Py, B.F., Molinaro, A., et al. (2018). Human caspase-4 detects tetra-acylated LPS and cytosolic Francisella and functions differently from murine caspase-11. Nat. Commun. *9*.

Lampe, E.O., Brenz, Y., Herrmann, L., Repnik, U., Griffiths, G., Zingmark, C., Sjöstedt, A., Winther-Larsen, H.C., and Hagedorn, M. (2015). Dissection of Francisella-Host Cell Interactions in Dictyostelium discoideum. Appl. Environ. Microbiol. *82*, 1586–1598.

Larson, M.H., Gilbert, L.A., Wang, X., Lim, W.A., Weissman, J.S., and Qi, L.S. (2013). CRISPR interference (CRISPRi) for sequence-specific control of gene expression. Nat. Protoc. *8*, 2180–2196.

Larsson, P., Elfsmark, D., Svensson, K., Wikström, P., Forsman, M., Brettin, T., Keim, P., and Johansson, A. (2009). Molecular evolutionary consequences of niche restriction in Francisella tularensis, a facultative intracellular pathogen. PLoS Pathog. *5*, e1000472.

Lasica, A.M., Ksiazek, M., Madej, M., and Potempa, J. (2017). The Type IX Secretion System (T9SS): Highlights and Recent Insights into Its Structure and Function. Front. Cell. Infect. Microbiol. *7*, 215.

Laventie, B.-J., Sangermani, M., Estermann, F., Manfredi, P., Planes, R., Hug, I., Jaeger, T., Meunier, E., Broz, P., and Jenal, U. (2019). A Surface-Induced Asymmetric Program Promotes Tissue Colonization by Pseudomonas aeruginosa. Cell Host Microbe *25*, 140-152.e6.

Lawson, M.J., Camsund, D., Larsson, J., Baltekin, Ö., Fange, D., and Elf, J. (2017). In situ genotyping of a pooled strain library after characterizing complex phenotypes. Mol. Syst. Biol. *13*, 947.

Lazzaro, M., Feldman, M.F., and García Véscovi, E. (2017). A Transcriptional Regulatory Mechanism Finely Tunes the Firing of Type VI Secretion System in Response to Bacterial Enemies. MBio *8*, e00559-17.

Ledvina, H.E., Kelly, K.A., Eshraghi, A., Plemel, R.L., Peterson, S.B., Lee, B., Steele, S., Adler, M., Kawula, T.H., Merz, A.J., et al. (2018). A Phosphatidylinositol 3-Kinase Effector Alters Phagosomal Maturation to Promote Intracellular Growth of Francisella. Cell Host Microbe *24*, 285-295.e8.

Leiman, P.G., Basler, M., Ramagopal, U.A., Bonanno, J.B., Sauder, J.M., Pukatzki, S., Burley, S.K., Almo, S.C., and Mekalanos, J.J. (2009). Type VI secretion apparatus and phage tail-associated protein complexes share a common evolutionary origin. Proc. Natl. Acad. Sci. U. S. A. *106*, 4154–4159.

Leiman, P.G., Arisaka, F., van Raaij, M.J., Kostyuchenko, V.A., Aksyuk, A.A., Kanamaru, S., and Rossmann, M.G. (2010). Morphogenesis of the T4 tail and tail fibers. Virol. J. *7*, 355.

Lenarcic, R., Halbedel, S., Visser, L., Shaw, M., Wu, L.J., Errington, J., Marenduzzo, D., and Hamoen, L.W. (2009). Localisation of DivIVA by targeting to negatively curved membranes. EMBO J. *28*, 2272–2282.

Lenco, J., Pavkova, I., Hubalek, M., and Stulik, J. (2005). Insights into the oxidative stress response in Francisella tularensis LVS and its mutant DeltaiglC1+2 by proteomics analysis. FEMS Microbiol. Lett. *246*, 47–54.

Lennings, J., Mayer, C., Makhlouf, M., Brötz-Oesterhelt, H., and Schwarz, S. (2019). Polar localization of the ATPase ClpV-5 occurs independent of type VI secretion system apparatus proteins in Burkholderia thailandensis. BMC Res. Notes *12*, 109.

LeRoux, M., Kirkpatrick, R.L., Montauti, E.I., Tran, B.Q., Peterson, S.B., Harding, B.N., Whitney, J.C., Russell, A.B., Traxler, B., Goo, Y.A., et al. (2015). Kin cell lysis is a danger signal that activates antibacterial pathways of Pseudomonas aeruginosa. ELife *4*.

Lesic, B., Starkey, M., He, J., Hazan, R., and Rahme, L.G. (2009). Quorum sensing differentially regulates Pseudomonas aeruginosa type VI secretion locus I and homologous loci II and III, which are required for pathogenesis. Microbiology *155*, 2845–2855.

Leung, K.Y., Siame, B.A., Snowball, H., and Mok, Y.-K. (2011). Type VI secretion regulation: crosstalk and intracellular communication. Curr. Opin. Microbiol. *14*, 9–15.

Li, D., Shao, L., Chen, B.-C., Zhang, X., Zhang, M., Moses, B., Milkie, D.E., Beach, J.R., Hammer, J.A., Pasham, M., et al. (2015). ADVANCED IMAGING. Extended-resolution structured illumination imaging of endocytic and cytoskeletal dynamics. Science *349*, aab3500.

Li, M., Le Trong, I., Carl, M.A., Larson, E.T., Chou, S., De Leon, J.A., Dove, S.L., Stenkamp, R.E., and Mougous, J.D. (2012). Structural basis for type VI secretion effector recognition by a cognate immunity protein. PLoS Pathog. *8*, e1002613.

Li, S., Li, T., Xu, Y., Zhang, Q., Zhang, W., Che, S., Liu, R., Wang, Y., and Bartlam, M. (2015). Structural insights into YfiR sequestering by YfiB in Pseudomonas aeruginosa PAO1. Sci. Rep. *5*, 16915.

Liang, X., Moore, R., Wilton, M., Wong, M.J.Q., Lam, L., and Dong, T.G. (2015). Identification of divergent type VI secretion effectors using a conserved chaperone domain. Proc. Natl. Acad. Sci. U. S. A. *112*, 9106–9111.

Liebl, D., Robert-Genthon, M., Job, V., Cogoni, V., and ATTREE, I. (2019). Baseplate component TssK and spatio-temporal assembly of T6SS in Pseudomonas aeruginosa. Front. Microbiol. *10*, 1615.

Lien, Y.-W., and Lai, E.-M. (2017). Type VI Secretion Effectors: Methodologies and Biology. Front. Cell. Infect. Microbiol. *7*, 254.

Lima, S., Guo, M.S., Chaba, R., Gross, C.A., and Sauer, R.T. (2013). Dual molecular signals mediate the bacterial response to outer-membrane stress. Science *340*, 837–841.

Lin, L., and Thanbichler, M. (2013). Nucleotide-independent cytoskeletal scaffolds in bacteria. Cytoskelet. Hoboken NJ *70*, 409–423.

Lin, J., Zhang, W., Cheng, J., Yang, X., Zhu, K., Wang, Y., Wei, G., Qian, P.-Y., Luo, Z.-Q., and Shen, X. (2017). A Pseudomonas T6SS effector recruits PQS-containing outer membrane vesicles for iron acquisition. Nat. Commun. *8*, 14888.

Lin, J.-S., Wu, H.-H., Hsu, P.-H., Ma, L.-S., Pang, Y.-Y., Tsai, M.-D., and Lai, E.-M. (2014). Fha Interaction with Phosphothreonine of TssL Activates Type VI Secretion in Agrobacterium tumefaciens. PLoS Pathog. *10*, e1003991.

Lin, J.-S., Pissaridou, P., Wu, H.-H., Tsai, M.-D., Filloux, A., and Lai, E.-M. (2018). TagF-mediated repression of bacterial type VI secretion systems involves a direct interaction with the cytoplasmic protein Fha. J. Biol. Chem.

Lin, L., Lezan, E., Schmidt, A., and Basler, M. (2019). Abundance of bacterial Type VI secretion system components measured by targeted proteomics. Nat. Commun. *10*, 2584.

Lindemann, S.R., Peng, K., Long, M.E., Hunt, J.R., Apicella, M.A., Monack, D.M., Allen, L.-A.H., and Jones, B.D. (2011). Francisella tularensis Schu S4 O-antigen and capsule biosynthesis gene mutants induce early cell death in human macrophages. Infect. Immun. *79*, 581–594.

Lindgren, H., Shen, H., Zingmark, C., Golovliov, I., Conlan, W., and Sjöstedt, A. (2007). Resistance of Francisella tularensis strains against reactive nitrogen and oxygen species with special reference to the role of KatG. Infect. Immun. *75*, 1303–1309.

Lindgren, M., Bröms, J.E., Meyer, L., Golovliov, I., and Sjöstedt, A. (2013). The Francisella tularensis LVS ΔpdpC mutant exhibits a unique phenotype during intracellular infection. BMC Microbiol. *13*, 20.

Lo, K.Y., Visram, S., Vogl, A.W., Shen, C.L.J., and Guttman, J.A. (2016). Morphological analysis of Francisella novicida epithelial cell infections in the absence of functional FipA. Cell Tissue Res. *363*, 449–459.

Long, M.E., Lindemann, S.R., Rasmussen, J.A., Jones, B.D., and Allen, L.-A.H. (2013). Disruption of Francisella tularensis Schu S4 iglI, iglJ, and pdpC Genes Results in Attenuation for Growth in Human Macrophages and In Vivo Virulence in Mice and Reveals a Unique Phenotype for pdpC. Infect. Immun. *81*, 850–861.

van Loosdrecht, M.C., Lyklema, J., Norde, W., and Zehnder, A.J. (1989). Bacterial adhesion: A physicochemical approach. Microb. Ecol. *17*, 1–15.

López-Marqués, R.L., Pérez-Castiñeira, J.R., Losada, M., and Serrano, A. (2004). Differential regulation of soluble and membrane-bound inorganic pyrophosphatases in the photosynthetic bacterium Rhodospirillum rubrum provides insights into pyrophosphate-based stress bioenergetics. J. Bacteriol. *186*, 5418–5426.

Lossi, N.S., Dajani, R., Freemont, P., and Filloux, A. (2011). Structure-function analysis of HsiF, a gp25-like component of the type VI secretion system, in Pseudomonas aeruginosa. Microbiol. Read. Engl. *157*, 3292–3305.

Lossi, N.S., Manoli, E., Simpson, P., Jones, C., Hui, K., Dajani, R., Coulthurst, S.J., Freemont, P., and Filloux, A. (2012). The archetype Pseudomonas aeruginosa proteins TssB and TagJ form a novel subcomplex in the bacterial type VI secretion system. Mol. Microbiol. *86*, 437–456.

LoVullo, E.D., Sherrill, L.A., Perez, L.L., and Pavelka, M.S. (2006). Genetic tools for highly pathogenic Francisella tularensis subsp. tularensis. Microbiology *152*, 3425–3435.

Ludu, J.S., de Bruin, O.M., Duplantis, B.N., Schmerk, C.L., Chou, A.Y., Elkins, K.L., and Nano, F.E. (2008). The Francisella pathogenicity island protein PdpD is required for full virulence and associates with homologues of the type VI secretion system. J. Bacteriol. *190*, 4584–4595.

Ma, J., Pan, Z., Huang, J., Sun, M., Lu, C., and Yao, H. (2017). The Hcp proteins fused with diverse extended-toxin domains represent a novel pattern of antibacterial effectors in type VI secretion systems. Virulence *8*, 1189–1202.

Ma, L.-S., Lin, J.-S., and Lai, E.-M. (2009). An IcmF family protein, ImpLM, is an integral inner membrane protein interacting with ImpKL, and its walker a motif is required for type VI secretion system-mediated Hcp secretion in Agrobacterium tumefaciens. J. Bacteriol. *191*, 4316–4329.

Ma, L.-S., Narberhaus, F., and Lai, E.-M. (2012). IcmF Family Protein TssM Exhibits ATPase Activity and Energizes Type VI Secretion. J. Biol. Chem. *287*, 15610–15621.

Mac Síomóin, R.A., Nakata, N., Murai, T., Yoshikawa, M., Tsuji, H., and Sasakawa, C. (1996). Identification and characterization of ispA, a Shigella flexneri chromosomal gene essential for normal in vivo cell division and intracellular spreading. Mol. Microbiol. *19*, 599–609.

Maier, T.M., Havig, A., Casey, M., Nano, F.E., Frank, D.W., and Zahrt, T.C. (2004). Construction and characterization of a highly efficient Francisella shuttle plasmid. Appl. Environ. Microbiol. *70*, 7511–7519.

Malone, J.G., Jaeger, T., Spangler, C., Ritz, D., Spang, A., Arrieumerlou, C., Kaever, V., Landmann, R., and Jenal, U. (2010). YfiBNR mediates cyclic di-GMP dependent small colony variant formation and persistence in Pseudomonas aeruginosa. PLoS Pathog. *6*, e1000804.

Malone, J.G., Jaeger, T., Manfredi, P., Dötsch, A., Blanka, A., Bos, R., Cornelis, G.R., Häussler, S., and Jenal, U. (2012). The YfiBNR signal transduction mechanism reveals novel targets for the evolution of persistent Pseudomonas aeruginosa in cystic fibrosis airways. PLoS Pathog. *8*, e1002760.

Masuda, N., Sakagawa, E., Ohya, S., Gotoh, N., Tsujimoto, H., and Nishino, T. (2000). Substrate Specificities of MexAB-OprM, MexCD-OprJ, and MexXY-OprM Efflux Pumps in Pseudomonas aeruginosa. Antimicrob. Agents Chemother. *44*, 3322–3327.

Mathee, K., Narasimhan, G., Valdes, C., Qiu, X., Matewish, J.M., Koehrsen, M., Rokas, A., Yandava, C.N., Engels, R., Zeng, E., et al. (2008). Dynamics of Pseudomonas aeruginosa genome evolution. Proc. Natl. Acad. Sci. U. S. A. *105*, 3100–3105.

Matthysse, A.G. (1987). Characterization of nonattaching mutants of Agrobacterium tumefaciens. J. Bacteriol. *169*, 313–323.

McLendon, M.K., Apicella, M.A., and Allen, L.-A.H. (2006). Francisella tularensis: Taxonomy, Genetics, and Immunopathogenesis of a Potential Agent of Biowarfare. Annu. Rev. Microbiol. *60*, 167–185.

McNally, L., Bernardy, E., Thomas, J., Kalziqi, A., Pentz, J., Brown, S.P., Hammer, B.K., Yunker, P.J., and Ratcliff, W.C. (2017). Killing by Type VI secretion drives genetic phase separation and correlates with increased cooperation. Nat. Commun. *8*, 14371.

Megaw, J., Thompson, T.P., Lafferty, R.A., and Gilmore, B.F. (2015). Galleria mellonella as a novel in vivo model for assessment of the toxicity of 1-alkyl-3-methylimidazolium chloride ionic liquids. Chemosphere *139*, 197–201.

Meibom, K.L., Dubail, I., Dupuis, M., Barel, M., Lenco, J., Stulik, J., Golovliov, I., Sjöstedt, A., and Charbit, A. (2008). The heat-shock protein ClpB of Francisella tularensis is involved in stress tolerance and is required for multiplication in target organs of infected mice. Mol. Microbiol. *67*, 1384–1401.

Meibom, K.L., Forslund, A.-L., Kuoppa, K., Alkhuder, K., Dubail, I., Dupuis, M., Forsberg, A., and Charbit, A. (2009). Hfq, a novel pleiotropic regulator of virulence-associated genes in Francisella tularensis. Infect. Immun. *77*, 1866–1880.

Merdanovic, M., Clausen, T., Kaiser, M., Huber, R., and Ehrmann, M. (2011). Protein quality control in the bacterial periplasm. Annu. Rev. Microbiol. *65*, 149–168.

Meunier, E., Wallet, P., Dreier, R.F., Costanzo, S., Anton, L., Ruhl, S., Dussurgey, S., Dick, M.S., Kistner, A., Rigard, M., et al. (2015). Guanylate-binding proteins promote activation of the AIM2 inflammasome during infection with Francisella novicida. Nat Immunol *advance online publication*.

Meyer, L., Bröms, J.E., Liu, X., Rottenberg, M.E., and Sjöstedt, A. (2015). Microinjection of Francisella tularensis and Listeria monocytogenes reveals the importance of bacterial and host factors for successful replication. Infect. Immun. *83*, 3233–3242.

Mitri, S., Xavier, J.B., and Foster, K.R. (2011). Social evolution in multispecies biofilms. Proc. Natl. Acad. Sci. U. S. A. *108 Suppl 2*, 10839–10846.

Miyata, S.T., Bachmann, V., and Pukatzki, S. (2013). Type VI secretion system regulation as a consequence of evolutionary pressure. J. Med. Microbiol. *62*, 663–676.

Moradali, M.F., Ghods, S., and Rehm, B.H.A. (2017). Pseudomonas aeruginosa Lifestyle: A Paradigm for Adaptation, Survival, and Persistence. Front. Cell. Infect. Microbiol. *7*, 39.

Morgan, J.K., Luedtke, B.E., and Shaw, E.I. (2010). Polar localization of the Coxiella burnetii type IVB secretion system. FEMS Microbiol. Lett. *305*, 177–183.

Morlot, C., Uehara, T., Marquis, K.A., Bernhardt, T.G., and Rudner, D.Z. (2010). A highly coordinated cell wall degradation machine governs spore morphogenesis in Bacillus subtilis. Genes Dev. *24*, 411–422.

Motley, S.T., and Lory, S. (1999). Functional characterization of a serine/threonine protein kinase of Pseudomonas aeruginosa. Infect. Immun. *67*, 5386–5394.

Mougous, J.D., Cuff, M.E., Raunser, S., Shen, A., Zhou, M., Gifford, C.A., Goodman, A.L., Joachimiak, G., Ordoñez, C.L., Lory, S., et al. (2006). A Virulence Locus of Pseudomonas aeruginosa Encodes a Protein Secretion Apparatus. Science *312*, 1526–1530.

Mougous, J.D., Gifford, C.A., Ramsdell, T.L., and Mekalanos, J.J. (2007). Threonine phosphorylation post-translationally regulates protein secretion in Pseudomonas aeruginosa. Nat Cell Biol *9*, 797–803.

Nakata, N., Sasakawa, C., Okada, N., Tobe, T., Fukuda, I., Suzuki, T., Komatsu, K., and Yoshikawa, M. (1992). Identification and characterization of virK, a virulence-associated large plasmid gene essential for intercellular spreading of Shigella flexneri. Mol. Microbiol. *6*, 2387–2395.

Nano, F.E., and Schmerk, C. (2007). The Francisella pathogenicity island. Ann. N. Y. Acad. Sci. *1105*, 122–137.

Nano, F.E., Zhang, N., Cowley, S.C., Klose, K.E., Cheung, K.K.M., Roberts, M.J., Ludu, J.S., Letendre, G.W., Meierovics, A.I., Stephens, G., et al. (2004). A Francisella tularensis Pathogenicity Island Required for Intramacrophage Growth. J. Bacteriol. *186*, 6430–6436.

Narita, S., and Tokuda, H. (2006). An ABC transporter mediating the membrane detachment of bacterial lipoproteins depending on their sorting signals. FEBS Lett. *580*, 1164–1170.

Narita, S., and Tokuda, H. (2007). Amino Acids at Positions 3 and 4 Determine the Membrane Specificity of Pseudomonas aeruginosa Lipoproteins. J. Biol. Chem. *282*, 13372–13378.

Nazarov, S., Schneider, J.P., Brackmann, M., Goldie, K.N., Stahlberg, H., and Basler, M. (2018). Cryo-EM reconstruction of Type VI secretion system baseplate and sheath distal end. EMBO J. *37*.

Neumann, S., Wessels, H.J.C.T., Rijpstra, W.I.C., Sinninghe Damsté, J.S., Kartal, B., Jetten, M.S.M., and van Niftrik, L. (2014). Isolation and characterization of a prokaryotic cell organelle from the anammox bacterium Kuenenia stuttgartiensis. Mol. Microbiol. *94*, 794–802.

Nguyen, J.Q., Gilley, R.P., Zogaj, X., Rodriguez, S.A., and Klose, K.E. (2014). Lipidation of the FPI protein IglE contributes to Francisella tularensis ssp. novicida intramacrophage replication and virulence. Pathog. Dis. *72*, 10–18.

Nguyen, V.S., Logger, L., Spinelli, S., Legrand, P., Huyen Pham, T.T., Nhung Trinh, T.T., Cherrak, Y., Zoued, A., Desmyter, A., Durand, E., et al. (2017). Type VI secretion TssK baseplate protein exhibits structural similarity with phage receptor-binding proteins and evolved to bind the membrane complex. Nat. Microbiol. *2*, 17103.

Nguyen, V.S., Douzi, B., Durand, E., Roussel, A., Cascales, E., and Cambillau, C. (2018). Towards a complete structural deciphering of Type VI secretion system. Curr. Opin. Struct. Biol. *49*, 77–84.

Nikaido, H. (2003). Molecular basis of bacterial outer membrane permeability revisited. Microbiol. Mol. Biol. Rev. MMBR *67*, 593–656.

Nikolaus, T., Deiwick, J., Rappl, C., Freeman, J.A., Schröder, W., Miller, S.I., and Hensel, M. (2001). SseBCD proteins are secreted by the type III secretion system of Salmonella pathogenicity island 2 and function as a translocon. J. Bacteriol. *183*, 6036–6045.

Norqvist, A., Kuoppa, K., and Sandström, G. (1996). Construction of a shuttle vector for use in Francisella tularensis. FEMS Immunol. Med. Microbiol. *13*, 257–260.

Nowak, M.A. (2006). Five rules for the evolution of cooperation. Science *314*, 1560–1563.

Nuñez, I.N., Matute, T.F., Del Valle, I.D., Kan, A., Choksi, A., Endy, D., Haseloff, J., Rudge, T.J., and Federici, F. (2016). Artifical Symmetry-Breaking for Morphogenetic Engineering Bacterial Colonies. ACS Synth. Biol. *6*, 256–265.

Okuda, S., and Tokuda, H. (2011). Lipoprotein sorting in bacteria. Annu. Rev. Microbiol. *65*, 239–259.

Olshausen, P.V., Defeu Soufo, H.J., Wicker, K., Heintzmann, R., Graumann, P.L., and Rohrbach, A. (2013). Superresolution imaging of dynamic MreB filaments in B. subtilis--a multiple-motor-driven transport? Biophys. J. *105*, 1171–1181.

Ostrowski, A., Cianfanelli, F.R., Porter, M., Mariano, G., Peltier, J., Wong, J.J., Swedlow, J.R., Trost, M., and Coulthurst, S.J. (2018). Killing with proficiency: Integrated post-translational regulation of an offensive Type VI secretion system. PLoS Pathog. *14*, e1007230.

Oyston, P.C.F., Sjostedt, A., and Titball, R.W. (2004). Tularaemia: bioterrorism defence renews interest in Francisella tularensis. Nat. Rev. Microbiol. *2*, 967–978.

Ozanic, M., Marecic, V., Abu Kwaik, Y., and Santic, M. (2015). The Divergent Intracellular Lifestyle of Francisella tularensis in Evolutionarily Distinct Host Cells. PLoS Pathog. *11*, e1005208.

Ozanic, M., Marecic, V., Lindgren, M., Sjöstedt, A., and Santic, M. (2016). Phenotypic characterization of the Francisella tularensis ΔpdpC and ΔiglG mutants. Microbes Infect. *18*, 768–776.

Palmer, T., and Berks, B.C. (2012). The twin-arginine translocation (Tat) protein export pathway. Nat. Rev. Microbiol. *10*, 483–496.

Park, K.-T., Wu, W., Battaile, K.P., Lovell, S., Holyoak, T., and Lutkenhaus, J. (2011). The Min oscillator uses MinD-dependent conformational changes in MinE to spatially regulate cytokinesis. Cell *146*, 396–407.

Park, Y.-J., Lacourse, K.D., Cambillau, C., DiMaio, F., Mougous, J.D., and Veesler, D. (2018). Structure of the type VI secretion system TssK-TssF-TssG baseplate subcomplex revealed by cryo-electron microscopy. Nat. Commun. *9*, 5385.

Parsons, D.A., and Heffron, F. (2005). sciS, an icmF homolog in Salmonella enterica serovar Typhimurium, limits intracellular replication and decreases virulence. Infect. Immun. *73*, 4338–4345.

de Pedro, M.A., Grünfelder, C.G., and Schwarz, H. (2004). Restricted Mobility of Cell Surface Proteins in the Polar Regions of Escherichia coli. J. Bacteriol. *186*, 2594–2602.

Peters, J.M., Colavin, A., Shi, H., Czarny, T.L., Larson, M.H., Wong, S., Hawkins, J.S., Lu, C.H.S., Koo, B.-M., Marta, E., et al. (2016). A Comprehensive, CRISPR-based Functional Analysis of Essential Genes in Bacteria. Cell *165*, 1493–1506.

Peters, N.T., Dinh, T., and Bernhardt, T.G. (2011). A fail-safe mechanism in the septal ring assembly pathway generated by the sequential recruitment of cell separation amidases and their activators. J. Bacteriol. *193*, 4973–4983.

Pietrosiuk, A., Lenherr, E.D., Falk, S., Bönemann, G., Kopp, J., Zentgraf, H., Sinning, I., and Mogk, A. (2011). Molecular basis for the unique role of the AAA+ chaperone ClpV in type VI protein secretion. J. Biol. Chem. *286*, 30010–30021.

Planamente, S., Salih, O., Manoli, E., Albesa-Jové, D., Freemont, P.S., and Filloux, A. (2016). TssA forms a gp6-like ring attached to the type VI secretion sheath. EMBO J. *35*, 1613–1627.

Pukatzki, S., Ma, A.T., Sturtevant, D., Krastins, B., Sarracino, D., Nelson, W.C., Heidelberg, J.F., and Mekalanos, J.J. (2006). Identification of a conserved bacterial protein secretion system in Vibrio cholerae using the Dictyostelium host model system. Proc. Natl. Acad. Sci. U. S. A. *103*, 1528–1533.

Pukatzki, S., Ma, A.T., Revel, A.T., Sturtevant, D., and Mekalanos, J.J. (2007). Type VI secretion system translocates a phage tail spike-like protein into target cells where it cross-links actin. Proc. Natl. Acad. Sci. U. S. A. *104*, 15508–15513.

Qin, A., Zhang, Y., Clark, M.E., Moore, E.A., Rabideau, M.M., Moreau, G.B., and Mann, B.J. (2016). Components of the type six secretion system are substrates of Francisella tularensis Schu S4 DsbA-like FipB protein. Virulence *7*, 882–894.

Qiu, J., and Luo, Z.-Q. (2017). Legionella and Coxiella effectors: strength in diversity and activity. Nat. Rev. Microbiol. *15*, 591–605.

Quintela, J.C., de Pedro, M.A., Zöllner, P., Allmaier, G., and Garcia-del Portillo, F. (1997). Peptidoglycan structure of Salmonella typhimurium growing within cultured mammalian cells. Mol. Microbiol. *23*, 693–704.

Ramamurthi, K.S., Lecuyer, S., Stone, H.A., and Losick, R. (2009). Geometric cue for protein localization in a bacterium. Science *323*, 1354–1357.

Ramarao, N., Nielsen-Leroux, C., and Lereclus, D. (2012). The insect Galleria mellonella as a powerful infection model to investigate bacterial pathogenesis. J. Vis. Exp. JoVE e4392.

Ramond, E., Gesbert, G., Guerrera, I.C., Chhuon, C., Dupuis, M., Rigard, M., Henry, T., Barel, M., and Charbit, A. (2015). Importance of host cell arginine uptake in Francisella phagosomal escape and ribosomal protein amounts. Mol. Cell. Proteomics MCP *14*, 870–881.

Rapisarda, C., Cherrak, Y., Kooger, R., Schmidt, V., Pellarin, R., Logger, L., Cascales, E., Pilhofer, M., Durand, E., and Fronzes, R. (2019). In situ and high-resolution cryo-EM structure of a bacterial type VI secretion system membrane complex. EMBO J.

Raskin, D.M., and de Boer, P.A. (1999). MinDE-dependent pole-to-pole oscillation of division inhibitor MinC in Escherichia coli. J. Bacteriol. *181*, 6419–6424.

Ratner, H.K., Escalera-Maurer, A., Le Rhun, A., Jaggavarapu, S., Wozniak, J.E., Crispell, E.K., Charpentier, E., and Weiss, D.S. (2019). Catalytically Active Cas9 Mediates Transcriptional Interference to Facilitate Bacterial Virulence. Mol. Cell.

Ray, H.J., Chu, P., Wu, T.H., Lyons, C.R., Murthy, A.K., Guentzel, M.N., Klose, K.E., and Arulanandam, B.P. (2010). The Fischer 344 rat reflects human susceptibility to francisella pulmonary challenge and provides a new platform for virulence and protection studies. PloS One *5*, e9952.

Read, A., Vogl, S.J., Hueffer, K., Gallagher, L.A., and Happ, G.M. (2008). Francisella genes required for replication in mosquito cells. J. Med. Entomol. *45*, 1108–1116.

Renault, M.G., Zamarreno Beas, J., Douzi, B., Chabalier, M., Zoued, A., Brunet, Y.R., Cambillau, C., Journet, L., and Cascales, E. (2018). The gp27-like Hub of VgrG Serves as Adaptor to Promote Hcp Tube Assembly. J. Mol. Biol. *430*, 3143–3156.

Rick Lyons, C., and Wu, T.H. (2007). Animal models of Francisella tularensis infection. Ann. N. Y. Acad. Sci. *1105*, 238–265.

Rietsch, A., Vallet-Gely, I., Dove, S.L., and Mekalanos, J.J. (2005). ExsE, a secreted regulator of type III secretion genes in Pseudomonas aeruginosa. Proc. Natl. Acad. Sci. U. S. A. *102*, 8006–8011.

Rigard, M., Bröms, J.E., Mosnier, A., Hologne, M., Martin, A., Lindgren, L., Punginelli, C., Lays, C., Walker, O., Charbit, A., et al. (2016). Francisella tularensis IglG Belongs to a Novel Family of PAAR-Like T6SS Proteins and Harbors a Unique N-terminal Extension Required for Virulence. PLoS Pathog. *12*, e1005821.

Ringel, P.D., Hu, D., and Basler, M. (2017). The Role of Type VI Secretion System Effectors in Target Cell Lysis and Subsequent Horizontal Gene Transfer. Cell Rep. *21*, 3927–3940.

Ringgaard, S., van Zon, J., Howard, M., and Gerdes, K. (2009). Movement and equipositioning of plasmids by ParA filament disassembly. Proc. Natl. Acad. Sci. U. S. A. *106*, 19369–19374.

Robb, C.S., Nano, F.E., and Boraston, A.B. (2012). The structure of the conserved type six secretion protein TssL (DotU) from Francisella novicida. J. Mol. Biol. *419*, 277–283.

Rosch, J., and Caparon, M. (2004). A microdomain for protein secretion in Gram-positive bacteria. Science *304*, 1513–1515.

Rosch, J.W., and Caparon, M.G. (2005). The ExPortal: an organelle dedicated to the biogenesis of secreted proteins in Streptococcus pyogenes. Mol. Microbiol. *58*, 959–968.

Rossetti, V., Schirrmeister, B.E., Bernasconi, M.V., and Bagheri, H.C. (2010). The evolutionary path to terminal differentiation and division of labor in cyanobacteria. J. Theor. Biol. *262*, 23–34.

Rowlett, V.W., and Margolin, W. (2013). The bacterial Min system. Curr. Biol. CB *23*, R553-556.

Rudge, T.J., Steiner, P.J., Phillips, A., and Haseloff, J. (2012). Computational Modeling of Synthetic Microbial Biofilms. ACS Synth. Biol. *1*, 345–352.

Rudge, T.J., Steiner, P.J., Kan, A., and Haseloff, J. (2013). Cell Polarity-Driven Instability Generates Self-Organized, Fractal Patterning of Cell Layers. ACS Synth Biol 705–714.

Ruiz, N., Kahne, D., and Silhavy, T.J. (2009). Transport of lipopolysaccharide across the cell envelope: the long road of discovery. Nat. Rev. Microbiol. *7*, 677–683.

Russell, A.B., Hood, R.D., Bui, N.K., LeRoux, M., Vollmer, W., and Mougous, J.D. (2011). Type VI secretion delivers bacteriolytic effectors to target cells. Nature *475*, 343–347.

Russell, A.B., LeRoux, M., Hathazi, K., Agnello, D.M., Ishikawa, T., Wiggins, P.A., Wai, S.N., and Mougous, J.D. (2013). Diverse type VI secretion phospholipases are functionally plastic antibacterial effectors. Nature *496*, 508–512.

Russell, A.B., Wexler, A.G., Harding, B.N., Whitney, J.C., Bohn, A.J., Goo, Y.A., Tran, B.Q., Barry, N.A., Zheng, H., Peterson, S.B., et al. (2014). A type VI secretion-related pathway in Bacteroidetes mediates interbacterial antagonism. Cell Host Microbe *16*, 227–236.

Saberi, S., and Emberly, E. (2010). Chromosome driven spatial patterning of proteins in bacteria. PLoS Comput. Biol. *6*, e1000986.

Salih, O., He, S., Planamente, S., Stach, L., MacDonald, J.T., Manoli, E., Scheres, S.H.W., Filloux, A., and Freemont, P.S. (2018). Atomic Structure of Type VI Contractile Sheath from Pseudomonas aeruginosa. Struct. Lond. Engl. 1993 *26*, 329-336.e3.

Sampson, T.R., Napier, B.A., Schroeder, M.R., Louwen, R., Zhao, J., Chin, C.-Y., Ratner, H.K., Llewellyn, A.C., Jones, C.L., Laroui, H., et al. (2014). A CRISPR-Cas system enhances envelope integrity mediating antibiotic resistance and inflammasome evasion. Proc. Natl. Acad. Sci. U. S. A. *111*, 11163–11168.

Sangermani, M., Hug, I., Sauter, N., Pfohl, T., and Jenal, U. (2019). Tad pili play a dynamic role in Caulobacter crescentus surface colonization. BioRxiv 526160.

Santic, M., Molmeret, M., Klose, K.E., Jones, S., and Kwaik, Y.A. (2005). The Francisella tularensis pathogenicity island protein IglC and its regulator MglA are essential for modulating phagosome biogenesis and subsequent bacterial escape into the cytoplasm. Cell. Microbiol. *7*, 969–979.

Santic, M., Asare, R., Skrobonja, I., Jones, S., and Abu Kwaik, Y. (2008). Acquisition of the Vacuolar ATPase Proton Pump and Phagosome Acidification Are Essential for Escape of Francisella tularensis into the Macrophage Cytosol. Infect. Immun. *76*, 2671–2677.

Santic, M., Ozanic, M., Semic, V., Pavokovic, G., Mrvcic, V., and Kwaik, Y.A. (2011). Intra-Vacuolar Proliferation of F. Novicida within H. Vermiformis. Front. Microbiol. *2*, 78.

Santin, Y.G., and Cascales, E. (2017). Domestication of a housekeeping transglycosylase for assembly of a Type VI secretion system. EMBO Rep. *18*, 138–149.

Santin, Y.G., Doan, T., Lebrun, R., Espinosa, L., Journet, L., and Cascales, E. (2018). In vivo TssA proximity labelling during type VI secretion biogenesis reveals TagA as a protein that stops and holds the sheath. Nat. Microbiol. *3*, 1304–1313.

Santin, Y.G., Camy, C.E., Zoued, A., Doan, T., Aschtgen, M.-S., and Cascales, E. (2019). Role and recruitment of the TagL peptidoglycan-binding protein during Type VI secretion system biogenesis. J. Bacteriol.

Savage, D.F., Afonso, B., Chen, A.H., and Silver, P.A. (2010). Spatially ordered dynamics of the bacterial carbon fixation machinery. Science *327*, 1258–1261.

Schermelleh, L., Ferrand, A., Huser, T., Eggeling, C., Sauer, M., Biehlmaier, O., and Drummen, G.P.C. (2019). Super-resolution microscopy demystified. Nat. Cell Biol. *21*, 72–84.

Scheurwater, E.M., and Burrows, L.L. (2011). Maintaining network security: how macromolecular structures cross the peptidoglycan layer. FEMS Microbiol. Lett. *318*, 1–9.

Scheurwater, E., Reid, C.W., and Clarke, A.J. (2008). Lytic transglycosylases: bacterial space-making autolysins. Int. J. Biochem. Cell Biol. *40*, 586–591.

Schindelin, J., Arganda-Carreras, I., Frise, E., Kaynig, V., Longair, M., Pietzsch, T., Preibisch, S., Rueden, C., Saalfeld, S., Schmid, B., et al. (2012). Fiji: an open-source platform for biological-image analysis. Nat. Methods *9*, 676–682.

Schmitt, D.M., Barnes, R., Rogerson, T., Haught, A., Mazzella, L.K., Ford, M., Gilson, T., Birch, J.W.-M., Sjöstedt, A., Reed, D.S., et al. (2017). The Role and Mechanism of Erythrocyte Invasion by Francisella tularensis. Front. Cell. Infect. Microbiol. *7*, 173.

Schneider, J.P., and Basler, M. (2016). Shedding light on biology of bacterial cells. Philos. Trans. R. Soc. Lond. B. Biol. Sci. *371*.

Schneider, P.J., and Eberly, D.H. (2002). Geometric Tools For Computer Graphics (Elsevier).

Schneider, J.P., Nazarov, S., Adaixo, R., Liuzzo, M., Ringel, P.D., Stahlberg, H., and Basler, M. (2019). Diverse roles of TssA-like proteins in the assembly of bacterial type VI secretion systems. EMBO J. *0*, e100825.

Schwarz, S., West, T.E., Boyer, F., Chiang, W.-C., Carl, M.A., Hood, R.D., Rohmer, L., Tolker-Nielsen, T., Skerrett, S.J., and Mougous, J.D. (2010). Burkholderia type VI secretion systems have distinct roles in eukaryotic and bacterial cell interactions. PLoS Pathog. *6*, e1001068.

Schwarz, S., Singh, P., Robertson, J.D., LeRoux, M., Skerrett, S.J., Goodlett, D.R., West, T.E., and Mougous, J.D. (2014). VgrG-5 is a Burkholderia type VI secretion system-exported protein required for multinucleated giant cell formation and virulence. Infect. Immun. *82*, 1445–1452.

Scott, M.E., Dossani, Z.Y., and Sandkvist, M. (2001). Directed polar secretion of protease from single cells of Vibrio cholerae via the type II secretion pathway. Proc. Natl. Acad. Sci. U. S. A. *98*, 13978–13983.

Scribano, D., Petrucca, A., Pompili, M., Ambrosi, C., Bruni, E., Zagaglia, C., Prosseda, G., Nencioni, L., Casalino, M., Polticelli, F., et al. (2014). Polar localization of PhoN2, a periplasmic virulence-associated factor of Shigella flexneri, is required for proper IcsA exposition at the old bacterial pole. PloS One *9*, e90230.

Senf, F., Tommassen, J., and Koster, M. (2008). Polar secretion of proteins via the Xcp type II secretion system in Pseudomonas aeruginosa. Microbiol. Read. Engl. *154*, 3025–3032.

Seufferheld, M., Vieira, M.C.F., Ruiz, F.A., Rodrigues, C.O., Moreno, S.N.J., and Docampo, R. (2003). Identification of organelles in bacteria similar to acidocalcisomes of unicellular eukaryotes. J. Biol. Chem. *278*, 29971–29978.

Seydel, A., Gounon, P., and Pugsley, A.P. (1999). Testing the "+2 rule" for lipoprotein sorting in the Escherichia coli cell envelope with a new genetic selection. Mol. Microbiol. *34*, 810–821.

Shapiro, L., McAdams, H.H., and Losick, R. (2009). Why and How Bacteria Localize Proteins. Science *326*, 1225–1228.

Shneider, M.M., Buth, S.A., Ho, B.T., Basler, M., Mekalanos, J.J., and Leiman, P.G. (2013). PAAR-repeat proteins sharpen and diversify the type VI secretion system spike. Nature *500*, 350–353.

Si, M., Zhao, C., Burkinshaw, B., Zhang, B., Wei, D., Wang, Y., Dong, T.G., and Shen, X. (2017). Manganese scavenging and oxidative stress response mediated by type VI secretion system in Burkholderia thailandensis. Proc. Natl. Acad. Sci. U. S. A. *114*, E2233–E2242.

Silhavy, T.J., Kahne, D., and Walker, S. (2010). The bacterial cell envelope. Cold Spring Harb. Perspect. Biol. *2*, a000414.

Silverman, J.M., Austin, L.S., Hsu, F., Hicks, K.G., Hood, R.D., and Mougous, J.D. (2011). Separate inputs modulate phosphorylation-dependent and -independent type VI secretion activation. Mol. Microbiol. *82*, 1277–1290.

Smith, W.P.J., Davit, Y., Osborne, J.M., Kim, W., Foster, K.R., and Pitt-Francis, J.M. (2016). Cell morphology drives spatial patterning in microbial communities. Proc. Natl. Acad. Sci. E280–E286.

Smith, W.P.J., Vettiger, A., Winter, J., Ryser, T., Comstock, L.E., Basler, M., and Foster, K.R. (2019). The Evolution of the Type VI Secretion System as a Lytic Weapon. TBC.

Spreitzer, R.J., and Salvucci, M.E. (2002). Rubisco: structure, regulatory interactions, and possibilities for a better enzyme. Annu. Rev. Plant Biol. *53*, 449–475.

Steinhauer, J., Agha, R., Pham, T., Varga, A.W., and Goldberg, M.B. (1999). The unipolar Shigella surface protein IcsA is targeted directly to the bacterial old pole: IcsP cleavage of IcsA occurs over the entire bacterial surface. Mol. Microbiol. *32*, 367–377.

Stewart, E.J., Madden, R., Paul, G., and Taddei, F. (2005). Aging and death in an organism that reproduces by morphologically symmetric division. PLoS Biol. *3*, e45.

Strahl, H., Ronneau, S., González, B.S., Klutsch, D., Schaffner-Barbero, C., and Hamoen, L.W. (2015). Transmembrane protein sorting driven by membrane curvature. Nat. Commun. *6*, 8728.

Su, J., Yang, J., Zhao, D., Kawula, T.H., Banas, J.A., and Zhang, J.-R. (2007). Genome-wide identification of Francisella tularensis virulence determinants. Infect. Immun. *75*, 3089–3101.

Sun, P., Austin, B.P., Schubot, F.D., and Waugh, D.S. (2007). New protein fold revealed by a 1.65 Å resolution crystal structure of Francisella tularensis pathogenicity island protein IglC. Protein Sci. *16*, 2560–2563.

Surovtsev, I.V., and Jacobs-Wagner, C. (2018). Subcellular Organization: A Critical Feature of Bacterial Cell Replication. Cell *172*, 1271–1293.

Swedlow, J.R. (2013). Quantitative fluorescence microscopy and image deconvolution. Methods Cell Biol. *114*, 407–426.

Sycuro, L.K., Pincus, Z., Gutierrez, K.D., Biboy, J., Stern, C.A., Vollmer, W., and Salama, N.R. (2010). Peptidoglycan crosslinking relaxation promotes Helicobacter pylori's helical shape and stomach colonization. Cell *141*, 822–833.

Szwedziak, P., and Pilhofer, M. (2019). Bidirectional contraction of a type six secretion system. Nat. Commun. *10*, 1565.

Tang, H. (2009). Regulation and function of the melanization reaction in Drosophila. Fly (Austin) *3*, 105–111.

Taylor, N.M.I., Prokhorov, N.S., Guerrero-Ferreira, R.C., Shneider, M.M., Browning, C., Goldie, K.N., Stahlberg, H., and Leiman, P.G. (2016). Structure of the T4 baseplate and its function in triggering sheath contraction. Nature *533*, 346–352.

Taylor, N.M.I., van Raaij, M.J., and Leiman, P.G. (2018). Contractile injection systems of bacteriophages and related systems. Mol. Microbiol. *108*, 6–15.

Thelaus, J., Lundmark, E., Lindgren, P., Sjödin, A., and Forsman, M. (2018). Galleria mellonella Reveals Niche Differences Between Highly Pathogenic and Closely Related Strains of Francisella spp. Front. Cell. Infect. Microbiol. *8*.

Thibault G. Sana, C.B., Andreas Merdes, C.S., Thomas Rattei, A.H., Cerith Jones, K.L.B., Alain Filloux, G.S.-F., and Romé Voulhoux, S.B. (2015). Internalization of Pseudomonas aeruginosa Strain PAO1 into Epithelial Cells Is Promoted by Interaction of a T6SS Effector with the Microtubule Network. MBio *Volume 6*.

Thiem, S., and Sourjik, V. (2008). Stochastic assembly of chemoreceptor clusters in Escherichia coli. Mol. Microbiol. *68*, 1228–1236.

Thurston, T.L.M., Matthews, S.A., Jennings, E., Alix, E., Shao, F., Shenoy, A.R., Birrell, M.A., and Holden, D.W. (2016). Growth inhibition of cytosolic Salmonella by caspase-1 and caspase-11 precedes host cell death. Nat. Commun. *7*, 13292.

Toesca, I.J., French, C.T., and Miller, J.F. (2014). The Type VI secretion system spike protein VgrG5 mediates membrane fusion during intercellular spread by pseudomallei group Burkholderia species. Infect. Immun. *82*, 1436–1444.

Trivers, R.L. (1971). The Evolution of Reciprocal Altruism. Q. Rev. Biol. *46*, 35–57.

Trunk, K., Peltier, J., Liu, Y.-C., Dill, B.D., Walker, L., Gow, N.A.R., Stark, M.J.R., Quinn, J., Strahl, H., Trost, M., et al. (2018). The type VI secretion system deploys antifungal effectors against microbial competitors. Nat. Microbiol. *3*, 920–931.

Tsai, C.J.-Y., Loh, J.M.S., and Proft, T. (2016). Galleria mellonella infection models for the study of bacterial diseases and for antimicrobial drug testing. Virulence *7*, 214–229.

Tsirigotaki, A., De Geyter, J., Šoštaric, N., Economou, A., and Karamanou, S. (2017). Protein export through the bacterial Sec pathway. Nat. Rev. Microbiol. *15*, 21–36.

Typas, A., Banzhaf, M., Gross, C.A., and Vollmer, W. (2011). From the regulation of peptidoglycan synthesis to bacterial growth and morphology. Nat. Rev. Microbiol. *10*, 123–136.

Uda, A., Sekizuka, T., Tanabayashi, K., Fujita, O., Kuroda, M., Hotta, A., Sugiura, N., Sharma, N., Morikawa, S., and Yamada, A. (2014). Role of Pathogenicity Determinant Protein C (PdpC) in Determining the Virulence of the Francisella tularensis Subspecies tularensis SCHU. PLOS ONE *9*, e89075.

Unterweger, D., Kostiuk, B., Ötjengerdes, R., Wilton, A., Diaz-Satizabal, L., and Pukatzki, S. (2015). Chimeric adaptor proteins translocate diverse type VI secretion system effectors in Vibrio cholerae. EMBO J. *34*, 2198–2210.

Updegrove, T.B., and Ramamurthi, K.S. (2017). Geometric protein localization cues in bacterial cells. Curr. Opin. Microbiol. *36*, 7–13.

Vecchiarelli, A.G., Li, M., Mizuuchi, M., Hwang, L.C., Seol, Y., Neuman, K.C., and Mizuuchi, K. (2016). Membrane-bound MinDE complex acts as a toggle switch that drives Min oscillation coupled to cytoplasmic depletion of MinD. Proc. Natl. Acad. Sci. U. S. A. *113*, E1479-1488.

Vettiger, A., and Basler, M. (2016). Type VI Secretion System Substrates Are Transferred and Reused among Sister Cells. Cell *167*, 99-110.e12.

Vettiger, A., Winter, J., Lin, L., and Basler, M. (2017). The type VI secretion system sheath assembles at the end distal from the membrane anchor. Nat. Commun. *8*, 16088.

Vogel, H., Altincicek, B., Glöckner, G., and Vilcinskas, A. (2011). A comprehensive transcriptome and immune-gene repertoire of the lepidopteran model host Galleria mellonella. BMC Genomics *12*, 308.

Vollmer, W., and Bertsche, U. (2008). Murein (peptidoglycan) structure, architecture and biosynthesis in Escherichia coli. Biochim. Biophys. Acta *1778*, 1714–1734.

Vollmer, W., Joris, B., Charlier, P., and Foster, S. (2008). Bacterial peptidoglycan (murein) hydrolases. FEMS Microbiol. Rev. *32*, 259–286.

Wadhams, G.H., Warren, A.V., Martin, A.C., and Armitage, J.P. (2003). Targeting of two signal transduction pathways to different regions of the bacterial cell. Mol. Microbiol. *50*, 763–770.

Wang, J., Brackmann, M., Castaño-Díez, D., Kudryashev, M., Goldie, K.N., Maier, T., Stahlberg, H., and Basler, M. (2017). Cryo-EM structure of the extended type VI secretion system sheath-tube complex. Nat. Microbiol. *2*, 1507–1512.

Wang, J., Brodmann, M., and Basler, M. (2019). Assembly and Subcellular Localization of Bacterial Type VI Secretion Systems. Annu. Rev. Microbiol.

Wang, T., Si, M., Song, Y., Zhu, W., Gao, F., Wang, Y., Zhang, L., Zhang, W., Wei, G., Luo, Z.-Q., et al. (2015). Type VI Secretion System Transports Zn2+ to Combat Multiple Stresses and Host Immunity. PLoS Pathog. *11*, e1005020.

Weber, B.S., Hennon, S.W., Wright, M.S., Scott, N.E., de Berardinis, V., Foster, L.J., Ayala, J.A., Adams, M.D., and Feldman, M.F. (2016). Genetic Dissection of the Type VI Secretion System in Acinetobacter and Identification of a Novel Peptidoglycan Hydrolase, TagX, Required for Its Biogenesis. MBio *7*.

Wehbi, H., Portillo, E., Harvey, H., Shimkoff, A.E., Scheurwater, E.M., Howell, P.L., and Burrows, L.L. (2011). The peptidoglycan-binding protein FimV promotes assembly of the Pseudomonas aeruginosa type IV pilus secretin. J. Bacteriol. *193*, 540–550.

Wehrly TD, C.A., Virtaneva K, S.D., Child R, E.J., Brouwer D, N.V., Fischer ER, W.L., Curda AJ, K.J. 3rd, Martens C, C.D., Bosio CM, P.S., and Celli J (2009). Intracellular biology and virulence determinants of Francisella tularensis revealed by transcriptional profiling inside macrophages. Cell Microbiol.

van Wely, K.H., Swaving, J., Freudl, R., and Driessen, A.J. (2001). Translocation of proteins across the cell envelope of Gram-positive bacteria. FEMS Microbiol. Rev. *25*, 437–454.

Wexler, A.G., Bao, Y., Whitney, J.C., Bobay, L.-M., Xavier, J.B., Schofield, W.B., Barry, N.A., Russell, A.B., Tran, B.Q., Goo, Y.A., et al. (2016). Human symbionts inject and neutralize antibacterial toxins to persist in the gut. Proc. Natl. Acad. Sci. U. S. A. *113*, 3639–3644.

Williams, S.G., Varcoe, L.T., Attridge, S.R., and Manning, P.A. (1996). Vibrio cholerae Hcp, a secreted protein coregulated with HlyA. Infect. Immun. *64*, 283–289.

Wilton, M., Wong, M.J.Q., Tang, L., Liang, X., Moore, R., Parkins, M.D., Lewenza, S., and Dong, T.G. (2016). Chelation of Membrane-Bound Cations by Extracellular DNA Activates the Type VI Secretion System in Pseudomonas aeruginosa. Infect. Immun. *84*, 2355–2361.

Winchell, C.G., Graham, J.G., Kurten, R.C., and Voth, D.E. (2014). Coxiella burnetii type IV secretion-dependent recruitment of macrophage autophagosomes. Infect. Immun. *82*, 2229–2238.

Winnen, B., Schlumberger, M.C., Sturm, A., Schüpbach, K., Siebenmann, S., Jenny, P., and Hardt, W.-D. (2008). Hierarchical effector protein transport by the Salmonella Typhimurium SPI-1 type III secretion system. PloS One *3*, e2178.

Wirth, S.E., Krywy, J.A., Aldridge, B.B., Fortune, S.M., Fernandez-Suarez, M., Gray, T.A., and Derbyshire, K.M. (2012). Polar assembly and scaffolding proteins of the virulence-associated ESX-1 secretory apparatus in mycobacteria. Mol. Microbiol. *83*, 654–664.

Wittwer, M., Altpeter, E., Pilo, P., Gygli, S.M., Beuret, C., Foucault, F., Ackermann-Gäumann, R., Karrer, U., Jacob, D., Grunow, R., et al. (2018). Population Genomics of Francisella tularensis subsp. holarctica and its Implication on the Eco-Epidemiology of Tularemia in Switzerland. Front. Cell. Infect. Microbiol. *8*, 89.

Woese, C.R., Kandler, O., and Wheelis, M.L. (1990). Towards a natural system of organisms: proposal for the domains Archaea, Bacteria, and Eucarya. Proc. Natl. Acad. Sci. U. S. A. *87*, 4576–4579.

Wong, M.J.Q., Liang, X., Smart, M., Tang, L., Moore, R., Ingalls, B., and Dong, T.G. (2016). Microbial Herd Protection Mediated by Antagonistic Interaction in Polymicrobial Communities. Appl. Environ. Microbiol. *82*, 6881–6888.

Wu, L.J., and Errington, J. (2011). Nucleoid occlusion and bacterial cell division. Nat. Rev. Microbiol. *10*, 8–12.

Yahr, T.L., and Wolfgang, M.C. (2006). Transcriptional regulation of the Pseudomonas aeruginosa type III secretion system. Mol. Microbiol. *62*, 631–640.

Yamaichi, Y., Bruckner, R., Ringgaard, S., Möll, A., Cameron, D.E., Briegel, A., Jensen, G.J., Davis, B.M., and Waldor, M.K. (2012). A multidomain hub anchors the chromosome segregation and chemotactic machinery to the bacterial pole. Genes Dev. *26*, 2348–2360.

Yang, Z., Zhou, X., Ma, Y., Zhou, M., Waldor, M.K., Zhang, Y., and Wang, Q. (2018). Serine/threonine kinase PpkA coordinates the interplay between T6SS2 activation and quorum sensing in the marine pathogen Vibrio alginolyticus. Environ. Microbiol.

Yin, M., Yan, Z., and Li, X. (2019). Architecture of type VI secretion system membrane core complex. Cell Res. *29*, 251–253.

Young, K.D. (2006). The selective value of bacterial shape. Microbiol. Mol. Biol. Rev. MMBR *70*, 660–703.

Zhang, H., and Perc, M. (2016). Evolution of conditional cooperation under multilevel selection. Sci. Rep. *6*, 23006.

Zhao, W., Caro, F., Robins, W., and Mekalanos, J.J. (2018). Antagonism toward the intestinal microbiota and its effect on Vibrio cholerae virulence. Science *359*, 210–213.

Zheng, J., and Leung, K.Y. (2007). Dissection of a type VI secretion system in Edwardsiella tarda. Mol. Microbiol. *66*, 1192–1206.

Zheng, J., Ho, B., and Mekalanos, J.J. (2011). Genetic analysis of anti-amoebae and anti-bacterial activities of the type VI secretion system in Vibrio cholerae. PloS One *6*, e23876.

Zimmermann, L., Stephens, A., Nam, S.-Z., Rau, D., Kübler, J., Lozajic, M., Gabler, F., Söding, J., Lupas, A.N., and Alva, V. (2018). A Completely Reimplemented MPI Bioinformatics Toolkit with a New HHpred Server at its Core. J. Mol. Biol. *430*, 2237–2243.

Zogaj, X., Wyatt, G.C., and Klose, K.E. (2012). Cyclic di-GMP stimulates biofilm formation and inhibits virulence of Francisella novicida. Infect. Immun. *80*, 4239–4247.

Zoued, A., Durand, E., Brunet, Y.R., Spinelli, S., Douzi, B., Guzzo, M., Flaugnatti, N., Legrand, P., Journet, L., Fronzes, R., et al. (2016). Priming and polymerization of a bacterial contractile tail structure. Nature *531*, 59–63.

VII. APPENDIX

7.1.

Assembly and Subcellular Localization of Bacterial Type VI Secretion Systems

Jing Wang, Maj Brodmann, and Marek Basler*

Biozentrum, University of Basel, Basel, Switzerland

* **Correspondence:** Dr. Marek Basler, marek.basler@unibas.ch

Annual Reviews in Microbiology

Review in Advance first posted on June 21, 2019.

Statement of contribution:

I prepared figure 5 and wrote chapter 3 together with Marek Basler. I reviewed and edited the whole manuscript together with the other authors.

MI73CH28_Basler ARjats.cls June 10, 2019 14:25

ANNUAL REVIEWS

Annual Review of Microbiology

Assembly and Subcellular Localization of Bacterial Type VI Secretion Systems

Jing Wang,* Maj Brodmann,* and Marek Basler

Biozentrum, University of Basel, CH 4056 Basel, Switzerland;
email: marek.basler@unibas.ch

Annu. Rev. Microbiol. 2019. 73:28.1–28.18

The *Annual Review of Microbiology* is online at micro.annualreviews.org

https://doi.org/10.1146/annurev-micro-020518-115420

*These authors contributed equally to this article

Keywords

bacterial secretion systems, contractile nanomachines, subcellular localization, sensing and signaling cascades

Abstract

Bacteria need to deliver large molecules out of the cytosol to the extracellular space or even across membranes of neighboring cells to influence their environment, prevent predation, defeat competitors, or communicate. A variety of protein-secretion systems have evolved to make this process highly regulated and efficient. The type VI secretion system (T6SS) is one of the largest dynamic assemblies in gram-negative bacteria and allows for delivery of toxins into both bacterial and eukaryotic cells. The recent progress in structural biology and live-cell imaging shows the T6SS as a long contractile sheath assembled around a rigid tube with associated toxins anchored to a cell envelope by a baseplate and membrane complex. Rapid sheath contraction releases a large amount of energy used to push the tube and toxins through the membranes of neighboring target cells. Because reach of the T6SS is limited, some bacteria dynamically regulate its subcellular localization to precisely aim at their targets and thus increase efficiency of toxin translocation.

Review in Advance first posted on June 21, 2019. (Changes may still occur before final publication.)

MI73CH28_Basler ARjats.cls June 10, 2019 14:25

Contents

1. T6SS MODE OF ACTION

The bacterial type VI secretion system (T6SS) shares its evolutionary origin with contractile phage tails and other extracellular contractile protein-translocation nanomachines such as R-type pyocins (8, 45, 49, 72, 73). The T6SS apparatus is composed of 13 core proteins, with a set of regulatory and accessory proteins for specialized functions (11). The whole T6SS was visualized in bacteria by cryo–electron tomography (ET) (7, 21), which shows that the T6SS is tethered to the cell envelope by a membrane complex (30), a platform for assembly of a phage-like baseplate with a central spike and effectors (24, 66, 69). Baseplate assembly initiates copolymerization of a contractile sheath around a rigid inner tube (92, 100). Upon an unknown signal, the long spring-like sheath quickly contracts, starting likely from the baseplate and progressing to the distal end. This physically pushes the inner tube and spike with effectors out of the cell and through the membrane of a neighboring cell (26, 47, 100) (**Figure 1**; **Supplemental Movie 1**).

An important advantage of the T6SS mode of action is that the sheath contraction releases a large amount of energy that can be used to penetrate physical barriers. Single-sheath contraction, which happens in less than 2 ms (99), could release the same amount of energy as the conversion of 1,000 molecules of ATP to ADP (100). While effector delivery to gram-positive bacteria has not been reported so far, the T6SS can deliver large hydrophilic effectors across target eukaryotic membranes, bacterial outer membranes, and even two membranes and the peptidoglycan layer of gram-negative bacterial cells (98). The T6SS mode of action also has significant drawbacks. Most T6SS substrates are secreted by binding to the spike components, and thus with every firing of T6SS only a few copies of the cargo proteins are secreted (25, 72, 89). In addition, even the most active bacteria fire the T6SS only approximately once per minute (6, 7, 14, 30, 38, 68, 78, 85). The extended sheath is assembled around the inner tube, which is mostly lost upon firing and has to be resynthesized (100, 92). Furthermore, the contracted sheath cannot be directly used for a new assembly, and the sheath subunits have to be unfolded by a dedicated ATPase (ClpV or ClpB) (6, 10, 14). Finally, since T6SS substrates are directly pushed across the target membrane by the tube, the T6SS has a limited reach and proteins can be delivered only if the target cell is in close proximity and the T6SS fires in the right direction (5, 41, 98).

Here, we review recent insights into the structure and assembly of the T6SS and the mechanisms that evolved in certain bacteria to dynamically localize the T6SS to minimize costs and increase efficiency of toxin translocation and target-cell killing.

MI73CH28_Basler ARjats.cls June 10, 2019 14:25

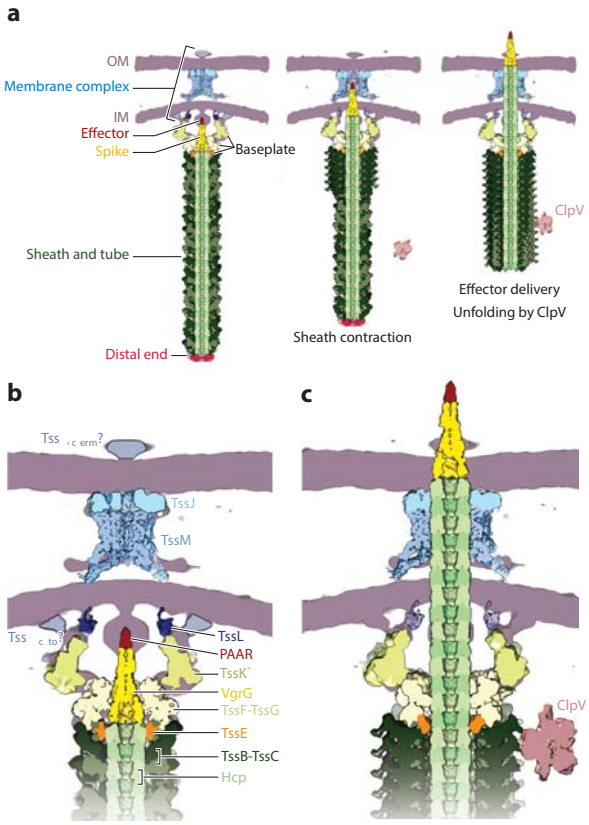

Figure 1

Overview of T6SS assembly and mode of action. (*a*) The T6SS consists of a membrane complex (*blue*), a baseplate assembled around a central spike (*yellow*), and a contractile sheath wrapping around a rigid tube (*green*). The distal end of the sheath is capped (*red*). Upon activation, the membrane complex opens up to allow the passage of spike and tube. The baseplate reorients to trigger contraction, and the tube is pushed out of the cell by the contracting sheath. The contracted sheath is unfolded by ClpV. (*b*) The T6SS in the prefiring state. Membrane complex: TssJ/TssL/TssM in the closed state (EMD-0265, PDB 3U66). Baseplate: PAAR (PDB 4JIV), VgrG (PDB 6H3L), TssK, TssF/TssG (PDB 6GIY and 6N38), and TssE (PDB 6GJ1). Extended sheath: TssB/TssC. The tube: Hcp (PDB 5MXN). The sheath-tube complex and the spike are modeled by fitting atomic structures to the EM map of the T6SS baseplate of *Vibrio cholerae* (EMD-3879). The wedge of the T6SS in the prefiring state was modeled by fitting the core bundle of TssF/TssG to the T4 phage extended baseplate gp6/gp7 core-bundle (PDB 5IV5). The composite structure is superimposed with the subtomogram average of T6SS in *Myxococcus xanthus* (EMD-8600). (*c*) Both the membrane complex and the baseplate undergo significant reorientation to allow the passage of the tube. After contraction, the sheath exposes the surface domain to recruit ClpV (modeled based on ClpB EMD-3776). Abbreviations: EM, electron microscopy; EMD, Electron Microscopy Data Bank ID; IM, inner membrane; OM, outer membrane; PAAR, proline, alanine, alanine, arginine; PDB, Protein Data Bank ID.

MI73CH28_Basler ARjats.cls June 10, 2019 14:25

2. T6SS STRUCTURE AND ASSEMBLY

2.1. Membrane Complex

The membrane complex is composed of three proteins, TssJ, TssL, and TssM. TssJ is a lipoprotein anchored to the outer membrane (OM) by N-terminal cysteine acylation (3). The protein itself is confined within the periplasm and folds as a β sandwich resembling transthyretin with an additional helical domain and a protruding loop (L1–2 loop) (32, 75, 79) (**Figure 2*a***). The helical domain stabilizes TssJ, and the L1–2 loop interacts with TssM (32). TssJ is required for assembly of the other membrane complex components TssL and TssM (30); however, the high-order assembly of TssJ seems to be driven by TssM (**Figure 2*b,c***) (76).

TssM was early identified as a T4SS IcmF-like protein (4, 19, 59). The N terminus of TssM is flanked by transmembrane helices and forms a large cytosolic domain with NTPase activity

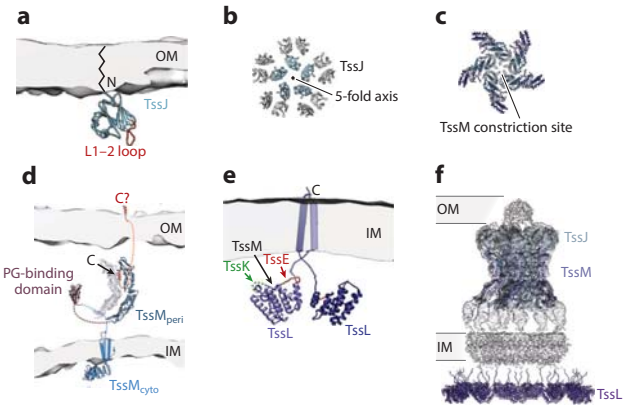

Figure 2

Membrane complex structure. (*a*) TssJ is anchored to the OM by N-terminal acylation. The L1–2 loop (*red*) is required for TssM binding. (*b*) Fifteen copies of TssJ (PDB 4Y7O) molecules cap the top of the membrane complex, with three copies of TssJ on top of each pillar-like TssM dimer. Adjacent TssJ trimers do not make contact for the fivefold oligomerization. (*c*) TssM dimers oligomerize in the periplasm. Cross section of the TssM pillars shows the periplasmic gate. Five pairs of TssM pillars form a narrow central channel with minimal pore size less than 5 Å. (*d*) TssM anchors to the IM by three N-terminal transmembrane helices. The TssM cytosolic domain is modeled after NTPase-like domain EngB (PDB 4DHE) followed by a helical extension modeled after DPY-30 (PDB 3G36) as described in Reference 56. The periplasmic domain of TssM carries a putative peptidoglycan-binding motif, modeled after the OmpA domain (5U1H), followed by a long helical domain traversing the entire periplasm. The very C terminus of TssM (*red*) may extend to the extracellular space in the native membrane complex. Each TssM pillar consists of two copies of TssM (*blue* and *gray*). A full-length model of TssM is shown for the blue copy only. (*e*) The cytosolic domain of TssL (PDB 3U66) anchors to the IM by a C-terminal transmembrane helix. The transmembrane helix is responsible for dimerization, and the cytosolic domain interacts with both the baseplate (*red loop* interacts with TssE, *green loop* interacts with TssK) and TssM (*central cleft*). (*f*) Cryo-EM density of the full transenvelope complex (EMD-0265) accounting for the density of TssJ and the helical domain (residues 569–1129) of the enteroaggregative *Escherichia coli* TssM periplasmic domain (residues 382–1129). TssL is positioned in the cytoplasmic side of the complex. Abbreviations: EM, electron microscopy; EMD, Electron Microscopy Data Bank ID; IM, inner membrane; OM, outer membrane; PDB, PDB, Protein Data Bank ID; PG, peptidoglycan.

MI73CH28_Basler ARjats.cls June 10, 2019 14:25

in some organisms (60) (**Figure 2*d***). The C-terminal domain traverses the entire periplasm and reaches the OM by contacting TssJ (30). This periplasmic domain has an OmpA-like peptidoglycan-binding motif and oligomerizes as the core of the membrane complex (4, 76, 104). Density corresponding to the OmpA-like domain is missing in the membrane complex in situ cryo-ET structure, indicating that it is rather flexible compared to the rest of the membrane complex (76). The very C terminus of TssM is exposed on the cell surface, and part of the TssM β-stranded domain can breach the OM transiently during T6SS firing (30). In the recent membrane complex structure, the TssM C-terminal extremity folds within the periplasm domain as an α helix that connects to the rest of the TssM by a 20-amino-acid-long linker (76). The TssM C terminus may extend outside of the cell in the native state and thus be responsible for sensing environmental clues to activate the T6SS assembly.

TssL is an inner membrane (IM) protein homologous to IcmH (DotU) of the T4bSS (31). Its function requires dimerization controlled mainly by the N-terminal transmembrane segment. The TssL cytosolic domain is necessary for interactions with the baseplate as well as the membrane complex (**Figure 2*e***), and substitutions in loops and cleft of this domain abolish the TssF binding (31, 108). The baseplate-binding loops are not conserved among the TssL proteins and may determine specificity during T6SS assembly in the organisms encoding several T6SSs (31).

Overexpression of *Escherichia coli* [enteroaggregative *E. coli* (EAEC)] TssJ, TssM, and TssL allowed in situ visualization of the membrane complex by cryo-ET (**Figure 2*f***); however, TssL was poorly resolved and thus its exact orientation remains unclear. A Y-shaped core of the membrane complex spanning the periplasm is flanked by a cap embedded in the OM and a base embedded in the IM (76). Interestingly, cryo-ET and single-particle analysis of the EAEC T6SS membrane complex revealed a fivefold symmetry structure. This is in contrast to the rest of the T6SS apparatus, which follows a C6 symmetry [except C3 for VgrG and C1 for PAAR (proline, alanine, alanine, arginine)]. Therefore, this symmetry mismatch will have to be resolved between TssL/TssM and the binding partners in the baseplate, such as TssK. This might require more flexible binding sites and might explain why the cytoplasmic part of the complex shows heterogeneous density that fails to yield any consensus structure upon averaging. Alternatively, assembly of the membrane complex with C6 symmetry might be facilitated by a scaffold protein or chaperone-like activity of other T6SS components such as TssA, which were absent in the *E. coli* strain overexpressing TssJ/TssL/TssM (76, 104, 112). The in situ structure of the membrane complex is likely in a closed conformation, since the periplasm channel is constricted by a TssM loop protruding into the central lumen (**Figure 2*c***) (76, 104). This constriction could be displaced by a TssM conformational change triggered by movement in the baseplate during initiation of sheath contraction or it could simply be forced open during tube/spike secretion through the membrane complex (30).

2.2. Baseplate Structure

Similarly to the baseplates of contractile phages, the T6SS baseplate comprises a central hub surrounded by six wedges (**Figure 3*a***). It initiates the assembly of the Hcp tube and sheath in an extended high-energy state, and change in baseplate structure is likely required for triggering sheath contraction (24, 50, 66, 69). The central hub is made of a trimeric VgrG, which connects the wedges and initiates Hcp tube assembly. The base of the VgrG structure has a similar fold as an Hcp dimer (49). Therefore, a VgrG trimer with a pseudohexameric structure provides a platform to seed Hcp polymerization (77). Several loops of Hcp absent from X-ray structures become ordered in the Hcp tube (100). These unstructured regions could be preventing Hcp stacking but may readily fold and initiate polymerization when initiator complex is bound (VgrG, TssE,

MI73CH28_Basler ARjats.cls June 10, 2019 14:25

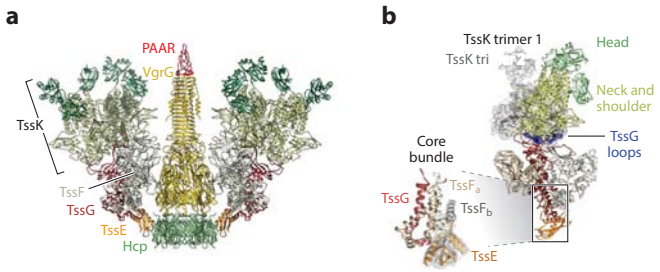

Figure 3

Baseplate structure. (*a*) The T6SS prefiring baseplate is modeled after the T4 phage baseplate in the preattachment state (EMD-3374). Both baseplates use a three-helix core-bundle motif for wedge assembly and its attachment to the central hub. The T6SS is modeled by matching the $(TssF)_2$/TssG core bundle to the $(gp6)_2$/gp7 core bundle. (*b*) Atomic structure of the T6SS wedge (one TssE and one TssG and two TssF and two TssK trimers). TssK trimers attach to hydrophobic TssG loops (highlighted *blue* surface). The head domain of TssK (*green*) is flexible. Two copies of TssF (*tan* and *gray*) encircle the TssG (*red*). The TssE attaches to the rest of the wedge by interacting with the core bundle (*inset*), which comprises three helices from the N termini of TssF and TssG.

and sheath). The needle domain of T6SS VgrG lacks a sharp point for membrane piercing (91); however, this blunt end binds a small protein with a characteristic PAAR domain sequence. The VgrG/PAAR complex then serves as a docking structure for many effectors that may require help of chaperones or adaptor proteins to assemble (9, 16, 52, 74, 96). Diversity of effectors and their functions was reviewed elsewhere (1, 53).

The wedge of T6SS contains TssE/TssF/TssG/TssK at 1:2:1:6 stoichiometry (24, 69) (**Figure 3*b***). TssE is a universally conserved gp25-like protein in contractile injection systems (50, 57) resembling the handshake domain of TssB/TssC (see below) and was suggested to play an important role in the initiation of sheath assembly to the extended state. Somewhat surprisingly, a *tssE*-negative strain of *Vibrio cholerae* assembles functional T6SS, albeit at a much lower frequency (7, 98). Whether another protein can complement the absence of TssE is unknown.

TssF folds as a three-domain wing-like structure (24, 69). Two TssF molecules within a single wedge interact with a conserved EPR motif of TssE (93) and TssG (24, 69). TssG has a fold similar to that of TssF, except it lacks the large TssF central wing-like domain. TssG also features two TssK-binding loops that are absent in TssF (**Figure 3*b***) (24, 69). The C-terminal fold of TssG can be superimposed with the TssF C-terminal domain, suggesting that these proteins evolved from a common ancestor by gene duplication (69). $(TssF)_2$/TssG heterotrimer is tightly interdigitated. Their N-terminal domains form a three-helix bundle resembling the core bundle of phage T4, and their C-terminal domains form a triangular core resembling the T4 trifurcation unit (69, 93) (**Figure 3*b***).

In phage T4, a LysM-domain-containing protein gp53 functions as an interwedge clamp that joins the wedges into the baseplate (2). The T6SS lacks gp53 orthologs, maybe to allow quick baseplate disassembly upon sheath contraction. It is unclear what triggers and stabilizes the assembly of six wedges around the central hub. It could be interaction with the membrane complex or in some cases even be facilitated by additional proteins such as TssA of *Pseudomonas aeruginosa* (71).

Unlike other T6SS baseplate components, which share common evolutionary origin with contractile phages (12, 66), TssK is clearly a homolog of the receptor-binding protein (RBP) from

MI73CH28_Basler ARjats.cls June 10, 2019 14:25

noncontractile phages (67). The main difference between TssK and phage RBP lies in the C-terminal head domain that recognizes the binding partner. Based on the isolated wedge structure, each wedge complex contains two TssK trimers attaching to one of the two extended loops of TssG (**Figure 3*b***) (24, 69). The conserved loops of TssG interact by complementary surfaces with the hydrophobic N termini of TssK. Binding of TssK to TssG is reminiscent of the attachment observed for RBP to phage baseplates, such as in TP901–1 (97) and P2 (87). TssK plays a central role in T6SS assembly by docking the baseplate to the membrane complex as it interacts directly with cytosolic domains of TssL and TssM (110). The self-association of TssM and TssL as a dimer is critical for T6SS function (24, 31, 109), suggesting that matching dimers of TssK and TssL/TssM mediate the baseplate-to-membrane-complex interaction. TssK trimer is mobile relative to the $(TssF)_2$/TssG module, as revealed by cryo–electron microscopy (EM) (69). One can envision that TssK detects the mechanical distortion from the membrane complex undergoing conformational change and propagates it to downstream baseplate components. The resulting reorganization of the baseplate eventually leads to sheath contraction. Alternatively, cytosolic signaling pathways or interactions with other proteins might modulate the affinity of TssK to the membrane complex and thus precisely control the timing of T6SS assembly or contraction.

2.3. Tube-Sheath Complex

During T6SS assembly, sheath subunits (TssB/TssC) polymerize in a metastable, extended state that requires the presence of baseplate and tube (Hcp). Contraction of the sheath provides energy to push and rotate the inner tube out of the bacterial cell envelope for effector delivery. The structures of contracted T6SS sheath from several bacteria have been determined by cryo-EM (26, 47, 81). Despite sequence variations, the overall structure and the assembly of the T6SS sheath is conserved (**Figure 4*b,d***). Each sheath subunit consists of two proteins, TssB (VipA) and TssC (VipB), which fold into three domains (**Figure 4*a***). Domains 1 and 2 of the sheath subunit are similar to those of other contractile injection systems, and they connect sheath subunits as a meshwork (12). However, the third α-helical domain inserted into domain 2 is T6SS specific. Domain 3 assembles from the TssB C terminus and TssC N terminus, which includes the ClpV-binding site (47).

To obtain a structure of the extended sheath, a noncontractile sheath was generated by elongating the TssB linker, allowing an aberrant connectivity of the sheath meshwork and preventing its contraction during purification from cells (**Figure 4*a,c***) (13). This noncontractile sheath contains a wild-type Hcp tube, which is made of stacked Hcp hexamers following the helical symmetry of the extended sheath. The free solvation energy stabilizing the Hcp tube is weaker compared to tubes of T4 phage and R-type pyocin (100), which may explain why the Hcp tube was never isolated and apparently disassembles after secretion out of cells (92).

Comparison of the extended T6SS tube-sheath complex with the contracted sheath suggests a mechanism by which sheath contraction is coupled to the translocation of the inner tube. Upon contraction, the sheath expands radially to release the Hcp tube and compresses along the long axis to push the tube forward. The difference in the helical parameters of the extended and contracted sheath shows that T6SS functions as a powerful drill. Contraction of a 1-μm-long sheath would push the Hcp tube by 420 nm and rotate it by 4.2 turns within a few milliseconds (47, 99, 100).

Importantly, domain 3 is folded on the surface of the extended sheath, making the ClpV-binding site on TssC inaccessible (70, 100) (**Figure 4*e,f***). During sheath contraction domain 3 becomes unstructured to allow ClpV binding and specific refolding of the contracted sheath (6). ClpV is a hexameric AAA+ ATPase that pulls on the exposed N terminus of TssC and releases it from the contracted sheaths to replenish the pool of sheath subunits for new rounds of assembly

MI73CH28_Basler ARjats.cls June 10, 2019 14:25

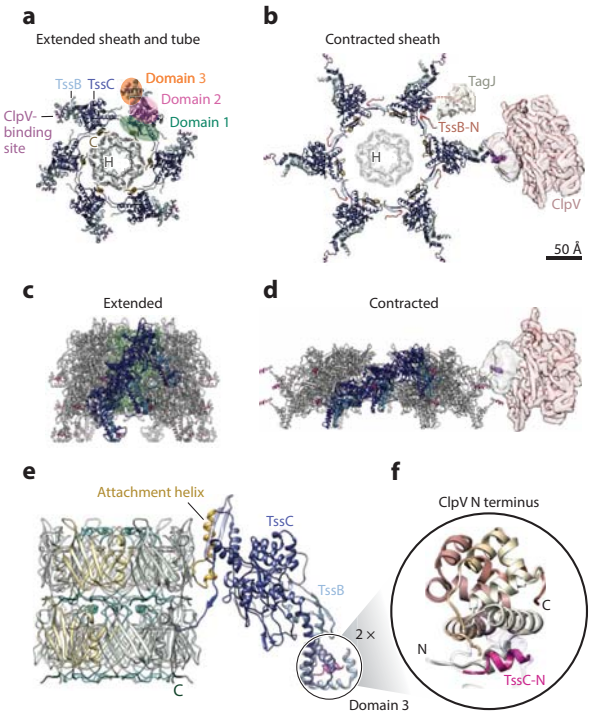

Figure 4

Structure of the sheath and tube. (*a*) In the extended state (*top view*, single ring), the sheath protomer (TssB and TssC, *light blue and dark blue*) contacts Hcp (*gray*) with a C-terminal helix (*yellow*) of TssC. Sheath subunit connection is accomplished by interwoven domain 1. The ClpV-binding site (*purple*) of TssC is tucked inside domain 3 on the sheath surface. (*b*) Upon contraction, the sheath protomer rotates and detaches from the Hcp tube (*top view*, single ring). The ClpV-binding site is exposed for ClpV docking. In some T6SSs, the N terminus of TssB engages TagJ to facilitate ClpV association. (*c,d*) The side views of three rings of the sheath in extended and contracted states. (*e*) Two rings of Hcp with one sheath protomer. The unstructured loops (residues 50–63, 129–139) and C terminus (166–172) (*dark green*) become ordered once they stack into a functional tube. One Hcp is colored yellow to show the helical packing. The domain 3 (*black circle*) of the extended sheath shields the ClpV-binding site of TssC. (*f*) Structure of the ClpV N terminus (PDB 3ZRJ) binding to the TssC positioned in the same orientation as in panel *e*. Abbreviation: PDB, PDB, Protein Data Bank ID.

(6, 10, 70). In *Francisella novicida*, where a canonical ClpV is missing, the contracted sheath of T6SS is disassembled by a general-purpose unfoldase ClpB (14). Several recent structures of ClpB have demonstrated a general mechanism by which unfoldase couples sequential ATP hydrolysis to substrate threading during disaggregation (27, 36, 105). Interestingly, in some organisms like *P. aeruginosa*, an additional protein, TagJ, was shown to interact with both the sheath (TssB) and ClpV; however, the exact role of TagJ is unclear, as its deletion has no obvious influence on T6SS activity (33, 58) (**Figure 4*b***).

MI73CH28_Basler ARjats.cls June 10, 2019 14:25

2.4. TssA and TagA Proteins

Proteins possessing a conserved N-terminal ImpA_N region are considered members of the TssA family. The C-terminal sequences of TssA are highly diverse, dividing members of TssA into separate classes with different functions and localization (29, 71, 111). *P. aeruginosa* TssA interacts with baseplate components, ClpV and TagJ (71), whereas *Burkholderia cenocepacia* TssA (29) and *E. coli* TssA (111) interact with the baseplate, the membrane complex, and the sheath-tube complex. In addition, *E. coli* TssA was shown to coordinate copolymerization of the sheath and tube (111). The overall architecture of the TssA-assembled complexes varies depending on the TssA class and may be a 5-fold-symmetry decamer, a 6-fold-symmetry dodecamer, or a 16-fold-symmetry 32-mer (29, 71, 111). Interestingly, another N-terminal ImpA-domain-containing protein is membrane-associated TagA, which arrests sheath polymerization and stabilizes the extended sheath (83, 92).

3. SUBCELLULAR LOCALIZATION OF T6SS ASSEMBLY

Regulation of T6SS activity mainly involves regulation of expression of the T6SS genes on a transcriptional or posttranscriptional level as a response to diverse environmental stimuli (23, 46, 51, 61). Interestingly, live-cell imaging of TssB or ClpV dynamics showed that bacteria have different T6SS assembly patterns and may dynamically localize the T6SS within the bacterial cell. *V. cholerae* and *Acinetobacter baylyi* build several T6SS sheaths per cell and fire constantly in apparently random directions (6, 78). EAEC repeatedly assembles the Sci-1 T6SS at one or two apparently random positions within the cell (30). *P. aeruginosa* assembles one of its three T6SS within seconds of an attack from other bacteria at the site of the inflicted damage to quickly retaliate (5). The majority of *Serratia marcescens* cells assemble one T6SS sheath at random positions in the cell; however, they rely on regulated T6SS assembly for efficient killing of prey cells (38, 68). In addition, intracellular pathogens *F. novicida* and *Burkholderia thailandensis* assemble their antieukaryotic T6SS on the poles (14, 85).

3.1. Threonine Phosphorylation Pathway Mediates T6SS Repositioning

The first example of posttranslational regulation of T6SS assembly by a threonine phosphorylation pathway (TPP) was described in *P. aeruginosa* (64). Later, TPPs were shown to regulate initiation and positioning of T6SS assembly in several organisms (5, 35, 54, 68) (**Figure 5**). TPPs have a sensor module that senses a signal and activates a kinase (PpkA). An activated kinase then phosphorylates a target protein, which in turn initiates T6SS assembly. Finally, a phosphatase (PppA) dephosphorylates the target protein and thus prevents further T6SS assembly initiation. *P. aeruginosa* cluster H1-T6SS encodes a complete TPP with a sensor module composed of TagQ/TagR/TagS/TagT; a kinase PpkA phosphorylating Fha; and a cognate phosphatase, PppA. Other species like *S. marcescens* and *Agrobacterium tumefaciens* possess only PpkA, PppA, and Fha. In addition, T6SS assembly in these three organisms is blocked by TagF, and deactivation of TagF can trigger T6SS assembly in a TPP-independent manner (54, 55, 68, 90).

3.1.1. Signal sensing and kinase activation. The sensor module TagQ/TagR/TagS/TagT in *P. aeruginosa* was shown to be required for sensing T6SS attacks from either sister cells or other bacteria as well as cell envelope stress induced by polymyxin B, the type 4 secretion system, chelation of ions, or extracellular DNA (5, 6, 40, 102). Lipoprotein TagQ with a conserved lipobox is anchored to the periplasmic side of the OM and binds periplasmic TagR (18). Interaction of TagR with the periplasmic domain of PpkA might result in activation of its kinase activity (42).

MI73CH28_Basler ARjats.cls June 10, 2019 14:25

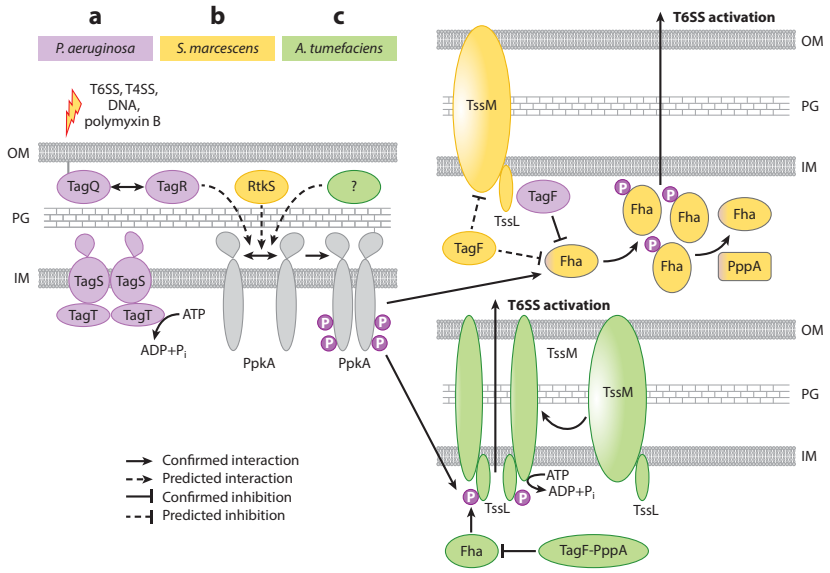

Figure 5

Posttranslational regulation of T6SS activity. (*a*) In *Pseudomonas aeruginosa* (*purple*), membrane damage (*lightning bolt*) leads to activation of PpkA by TagQ/TagR/TagS/TagT and to phosphorylation of Fha. Phosphorylated Fha multimerizes and promotes T6SS assembly. PppA dephosphorylates Fha and stops T6SS assembly. TagF represses T6SS activity independently of the threonine phosphorylation pathway by interacting with Fha. (*b*) In *Serratia marcescens* (*yellow*), PpkA interacts with RtkS and subsequently phosphorylates Fha, which multimerizes and activates T6SS assembly. PppA dephosphorylates Fha and thus blocks T6SS activity. TagF blocks T6SS activity, likely by acting on the membrane complex. (*c*) In *Agrobacterium tumefaciens* (*green*), PpkA phosphorylates TssL, which triggers a conformational change in TssM and ATP hydrolysis. Binding of Fha to phosphorylated TssL induces T6SS activity. TagF-PppA blocks T6SS activity by interaction with Fha. Abbreviations: IM, inner membrane; OM, outer membrane; PG, peptidoglycan.

This suggests that TagQ might be sequestering TagR to the OM to prevent its binding to PpkA and thus T6SS activation; however, TagQ likely has an additional role since deletion of either TagQ or TagR prevents T6SS assembly (18).

The components TagS and TagT form a putative ABC transporter with homology to the Lol complex, which transports lipoproteins (65). TagS forms an integral membrane protein with a long periplasmic loop, and TagT is an ATPase and contains Walker A and B motifs, which are required to hydrolyze ATP in vitro (18). TagS or TagT is required for full T6SS activation (5, 18); however, despite homology to the Lol complex, it is unclear whether TagS and TagT transport any substrates. An obvious candidate would be TagQ or TssJ; however, deletion of TagS and TagT does not seem to alter their membrane localization (18).

In *S. marcescens*, periplasmic RtkS (regulator of T6SS kinase in *Serratia*) was shown to be required for efficient killing of prey cells but dispensable for T6SS activity in liquid culture. Signals sensed by RtkS are unknown, and it is also unclear whether RtkS directly interacts with PpkA; however, deletion of *rtkS* resulted in destabilization and degradation of PpkA (68).

The serine/threonine kinase PpkA is an IM protein with a periplasmic domain and cytosolic kinase domain. PpkA may be activated by interaction with a periplasmic protein (e.g., TagR) that

results in PpkA dimerization. The PpkA dimer autophosphorylates and activates T6SS assembly by phosphorylating a T6SS component (35, 42, 55, 63, 64). While the kinase domain is conserved, the structure of the periplasmic domain differs between *S. marcescens* and *P. aeruginosa* (35). This is likely because each PpkA responds to a different signal and binds a different periplasmic protein.

3.1.2. Activation of T6SS assembly by protein phosphorylation. In both *P. aeruginosa* and *S. marcescens*, activated PpkA phosphorylates Fha, which likely recognizes phosphorylated PpkA via its forkhead-associated (FHA) domain, known to bind phosphopeptides (64). However, it is unclear how phosphorylation of Fha promotes T6SS assembly (42, 64, 68). Interestingly, Fha forms foci in *P. aeruginosa* independently of its phosphorylation status (64); however, membrane-anchored PpkA is still required for formation of these foci (42). This suggests that PpkA might have an additional structural role in Fha foci formation and T6SS assembly initiation. In *P. aeruginosa*, Fha phosphorylation is increased when cells are incubated on a solid surface, suggesting that cell-cell interactions result in PpkA activation (18). This activation might be a consequence of T6SS dueling between sister cells (6). In contrast, the majority of Fha in *S. marcescens* is phosphorylated also in liquid culture, where there are minimal or no cell-cell interactions (35).

In *A. tumefaciens*, PpkA phosphorylates the membrane complex component TssL, leading to a conformational change in TssM (55). TssM is an IM ATPase with Walker A and B motifs, and the conformational change triggers ATP hydrolysis. However, TssL-TssM interaction is independent of ATPase activity of TssM (60). Phosphorylated TssL interacts with Fha, and the Fha-pTssL complex promotes recruitment of secretion substrates Hcp and effector Atu4347 to TssL (55). It is unclear how ATPase activity of TssM is involved in recruiting the secreted proteins and whether formation of this complex requires additional proteins (55, 60). TssM of *P. aeruginosa*, *V. cholerae*, and *Edwardsiella tarda* also contains Walker A and B motifs (60); however, ATP hydrolysis does not seem to be important for T6SS activity in *E. tarda* (107).

An interesting case is *Vibrio alginolyticus*, which uses the TPP of its second T6SS cluster to regulate T6SS assembly as well as gene expression. As in *A. tumefaciens*, PpkA phosphorylates TssL, which results in binding of Fha and an increase in T6SS activity. In addition, PpkA phosphorylates a non-T6SS substrate, VtsR. Phosphorylated VtsR activates LuxO and subsequently promotes expression of T6SS-2 and quorum sensing (103).

3.1.3. T6SS assembly deactivation. In *P. aeruginosa* and *S. marcescens*, phosphatase PppA is responsible for dephosphorylation of Fha and thus shutting down T6SS activity. Since T6SS activity is low in *P. aeruginosa*, deletion of PppA results in an increase of T6SS activity and Hcp secretion (5, 18, 42, 64). However, in *S. marcescens*, deletion of PppA does not increase Hcp secretion in liquid medium, suggesting that the system is already at maximum activity. Interestingly, in both species, *pppA* deletion strains repeatedly assemble T6SS at the same location within the cells for several rounds of firing (5, 68). This has a major consequence for interaction with competing bacteria, because a *P. aeruginosa pppA*-negative strain cannot distinguish between T6SS-positive attackers and T6SS-negative bystander cells and kills both to a similar extent. Importantly, the killing rate of T6SS-positive attackers by a *pppA*-negative strain is low, even though a *pppA*-negative strain secretes significantly more effectors than the wild-type strain (5, 40). A similar observation was also made for *S. marcescens*, where a *pppA*-negative strain kills prey cells poorly despite high T6SS activity (35, 68). This suggests that PppA activity is important to preventing excessive firing of T6SS in one direction and by stopping the assembly allows T6SS to reposition to a new subcellular location upon sensing a signal, which in turn is required for efficient killing of target cells.

MI73CH28_Basler ARjats.cls June 10, 2019 14:25

3.2. TPP-Independent Regulation

In addition to the TPP, TagF regulates T6SS assembly in *P. aeruginosa* and *S. marcescens*, by a poorly understood mechanism. For *P. aeruginosa*, it was shown that TagF sequesters Fha to prevent T6SS assembly (54), and indeed, deletion of TagF activates T6SS even in the absence of TagQ/TagR/TagS/TagT and PpkA (90). Importantly, even strains lacking TPP, like *V. cholerae*, also require Fha for T6SS activity, suggesting that Fha is an important scaffold protein for assembly of other T6SS components (106). Similarly to the case of *P. aeruginosa*, when *tagF* is deleted in the *ppkA*-negative strain of *S. marcescens*, T6SS assembly is restored. It is, however, unclear whether TagF interacts with Fha or other T6SS components.

In *A. tumefaciens*, TagF and PppA are fused into a single polypeptide; however, both independently block T6SS activity (54, 55). The TagF domain binds Fha; however, this seems insufficient to prevent T6SS assembly, as a TagF domain mutant, which is still able to bind Fha, loses its ability to repress T6SS activity. This suggests that the TagF domain is also involved in Fha-independent repression (54). Similarly to the case of *S. marcescens*, efficiency of target-cell killing is decreased in the absence of PpkA and TagF-PppA even though the overall T6SS activity remains high (54), suggesting that TPP components and TagF are important for sensing prey cells and/or repositioning the T6SS apparatus.

3.3. Regulation of T6SS Localization by Peptidoglycan-Cleaving Enzymes

Many cell envelope–spanning complexes, like flagella, the T3SS, or the T4SS, require specialized lytic transglycosylases for insertion into the peptidoglycan layer (28, 84, 95). Interestingly, two dedicated peptidoglycan-cleaving enzymes were shown to be required for T6SS assembly, and thus their control in response to certain signals or stimuli might, in principle, allow for dynamic localization of T6SS assembly. EAEC requires the general lytic transglycosylase MltE to insert membrane complexes of the Sci-1 T6SS. The lipoprotein MltE is located at the OM and interacts with the periplasmic domain of TssM. How MltE is activated by TssM and whether additional components are required is unknown (82). In *Acinetobacter*, the L,D-endopeptidase TagX is encoded in the T6SS cluster and is required for T6SS activity (78, 101). Since T6SS assembles at low frequency also in a *tagX*-negative strain, it is likely that additional mechanisms allow for assembly initiation or peptidoglycan cleavage and that TagX is only required for integration of the T6SS apparatus into the peptidoglycan layer and not for T6SS function (78).

3.4. Polar Localization of T6SS

Polar localization is a potential mechanism for bacteria to coordinate function of multiple protein complexes, such as pili, flagella, or secretion systems. Positioning of macromolecular assemblies on the bacterial pole is achieved by several distinct mechanisms, some of which are well understood (48). Strikingly, polar localization was shown for almost all types of secretion systems, most of which are required for host-pathogen interactions (17, 20, 22, 43, 44, 62, 80, 88). Polar localization of the T4SS is achieved by positioning of DotU and IcmF, homologs of the T6SS proteins TssL and TssM, and this is required for successful effector translocation and progression of infection in *Legionella pneumophila* (39, 44). In addition, secretion of typhoid toxin from *Salmonella enterica* serovar Typhi requires localized cleavage of peptidoglycan, which is specifically edited on the bacterial pole to contain LD-cross-links (37).

B. thailandensis and *F. novicida* were shown to assemble a polarly localized T6SS required for host-pathogen interactions (14, 85). *B. thailandensis* T6SS-5 is required for formation of a

multinucleated giant cell (34, 85, 86, 94), while *F. novicida* requires the T6SS for phagosomal escape and assembles one polar T6SS per cell in vitro and inside macrophages (14, 15). For the T6SS, sheath length defines the reach of T6SS attack, as the sheath contracts to half of its extended length (7). Therefore, polar T6SS assembly might allow assembly of longer sheaths in rod-shaped bacteria and thus increase efficiency of effector delivery. In the case of *F. novicida* it would be delivery across a phagosomal membrane, and in the case of *B. thailandensis* it would be the ability to induce membrane fusion of neighboring host cells. However, polar localization could also be required for coordination with other polarly localized complexes such as adhesins or pili to bring the target membrane closer to the bacterial cell and thus facilitate protein translocation by the T6SS.

4. CONCLUDING REMARKS

Tremendous progress has been achieved in understanding the mode of action of the T6SS; however, it is clear that there are still many open questions that need to be solved. We need an atomic model of the whole assembly; however, since the T6SS is both dynamic and regulated, we also need to solve high-resolution structures of the individual steps of the assembly process. This will be challenging especially for the membrane complex but also for the transient complexes forming, for example, during sheath-tube copolymerization. Since live-cell imaging shows that T6SS localization and assembly dynamics can vary significantly between species or under various conditions, more effort will have to be devoted to the accessory proteins, which are in some bacteria required for aiming of the T6SS. This will certainly reveal novel fascinating mechanisms of dynamic localization of proteins within bacterial cells, which will have implications reaching beyond the T6SS field.

DISCLOSURE STATEMENT

The authors are not aware of any affiliations, memberships, funding, or financial holdings that might be perceived as affecting the objectivity of this review.

ACKNOWLEDGMENTS

We would like to thank Dr. Chiara Rapisarda and Dr. Rémi Fronzes for sharing the structures of the membrane complex prior publication. The work on this review was supported by Swiss National Science Foundation grants BSSGI0_155778 and 31003A_159525.

LITERATURE CITED

1. Alcoforado Diniz J, Liu Y, Coulthurst SJ. 2015. Molecular weaponry: diverse effectors delivered by the Type VI secretion system. *Cell. Microbiol.* 17(12):1742–51
2. Arisaka F, Yap ML, Kanamaru S, Rossmann MG. 2016. Molecular assembly and structure of the bacteriophage T4 tail. *Biophys. Rev.* 8(4):385–96
3. Aschtgen M-S, Bernard CS, Bentzmann SD, Lloubès R, Cascales E. 2008. SciN is an outer membrane lipoprotein required for type VI secretion in enteroaggregative *Escherichia coli*. *J. Bacteriol.* 190(22):7523–31
4. Aschtgen M-S, Gavioli M, Dessen A, Lloubès R, Cascales E. 2010. The SciZ protein anchors the enteroaggregative *Escherichia coli* Type VI secretion system to the cell wall. *Mol. Microbiol.* 75(4):886–99
5. Basler M, Ho BT, Mekalanos JJ. 2013. Tit-for-tat: type VI secretion system counterattack during bacterial cell-cell interactions. *Cell* 152(4):884–94

MI73CH28_Basler ARjats.cls June 10, 2019 14:25

6. Basler M, Mekalanos JJ. 2012. Type 6 secretion dynamics within and between bacterial cells. *Science* 337(6096):815
7. Basler M, Pilhofer M, Henderson GP, Jensen GJ, Mekalanos JJ. 2012. Type VI secretion requires a dynamic contractile phage tail-like structure. *Nature* 483(7388):182–86
8. Böck D, Medeiros JM, Tsao H-F, Penz T, Weiss GL, et al. 2017. In situ architecture, function, and evolution of a contractile injection system. *Science* 357(6352):713–17
9. Bondage DD, Lin JS, Ma LS, Kuo CH, Lai EM. 2016. VgrG C terminus confers the type VI effector transport specificity and is required for binding with PAAR and adaptor-effector complex. *PNAS* 113:E3931–40
10. Bönemann G, Pietrosiuk A, Diemand A, Zentgraf H, Mogk A. 2009. Remodelling of VipA/VipB tubules by ClpV-mediated threading is crucial for type VI protein secretion. *EMBO J.* 28(4):315–25
11. Boyer F, Fichant G, Berthod J, Vandenbrouck Y, Attree I. 2009. Dissecting the bacterial type VI secretion system by a genome wide in silico analysis: what can be learned from available microbial genomic resources? *BMC Genom*. 10:104
12. Brackmann M, Nazarov S, Wang J, Basler M. 2017. Using force to punch holes: mechanics of contractile nanomachines. *Trends Cell Biol*. 27(9):623–32
13. Brackmann M, Wang J, Basler M. 2018. Type VI secretion system sheath inter-subunit interactions modulate its contraction. *EMBO Rep*. 19(2):225–33
14. Brodmann M, Dreier RF, Broz P, Basler M. 2017. *Francisella* requires dynamic type VI secretion system and ClpB to deliver effectors for phagosomal escape. *Nat. Commun.* 8:15853
15. Bröms JE, Sjöstedt A, Lavander M. 2010. The role of the *Francisella tularensis* pathogenicity island in type VI secretion, intracellular survival, and modulation of host cell signaling. *Front. Microbiol.* 1:136
16. Burkinshaw BJ, Liang X, Wong M, Le ANH, Lam L, Dong TG. 2018. A type VI secretion system effector delivery mechanism dependent on PAAR and a chaperone-co-chaperone complex. *Nat. Microbiol.* 3:632–40
17. Carlsson F, Joshi SA, Rangell L, Brown EJ. 2009. Polar localization of virulence-related Esx-1 secretion in mycobacteria. *PLOS Pathog*. 5(1):e1000285
18. Casabona MG, Silverman JM, Sall KM, Boyer F, Couté Y, et al. 2013. An ABC transporter and an outer membrane lipoprotein participate in posttranslational activation of type VI secretion in *Pseudomonas aeruginosa*. *Environ. Microbiol*. 15(2):471–86
19. Cascales E. 2008. The type VI secretion toolkit. *EMBO Rep*. 9(8):735–41
20. Chakravortty D, Rohde M, Jäger L, Deiwick J, Hensel M. 2005. Formation of a novel surface structure encoded by *Salmonella* Pathogenicity Island 2. *EMBO J.* 24(11):2043–52
21. Chang Y-W, Rettberg LA, Ortega DR, Jensen GJ. 2017. In vivo structures of an intact type VI secretion system revealed by electron cryotomography. *EMBO Rep*. 18(7):1090–99
22. Charles M, Pérez M, Kobil JH, Goldberg MB. 2001. Polar targeting of *Shigella* virulence factor IcsA in Enterobacteriacae and *Vibrio*. *PNAS* 98(17):9871–76
23. Chen L, Zou Y, She P, Wu Y. 2015. Composition, function, and regulation of T6SS in *Pseudomonas aeruginosa*. *Microbiol. Res*. 172:19–25
24. Cherrak Y, Rapisarda C, Pellarin R, Bouvier G, Bardiaux B, et al. 2018. Biogenesis and structure of a type VI secretion baseplate. *Nat. Microbiol.* 3(12):1404–16
25. Cianfanelli FR, Alcoforado Diniz J, Guo M, De Cesare V, Trost M, Coulthurst SJ. 2016. VgrG and PAAR proteins define distinct versions of a functional Type VI secretion system. *PLOS Pathog*. 12(6):e1005735
26. Clemens DL, Ge P, Lee B-Y, Horwitz MA, Zhou ZH. 2015. Atomic structure of T6SS reveals interlaced array essential to function. *Cell* 160(5):940–51
27. Deville C, Carroni M, Franke KB, Topf M, Bukau B, et al. 2017. Structural pathway of regulated substrate transfer and threading through an Hsp100 disaggregase. *Sci. Adv.* 3(8):e1701726
28. Dik DA, Marous DR, Fisher JF, Mobashery S. 2017. Lytic transglycosylases: concinnity in concision of the bacterial cell wall. *Crit. Rev. Biochem. Mol. Biol.* 52(5):503–42
29. Dix SR, Owen HJ, Sun R, Ahmad A, Shastri S, et al. 2018. Structural insights into the function of type VI secretion system TssA subunits. *Nat Commun*. 9(1):4765

30. Durand E, Nguyen VS, Zoued A, Logger L, Péhau-Arnaudet G, et al. 2015. Biogenesis and structure of a type VI secretion membrane core complex. *Nature* 523(7562):555–60
31. Durand E, Zoued A, Spinelli S, Watson PJH, Aschtgen M-S, et al. 2012. Structural characterization and oligomerization of the TssL protein, a component shared by bacterial type VI and type IVb secretion systems. *J. Biol. Chem.* 287(17):14157–68
32. Felisberto-Rodrigues C, Durand E, Aschtgen M-S, Blangy S, Ortiz-Lombardia M, et al. 2011. Towards a structural comprehension of bacterial type VI secretion systems: characterization of the TssJ-TssM complex of an *Escherichia coli* pathovar. *PLOS Patbog*. 7(11):e1002386
33. Förster A, Planamente S, Manoli E, Lossi NS, Freemont PS, Filloux A. 2014. Coevolution of the ATPase ClpV, the sheath proteins TssB and TssC, and the accessory protein TagJ/HsiE1 distinguishes type VI secretion classes. *J. Biol. Chem.* 289(47):33032–43
34. French CT, Toesca IJ, Wu T-H, Teslaa T, Beaty SM, et al. 2011. Dissection of the *Burkholderia* intracellular life cycle using a photothermal nanoblade. *PNAS* 108(29):12095–100
35. Fritsch MJ, Trunk K, Diniz JA, Guo M, Trost M, Coulthurst SJ. 2013. Proteomic identification of novel secreted antibacterial toxins of the *Serratia marcescens* type VI secretion system. *Mol. Cell. Proteom.* 12(10):2735–49
36. Gates SN, Yokom AL, Lin J, Jackrel ME, Rizo AN, et al. 2017. Ratchet-like polypeptide translocation mechanism of the AAA+ disaggregase Hsp104. *Science* 357(6348):273–79
37. Geiger T, Pazos M, Lara-Tejero M, Vollmer W, Galán JE. 2018. Peptidoglycan editing by a specific LD-transpeptidase controls the muramidase-dependent secretion of typhoid toxin. *Nat. Microbiol.* 3(11):1243–54
38. Gerc AJ, Diepold A, Trunk K, Porter M, Rickman C, et al. 2015. Visualization of the *Serratia* Type VI secretion system reveals unprovoked attacks and dynamic assembly. *Cell Rep*. 12(12):2131–42
39. Ghosal D, Jeong KC, Chang Y-W, Gyore J, Teng L, et al. 2019. Molecular architecture, polar targeting and biogenesis of the *Legionella* Dot/Icm T4SS. *Nat. Microbiol.* In press. **https://doi.org/10.1038/s41564-019-0427-4**
40. Ho BT, Basler M, Mekalanos JJ. 2013. Type 6 secretion system-mediated immunity to type 4 secretion system-mediated horizontal gene transfer. *Science* 342(6155):250–53
41. Ho BT, Dong TG, Mekalanos JJ. 2014. A view to a kill: the bacterial type VI secretion system. *Cell Host Microbe* 15(1):9–21
42. Hsu F, Schwarz S, Mougous JD. 2009. TagR promotes PpkA-catalyzed type VI secretion activation in *Pseudomonas aeruginosa*. *Mol. Microbiol*. 72(5):1111–25
43. Jain S, van Ulsen P, Benz I, Schmidt MA, Fernandez R, et al. 2006. Polar localization of the autotransporter family of large bacterial virulence proteins. *J. Bacteriol.* 188(13):4841–50
44. Jeong KC, Ghosal D, Chang Y-W, Jensen GJ, Vogel JP. 2017. Polar delivery of *Legionella* type IV secretion system substrates is essential for virulence. *PNAS* 114(30):8077–82
45. Jiang F, Li N, Wang X, Cheng J, Huang Y, et al. 2019. Cryo-EM structure and assembly of an extracellular contractile injection system. *Cell* 177(2):370–83.e15
46. Joshi A, Kostiuk B, Rogers A, Teschler J, Pukatzki S, Yildiz FH. 2017. Rules of engagement: the type VI secretion system in *Vibrio cholerae*. *Trends Microbiol*. 25:426–79
47. Kudryashev M, Wang RY-R, Brackmann M, Scherer S, Maier T, et al. 2015. Structure of the type VI secretion system contractile sheath. *Cell* 160(5):952–62
48. Laloux G, Jacobs-Wagner C. 2014. How do bacteria localize proteins to the cell pole? *J. Cell Sci.* 127(Part 1):11–19
49. Leiman PG, Basler M, Ramagopal UA, Bonanno JB, Sauder JM, et al. 2009. Type VI secretion apparatus and phage tail-associated protein complexes share a common evolutionary origin. *PNAS* 106(11):4154–59
50. Leiman PG, Shneider MM. 2012. Contractile tail machines of bacteriophages. *Adv. Exp. Med. Biol.* 726:93–114
51. Leung KY, Siame BA, Snowball H, Mok Y-K. 2011. Type VI secretion regulation: crosstalk and intracellular communication. *Host-Microbe Interact*. 14(1):9–15

MI73CH28_Basler ARjats.cls June 10, 2019 14:25

52. Liang X, Moore R, Wilton M, Wong MJ, Lam L, Dong TG. 2015. Identification of divergent type VI secretion effectors using a conserved chaperone domain. *PNAS* 112:9106–11
53. Lien Y-W, Lai E-M. 2017. Type VI secretion effectors: methodologies and biology. *Front. Cell. Infect. Microbiol.* 7:254
54. Lin J-S, Pissaridou P, Wu H-H, Tsai M-D, Filloux A, Lai E-M. 2018. TagF-mediated repression of bacterial type VI secretion systems involves a direct interaction with the cytoplasmic protein Fha. *J. Biol. Chem.* 293:8829–42
55. Lin J-S, Wu H-H, Hsu P-H, Ma L-S, Pang Y-Y, et al. 2014. Fha interaction with phosphothreonine of TssL activates type VI secretion in *Agrobacterium tumefaciens*. *PLOS Pathog*. 10(3):e1003991
56. Logger L, Aschtgen M-S, Guérin M, Cascales E, Durand E. 2016. Molecular dissection of the interface between the type VI secretion TssM cytoplasmic domain and the TssG baseplate component. *J. Mol. Biol.* 428(22):4424–37
57. Lossi NS, Dajani R, Freemont P, Filloux A. 2011. Structure-function analysis of HsiF, a gp25-like component of the type VI secretion system, in *Pseudomonas aeruginosa*. *Microbiology* 157:3292–305
58. Lossi NS, Manoli E, Simpson P, Jones C, Hui K, et al. 2012. The archetype *Pseudomonas aeruginosa* proteins TssB and TagJ form a novel subcomplex in the bacterial type VI secretion system. *Mol. Microbiol.* 86(2):437–56
59. Ma L-S, Lin J-S, Lai E-M. 2009. An IcmF family protein, ImpLM, is an integral inner membrane protein interacting with ImpKL, and its Walker A motif is required for type VI secretion system-mediated Hcp secretion in *Agrobacterium tumefaciens*. *J. Bacteriol*. 191(13):4316–29
60. Ma L-S, Narberhaus F, Lai E-M. 2012. IcmF family protein TssM exhibits ATPase activity and energizes type VI secretion. *J. Biol. Chem.* 287(19):15610–21
61. Miyata ST, Bachmann V, Pukatzki S. 2013. Type VI secretion system regulation as a consequence of evolutionary pressure. *J. Med. Microbiol.* 62(Part 5):663–76
62. Morgan JK, Luedtke BE, Shaw EI. 2010. Polar localization of the *Coxiella burnetii* type IVB secretion system. *FEMS Microbiol. Lett.* 305(2):177–83
63. Motley ST, Lory S. 1999. Functional characterization of a serine/threonine protein kinase of *Pseudomonas aeruginosa*. *Infect. Immun*. 67(10):5386–94
64. Mougous JD, Gifford CA, Ramsdell TL, Mekalanos JJ. 2007. Threonine phosphorylation post-translationally regulates protein secretion in *Pseudomonas aeruginosa*. *Nat. Cell Biol*. 9(7):797–803
65. Narita S, Tokuda H. 2006. An ABC transporter mediating the membrane detachment of bacterial lipoproteins depending on their sorting signals. *FEBS Lett*. 580(4):1164–70
66. Nazarov S, Schneider JP, Brackmann M, Goldie KN, Stahlberg H, Basler M. 2018. Cryo-EM reconstruction of Type VI secretion system baseplate and sheath distal end. *EMBO J*. 37(4):e97103
67. Nguyen VS, Logger L, Spinelli S, Legrand P, Huyen Pham TT, et al. 2017. Type VI secretion TssK baseplate protein exhibits structural similarity with phage receptor-binding proteins and evolved to bind the membrane complex. *Nat. Microbiol.* 2(9):17103
68. Ostrowski A, Cianfanelli FR, Porter M, Mariano G, Peltier J, et al. 2018. Killing with proficiency: integrated post-translational regulation of an offensive Type VI secretion system. *PLOS Pathog*. 14(7):e1007230
69. Park Y-J, Lacourse KD, Cambillau C, DiMaio F, Mougous JD, Veesler D. 2018. Structure of the type VI secretion system TssK-TssF-TssG baseplate subcomplex revealed by cryo-electron microscopy. *Nat. Commun*. 9(1):5385
70. Pietrosiuk A, Lenherr ED, Falk S, Bönemann G, Kopp J, et al. 2011. Molecular basis for the unique role of the AAA+ chaperone ClpV in type VI protein secretion. *J. Biol. Chem.* 286(34):30010–21
71. Planamente S, Salih O, Manoli E, Albesa-Jové D, Freemont PS, Filloux A. 2016. TssA forms a gp6-like ring attached to the type VI secretion sheath. *EMBO J*. 35(15):1613–27
72. Pukatzki S, Ma AT, Revel AT, Sturtevant D, Mekalanos JJ. 2007. Type VI secretion system translocates a phage tail spike-like protein into target cells where it cross-links actin. *PNAS* 104(39):15508–13
73. Pukatzki S, Ma AT, Sturtevant D, Krastins B, Sarracino D, et al. 2006. Identification of a conserved bacterial protein secretion system in *Vibrio cholerae* using the *Dictyostelium* host model system. *PNAS* 103(5):1528–33

74. Quentin D, Ahmad S, Shanthamoorthy P, Mougous JD, Whitney JC, Raunser S. 2018. Mechanism of loading and translocation of type VI secretion system effector Tse6. *Nat. Microbiol.* 3(10):1142–52
75. Rao VA, Shepherd SM, English G, Coulthurst SJ, Hunter WN. 2011. The structure of *Serratia marcescens* Lip, a membrane-bound component of the type VI secretion system. *Acta Crystallogr. D Biol. Crystallogr.* 67(12):1065–72
76. Rapisarda C, Cherrak Y, Kooger R, Schmidt V, Pellarin R. 2019. In situ and high-resolution cryo-EM structure of a bacterial type VI secretion system membrane complex. *EMBO J.* 38:e100886
77. Renault MG, Zamarreno Beas J, Douzi B, Chabalier M, Zoued A, et al. 2018. The gp27-like hub of VgrG serves as adaptor to promote hcp tube assembly. *J. Mol. Biol.* 430(18 Part B):3143–56
78. Ringel PD, Hu D, Basler M. 2017. The role of type VI secretion system effectors in target cell lysis and subsequent horizontal gene transfer. *Cell Rep.* 21(13):3927–40
79. Robb CS, Nano FE, Boraston AB. 2010. Cloning, expression, purification, crystallization and preliminary X-ray diffraction analysis of intracellular growth locus E (IglE) protein from *Francisella tularensis* subsp. *novicida*. *Acta Crystallograph. F Struct. Biol. Cryst. Commun.* 66(12):1596–98
80. Rosch J, Caparon M. 2004. A microdomain for protein secretion in Gram-positive bacteria. *Science* 304(5676):1513–15
81. Salih O, He S, Planamente S, Stach L, MacDonald JT, et al. 2018. Atomic structure of type VI contractile sheath from *Pseudomonas aeruginosa*. *Structure* 26(2):329–36.e3
82. Santin YG, Cascales E. 2017. Domestication of a housekeeping transglycosylase for assembly of a Type VI secretion system. *EMBO Rep.* 18(1):138–49
83. Santin YG, Doan T, Lebrun R, Espinosa L, Journet L, Cascales E. 2018. In vivo TssA proximity labelling during type VI secretion biogenesis reveals TagA as a protein that stops and holds the sheath. *Nat. Microbiol.* 3(11):1304
84. Scheurwater EM, Burrows LL. 2011. Maintaining network security: how macromolecular structures cross the peptidoglycan layer. *FEMS Microbiol. Lett.* 318(1):1–9
85. Schwarz S, Singh P, Robertson JD, LeRoux M, Skerrett SJ, et al. 2014. VgrG-5 is a *Burkholderia* type VI secretion system-exported protein required for multinucleated giant cell formation and virulence. *Infect. Immun.* 82(4):1445–52
86. Schwarz S, West TE, Boyer F, Chiang W-C, Carl MA, et al. 2010. *Burkholderia* type VI secretion systems have distinct roles in eukaryotic and bacterial cell interactions. *PLOS Pathog.* 6(8):e1001068
87. Sciara G, Bebeacua C, Bron P, Tremblay D, Ortiz-Lombardia M, et al. 2010. Structure of lactococcal phage p2 baseplate and its mechanism of activation. *PNAS* 107(15):6852–57
88. Scott ME, Dossani ZY, Sandkvist M. 2001. Directed polar secretion of protease from single cells of *Vibrio cholerae* via the type II secretion pathway. *PNAS* 98(24):13978–83
89. Shneider MM, Buth SA, Ho BT, Basler M, Mekalanos JJ, Leiman PG. 2013. PAAR-repeat proteins sharpen and diversify the type VI secretion system spike. *Nature* 500(7462):350–53
90. Silverman JM, Austin LS, Hsu F, Hicks KG, Hood RD, Mougous JD. 2011. Separate inputs modulate phosphorylation-dependent and -independent type VI secretion activation. *Mol. Microbiol.* 82(5):1277–90
91. Spínola-Amilibia M, Davó-Siguero I, Ruiz FM, Santillana E, Medrano FJ, Romero A. 2016. The structure of VgrG1 from *Pseudomonas aeruginosa*, the needle tip of the bacterial type VI secretion system. *Acta Crystallogr. D Struct. Biol.* 72(Part 1):22–33
92. Szwedziak P, Pilhofer M. 2019. Bidirectional contraction of a type six secretion system. *Nat. Commun.* 10:1565
93. Taylor NMI, Prokhorov NS, Guerrero-Ferreira RC, Shneider MM, Browning C, et al. 2016. Structure of the T4 baseplate and its function in triggering sheath contraction. *Nature* 533(7603):346
94. Toesca IJ, French CT, Miller JF. 2014. The Type VI secretion system spike protein VgrG5 mediates membrane fusion during intercellular spread by pseudomallei group *Burkholderia* species. *Infect. Immun.* 82(4):1436–44
95. Typas A, Banzhaf M, Gross CA, Vollmer W. 2011. From the regulation of peptidoglycan synthesis to bacterial growth and morphology. *Nat. Rev. Microbiol.* 10(2):123–36

MI73CH28_Basler ARjats.cls June 10, 2019 14:25

96. Unterweger D, Kostiuk B, Ötjengerdes R, Wilton A, Diaz-Satizabal L, Pukatzki S. 2015. Chimeric adaptor proteins translocate diverse type VI secretion system effectors in *Vibrio cholerae*. *EMBO J.* 34:2198–210
97. Veesler D, Spinelli S, Mahony J, Lichière J, Blangy S, et al. 2012. Structure of the phage TP901–1 1.8 MDa baseplate suggests an alternative host adhesion mechanism. *PNAS* 109(23):8954–58
98. Vettiger A, Basler M. 2016. Type VI secretion system substrates are transferred and reused among sister cells. *Cell* 167(1):99–110.e12
99. Vettiger A, Winter J, Lin L, Basler M. 2017. The type VI secretion system sheath assembles at the end distal from the membrane anchor. *Nat. Commun.* 8:16088
100. Wang J, Brackmann M, Castaño-Díez D, Kudryashev M, Goldie KN, et al. 2017. Cryo-EM structure of the extended type VI secretion system sheath-tube complex. *Nat. Microbiol.* 2(11):1507–12
101. Weber BS, Hennon SW, Wright MS, Scott NE, de Berardinis V, et al. 2016. Genetic dissection of the type VI secretion system in *Acinetobacter* and identification of a novel peptidoglycan hydrolase, TagX, required for its biogenesis. *mBio* 7(5):e01253-16
102. Wilton M, Wong MJQ, Tang L, Liang X, Moore R, et al. 2016. Chelation of membrane-bound cations by extracellular DNA activates the type VI secretion system in *Pseudomonas aeruginosa*. *Infect. Immun.* 84(8):2355–61
103. Yang Z, Zhou X, Ma Y, Zhou M, Waldor MK, et al. 2018. Serine/threonine kinase PpkA coordinates the interplay between T6SS2 activation and quorum sensing in the marine pathogen *Vibrio alginolyticus*. *Environ. Microbiol.* 20:903–19
104. Yin M, Yan Z, Li X. 2019. Architecture of type VI secretion system membrane core complex. *Cell Res.* 29:251–52
105. Yu H, Lupoli TJ, Kovach A, Meng X, Zhao G, et al. 2018. ATP hydrolysis-coupled peptide translocation mechanism of *Mycobacterium tuberculosis* ClpB. *PNAS* 115(41):E9560–69
106. Zheng J, Ho B, Mekalanos JJ. 2011. Genetic analysis of anti-amoebae and anti-bacterial activities of the type VI secretion system in *Vibrio cholerae*. *PLOS ONE* 6(8):e23876
107. Zheng J, Leung KY. 2007. Dissection of a type VI secretion system in *Edwardsiella tarda*. *Mol. Microbiol.* 66(5):1192–206
108. Zoued A, Cassaro CJ, Durand E, Douzi B, España AP, et al. 2016. Structure-function analysis of the TssL cytoplasmic domain reveals a new interaction between the type VI secretion baseplate and membrane complexes. *J. Mol. Biol.* 428(22):4413–23
109. Zoued A, Duneau J-P, Durand E, España AP, Journet L, et al. 2018. Tryptophan-mediated dimerization of the TssL transmembrane anchor is required for type VI secretion system activity. *J. Mol. Biol.* 430(7):987–1003
110. Zoued A, Durand E, Bebeacua C, Brunet YR, Douzi B, et al. 2013. TssK is a trimeric cytoplasmic protein interacting with components of both phage-like and membrane anchoring complexes of the type VI secretion system. *J. Biol. Chem.* 288(38):27031–41
111. Zoued A, Durand E, Brunet YR, Spinelli S, Douzi B, et al. 2016. Priming and polymerization of a bacterial contractile tail structure. *Nature* 531(7592):59–63
112. Zoued A, Durand E, Santin YG, Journet L, Roussel A, et al. 2017. TssA: the cap protein of the Type VI secretion system tail. *BioEssays* 39(10):1600262